

**Development of 2-Aminoquinoline  
Derivatives with Improved Drug-Like  
Character as Small Molecule Inhibitors  
for a Protein-Protein Interaction  
Domain**

Ellen Lillian Swan

February 2023

A thesis submitted for the degree of  
Doctor of Philosophy



Department of Chemistry

School of Physics, Chemistry and Earth Sciences

The University of Adelaide



# Contents

<b>List of Publications</b>	<b>viii</b>
<b>List of Figures</b>	<b>ix</b>
<b>List of Tables</b>	<b>xviii</b>
<b>List of Schemes</b>	<b>xxii</b>
<b>Abstract</b>	<b>xxviii</b>
<b>Declaration</b>	<b>xxx</b>
<b>Acknowledgments</b>	<b>xxxi</b>
<b>List of Communications &amp; Presentations</b>	<b>xxxiii</b>
<b>List of Abbreviations</b>	<b>xxxiv</b>
<b>1 Introduction</b>	<b>1</b>
1.1 Contextual statement . . . . .	1
1.2 Statement of Authorship and associated publication . . . . .	2
1.3 SH3 Domains . . . . .	26
1.3.1 Tec kinase family . . . . .	26
1.3.2 Native Tec SH3 domain ligands . . . . .	27
1.4 Small molecule ligand design for targeting a SH3 domain . . . . .	27
1.4.1 Rational drug design methodologies . . . . .	27
1.5 Structure-based drug design for targeting the Tec SH3 domain . . . . .	29
1.5.1 Binding affinity determination and initial SAR studies . . . . .	30
1.5.2 Binding model development . . . . .	33
1.5.3 Early SAR-guided ligand design . . . . .	36
1.5.4 Towards selective SH3 domain inhibitors . . . . .	39
1.5.5 SAR-guided design of 6-position substituted 2-aminoquinoline ligands . . . . .	41
1.5.6 Limitations of previous lead compounds . . . . .	44

1.5.7	Limitations of previous ligand binding assays . . . . .	44
1.6	Project aims . . . . .	45
1.6.1	Synthetic targets . . . . .	45
<b>2</b>	<b>Ligand binding assay validation and optimisation</b>	<b>47</b>
2.1	Introduction . . . . .	47
2.1.1	Surface Plasmon Resonance assays — General theory . . . . .	49
2.2	Proposed optimisation of the SPR binding assay . . . . .	55
2.3	Protein expression and purification . . . . .	56
2.3.1	Expression and purification of GST-Tec SH3 and GST-Tec SH3 D196A proteins . . . . .	57
2.3.2	Purification of Tec SH3 . . . . .	64
2.4	SPR binding assay validation . . . . .	67
2.4.1	Binding to GST-SH3 . . . . .	67
2.4.1.1	Introduction: Chip surface preparation and immobilisation . . . . .	67
2.4.1.2	Immobilisation of GST and GST-Tec SH3 . . . . .	69
2.4.1.3	Binding affinity assays with GST-Tec SH3 . . . . .	72
2.4.2	Binding to GST-Tec SH3 D196A mutant . . . . .	72
2.4.2.1	Immobilisation of GST and GST-Tec SH3 D196A . . . . .	72
2.4.2.2	Binding affinity assays with GST-Tec SH3 D196A mutant . . . . .	74
2.4.3	Binding to Tec SH3 . . . . .	76
2.4.3.1	Immobilisation of Tec SH3 . . . . .	76
2.4.3.2	Binding affinity assays with Tec SH3 . . . . .	80
2.5	Protein structure determination: X-ray crystallography . . . . .	87
2.5.1	Introduction to protein crystallography in rational drug design . . . . .	87
2.5.2	Introduction to crystallisation of GST-containing proteins . . . . .	87
2.5.3	Attempted crystallisation of GST-Tec SH3 . . . . .	89
2.5.4	Introduction to crystallisation of SH3 domains . . . . .	89
2.5.5	Attempted crystallisation of Tec SH3 . . . . .	90
2.6	Preparation of control ligands: general synthetic pathway . . . . .	91
2.7	Synthesis of control 2-aminoquinoline ligands with a pyridyl substituent . . . . .	95



2.7.1	Synthesis of arylmethyl piperidine derivatives . . . . .	95
2.7.2	Synthesis of 6-position substituted 2-chloroquinolines via selective Buchwald-Hartwig coupling . . . . .	100
2.7.3	Synthesis of 6-position substituted 2-aminoquinolines via Buchwald-Hartwig coupling . . . . .	107
2.7.4	Synthesis of reduced 6-position substituted 2-aminoquinolines via Buchwald-Hartwig coupling . . . . .	114
<b>3</b>	<b>Synthesis of simple 6-position substituted 2-aminoquinoline ligands</b>	<b>117</b>
3.1	Introduction . . . . .	117
3.2	General synthetic pathway . . . . .	120
3.3	Synthesis of simple 6-arylamidopiperaziny1-2-aminoquinolines . . . . .	122
3.3.1	Synthesis of 6-position substituted 2-chloroquinoline derivatives . . . . .	122
3.3.2	Synthesis of amidopiperaziny1 2-aminoquinoline derivatives . . . . .	140
3.4	SPR binding studies of 6-arylamidopiperaziny1-2-aminoquinoline derivatives . . . . .	147
3.4.1	SPR binding assay aims . . . . .	147
3.4.2	Results of SPR binding assays with GST-Tec SH3 and Tec SH3 . . . . .	148
3.4.3	Analysis of trends in SPR binding assay data with GST-Tec SH3 . . . . .	152
3.4.4	Results of SPR binding assays with GST-Tec SH3 D196A mutant . . . . .	154
3.5	Synthesis of simple 6-benzylpiperaziny1-2-aminoquinolines . . . . .	157
3.5.1	Synthesis of 6-position substituted 2-chloroquinoline derivatives . . . . .	157
3.5.2	Synthesis of 6-position substituted 2-aminoquinoline derivatives . . . . .	161
3.5.3	Derivatisation of nitrile-containing 2-aminoquinoline ligands . . . . .	165
3.6	SPR binding studies of 6-benzylpiperaziny1-2-aminoquinoline derivatives . . . . .	169
3.6.1	SPR binding assay aims . . . . .	169
3.6.2	Results of SPR binding assays with GST-Tec SH3 . . . . .	169
3.6.3	Analysis of trends in SPR binding assay data with GST-Tec SH3 . . . . .	175
3.6.4	Results of SPR binding assays with GST-Tec SH3 D196A mutant . . . . .	178
3.6.5	Summary - Results of SPR binding assays and insights into binding model	180

<b>4</b>	<b>Synthesis of complex 6-position substituted 2-aminoquinoline ligands</b>	<b>183</b>
4.1	Introduction . . . . .	183
4.2	Proposed ligands and general synthetic pathways . . . . .	187
4.3	Synthesis of complex ligands containing biaryl and 4-amido functional groups . . .	191
4.3.1	Proposed synthetic pathways of complex ligands containing biaryl and 4-amido functional groups . . . . .	191
4.3.2	Synthesis of methylenepiperidinyl derivatives containing biaryl and 4-nitrile functional groups . . . . .	194
4.3.3	Synthesis of methylenepiperidinyl-substituted quinoline derivatives containing biaryl and 4-nitrile functional groups . . . . .	208
4.3.4	Synthesis of benzylpiperazinyl derivatives containing biaryl and 4-nitrile functional groups . . . . .	213
4.3.4.1	Synthesis of benzylpiperazinyl derivatives containing biaryl and 4-nitrile functional groups via alternative protecting group strategy	218
4.4	Synthesis of complex ligands containing biaryl and 2-pyridyl functional groups . .	226
4.4.1	Proposed synthetic pathways of complex ligands containing biaryl and 2-pyridyl functional groups . . . . .	226
4.4.1.1	Synthesis of methylene piperidinyl derivatives containing 2-pyridyl and biaryl functional groups . . . . .	228
4.4.1.2	Synthesis of methylpiperidine-substituted quinoline derivatives containing 2-pyridyl and biaryl functional groups . . . . .	236
4.4.1.3	Synthesis of methylpiperazine-substituted quinoline derivatives containing 2-pyridyl and biaryl functional groups . . . . .	240
4.5	Synthesis of complex ligands containing 2-pyridyl and 4-amido functional groups .	246
4.5.1	Proposed synthetic pathways of complex ligands containing 2-pyridyl and 4-amido functional groups . . . . .	246
4.5.1.1	Synthesis of methylene piperidinyl derivatives containing 2-pyridyl and 4-nitrile functional groups . . . . .	249
4.5.1.2	Synthesis of methylpiperazine-substituted derivatives containing 2-pyridyl and 4-nitrile functional groups . . . . .	253
4.6	SPR binding studies of complex 6-position substituted 2-aminoquinoline ligands .	258

4.6.1	SPR binding assay aims . . . . .	258
4.6.2	Results of SPR binding assays with GST-Tec SH3 and insights into binding model . . . . .	258
<b>5</b>	<b>Conclusions and Future Directions</b>	<b>262</b>
5.1	SPR ligand binding assay . . . . .	262
5.2	Protein crystallisation . . . . .	263
5.3	Simple 6-substituted 2-aminoquinoline ligands containing a piperazine component	263
5.4	Complex 6-substituted 2-aminoquinoline ligands . . . . .	265
5.5	Proposed future work . . . . .	266
5.5.1	Optimisation of Tec SH3 protein yields . . . . .	266
5.5.2	Elucidation of the ligand-protein binding model . . . . .	267
5.5.3	SPR binding assay optimisation . . . . .	269
5.5.4	Synthesis of additional complex 6-substituted 2-aminoquinoline ligands . .	270
5.5.5	Synthesis of ligands with variable heterocycle geometry . . . . .	271
<b>6</b>	<b>Experimental</b>	<b>274</b>
6.1	General procedures - chemistry . . . . .	274
6.2	General synthetic methods . . . . .	275
6.3	Synthesis of control ligands . . . . .	281
6.3.1	Synthesis of arylmethyl and arylmethylene piperidine derivatives . . . . .	281
6.3.2	Synthesis of arylmethyl and arylmethylene piperidine 2-chloroquinoline derivatives . . . . .	287
6.3.3	Synthesis of arylmethyl and arylmethylene piperidine 2-aminoquinoline derivatives . . . . .	293
6.4	Synthesis of simple 6-position substituted 2-aminoquinoline ligands . . . . .	296
6.4.1	Synthesis of simple 6-arylpiperazinyl-2-aminoquinoline derivatives . . . .	296
6.4.2	Synthesis of simple 6-arylmethylpiperazinyl-2-aminoquinoline derivatives .	323
6.5	Synthesis of complex 6-substituted-2-aminoquinoline ligands . . . . .	340
6.5.1	Synthesis of a complex 6-benzylpiperidinyl 2-aminoquinoline ligand containing biaryl and nitrile components . . . . .	340

6.5.2	Synthesis of a complex 6-benzylpiperazinyl 2-aminoquinoline ligand containing biaryl and nitrile components . . . . .	349
6.5.3	Synthesis of a complex 6-arylmethylpiperidine ligand containing biaryl and 2-pyridyl components . . . . .	354
6.5.4	Synthesis of a complex 6-arylmethylpiperazinyl ligand containing biaryl and 2-pyridyl components . . . . .	361
6.5.5	Towards the synthesis of a 6-arylmethylpiperidinyl 2-aminoquinoline ligand containing 4-amido and 2-pyridyl components . . . . .	364
6.5.6	Towards the synthesis of a 6-arylmethylpiperazinyl 2-aminoquinoline ligand containing 4-amido and 2-pyridyl components . . . . .	366
6.6	Protein Methods: Expression and purification . . . . .	367
6.6.1	Comment on general protein methods . . . . .	367
6.6.1.1	Common buffers and solutions . . . . .	368
6.6.1.2	Purification of GST-SH3 fusion proteins by agarose/glutathione column chromatography . . . . .	368
6.6.1.3	Determination of protein concentration using Bradford dye binding assay . . . . .	369
6.6.1.4	PD10 buffer exchange chromatography . . . . .	369
6.6.1.5	Thrombin digestion . . . . .	370
6.6.1.6	Size exclusion chromatography . . . . .	370
6.6.1.7	SDS-PAGE: sodium dodecyl sulfate-polyacrylamide gel electrophoresis . . . . .	371
6.6.2	Protein preparation methods . . . . .	372
6.6.2.1	Bacterial growth media . . . . .	372
6.6.2.2	Procedure for preparation of GST-Tec SH3 fusion proteins for SPR experiments and x-ray crystallography . . . . .	372
6.6.3	Procedure for preparation of Tec SH3 protein for x-ray crystallography experiments . . . . .	373
6.7	Protein Methods: SPR ligand binding assays . . . . .	373
6.7.1	Preparation of GST protein . . . . .	373

6.7.2	Ligand-binding assays with GST-SH3 fusion proteins and Tec SH3 domain using SPR experiments . . . . .	374
6.7.3	Optimisation of protein pre-concentration conditions by pH scouting . . . . .	376
6.8	Protein Methods: X-ray crystallography . . . . .	376
6.8.1	Automated preparation of screening trays . . . . .	376
6.8.2	Manual preparation of screening trays . . . . .	377
6.8.3	Preparation of optimisation trays . . . . .	377
<b>Appendix A: Summary of SPR-derived ligand binding affinities</b>		<b>377</b>
<b>Appendix B: Hansch plot analysis of trends in SPR binding assay data with GST-Tec SH3</b>		<b>386</b>
<b>Bibliography</b>		<b>391</b>

# List of Publications

1. **Swan, E. L.**; Jayne, S.; Pyke, S. M., Recent Developments in Targeting “Undruggable” SH3 Domains. In 2021 Medicinal Chemistry Reviews, Bronson, J. J., Ed. Medicinal Chemistry Division of the American Chemical Society: 1155 Sixteenth Street, NW, Washington, DC 20036, USA, 2021; Vol. 56, pp 389-411.

# List of Figures

1.1	Simplified gene sequence of the human Tec tyrosine kinase. . . . .	26
1.2	Small molecule compounds identified from LUDI screening as potential ligands for the Tec SH3 domain. . . . .	30
1.3	Example NMR spectrum overlay from 2D HSQC chemical shift perturbation assays for a ligand in fast exchange. . . . .	31
1.4	Example of normalised binding isotherm generated from NMR chemical shift perturbation assay with the Tec SH3 domain, and representation of amino acid residues affected during the binding interaction. . . . .	33
1.5	Proposed binding model between 2-aminoquinoline and the Tec SH3 domain, through a $\pi$ - $\pi$ stacking interaction with W215 and salt-bridge formation with D196. . . . .	34
1.6	Extended proposed binding model of 2-aminoquinoline with the Tec SH3 domain, indicating proximal residues to the ligand binding site. . . . .	36
1.7	Accessible rotamers for <i>N</i> -substituted 2-aminoquinoline derivatives and proposed interactions with D196 of the Tec SH3 domain. . . . .	37
1.8	Structure and reported binding affinities of 3-substituted 2-aminoquinoline ligands, as determined by NMR chemical shift perturbation assays. . . . .	37
1.9	Structures and reported binding affinities of 4-substituted 2-aminoquinoline ligands, as determined by NMR chemical shift perturbation assays. . . . .	38
1.10	Structure of 6-substituted 2-aminoquinoline ligand scaffold containing an acetal group for targeting the Tec SH3 domain . . . . .	39
1.11	Reported structures and binding affinities of 6-phenylphenoxy substituted 2-aminoquinolone ligands for the Tec SH3 domain. . . . .	42
1.12	General structures of proposed benzylpiperazinyl-based ligands. . . . .	46
1.13	General proposed structure of 2-aminoquinoline ligands with a complex 6-position extension. . . . .	46
2.1	Schematic representation of immobilised protein to the SPR sensor chip surface. . .	49
2.2	Schematic representation of total internal reflection condition of incident light against an SPR chip. . . . .	50

2.3	Schematic representation of binding interaction upon SPR sensor chip surface, and the resulting change in SPR angle. . . . .	51
2.4	General workflow for ligand binding affinity assays by SPR. . . . .	52
2.5	Example SPR sensorgrams for binding of 2-aminoquinoline ligand to GST-Tec SH3 protein. . . . .	53
2.6	Example binding isotherm derived from SPR sensorgrams of 2-aminoquinoline ligand binding to GST-Tec SH3 protein. . . . .	54
2.7	Simulated SPR sensorgrams displaying the different responses observed for either a one-site or multi-site ligand binding model. . . . .	55
2.8	Structures of proposed control 6-heterocycle substituted 2-aminoquinoline ligands. . . . .	56
2.9	Representation of cloned pGEX-4T-2 plasmid vector utilised for expression of GST-tagged Tec SH3 domain. . . . .	58
2.10	Purification of GST-Tec SH3 protein by agarose/glutathione chromatography. . . . .	60
2.11	Purification of GST-Tec SH3 protein by size-exclusion chromatography. . . . .	61
2.12	Deconvoluted mass spectrum of GST-Tec SH3 fusion protein. . . . .	62
2.13	Deconvoluted mass spectrum of GST-Tec SH3 D196A fusion protein. . . . .	63
2.14	Purification of Tec SH3 protein by size-exclusion chromatography following thrombin digest of GST-Tec SH3 fusion protein. . . . .	65
2.15	Deconvoluted mass spectrum of Tec SH3 protein. . . . .	66
2.16	Relative (normalised) response during pre-conditioning of a flow channel on a CM5 SPR sensor chip. . . . .	67
2.17	Schematic representation of utilising amine coupling methods to immobilise the target protein to the SPR sensor chip surface. . . . .	69
2.18	SPR sensorgram displaying pH scouting and protein immobilisation of GST. . . . .	70
2.19	SPR Sensorgram displaying pH scouting and protein immobilisation of GST-Tec SH3 D196A. . . . .	73
2.20	SPR sensorgrams and derived isotherm for binding of control ligands to GST-Tec SH3 or GST-Tec SH3 D196A. . . . .	75
2.21	SPR Sensorgram displaying surface activation and blocking. . . . .	77
2.22	Solution structure of the Tec SH3 domain (PDB ID: 1GL5), highlighting lysine residues available for amine coupling via SPR. . . . .	78



2.23	SPR Sensorgram displaying pH scouting and immobilisation of Tec SH3. . . . .	79
2.24	SPR Sensorgrams for binding of control ligands to Tec SH3. . . . .	81
2.25	Violin plot comparison of normalised $\Delta$ RU values for control ligands binding to either GST-Tec SH3 or Tec SH3 proteins. . . . .	83
2.26	Hydrophobicity analysis of Tec SH3 protein sequence. . . . .	84
2.27	Hydrophobicity surface analysis of Tec SH3 protein. . . . .	84
2.28	Hydrophobicity analysis of GST-Tec SH3 fusion protein sequence. . . . .	85
2.29	Violin plot comparison of normalised $\Delta$ RU values for control ligands binding to either GST-Tec SH3 or Tec SH3 proteins. . . . .	86
2.30	General structures of possible products from Buchwald-Hartwig coupling of heterocyclic amines and 6-bromo-2-chloroquinoline. . . . .	93
2.31	Excerpts of $^1\text{H}$ and $^{13}\text{C}$ NMR spectra indicating broadened signals due to restricted conformation of the piperidinyl ring and slow rotation of the Boc protecting group in pyridylmethylene piperidinyl derivatives. . . . .	99
2.32	Structural analysis of a 6-position coupled 2-chloroquinoline derivative, from ROESY and HMBC 2D NMR spectra. . . . .	106
2.33	Structural analysis of a 2-position coupled 6-bromoquinoline derivative, from HMBC 2D NMR spectra. . . . .	107
2.34	Comparison of $^1\text{H}$ NMR spectra indicating increased piperidinyl ring signal complexity upon alkene bond reduction by hydrogenation. . . . .	111
2.35	Comparison of $^1\text{H}$ NMR spectra of differentially substituted piperidine derivatives, demonstrating the effects of steric bulk, altered ring-flipping and chair-like structure on signal resolution. . . . .	113
2.36	Comparison of truncated $^1\text{H}$ NMR spectra of control 2-aminoquinoline ligands. . .	116
3.1	Proposed 6-position substituted 2-aminoquinoline ligand families with calculated <i>logP</i> values to investigate a more hydrophilic benzylpiperidinyl derivative. . . . .	120
3.2	Comparison of $^1\text{H}$ NMR spectra displaying characteristic upfield shifts for C(5)H and C(7)H for 6-substituted 2-chloroquinoline derivatives. . . . .	124
3.3	Normalised and overlaid $^1\text{H}$ NMR spectra showing comparison of piperazinyl H signal broadness in substituted amidopiperazines. . . . .	127

3.4	ROESY correlations (green) between piperazinyl ring hydrogens (C(2'/6')H) and quinolinyl ring hydrogens (C(5)H, C(7)H), indicating successful formation of the amidopiperazinyl-substituted 2-chloroquinoline. . . . .	127
3.5	Stacked comparison of normalised <sup>1</sup> H NMR spectra showing differences in shape, resolution and coalescence of some piperazinyl ring H signals. . . . .	135
3.6	Representation of rotamers accessible through amide group rotation, highlighting amide group partial double bond character in amide-substituted piperazinyl rings. . . . .	136
3.7	HSQC correlations (blue) between piperazinyl ring hydrogens and corresponding carbons, displaying 4 distinct chemical environments for each piperazinyl ring CH <sub>2</sub> group. . . . .	138
3.8	Stacked comparison of normalised <sup>1</sup> H NMR spectra of various amidopiperazinyl 2-chloroquinoline derivatives listed from lowest to highest value Hammett constants, illustrating differences in piperazinyl ring H signal resolution (on the NMR timescale). . . . .	139
3.9	Stacked & normalised <sup>13</sup> C NMR spectra obtained at variable temperatures to investigate piperazinyl ring dynamics. . . . .	142
3.10	Proposed mechanism of Pd sequestration for 2-pyridyl aminopiperazine derivatives during Buchwald-Hartwig coupling reactions. . . . .	144
3.11	Stacked & normalised <sup>1</sup> H NMR spectra of various amidopiperazinyl 2-aminoquinoline ligands, indicating key signals for product formation and unique signals indicating formamide side-product formation. . . . .	146
3.12	SPR sensorgrams and derived isotherms for binding of an amidopiperazinyl 2-aminoquinoline ligand to GST-Tec SH3 or Tec SH3. . . . .	151
3.13	Hansch plots displaying relationships between Hammett constants, molar refractivity and logP values for amidopiperazinyl 2-aminoquinoline ligands. . . . .	153
3.14	SPR sensorgrams and derived isotherm for binding of an amidopiperazinyl 2-aminoquinoline ligand to GST-Tec SH3 D196A mutant protein. . . . .	156
3.15	HMBC correlations between benzyl methylene group hydrogens and piperazinyl & benzyl carbons in a benzylpiperazinyl 2-chloroquinoline derivative. . . . .	158
3.16	Stacked comparison of normalised <sup>1</sup> H NMR spectra of benzylpiperazinyl-substituted-2-chloroquinoline and 2-aminoquinoline derivatives. . . . .	162

3.17	Proposed mechanism of Pd sequestration during synthesis of a 2-pyridylmethyl piperazinyl-substituted 2-aminoquinoline ligand, indicating undesired coordination of the Pd species. . . . .	165
3.18	Structures of proposed simple amide-substituted 2-aminoquinoline ligands. . . . .	165
3.19	Stacked comparison of normalised <sup>1</sup> H NMR spectra of benzylpiperazinyl-substituted 2-aminoquinoline derivatives, indicating emergence of two distinct, broad amide NH signals following nitrile hydrolysis. . . . .	168
3.20	SPR sensorgrams and derived isotherm for binding of 2-pyridylmethyl piperazinyl 2-aminoquinoline ligand binding to GST-Tec SH3. . . . .	172
3.21	Example sensorgram with sufficient curvature for kinetic model fitting. . . . .	173
3.22	Overlaid sensorgrams and fitted 1:1 kinetic model for pyridylmethylpiperazinyl ligand and with slower association and dissociation. . . . .	173
3.23	Residuals plot of 1:1 fitted kinetics model for binding of 2-pyridylmethyl piperazinyl 2-aminoquinoline ligand to GST-Tec SH3. . . . .	174
3.24	Hansch plots displaying relationships between Hammett constants, molar refractivity and <i>logP</i> values for benzylpiperazinyl 2-aminoquinoline ligands. . . . .	176
3.25	SPR sensorgrams and derived isotherms for binding of a benzylpiperazinyl-substituted 2-aminoquinoline ligand to GST-Tec SH3 D196A mutant. . . . .	180
3.26	Structures of strongest binding piperazinyl 2-aminoquinoline ligands for the Tec SH3 domain, as determined by SPR assays. . . . .	181
4.1	Proposed general structures for complex 2-aminoquinoline ligands. . . . .	187
4.2	Proposed general retrosynthesis for substituted benzylpiperidinyl 2-aminoquinoline ligands. . . . .	188
4.3	Proposed general retrosynthesis for substituted benzylpiperazinyl 2-aminoquinoline ligands. . . . .	188
4.4	Commercially-available starting materials for the synthesis of complex 2-aminoquinoline ligands. . . . .	189
4.5	Proposed synthetic pathway for synthesis of a complex benzylpiperidinyl ligand containing 4-amido and biaryl substituents. . . . .	192
4.6	Proposed synthetic pathway for synthesis of a complex benzylpiperazinyl ligand containing 4-amido and biaryl substituents. . . . .	193

4.7	Proposed alternative synthetic pathway for synthesis of benzylpiperazinyl-substituted 2-chloroquinoline derivatives, to avoid polyalkylation from benzyl bromide derivatives. . . . .	194
4.8	Comparison of normalised <sup>1</sup> H NMR, indicating successful Suzuki cross-coupling reaction towards the synthesis of a nitrile-containing substituted tolyl derivative. . .	195
4.9	Structures of di-brominated side products detected following radical brominations of substituted tolyl derivatives containing a nitrile substituent. . . . .	197
4.10	Comparison of normalised and overlaid <sup>1</sup> H NMR spectra following radical bromination of 4-methyl-3-(pyrimidin-5-yl)benzonitrile. . . . .	198
4.11	HMBC correlations (red) between methyl group hydrogens (CH <sub>2</sub> ) and phenyl ring carbons C(3), C(4) and C(5), indicating successful formation of a benzyl bromide derivative containing nitrile and bromo- functional groups. . . . .	198
4.12	Stacked and normalised <sup>1</sup> H NMR spectra of attempted Wittig reaction with a stabilised ylide. . . . .	200
4.13	Proposed mechanisms for stabilisation of ylides containing an electron-withdrawing substituent. . . . .	201
4.14	Proposed mechanism for quenching of stabilised ylides with water, to form substituted tolyl starting materials. . . . .	202
4.15	<sup>1</sup> H NMR Spectra indicating successful Wittig reaction from a stabilised ylide with benzaldehyde. . . . .	203
4.16	Structural analysis of a methylenepiperidine derivative, from HMBC and ROESY 2D NMR spectra. . . . .	205
4.17	Stacked and normalised <sup>1</sup> H NMR spectra, indicating successful Boc group removal for a nitrile & biaryl substituted benzylpiperidinyl derivative. . . . .	207
4.18	Comparison of stacked and normalised <sup>1</sup> H NMR spectra, indicating different quinoliny ring chemical shifts between 2- and 6-substituted quinoline derivatives containing a methylene piperidine substituent, with biaryl and 4-nitrile functional groups.	209
4.19	Structural analysis of a methylenepiperidine-substituted 2-chloroquinoline derivative, from HMBC and ROESY 2D NMR spectra. . . . .	210
4.20	<sup>1</sup> H NMR spectra of a methylene piperidinyl derivative and its corresponding tetrahydropyridine isomer. . . . .	210

4.21	Stacked comparison of truncated and normalised $^1\text{H}$ NMR spectra for methylene piperidinyl quinoline derivatives containing biaryl and nitrile substituents, indicating an upfield movement in chemical shift for C(3)H of the quinolinyl ring in 2-aminoquinoline derivatives. . . . .	212
4.22	Structural analysis of a benzylpiperazine-substituted 2-chloroquinoline derivative, from HMBC and ROESY 2D NMR spectra. . . . .	215
4.23	Stacked comparison of truncated and normalised $^1\text{H}$ NMR spectra for benzylpiperazinyl quinoline derivatives containing biaryl and nitrile substituents, indicating an upfield movement in chemical shift for C(3)H of the quinolinyl ring in 2-aminoquinoline derivatives. . . . .	216
4.24	Stacked comparison of truncated and normalised $^1\text{H}$ NMR spectra for Boc-protected piperazine-substituted quinoline derivatives, indicating a downfield movement in chemical shift for C(3)H of the quinolinyl ring in 2-acetamidoquinoline derivatives. . . . .	220
4.25	Stacked comparison of truncated and normalised $^1\text{H}$ NMR spectra indicating resolution of acetyl $\text{CH}_3$ signals, and the corresponding downfield chemical shifts and signal broadening for C(3)H of the quinolinyl ring following Boc group removal. . . . .	222
4.26	Stacked comparison of normalised $^1\text{H}$ NMR spectra following attempted nucleophilic substitution reaction with a diacylated 2-aminoquinoline derivative, indicating only trace amounts of the desired product had formed. . . . .	224
4.27	Proposed synthetic pathway for synthesis of a complex benzylpiperidinyl-derived ligand containing 2-pyridyl and biaryl substituents. . . . .	226
4.28	Proposed synthetic pathway for synthesis of a complex benzylpiperazinyl-derived ligand containing 2-pyridyl and biaryl substituents. . . . .	228
4.29	Structural analysis of a biaryl methylpyridine derivative by 2D HMBC NMR spectra. . . . .	229
4.30	Stacked comparison of normalised and truncated $^1\text{H}$ NMR spectra of 2,6-lutidine following radical bromination reaction, indicating formation of a distinct bromomethyl $\text{CH}_2$ singlet. . . . .	230
4.31	Structural analysis of a biaryl pyridylmethylene piperidine derivative by 2D HMBC NMR spectra. . . . .	234

4.32	Stacked comparison of normalised $^1\text{H}$ NMR spectra indicating deconvolution of piperidinyl ring signals into pseudo-axial and pseudo-equatorial chemical environments upon alkene reduction of a biaryl 2-pyridylmethylene piperidine derivative. . . . .	235
4.33	Structural analysis of a biaryl 2-pyridylmethyl piperidinyl 2-chloroquinoline derivative via 2D ROESY NMR spectra. . . . .	237
4.34	Structural analysis of a methylpiperidine-substituted 2-chloroquinoline derivative, from HMBC and ROESY 2D NMR spectra. . . . .	238
4.35	Comparison of truncated and normalised $^1\text{H}$ NMR spectra, indicating successful formation of a biaryl 2-pyridylmethyl piperidine-substituted 2-aminoquinoline ligand.	239
4.36	Stacked comparison of normalised $^1\text{H}$ NMR spectra, indicating the emergence of additional, non-piperazinyl alkyl signals for a succinimide-containing side product.	243
4.37	Structural analysis of proposed succinimide side product via 2D NMR spectra, with COSY correlations indicated by pink arrows. . . . .	243
4.38	Comparison of truncated and normalised $^1\text{H}$ NMR spectra, indicating successful formation of a biaryl 2-pyridylmethyl piperazine-substituted 2-aminoquinoline ligand.	245
4.39	Proposed synthetic pathway for the synthesis of a complex piperidinyl-containing ligand with 2-pyridyl and 4-amido substituents. . . . .	247
4.40	Proposed synthetic pathway for the synthesis of a complex piperazinyl-containing ligand with 2-pyridyl and 4-amido substituents. . . . .	248
4.41	Stacked $^1\text{H}$ NMR spectra of attempted Wittig reaction with a stabilised ylide containing a 2-pyridyl aryl group. . . . .	250
4.42	Possible resonance contributors in a pyridyl methylene phenyl derivative, indicating deshielding of alkene chemical environments through electron delocalisation. . . . .	251
4.43	Structural analysis of a pyridyl methyl phenyl derivative, from COSY and HMBC 2D NMR spectra. . . . .	252
4.44	Structural analysis of proposed piperazinyl 2-chloroquinoline derivative containing 2-pyridyl and 4-nitrile substituents via 2D NMR spectra, with HMBC correlations indicated by pink arrows. . . . .	254
4.45	Stacked comparison of truncated and normalised $^1\text{H}$ NMR spectra indicating benzyl protecting group removal during attempted Buchwald-Hartwig coupling reaction. . . . .	256

5.1	Structures of strongest binding simple 6-substituted piperazinyl 2-aminoquinoline ligands for the Tec SH3 domain (determined by SPR assays) for work in this thesis.	264
5.2	Structures of complex 6-substituted 2-aminoquinoline ligands which were successfully synthesised for testing in SPR ligand binding assays.	266
5.3	Structures of complex ligands of interest containing a 2-pyridyl ring and 4-amido group.	270
5.4	Possible synthetic pathways for synthesis of a pyridylmethylene piperidine derivative containing a nitrile substituent.	271
5.5	General proposed structure indicating the cycloalkyl group to be investigated in 6-substituted 2-aminoquinoline ligands.	272
5.6	Proposed structures of cyclohexane-containing ligands for investigating how chair-like geometry impacts ligand binding affinity for Tec SH3 domain.	272
5.7	Comparison of <i>clogP</i> values for 2-aminoquinoline ligands containing variable 6-position substituents.	273
6.1	SDS-PAGE analysis of protein samples at different timepoints during thrombin digest.	370
B.1	Hansch plots displaying relationships between Hammett constants, molar refractivity and <i>clogP</i> values for amidopiperazinyl 2-aminoquinoline ligands, and fitted simple linear equations.	388
B.2	Hansch plots displaying relationships between Hammett constants, molar refractivity and <i>clogP</i> values for benzylpiperazinyl 2-aminoquinoline ligands, and fitted simple linear equations.	389

# List of Tables

1.1	Summary of guidelines for improving ligand (oral) bioavailability proposed through the Rule of Five, Veber's Rules and QED. . . . .	28
1.2	Experimentally determined $K_d$ values from initial NMR chemical shift perturbation assays. . . . .	33
1.3	Structure and binding affinities of <i>N</i> -substituted 2-aminoquinoline derivatives, as determined by NMR chemical shift perturbation assays. . . . .	36
1.4	Reported $EC_{50}$ values of small molecule ligands for displacing a known peptide binding partner (fPRP-1) from the Tec SH3 domain, determined by FP assays (in triplicate). . . . .	39
1.5	Protein sequence alignment for various SH3 domains. . . . .	40
1.6	Reported $EC_{50}$ values from specificity FP competition binding studies with synthesised ligands and various SH3 domains. . . . .	40
1.7	Structure and reported binding affinities for various 6-substituted 2-aminoquinoline ligands for binding the Tec SH3 domain. . . . .	41
1.8	Structures and binding affinities of 2,5-pyrimidinyl-substituted 6-benzylpiperidinyl 2-aminoquinoline ligands for the Tec SH3 domain . . . . .	43
2.1	Key for deconvoluted mass spectrum of GST-Tec SH3 fusion protein. . . . .	62
2.2	Key for deconvoluted mass spectrum of GST-Tec SH3 D196A fusion protein. . . . .	63
2.3	Calculated yields for purified GST-Tec SH3 fusion proteins. . . . .	64
2.4	Key for deconvoluted mass spectrum of Tec SH3 protein. . . . .	66
2.5	Calculated yields for purified Tec SH3 protein. . . . .	66
2.6	Calculated target protein immobilisation levels for SPR assays. . . . .	68
2.7	Comparison of current and previously reported binding affinities of control ligands for GST-Tec SH3 protein. . . . .	72
2.8	Comparison of binding affinities for control ligands to GST-Tec SH3 and GST-Tec SH3 D196A proteins. . . . .	74
2.9	Comparison of binding affinities for control ligands to GST-Tec SH3 and Tec SH3 proteins. . . . .	81



2.10	Comparison of determined binding affinities of control ligands for various Tec SH3 domain-containing proteins by SPR. . . . .	86
2.11	Examples of crystallisation conditions for GST proteins reported in the Protein Data Bank. . . . .	88
2.12	Examples of crystallisation conditions for SH3 proteins reported in the Protein Data Bank. . . . .	90
2.13	Yields for phosphonium salt synthesis towards control ligands. . . . .	96
2.14	Yields for synthesis of pyridylmethylene Boc-protected piperidines via Wittig reaction. . . . .	97
2.15	Observed product distributions from employing various literature procedures for the synthesis of quinolones. . . . .	102
2.16	Observed products and yields from selective Buchwald-Hartwig coupling reaction between 6-bromo-2-chloroquinoline and pyridylmethylene piperidine derivative. . . . .	105
2.17	Yields for pyridylmethyl Boc-protected piperidine derivative formation via hydrogenation. . . . .	110
2.18	Yields for pyridylmethyl piperidine derivative liberation from Boc-protected pyridylmethyl piperidine derivatives. . . . .	112
2.19	Yields for synthesis of pyridylmethyl piperidine-substituted quinolines via Buchwald-Hartwig coupling reaction. . . . .	114
2.20	Yields for synthesis of pyridylmethyl piperidine-substituted 2-aminoquinolines via Buchwald-Hartwig coupling reaction. . . . .	115
3.1	Binding affinities of previously reported 6-heterocycle substituted 2-aminoquinoline derivatives, with high binding affinity for the Tec SH3 domain (determined by SPR assays). . . . .	118
3.2	Binding affinities of previously reported 6-heterocycle substituted 2-aminoquinoline derivatives (determined by 2D NMR chemical shift perturbation assays) and calculated <i>logP</i> values. . . . .	119
3.3	Effect of reaction solvent upon isolated yields of products from Buchwald-Hartwig coupling reactions between Boc-piperazine and 6-bromo-2-chloroquinoline. . . . .	123
3.4	Attempted amidations of piperazine-coupled 2-chloroquinoline derivatives via <i>in situ</i> formation of acid chlorides from benzoic acid derivatives. . . . .	129

3.5	Synthesis and yields of amidopiperazine-substituted 2-chloroquinoline derivatives via stepwise acid chloride formation and amidation. . . . .	131
3.6	Results of stepwise acid chloride formation from benzoic acid derivatives and subsequent amidation with piperazine-coupled 2-chloroquinoline to afford amidopiperazinyl 2-chloroquinoline derivatives. . . . .	133
3.7	Results of stepwise acid chloride formation from pyridyl carboxylic acid derivatives and subsequent amidation with piperazine-coupled 2-chloroquinoline to afford amidopiperazinyl 2-chloroquinoline derivatives. . . . .	134
3.8	Results and yields of synthesis of amidopiperazinyl 2-aminoquinoline derivatives via Buchwald-Hartwig coupling reaction. . . . .	141
3.9	Results and yields of synthesis of pyridyl-containing amidopiperazinyl 2-aminoquinoline derivatives via Buchwald-Hartwig coupling reaction. . . . .	144
3.10	Binding affinities of amidopiperazinyl derivative ligands determined by SPR for binding GST-tagged- and naked Tec SH3. . . . .	148
3.11	Binding affinities of 6-arylamidopiperazinyl-2-aminoquinoline ligands for GST-Tec SH3 D196A mutant protein, as determined by SPR. N.D. denotes not determined as the ligand was not soluble under assay conditions. . . . .	155
3.12	Yields from synthesis of benzylpiperazinyl 2-chloroquinoline derivatives via reductive amination with benzaldehyde derivatives. . . . .	160
3.13	Yields from synthesis of pyridylmethyl piperazinyl-substituted 2-chloroquinoline derivatives via reductive amination with benzaldehyde derivatives. . . . .	161
3.14	Results and yields of Buchwald-Hartwig coupling reactions for amination of benzylpiperazinyl-substituted 2-chloroquinoline derivatives. . . . .	163
3.15	Results and yields of Buchwald-Hartwig coupling reactions for amination of pyridylmethyl piperazinyl-substituted 2-chloroquinoline derivatives. . . . .	164
3.16	Results and yields of nitrile hydrolysis of nitrile-containing 2-aminoquinoline derivatives to the corresponding amide-containing 2-aminoquinoline ligands. . . . .	167
3.17	Binding affinities of benzylpiperazinyl-substituted and pyridylmethyl piperazinyl-substituted 2-aminoquinoline ligands for GST-Tec SH3 protein, determined by SPR. . . . .	170
3.18	Binding affinities of benzylpiperazinyl-substituted and pyridylmethyl-substituted 2-aminoquinoline ligands to GST-Tec SH3 D196A mutant. . . . .	178

4.1	Binding affinities of previously reported 6-heterocycle piperidinyl and piperazinyl substituted 2-aminoquinoline derivatives, with high binding affinity for the Tec SH3 domain (determined by SPR assays). . . . .	184
4.2	Structures of target combinatorial ligands for synthesis. . . . .	190
4.3	Results of radical bromination of substituted tolyl derivatives containing a nitrile substituent. . . . .	197
4.4	Results from the attempted synthesis of an acetyl-protected 2-aminoquinoline derivative via alkylation reaction using various bases. . . . .	223
4.5	Binding affinities of compounds determined by SPR for binding GST-Tec SH3. . .	259
A.1	Binding affinities of ligands synthesised in this work, as determined by SPR for binding GST-Tec SH3. . . . .	378
A.2	Binding affinities of ligands synthesised in this work, as determined by SPR for binding GST-Tec SH3 D196A. . . . .	382
A.3	Comparison of binding affinities of ligands synthesised in this work, as determined by SPR for binding to either GST-Tec SH3 or Tec SH3. . . . .	385

# List of Schemes

2.1	Proposed general retrosynthetic plan for the synthesis of control ligands. . . . .	92
2.2	General workflow of sequential Buchwald-Hartwig coupling reactions for synthesis o control ligands. . . . .	92
2.3	General synthetic pathway for the synthesis of 6-benzylpiperidinyl 2-aminoquinoline ligands. . . . .	94
2.4	Literature attempts towards the synthesis of pyridylmethylene piperidinyl deriva- tives via Wittig and Horner-Emmons reactions. . . . .	95
2.5	Synthesis of pyridylmethyl phosphonium salts towards control ligands. . . . .	96
2.6	Previously attempted synthesis of electron-deficient benzylpiperidinyl derivatives via Horner Emmons reaction and tetrahydropyridine isomer formation. . . . .	97
2.7	Synthesis of pyridylmethylene Boc-protected piperidine derivatives via Wittig re- action. . . . .	97
2.8	Representation of Boc-protecting group partial double bond character in benzyl piperidinyl derivatives. . . . .	98
2.9	Boc-deprotection of pyridylmethylene Boc-protected piperidines. . . . .	100
2.10	Reaction scheme for synthesis of cinnamanilide derivative. . . . .	101
2.11	Proposed synthesis of 6-bromo-2-chloroquinoline. . . . .	101
2.12	Possible synthetic pathways for the synthesis of quinolones from cinnamanilide derivatives. . . . .	102
2.13	Optimised reaction conditions for synthesis of 6-bromo-2-chloroquinoline. . . . .	103
2.14	Previously optimised Buchwald-Hartwig reaction conditions for the selective cou- pling of heterocyclic amines at the 6-position of 6-bromo-2-chloroquinoline. . . . .	104
2.15	Reported attempted selective Buchwald-Hartwig coupling reaction with 6-bromo- 2-chloroquinoline and a pyridylmethylene piperidine derivative. . . . .	105
2.16	Selective coupling of 6-bromo-2-chloroquinoline and a pyridylmethylene piperidine derivative, via Buchwald-Hartwig coupling reaction. . . . .	105
2.17	Previously reported reaction conditions for the introduction of the 2-amine func- tionality for 6-substituted 2-chloroquinoline derivatives. . . . .	108

2.18	Synthesis of a methylenepiperidine-containing 2-aminoquinoline derivative via Buchwald-Hartwig coupling, and THP isomer formation. . . . .	108
2.19	Previously reported reactions with hydroxide-containing or hydroxide-producing bases to afford THP formation. . . . .	109
2.20	Synthesis of pyridylmethyl Boc-protected piperidine derivatives via hydrogenation. . . . .	110
2.21	Synthesis of pyridylmethyl piperidines via Boc deprotection. . . . .	112
2.22	Synthesis of pyridylmethyl piperidine-substituted quinolines via Buchwald-Hartwig coupling reaction. . . . .	114
2.23	Synthesis of pyridylmethyl piperidine-substituted 2-aminoquinolines via Buchwald-Hartwig coupling reaction. . . . .	115
3.1	Proposed general synthetic pathways for the synthesis of benzylpiperazinyl-derived ligand families. . . . .	121
3.2	Obtained products from various Buchwald-Hartwig coupling reactions with Boc-piperazine and 6-bromo-2-chloroquinoline. . . . .	123
3.3	Reaction scheme for Boc deprotection of Boc-piperazine coupled-2-chloroquinoline. . . . .	125
3.4	General scheme for amidation of piperazine-coupled 2-chloroquinoline with acid chlorides. . . . .	125
3.5	Proof-of-concept reaction for general amidation conditions with benzoyl chloride. . . . .	126
3.6	Literature synthesis of tertiary amides via <i>in situ</i> acid chloride formation. . . . .	128
3.7	Proposed mechanism for acid chloride synthesis from benzoic acids. . . . .	132
3.8	General reaction conditions for the synthesis of amidopiperazinyl-substituted 2-chloroquinoline derivatives. . . . .	133
3.9	General reaction conditions for the synthesis of pyridyl amidopiperazinyl-substituted 2-chloroquinoline derivatives. . . . .	134
3.10	General reaction conditions for amination of amidopiperazinyl 2-chloroquinoline derivatives via Buchwald-Hartwig coupling reaction. . . . .	140
3.11	General reaction conditions for amination of pyridyl-containing amidopiperazinyl 2-chloroquinoline derivatives via Buchwald-Hartwig coupling reaction. . . . .	143
3.12	Previously reported reaction conditions for the synthesis of 4-(phenylamino)piperidinyl derivatives via reductive amination with aniline derivatives and Boc-piperidine. . . . .	157

3.13	Proof-of-concept reaction conditions and isolated yield for the synthesis of benzylpiperazinyl 2-chloroquinoline derivatives via reductive amination with benzaldehyde. . . . .	158
3.14	Reaction scheme showing formation of reduced benzyl alcohol following treatment of benzaldehyde under reductive amination conditions. . . . .	159
3.15	General reaction conditions for the synthesis of benzylpiperazinyl-substituted 2-chloroquinoline derivatives via reductive amination. . . . .	159
3.16	General reaction conditions for the synthesis of pyridylmethyl piperazinyl-substituted 2-chloroquinoline derivatives via reductive amination. . . . .	160
3.17	Proof-of-concept Buchwald-Hartwig coupling reaction conditions for synthesis of 2-aminoquinoline ligands via amination of benzylpiperazinyl-substituted 2-chloroquinoline derivatives, using LiHMDS as an ammonia equivalent. . . . .	162
3.18	General Buchwald-Hartwig coupling reaction conditions for amination of benzylpiperazinyl-substituted 2-chloroquinoline derivatives, using LiHMDS as an ammonia equivalent.	163
3.19	General Buchwald-Hartwig coupling reaction conditions for amination of pyridylmethyl piperazinyl-substituted 2-chloroquinoline derivatives. . . . .	164
3.20	Literature synthesis of benzamide by selective hydrolysis of benzonitrile. . . . .	166
3.21	General reaction conditions for hydrolysis of nitrile-containing 2-aminoquinoline derivatives to the corresponding amide-containing 2-aminoquinoline ligands. . . .	166
4.1	Reaction conditions and yield for synthesis of a biaryl derivative containing a nitrile substituent via Suzuki cross-coupling reaction. . . . .	195
4.2	Literature radical bromination conditions for the synthesis of bromomethyl quinolyl derivatives. . . . .	196
4.3	General proposed conditions for synthesis of benzyl bromide derivatives via radical bromination with <i>N</i> -bromosuccinimide (NBS) and benzoyl peroxide (BPO) in BTF.	197
4.4	Reaction conditions and yield for synthesis of substituted tolyl phosphonium salts.	199
4.5	Reaction conditions for attempted synthesis of a phenylmethylene piperidine derivative containing bromo and nitrile substituents, via Wittig reaction. . . . .	200
4.6	Reaction conditions for the synthesis of a benzyl methylene derivative via Wittig reaction with benzaldehyde and a phosphonium salt containing a 4-nitrile substituent.	202

4.7	Reaction conditions and yield for synthesis of a benzyl phosphonate derivative via Michaelis-Arbuzov rearrangement. . . . .	203
4.8	Reaction conditions and yield for synthesis of a phenylmethylene piperidine derivative containing bromo and nitrile groups via Horner-Emmons reaction. . . . .	204
4.9	Reaction conditions and yield for synthesis of a biaryl methylene piperidine derivative containing a nitrile substituent via Suzuki cross-coupling reaction. . . . .	205
4.10	Reaction conditions and yield for Boc group deprotection of a biaryl methylenepiperidine derivative containing a nitrile substituent. . . . .	206
4.11	Reaction conditions and yield for synthesis of a piperidine-coupled 2-chloroquinoline derivative containing biaryl and 4-nitrile groups via Buchwald-Hartwig coupling reaction. . . . .	208
4.12	Reaction conditions and yield for synthesis of 2-aminoquinoline derivatives containing biaryl and nitrile substituents via Buchwald-Hartwig coupling reaction. . .	211
4.13	Literature conditions for synthesis of a benzylpiperazine derivative via nucleophilic substitution. . . . .	214
4.14	Reaction conditions and yield for synthesis of a benzylpiperazine-substituted 2-chloroquinoline derivative containing biaryl and nitrile functional groups, via nucleophilic substitution. . . . .	214
4.15	Reaction conditions and yield for synthesis of a benzylpiperazine-substituted 2-aminoquinoline derivative containing biaryl and nitrile functional groups, via Buchwald-Hartwig coupling reaction. . . . .	215
4.16	Proposed alternative synthetic pathways for the synthesis of arylmethylpiperazinyl 2-aminoquinoline ligands. . . . .	217
4.17	Reaction conditions and yield for synthesis of a Boc-piperazine-coupled 2-aminoquinoline derivative via Buchwald-Hartwig coupling reaction. . . . .	218
4.18	Reaction conditions for the attempted synthesis of an acetyl-protected 2-aminoquinoline derivative via amide formation with acetyl chloride. . . . .	219
4.19	Reaction condition and yield for Boc group deprotection of a Boc-piperazine 2-aminoquinoline derivative. . . . .	221
4.20	Attempted nucleophilic substitution reaction using TEA as the base, and likely product from proposed Menshutkin reaction. . . . .	225

4.21	Reaction conditions and yield for synthesis of a biaryl 2-pyridyl methyl derivative by Suzuki cross-coupling reaction. . . . .	228
4.22	Proof-of-concept reaction for synthesis of halomethylpyridines via radical bromination of 2,6-lutidine. . . . .	230
4.23	Reaction conditions for the attempted synthesis of a biaryl 2-pyridylmethyl bromide derivative by radical bromination reaction. . . . .	231
4.24	Reaction conditions and yield for synthesis of a 2-pyridyl phosphonium salt via 2-pyridylmethyl chloride intermediate. . . . .	232
4.25	Reaction conditions and yield for synthesis of 2-pyridyl methylenepiperidine derivative. . . . .	233
4.26	Reaction conditions and yield for synthesis of a biaryl 2-pyridyl methylenepiperidine derivative by Suzuki cross-coupling reaction. . . . .	233
4.27	Reaction conditions and yield for alkene reduction of a biaryl 2-pyridylmethylene piperidine derivative. . . . .	234
4.28	Reaction conditions and yield for Boc group deprotection of a biaryl 2-pyridylmethyl piperidine derivative. . . . .	236
4.29	Reaction conditions and yield for synthesis of a biaryl 2-pyridylmethyl piperidine-coupled 2-chloroquinoline derivative via selective Buchwald-Hartwig coupling reaction. . . . .	237
4.30	Reaction conditions and yield for synthesis of a biaryl 2-pyridylmethyl piperidinyl 2-aminoquinoline derivative via Buchwald-Hartwig coupling reaction. . . . .	239
4.31	Reaction conditions and yield for synthesis of a biaryl 2-pyridylmethyl chloride via radical chlorination reaction. . . . .	240
4.32	Reaction conditions for attempted synthesis of a biaryl 2-pyridylmethyl piperazinyl 2-chloroquinoline derivative via radical chlorination followed by nucleophilic substitution reaction with a crude biaryl 2-pyridylmethyl chloride derivative, and formation of a succinimide-containing side product. . . . .	241
4.33	Reaction conditions and yield for synthesis of a biaryl 2-pyridylmethyl piperazine 2-chloroquinoline derivative via nucleophilic substitution. . . . .	244
4.34	Reaction conditions and yield for synthesis of a biaryl 2-pyridylmethyl piperazinyl 2-aminoquinoline derivative via Buchwald-Hartwig coupling reaction. . . . .	245



4.35	Reaction conditions and yield for synthesis of a 2-pyridyl 4-nitrilo phosphonium salt via 2-pyridylmethyl chloride intermediate. . . . .	249
4.36	Reaction conditions for attempted synthesis of a methylene piperidinyll derivative containing 2-pyridyl and 4-amido substituents, via Wittig reaction. . . . .	249
4.37	Reaction conditions and yield for the synthesis of a benzyl methylene derivative via Wittig reaction with benzaldehyde and a phosphonium salt containing a 4-nitrile and 2-pyridyl substituent. . . . .	251
4.38	Reaction conditions and yield for synthesis of a 2-pyridyl, 4-nitrile substituted piperazinyl-2-chloroquinoline derivative via radical chlorination of a substituted tolyl derivative, and subsequent nucleophilic substitution reaction. . . . .	253
4.39	Attempted synthesis of piperazinyl 2-aminoquinoline derivative containing 2-pyridyl and 4-nitrile substituents via Buchwald-Hartwig coupling reaction. . . . .	255

# Abstract

Protein-protein interactions (PPIs) involve the physical interaction between two distinct protein surfaces to form protein complexes, which propagate cell signalling pathways and control of biological function. If PPIs are dysregulated, disease often ensues; PPIs are therefore attractive therapeutic targets. Historically, PPIs have been considered “undruggable”; they generally contain few defined sites for selective inhibitor targeting, and PPI interfaces are often hydrophobic.

Src Homology 3 (SH3) domains facilitate cell signalling pathways through PPIs with proline-rich regions in their native binding partners; signalling pathways controlled by SH3 domains have roles in the progression of diseases (including cancers). With over 200 proteins in the human proteome containing a SH3 domain, there is good scope for selective targeting of specific SH3 domains.

The work described in this thesis contributes to a structure-based drug discovery program for SH3 domains. The small molecule 2-aminoquinoline was identified as a ligand for the murine Tec SH3 domain, and a ligand-protein binding model was proposed. Development of this ligand scaffold yielded identification of 6-position extended 2-aminoquinoline derivatives with improved binding affinity and SH3 domain selectivity over 2-aminoquinoline. However, the lead ligands were largely hydrophobic and presented limited opportunities for ligand modification.

This thesis describes the development of novel small molecule ligands for the Tec SH3 domain with improved hydrophilicity (i.e., drug-like character) compared to those reported previously. As the strongest reported ligands for the Tec SH3 domain contain a benzylpiperidine substituent, the primary focus of this work investigated the synthesis (via general synthetic pathways) and binding activities of benzylpiperazinyl- and phenylamidopiperazinyl-analogues of previously reported 6-substituted 2-aminoquinoline ligands. Furthermore, the synthesis and binding activities of more complex ligands containing combinations of favourable structural features were investigated. A broad general synthetic pathway was developed for each complex ligand family, which was tailored as required for each derivative.

A surface plasmon resonance (SPR) binding assay was previously used to determine ligand binding affinities for the Tec SH3 domain, however this assay derived binding affinities which were agnostic

to the location of the ligand-protein binding interaction. A secondary focus of the work in this thesis involved validating the SPR binding assay by investigating the location of the measured ligand-protein binding interaction. Separately, efforts towards elucidation of the proposed ligand-protein binding model were made, but were unsuccessful.

The binding affinities of all novel ligands in this work were investigated using SPR binding assays. None of the assayed ligands exhibited improved binding affinity for the Tec SH3 domain, although some benzylpiperazine-containing ligands displayed binding affinities comparable to the current lead compounds. Ligand solubilisation under biologically-relevant assay conditions was achieved in all but two cases, indicating the ligands had improved drug-like character. Importantly, the SPR binding assay was validated; it was conclusively shown to measure a binding interaction consistent with the previously proposed ligand-protein binding model.

These results report a more drug-like, equipotent small molecule ligand scaffold, which can be derivatised further for identification of stronger binding SH3 domain ligands and supports the notion of targeting PPIs with small molecules generally.

# Declaration

I certify that this work contains no material which has been accepted for the award of any other degree or diploma in my name, in any university or other tertiary institution and, to the best of my knowledge and belief, contains no material previously published or written by another person, except where due reference has been made in the text. In addition, I certify that no part of this work will, in the future, be used in a submission in my name, for any other degree or diploma in any university or other tertiary institution without the prior approval of the University of Adelaide and where applicable, any partner institution responsible for the joint award of this degree.

The author acknowledges that copyright of published works contained within the thesis resides with the copyright holder(s) of those works.

I give permission for the digital version of my thesis to be made available on the web, via the University's digital research repository, the Library Search and also through web search engines, unless permission has been granted by the University to restrict access for a period of time.

I acknowledge the support I have received for my research through the provision of an Australian Government Research Training Program Scholarship.

Ellen Lillian Swan

February 2023

# Acknowledgements

First and foremost, my deepest thanks go to my primary supervisor, Professor Simon Pyke. The last few years have not been without their challenges (with a pandemic for good measure!), and I cannot thank you enough for your ongoing support and encouragement, both in and out of the lab. Thank you for providing the freedom for me to pursue the biological aspects of my project, which has made my PhD journey that much more rewarding. Thank you especially for pushing me, challenging my ideas, and for sharing your time, knowledge, wisdom, and experience — I really appreciate it. Thank you also for your understanding and flexibility over the last 12 months while I juggled part-time study and work.

I would also like to thank my co-supervisors, Professor Grant Booker and Dr John Bruning. Grant, thank you for taking me in as a fresh chemistry PhD student and allowing me access to your lab, I hope you're enjoying your well-deserved retirement! John, thank you for taking me in after Grant's departure and for introducing me to the wonderful world of protein crystallography. Thank you especially for making the time for our discussions, for access to your lab, and for sharing your advice and knowledge on all things protein.

A big thank you goes to the members (past and present) of Lab 3. Sam Dama, I am so glad to have embarked on this PhD journey alongside you. Thank you for your help in the lab and for keeping me grounded. Special thanks for keeping the lab well-fed with cupcakes, and importantly for being a good friend. Steph Jayne, thank you for sharing your enthusiasm for this project, and for your help and advice for all things synthetic chemistry. Jess Limongelli, you are a wonderful friend and are truly sunlight in human form. Thank you for bringing the energy to a lab full of introverts.

I would also like to thank Associate Professor Tara Pukala for allowing me to access your lab spaces as required. A special thank you goes to Dr Blagojce (BJ) Jovcevski, for teaching me how to express and purify protein, pour gels for SDS-PAGE, and all the other small things. Thank you especially for your time and friendship, and for reminding me not to sweat the small things. Thank you also to Lewis McFarlane for deconvoluting my protein mass spectra.

Thanks also go to Dr Louise Sternicki and Dr Mehrnaz Keyhanfar from the Booker group, who generously introduced me to SPR. From the Bruning group, thank you to Jordan Pederick for your

assistance with my SPR and Biacore queries, and to Dan McDougal for your advice on protein expression aspects, and for the conversations on those inevitable late nights in the lab.

I'm extremely grateful for the support staff within the Department of Chemistry, particularly Phil Clements, and later Matt Bull for maintaining the NMR and MS facilities, which were critical for this project. Thank you both for your assistance and patience while teaching me various aspects of the NMR and MS software and hardware, and for running the occasional sample for me. Thanks also go to Dr Jesse Teo for lending me equipment without hesitation.

Finally, I must thank my family, particularly my Mum. I am so grateful for your constant love, support, and belief in me — you inspire me more than you know. To my fiancé Brad, I appreciate you so much! Thank you for listening to my chemistry problems, even though they made no sense to you whatsoever. Thank you (and Boris & Slinky) for your unwavering support, pep talks and encouragement over the last few years, and especially over the last few months — you are such a good egg.

# List of Communications & Presentations

**Swan, E.**, Small Molecules, Big Potential: Ligand Development for Targeting a Protein-Protein Interaction Domain; 2022. *RACI National Congress, Brisbane, Queensland, Australia*. Oral Presentation.

**Swan, E.**, Drugging the “Undruggable” with Small Molecules; 2021. *The University of Adelaide — Ingenuity, Adelaide, South Australia, Australia*. Poster Presentation.

**Swan, E.**, Not so Undruggable: Design and Synthesis of Novel Small Molecule Ligands for a Non-Traditional Therapeutic Target; 2021. *RACI SA One-Day Synthesis Symposium, Adelaide, South Australia, Australia*. Oral Presentation.

**Swan, E. L.**; Jayne, S.; Sternicki, L. M.; Limongelli, J. S.; Booker, G. W.; Pyke, S. M., Small Molecules Can Effectively Bind a Protein-Protein Interaction Domain; 2021. *Drug Discovery and Development SA Symposium, Adelaide, South Australia, Australia*. Poster Presentation.

# List of Abbreviations

ATP	Adenosine 5'-triphosphate
BLAST	Basic Local Alignment Search Tool
Boc	<i>tert</i> -Butoxycarbonyl
BCL-2	B-cell lymphoma-2
BPO	Benzoyl peroxide
BTF	$\alpha,\alpha,\alpha$ -Trifluorotoluene
COSY	Correlated Spectroscopy
DCM	Dichloromethane
DMAP	4-Dimethylaminopyridine
DMF	<i>N,N</i> -Dimethylformamide
DMSO	Dimethylsulfoxide
DNA	Deoxyribonucleic acid
DREF	DNA replication-related element-binding factor
DTT	Dithiothreitol
EC	Effective Concentration
EDC	1-Ethyl-3-(3-dimethylaminopropyl)carbodiimide hydrochloride
EGTA	Ethylene glycol-bis( $\beta$ -aminoethyl ether)- <i>N,N,N',N'</i> -tetraacetic acid
ESI	Electrospray Ionisation
EVH1	Enabled/vasodilator-stimulated phosphoprotein homology 1
FDA	Food and Drug Administration
FP	Fluorescence Polarisation
FPLC	Fast Protein Liquid Chromatography
FT	Fluorescence titration
GPCR	G-protein coupled-receptor
GST	Glutathione <i>S</i> -transferase
HEPES	2-[4-(2-Hydroxyethyl)piperazin-1-yl]ethane-1-sulfonic acid
HMBC	Heteronuclear Multiple Bond Correlation
HMQC	Heteronuclear Multiple Quantum Coherence
HRMS	High Resolution Mass Spectrometry



HSQC	Heteronuclear Single Quantum Coherence
HTS	High-throughput screening
IL-2	Interleukin-2
IPTG	Isopropyl- $\beta$ -D-thiogalactopyranoside
IR	Infra-red
ITC	Isothermal titration calorimetry
LB	Luria-Bertani
LC/MS	Liquid chromatography / Mass Spectrometry
LE	Ligand efficiency
LiHMDS	Lithium bis(trimethylsilylamine)
MDM2	Mouse double minute 2 homolog
MES	2-( <i>N</i> -morpholino)ethanesulfonic acid
MPD	2-Methyl-2,4-pentanediol
MQ	Milli-Q
MW	Molecular weight
MWCO	Molecular weight cut-off
NBS	<i>N</i> -Bromosuccinimide
NCS	<i>N</i> -Chlorosuccinimide
NHS	<i>N</i> -Hydroxysuccinimide
NMR	Nuclear Magnetic Resonance
NOESY	Nuclear Overhauser Effect Spectroscopy
OD	Optical density
PAINS	Pan-assay interference compounds
PBS	Phosphate-buffered saline
PDB	Protein Data Bank
PEG	Polyethylene glycol
PG	Protecting group
PH	Pleckstrin homology
PMB	<i>para</i> -Methoxybenzylamine
PMSF	Phenylmethylsulfonyl fluoride
PPI	Protein-protein interaction

PRP	Proline-rich peptide
PRR	Proline-rich region
PTK	Protein tyrosine kinase
QED	Quantitative Estimate of Druglikeness
RI	Refractive index
Ro5	Lipinski's Rule of Five
ROESY	Rotating Frame Overhauser Enhancement Spectroscopy
RT	Room temperature
RU	Response units
SAR	Structure-Activity Relationship
SDS	Sodium dodecyl sulfate
SDS-PAGE	Sodium dodecyl-sulfate polyacrylamide gel electrophoresis
SH1	Src Homology 1
SH2	Src Homology 2
SH3	Src Homology 3
SPR	Surface Plasmon Resonance
SOS	Son of sevenless homolog 1
TBS	Tris-buffered saline
TCEP	Tris(2-carboxyethyl)phosphine
TEA	Triethylamine
TEMED	<i>N,N,N',N'</i> -Tetramethylethylenediamine
TEV	Tobacco Etch Virus
TFA	Trifluoroacetic acid
TGS	Tris-glycine SDS
TH	Tec homology
THF	Tetrahydrofuran
THP	Tetrahydropyridine
TLC	Thin-layer chromatography
TOF	Time of flight
TTBS	TBS + 0.1% Triton, pH 8



# 1 | Introduction

## 1.1 Contextual statement

This chapter is comprised of two parts.

The first part is included in the form of a review, published as a book chapter. This publication will contextualise the aims of the project more broadly, through discussing the biological structure and function of SH3 domains, and why they would be considered attractive therapeutic targets. It includes a discussion about how the features of SH3 domains have historically lent them the title “undruggable”. This is followed by a brief summary of various strategies for targeting SH3 domains reported in the literature from ~2016-2021.

The second part is included as a traditional section of a conventional thesis chapter, and will present the specific SH3 domain target of interest (Tec SH3 domain), as well as the literature surrounding inhibitors developed for the Tec SH3 domain. It will also contextualise the aims for the work described in this thesis.

## 1.2 Statement of Authorship and associated publication

### Statement of Authorship

Title of Paper	Recent Developments in Targeting "Undruggable" SH3 Domains
Publication Status	<input checked="" type="checkbox"/> Published <input type="checkbox"/> Accepted for Publication <input type="checkbox"/> Submitted for Publication <input type="checkbox"/> Unpublished and Unsubmitted work written in manuscript style
Publication Details	Swan, E. L.; Jayne, S.; Pyke, S. M., Recent Developments in Targeting "Undruggable" SH3 Domains. In <i>2021 Medicinal Chemistry Reviews</i> , Bronson, J. J., Ed. Medicinal Chemistry Division of the American Chemical Society: 1155 Sixteenth Street, NW, Washington, DC 20036, USA, 2021; Vol. 56, pp 389-411.

#### Principal Author

Name of Principal Author (Candidate)	Ellen Lillian Swan		
Contribution to the Paper	Proposed review to all authors, led structure of the review, sourcing citations, writing of most sections and major drafting/editing.		
Overall percentage (%)	65%		
Certification:	This paper reports on original research I conducted during the period of my Higher Degree by Research candidature and is not subject to any obligations or contractual agreements with a third party that would constrain its inclusion in this thesis. I am the primary author of this paper.		
Signature		Date	12 <sup>th</sup> October 2022

#### Co-Author Contributions

By signing the Statement of Authorship, each author certifies that:

- the candidate's stated contribution to the publication is accurate (as detailed above);
- permission is granted for the candidate to include the publication in the thesis; and
- the sum of all co-author contributions is equal to 100% less the candidate's stated contribution.

Name of Co-Author	Stephanie Jayne		
Contribution to the Paper	Assistance with structure of review, including sourcing citations and initial drafting of some sections.		
Signature		Date	8 <sup>th</sup> October 2022

Name of Co-Author	Simon Matthew Pyke		
Contribution to the Paper	Evaluation and editing of the manuscript, acted as corresponding author.		
Signature		Date	6 <sup>th</sup> October 2022

Please cut and paste additional co-author panels here as required.

# RECENT DEVELOPMENTS IN TARGETING “UNDRUGGABLE” SH3 DOMAINS

**Ellen Lillian Swan, Stephanie Jayne  
and Simon Matthew Pyke**

The University of Adelaide, Adelaide, Australia

## Contents

1.	Introduction	389
2.	Protein-Protein Interactions and SH3 Domains	390
2.1	Protein-Protein Interactions in Biology	390
2.2	Protein-Protein Interactions as Challenging, Non-Traditional Therapeutic Targets	392
2.3	SH3 Domain Structure and Function	395
2.4	SH3 Domains as Potential Therapeutic Targets	395
3.	Recent Developments in Targeting SH3 Domains	395
3.1	Peptide Ligands	396
3.2	Peptide-Based or “Peptoid” Ligands	398
3.3	Small-Molecule Ligands	399
3.4	Organic-Inorganic Hybrid Ligands	403
4.	Conclusions	405

## 1. INTRODUCTION

Therapeutic design methodologies have traditionally been applied to biomolecular targets containing well-defined sites in their three-dimensional structures (e.g., enzyme active sites, receptors). An expansion of the druggable therapeutic target space would increase and diversify the scope of ligand development and aid in the discovery of modulators to impact function. This would include targeting protein-protein interactions (PPIs), which have historically been less amenable to intervention by therapeutic agents. The landscape has changed in recent years with PPI inhibitors increasingly reaching clinical trials<sup>1-4</sup> and becoming FDA-approved,<sup>5</sup> thus revising the prior understanding of what constitutes a druggable target. While various PPIs mediated by Src Homology 3 (SH3)

domains are linked to disease progression, SH3 domains have previously been labeled “undruggable” in the literature.<sup>6</sup> This chapter will reflect on the current understanding of these challenging targets and consider strategies and successes in development of PPI inhibitors for SH3 domains.

## 2. PROTEIN-PROTEIN INTERACTIONS AND SH3 DOMAINS

### 2.1 Protein-Protein Interactions in Biology

PPIs describe the physical interaction between two distinct protein interfaces (domains). With over 20,000 proteins in the human proteome (assuming one gene encodes one protein),<sup>7</sup> PPIs are vital for regulating most facets of cellular communication and signalling pathways in biological systems, including cell proliferation, apoptosis, and growth and development. Consequently, when PPIs are dysregulated, disease often ensues.<sup>8,9</sup>

PPI interface surfaces are generally quite large (1,000-2,000 Å<sup>2</sup>)<sup>10</sup> and are often relatively flat in contrast to the structurally defined binding pockets of enzymes.<sup>11</sup> PPIs are typically comprised of several small, weak interactions dispersed across clustered, hydrophobic residues (“hot-spots” and “hot-sequences”)<sup>10,12</sup> of the interface surface, with limited opportunities for strong hydrogen bonding. The surface and binding topology of PPIs has been further described elsewhere.<sup>13</sup>

The nature of PPIs can vary substantially based on the surface architecture of the protein interfaces involved: PPIs can occur between a short, linear peptide component of a protein surface and a small, “hot-spot”-containing region (250-900 Å<sup>2</sup>)<sup>10,14,15</sup> of a partner protein; conversely, they may occur between the surfaces of a pair of large, globular proteins. In addition, the number of PPIs a single protein can facilitate, potentially simultaneously, can vary. Some proteins may contain a single PPI domain, while others (e.g., adapter proteins) contain several PPI domains, and generally function to facilitate multi-protein complex formation (e.g., Grb2).<sup>16</sup>

### 2.2 Protein-Protein Interactions as Challenging, Non-Traditional Therapeutic Targets

Regulated cellular communication is required to facilitate normal processes of cell and organism survival. This is achieved through a complex

network of cell signalling pathways, mediated largely by PPIs. While this function can render PPIs as potential therapeutic targets, there are limited examples of PPI modulators in the literature, primarily due to the uniquely challenging mechanisms of their binding interactions. This has led to the historical assumption that PPIs are intractable therapeutic targets.<sup>6,17</sup> Often, therapeutic design for PPI domains presents challenges that are less often encountered when targeting traditional therapeutic targets. Enzymes and receptors have proven more amenable to modulator design, as they often contain deep binding pockets and the capacity for a “lock-and-key” binding mode due to a high density of functional groups that facilitate specific binding interactions.<sup>11,18</sup> As such, enzymes and receptors are often readily targeted with orally available small molecules, as well as peptides and other biologics. Conversely, the relatively flat binding surfaces (targetable “hot-spots”) of PPI interfaces are generally dispersed over a larger area, so it becomes more difficult for small molecules to make comparably strong interactions with PPI domains (Figure 1).<sup>19,20</sup>

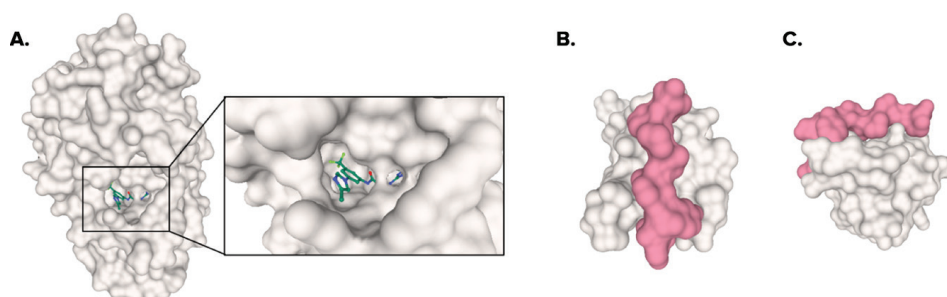


**Figure 1** Structural comparison of inhibitor interactions with a “traditional” therapeutic target (**A**) and “non-traditional” PPI therapeutic target (**B** and **C**). **A**: Co-crystal structure of the Abl kinase domain (white) in complex with the small-molecule inhibitor nilotinib (PDB ID: 3CS9).<sup>21</sup> **B** and **C**: Co-crystal structure of the SH3 domain of Abl kinase (white) in complex with a non-native peptide ligand (pink) (PDB ID: 1BBZ).<sup>22-25</sup>

Consequently, ligands designed for targeting PPIs are often larger and contain more hydrophobic features than ligands designed for traditional therapeutic targets. Small-molecule PPI ligands are less likely to conform to traditional drug design metrics (e.g., Lipinski’s Rule of 5 (Ro5), or Veber’s rules for predicting oral availability),<sup>26-28</sup> and it is not uncommon for small-molecule inhibitors of PPIs to be in violation of at least one of the Ro5, although oral availability can still be achieved. Examples include the FDA-approved small-molecule inhibitor venetoclax (**1**) (targeting the BCL-2/



BH3 PPI) and nutlin-derived compounds RG7112 (**2**) and RG7338 (**3**) (each targeting the p53/MDM2 PPI) recently in clinical trials (Figure 2).<sup>1,5,29-31</sup>

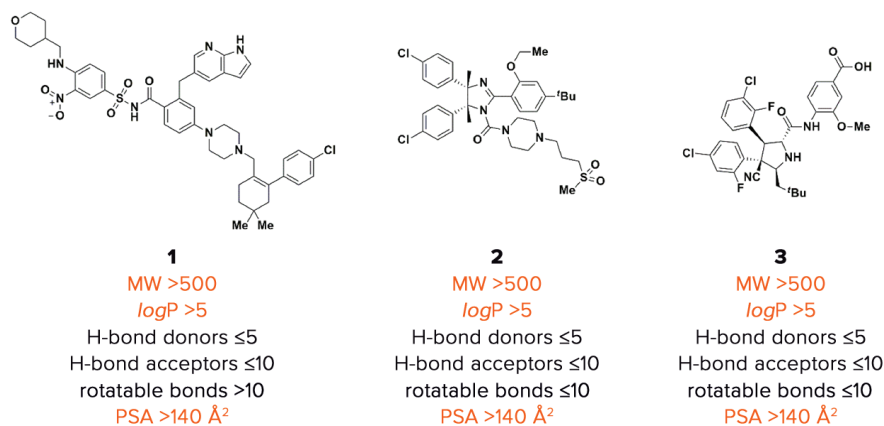


**Figure 2** Structures of orally available small-molecule PPI inhibitors **1**,<sup>5</sup> **2**<sup>1</sup> and **3**<sup>29</sup> and their compliance with Ro5 and Veber's rules.<sup>27,28</sup> Compound metrics violating Ro5 or Veber's rules indicated in orange. Metrics calculated using pkCSM and Marvin.<sup>32,33</sup>

High-throughput screening (HTS) of small-molecule libraries has been effectively employed in the development of ligands against traditional therapeutic targets. However, HTS with these same libraries against PPI targets has often been unsuccessful<sup>34</sup> or provides less tractable hits that are more difficult to develop into lead compounds, though some successful outcomes have been achieved.<sup>35,36</sup> Thus, targeting PPIs poses unique challenges, as traditionally employed methods for identifying lead compounds are generally not as efficient, and traditional small-molecule libraries may not sample an appropriate chemical space for targeting PPIs (e.g., less hydrophobic, fewer rotatable bonds).<sup>37</sup> Considerable progress has been made when utilizing HTS of curated fragment libraries against PPI targets, particularly by utilizing NMR experiments to demonstrate binding.<sup>38,39</sup> However, further validation and optimization of lead fragments can require a considerable investment of time and resources to achieve a clinically viable molecule. It is apparent that conventional approaches for traditional enzyme and receptor targets are generally not as robust when the therapeutic target is a PPI.<sup>34</sup>

### 2.3 SH3 Domain Structure and Function

The human proteome encodes over 200 proteins containing at least one Src Homology 3 (SH3) domain,<sup>40,41</sup> which are non-catalytic protein domains

that specifically bind proline-rich helical peptide sequences of proteins. Proteins containing SH3 domains may also contain catalytic domains to assist in the protein’s biological function (e.g., Src kinases) or other non-catalytic domains (e.g., Src Homology 2 [SH2]) to form adapter proteins (e.g., Grb2, Nck). The resultant multi-protein/domain complexes (“protiplexes”) are implicated in cell signalling pathways through PPIs, including regulating cell growth and proliferation, and immune responses.<sup>42</sup>

The canonical SH3 domain is comprised of five  $\beta$ -strands, arranged in a characteristic  $\beta$ -barrel as two triple-stranded antiparallel  $\beta$ -sheets, with each  $\beta$ -strand connected by a loop or  $3_{10}$  helix (Figure 3).<sup>43-45</sup> The PPI binding site is comprised of three shallow grooves: the first two grooves contain conserved hydrophobic residues that selectively bind proline-rich peptide sequences, while the third (specificity) groove, located between the less conserved RT and nSrc loops, generally contains an acidic amino acid residue that can confer binding specificity through salt bridge formation with appropriate ligands.<sup>42</sup> In addition, the ALYDY motif in the RT loop, the PXXY motif in the  $3_{10}$  helix, and the core WW motif surround the binding site and enable the selectivity for proline-rich ligands (Table 1).<sup>46</sup>

SH3 domains typically bind to proline-rich sequences in their binding partners through recognition of a core “PXXP” motif. The PXXP motif has a left-handed helical structure, classified as a polyproline type II (PPII) helix. Left-handed proline rich helical peptides can be further defined into two classes based upon the relative orientation of the PXXP motif to the acidic residue in the specificity groove on the protein surface (Figure 3).<sup>42,47</sup>

Protein Class	Protein	SH3 domain sequence alignment
Tec family kinases	Tec	VV <b>AMY</b> DFQAAEGH DL RLERGQEYLI LEK-NDVH <b>WW</b> RARD-KYGN <b>E</b> GYIP <b>SNY</b> VTG
	Btk	VV <b>ALY</b> DYMPMNAN DL QLRKGDEYFI LEE-SNLP <b>WW</b> RARD-KNGQE GYIP <b>SNY</b> VTE
	Itk	V <b>I</b> ALY DYQTNDPQ EL ALRRNEEYCL LDS-SEIH <b>WW</b> RVQD-RNGHE GYV <b>PSS</b> YLVE
	Txk	V <b>K</b> ALY DFLPREPC NL ALRRAAEEYLI LEK-YNPH <b>WW</b> KARD-RLGN <b>E</b> GLIP <b>SNY</b> VTE
Src family kinases	Src	FV <b>ALY</b> DYESRTET DL SFKKGRLQI VNNT-EGD <b>WW</b> LAHSLSTGQT GYIP <b>SNY</b> VAP
	Fyn	FV <b>ALY</b> DYEARTED DL SFHKGEKFQI LNSS-EGD <b>WW</b> EARSLTTGET GYIP <b>SNY</b> VAP
	Hck	VV <b>ALY</b> DYEAIHHE DL SFQKGDQMVV LE-E-SGE <b>WW</b> KARSLATRKE GYIP <b>SNY</b> VAR
Adaptor proteins	Grb2	A <b>I</b> AKY DFKATADD EL SFKRGDILKV LNEECDQN <b>WY</b> KAE—LNGKD GFIP <b>KNY</b> IEM
	Nck1.2	AY <b>V</b> KF NYMAERED EL SLIKGTKVIV MEK-CSDG <b>WW</b> RGS—YNGQV GWF <b>PSNY</b> VTE
Other kinases	Abl1	FV <b>ALY</b> DVFASGDN T L SITKGEKLRV LGYNHNGE <b>WC</b> EAQ—TKNGQ GWV <b>PSNY</b> ITP

**Table 1** Protein sequence alignment for various SH3 domains. Key conserved motifs known to be important for binding have been indicated in orange. Nck1.2 refers to the second SH3 domain of the human Nck1 protein. Sequence alignment completed using BLAST.<sup>48</sup>

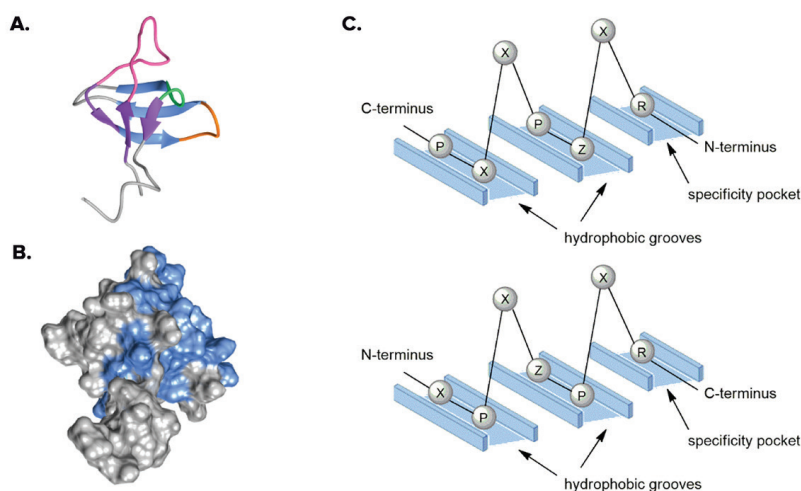


**Figure 3** SH3 Domain structure and interaction with native binding partners. **A:** Solution structure of *murine* Tec SH3 domain. Ribbon diagram indicating the  $\beta$ -strands forming the two  $\beta$ -sheets (indicated in purple and blue), RT loop (indicated in pink), nSrc loop (indicated in orange) and the  $3_{10}$  helix (indicated in green). **B:** Surface representation highlighting residues affected upon binding to proline-rich peptide binding partner (determined via 2D NMR HSQC chemical shift perturbation experiments), indicating binding region (blue) (PDB ID: 1GL5).<sup>45</sup> **C:** Schematic representation of Class I (upper) and Class II (lower) proline-rich helical peptide ligand binding to an SH3 domain (blue), where P refers to proline, R refers to a basic amino acid residue, and Z refers to an aliphatic amino acid residue.<sup>42</sup> Molecular graphics for **A** and **B** were created using UCSF Chimera, developed by the Resource for Biocomputing, Visualisation, and Informatics at the University of California, San Francisco, with support from NIH P41-GM103311.<sup>49</sup>

There are reports of atypical binding partners of SH3 domains that do not strictly contain a core PXXP motif. Their mechanism of binding still appears to be reliant upon recognition of a proline residue,<sup>50,51</sup> although at least one exception has been reported.<sup>52</sup> Interestingly, the PPI between the SH3 domain of Grb2 and SOS1 requires additional interactions beyond the canonical PXXP motif for strong binding affinity. SOS1-derived peptides containing the PXXP motif exhibited substantially weaker binding affinity for Grb2 SH3 domain when compared to full length SOS1. In addition, a peptide derived from the proline-rich region of SOS1 with the PXXP motifs deleted can still bind to Grb2 SH3, with affinity comparable to that of the native SOS1 sequence. This indicates that the Grb2 SH3 domain binding interactions were aided by, but not solely dependent upon, the core polyproline helix (PXXP motif).<sup>53</sup>

Approximately 25% of human proteins contain proline-rich sequences, providing a large array of possible partners for SH3 domains.<sup>54</sup> Despite this, both yeast<sup>55</sup> and human studies have shown that SH3 domains can be very selective for a particular peptide sequence in their native environment.<sup>54</sup> For example, the strongest natural ligand-SH3 interaction is between the Nef protein and the Hck SH3 domain ( $K_d = 0.130 \mu\text{M}$ ).<sup>56</sup> The binding affinity does not necessarily indicate selectivity, as most SH3 domain interactions with native protein binding partners exhibit binding with moderate to weak affinity (typical dissociation constants are  $K_d = 1\text{-}100 \mu\text{M}$ ). Even comparatively weak interactions can show high selectivity *in vivo*, and additional interactions outside the consensus PXXP motif improve the strength of the binding interaction.<sup>57-59</sup>

## 2.4 SH3 Domains as Potential Therapeutic Targets

SH3 domains are implicated in a wide range of vital cell signalling pathways.<sup>60</sup> Dysregulation of these pathways has been implicated in progression of diseases, including cancers and osteoporosis,<sup>61-64</sup> suggesting potential for SH3 domains as therapeutic targets. In addition, the small size of these domains (~60 amino acids, <10 kDa) has enabled structure determination by solution NMR spectroscopy and by x-ray crystallography,<sup>22</sup> indicating that structure-guided ligand development for SH3 domains is feasible. However, the same ubiquity that makes SH3 domains attractive therapeutic targets also creates challenges in elucidating their specific functions due to the relatively weak interactions with native binding partner proteins.<sup>43</sup> Additionally, SH3 domain surfaces are relatively flat and hydrophobic, and have a low density and high dispersion of any identifiable hydrogen-bonding opportunities or deeper pockets. Identification and development of ligands for SH3 domains, albeit challenging, may provide tools for investigating the role of specific SH3 domains in cellular processes, and potentially reveal novel therapeutic targets.

## 3. RECENT DEVELOPMENTS IN TARGETING SH3 DOMAINS

Several strategies highlighted below have been pursued in the development of ligands for targeting SH3 domains, with each strategy utilizing unique tools to address the issues of bioavailability, selectivity, and potency.

### 3.1 Peptide Ligands

SH3 domain selectivity for proteins containing proline-rich sequences has led to substantial investigation of short proline-rich peptide sequences of SH3 domain binding partners as potential ligands for SH3 domain targets. Studies of short peptide sequences directly derived from native SH3 domain binding proteins, however, consistently show that the polyproline type II helix formed by proline-rich peptides is not sufficient to ensure SH3 domain binding specificity or potency.<sup>53,65</sup>

Some notable peptide SH3 domain inhibitors are evident in the literature, including development of a cell-permeable inhibitor based upon a peptide sequence directly derived from a native SH3 ligand. The competitive Fyn SH3 inhibitor **4** was derived largely from a proline-rich region of Tau (**5**), but with an appended peptide sequence included specifically to improve cell permeability (Table 2).<sup>66</sup> Significant inhibition of the Tau/Fyn SH3 PPI was achieved by *in vitro* treatment of mammalian cells with **4**, leading to amelioration of amyloid- $\beta$  toxicity and therefore demonstrating the therapeutic potential of SH3 inhibitors in the treatment of amyloid- $\beta$ -associated conditions such as Alzheimer's disease. The proximity ligation assay (PLA) methodology developed in this study effectively measured the competitive inhibition in cells and demonstrated the ability of this method to probe *in vitro* activity of SH3 domain inhibitors.

Compound	Peptide sequence
<b>4</b>	RRRQRRKKRGRSRTPSLTPPTREPCK
<b>5</b>	RSRTPSLTPPTREPCK

**Table 2** Sequences of Tau-derived peptide ligands **4** and **5**, where **4** contains an appended transactivator of transcription (TAT) tag (orange) for improved cell permeability.<sup>66</sup>

Other peptide strategies have comprised identification of the required peptide motifs to bind SH3 domain targets, followed by optimization to exploit specific pockets and other interactions to achieve greater specificity and potency. An early example was the development of a peptide ligand for the SH3 domain of Src kinase. Using a combinatorial library approach, the peptide motif necessary for Src kinase binding was identified (**6**).<sup>67</sup> Addition of five additional amino acid residues to the *N*-terminus of the peptide targeted the specificity pocket, resulting in increased binding affinity compared to the core motif (**7**, Table 3).<sup>68</sup>

Compound	Peptide sequence	$K_d$ ( $\mu\text{M}$ )
<b>6</b>	RPLPPLP	17.7 <sup>67</sup>
<b>7</b>	VSLARPLPPLP	0.45 <sup>68</sup>

**Table 3** Core Src SH3 domain peptide binding motif **6** and improved binding ligand **7** for targeting the Src SH3 domain.<sup>67,68</sup> Additional amino acids conferring improved affinity in **7** highlighted in orange.

Further studies have also shown the effect of changing adjacent or “flanking” residues of the core PXXP SH3 binding motif to improve binding to the specificity pocket. Through investigation of c-Crk SH3 domain ligand **8**, it was discovered that charged arginine residues at the C-terminus improved binding with the specificity pocket, and therefore enabled more potent binding as well as improved selectivity for c-Crk SH3 over the N-Grb2 SH3 domain (**9**, Table 4).<sup>69</sup>

Compound	Peptide sequence	$K_d$ ( $\mu\text{M}$ )	SH3 domain target	Selectivity for c-Crk over N-Grb2
<b>8</b>	PPPALPKKR	1.90	c-Crk	~75 fold
		142	N-Grb2	
<b>9</b>	PPPALPLRRR	0.110	c-Crk	~200 fold
		21.8	N-Grb2	

**Table 4** Core peptide binding motif **8** and improved binding ligand **9** for targeting the c-Crk SH3 domain.<sup>69</sup> Additional amino acids conferring selectivity and improved affinity in **9** highlighted in orange.

Despite the challenges of degradation and cell permeability, peptide SH3 domain ligands are of great importance in medicinal chemistry research as these peptide ligands can be rapidly identified and utilized to study the roles of SH3 domains. Recently, phage display library screening identified novel selective N1-Src SH3 inhibitors and subsequently demonstrated a role for the N1-Src SH3 domain in neuron development through use of a tool ligand that was selective for the N1-Src SH3 domain over the splice variant from the C-Src SH3 domain. Progress in development of such highly selective SH3 domain ligands overcomes one of the most significant challenges of developing SH3 inhibitors.<sup>70</sup>

### 3.2 Peptide-Based or “Peptoid” Ligands

The structures of potent and selective peptide SH3 ligands have been utilized as inspiration for development of non-peptide therapeutics. Investigations of the SH3 binding model with proline-rich sequences indicated that the interaction is primarily mediated by recognition of *N*-substituted amino acid residues in the peptide backbone<sup>71</sup>—a feature that is unique to proline among naturally occurring amino acids. Peptoid ligands are based on the structure of peptides and have at least one amino acid with the sidechain attached to the peptide backbone nitrogen rather than the  $\alpha$ -carbon (Figure 4). Due to the range of possibilities for sidechain manipulation and subsequent specificity scope, there is great potential in the field of peptoid therapeutics for targeting PPIs.

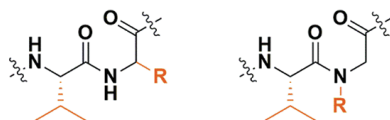


**Figure 4** Structural comparison of peptides (left) and peptoids (right), R groups shown in orange. These peptoids mimic a proline-rich peptide by incorporating unnatural *N*-substituted amino acids.

Research targeting the Grb2 SH3 domain has demonstrated the utility of this approach for developing more potent and selective SH3 domain inhibitors from known peptide ligands, in comparison to native binding partners.<sup>59,71</sup>

More recently, the design and synthesis of peptide-peptoid inhibitors for targeting the human osteoclast-stimulating factor (hOSF) SH3 domain was reported.<sup>72</sup> Initial design of the ligands was achieved by computational modelling, first by generating an artificial hOSF SH3-peptide complex derived from the crystal structure of another SH3-peptide complex, followed by computational mutations of the peptide. The generated theoretical peptoid structures were based upon the native Sam8 ligand; subsequent calculations were performed to predict the affinity of the SH3-peptoid complexes. Experimental assays showed two of the designed peptoids (**10** and **11**, Figure 5) exhibited comparable or increased affinity compared to the Sam8-native ligand template (**12**),<sup>72</sup> demonstrating again that binding affinity can be retained with these peptide-peptoid mimics of native ligand-derived peptides. The development of this computational modelling approach for design of peptide-peptoid SH3 domain ligands is a significant

achievement, with great promise in the rational design and development of peptide-based SH3 domain ligands.

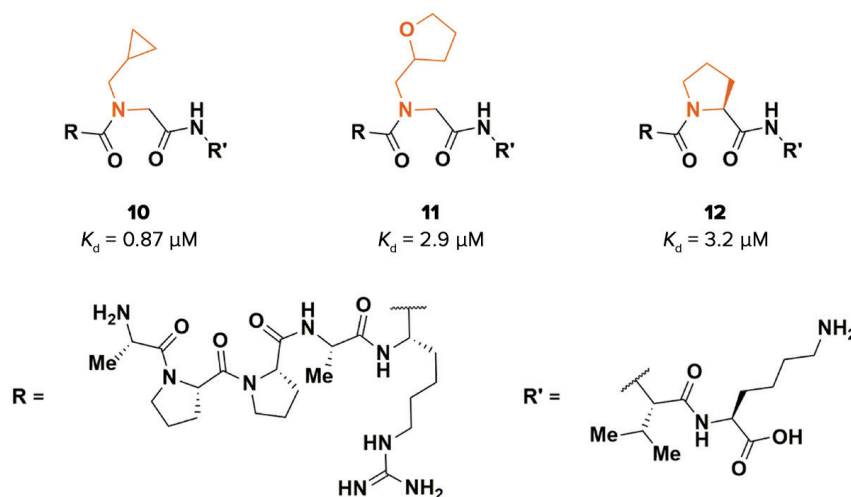


**Figure 5** Structures and binding affinities of peptoid ligands **10** and **11** derived from the Sam68 peptide **12** against the hOSF SH3 domain.<sup>72</sup> Proline residue altered in peptoid ligands indicated in orange.

While peptide and peptide-peptoid ligands may achieve strong binding affinity and some specificity in their interactions, the use of peptide-based compounds as therapeutics is still limited due to the susceptibility to hydrolysis and low cell membrane permeability. Entirely peptoid or non-peptide SH3 domain ligands may overcome these bioavailability challenges and reach the intended protein target; however, none have yet been developed.

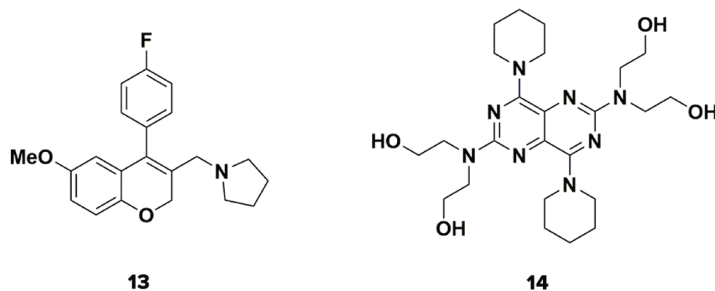
### 3.3 Small-Molecule Ligands

Small-molecule inhibitors can offer significant advantages over peptidic therapeutics, particularly from an oral bioavailability and pharmacokinetic perspective.<sup>26-28</sup> The advances towards small-molecule ligand development for SH3 domains discussed in this section indicate that targeting these domains, and PPIs in general, with small molecules is becoming an achievable reality.

One significant SH3-containing target is the Nck adaptor protein, which amplifies T-cell receptor signalling pathways to afford T-cell activation in autoimmune diseases.<sup>73,74</sup> A PPI between the Nck *N*-terminal SH3 domain



(SH3.1) and a proline-rich sequence of CD3 $\epsilon$  is implicated in Nck activity.<sup>73,74</sup> Progress towards a Nck SH3.1 inhibitor was achieved through *in silico* screening targeting a hydrophobic pocket on the protein surface, which identified a substituted 2*H*-benzopyran structure as a hit. Subsequent SAR studies provided the lead compound (AX-024, **13**). Binding of **13** to the proposed binding site was studied with several biophysical techniques (NMR, surface plasmon resonance [SPR]), and **13** was reported to inhibit T-cell proliferation.<sup>75</sup> The selectivity of **13** for the Nck SH3.1/CD3 $\epsilon$  PPI has been studied further, and it was proposed that **13** may be inhibiting T-cell proliferation through another target.<sup>76</sup> More recent investigations of **13** have also produced conflicting results,<sup>77</sup> and it is therefore noted that further work is required to determine the specific mode of inhibiting cell proliferation in this case.



ABL kinase is another SH3 domain-containing protein that has been extensively researched, often in the context of the gene translocation product BCR-ABL in several types of leukemias. Many approaches target the ATP-binding site of the kinase; unfortunately, the BCR-ABL gene is known to undergo mutations, affording conformational changes and eliminating key residues in the ATP binding site that result in reduced affinity of inhibitors.<sup>78</sup> Recent research has investigated the feasibility of targeting a non-conserved, regulatory component of ABL kinase, such as the ABL SH3 domain, which is also present in BCR-ABL. The ABL SH3 domain autoregulates ABL kinase activity through a PPI with a proline-rich sequence in the N-lobe of the kinase domain. Disruption of this PPI activates ABL kinase,<sup>79</sup> facilitating interactions with modulators of DNA repair and DNA damage-induced apoptosis as appropriate.<sup>80</sup> The small molecule dipyrimidole (**14**, currently FDA-approved as an antithrombotic drug),<sup>81</sup> was identified as a lead compound for targeting the ABL SH3 domain by HTS, and extensive follow-up assays indicated binding of **14** to the SH3 domain surface at the native ligand binding site, displacing a polyproline

type II helix.<sup>36</sup> Importantly, this approach could be applied to other multi-domain kinases with similar SH3 domain-containing regulatory features, including the Src and Tec families.

More recently, a small-molecule inhibitor containing the dimeric structure **15** was reported for targeting the p47phox-22phox PPI, a PPI with widespread implications in diseases stemming from excessive oxidative stress, including inflammation, diabetes, and some cancers (Figure 6). Using a comprehensive fragment-based drug discovery workflow, the fragments 2-aminoquinoline (**16**) and 2-methyl-4-(piperazin-1-yl)quinoline (**17**) were identified as lead compounds for targeting both SH3 domains of p47phox. Of note, **16** had been reported earlier as a small-molecule SH3 domain ligand,<sup>82,83</sup> and subsequently used as inspiration for development of ligands for a different SH3 domain,<sup>84</sup> suggesting this fragment may be potentially useful as a lead compound for targeting SH3 domains more generally. As the fragments displayed binding to both p47phox SH3 domains, a dimeric molecule with a flexible linker was synthesized, and both fluorescence polarization (FP) and SPR experiments identified **15** (Figure 6) as the small-molecule ligand with the strongest binding affinity to date for targeting the p47phox SH3 domains.<sup>85</sup>

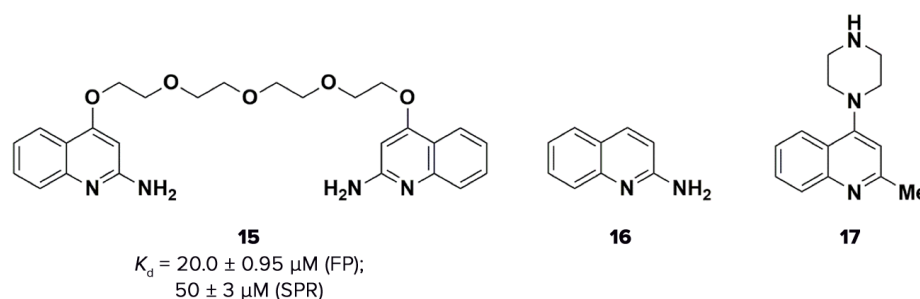
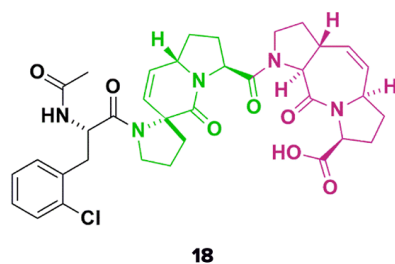


**Figure 6** Structures of precursors **16** and **17** to the dimeric small-molecule ligand **15**. Binding affinities for **15** reported for targeting the p47phox SH3 domain.<sup>85</sup>

While **15** is not the first example of a multi-unit ligand for targeting SH3 domains, it is the first entirely non-peptide inhibitor of this type: the previously reported bivalent “chimera” inhibitors were comprised of both peptide and small-molecule components attached to a central protein unit.<sup>86,87</sup> Again, the challenges of PPI development are highlighted—the workflow employed in this study included thermal shift assays, NMR, FP, SPR, and small-angle X-ray scattering; such an extensive range of techniques

raises questions about the general applicability of this process. Considering the extended structure and high number of rotatable bonds within **15**, this compound does not obey traditional predictors of oral availability (e.g., Veber's rules); however, these encouraging results will likely form a scaffold for a more drug-like ligand for the p47phox SH3 domains.

Although targeting specific SH3 domains has produced relatively potent modulators, the workflows applied to ligand optimization are generally target-specific. Consequently, development of a more universal drug design workflow for targeting SH3 domains would be beneficial. It has been suggested that targeting proline-rich sequence binding domains (including SH3 domains) by synthesizing a curated toolkit of fragments designed to mimic conserved prolines in recognition motifs (i.e., PXXP, PX and XP pairs) could provide a valuable foundation for SH3 domain ligands in general. Similarly to SH3 domains, enabled/vasodilator-stimulated phosphoprotein (Ena/VASP) homology 1 (EVH1) domains also bind proline-rich peptide sequences; Ena/VASP family proteins contain EVH1 domains and function to modulate actin cytoskeleton rearrangements.<sup>88</sup> A proof-of-concept study was conducted against the EVH1 domains of Ena/VASP proteins (VASP, EnaH and EVL).<sup>89</sup> Through consideration of the recognition sequence of EVH1 domains to their native binding partners, a series of peptide-derived small-molecule conjugates were synthesized in which each conjugate was



Technique	$K_d \pm SE$ ( $\mu\text{M}$ )		
	VASP-EVH1	EnaH-EVH1	EVL-EVH1
ITC	$3.8 \pm 0.1$	$2.4 \pm 0.1$	$2.2 \pm 0.2$
FT	$2.7 \pm 0.7$	$2.3 \pm 0.2$	$1.4 \pm 0.2$

**Figure 7** Structure and binding affinities ( $K_d$ ) of the most potent peptide-derived small-molecule conjugate ligand to date for targeting Ena/VASP EVH1 domains, with fragments designed to mimic conserved proline recognition motifs. Individual fragments from the curated toolkit indicated in black, green and magenta.<sup>89</sup>

comprised of a non-natural phenylalanine residue with at least one fragment from the toolkit. The most potent conjugate (**18**, Figure 7) exhibited at least 180-fold improved binding affinity for these EVH1 domains over a peptide derived from the native recognition sequence (as determined by isothermal titration calorimetry [ITC] and fluorescence titration [FT]), and additionally exhibited greater than 80-fold selectivity for these EVH1 domains over the Fyn SH3 domain. While this toolkit of fragments is currently quite small, there is potential for this methodology in targeting other proline-rich sequence binding domains. However, this methodology is yet to be applied to the development of an inhibitor for a SH3 domain.

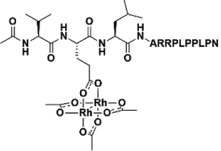
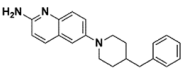
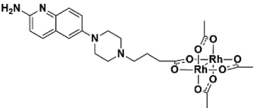
### 3.4 Organic-Inorganic Hybrid Ligands

Perhaps the most significant progress in development of highly selective SH3 domain ligands has been achieved with organic-inorganic hybrids, particularly dirhodium conjugates of known peptide or small-molecule SH3 ligands.

Dirhodium complexes have been investigated for several decades as potential antitumor drugs, with inhibitory activity demonstrated against various cancer targets,<sup>90-92</sup> although their exact mechanism of action is still under investigation.<sup>93,94</sup> Despite their antitumor activity, the toxicity of dirhodium complexes has largely prevented their therapeutic use. The toxic effects of dirhodium carboxylates can potentially be mediated in some cases by incorporation of less labile coordinating ligands.<sup>95</sup> No dirhodium drug candidates have yet progressed through clinical trials, though the incorporation of dirhodium structures into metallopeptides has more recently been investigated, with significant achievements in targeting the CAL PDZ domain and MDM2 interactions.<sup>96,97</sup> The dirhodium core of the metallopeptide binds to histidine or other Lewis-base residues of the protein target; SH3 domain targets with non-conserved histidine residues are therefore potential targets for metallopeptide inhibitor development.

Modification of a previously reported non-specific SH3 peptide ligand, VSLARRPLPPLPGGK (**19**),<sup>67,98</sup> with the dirhodium core at various positions resulted in ligands with tunable selectivity for several human SH3 domains. The most successful metallopeptide hybrid ligand, **20**, had strongest affinity for Lyn SH3 ( $K_d = 6.1$  nM) and exhibited substantial selectivity for Lyn over other human SH3 domains tested (Table 5).<sup>99</sup> Ligands with observed

selectivity for other human SH3 domains (Lck or Hck) were also successfully prepared by varying the attachment position of the dirhodium core to optimally bind non-conserved histidine residues.

Compound	Structure/peptide sequence	$K_d$ (nM)	SH3 domain target	Reference
<b>19</b>	VSLARRPLPLPGGK	2,800 ± 660	Lyn	67
		600 ± 100	Fyn	
<b>20</b>		6.1	Lyn	99
		769	Fyn	
<b>21</b>		9,000 ± 1	Tec	83
		37,000 ± 22	Lyn	84
		127,000 ± 25	Fyn	
<b>22</b>		27 ± 12	Lyn	84
		9,600 ± 1100	Fyn	

**Table 5** Binding affinities and selectivity of SH3 domain ligands, including dirhodium conjugates **20** and **22**<sup>84,99</sup> and their precursors **19** and **21**.<sup>67,83,84</sup>

Further expanding upon these promising results, metal-small molecule hybrids targeting the Lyn SH3 domain were also investigated.<sup>84</sup> Extended 2-aminoquinoline compounds (including **21**) had been previously reported as entirely small-molecule ligands for the Tec SH3 domain; based upon the proposed binding model of these compounds, the dirhodium core was therefore strategically appended to an analog of **21**.<sup>83</sup> While **21** exhibited 4-fold weaker interactions for Lyn SH3<sup>84</sup> compared to the reported activity for Tec SH3 domain,<sup>83</sup> it was found that the dirhodium metallo-organic ligand **22** exhibited dramatically improved binding affinity for Lyn SH3 (Table 5). High selectivity for Lyn SH3 over Fyn SH3 was demonstrated; however, binding of **22** with Tec SH3, the target of **21**, has not yet been tested.

The promising results of this organic-inorganic hybrid strategy demonstrate the potential of hybrid compounds to overcome the key challenges of SH3 domain potency and selectivity. Studies with other dirhodium-small

molecule hybrids have shown favourable cell membrane permeability, suggesting potential bioavailability for these types of ligands.<sup>100</sup> This method of SH3 domain ligand development, however, requires prior investigation of the binding model of the organic component of an organic-inorganic hybrid with an SH3 domain target and is therefore limited by the current scope of reported small-molecule SH3 domain ligands.

## 4. CONCLUSIONS

SH3 domains, which facilitate numerous PPIs, have typically been overlooked as therapeutic targets due to a lack of traditionally “druggable” structural features. However, this idea continues to be challenged by many researchers. Recent literature suggests that targeting the SH3 domain as a regulatory component of multi-domain kinases may be an alternative therapeutic target for several cancers and neurodegenerative diseases. There is still much to investigate; although reported ligands often have comparable or improved binding affinities (and specifically for dirhodium unit-containing ligands, improved selectivity) for their target SH3 domains over native binding partners, often these ligands are larger, more hydrophobic, and more flexible than ligands for traditional therapeutic targets. As effective PPI inhibitors often do not conform to traditional drug design metrics, the task of balancing ligand binding affinity and bioavailability is further complicated. However, the general applicability of workflows for the development of SH3 (and more specifically, PPI) ligands appears to be improving, particularly in the peptide-derived ligand space. The exciting development of versatile curated fragment toolkits also suggests that ligand development for SH3 domains may become more efficient in future. While PPIs are still considered challenging therapeutic targets, the increasing number of PPI inhibitors progressing to clinical trials indicates this perception may be changing.

## References

1. Andreeff, M.; Kelly, K. R.; Yee, K.; Assouline, S.; Strair, R.; Popplewell, L.; Bowen, D.; Martinelli, G.; Drummond, M. W.; Vyas, P.; Kirschbaum, M.; Iyer, S. P.; Ruvolo, V.; González, G. M. N.; Huang, X.; Chen, G.; Graves, B.; Blotner, S.; Bridge, P.; Jukofsky, L.; Middleton, S.; Reckner, M.; Rueger, R.; Zhi, J.; Nichols, G.; Kojima, K. Results of the Phase I Trial of RG7112, a Small-Molecule MDM2 Antagonist in Leukemia. *Clin. Cancer Res.* **2016**, *22*, 868-876.
2. Li, Z.; He, S.; Look, A. T. The Mcl1-Specific Inhibitor S63845 Acts Synergistically with Venetoclax/ABT-199 to Induce Apoptosis in T-Cell Acute Lymphoblastic Leukemia Cells. *Leukemia* **2019**, *33*, 262-266.

3. Skalniak, L.; Kocik, J.; Polak, J.; Skalniak, A.; Rak, M.; Wolnicka-Glubisz, A.; Holak, T. A. Prolonged Idasanutlin (RG7388) Treatment Leads to the Generation of p53-Mutated Cells. *Cancers (Basel)* **2018**, *10*, 396.
4. Szlavik, Z.; Csekei, M.; Paczal, A.; Szabo, Z. B.; Sipos, S.; Radics, G.; Proszenyak, A.; Balint, B.; Murray, J.; Davidson, J.; Chen, I.; Dokurno, P.; Surgenor, A. E.; Daniels, Z. M.; Hubbard, R. E.; Le Toumelin-Braizat, G.; Claperon, A.; Lysiak-Auvity, G.; Girard, A.-M.; Bruno, A.; Chanrion, M.; Colland, F.; Maragno, A.-L.; Demarles, D.; Geneste, O.; Kotschy, A. Discovery of S64315, a Potent and Selective Mcl-1 Inhibitor. *J. Med. Chem.* **2020**, *63*, 13762-13795.
5. Souers, A. J.; Levenson, J. D.; Boghaert, E. R.; Ackler, S. L.; Catron, N. D.; Chen, J.; Dayton, B. D.; Ding, H.; Enschede, S. H.; Fairbrother, W. J.; Huang, D. C. S.; Hymowitz, S. G.; Jin, S.; Khaw, S. L.; Kovar, P. J.; Lam, L. T.; Lee, J.; Maecker, H. L.; Marsh, K. C.; Mason, K. D.; Mitten, M. J.; Nimmer, P. M.; Oleksijew, A.; Park, C. H.; Park, C. M.; Phillips, D. C.; Roberts, A. W.; Sampath, D.; Seymour, J. F.; Smith, M. L.; Sullivan, G. M.; Tahir, S. K.; Tse, C.; Wendt, M. D.; Xiao, Y.; Xue, J. C.; Zhang, H.; Humerickhouse, R. A.; Rosenberg, S. H.; Elmore, S. W. ABT-199, a Potent and Selective Bcl-2 Inhibitor, Achieves Antitumor Activity While Sparing Platelets. *Nat. Med.* **2013**, *19*, 202-208.
6. Mayer, J. P.; DiMarchi, R. D. Drugging the Undruggable. *Chem. Biol.* **2005**, *12*, 860-861.
7. Ponomarenko, E. A.; Poverennaya, E. V.; Ilgisonis, E. V.; Pyatnitskiy, M. A.; Kopylov, A. T.; Zgoda, V. G.; Lisitsa, A. V.; Archakov, A. I. The Size of the Human Proteome: The Width and Depth. *Int. J. Anal. Chem.* **2016**, *2016*, 7436849-7436849.
8. Ruffner, H.; Bauer, A.; Bouwmeester, T. Human Protein-Protein Interaction Networks and the Value for Drug Discovery. *Drug Discov. Today* **2007**, *12*, 709-716.
9. Westermark, J.; Ivaska, J.; Corthals, G. L. Identification of Protein Interactions Involved in Cellular Signaling. *Mol. Cell. Proteom.* **2013**, *12*, 1752-1763.
10. Arkin, Michelle R.; Tang, Y.; Wells, James A. Small-Molecule Inhibitors of Protein-Protein Interactions: Progressing toward the Reality. *Chem. Biol.* **2014**, *21*, 1102-1114.
11. Fuller, J. C.; Burgoyne, N. J.; Jackson, R. M. Predicting Druggable Binding Sites at the Protein-Protein Interface. *Drug Discov. Today* **2009**, *14*, 155-161.
12. London, N.; Raveh, B.; Schueler-Furman, O. Druggable Protein-Protein Interactions— from Hot Spots to Hot Segments. *Curr. Opin. Chem. Biol.* **2013**, *17*, 952-959.
13. Jones, S.; Thornton, J. M. Principles of Protein-Protein Interactions. *Proc. Natl. Acad. Sci. U.S.A.* **1996**, *93*, 13.
14. Basse, M. J.; Betzi, S.; Bourgeas, R.; Bouzidi, S.; Chetrit, B.; Hamon, V.; Morelli, X.; Roche, P. 2P2Idb: A Structural Database Dedicated to Orthosteric Modulation of Protein-Protein Interactions. *Nucleic Acids Res.* **2013**, *41*, D824-D827.
15. Smith, M. C.; Gestwicki, J. E. Features of Protein-Protein Interactions That Translate into Potent Inhibitors: Topology, Surface Area and Affinity. *Expert Rev. Mol. Med.* **2012**, *14*, e16-e16.
16. Maignan, S.; Guilloteau, J.-P.; Fromage, N.; Arnoux, B.; Becquart, J.; Ducruix, A. Crystal Structure of the Mammalian Grb2 Adaptor. *Science* **1995**, *268*, 291-293.
17. Hopkins, A. L.; Groom, C. R. The Druggable Genome. *Nat. Rev. Drug Discov.* **2002**, *1*, 727-730.
18. Liang, J.; Edelsbrunner, H.; Woodward, C. Anatomy of Protein Pockets and Cavities: Measurement of Binding Site Geometry and Implications for Ligand Design. *Protein Sci.* **1998**, *7*, 1884-1897.
19. Arkin, M. R.; Wells, J. A. Small-Molecule Inhibitors of Protein-Protein Interactions: Progressing Towards the Dream. *Nat. Rev. Drug Discov.* **2004**, *3*, 301-317.
20. Jubb, H.; Blundell, T. L.; Ascher, D. B. Flexibility and Small Pockets at Protein-Protein Interfaces: New Insights into Druggability. *Prog. Biophys. Mol. Biol.* **2015**, *119*, 2-9.



21. Weisberg, E.; Manley, P. W.; Breitenstein, W.; Brügger, J.; Cowan-Jacob, S. W.; Ray, A.; Huntly, B.; Fabbro, D.; Fendrich, G.; Hall-Meyers, E.; Kung, A. L.; Mestan, J.; Daley, G. Q.; Callahan, L.; Catley, L.; Cavazza, C.; Mohammed, A.; Neuberg, D.; Wright, R. D.; Gilliland, D. G.; Griffin, J. D. Characterization of AMN107, a Selective Inhibitor of Native and Mutant Bcr-Abl. *Cancer Cell* **2005**, *7*, 129-141.
22. Berman, H. M.; Westbrook, J.; Feng, Z.; Gilliland, G.; Bhat, T. N.; Weissig, H.; Shindyalov, I. N.; Bourne, P. E. The Protein Data Bank. *Nucleic Acids Res.* **2000**, *28*, 235-242.
23. Pisabarro, M. T.; Serrano, L.; Wilmanns, M. Crystal Structure of the Abl-SH3 Domain Complexed with a Designed High-Affinity Peptide Ligand: Implications for SH3-Ligand Interactions. *J. Mol. Biol.* **1998**, *281*, 513-521.
24. Sehnal, D.; Rose, A. S.; Koča, J.; Burley, S. K.; Velankar, S. Mol\*: Towards a Common Library and Tools for Web Molecular Graphics. In *Proceedings of the Workshop on Molecular Graphics and Visual Analysis of Molecular Data*, Eurographics Association: Brno, Czech Republic, 2018; pp 29-33.
25. Bioinformatics, R. C. f. S. Protein Data Bank (PDB). 2021.
26. Lipinski, C. A. Drug-Like Properties and the Causes of Poor Solubility and Poor Permeability. *J. Pharmacol. Toxicol. Methods* **2000**, *44*, 235-249.
27. Lipinski, C. A.; Lombardo, F.; Dominy, B. W.; Feeney, P. J. Experimental and Computational Approaches to Estimate Solubility and Permeability in Drug Discovery and Development Settings. *Adv. Drug Deliv. Rev.* **1997**, *23*, 3-25.
28. Veber, D. F.; Johnson, S. R.; Cheng, H.-Y.; Smith, B. R.; Ward, K. W.; Kopple, K. D. Molecular Properties That Influence the Oral Bioavailability of Drug Candidates. *J. Med. Chem.* **2002**, *45*, 2615-2623.
29. Ding, Q.; Zhang, Z.; Liu, J.-J.; Jiang, N.; Zhang, J.; Ross, T. M.; Chu, X.-J.; Bartkovitz, D.; Podlaski, F.; Janson, C.; Tovar, C.; Filipovic, Z. M.; Higgins, B.; Glenn, K.; Packman, K.; Vassilev, L. T.; Graves, B. Discovery of RG7388, a Potent and Selective p53-MDM2 Inhibitor in Clinical Development. *J. Med. Chem.* **2013**, *56*, 5979-5983.
30. Doak, B. C.; Over, B.; Giordanetto, F.; Kihlberg, J. Oral Druggable Space Beyond the Rule of 5: Insights from Drugs and Clinical Candidates. *Chem. Biol.* **2014**, *21*, 1115-1142.
31. Lipinski, C. A. Rule of Five in 2015 and Beyond: Target and Ligand Structural Limitations, Ligand Chemistry Structure and Drug Discovery Project Decisions. *Adv. Drug Deliv. Rev.* **2016**, *101*, 34-41.
32. ChemAxon *Marvin*, 19.8.0; 2019.
33. Pires, D. E. V.; Blundell, T. L.; Ascher, D. B. pkCSM: Predicting Small-Molecule Pharmacokinetic and Toxicity Properties Using Graph-Based Signatures. *J. Med. Chem.* **2015**, *58*, 4066-4072.
34. Magee, T. V. Progress in Discovery of Small-Molecule Modulators of Protein-Protein Interactions Via Fragment Screening. *Bioorg. Med. Chem. Lett.* **2015**, *25*, 2461-2468.
35. Wadsworth, P. A.; Folorunso, O.; Nguyen, N.; Singh, A. K.; D'Amico, D.; Powell, R. T.; Brunell, D.; Allen, J.; Stephan, C.; Laezza, F. High-Throughput Screening against Protein: Protein Interaction Interfaces Reveals Anti-Cancer Therapeutics as Potent Modulators of the Voltage-Gated Na<sup>+</sup> Channel Complex. *Scientific Reports* **2019**, *9*, 16890.
36. Grover, P.; Shi, H.; Baumgartner, M.; Camacho, C. J.; Smithgall, T. E. Fluorescence Polarization Screening Assays for Small Molecule Allosteric Modulators of Abl Kinase Function. *PLOS ONE* **2015**, *10*, e0133590.
37. Makley, L. N.; Gestwicki, J. E. Expanding the Number of "Druggable" Targets: Non-Enzymes and Protein-Protein Interactions. *Chem. Biol. Drug Des.* **2013**, *81*, 22-32.
38. Erlanson, D. A.; Davis, B. J.; Jahnke, W. Fragment-Based Drug Discovery: Advancing Fragments in the Absence of Crystal Structures. *Cell Chem. Biol.* **2019**, *26*, 9-15.
39. Bainan, W.; Elisa, B.; Surya, K. D.; Jun, W.; Angela, P.; Maurizio, P. High-Throughput Screening by Nuclear Magnetic Resonance (HTS by NMR) for the Identification of PPIs Antagonists. *Curr. Top. Med. Chem.* **2019**, *15*, 2032-2042.



40. Letunic, I.; Bork, P. 20 Years of the Smart Protein Domain Annotation Resource. *Nucleic Acids Res.* **2017**, *46*, D493-D496.
41. Letunic, I.; Doerks, T.; Bork, P. Smart: Recent Updates, New Developments and Status in 2015. *Nucleic Acids Res.* **2014**, *43*, D257-D260.
42. Mayer, B. J. SH3 Domains: Complexity in Moderation. *J. Cell Sci.* **2001**, *114*, 1253-1263.
43. Gmeiner, W. H.; Horita, D. A. Implications of SH3 Domain Structure and Dynamics for Protein Regulation and Drug Design. *Cell Biochem. Biophys.* **2001**, *35*, 127-140.
44. Pursglove, S. E.; Mulhern, T. D.; Hinds, M. G.; Norton, R. S.; Booker, G. W. Assignment of <sup>1</sup>H and <sup>15</sup>N Resonances of Murine Tec SH3 Domain. *J. Biomol. NMR* **1998**, *12*, 461-462.
45. Pursglove, S. E.; Mulhern, T. D.; MacKay, J. P.; Hinds, M. G.; Booker, G. W. The Solution Structure and Intramolecular Associations of the Tec Kinase Src Homology 3 Domain. *J. Biol. Chem.* **2002**, *277*, 755-762.
46. Luccarelli, J.; Thompson, S.; Hamilton, A. D. SH3 Domains as Drug Targets. In *Protein-Protein Interactions in Drug Discovery* **2013**; pp 101-128.
47. Chen, J. K.; Lane, W. S.; Brauer, A. W.; Tanaka, A.; Schreiber, S. L. Biased Combinatorial Libraries: Novel Ligands for the SH3 Domain of Phosphatidylinositol 3-Kinase. *J. Am. Chem. Soc.* **1993**, *115*, 12591-12592.
48. Altschul, S. F.; Gish, W.; Miller, W.; Myers, E. W.; Lipman, D. J. Basic Local Alignment Search Tool. *J. Mol. Biol.* **1990**, *215*, 403-410.
49. Pettersen, E. F.; Goddard, T. D.; Huang, C. C.; Couch, G. S.; Greenblatt, D. M.; Meng, E. C.; Ferrin, T. E. UCSF Chimera—a Visualization System for Exploratory Research and Analysis. *J. Comput. Chem.* **2004**, *25*, 1605-1612.
50. Mongioli, A. M.; Romano, P. R.; Panni, S.; Mendoza, M.; Wong, W. T.; Musacchio, A.; Cesareni, G.; Di Fiore, P. P. A Novel Peptide-SH3 Interaction. *EMBO J.* **1999**, *18*, 5300-5309.
51. Tian, L.; Chen, L.; McClafferty, H.; Sailer, C. A.; Ruth, P.; Knaus, H.-G.; Shipston, M. J. A Noncanonical SH3 Domain Binding Motif Links BK Channels to the Actin Cytoskeleton Via the SH3 Adapter Cortactin. *FASEB J.* **2006**, *20*, 2588-2590.
52. Stamenova, S. D.; French, M. E.; He, Y.; Francis, S. A.; Kramer, Z. B.; Hicke, L. Ubiquitin Binds to and Regulates a Subset of SH3 Domains. *Mol. Cell* **2007**, *25*, 273-284.
53. Bartelt, R. R.; Light, J.; Vacaflores, A.; Butcher, A.; Pandian, M.; Nash, P.; Houtman, J. C. D. Regions Outside of Conserved PxxPxR Motifs Drive the High Affinity Interaction of Grb2 with SH3 Domain Ligands. *Biochim. Biophys. Acta, Mol. Cell Res.* **2015**, *1853*, 2560-2569.
54. Li, H.; Lawrence, D. S. Acquisition of Fyn-Selective SH3 Domain Ligands via a Combinatorial Library Strategy. *Chem. Biol.* **2005**, *12*, 905-912.
55. Zarrinpar, A.; Park, S.-H.; Lim, W. A. Optimization of Specificity in a Cellular Protein Interaction Network by Negative Selection. *Nature* **2003**, *426*, 676-680.
56. Lee, C. H.; Leung, B.; Lemmon, M. A.; Zheng, J.; Cowburn, D.; Kuriyan, J.; Saksela, K. A Single Amino Acid in the SH3 Domain of Hck Determines Its High Affinity and Specificity in Binding to HIV-1 Nef Protein. *EMBO J.* **1995**, *14*, 5006-5015.
57. Dalgarno, D. C.; Botfield, M. C.; Rickles, R. J. SH3 Domains and Drug Design: Ligands, Structure, and Biological Function. *Biopolymers* **1998**, *43*, 383-400.
58. Kay, B. K.; Williamson, M. P.; Sudol, M. The Importance of Being Proline: The Interaction of Proline-Rich Motifs in Signaling Proteins with Their Cognate Domains. *FASEB J.* **2000**, *14*, 231-241.
59. Nguyen, J. T.; Porter, M.; Amoui, M.; Miller, W. T.; Zuckermann, R. N.; Lim, W. A. Improving SH3 Domain Ligand Selectivity Using a Non-Natural Scaffold. *Chem. Biol.* **2000**, *7*, 463-473.
60. Kurochkina, N.; Guha, U. SH3 Domains: Modules of Protein-Protein Interactions. *Biophys. Rev.* **2013**, *5*, 29-39.

61. Frame, M. C. Src in Cancer: Deregulation and Consequences for Cell Behavior. *Biochim. Biophys. Acta, Rev. Cancer* **2002**, *1602*, 114-130.
62. Kaplan, K. B.; Bibbins, K. B.; Swedlow, J. R.; Arnaud, M.; Morgan, D. O.; Varmus, H. E. Association of the Amino-Terminal Half of C-Src with Focal Adhesions Alters Their Properties and Is Regulated by Phosphorylation of Tyrosine 527. *EMBO J.* **1994**, *13*, 4745-4756.
63. Kaplan, K. B.; Swedlow, J. R.; Morgan, D. O.; Varmus, H. E. C-Src Enhances the Spreading of Src-/- Fibroblasts on Fibronectin by a Kinase-Independent Mechanism. *Genes Dev.* **1995**, *9*, 1505-1517.
64. Schwartzberg, P.; Xing, L.; Hoffmann, O.; Lowell, C.; Garrett, L.; Boyce, B.; Varmus, H. Rescue of Osteoclast Function by Transgenic Expression of Kinase-Deficient Src in Src-/- Mutant Mice. *Genes Dev.* **1997**, *11*, 2835-44.
65. Lim, W. A.; Richards, F. M.; Fox, R. O. Structural Determinants of Peptide-Binding Orientation and of Sequence Specificity in SH3 Domains. *Nature* **1994**, *372*, 375-379.
66. Rush, T.; Roth, J. R.; Thompson, S. J.; Aldaher, A. R.; Cochran, J. N.; Roberson, E. D. A Peptide Inhibitor of Tau-SH3 Interactions Ameliorates Amyloid- $\beta$  Toxicity. *Neurobiol. Dis.* **2020**, *134*, 104668.
67. Rickles, R. J.; Botfield, M. C.; Zhou, X. M.; Henry, P. A.; Brugge, J. S.; Zoller, M. J. Phage Display Selection of Ligand Residues Important for Src Homology 3 Domain Binding Specificity. *Proc. Natl. Acad. Sci. U.S.A.* **1995**, *92*, 10909-10913.
68. Feng, S.; Kasahara, C.; Rickles, R. J.; Schreiber, S. L. Specific Interactions Outside the Proline-Rich Core of Two Classes of Src Homology 3 Ligands. *Proc. Natl. Acad. Sci. U.S.A.* **1995**, *92*, 12408-12415.
69. Posern, G.; Zheng, J.; Knudsen, B. S.; Kardinal, C.; Müller, K. B.; Voss, J.; Shishido, T.; Cowburn, D.; Cheng, G.; Wang, B.; Kruh, G. D.; Burrell, S. K.; Jacobson, C. A.; Lenz, D. M.; Zamborelli, T. J.; Adermann, K.; Hanafusa, H.; Feller, S. M. Development of Highly Selective SH3 Binding Peptides for Crk and Crkl Which Disrupt Crk-Complexes with Dock180, SoS and C3G. *Oncogene* **1998**, *16*, 1903-1912.
70. Keenan, S.; Wetherill, S. J.; Ugbode, C. I.; Chawla, S.; Brackenbury, W. J.; Evans, G. J. O. Inhibition of N1-Src Kinase by a Specific SH3 Peptide Ligand Reveals a Role for N1-Src in Neurite Elongation by L1-Cam. *Sci. Rep.* **2017**, *7*, 43106.
71. Nguyen, J. T.; Turck, C. W.; Cohen, F. E.; Zuckermann, R. N.; Lim, W. A. Exploiting the Basis of Proline Recognition by SH3 and WW Domains: Design of N-Substituted Inhibitors. *Science* **1998**, *282*, 2088-2092.
72. Han, S.; Liu, Q.; Wang, F.; Yuan, Z. Targeting the SH3 Domain of Human Osteoclast-Stimulating Factor with Rationally Designed Peptoid Inhibitors. *J. Pept. Sci.* **2016**, *22*, 533-539.
73. Gil, D.; Schamel, W. W. A.; Montoya, M.; Sánchez-Madrid, F.; Alarcón, B. Recruitment of Nck by CD3 $\epsilon$ ; Reveals a Ligand-Induced Conformational Change Essential for T Cell Receptor Signaling and Synapse Formation. *Cell* **2002**, *109*, 901-912.
74. Lettau, M.; Pieper, J.; Gemeth, A.; Lengl-Janßen, B.; Voss, M.; Linkermann, A.; Schmidt, H.; Gelhaus, C.; Leippe, M.; Kabelitz, D.; Janssen, O. The Adapter Protein Nck: Role of Individual SH3 and SH2 Binding Modules for Protein Interactions in T Lymphocytes. *Protein Sci.* **2010**, *19*, 658-669.
75. Borroto, A.; Reyes-Garau, D.; Jiménez, M. A.; Carrasco, E.; Moreno, B.; Martínez-Pasamar, S.; Cortés, J. R.; Perona, A.; Abia, D.; Blanco, S.; Fuentes, M.; Arellano, I.; Lobo, J.; Heidarieh, H.; Rueda, J.; Esteve, P.; Cibrián, D.; Martínez-Riaño, A.; Mendoza, P.; Prieto, C.; Calleja, E.; Oeste, C. L.; Orfao, A.; Fresno, M.; Sánchez-Madrid, F.; Alcamí, A.; Bovolenta, P.; Martín, P.; Villoslada, P.; Morreale, A.; Messeguer, A.; Alarcon, B. First-in-Class Inhibitor of the T Cell Receptor for the Treatment of Autoimmune Diseases. *Sci. Transl. Med.* **2016**, *8*, 370ra184.

76. Szymczak, A. L.; Workman, C. J.; Gil, D.; Dilioglou, S.; Vignali, K. M.; Palmer, E.; Vignali, D. A. A. The CD3 $\epsilon$  Proline-Rich Sequence, and Its Interaction with Nck, Is Not Required for T Cell Development and Function. *J. Immunol.* **2005**, *175*, 270-275.
77. Richter, K.; Rufer, A. C.; Muller, M.; Burger, D.; Casagrande, F.; Grossenbacher, T.; Huber, S.; Hug, M. N.; Koldewey, P.; D'Oswaldo, A.; Schlatter, D.; Stoll, T.; Rudolph, M. G. Small Molecule AX-024 Reduces T Cell Proliferation Independently of CD3 $\epsilon$ /Nck1 Interaction, Which Is Governed by a Domain Swap in the Nck1-SH3.1 Domain. *J. Biol. Chem.* **2020**, *295*, 7849-7864.
78. von Bubnoff, N.; Schneller, F.; Peschel, C.; Duyster, J. Bcr-Abl Gene Mutations in Relation to Clinical Resistance of Philadelphia-Chromosome-Positive Leukaemia to ST1571: A Prospective Study. *The Lancet* **2002**, *359*, 487-491.
79. Barilá, D.; Superti-Furga, G. An Intramolecular SH3-Domain Interaction Regulates C-Abl Activity. *Nat. Genet.* **1998**, *18*, 280-282.
80. Maiani, E.; Diederich, M.; Gonfloni, S. DNA Damage Response: The Emerging Role of C-Abl as a Regulatory Switch? *Biochem. Pharmacol.* **2011**, *82*, 1269-1276.
81. U.S. Food and Drug Administration <https://www.accessdata.fda.gov/scripts/cder/daf/index.cfm> (accessed Feb. 15, 2021).
82. Inglis, S. R.; Stojkoski, C.; Branson, K. M.; Cawthray, J. F.; Fritz, D.; Wiadrowski, E.; Pyke, S. M.; Booker, G. W. Identification and Specificity Studies of Small-Molecule Ligands for SH3 Protein Domains. *J. Med. Chem.* **2004**, *47*, 5405-5417.
83. Smith, J. A.; Jones, R. K.; Booker, G. W.; Pyke, S. M. Sequential and Selective Buchwald-Hartwig Amination Reactions for the Controlled Functionalization of 6-Bromo-2-Chloroquinoline: Synthesis of Ligands for the Tec Src Homology 3 Domain. *J. Org. Chem.* **2008**, *73*, 8880-8892.
84. Martin, S. C.; Ball, Z. T. Aminoquinoline-Rhodium(II) Conjugates as Src-Family SH3 Ligands. *ACS Med. Chem. Lett.* **2019**, *10*, 1380-1385.
85. Solbak, S. M. O.; Zang, J.; Narayanan, D.; Hoej, L. J.; Bucciarelli, S.; Softley, C.; Meier, S.; Langkilde, A. E.; Gotfredsen, C. H.; Sattler, M.; Bach, A. Developing Inhibitors of the p47phox-p22phox Protein-Protein Interaction by Fragment-Based Drug Discovery. *J. Med. Chem.* **2020**, *63*, 1156-1177.
86. Hill, Z. B.; Perera, B. G. K.; Maly, D. J. A Chemical Genetic Method for Generating Bivalent Inhibitors of Protein Kinases. *J. Am. Chem. Soc.* **2009**, *131*, 6686-6688.
87. Tiwari, R.; Parang, K. Protein Conjugates of SH3-Domain Ligands and ATP-Competitive Inhibitors as Bivalent Inhibitors of Protein Kinases. *Chem. Bio. Chem.* **2009**, *10*, 2445-2448.
88. Ball, L. J.; Jarchau, T.; Oschkinat, H.; Walter, U. EVH1 Domains: Structure, Function and Interactions. *FEBS Lett.* **2002**, *513*, 45-52.
89. Opitz, R.; Müller, M.; Reuter, C.; Barone, M.; Soicke, A.; Roske, Y.; Piotukh, K.; Huy, P.; Beerbaum, M.; Wiesner, B.; Beyermann, M.; Schmieder, P.; Freund, C.; Volkmer, R.; Oschkinat, H.; Schmalz, H.-G.; Kühne, R. A Modular Toolkit to Inhibit Proline-Rich Motif-Mediated Protein-Protein Interactions. *Proc. Natl. Acad. Sci. U.S.A.* **2015**, *112*, 5011-5016.
90. Bear, J. L.; Gray, H. B.; Rainen, L.; Chang, I. M.; Howard, R.; Serio, G.; Kimball, A. P. Interaction of Rhodium(II) Carboxylates with Molecules of Biologic Importance. *Cancer Chemother. Rep.* **1975**, *59*, 611-620.
91. Fimiani, V.; Ainis, T.; Cavallaro, A.; Piraino, P. Antitumor Effect of the New Rhodium(II) Complex: Rh<sub>2</sub>(Form)<sub>2</sub>(O<sub>2</sub>CCF<sub>3</sub>)<sub>2</sub>(H<sub>2</sub>O)<sub>2</sub> (Form = N,N'-di-p-Tolylformamidinate). *J. Chemother.* **1990**, *2*, 319-326.
92. Esposito, B.; Zyngier, S.; Souza, A.; Najjar, R. Rh<sub>2</sub>(CF<sub>3</sub>CONH)<sub>4</sub>: The First Biological Assays of a Rhodium(II) Amidate. *Metal-Based Drugs* **1997**, *4*, 333-338.

93. Chifotides, H. T.; Dunbar, K. R. Interactions of Metal–Metal-Bonded Antitumor Active Complexes with DNA Fragments and DNA. *Acc. Chem. Res.* **2005**, *38*, 146-156.
94. Siu, F.-M.; Lin, I. W.-S.; Yan, K.; Lok, C.-N.; Low, K.-H.; Leung, T. Y.-C.; Lam, T.-L.; Che, C.-M. Anticancer Dirhodium(II,II) Carboxylates as Potent Inhibitors of Ubiquitin-Proteasome System. *Chem. Sci.* **2012**, *3*, 1785-1793.
95. Angeles-Boza, A. M.; Chifotides, H. T.; Aguirre, J. D.; Chouai, A.; Fu, P. K. L.; Dunbar, K. R.; Turro, C. Dirhodium(II,II) Complexes: Molecular Characteristics That Affect in Vitro Activity. *J. Med. Chem.* **2006**, *49*, 6841-6847.
96. Kundu, R.; Cushing, P. R.; Popp, B. V.; Zhao, Y.; Madden, D. R.; Ball, Z. T. Hybrid Organic-Inorganic Inhibitors of a PDZ Interaction That Regulates the Endocytic Fate of CFTR. *Angew. Chem. Int. Ed. Engl.* **2012**, *51*, 7217-7220.
97. Zaykov, A. N.; Ball, Z. T. A General Synthesis of Dirhodium Metallopeptides as MDM2 Ligands. *Chem. Commun.* **2011**, *47*, 10927-10929.
98. Moroco, J. A.; Craigo, J. K.; Iacob, R. E.; Wales, T. E.; Engen, J. R.; Smithgall, T. E. Differential Sensitivity of Src-Family Kinases to Activation by SH3 Domain Displacement. *PLOS ONE* **2014**, *9*, e105629.
99. Vohidov, F.; Knudsen, S. E.; Leonard, P. G.; Ohata, J.; Wheadon, M. J.; Popp, B. V.; Ladbury, J. E.; Ball, Z. T. Potent and Selective Inhibition of SH3 Domains with Dirhodium Metalloinhibitors. *Chem. Sci.* **2015**, *6*, 4778-4783.
100. Minus, M. B.; Kang, M. K.; Knudsen, S. E.; Liu, W.; Krueger, M. J.; Smith, M. L.; Redell, M. S.; Ball, Z. T. Assessing the Intracellular Fate of Rhodium(II) Complexes. *Chem. Commun.* **2016**, *52*, 11685-11688.

## 1.3 SH3 Domains

### 1.3.1 Tec kinase family

Tec is the second largest family of protein tyrosine kinases (PTKs), and is comprised of five members: Tec, Btk, Bmx, Itk and Txk. Each member contains five specific protein domains: pleckstrin homology (PH), which facilitates phospholipid binding and consequently lipid membrane localisation;<sup>1</sup> Tec homology (TH), which is comprised of a Btk (Zn binding) motif and proline-rich region (PRR), allowing binding to heterotrimeric G-proteins,<sup>2</sup> as well as intra- and intermolecular protein interactions;<sup>3</sup> SH3 domain, which binds proline-rich helical peptides as described previously; SH2 domain, which binds phosphorylated tyrosine residues, permitting self-regulation of kinase activity;<sup>4</sup> and the SH1 (kinase) domain, which phosphorylates tyrosine amino acid residues.<sup>5</sup> A simplified gene sequence for Tec PTKs is shown in Figure 1.1.

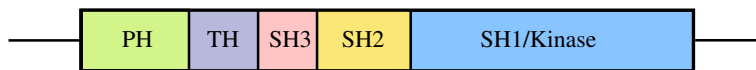


Figure 1.1: Simplified gene sequence of the human Tec tyrosine kinase.<sup>6</sup>

Functional studies investigating Tec family kinases have revealed their role in immunity through mediation of B- and T-cell development and activity. Specifically, Btk is involved in signalling pathways controlling  $\text{Ca}^{2+}$  mobilisation and B-cell development. In some cancers, B-cell signalling can be a driving factor for the propagation of malignancies, leading to the development of Btk inhibitors as anticancer therapeutics.<sup>7</sup> Other Tec family kinase members are generally expressed predominantly in T-cells and have roles in T-cell signalling and development.<sup>8</sup> Tec kinase is involved in both B- and T-cell development, with varying degrees of redundancy with other Tec family kinases.<sup>5</sup> In the case of B-cell development, Tec can partially recoup kinase activities for cells lacking Btk; in Tec-deficient mice, B-cells were sufficiently activated by Btk.<sup>8,9</sup> Interestingly, these Tec-deficient mice also exhibited an increased B-cell response to afford a mild autoimmune phenotype,<sup>10</sup> suggesting that while there is some circumstantial redundancy in kinase function, there are also roles for regulation and/or competition between Tec and Btk.

In addition, research has indicated that Tec kinase is involved in facilitating an immune response to fungal, but not bacterial pathogens in mice. Tec-deficient mice also appear to have increased

resistance to fungal sepsis through an ameliorative reduction of inflammatory response,<sup>11</sup> indicating Tec is a potential therapeutic target for antifungal drug development.

### 1.3.2 Native Tec SH3 domain ligands

Generally, native SH3 domain ligands containing a core 'PXXP' motif bind their cognate SH3 domain(s) with moderate to weak affinity ( $K_d = 1\text{-}100\ \mu\text{M}$ ).<sup>12-14</sup> The Tec SH3 domain participates as a binding partner in several chemokine pathways, including those which facilitate cytoskeleton rearrangement.<sup>15</sup> Therefore, native ligands of the Tec SH3 domain include CD28, a T-cell co-stimulatory receptor protein that is implicated in T-cell development<sup>16</sup> and survival through interleukin-2 (IL-2) production. This occurs via a PPI involving the Tec SH3 domain, and the PRR in the cytoplasmic tail of CD28.<sup>17,18</sup>

The Tec SH3 domain also facilitates self-regulation of kinase activity. It can intramolecularly bind the PRR in the adjacent TH domain, preventing binding to other native binding partners.<sup>19</sup> Alternatively, two Tec kinase proteins can form a homodimer through SH3-PRR interactions, effectively functioning as co-repressors.<sup>3,20</sup>

## 1.4 Small molecule ligand design for targeting a SH3 domain

### 1.4.1 Rational drug design methodologies

Approaches for rational design of small molecule inhibitors are generally classed as either ligand- or structure-based: the former relies upon structural information about native ligands of the therapeutic target; the latter utilises structural information about the therapeutic target to guide ligand design. Structure-based drug design can be further classified into either small molecules or fragments, based upon the nature of the ligand screening libraries utilised. In each case, experimentally-determined three-dimensional structural information of the therapeutic target is preferred.<sup>21</sup> Screening methods can also be conducted computationally, either by *ab initio* ligand development, or library screening *in silico*.<sup>22,23</sup> However, computational high-throughput screening (HTS) efforts of traditional small molecule libraries against PPI targets are often unsuccessful<sup>24</sup> — traditional small molecule libraries were compiled with the intent of inhibiting 'traditional' therapeutic targets, such as enzyme active sites and GPCRs. Given the stark structural differences between traditional therapeutic targets and PPIs (e.g., binding interface surface area, hydrophobicity),<sup>25-27</sup> it is likely that the small

## 1.4. SMALL MOLECULE LIGAND DESIGN FOR TARGETING A SH3 DOMAIN

---

molecule libraries are not sufficiently diverse to sample an appropriate range of chemical space for interactions with PPI targets. Consequently, it is not unusual for structure- or fragment-based drug development of PPI inhibitors to be guided strongly by data from biophysical techniques (e.g., NMR, surface plasmon resonance (SPR), fluorescence polarisation (FP)).<sup>28–31</sup>

In order for inhibitors to be clinically effective as therapeutics, they must be selective, have low associated toxicity, and be biologically available in effective quantities. While the success of these factors for an inhibitor is determined experimentally in pre-clinical studies, several guidelines are widely accepted as predictors of favourable oral bioavailability for small molecules, the most prominent being the Rule of Five<sup>32,33</sup> (or for fragments, Rule of Three),<sup>34</sup> Veber’s Rules<sup>35</sup> and Quantitative Estimate of Druglikeness (QED), a universal scoring system developed by Bickerton *et al.*<sup>36</sup> These guidelines are summarised in Table 1.1.

Table 1.1: Summary of guidelines for improving ligand bioavailability proposed through the Rule of Five,<sup>32,33</sup> Veber’s Rules,<sup>35</sup> and QED.<sup>36</sup> PSA refers to polar surface area; structural alerts refer to functional groups that confer toxicity to the host through metabolism; PAINS refer to Pan-assay inference compounds, which give false positives in binding assays due to non-specific binding.<sup>37</sup>

Metric	Recommendation	Outcome
H-Bond donors	$\leq 5$	Increased likelihood of cell membrane permeation
H-Bond acceptors	$\leq 10$	Limits the degree of ligand-water complexation; increases likelihood of cell membrane permeation
MW	$\leq 500 \text{ gmol}^{-1}$	Decreased likelihood of excess hydrophobicity
<i>logP</i>	$\leq 5$	Confers appropriate hydrophilicity for biological systems
PSA	$\leq 140 \text{ \AA}$	Limits the degree of ligand-water complexation; increases likelihood of cell membrane permeation
Rotatable bonds	$\leq 10$	Increases ligand rigidity, limits entropic penalties
Aromatic rings	$\leq 3$	Controls molecular flexibility
Structural alerts	Minimal	Minimises host toxicity
PAINS	0	Avoids non-specific binding

Inhibitor efficacy can generally be predicted through calculating a ligand efficiency (LE) value, with a premise of ensuring that there is an appropriate gain in binding affinity for the number of heavy atoms (HA) added to a ligand scaffold (Equation 1.1).<sup>38</sup> For traditional therapeutic targets, it is suggested that for small molecules, lead compounds should have a LE of  $\sim 0.3$ , whilst optimised

ligands should aim for a LE of  $\sim 0.5$ . In the case of PPI inhibitors, it is understood that ligands are more hydrophobic, so lower LE values are acceptable.<sup>39</sup>

$$LE = \frac{\Delta G}{HA}$$
$$\Delta G = -RT \ln K_d \text{ or } -RT \ln K_i \text{ or } -RT \ln IC_{50}; \quad (1.1)$$

LE = ligand efficiency, HA = heavy atom count

Whilst LE is a useful metric, it has come under scrutiny several times in the literature.<sup>40–42</sup> Similarly to the “rules” for predicting bioavailability, in many cases LE may be better suited as a guideline, rather than a determinant metric.

### 1.5 Structure-based drug design for targeting the Tec SH3 domain

A range of SH3 domain structures have previously been determined by x-ray crystallography or solution NMR studies, and deposited into the Protein Data Bank (PDB);<sup>43</sup> this wealth of structural information presents SH3 domains as accessible therapeutics targets for structure-based drug design projects. The suitability of a therapeutic target for investigation is also increased if a binding partner for the proposed target has been previously identified and characterised, providing an opportunity for competitive binding assays with developed small molecule inhibitors. The *murine* Tec IV SH3 domain was identified as a suitable therapeutic target for structure-based drug design with small molecule inhibitors, as the solution NMR structure had been solved previously.<sup>44</sup> In addition, a proline-rich peptide had previously been identified as a binding partner to the Tec SH3 domain, providing scope for competition binding assays.<sup>3</sup>

Using the structural information of the Tec SH3 domain,<sup>3,44</sup> the fragment screening software LUDI<sup>45</sup> was used to identify small molecules that were likely to competitively bind to the SH3 domain surface, and displace native binding partners.<sup>46</sup> Briefly, the LUDI software screens and fits a library of small (“micro”) fragments to the protein surface. The software then maps and identifies potential favourable binding sites on the protein surface, and attempts to fit molecular fragments into these sites to form favourable interactions (e.g., hydrophobic fragments in hydrophobic regions, hydrogen bond donors in regions with available hydrogen-bonding opportunities) in a realistic geometry that maximises the number of favourable interactions. Favourable fragments that are fitted suitably close



in three-dimensional space are then linked together to form chemically reasonable small molecules, using simple chemical linker fragments if required. The list of potential compounds suggested by the software was then scrutinised by a chemist, to discard any chemically possible, but non-viable hits (e.g., insufficient stability, biological incompatibility, PAINS).

Of the small molecule hits suggested by LUDI, 2-aminoquinazoline **1** was identified as a suitable lead compound, and selected for further investigation. The structural analogue 2-aminoquinoline **2** was also available, so was also explored as a potential inhibitor for the Tec SH3 domain (Figure 1.2).

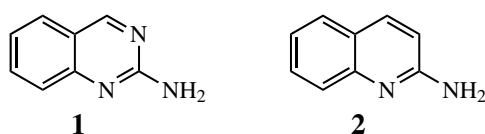


Figure 1.2: Small molecule compounds identified from LUDI screening as potential ligands for the Tec SH3 domain.<sup>46</sup>

### 1.5.1 Binding affinity determination and initial SAR studies

Initial binding studies utilised [<sup>1</sup>H,<sup>15</sup>N] HSQC NMR chemical shift perturbation assays to investigate structure-activity relationships (SAR) between the Tec SH3 domain, and **1** & **2**.<sup>46-48</sup> In these NMR assays, the experimental data provides information regarding both the ligand binding affinity and the location of the ligand-protein binding interaction, through identification of amino acids residues which are affected (either directly or indirectly) during the binding interaction. Throughout the experiment, a constant concentration of uniformly <sup>15</sup>N-labelled protein is titrated with a small molecule ligand, and a [<sup>1</sup>H,<sup>15</sup>N] HSQC NMR spectrum is obtained after each ligand aliquot is added. The process is repeated with increasing concentrations of ligand, which ideally induce incremental changes in the chemical shifts of the amino acid residues involved in the binding interaction, until saturation is reached (i.e. no further change in chemical shift is observed, Figure 1.3). The observed chemical shift is the weighted average of both ligand-bound and free protein, and can be defined as per Equation 1.2, where  $\delta$  refers to the chemical shift for a given species, and X refers to the mole fraction.

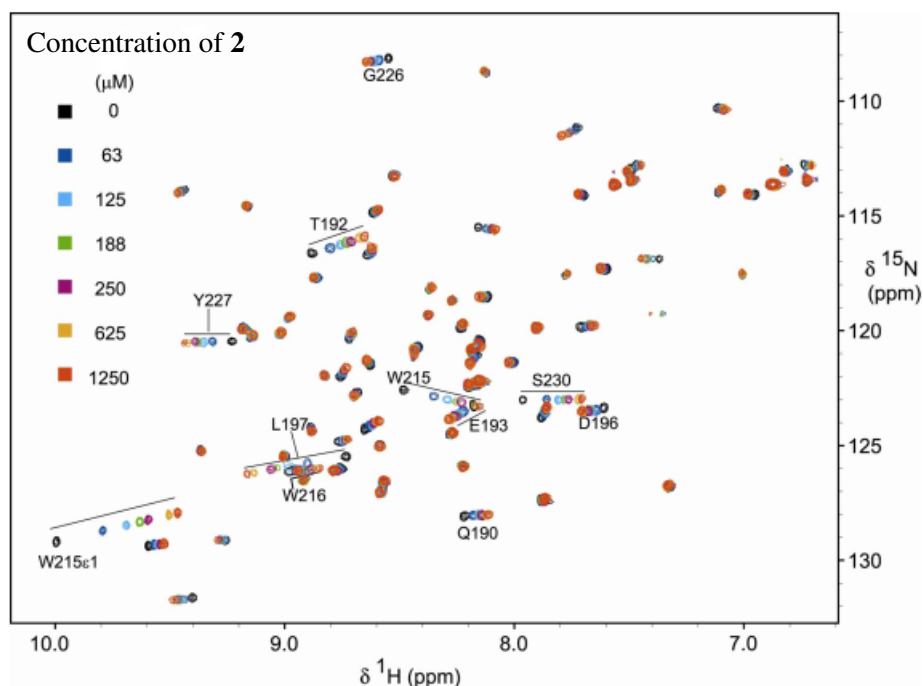


Figure 1.3: Example  $[^1\text{H}, ^{15}\text{N}]$  NMR spectrum overlay from HSQC chemical shift perturbation assays for a ligand in fast exchange. Chemical shifts are labelled corresponding to their representative amino acid residue. Example spectra shows **2** binding the Tec SH3 domain.<sup>46</sup> Reprinted (adapted) with permission from Inglis, S. R.; Stojkoski, C.; Branson, K. M.; Cawthray, J. F.; Fritz, D.; Wiadrowski, E.; Pyke, S. M.; Booker, G. W. Identification and Specificity Studies of Small Molecule Ligands for SH3 Protein Domains, *J. Med. Chem.* **2004**, 47(22), 5405–5417. Copyright 2004 American Chemical Society.

$$\delta_{\text{observed}} = X_P \delta_P + X_{PL} \delta_{PL} \quad (1.2)$$

For a 1:1 binding model, the nature of the protein-ligand binding interaction can be represented by Equation 1.3, where the rate of protein (P) and ligand (L) complexation (PL) is defined by the kinetic rates  $k_{\text{on}}$  and  $k_{\text{off}}$ . Given the reversibility of complex formation, the ratio of protein-ligand complex to unbound protein at any given point is indicated in Equation 1.4, and is determined by the association ( $K_a$ ) or dissociation constant ( $K_d$ ).



When  $k_{\text{on}} = k_{\text{off}}$ , the system is at equilibrium. Furthermore, when the concentration of free protein is equal to the concentration of ligand-bound protein, then  $K_d$  is equal to the ligand concentration (Equation 1.5). Thus, the  $K_d$  value described in this thesis represents the ligand concentration required for 50% saturation (i.e., occupancy) of available binding sites on the protein surface, so a lower  $K_d$  value indicates a stronger binding affinity.

$$K_d = \frac{[P][L]}{[PL]}$$

(1.5)

when  $[P] = [PL]$ ,  $K_d = [L]$

$$\therefore K_d = [L] \approx \frac{k_{\text{off}}}{k_{\text{on}}}$$

The above derivation of  $K_d$  is only applicable for ligands in fast exchange (on the NMR timescale) at the protein surface, typically observed for binding affinities weaker than  $10^{-6}$  M (i.e., typically between  $10^{-3}$  and  $10^{-6}$  M).<sup>49</sup> For ligands in intermediate or slow exchange, there is either a partial or complete absence of chemical shift resonances from interim protein-ligand bound populations. In the case of intermediate exchange, chemical shift resonances may disappear at certain ligand titrations, only to reappear at higher concentration; in slow exchange, only two signals are observed in the NMR spectrum, corresponding to unbound and bound protein. Qualitatively, the approximate binding affinities for these rates of ligand exchange are 10-100  $\mu\text{M}$  and  $<10^{-6}$  M, respectively.<sup>49</sup> With the goal of identifying a strong inhibitor that can compete with native ligands of the Tec SH3 domain (binding affinities  $\approx$  1-100  $\mu\text{M}$ ),<sup>12-14</sup> it is desirable to develop a ligand that binds the Tec SH3 domain in slow exchange on the NMR timescale. For ligands binding in slow exchange, it is anticipated that there would be a sufficient period for Nuclear Overhauser effect (NOE) buildup and transfer between the ligand and protein, allowing the three-dimensional solution structure of the ligand-protein complex to be determined, and providing valuable insight into the nature of the binding interaction.

From the NMR chemical shift perturbation assays of **1** and **2**, both ligands were observed to bind the protein surface in fast exchange, allowing the derivation of a normalised binding isotherm from significantly perturbed chemical shifts ( $\Delta\delta_{\text{H}} > \sim 0.1$  ppm) and binding affinity through  $K_d$  interpolation. (Figure 1.4).

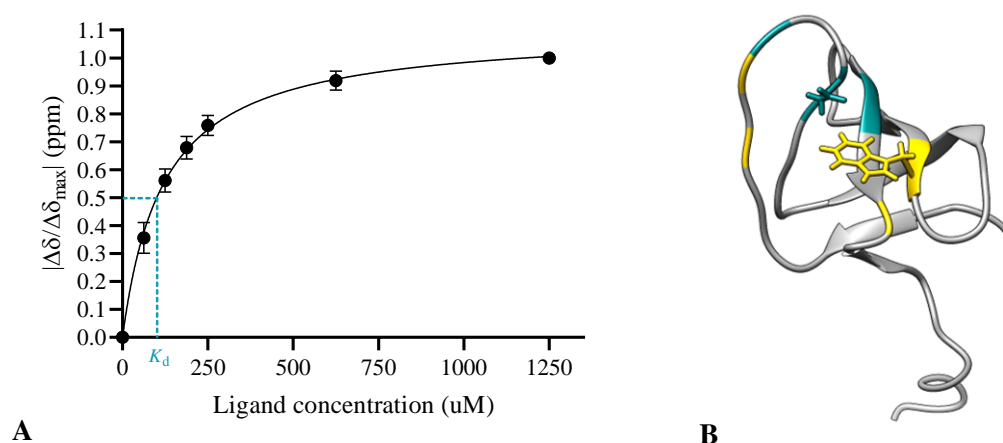


Figure 1.4: (A) Example of normalised binding isotherm generated from NMR chemical shift perturbation data of **2** with the Tec SH3 domain, used to derive the dissociation constant,  $K_d$ .<sup>50</sup> Chemical shift perturbations were normalised for each significantly perturbed residue, and the average perturbation at each ligand concentration plotted. Dataset was fitted with a one-site specific binding analyses in GraphPad.<sup>51</sup> (B) Residues of the Tec SH3 domain significantly shifted during NMR chemical shift perturbation assays (deshielded residues in teal, shielded residues in yellow). Structures of key amino acid residues D196 and W215 are shown.<sup>46,52</sup>

From the NMR chemical shift perturbation experiments, **2** exhibited a 6-fold stronger binding affinity for the Tec SH3 domain over **1** (Table 1.2), and consequently **2** was adopted as the lead compound for ligand design.

Table 1.2: Experimentally determined  $K_d$  values from initial NMR chemical shift perturbation assays.<sup>46</sup>

Compound	Structure	$K_d$ ( $\mu\text{M}$ )
<b>1</b>		800
<b>2</b>		125

## 1.5.2 Binding model development

NMR Chemical shift perturbation experiments can provide valuable insight into the amino acid residues that are implicated in the binding interaction, through analysis of their degree of perturbation. For the binding event between **2** and the Tec SH3 domain, two key amino acids were identified: tryptophan 215 (W215), which displayed a significant upfield shift ( $^1\text{H}$ ) upon ligand binding; and aspartic acid 196 (D196), which displayed a significant downfield shift ( $^1\text{H}$ ) upon ligand binding. Due to the direction of the chemical shift perturbations, it was proposed that **2** was forming a  $\pi$ - $\pi$  stacking interaction with W215, whereby the stacked electron cloud would induce an

## 1.5. STRUCTURE-BASED DRUG DESIGN FOR TARGETING THE TEC SH3 DOMAIN

anisotropic shielding effect in nearby H atoms; while a salt-bridge was proposed to form between the amino functional group (protonated under assay conditions) and D196, causing a decrease in electron density about D196 and subsequent deshielding of local H atoms (Figure 1.5).<sup>46</sup>

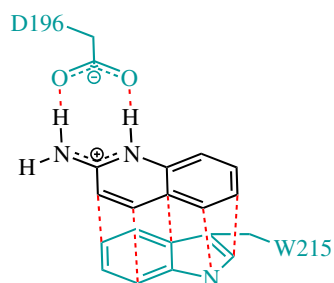


Figure 1.5: Proposed binding model for **2** (black) and the Tec SH3 domain (teal), through a  $\pi$ - $\pi$  stacking interaction with W215 and salt-bridge formation with D196.<sup>46</sup>

To investigate the importance of W215 and D196 residues in the binding interaction, two approaches were undertaken. The binding affinities of a series of ligands with systematically altered ring structures relative to **2** (e.g. removing one aromatic ring, reducing conjugation, changing ring size, removing heteroaromaticity, altering 2-amino substituents)<sup>46,53</sup> were investigated by NMR chemical shift perturbation assays. It was revealed that an aromatic, bicyclic ring structure containing a pyridyl nitrogen was required for binding — smaller ring systems could not form a sufficiently strong hydrophobic interaction with the protein domain due to a reduced contact area for forming a  $\pi$ - $\pi$  stack with W215, and the absence of both a pyridyl nitrogen and primary 2-amino functionality precluded salt bridge formation with D196.

The role of the D196 residue in **2** ligand binding was investigated by a fluorescence polarisation (FP) ligand displacement assay; this displacement assay requires a fluorescently-labelled native binding partner to be displaced by an incoming ligand — a proline-rich peptide (PRP-1) known to bind the Tec SH3 domain through W215 and D196 was available,<sup>3</sup> and was amenable to fluorescent labelling with a fluorescein tag (fPRP-1). The principle of the FP displacement assay relies on the altered kinetics of large biomolecules/complexes (compared to small molecules) in solution — a strong light source is passed through a polarisation filter, and the polarised light wave (excitatory wave) is directed through a sample containing Tec SH3 and fPRP-1. The excitatory wave then excites the fluorophore in the fPRP-1 fluorescein tag, which then emits a light wave (emitted wave) in the same orientation as the excitatory wave. The emitted wave is then passed through a second polarisation filter, which filters light in the same orientation as the first polarisation filter. Hypothetically, for

a static biomolecular complex, the emitted wave from the bound Tec SH3/fPRP-1 biomolecular complex will pass through the second polarisation filter and be detected at an intensity of 100%. However, as the molecules inevitably tumble in solution, the orientation of the emitted wave will differ from the excitatory wave, and therefore the emitted wave may not pass through the second polarisation filter as efficiently, so a lower polarised light intensity is recorded. The weight of the biomolecular complex influences the kinetics of the biomolecule in solution — a heavier biomolecular complex (i.e., Tec SH3 bound to fPRP-1) will move more slowly in solution than free fPRP-1, so the detected light intensity should be greater for the Tec SH3/fPRP-1 complex. Therefore, if an incoming ligand displaces fPRP-1 from the Tec SH3 domain, the free (displaced) fPRP-1 in solution would be represented as a reduction of intensity of detected polarised light.

A series of Tec SH3 D196 variants (including D196A, D196E, D196N and D196T; each generated by site-directed mutagenesis) were expressed and purified for use in the FP ligand displacement assay. In a 96-well plate, each well contained constant concentrations of the Tec SH3 protein (or variant) and fPRP-1, while **2** was added to each well at varying concentrations — this allowed for a relative determination of binding competition of the titrated ligand with fPRP-1, through calculation of an EC<sub>50</sub> value (defined as the effective concentration of titrated ligand, at which 50% of the native ligand is displaced).<sup>46,54</sup> For wild type Tec SH3, **2** showed effective competitive binding over fPRP-1 (EC<sub>50</sub> = 160 ± 36 μM, c.f., K<sub>d</sub> = 125 μM).<sup>46</sup> Importantly, **2** could not displace fPRP-1 from any of the Tec SH3 D196 variants, therefore the binding activity of **2** was abolished, suggesting salt-bridge formation between **2** and D196 is imperative to facilitate the binding interaction.<sup>46,54</sup> More recently, computational docking models reported by Ball and colleagues also support the proposed binding model through appropriate energy levels and geometries, providing further evidence that the model proposed in Figure 1.5 is indeed the preferred binding mode of **2** to the Tec SH3 domain.<sup>55</sup>

By considering the proposed binding model of **2** and the solution structure of the Tec SH3 domain, it is possible to identify amino acids which might be in the vicinity of the binding site. Small molecule ligands could then be designed to target these proximal residues, with the aim of improving both ligand binding affinity and selectivity over other SH3 domains. For example, from Figure 1.6 it would be reasonable to consider decoration of the quinoline ring in **2** to form hydrophobic interactions with the sidechains of F189 and L213, or polar charged/uncharged interactions with the sidechains of T192, Q190, H214, N211 and D212.

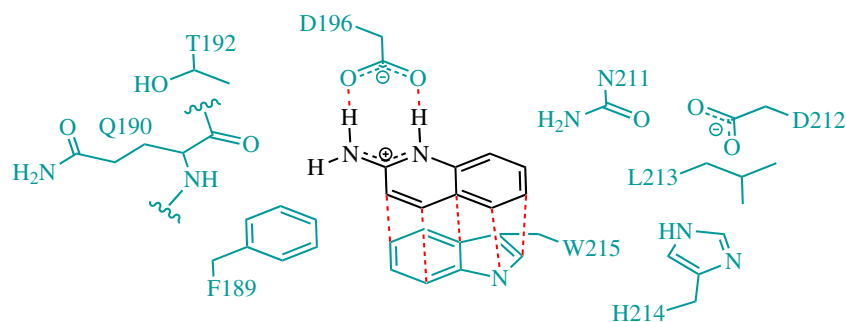


Figure 1.6: Extended proposed binding model of **2** (black) and the Tec SH3 domain (teal), based upon proximal residues.<sup>44,46</sup>

### 1.5.3 Early SAR-guided ligand design

Early research investigated the binding affinities of *N*-substituted 2-aminoquinolines to the Tec SH3 domain. Unfortunately, substitution of the the 2-amino nitrogen was detrimental, with the binding affinities of *N*-substituted 2-aminoquinoline ligands being reduced in all cases (Table 1.3).

Table 1.3: Structure and binding affinities of *N*-substituted 2-aminoquinoline derivatives, as determined by NMR chemical shift perturbation assays.<sup>46,53</sup>

Compound	R =	$K_d$ ( $\mu\text{M}$ )
<b>2</b>	H	125
<b>3</b>	Me	380
<b>4</b>	Bn	193
<b>5</b>	Ac	no binding

It was proposed that the poor binding affinities of *N*-substituted 2-aminoquinoline ligands was caused by a reduction of the number of possible rotamers capable of forming a salt-bridge with D196 of Tec SH3 (Figure 1.7). However, it appeared that some binding affinity was regained when a larger hydrophobic substituent (e.g., **4**) is attached to the 2-amino group, and further chemical shift perturbation analysis revealed an interaction between **4** and F189, an amino acid residue previously unaffected by binding with **2**.<sup>46,53</sup>

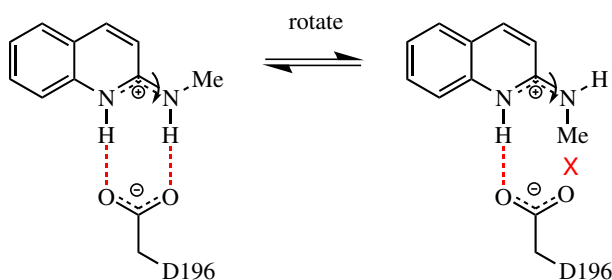
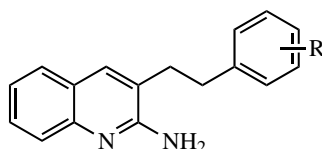


Figure 1.7: Rotation of the methyl-substituted 2-amino group in **3** disrupts salt-bridge formation with D196, lowering binding affinity. Hydrogen bonds shown in red (dashed), bond rotation shown in black (arrow).<sup>53</sup>

From the NMR chemical shift perturbation assay data with **4**, it was plausible that a similar interaction with F189 could be achieved through substitution of a hydrophobic component at the 3-position of the quinoline ring. This yielded positive results; SAR studies revealed that a phenethyl group at the 3-position of the quinoline ring was tolerated, with **6**, **7** and **8** binding with similar affinities to **2** (Figure 1.8). The presence of a bulky lipophilic group in the *para*-position of the phenyl ring also improved binding affinity, suggesting an additional hydrophobic contact was made.<sup>48</sup>

Attempts were made to exploit the lipophilic interaction made by **9** through substitution of the *tert*-butyl group for an aryl ring. However, none of the investigated 3-position substituted 2-aminoquinoline ligands containing a biaryl substituent had improved binding affinity over **9**.<sup>56</sup>

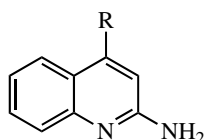


Compound	R =	$K_d$ ( $\mu\text{M}$ )
<b>6</b>	H	$128 \pm 8$
<b>7</b>	4-Me	$74 \pm 18$
<b>8</b>	3-Me	$84 \pm 5$
<b>9</b>	4- <i>tert</i> -Butyl	$40 \pm 7$

Figure 1.8: Structure and reported binding affinities of 3-substituted 2-aminoquinoline ligands, as determined by NMR chemical shift perturbation assays.<sup>48</sup>

Some brief investigations into 4-substituted 2-aminoquinoline ligands have previously been undertaken. From the few ligands that were assayed, it was revealed that a small hydrophobic substituent (e.g., Me) was tolerated in this position (Figure 1.9).<sup>57</sup> This suggests that a small or more flexible substituent might be better tolerated, however this avenue has not been pursued further.





Compound	R =	$K_d$ ( $\mu\text{M}$ )
<b>10</b>	Me	65
<b>11</b>	4-tolyl	350

Figure 1.9: Structures and reported binding affinities of 4-substituted 2-aminoquinoline ligands, as determined by NMR chemical shift perturbation assays.<sup>57</sup>

The binding affinities of a range of 5-substituted 2-aminoquinoline ligands were also investigated by NMR chemical shift perturbation assays; the strongest ligand indicated similar binding affinities to **2**, however no additional contacts with the Tec SH3 domain were observed upon binding of these ligands.<sup>58</sup> This is not surprising, as the proposed binding model suggests that substituents at the 5-position of the quinoline ring would be directed away from the protein surface, so are not expected to form any favourable contacts. It is noted that one derivative containing a H-bond donor had slightly improved affinity relative to **2**.<sup>58</sup>

A range of 7-substituted 2-aminoquinoline ligands were also investigated, given their accessibility from the synthetic methods used for production of 5-substituted 2-aminoquinoline derivatives.<sup>58</sup> Considering the results from the 5-substituted 2-aminoquinoline ligands (and considering the proposed ligand-protein binding model), it was anticipated that 7-substituted 2-aminoquinoline ligands would be directed into the protein surface, leading to displacement of the ligand from the optimal binding geometry and reducing binding affinity. This is consistent with what was observed — for all 7-substituted 2-aminoquinoline ligands investigated, a reduction in binding affinity relative to **2** was observed.<sup>58</sup> Similarly, it was expected that 8-position substituted 2-aminoquinoline ligands would also be directed into the protein surface; given the negative results obtained from binding assays between the Tec SH3 domain and 7-substituted 2-aminoquinoline ligands, investigations of 8-substituted 2-aminoquinoline ligands were not undertaken.

Separately, a range of 6-substituted 2-aminoquinoline ligands with predominately lipophilic components were synthesised and assayed by FP and NMR chemical shift perturbation assays. Serendipitously, the 6-acetal substituted 2-aminoquinoline intermediate **12** (Figure 1.10,  $K_d = 22 \mu\text{M}$ ) exhibited significantly improved affinity over **2**, with NMR chemical shift perturbation spectra revealing

an additional hydrophobic contact was made between **12** and the protein surface.<sup>46,58</sup> While **12** contains an acetal group which is labile under physiological conditions,<sup>50</sup> the overall structure of **12** provided a promising ligand scaffold for further development.

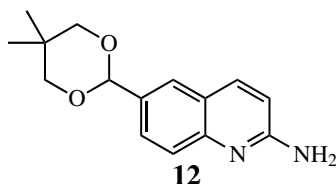
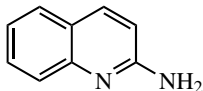
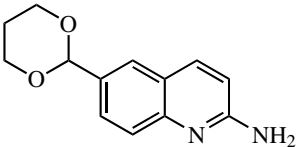


Figure 1.10: Structure of 6-substituted 2-aminoquinoline ligand scaffold containing an acetal group for targeting the Tec SH3 domain.<sup>46,58</sup>

#### 1.5.4 Towards selective SH3 domain inhibitors

Whilst preliminary SAR studies showed promising results for the development of an inhibitor for targeting the Tec SH3 domain, the ability for these developed ligands to selectively displace native binding partners needed to be established. It was envisaged that the FP ligand displacement assay (see Section 1.5.2) would be suitable to investigate this, using various SH3 domain proteins.<sup>46,54</sup> It was determined that the acetal-containing ligand **13** could effectively displace fPRP-1 from the Tec SH3 domain, with greater efficiency than for **2** (Table 1.4).<sup>46</sup>

Table 1.4: Reported EC<sub>50</sub> values of small molecule ligands for displacing a known peptide binding partner (fPRP-1) from the Tec SH3 domain, determined by FP assays (in triplicate).<sup>46</sup>

Compound	Structure	EC <sub>50</sub> (μM)
<b>2</b>		160 ± 36
<b>13</b>		26 ± 6

The amino acid residues W215 and D196 which facilitate the binding interaction between the Tec SH3 domain and **2** & **13**, and PRP-1 are highly conserved amongst SH3 domains (Table 1.5). Furthermore, there is a high degree of conservation for tryptophan residues in SH3 domains at the analogous position to 215 in Tec SH3. Conversely, there is slightly more variation amongst SH3 domains for the amino acid residue corresponding to position 196 in Tec SH3, but it is generally replaced with a charged or similarly lipophilic amino acid residue.<sup>59</sup>

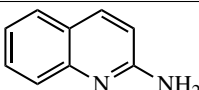
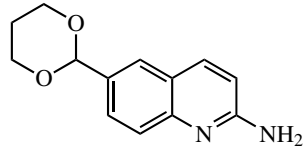
## 1.5. STRUCTURE-BASED DRUG DESIGN FOR TARGETING THE TEC SH3 DOMAIN

Table 1.5: Protein sequence alignment for various SH3 domains discussed in this thesis. Sequences highlighted in blue indicate SH3 domains used in FP selectivity assays. Conserved W215 and D196 amino acid residues (relative to the *murine* Tec SH3 domain) in magenta. Nck1(2) refers to the second SH3 domain of the human Nck1 protein. Sequence alignment completed using BLAST.<sup>59</sup> Adapted from Jayne and Inglis *et al.*<sup>46,56</sup>

Classification	Protein	SH3 domain sequence alignment
<i>murine</i>	<b>Tec</b>	VVAMY DFQATEAHDL RLERGQEYII LEK-NDLHWW RARD-KYGSE GYIPSNYVTG
<b>Human Tec</b>	<b>Tec</b>	VVAMY DFQAAEGHDL RLERGQEYLI LEK-NDVHWW RARD-KYGNE GYIPSNYVTG
<b>family kinases</b>	<b>Btk</b>	VVALY DYMPMNANDL QLRKGDEYFI LEE-SNLPWW RARD-KNGQE GYIPSNYVTE
	<b>Itk</b>	VIALY DYQTNDPQEL ALRRNEEYCL LDS-SEIHWW RVQD-RNGHE GYVPSSYLVE
	<b>Txk</b>	VKALY DFLPREPCNL ALRRAEEYLI LEK-YNPHWW KARD-RLGNE GLIPSNYVTE
<b>Human Src</b> <b>family kinases</b>	<b>Src</b>	FVALY DYESRTETDL SFKKGGERLQI VNNT-EGDWW LAHSLSTGQT GYIPSNYVAP
	<b>Fyn</b>	FVALY DYEARTEDDL SFHKGEKFQI LNSS-EGDWW EARSLTTGET GYIPSNYVAP
	<b>Hck</b>	VVALY DYEAIHHDLD SFQKGDQMVV LE-E-SGEWW KARSLATRKE GYIPSNYVAR
<b>Human adaptor</b> <b>proteins</b>	<b>Grb2</b>	AIKY DFKATADDEL SFKRGDILKV LNEECDQNWY KAE--LNGKD GFIPKNYIEM
	<b>Nck1(2)</b>	AYVKF NYMAEREDL SLIKGTVIV MEK-CSDGWW RGS--YNGQV GWFPSNYVTE

A series of FP ligand displacement assays were used to determine the ability of **2** and **13** to selectively displace a known, fluorescently-tagged binding partner from a range of human SH3 domains with similar sequence homology to the target *murine* Tec SH3 domain. Pleasingly, **2** displayed selectivity for Tec over Fyn and Hck SH3 domains, and **13** displayed improved selectivity for *murine* Tec SH3 domain compared to **2** (Table 1.6),<sup>46</sup> suggesting that the SAR-guided ligand design was effective. It is expected that future ligand design will involve targeting non-conserved amino acid residues on the protein surface, which would increase selectivity for the Tec SH3 domain over other SH3 domain-containing proteins. Overall, this yielded promising selectivity for the target Tec SH3 domain over human SH3 domains with similar sequence homology.

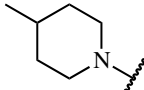
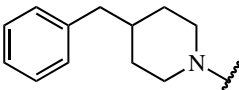
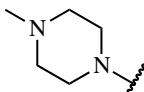
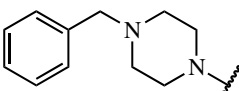
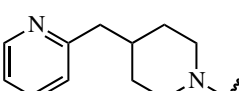
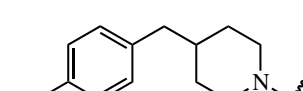
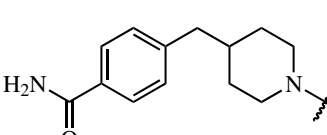
Table 1.6: Reported EC<sub>50</sub> values from specificity FP competition binding studies with synthesised ligands various SH3 domains. <sup>a</sup> *murine* Isoform (IV).<sup>46</sup>

Compound	Structure	EC <sub>50</sub> (μM)			
		Tec SH3 <sup>a</sup>	Nck-1(2) SH3	Fyn SH3	Hck SH3
<b>2</b>		160	150	>1000	no activity
<b>13</b>		26	>500	-	-

### 1.5.5 SAR-guided design of 6-position substituted 2-aminoquinoline ligands

Given the biological incompatibility of the acetal group in the then-lead ligand **12**, further development was required on the **12** scaffold to identify a ligand with improved binding affinity and (predicted) bioavailability. In an attempt to replicate the hydrophobic interaction made by the acetal group in **12** with the Tec SH3 domain, an initial range of 6-position heterocyclic 2-aminoquinoline ligands were synthesised, and their binding affinities determined by NMR chemical shift perturbation assays (Table 1.7).<sup>47</sup> Favourably, significant improvements were observed in binding affinity compared to **12**, particularly for 4-piperidinyl-containing 2-aminoquinoline derivatives (**14**, **15**). It is also noted that the piperazinyl-containing ligands **16** and **17** exhibited improvements in binding affinity compared to **12**, albeit to a lesser extent than the piperidinyl ligands **14** and **15**.<sup>47</sup>

Table 1.7: Structure and reported binding affinities for various 6-substituted 2-aminoquinoline ligands for binding the Tec SH3 domain. <sup>a</sup> refers to binding affinities determined by NMR chemical shift perturbation assays,<sup>47</sup> <sup>b</sup> Binding affinities determined by SPR assays.<sup>56</sup>

R =	Compound	K <sub>d</sub> (μM)
	<b>14</b>	12 ± 2 <sup>a</sup>
	<b>15</b>	9 ± 1 <sup>a</sup>
	<b>16</b>	67 ± 18 <sup>a</sup>
	<b>17a</b>	28 ± 8 <sup>a</sup>
	<b>18a</b>	5 ± 1 <sup>b</sup>
	<b>19</b>	2.0 ± 0.5 <sup>b</sup>
	<b>20</b>	2.0 ± 0.1 <sup>b</sup>

During this first round of **12** ligand optimisation, the strongest identified ligand **15** contained a benzylpiperidine substituent at the 6-position of the quinoline ring.<sup>47</sup> Whilst a substantial gain in binding affinity was achieved (**15**  $K_d = 9 \mu\text{M}$ , c.f., **12**  $K_d = 22 \mu\text{M}$ ),<sup>46,47</sup> identification of a ligand with sub-micromolar binding affinity is desirable, to enable competitive binding with the Tec SH3 domain in a biological system (typical SH3 native ligand binding affinities  $\sim 1\text{-}100 \mu\text{M}$ ).<sup>13,14</sup> Subsequently, further ligand optimisation towards improved binding affinity was undertaken based upon the **15** ligand scaffold. A large number of ligands were synthesised in this endeavour, which required a higher throughput screening method than NMR chemical shift perturbation assays — binding affinity for this cohort of ligands was therefore determined by SPR binding assays (described further in Chapter 2), as shown in Table 1.7.<sup>56</sup> These results suggest that 6-arylmethylpiperidinyl-substituted 2-aminoquinoline ligands bind the Tec SH3 domain with improved affinity compared to **15** when the arylmethyl group contains either an electron-deficient aromatic ring (**18a**), or an electron-withdrawing by resonance substituent on the aromatic ring (**19**, **20**). Importantly, this yielded identification of **19** and **20** as the strongest binding ligands for the Tec SH3 domain to date.<sup>56</sup>

An alternative approach to replicate the hydrophobic interaction by the acetal group in **12** led to the design and synthesis of a small number of 6-phenylphenoxy substituted 2-aminoquinoline ligands. The increased size of these structures and higher number of rotatable bonds compared to **12** and **15**, incurs an entropic penalty, where variable ligand orientations are accessible for sampling the binding site of the Tec SH3 domain. Following investigation of these 6-phenylphenoxy substituted 2-aminoquinoline ligands by NMR chemical shift perturbation assays, **21** and **22** were initially identified with improved binding affinity for the Tec SH3 domain compared to **12** (Figure 1.11).<sup>47</sup>

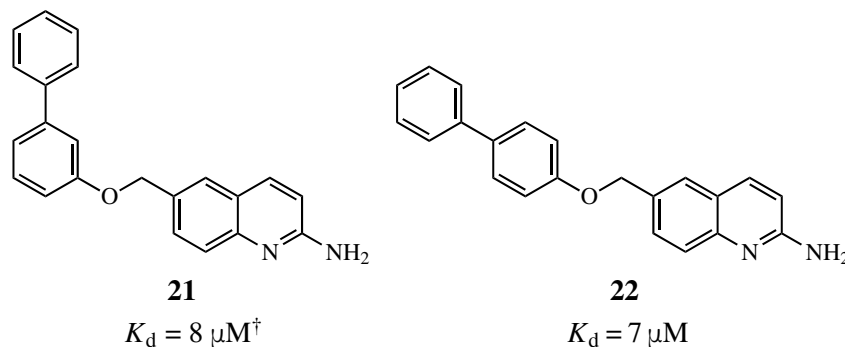
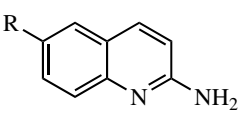


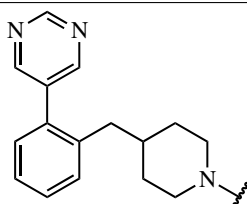
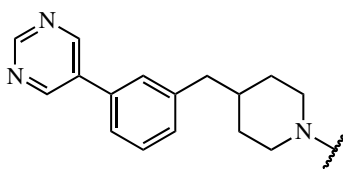
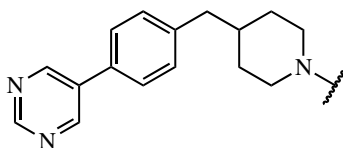
Figure 1.11: Reported structures and binding affinities of 6-phenylphenoxy substituted 2-aminoquinoline ligands for the Tec SH3 domain, determined by NMR chemical shift perturbation assays. <sup>†</sup>  $K_d$  assayed ligand was a 7:1 mixture with **22**.<sup>60</sup>

Upon closer investigation, the observed chemical shift perturbations induced by **21** and **22** were subtly different to that of the previously assayed ligands, appearing to access separate regions of the protein surface alternately, thus suggesting more than one favourable binding orientation.<sup>60</sup> As a result, the reported  $K_d$  values are potentially inaccurate as they were derived on the assumption of a one-site binding model.

Whilst definitive  $K_d$  values could not be determined for the 6-phenylphenoxy substituted 2-aminoquinoline ligands, the chemical shift perturbations suggested that there was an additional hydrophobic region of the protein surface that might be accessible for ligand binding. Utilising this SAR information, a series of aryl-substituted 6-benzylpiperidiny 2-aminoquinoline ligands (**23-25**) were synthesised, and their binding affinities determined by SPR experiments. From Table 1.8, binding affinity of 2,5-pyrimidinyl-substituted 6-benzylpiperidiny 2-aminoquinolines was either comparable or improved in all cases, with little discrimination in regards to the position of the 2,5-pyrimidinyl group.<sup>56</sup> This suggests that there is a relatively wide, hydrophobic region suitable for investigation in further SAR studies.

Table 1.8: Structures and binding affinities of 2,5-pyrimidinyl-substituted 6-benzylpiperidiny 2-aminoquinoline ligands for the Tec SH3 domain, determined by SPR assays.<sup>56</sup>



R =	Compound	$K_d$ ( $\mu\text{M}$ )
	<b>23</b>	$7 \pm 1$
	<b>24</b>	$4.1 \pm 0.7$
	<b>25</b>	$2.4 \pm 0.2$

### 1.5.6 Limitations of previous lead compounds

There is significant data to suggest that the Tec SH3 domain can be successfully targeted with small molecule inhibitors, with current ligands exhibiting low micromolar  $K_d$  values. However, to compete with native ligands of the Tec SH3 domain, further improvements to binding affinity are required. This could be achieved through more targeted ligand design for non-conserved amino acid residues on the Tec SH3 domain, ideally through 3D structural analysis of the ligand-protein binding interaction. At present, previously assayed ligands have bound in fast or intermediate, but not slow exchange on the NMR timescale, precluding structure determination by NMR spectroscopic methods.<sup>46,47</sup> Without a 3D ligand-protein bound structure, it is challenging to rationally design ligands for testing.

Another challenge in the development of PPI inhibitors is the increased hydrophobicity of the binding surface (compared to 'traditional' drug targets e.g., enzyme active sites). Whilst  $K_d$  values have been reported for many ligands for the Tec SH3 domain, there were several instances where despite a calculated  $\log P$  value ( $clogP$ )  $< 5$ ,<sup>61</sup> a ligand could not be assayed for binding affinity due to insolubility under biologically-relevant assay conditions (data not shown).<sup>56</sup> This indicates that significant efforts are still required to reduce ligand  $clogP$  values, and thus increase the drug-like character of future potential ligands and scaffolds. This is important for future SAR studies, where extension of a ligand scaffold, and therefore an inevitable increase in hydrophobicity, is required.

### 1.5.7 Limitations of previous ligand binding assays

Both NMR chemical shift perturbation and SPR binding assays have previously been used to determine ligand binding affinity (as  $K_d$  values) in previous work. NMR Chemical shift perturbation assays are insightful regarding ligand binding affinity and the location of the ligand-protein binding interaction, but are low throughput and require large amounts of  $^{13}\text{C}$ - or  $^{15}\text{N}$ -labelled protein. Alternatively, SPR assays are comparatively higher throughput and do not require labelled protein. However, the SPR binding assays utilised in previous work did not explicitly interrogate the position of the ligand-protein binding interaction on the protein surface.<sup>56</sup> Therefore, the previously reported ligand binding affinities for the Tec SH3 domain (determined by SPR)<sup>56</sup> were not directly comparable to those determined by NMR chemical shift perturbation assays,<sup>46-48</sup> as no formal comparison regarding the position of the ligand-protein binding site was undertaken.

## 1.6 Project aims

The primary aim of this project is to synthesise small molecule ligands for the Tec SH3 domain with 1) increased binding affinity and 2) improved drug-like character (measured by *clogP* value). As previous results suggest favourable binding is achieved in 6-substituted 2-aminoquinoline ligands with either electron-deficient aromatic rings or extended biaryl structures, it would be prudent to combine these features in a single (or class of) ligand, to determine their compatibility.

A secondary aim of this project is to validate the previously reported SPR ligand binding assay.<sup>56</sup> While the SPR assay was used for determination of ligand binding affinity in previous work,<sup>56</sup> the assay was conducted with GST-Tec SH3 fusion protein only. The response measured upon ligand binding in this SPR assay is agnostic to the location of the binding interaction on the protein surface (i.e., GST-Tec SH3), so the previously reported data<sup>56</sup> could reflect a binding affinity for an alternative ligand-protein binding interaction compared to the proposed ligand-protein binding model.<sup>46</sup> Therefore, it is desirable to investigate the location of binding interaction measured by SPR, to confirm whether the measured ligand-protein binding interaction is consistent with the proposed ligand-protein binding model,<sup>46</sup> and if the previously reported assay results are comparable with those binding affinities reported previously.<sup>46-48</sup>

A subsidiary aim of this project is to substantiate the proposed ligand-protein binding model for 2-aminoquinoline ligands with the Tec SH3 domain. This could be achieved by several means: if a suitably strong-binding ligand is identified (i.e., binding in slow exchange on the NMR timescale), then a three-dimensional ligand-bound protein structure may be determined by NOE-based NMR experiments. Alternatively, if the Tec SH3 domain is amenable to crystallisation, then the structure may be determined by x-ray crystallographic methods, through determination of the ligand-bound protein structure via diffusion. Considering the successful crystallisation and structure determination of SH3 domains reported over the last few years,<sup>43</sup> this is a reasonable approach.

### 1.6.1 Synthetic targets

#### 2-Aminoquinoline derivatives with simple 6-benzylpiperidinyl-derived substituents

Previous studies indicate that 2-aminoquinoline ligands with a 6-benzylpiperidinyl derived substituent (e.g. **19**, **20** and **25**) are among the strongest ligands to date.<sup>56</sup> However, further SAR



studies would likely require modification or extension of these scaffolds, which would confer an increase in overall ligand hydrophobicity and reduction of drug-like character. It would be useful to increase the drug-like character of this lead ligand scaffold (i.e., ensure a *clogP* value  $<5$ ),<sup>32,61</sup> whilst either maintaining or preferably improving ligand binding affinity. The structurally similar benzylpiperazinyl derivatives should have approximately the same shape as ligands derived from **15** whilst also possessing increased hydrophilicity through incorporation of an additional amine group, and thus will constitute the first class of target ligands to be explored. In addition, given the positive relationship between ligand binding affinity and electron-deficient arylmethyl groups shown in Table 1.7, it would be useful to investigate incorporation of an arylamido group, as shown in Figure 1.12. The binding data from these proposed ligand families will also provide SAR information regarding the geometry of the heterocycle and methylene group upon ligand binding.

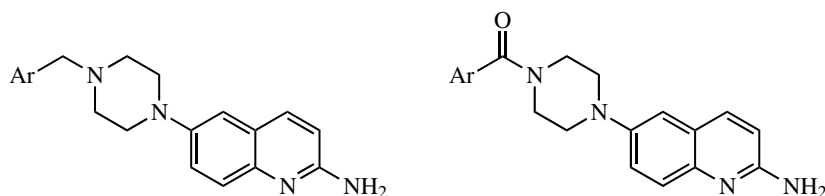


Figure 1.12: General structures of proposed benzylpiperazinyl-based ligands. Ar = aryl group.

### 2-Aminoquinoline derivatives with more complex 6-position extensions

An additional class of proposed ligands involves the combination of several favourable structural features into a single ligand, in an attempt to improve overall ligand binding affinity for the Tec SH3 domain in a cumulative manner. For example, from previous studies, it would be beneficial to consider synthesising a ligand where the arylmethyl component contains both an electron-deficient aromatic ring and a biaryl structure.<sup>56</sup> A general proposed target structure is provided in Figure 1.13; it is noted that the geometry and atomic composition about the X-Y group is subject to change based upon the binding assay results obtained for other piperazine-containing ligands in this thesis.

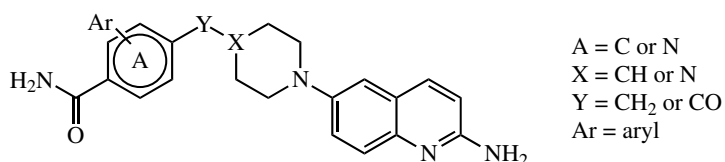


Figure 1.13: General proposed structure of 2-aminoquinoline ligands with a complex 6-position extension.

## 2 | Ligand binding assay validation and optimisation

### 2.1 Introduction

Investigation of small molecule ligand binding activity with the Tec SH3 domain has previously been achieved using a range of biophysical techniques; namely (2D) NMR chemical shift perturbation assays, FP ligand displacement (competition) assays, and SPR binding assays. Although each of these techniques can provide valuable information, due to the proposed number of ligands to be synthesised (see Chapter 3), each technique (NMR chemical shift perturbation assays, SPR and FP) has different capabilities regarding throughput of ligands and sensitivity of detection of ligand binding activities, therefore it would not be feasible to utilise all three techniques in this project. Furthermore, the interoperability of each of the biophysical techniques has not been closely scrutinised, therefore direct comparison of binding affinity data from two or more different techniques would not currently be viable.

To determine which biophysical technique would be most suitable to investigate the binding affinity of ligands in this project, the following aspects of each technique were considered:

1. Ability to determine binding affinity of the ligand for the protein;
2. Ability to determine the ligand binding site on the protein surface; and
3. Amenability to high-throughput screening of ligands.

2D NMR Chemical shift perturbation assays have the potential to provide a wealth of information regarding binding interactions, including binding affinity (as a dissociation constant,  $K_d$ ), binding site and potentially a 3-dimensional structure (each dependent on the nature of the binding interaction). However, only one compound can be assayed at a time, and is therefore not amenable to high-throughput screening of ligands. Additionally, the technique requires significant amounts of  $^{15}\text{N}$ -labelled protein, which can be quite expensive to produce; each assay requires a large amount of

protein (relative to other biophysical techniques), and expression of either  $^{15}\text{N}$  and/or  $^{13}\text{C}$ -labelled protein typically requires bacterial growth in minimal media supplemented with costly  $^{15}\text{N}$  and/or  $^{13}\text{C}$ -labelled salts and sugars, therefore protein yields are generally reduced compared to unlabelled protein which is typically grown in a rich media such as Luria-Bertani broth (LB).<sup>62,63</sup>

Similarly, FP is a valuable tool; unlike 2D NMR chemical shift perturbation assays, it is a relatively high-throughput method, as several compounds can be screened in a single 96-well-based plate assay. While some information can be obtained regarding the location of the binding site, the technique provides information regarding ligand displacement (as an  $\text{EC}_{50}$  value), therefore a binding affinity can only be inferred, not specifically determined. The technique also requires a fluorescently-labelled native ligand.

Alternatively, SPR can be used to directly determine binding affinities (as  $K_d$  values), also with the potential to investigate binding kinetics. Screening ligands by SPR is also a high-throughput process, with the ability to screen up to 11 compounds in a single run. Favourably, SPR is a direct, label-free technique (where label means radiolabel, fluorescent label etc.), and therefore a wider range of proteins and ligands are readily accessible for testing. While SPR doesn't provide specific information regarding the location of the binding interaction, the binding site could be readily investigated by conducting assays with rationally-designed protein variants constructed through site-directed mutagenesis experiments.

Consequently, SPR was chosen as the biophysical technique for investigating the binding activities of 2-aminoquinoline derivatives to the Tec SH3 domain in this project. If any ligands were identified to have substantially improved and/or favourable binding activity by SPR, then additional techniques (including 2D NMR chemical shift perturbation assays) may be considered for investigating those ligands only.

### 2.1.1 Surface Plasmon Resonance assays — General theory

SPR Assays utilise the principle of surface plasmon resonance to investigate real-time biomolecular interactions in solution, without the need for tags or labelling; the assays exploit the surface plasmons that exist between a metal layer (typically gold) that is plated on a glass surface. To conduct the SPR assays, the protein of interest must first be immobilised (covalently bonded or captured) to a chip comprised of gold layer supporting a dextran matrix, plated on a glass surface, as shown in Figure 2.1.

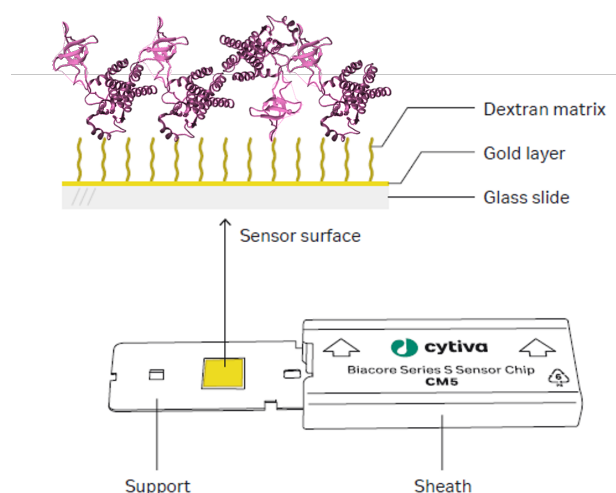


Figure 2.1: Representation of immobilised protein to the SPR chip, where chip components are labelled, and the protein target is indicated in pink. Adapted from Cytiva.<sup>64</sup> © 2022 Cytiva— Reproduced with Permission of Owner.

When light is directed at the glass surface of the chip, at a certain critical angle the photons achieve total internal reflection, where all of the incident light is reflected within the glass layer (Figure 2.2). In addition, upon reflection of light at the critical angle, the electric field of the photons extends just beyond the reflecting (glass) surface. When the glass layer is plated with gold (which is chemically inert and provides a SPR signal within a suitable range of wavelengths), if the photons are of a certain energy, they can interact with the free (outer shell) electrons on the gold surface. The photons are then absorbed by the gold, and their energy is transferred to the electrons on the gold surface, subsequently converting into surface plasmons. Through this surface plasmon generation by photon absorbance, a gap in the reflected light intensity at the glass surface is created. This minima in reflected light intensity is identified as the SPR angle, sometimes referred to as the resonance angle.

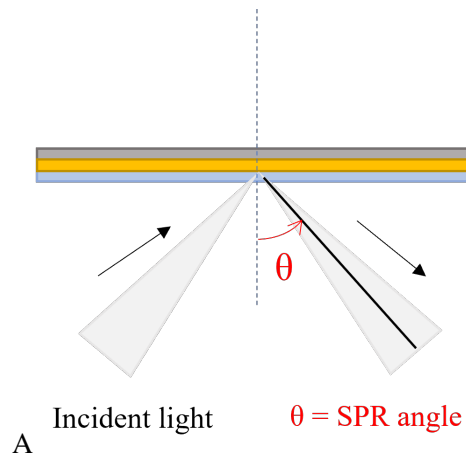


Figure 2.2: Schematic representation of total internal reflection condition of incident light against an SPR chip. Glass layer indicated in blue; gold layer indicated in gold; dextran matrix indicated in grey. SPR angle ( $\theta$ ) indicated in red, and minima in reflected light (at SPR angle) indicated by black line. Adapted from Cytiva.<sup>64</sup>

The SPR angle is extremely sensitive to alterations at the gold surface; the binding of molecules (ligands) to the immobilised protein is sufficient to alter the refractive index of the gold layer in a linear fashion. Thus, for each ligand that binds, an incremental change in SPR angle is observed (Figure 2.3). This change in SPR angle can be accurately quantified in arbitrary response units (RU) and plotted in a sensorgram, therefore allowing for quantitative analysis (including binding affinities and kinetic relationships) to be undertaken.

A general workflow describing the steps undertaken in a SPR assay to obtain and process a sensorgram, to eventually obtain ligand binding affinity data, is shown in Figure 2.4 and will be discussed in detail in the following text. For clarity, injections across the chip surface during assays are considered to be injections across both the reference and active flow channels.

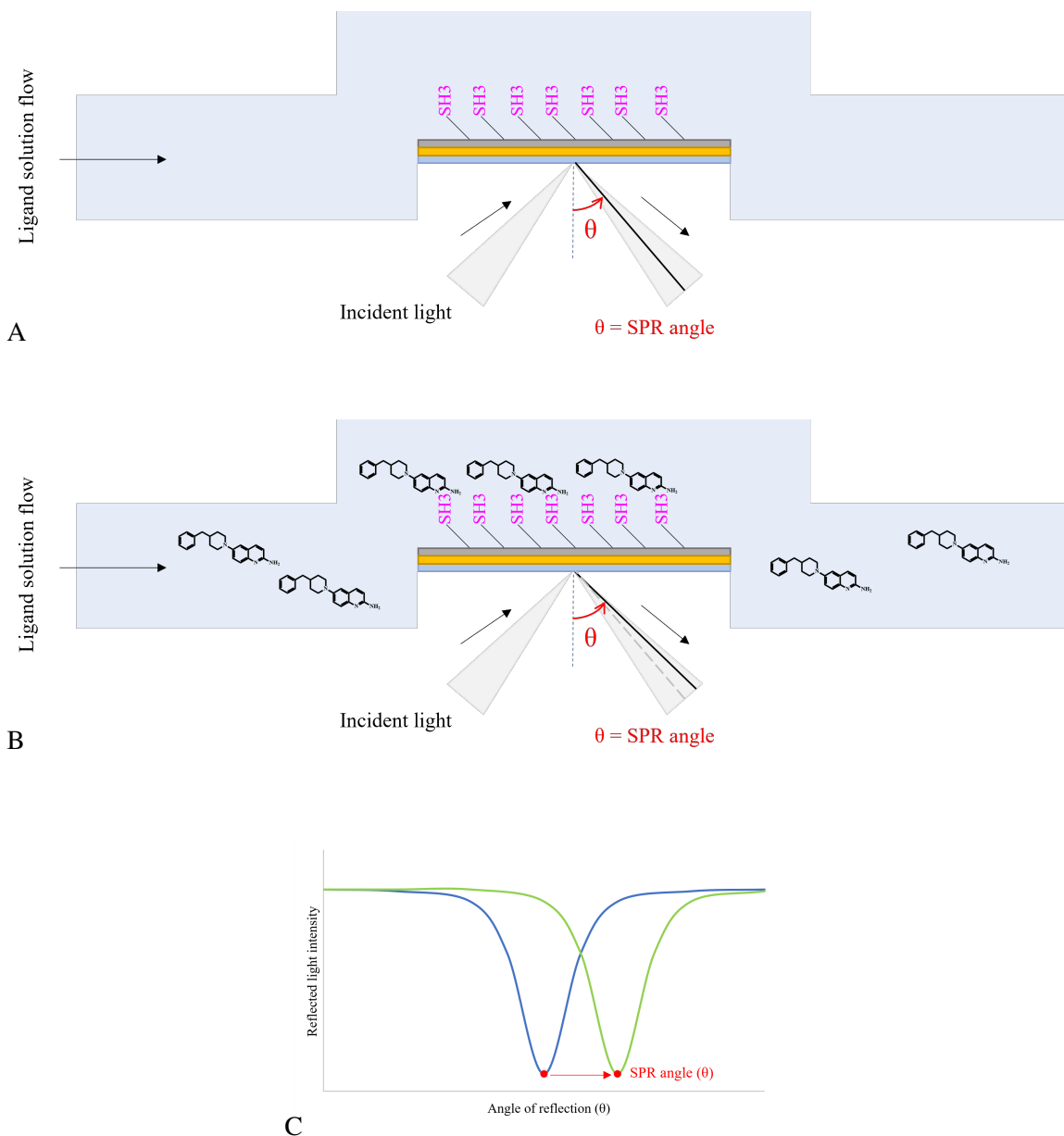


Figure 2.3: Schematic representation of binding interaction upon SPR sensor chip surface, and the resulting change in SPR angle, where the immobilised protein is SH3 domain (pink). (A) represents the baseline SPR angle when running buffer only (i.e., no ligand) is passed over the sensor chip surface. (B) represents the change in SPR angle upon ligand (black) binding to immobilised protein on the SPR sensor chip surface. (C) Graphical representation of change in SPR angle ( $\theta$ , red) and therefore minimum reflected light intensity, from baseline (blue, as for (A)) and upon ligand binding (green, as for (B)). Adapted from Cytiva.<sup>64</sup>

## 2.1. INTRODUCTION

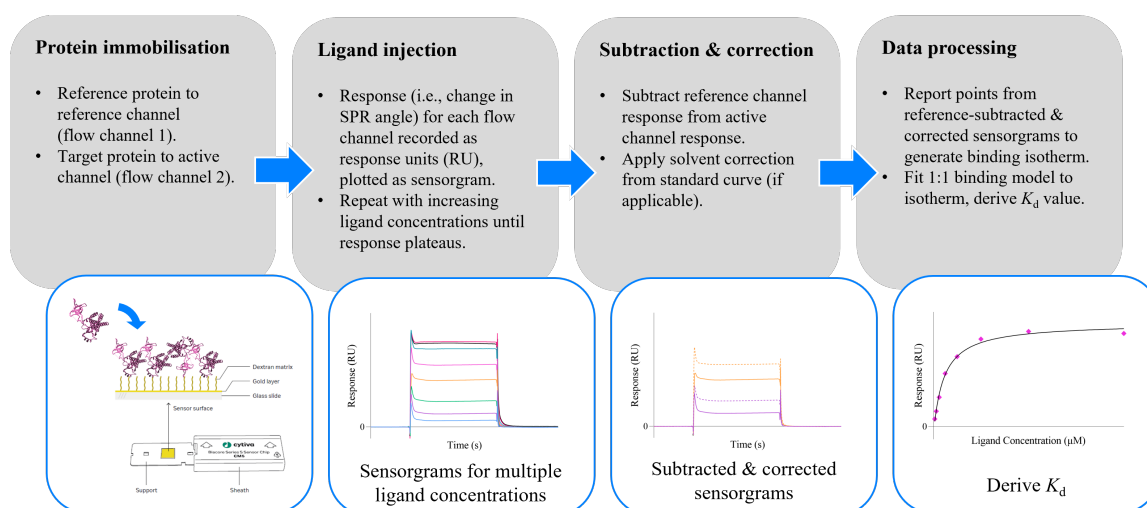


Figure 2.4: General workflow for ligand binding affinity assays by SPR. Some images adapted from Cytiva.<sup>64</sup> © 2022 Cytiva — Reproduced with Permission of Owner.

In a multi-cycle assay (as utilised in this thesis), several concentrations of ligand are injected over the chip surface and the SPR responses are measured over a fixed period, then the resulting sensorgrams are overlaid. In previous work, binding of the small molecule ligand **18a** (Figure 2.5) to the Tec SH3 domain was investigated by SPR.<sup>56</sup> With reference to Figure 2.5, an increase in response (RU) is observed upon ligand injection ('A'), indicating binding of the ligand to the protein immobilised on the chip. If the response following ligand injection stabilises ('B'), the ligand is considered to have achieved steady-state binding, where the on-rate of ligand binding is approximately equal to the off-rate. At the end of the injection ('C'), the response returns to baseline ('D', 'E') as the ligand dissociates from the protein. An additional wash procedure with 50% DMSO may be completed before injection of the next ligand (not pictured), to ensure that no "sticky" ligands remain bound to the sensor chip surface, without significantly impacting surface activity (i.e., protein folding or immobilisation). Sensor chip surface regeneration may be required if following the injection the ligand does not dissociate from the sensor chip surface at a reasonable rate. Notably, previous work investigating small molecule ligands for the Tec SH3 domain produced SPR sensorgrams with rapid association and dissociation (on-off rates) from the sensor chip surface (such as shown in Figure 2.5), therefore surface regeneration was not required, as the response returned to baseline ('E').<sup>56</sup> To undertake kinetic analyses of the binding interactions, the sensorgrams must display sufficient curvature during the association and dissociation phases;<sup>65</sup> given the square-wave sensorgrams observed for previously reported ligands (i.e., rapid on-off),<sup>56,66</sup> kinetic analyses could not be undertaken.

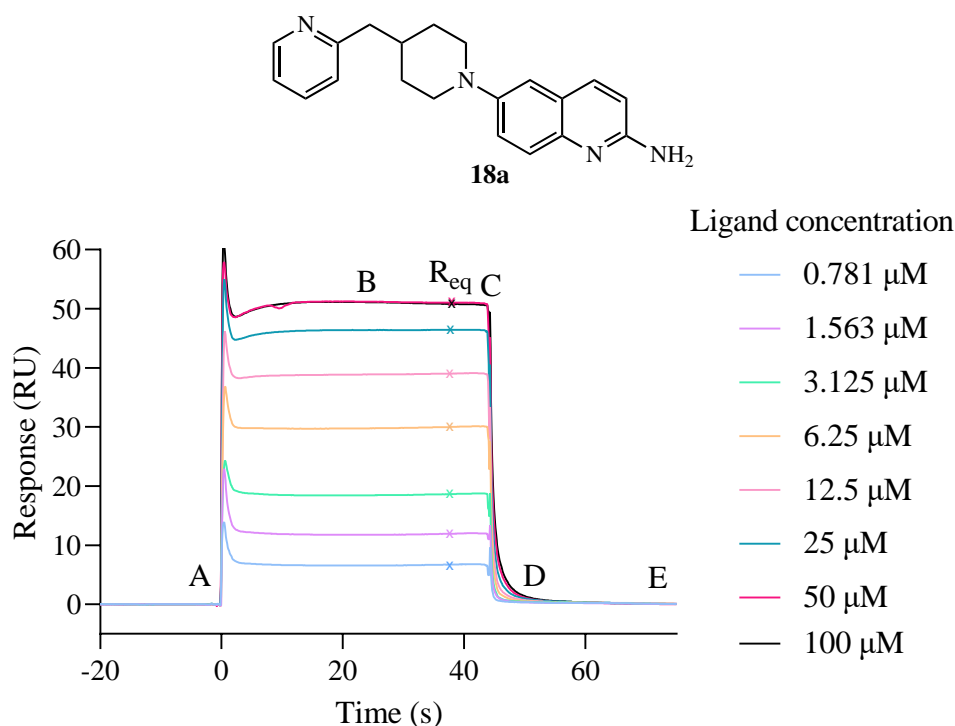


Figure 2.5: Example sensorgrams for binding of compound **18a** to GST-Tec SH3. SPR response indicated as response units (RU). ‘A’ indicates response at which **18a**<sup>56</sup> was injected over the sensor chip surface; ‘B’ indicates when the ligand-protein interaction has achieved steady-state binding (i.e., the SPR response is stable); ‘C’ indicates the SPR response drop at the end of the ligand injection; ‘D’ indicates a rapid SPR response drop upon ligand dissociation (typical of “fast-off” ligands); ‘E’ indicates the SPR response has returned to baseline, suggesting most of the ligand has been removed following the interaction.  $R_{eq}$  indicates the measured response at equilibrium binding (x), used to generate a binding isotherm.

Following sensorgram generation, post-run processing is conducted to reduce the observed response from off-site binding, and if organic solvents are used (e.g., DMSO), to correct bulk refractive index (RI) effects (compared to aqueous buffer). The latter occurs due to differences in the RI of the samples injected over the sensor chip surface — addition of 1% DMSO to buffer will give a bulk response of  $\sim 1200$  RU;<sup>65</sup> if the concentration of DMSO in the sample does not match the DMSO concentration of the running buffer, then an anomalous bulk response may be recorded. This is problematic when the ligands are small molecules, as the magnitude of response due to ligand binding is small in comparison to the magnitude of bulk response due to bulk RI effects. To minimise off-site binding effects, the response recorded upon ligand binding to the reference channel is subtracted from the response for ligand binding to the active channel (target) protein for each sensorgram. To minimise bulk RI effects, a solvent correction curve with varying concentrations of DMSO (a calibration curve) is applied to the sensorgram data, which is referenced to the observed response in the reference channel.



For a 1:1 binding model, a binding affinity for the ligand-protein binding interaction can be derived as a  $K_d$  value, as per Equations 1.3, 1.4 and 1.5 in Chapter 1. This is only applicable if the sensorgrams for each ligand concentration have reached steady-state (i.e., equilibrium) binding during the injection period. Subsequently, the steady-state response ( $R_{eq}$ , also see Figure 2.5) at each ligand concentration ( $C$ ) can be plotted to form a binding isotherm (Figure 2.6). Assuming a 1:1 ligand-protein (Langmuir) binding model, a non-linear regression (Equation 2.1) can be fitted to the binding isotherm to derive the binding affinity of the ligand,  $K_d$ .

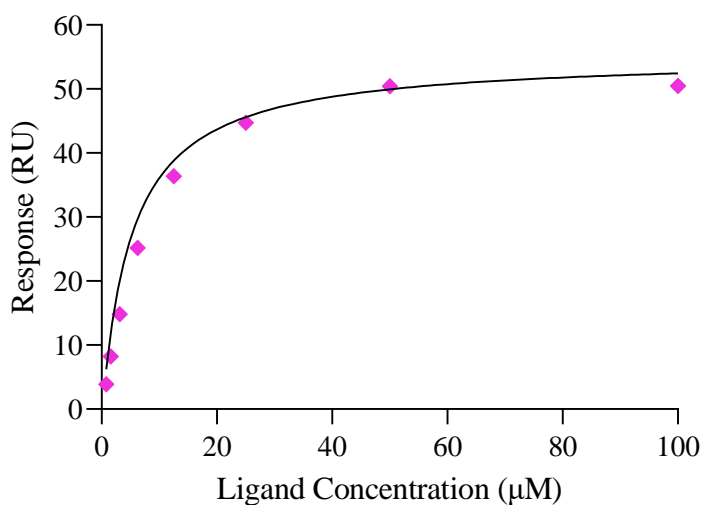


Figure 2.6: Example binding isotherm derived from sensorgrams of ligand (**18a**) binding to GST Tec-SH3 protein (Figure 2.5). SPR response indicated in response units (RU). Datapoints (pink) indicate raw data at given concentrations used to derive the fitted isotherm (black), based on Equation 2.1.

$$R_{eq} = \frac{C \cdot RU_{max}}{C + K_d} + R_O \quad (2.1)$$

The non-linear regression analysis calculates fitted values for the maximum SPR response upon ligand binding site saturation ( $RU_{max}$ ), equilibrium dissociation binding constant ( $K_d$ ), and SPR response offset (i.e., offset of the fitted equation on the y-axis,  $R_O$ ). These fitted values can be manually inspected to support or oppose the validity of the calculated  $K_d$  value, as the  $RU_{max}$  value can be compared to the theoretical  $RU_{max}$  based upon the amount of immobilised protein ( $RU_{max(theor.)}$ , see Section 2.4.1.1), and the SPR offset should be close to the origin of the binding isotherm, (0,0). In addition, the fitted nonlinear regression (isotherm) can be scrutinised by a calculated  $\chi^2$  value, to evaluate its closeness of fit to the experimentally-determined data. A well-fitting Langmuir isotherm should plateau at higher concentrations, indicating saturation of the available protein binding sites,

and therefore saturation binding has likely been achieved. In addition, the  $\chi^2$  value for the fitted isotherm should be low, indicating the model fits the experimental data well.<sup>65</sup>

While various modes of ligand binding are possible, the shape of the sensorgram is often indicative of the nature of the binding event that is occurring; typically, a 1:1 binding interaction will produce a box-shaped sensorgram due to reaching steady-state binding (i.e., rate of ligand association with target protein  $\approx$  rate of ligand dissociation from ligand-protein complex), whereas more complex binding interactions will not achieve steady state binding, so the sensorgram shape will differ (Figure 2.7).

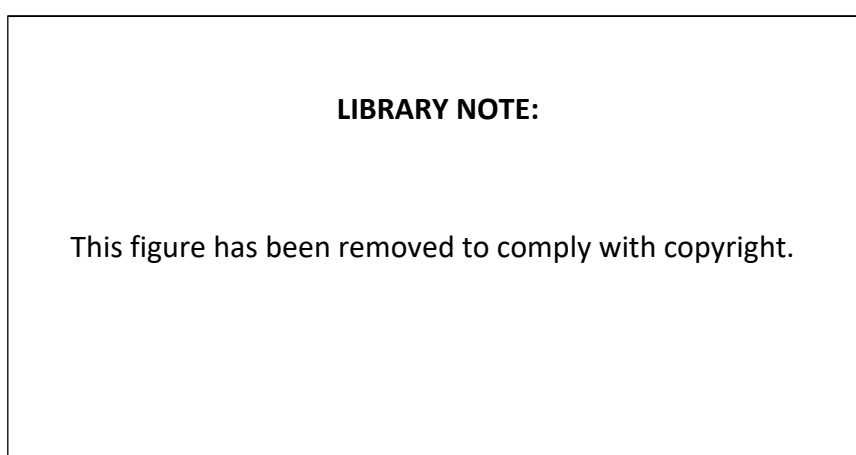


Figure 2.7: Simulated SPR sensorgrams displaying the different responses observed for either a one-site or multi-site ligand binding model. Taken from GE Healthcare Life Sciences Biacore Assay Handbook.<sup>67</sup>

## 2.2 Proposed optimisation of the SPR binding assay

SPR Assays detect mass changes at the protein (chip) surface, therefore they can be are indiscriminate to the location of ligand binding. It would be ideal to determine that the ligands are binding at the same site on the protein surface as those reported previously,<sup>46,47,58</sup> and investigation of the ligand-protein binding site will be made with reference to the previously proposed ligand-protein binding model, which identifies residues D196 and W215 of the Tec SH3 domain as crucial residues for ligand binding. Consequently, it would be desirable to test the binding activities of previously reported ligands<sup>56</sup> to a Tec SH3 D196 mutant; if no binding is observed to the Tec SH3 D196 mutant, then it is reasonable to suggest that the binding interaction being measured by SPR is consistent with the previously proposed ligand-protein binding model.<sup>54</sup> In addition, previous SPR binding assays conducted with Tec SH3 domain as a target tested ligand binding against GST-tagged SH3 protein (GST-Tec SH3),<sup>56,66</sup> which may have provided an opportunity for non-specific and/or off-

target binding to the GST tag. Although there are reports of similar small molecule ligands not binding significantly to the GST tag of GST-Tec SH3 protein,<sup>54</sup> it would be ideal to test the ligand binding against the Tec SH3 domain only, to conclusively investigate any non-specific and/or off-site binding interactions with the GST tag, and to ensure there are no cooperative effects between the GST and Tec SH3 protein domains. In each case, suitably high levels of protein are required for appropriate ligand binding, so optimisation of protein immobilisation will be required.

To facilitate assay optimisation, it would be beneficial to conduct the proposed SPR binding assays using previously assayed ligands, as this would provide a benchmark to previously reported data.<sup>56</sup> Compounds **18a**<sup>56</sup> and **18b**<sup>66</sup> (Figure 2.8) were selected as ideal control ligands to use for SPR protocol validation as their recorded binding affinities were highly reproducible and in the ideal range for analysis by SPR (i.e., sufficiently strong binding), they had reported improved stability over other previously reported benzylpiperdinyll derivatives, and reported syntheses of these compounds indicated high yields. The preparation of control ligands **18a** and **18b** is reported in Section 2.6.

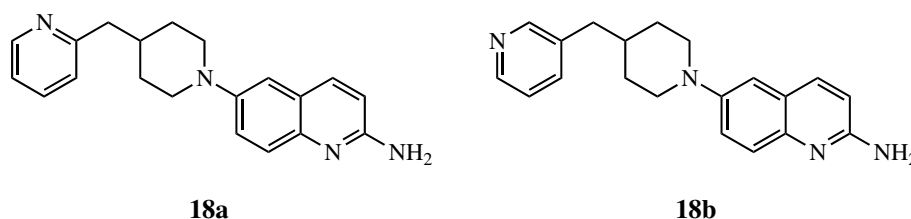


Figure 2.8: Control 6-heterocycle substituted 2-aminoquinoline ligands **18a**<sup>56</sup> and **18b**.<sup>66</sup>

## 2.3 Protein expression and purification

In preparation for SPR binding assay optimisation, expression and purification of three Tec SH3 domain derivatives was required for SPR binding assay optimisation:

1. GST-Tec SH3, which would allow for direct comparison to previous SPR binding assays;
2. Tec SH3, to conclusively identify any off-site binding to the GST tag; and
3. a Tec SH3 D196 mutant, to investigate whether the binding mode of current ligands is consistent with the previously proposed ligand-protein binding model.<sup>46</sup>

Earlier studies have successfully utilised the GST-Tec SH3 D196A mutant protein to investigate the proposed ligand-protein binding interaction,<sup>46</sup> therefore GST-Tec SH3 D196A was selected as the Tec SH3 D196 mutant protein for this work. *Escherichia coli* bacterial strain BL-21 (DE3) glycerol stocks which had been successfully transformed with the appropriate plasmids had been prepared previously,<sup>3,46,54</sup> and were used for the preparation of all Tec SH3-containing proteins described in this thesis.

A protein crystal structure could theoretically be used to elucidate the ligand-protein binding model by x-ray crystallography if suitable ligand soaking or co-crystallisation conditions were identified. Therefore, investigations into crystallisation of GST-Tec SH3 and the Tec SH3 domain were undertaken, including additional protein purification steps compared to those reported previously.<sup>50,56</sup>

### **2.3.1 Expression and purification of GST-Tec SH3 and GST-Tec SH3 D196A proteins**

The successful expression and purification of GST-Tec SH3 domain proteins (including GST-Tec SH3 D196A mutant protein) has been reported several times in the literature.<sup>3,46,47,54,60</sup> Previous preparation of these bacterial glycerol stocks involved the cloning and insertion of the sequence for the Tec SH3 domain into a pGEX-4T-2 plasmid vector. Notably, the selected insertion site into the plasmid meant the Tec-SH3 domain would be expressed with a GST tag appended to the N-terminus, which would aid protein expression through increased stability and facilitating protein folding,<sup>68</sup> and also provide an opportunity for GST-affinity purification. Between the GST tag and Tec SH3 domain lies a thrombin cleavage site, thus the Tec SH3 domain can be liberated from GST-Tec SH3 by incubation with the protease thrombin. Lastly, this plasmid construct contains an ampicillin-resistance gene; successful growth of bacteria containing the desired plasmid can be selected for by treatment with ampicillin (Figure 2.9).

### 2.3. PROTEIN EXPRESSION AND PURIFICATION

---

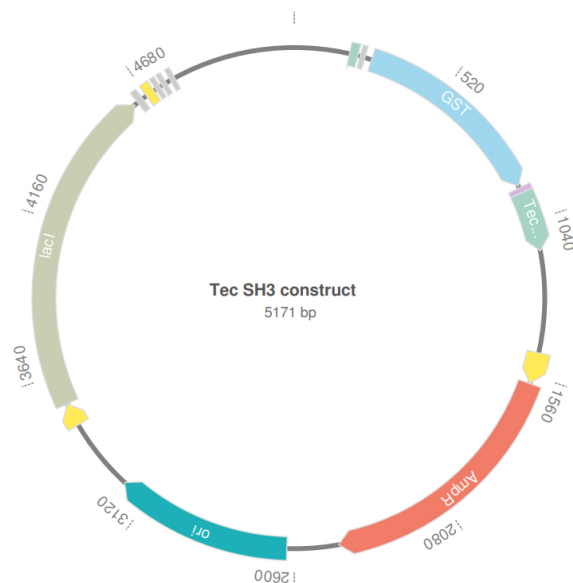
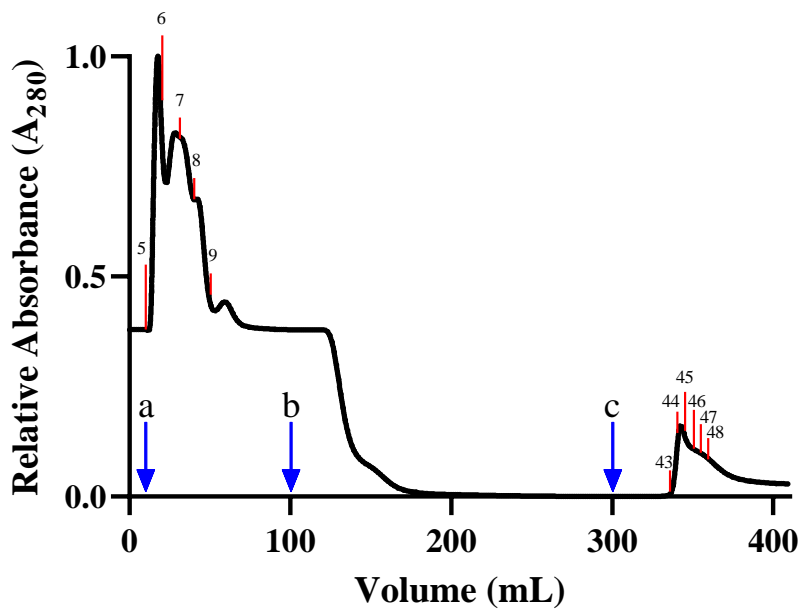


Figure 2.9: Representation of cloned pGEX-4T-2 plasmid vector utilised for expression of GST-tagged Tec SH3 domain. Total predicted vector size = 5171 bp. Regions of interested are highlighted as follows: GST tag sequence (257-911) indicated in blue; thrombin site sequence (917-935) indicated in purple; Tec SH3 domain sequence (936-1136) indicated in light green, ampicillin resistance gene (AmpR, 1578-2438) indicated in red. Figure created using GenSmart™ by GenScript.<sup>69</sup>

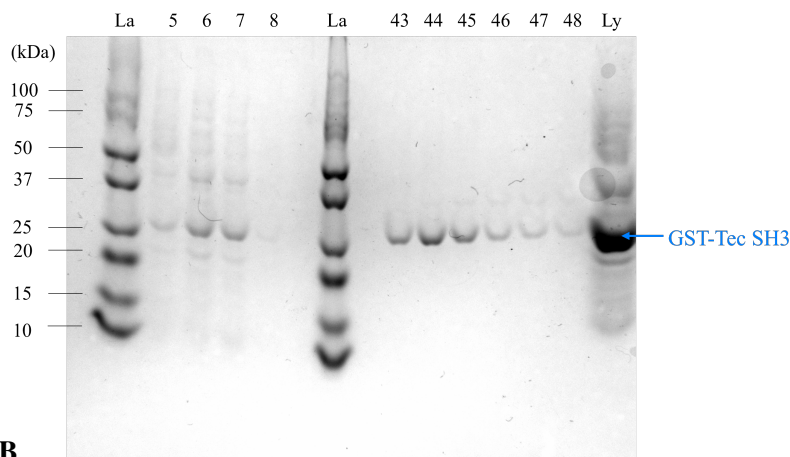
Following protein expression and purification methods reported previously,<sup>3,46,54</sup> *E. coli* BL-21 (DE3) transformed with either pGEX-4T-2 Tec SH3 or pGEX-4T-2 Tec SH3 D196A were grown at 37 °C until reaching OD<sub>600</sub> 0.6-0.8. Protein expression was then induced with isopropyl-β-D-thiogalactopyranoside (IPTG) to 0.2 mM, and grown at 37 °C over a further 4 hrs, before collection of the bacterial pellet. The bacterial pellet was re-suspended in lysis buffer (TTBS: TBS + 0.1% Triton, pH 8), and subjected to several freeze-thaw cycles (typically 3-4) before lysis by sonication and subsequent filtration. Analysis of the bacterial cell lysate by SDS-PAGE revealed an induced protein band at approximately 34 kDa, consistent with the sizes expected for fusion GST-Tec SH3 proteins (GST-Tec SH3 and GST-Tec SH3 D196A) (Figure 2.10). Fusion GST-Tec SH3 proteins were initially purified by agarose/glutathione affinity chromatography. In this technique, glutathione, a natural, specific substrate to GST, is immobilised to agarose. Upon passage of GST-containing proteins across the medium, proteins containing GST will bind through the GST tag to the medium. Following washing of unbound proteins, the desired GST-containing proteins can be displaced from the medium by eluting with an excess of reduced glutathione, which will competitively displace immobilised glutathione from the medium, allowing the GST-containing proteins to be collected. Filtered bacterial cell lysate was loaded onto an agarose/glutathione affinity column which had been pre-equilibrated into TTBS, and washed extensively with TTBS and TBS. The

GST-Tec SH3 protein was eluted with addition of 10 mM reduced glutathione in TBS, and the elution profile of GST-Tec SH3 is shown in Figure 2.10(A). Purity of the fractions collected by FPLC was analysed by SDS-PAGE under reducing conditions, and revealed a major product band at ~34 kDa, consistent with the desired GST-Tec SH3 protein (Figure 2.10(B)). The GST-Tec SH3 D196A mutant was also prepared following the same methods as for GST-Tec SH3 protein; subsequent purification of the cell lysate via FPLC (as described above) followed by analysis of FPLC fractions by SDS-PAGE revealed a major purified product band with a molecular weight of ~34 kDa, which is consistent with the molecular weight of the desired GST-Tec SH3 D196A mutant.

To avoid non-specific interactions in SPR assays, and to improve protein purity in preparation for crystallography studies, fractions containing GST-Tec SH3 were combined, concentrated from 120 mL to ~3 mL by centrifugation using 10 kDa MWCO filters, then purified by size-exclusion chromatography, eluting in TBS (pH 8). Analysis of the appropriate FPLC fractions by reducing SDS-PAGE revealed incomplete resolution of GST-Tec SH3 due to the presence of a minor protein band at approximately 37 kDa. Despite this, substantial resolution was observed overall, and the protein was considered sufficiently purified for both SPR and crystallography studies (Figure 2.11). Due to the incomplete resolution of GST-Tec SH3 by size-exclusion chromatography, the mutant GST-Tec SH3 D196A protein was purified by agarose/glutathione affinity chromatography only.



A



B

Figure 2.10: Purification of GST-Tec SH3 protein by agarose/glutathione chromatography. (A) Normalised FPLC elution profile following the purification of GST-Tec SH3 protein by agarose/glutathione affinity column chromatography. The column was equilibrated with at least two column volumes of TBS, followed by at least two column volumes of TTBS. The column was then loaded with no more than 4 mL of lysate, and washed with TTBS (indicated by blue arrow 'a') and TBS (blue arrow 'b'), as per Section 6.6.1.2. Bound GST-Tec SH3 was eluted by washing with 10 mM reduced glutathione in TBS (pH ~8) (blue arrow 'c'). Collected fractions indicated by red lines on chromatogram. (B) SDS-PAGE analysis of GST-Tec SH3 protein samples before and after purification by agarose-glutathione column chromatography, as indicated in (A). Reference ladder indicated by 'La', with size of reference proteins labelled (in kDa). Fraction numbers consistent with those labelled in (A). Bacterial lysate (loaded onto agarose/glutathione affinity column) indicated by 'Ly'.

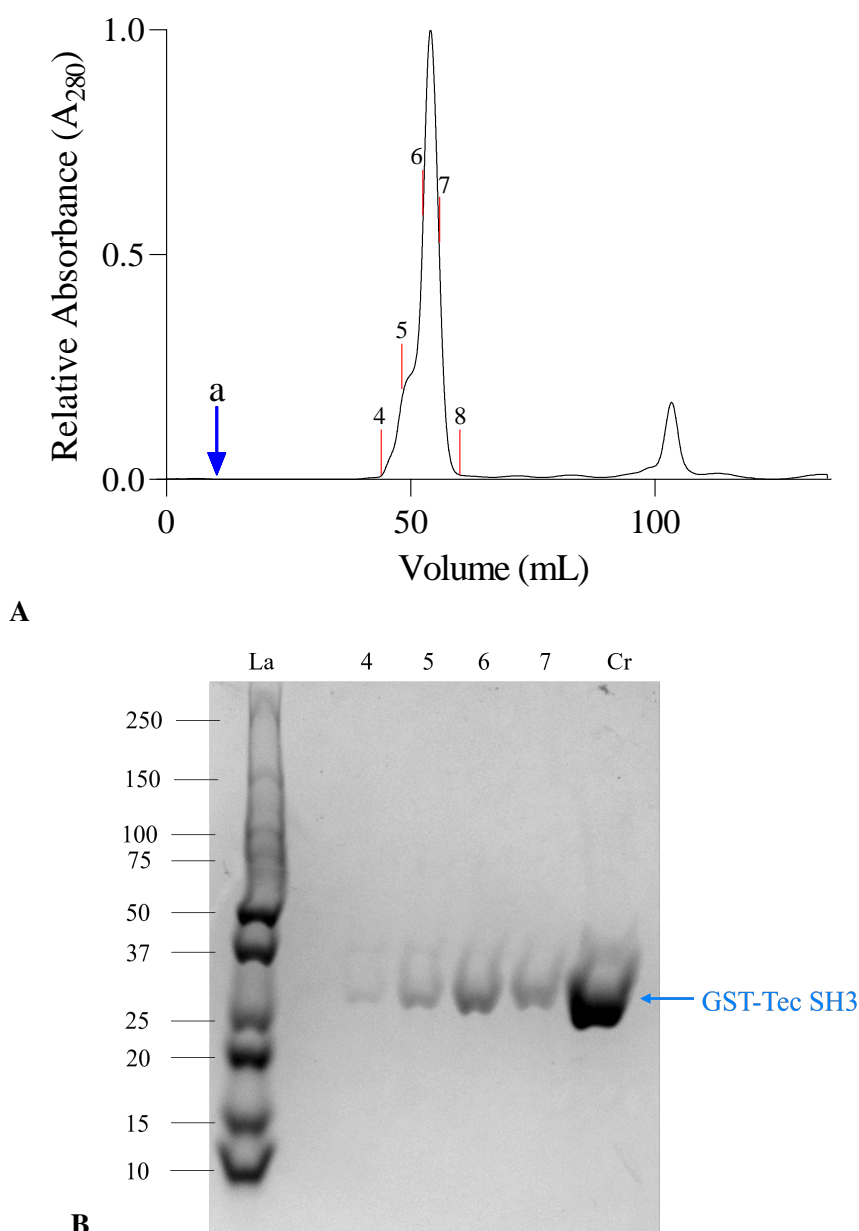


Figure 2.11: Purification of GST-Tec SH3 protein by size-exclusion chromatography. (A) Normalised FPLC elution profile following the purification of GST-Tec SH3 protein by size-exclusion chromatography. The column was equilibrated with at least two column volumes of TBS, before loading with no more than 2 mL of crude GST-Tec SH3 (indicated by blue arrow 'a'), then washing and eluting with TBS. Collected fractions indicated by red lines on chromatogram. (B) SDS-PAGE analysis of GST-Tec SH3 protein samples before and after purification by size-exclusion chromatography, as indicated in (A). Reference ladder indicated by 'La', with size of reference proteins labelled (in kDa). Fraction numbers consistent with those labelled in (A). Crude, concentrated GST-Tec SH3 (from the agarose/glutathione affinity column) indicated by 'Cr'.

To investigate whether the desired protein had been isolated, the purified GST-Tec SH3 protein was analysed by high-resolution mass spectrometry via electrospray ionisation (ESI) (Figure 2.12). Several major products were observed, however each of these are predicted to be the desired GST-Tec SH3 fusion protein, with bound glutathione molecules, and in some cases, loss of methionine



## 2.3. PROTEIN EXPRESSION AND PURIFICATION

via post-translational modification (Table 2.1). In each case, the presence of glutathione or absence of methionine is not expected to implicate binding activity.<sup>54</sup> glutathione is a small tripeptide that would be bound to the GST domain, therefore is highly unlikely to restrict access to the proposed ligand binding site on the Tec SH3 domain. Similarly, the methionine residue that is most likely cleaved is at the N-terminus of the protein (within the GST tag) and therefore not affecting the structure of the Tec SH3 domain. This loss of N-terminal methionine has also been reported previously, and did not interfere with subsequent protein binding assays.<sup>54</sup>

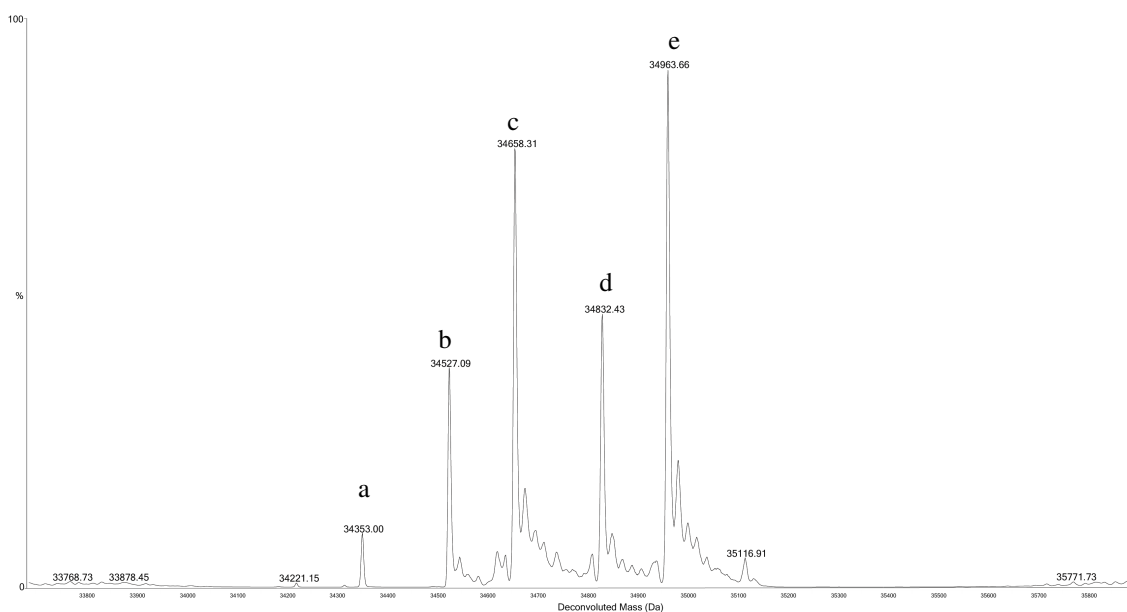


Figure 2.12: Deconvoluted mass spectrum of GST-Tec SH3 fusion protein. Major products are labelled, and relative abundances indicated. Mass spectra deconvoluted using UniDec version 5.0.0.beta<sup>70</sup>

Table 2.1: Key for deconvoluted mass spectrum of GST-Tec SH3 fusion protein (Figure 2.12). Predicted masses calculated assuming the following: GST-Tec SH3 = 34047 Da, glutathione = 306 Da, methionine = 131 Da. Obs. = observed.

Mass product	Predicted product	Predicted deconvoluted	Obs. deconvoluted
label	(GST-Tec SH3)	mass (Da)	mass (Da)
a	+ glutathione	34353	34353
b	+ 2 glutathione, - methionine	34528	34527
c	+ 2 glutathione	34659	34658
d	+ 3 glutathione, - methionine	34834	34832
e	+ 3 glutathione	34965	34964

Similarly, mass spectrometric analysis of the GST-Tec SH3 D196A mutant revealed a range of major deconvoluted mass products (Figure 2.13). Subsequent analysis revealed that again these masses were consistent with the presence of glutathione or loss of methionine (Table 2.2), supporting that the desired GST-Tec SH3 D196A mutant had also been isolated.

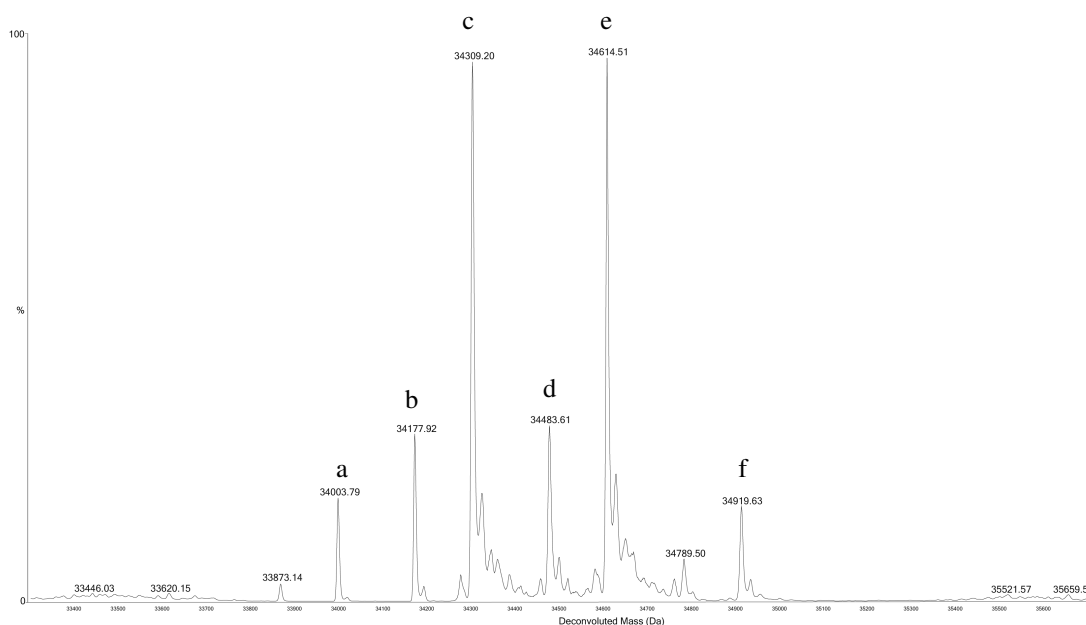


Figure 2.13: Deconvoluted mass spectrum of GST-Tec SH3 D196A fusion protein. Major products are labelled, and relative abundances indicated. Mass spectra deconvoluted using UniDec version 5.0.0.beta<sup>70</sup>

Table 2.2: Key for deconvoluted mass spectrum of GST-Tec SH3 D196A fusion protein (Figure 2.13). Predicted masses calculated assuming the following: GST-Tec SH3 D196A = 34003 Da, glutathione = 306 Da, methionine = 131 Da. Obs. = observed.

Mass product	Predicted product	Predicted deconvoluted	Obs. deconvoluted
label	(GST-Tec SH3 D196A)	mass (Da)	mass (Da)
a	no modifications	34004	34003
b	+ glutathione, - methionine	34178	34178
c	+ glutathione	34309	34309
d	+ 2 glutathione, - methionine	34484	34484
e	+ 2 glutathione	34615	34615
f	+ 3 glutathione	34921	34920

## 2.3. PROTEIN EXPRESSION AND PURIFICATION

---

In preparation for SPR binding assays, the GST-Tec SH3 proteins were concentrated, then buffer-exchanged into PBS (pH 7.4) using GE Healthcare PD-10 desalting columns (as per the manufacturer's instructions), followed by addition of 2% w/v sodium azide to a resultant concentration of 0.01% w/v. Typical protein yields as determined by Bradford assay are listed in Table 2.3. In each case, sufficient protein had been purified for SPR assays, and the yields for GST-Tec SH3 fusion protein were acceptable for preliminary crystallisation experiments.

Table 2.3: Calculated yields for purified GST-Tec SH3 fusion proteins, determined by Bradford assay.

Protein	Volume (mL)	Concentration (mg/mL)
GST-Tec SH3	3.5	6
GST-Tec SH3 D196A	5.5	2

### 2.3.2 Purification of Tec SH3

To liberate the Tec SH3 domain, purified GST-Tec SH3 fusion protein was diluted to  $\sim 2$  mg/mL, then cleaved with thrombin (Sigma T7009, 3U/mg GST-Tec SH3 protein), for a minimum of 18 hours. Generally, the reaction had not gone to completion at this time, however further incubation often resulted in lower yields due to non-specific proteolysis and protein precipitation. Following digestion, proteolysis was halted by addition of 100 mM phenylmethylsulfonyl fluoride (PMSF) in ethanol, to a resultant concentration of 1 mM. The protein digest was filtered, and isolation of the Tec SH3 domain was achieved by size exclusion chromatography on a GE Healthcare HiPrep 26/60 Sephacryl S-200 HR column. The Sephacryl beads effectively separated the Tec SH3 domain (8 kDa) from the GST tag (26 kDa), as indicated by SDS-PAGE (Figure 2.14).

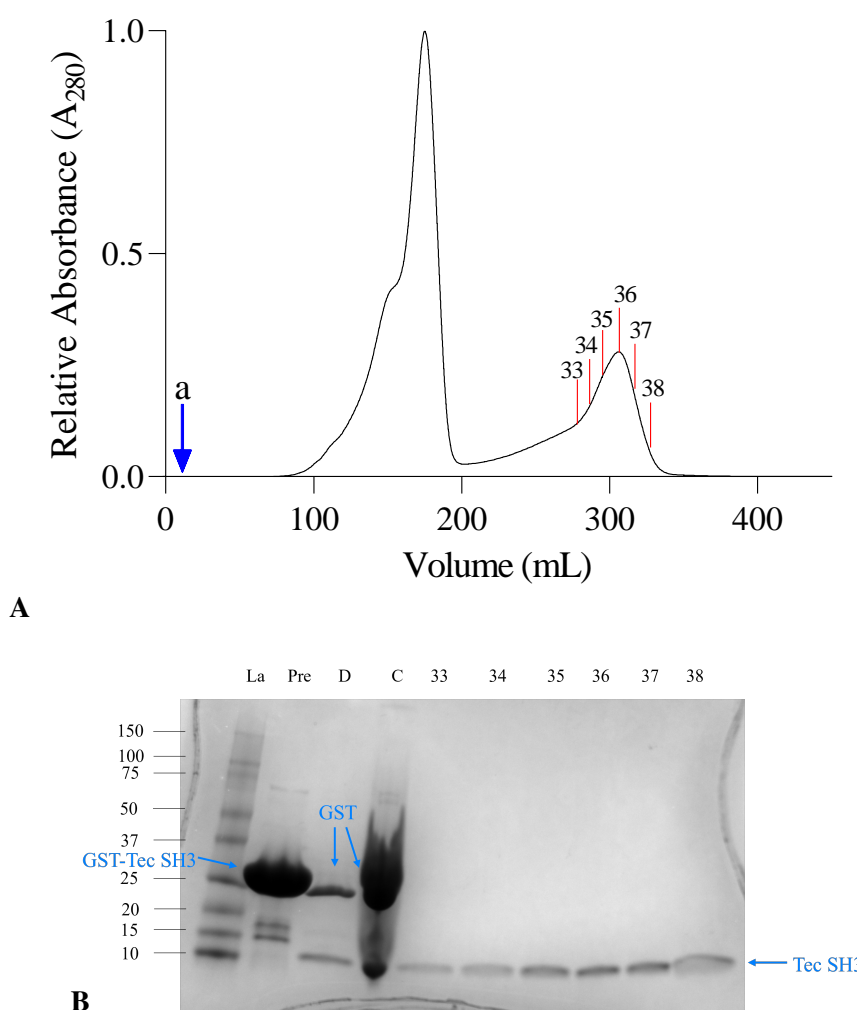


Figure 2.14: Purification of Tec SH3 protein by size-exclusion chromatography following thrombin digest of GST-Tec SH3 fusion protein. (A) Normalised FPLC elution profile of Tec SH3 by size exclusion chromatography. The column was equilibrated with at least two column volumes of TBS, before loading with no more than 10 mL of concentrated, digested GST-Tec SH3 fusion protein, indicated by blue arrow 'a' then washing and eluting with TBS. Fractions containing Tec SH3 indicated in red. (B) SDS-PAGE analysis of Tec SH3-containing protein samples before and after purification by size-exclusion chromatography, indicated in (A). Reference ladder indicated by 'La', with size of reference proteins labelled (in kDa). Fraction numbers consistent with those labelled in (A). 'Pre' indicates purified GST-Tec SH3 prior to digestion. 'D' indicates the dilute thrombin digest products. 'C' indicates the concentrated thrombin digest products, which were loaded onto the size-exclusion column.

Confirmation of the obtained protein product was again determined by high resolution mass spectrometry (ESI), revealing a deconvoluted mass product with  $m/z$  7899, consistent with that expected for the Tec SH3 domain (Figure 2.15, Table 2.4). No other major products were observed in the mass spectrum.

## 2.3. PROTEIN EXPRESSION AND PURIFICATION

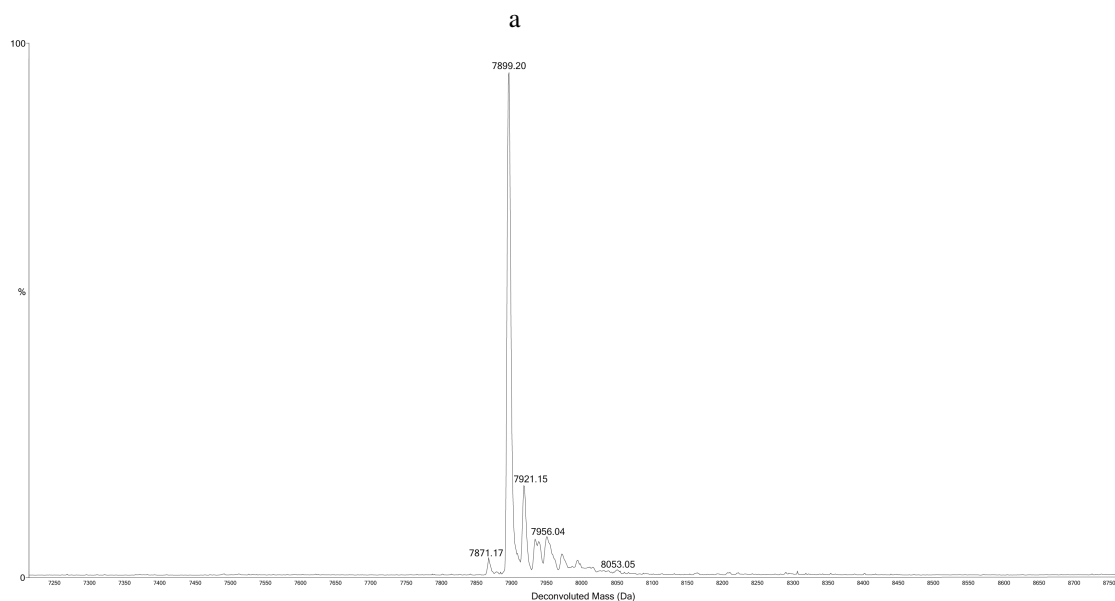


Figure 2.15: Deconvoluted mass spectrum of Tec SH3 protein. Major products are labelled, and relative abundance indicated. Mass spectra deconvoluted using UniDec version 5.0.0.beta<sup>70</sup>

Table 2.4: Key for deconvoluted mass spectrum of Tec SH3 protein (Figure 2.15).

Mass product label	Predicted product (GST-Tec SH3)	Predicted deconvoluted mass (Da)	Observed deconvoluted mass (Da)
a	no modifications	7899	7899

Similarly to the GST-Tec SH3 fusion protein, in preparation for SPR assays, Tec SH3 protein was concentrated, then buffer exchanged into PBS (pH 7.4) using GE Healthcare PD-10 desalting columns (as per the manufacturer's instructions), followed by addition of 2% w/v sodium azide to a resultant concentration of 0.01% w/v. Protein yield as determined by Bradford assay is listed in Table 2.5. Pleasingly, sufficient protein had been purified for both SPR assays and preliminary crystallisation experiments.

Table 2.5: Calculated yields for purified Tec SH3 protein, determined by Bradford assay.

Protein	Volume (mL)	Concentration (mg/mL)
Tec SH3	4	0.9

## 2.4 SPR binding assay validation

### 2.4.1 Binding to GST-SH3

#### 2.4.1.1 Introduction: Chip surface preparation and immobilisation

Previously reported ligands for the Tec SH3 domain that were assayed by SPR utilised GST-Tec SH3 as the protein binding partner, and GST as the reference protein to identify and correct for potential non-specific binding.<sup>56</sup> To ensure that the GST-Tec SH3 protein as prepared was sufficiently pure and correctly folded, it would be prudent to ensure that the synthesised ligands displayed similar binding activity to those reported previously. This would require investigation of the binding affinity through  $K_d$  comparison, and investigation of SPR chip surface preparation and protein immobilisation to the chip surface. In the first instance, CM5 SPR chips were investigated due to their general applicability for protein immobilisation.

The first step involved pre-conditioning of the chip surface to remove any non-specifically bound particles through sequential injections of various acids, bases and detergents, in order to ensure baseline stabilisation.<sup>71</sup> Pre-conditioning was conducted as previously reported;<sup>56</sup> following injection of each reagent, the response (RU) value returned to a stabilised baseline, indicating that no reagent molecules were adsorbed to the chip surface (Figure 2.16).

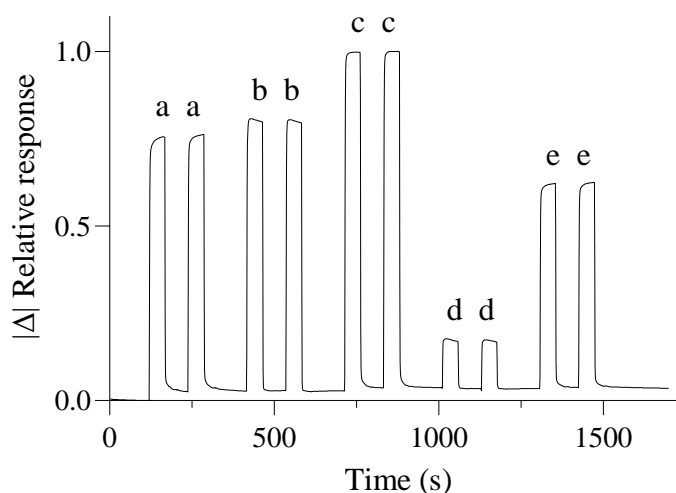


Figure 2.16: Relative (normalised) response during pre-conditioning of a flow channel on a CM5 sensor chip. Response changes upon injection of reagents over the flow channel. Reagents indicated by letters, as follows: a = 50 mM NaOH; b = 10 mM HCl; c = 0.1% w/v SDS; d = 0.85% v/v  $H_3PO_4$ ; e = 50 mM glycine, pH 9.5.

## 2.4. SPR BINDING ASSAY VALIDATION

---

Following pre-conditioning of the chip surface, the surface was primed for protein immobilisation via injection of a mixture of NHS and 1-ethyl-3-(3-dimethylaminopropyl)carbodiimide hydrochloride (EDC). Successful formation of NHS esters on the surface was indicated by a slight increase in RU value at the end of the injection.

In order to determine the desired amount of protein to be immobilised to the chip surface, reference to Equation 2.2 below is made — where, assuming a 1:1 binding stoichiometry,  $RU_{\max(\text{theor.})}$  is the theoretical maximum RU value,  $MW_{\text{ligand}}$  is the molecular weight of the ligand,  $MW_{\text{immob.}}$  is the molecular weight of the immobilised protein, and  $RU_{\text{immob.}}$  is the amount of immobilised protein, in RU. For SPR binding assays investigating the binding affinity of small molecules, typically a higher density of protein is immobilised to allow for sufficient signal to be produced upon ligand binding; from literature, the ideal  $RU_{\max(\text{theor.})}$  would be approximately 100 RU.<sup>67,72,73</sup> Considering the general structure of the small molecules (ligands) to be investigated throughout this thesis, the molecular weight of a ligand can generally be approximated at  $\sim 330 \text{ gmol}^{-1}$ . The required amounts of each protein to provide a  $RU_{\max(\text{theor.})}$  value of 100 RU (i.e., the target  $RU_{\text{immob.}}$ ) are shown in Table 2.6.

$$RU_{\max(\text{theor.})} = \frac{MW_{\text{ligand}}}{MW_{\text{immob.}}} \times RU_{\text{immob.}} \quad (2.2)$$

Table 2.6: Calculated target protein immobilisation levels for SPR assays as per Equation 2.2, assuming  $RU_{\max(\text{theor.})} = 100 \text{ RU}$ , ligand  $MW = 330 \text{ gmol}^{-1}$ .

Protein	MW ( $\text{gmol}^{-1}$ )	Target $RU_{\text{immob.}}$ (RU)
GST-Tec SH3	34353	10410
GST-Tec SH3 D196A	34004	10304
GST	26000	7878
Tec SH3	7899	2393

It was envisaged that the binding affinity of ligands **18a** and **18b** would first be established for GST-Tec SH3 protein. This would serve as a positive control to ensure that the assay system would behave consistently with previously reported results,<sup>56,66</sup> which is pertinent due to variation in protein purification protocols. Furthermore, it would be desirable to test and correct for any non-specific binding interactions — this may be achieved through immobilisation of a protein (of similar mass to the GST-Tec SH3 protein) to the reference flow channel prior to conducting ligand binding assays.

Consistent with previous reports,<sup>56</sup> GST protein was selected as a suitable protein to immobilise to the reference flow channel — GST has a similar molecular weight to GST-Tec SH3 fusion proteins (26 kDa vs. 34 kDa), and should also allow for any correction of non-specific binding to the GST tag on GST-Tec SH3 fusion proteins.

### 2.4.1.2 Immobilisation of GST and GST-Tec SH3

Due to their wide applicability, CM5 sensor chips were selected to be utilised for SPR binding affinity assays, and protein/ligand immobilisation would likely be achieved using amine coupling chemistry (Figure 2.17). Amine coupling generally occurs through either the protein N-terminus or amine group of lysine residue side-chains on the protein surface, however NHS esters have also been reported to react with the nucleophilic groups of other amino acid side-chains, including cysteine (S-H), histidine (imidazole N-H), and tyrosine (O-H).<sup>74</sup> Although amine coupling is less selective than other protein immobilisation or capture methods (e.g., biotin-streptavidin, antibody or aptamer capturing), these strategies require additional protein and/or ligand labelling, or additional purification steps. Alternatively, if the chip surface was immobilised with a high density of ligand protein by amine coupling, then theoretically there would be a higher chance that a sufficient amount of ligand protein molecules with accessible binding sites would be present, and allow ligand saturation binding to be achieved. Importantly, there do not appear to be any lysine residues within close proximity of the proposed ligand-protein binding site (see Section 2.4.3.1), therefore amine coupling chemistry was deemed a suitable method for protein immobilisation.

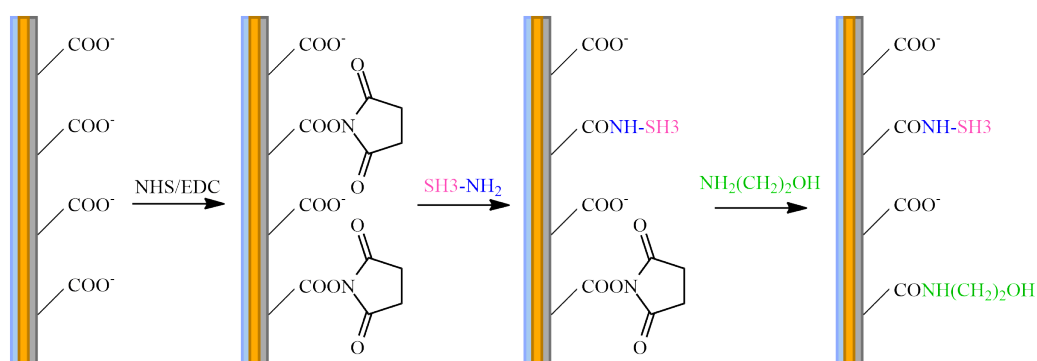


Figure 2.17: Schematic representation of utilising amine coupling methods to immobilise the target protein (SH3) to the SPR sensor chip surface. The carboxylate groups on the dextran surface are activated with both NHS and EDC to form the corresponding NHS ester. Nucleophilic amino acid groups (e.g., lysine residues) on the target protein surface displace the NHS esters to afford protein immobilisation. Remaining NHS esters are then blocked via injection of ethanolamine. The chip is comprised of: a glass layer (light blue), a gold layer (gold), and a dextran matrix (grey). The target protein is comprised of: the nucleophilic component of amino acid residues (i.e., amine group, blue); target protein (SH3, pink). Ethanolamine indicated in green. Adapted from Jayne<sup>56</sup> and Johnsson *et al.*<sup>75</sup>



## 2.4. SPR BINDING ASSAY VALIDATION

---

In the first instance, preparation of the reference flow channel was undertaken by immobilisation of GST protein; references to a typical sensorgram following protein immobilisation is shown in Figure 2.18, and the corresponding labels will be referred to in this section.

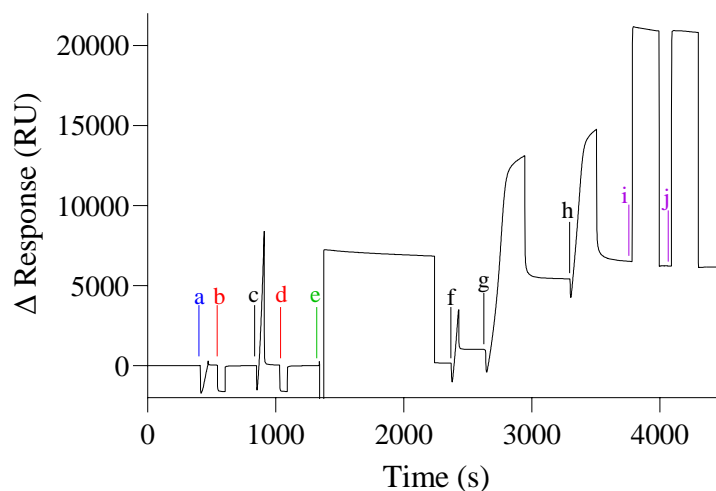


Figure 2.18: SPR sensorgram displaying pH scouting and protein immobilisation of GST. Significant events are labelled as follows: 'a' Injection of GST diluted to 1  $\mu\text{M}$  in 10 mM NaAc, pH 4.96; 'b' and 'd' Injection of 50 mM NaOH; 'c', 'f', 'g' and 'h' Injection of GST diluted to 1.5  $\mu\text{M}$  in 10 mM NaAc, pH 4.96; 'e' Injection of NHS (100 mM)/EDC (390 mM) mixture; 'i' and 'j' Injection of ethanolamine (1.0 M, pH 8.5). All injections were completed at a flow rate of 10  $\mu\text{L}/\text{min}$ , except for protein immobilisation injections (i.e., 'f', 'g' & 'h'), which were completed at 2  $\mu\text{L}/\text{min}$ .

Prior to activating the carboxydextran chip surface within a single (reference) flow channel for protein immobilisation, preliminary pH screening (scouting) steps were undertaken, to ensure sufficient electrostatic attraction and localisation of the protein to the chip surface. The pI of GST was predicted to be 6.32,<sup>76</sup> — to ensure the protein was sufficiently protonated but stable, it was diluted to 1  $\mu\text{M}$  in 10 mM NaAc, pH 4.96 then briefly injected across the chip surface ('a'). The initial drop in RU can be attributed to the rapid change in RI between running buffer (PBS, 0.05% T20) and diluted protein buffer (10 mM NaAc, pH 4.96) upon injection. Following injection, a steep increase in response is observed, indicating localisation of the protein to the chip surface. A small volume of 50 mM NaOH was then injected across the chip surface ('b'), to remove any non-specifically bound GST molecules.

To optimise GST localisation to the chip surface, pH scouting was again completed using 10 mM NaAc, pH 4.96, but instead diluting GST to only 1.5  $\mu\text{M}$ . Upon injection of the more concentrated protein over the chip surface ('c'), a significantly sharper increase in response was observed, sug-

gesting more effective protein localisation to the chip surface. The surface of the chip was again washed with 50 mM NaOH ('d'), and a mixture of NHS and EDC was injected across the chip surface ('e'), to allow formation of activated NHS esters with the carboxydextran matrix, therefore priming the surface for subsequent protein immobilisation. Following surface activation with NHS (100 mM)/EDC (390 mM), a slight increase ( $\sim 200$  RU) is observed relative to pre-surface activation, consistent with the addition of small NHS esters. A small volume of GST protein diluted to  $1.5 \mu\text{M}$  in 10 mM NaAc, pH 4.96 was then injected across the chip surface over a 60 second period ('f'). This short injection serves two purposes: firstly, it allows for GST protein to become immobilised to the chip surface; secondly, the efficiency of protein immobilisation can be inferred from this short injection, to inform how long subsequent protein injections should be to achieve the desired protein immobilisation levels. The amount of GST immobilised after a 60 sec injection was  $\sim 850$  RU, therefore to achieve a total immobilised protein level of  $\sim 8000$  RU, a subsequent 10 min injection of protein across the chip surface was undertaken ('g'). However, this 10 min injection was aborted early — as the injection proceeded, the RU increase appeared to gradually plateau, suggesting the chip surface was nearing saturation of protein molecules. A second 10 min injection of protein across the chip surface was undertaken ('h'), however this was also ceased prior to completion due to surface saturation. Confirmation of chip surface saturation can be inferred from the relative changes in RU (i.e., immobilised protein) following each "10 min" injection: after the first injection ('g'), the relative increase in RU is  $\sim 4000$  RU, while after the second injection ('h'), the increase in RU is modest, at  $\sim 1000$  RU. Following protein immobilisation, sequential injections of ethanolamine (1.0 M, pH 8.5) were conducted across the chip surface ('i', 'j'), to remove any non-specifically bound GST protein, and also to block any remaining activated NHS esters on the chip surface. The measured response stabilised following ethanolamine blocking, suggesting that the GST protein has been successfully immobilised and is not dissociating from the chip surface. The total immobilised protein value ( $\text{RU}_{\text{immob.}}$ ) was  $\sim 6000$  RU, which was acceptable in reference to the target immobilisation levels of 8000 RU (Table 2.6).

Following immobilisation of GST in the reference flow channel, a sample of GST-Tec SH3 protein was similarly diluted to  $\sim 1.5 \mu\text{M}$  in 10 mM NaAc, pH 4.96 then injected across the activated chip surface of the second (target) flow channel. A slightly lesser amount of total protein immobilisation following ethanolamine blocking was observed relative to that reported previously ( $\text{RU}_{\text{immob.}} = \sim 5000$  RU, c.f.,  $\sim 6000$ - $7000$  RU).<sup>56</sup> Despite this, the immobilised amount of GST-Tec SH3 was

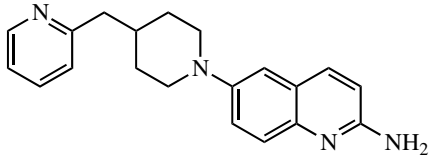
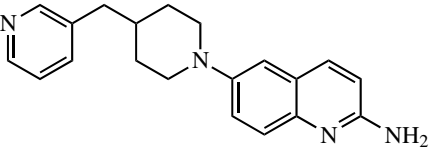
## 2.4. SPR BINDING ASSAY VALIDATION

expected to provide a suitable signal upon ligand binding (compared to the target  $RU_{\text{immob.}}$  value in Table 2.6), so was deemed suitable for binding assays.

### 2.4.1.3 Binding affinity assays with GST-Tec SH3

The binding affinities of **18a** and **18b** for the GST-Tec SH3 protein were investigated, to ascertain whether the synthesised ligands displayed similar binding affinities to those reported previously.<sup>56</sup> Favourably, the derived binding affinities (given as  $K_d$  values) were consistent with previous results (Table 2.7). Furthermore, the kinetics of the binding interaction were consistent, displaying box-shaped sensorgrams with fast on-off rates, similar to Figure 2.5.

Table 2.7: Comparison of current and previously reported binding affinities of control ligands **18a**<sup>56</sup> & **18b**<sup>66</sup> for GST-Tec SH3 protein.

Compound	Structure	$K_d \pm SD$ ( $\mu\text{M}$ ) (this work)	$K_d \pm SD$ ( $\mu\text{M}$ ) (previous work)
<b>18a</b>		$5.5 \pm 0.9$	$5 \pm 1^{56}$
<b>18b</b>		$3.0 \pm 0.7$	$2.8 \pm 1^{66}$

The consistent binding affinity data for **18a** and **18b** against GST-Tec SH3 protein indicates that the assay is performing as expected in comparison to previously determined values.<sup>56</sup> Therefore, it is reasonable to assume that there are no significant effects on ligand binding due to protein or ligand batch variability, and the ligand binding affinity data obtained in this thesis can be reasonably compared to previous results.<sup>56,66</sup>

## 2.4.2 Binding to GST-Tec SH3 D196A mutant

### 2.4.2.1 Immobilisation of GST and GST-Tec SH3 D196A

The results from binding assays with **18a** and **18b** against GST-Tec SH3 supported that the SPR assay was operating as anticipated. To validate the nature of the binding interaction, and particularly whether the ligands are binding at the hypothesised binding site on the Tec SH3 domain, it was

desired that similar binding assays be conducted against GST-Tec SH3 D196A mutant protein. Again, a reference protein needed to be selected to identify and correct for any non-specific binding interactions. Consistent with GST-Tec SH3 binding assays, GST was also selected as the reference protein of choice: the molecular weight of GST is comparable to GST-Tec SH3 D196A mutant protein (26 kDa, vs. 34 kDa); and also to provide correction for any non-specific binding to the GST-tag of GST-Tec SH3 D196A mutant protein. The GST reference protein was prepared and immobilised to a single (reference) flow channel on the chip surface as described in Section 2.4.1.2, to achieve a satisfactory  $RU_{\text{immob.}}$  value of 7000 RU (with reference to Table 2.6).

As the use of GST-Tec SH3 D196A had not previously been reported as a binding partner in SPR assays, investigations regarding the ideal protein immobilisation conditions were undertaken in a second (target) flow channel, again through pH scouting (Figure 2.19).

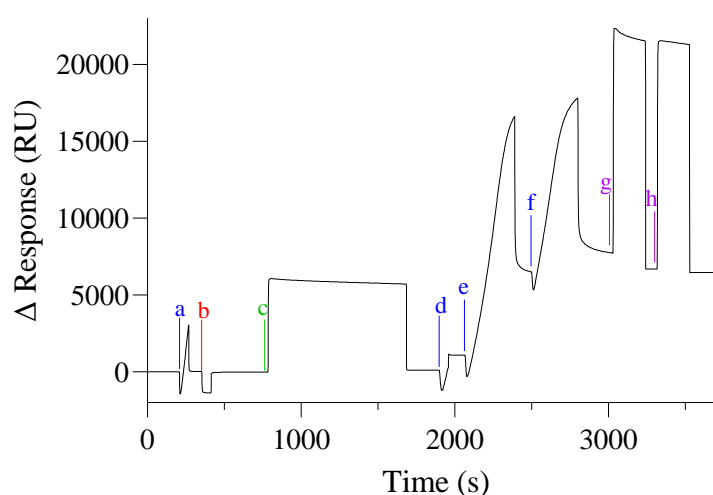


Figure 2.19: SPR Sensorgram displaying pH scouting and protein immobilisation of GST-Tec SH3 D196A. Significant events are labelled as follows: 'a', 'd', 'e' and 'f' Injection of GST-Tec SH3 D196A diluted to to 1  $\mu\text{M}$  in 10 mM NaAc, pH 4.96; 'b' Injection of 50 mM NaOH; 'c' Injection of NHS (100mM)/EDC (390 mM) mixture; 'i' and 'j' Injection of ethanolamine (1.0 M, pH 8.5). All injections were completed at a flow rate of 10  $\mu\text{L}/\text{min}$ , except for protein immobilisation injections (i.e., 'd', 'e' & 'f'), which were completed at 2  $\mu\text{L}/\text{min}$ .

The pI of GST-Tec SH3 D196A was predicted to be 5.95,<sup>76</sup> therefore to ensure the protein was sufficiently stable and protonated, it was diluted to  $\sim 1 \mu\text{M}$  in 10 mM NaAc, pH 4.96, and briefly injected across the chip surface. A sharp increase in response was observed following protein injection ('a'), indicating sufficiently strong electrostatic interactions were occurring to facilitate protein localisation to the chip surface. The chip surface was then washed with 50 mM NaOH ('b'), to remove any non-specifically bound protein molecules. Following this, the carboxydextran

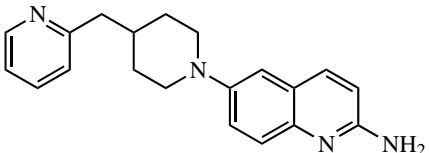
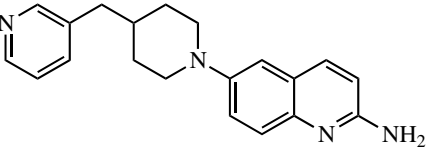
## 2.4. SPR BINDING ASSAY VALIDATION

chip surface was activated by injection of a mixture of NHS and EDC ('c'). As expected, a slight increase in response ( $\sim 200$  RU) was observed following chip surface activation. A small volume of GST-Tec SH3 D196A was diluted to  $1 \mu\text{M}$  in  $10 \text{ mM NaAc}$ ,  $\text{pH } 4.96$  before injection across the chip surface over a 60 second period ('d'), to achieve immobilisation of  $\sim 1000$  RU. Therefore to achieve a total immobilised protein level of  $\sim 8000$  RU, GST-Tec SH3 D196A was primed for injection over the chip surface for a period of 10 minutes ('e'). The injection was ceased after almost 7 minutes, as the rate of RU change suggested that the chip surface might be approaching saturation of protein molecules. A second protein injection was conducted over a period of 5 minutes ('f'), however the rate of RU change again supported that the chip surface was approaching saturation. The chip surface was then blocked with sequential injections of ethanolamine ('g', 'h') to afford sufficient immobilisation of GST-Tec SH3 D196A protein to the chip surface ( $\text{RU}_{\text{immob.}} = 6300 \text{ RU}$ ).

### 2.4.2.2 Binding affinity assays with GST-Tec SH3 D196A mutant

To investigate whether the current ligands were binding the Tec SH3 domain consistently with the previously proposed ligand-protein binding model,<sup>46,47,58</sup> **18a** and **18b** were assayed against GST-Tec SH3 D196A. Pleasingly, **18a** and **18b** did not exhibit any binding to GST-Tec SH3 D196A (Table 2.8). A comparison of the sensorgrams and derived isotherms for **18a** binding to both GST-Tec SH3, and GST-Tec SH3 D196A (with GST as a reference protein in both cases) is shown in Figure 2.20.

Table 2.8: Comparison of binding affinities for control ligands **18a** and **18b** to GST-Tec SH3 and GST-Tec SH3 D196A proteins. N.B. indicates no binding detected.

Compound	Structure	GST-Tec SH3	GST-Tec SH3
		$K_d \pm \text{SD} (\mu\text{M})$	D196A $K_d \pm \text{SD} (\mu\text{M})$
<b>18a</b>		$5.5 \pm 0.9$	N.B.
<b>18b</b>		$3.0 \pm 0.7$	N.B.

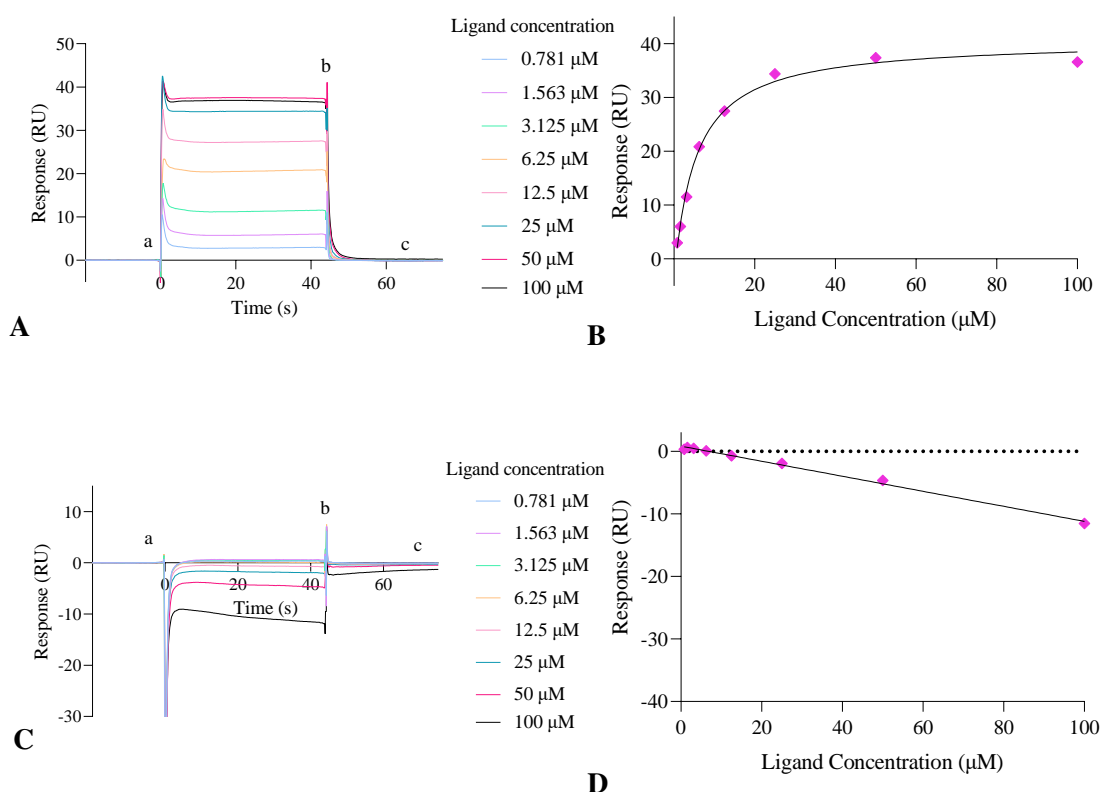


Figure 2.20: SPR sensorgrams and derived isotherm for binding of **18a** to GST-Tec SH3 or GST-Tec SH3 D196A. (A) Reference-subtracted and corrected sensorgrams for binding of **18a** to GST-Tec SH3, where ‘a’ indicates ligand injection, ‘b’ indicates the end of ligand injection, and ‘c’ indicates the approximate return of response to baseline following ligand injection. (B) Derived isotherm for binding of **18a** to GST-Tec SH3. (C) Reference-subtracted and corrected sensorgrams for binding of **18a** to GST-Tec SH3 D196A, where ‘a’ indicates ligand injection, ‘b’ indicates the end of ligand injection, and ‘c’ indicates the approximate return of response to baseline following ligand injection. (D) Derived isotherm for binding of **18a** to GST-Tec SH3 D196A.

When binding the target protein GST-Tec SH3 (Figure 2.20A), from the start of the injection (‘a’) there is a sharp increase in response (RU), indicating a mass increase at the chip surface, which is consistent with the ligand associating to and binding the immobilised GST-Tec SH3 protein. Similarly, upon ceasing ligand injection (‘b’), the RU value returns to baseline, indicating any mass increase at the chip surface has been lost, consistent with dissociation of the ligand from the immobilised GST-Tec SH3 protein. The corresponding isotherm derived from the sensorgrams of **18a** binding to GST-Tec SH3 (Figure 2.20B) can be closely fitted to a Langmuir 1:1 binding model, indicating the binding interaction is occurring as expected, consistent with the proposed ligand-protein binding model.

Conversely, the reference-subtracted and corrected sensorgrams observed for **18a** binding to GST-Tec SH3 D196A (Figure 2.20C) display a rapid decrease in RU value upon ligand injection (‘a’).

This is not indicative of mass loss at the chip surface, but rather that the degree of ligand binding to the reference channel protein (i.e., GST) is greater than that to GST-Tec SH3 D196A. Although the ligand displays stronger binding to GST than GST-Tec SH3 D196A, the change in RU value is quite small, indicating that the ligand-GST binding interaction is still weak. Furthermore, upon ceasing the ligand injection, the RU value returns to baseline ('d'), indicating that the immobilised protein on the chip surface has not been altered during the course of the injection. Lastly, the derived isotherm from sensorgrams of **18a** binding to GST-Tec SH3 D196A (Figure 2.20D) do not fit a Langmuir 1:1 binding model, but instead appears as a negative linear function, further supporting that the ligand is not binding the immobilised protein in any significant capacity. Therefore, the complete lack of ligand binding to GST-Tec SH3 D196A is consistent with the previously proposed ligand-protein binding model,<sup>46</sup> supporting that the current ligands are binding at the expected site on the protein surface throughout SPR binding assays.

### 2.4.3 Binding to Tec SH3

#### 2.4.3.1 Immobilisation of Tec SH3

From Section 2.4.2.2, SPR binding assays with GST-Tec SH3 D196A supported that the control ligands **18a** and **18b** bind the Tec SH3 domain at the proposed ligand-protein binding site. However, to investigate the comparability of the derived  $K_d$  values from ligand binding to GST-Tec SH3, and to conclusively investigate the effect of non-specific binding to the GST tag, it was preferable that SPR binding affinity assays with cleaved Tec SH3 domain be conducted.

A reference protein needed to be identified to correct for non-specific binding interactions. However, unlike for assays completed with GST-Tec SH3 fusion proteins, it was not appropriate to utilise GST as a reference protein due to its considerably larger mass compared to Tec SH3 (26 kDa, c.f. 8 kDa). There have been reports in the literature of SPR assays being conducted using an activated and blocked flow channel as the reference channel, with favourable results.<sup>77</sup> In the absence of any readily-available reference proteins with similar molecular weights to Tec SH3, this activation/blocking method was selected to correct for any non-specific binding. A single (reference) flow channel was therefore activated via injection of a mixture of NHS/EDC ('a'), then blocked by sequential injections of ethanolamine ('b' and 'c'), to afford a total of 47 RU immobilised ethanolamine in the reference channel (Figure 2.21).

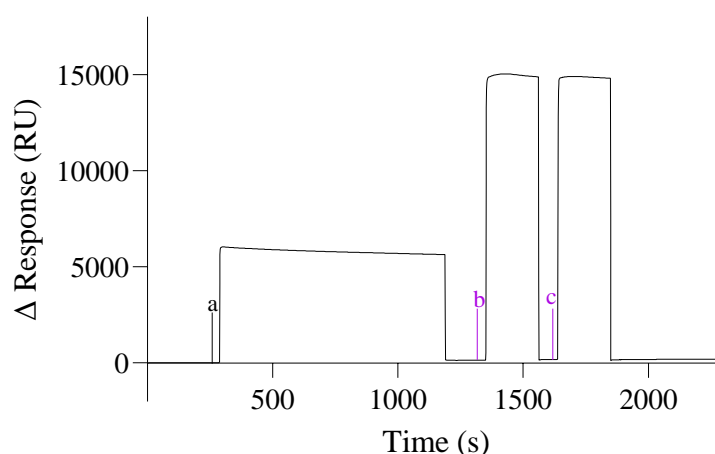


Figure 2.21: SPR Sensorgram displaying surface activation and blocking. Significant events indicated as: ‘a’ Injection of NHS (100 mM)/EDC (390 mM) mixture; ‘b’ and ‘c’ Injection of ethanolamine (1.0 M, pH 8.5). All injections were completed at a flow rate of 10  $\mu$ L/min.

The immobilisation of Tec SH3 to the target flow channel of the sensor chip was anticipated to require more rigorous optimisation than the GST-Tec SH3 fusion proteins discussed previously: the pI of Tec SH3 was predicted to be substantially lower than that of GST-Tec SH3 (4.94, c.f. 5.82);<sup>76</sup> typically the pH of the protein immobilisation buffer would be at least 1 pH unit below the protein pI to allow sufficient protonation for surface localisation,<sup>78</sup> therefore the previously utilised buffer of 10 mM NaAc pH 4.96 was unlikely to be effective. Furthermore, GST-Tec SH3 fusion proteins are significantly more amenable to amine coupling than Tec SH3 alone; amine coupling exploits the nucleophilicity of primary amine groups, specifically lysine residues in the context of proteins. GST-Tec SH3 fusion proteins contain 25 lysine residues (with 21/25 present in the GST tag), while Tec SH3 only contains 4 lysine residues. Coupling of Tec SH3 to the chip surface through any of these 4 lysine residues was not expected to impede the ligand-protein binding interaction, as none of the lysine residues were in close proximity to the proposed ligand-protein binding site (Figure 2.22). Despite the Tec SH3 domain containing fewer opportunities for efficient protein immobilisation using amine coupling chemistry, it was anticipated that increasing both relative protein concentration and protein injection periods during immobilisation might overcome this inefficiency, due to increased local protein concentration and contact time between Tec SH3 domain and the chip surface.



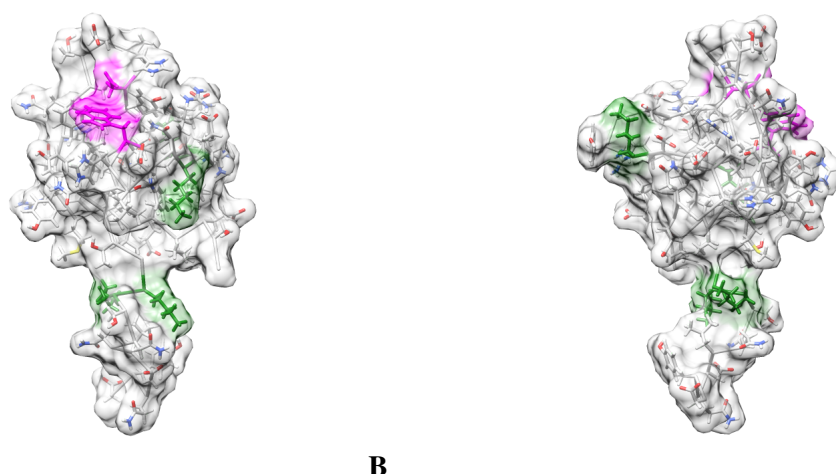


Figure 2.22: Solution structure of the Tec SH3 domain (PDB ID: 1GL5),<sup>3</sup> highlighting lysine residues available for amine coupling via SPR. Lysine residues are highlighted in green, proposed ligand-protein binding site residues (D196 and W215) are highlighted in pink. Structure (B) is rotated 140° relative to structure (A). Molecular graphics were created using UCSF Chimera, developed by the Resource for Biocomputing, Visualisation, and Informatics at the University of California, San Francisco, with support from NIH P41-GM103311.<sup>52</sup>

Investigations of the ideal immobilisation conditions for Tec SH3 protein were undertaken by pH scouting, as indicated in Figure 2.23. Tec SH3 protein was initially diluted to 1  $\mu\text{M}$  in 10 mM NaAc, pH 4.6 and injected over a second (target) flow channel ('a'), however the observed association of Tec SH3 to the chip surface was negligible, as indicated by the lack of response increase. To determine if the poor association was due to a low protein concentration, an aliquot of stock solution of Tec SH3 protein was then diluted to 2  $\mu\text{M}$  in 10 mM NaAc pH 4.6, and injected across the chip surface ('b'). The observed increase in response was slightly better than for ('a'), however the rate of protein association (i.e., response increase) was still not sufficient for protein immobilisation. This indicated that while the protein association to the chip surface was slightly improved by increasing the relative protein concentration, the main cause of poor association was likely poor pre-concentration (i.e., insufficient electrostatic attraction between the positively charged protein and negatively charged chip surface). Therefore, Tec SH3 protein was diluted to 1  $\mu\text{M}$  in 10 mM NaAc, pH 3.98, and injected across the chip surface ('c'). Under these conditions, favourable pre-concentration of the Tec SH3 protein to the chip surface was observed, as indicated by the relatively rapid increase in response. A 50 mM NaOH solution was briefly injected over the chip surface to remove any non-specifically bound molecules ('d'), and following this the chip surface was activated via injection of a mixture of NHS (100 mM)/EDC (390 mM) ('e'). A small increase in response

following surface activation was observed, consistent with that observed for GST-Tec SH3 fusion protein immobilisations.

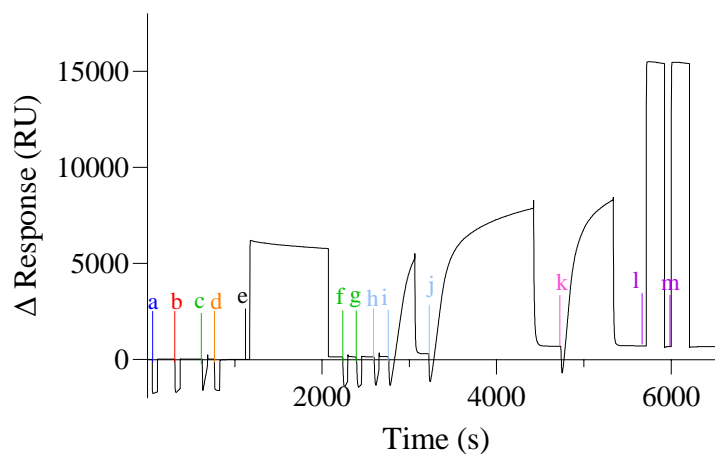


Figure 2.23: SPR Sensorgram displaying pH scouting and immobilisation of Tec SH3. Significant events are labelled as follows: 'a' Injection of Tec SH3 diluted to 1  $\mu\text{M}$  in 10 mM NaAc pH 4.6; 'b' Injection of Tec SH3 diluted to 2  $\mu\text{M}$  in NaAc pH 4.6; 'c' Injection of Tec SH3 diluted to 1  $\mu\text{M}$  in NaAc pH 3.98; 'd' Injection of 50 mM NaOH; 'e' Injection of NHS(100 mM)/EDC (390 mM) mixture; 'f' and 'g' Injection of Tec SH3 diluted to 1  $\mu\text{M}$  in NaAc pH 3.98; 'h', 'i' and 'j' Injection of Tec SH3 diluted to 2  $\mu\text{M}$  in NaAc pH 3.98; 'k' Injection of Tec SH3 diluted to 2.5  $\mu\text{M}$  in NaAc pH 3.98; 'l' and 'm' Injection of ethanolamine (1.0 M, pH 8.5). All injections were completed at a flow rate of 10  $\mu\text{L}/\text{min}$ , except for protein immobilisation injections (i.e., 'f', 'g', 'h', 'i', 'j', & 'k'), which were completed at 2  $\mu\text{L}/\text{min}$ .

The flow rate of buffer across the chip surface was reduced from 10  $\mu\text{L}/\text{min}$  to 2  $\mu\text{L}/\text{min}$ , as a slower flow rate may facilitate more effective protein-sensor chip surface interactions, and therefore more protein immobilisation. Based on the results of the pH scouting injections, Tec SH3 protein (from the aliquot used for pH scouting) was diluted to 1  $\mu\text{M}$  in 10 mM NaAc, pH 3.98, and injected over the chip surface for 60 seconds ('f'). Disappointingly, association of Tec SH3 protein at the lower flow rates (recommended for protein immobilisation) did not match the association that was observed during pH scouting ('c'). It was hypothesised that the Tec SH3 protein in this aliquot had possibly unfolded to a degree that would impede immobilisation while the chip surface was being activated (during 'e'), as the protein had been diluted in a slightly acidic buffer (pH 3.98). Consequently, a fresh aliquot of Tec SH3, diluted to 1  $\mu\text{M}$  in 10 mM NaAc, pH 3.98 was prepared and injected over the chip surface ('g'). Unfortunately, there was no significant difference in protein association to the chip surface, compared to ('f'). However, the similar association profiles between each Tec SH3 aliquot indicated that protein unfolding due to the acidic medium was unlikely to be the driving factor behind the poor association of the protein to the chip surface at lower flow rates. In an attempt to increase the relative protein concentration available for immobilisation at

## 2.4. SPR BINDING ASSAY VALIDATION

---

the chip surface, Tec SH3 was diluted to 2  $\mu\text{M}$  in 10 mM NaAc, pH 3.98 and injected across the chip surface (60 sec, 'h'). This offered a slight improvement on previous immobilisation attempts - while minimal Tec SH3 protein had immobilised to the sensor chip surface during this injection, the rate of association (i.e., increase in response) was substantially greater than that for ('f') and ('g'). In this instance, it was assumed that the protein was associating favourably with the chip surface, however minimal protein immobilisation had occurred, likely due to the small number of lysine residues (4) in Tec SH3 protein presenting limited opportunities for protein immobilisation. Theoretically, this could be overcome by increasing the period of the protein injection, through increasing the possible protein-sensor chip surface contact time. Therefore, Tec SH3 protein diluted to 2  $\mu\text{M}$  in 10 mM NaAc, pH 3.98 was again injected over the chip surface, but for a period of 5 minutes ('i'). Pleasingly, approximately 200 RU of Tec SH3 protein had immobilised to the chip surface. To work towards immobilisation of the optimal amount Tec SH3 (2500 RU), an additional injection of Tec SH3 diluted to 2  $\mu\text{M}$  in 10 mM NaAc, pH 3.98 was undertaken for a period of 20 minutes ('j'). During this period, association of the protein to the chip surface appeared to plateau, suggesting that the chip surface was approaching capacity. Despite approaching capacity, the amount of immobilised protein increased to approximately 400 RU. In a final attempt to reach the desired protein immobilisation level ( $\sim 2500$  RU), Tec SH3 was diluted to 2.5  $\mu\text{M}$  in 10 mM NaAc, pH 3.98, and injected over the chip surface for 10 minutes ('k'). Saturation of available sites for protein immobilisation to the chip surface (as indicated by response plateau) was again observed during this injection, with only a modest increase in immobilised protein observed. The chip surface was blocked with sequential injections of 1.0 M ethanolamine (pH 8.5) ('l', 'm'), to afford a total immobilisation of Tec SH3 protein to the chip surface of  $\text{RU}_{\text{immob.}} = \sim 530$  RU.

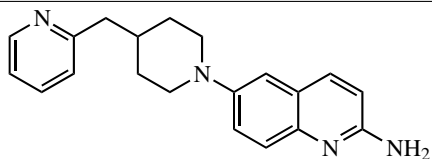
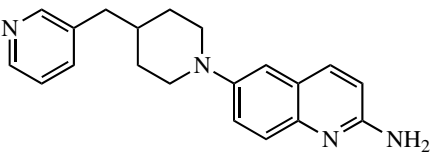
Although this was substantially lower than the desired protein immobilisation levels of 2500 RU (Table 2.6), it was anticipated that 530 RU of immobilised protein would be sufficient for the intended analyses. A limitation of less immobilised protein would be a reduced response upon upon ligand binding, however this could be remedied through shorter, but more frequent Tec SH3 injections during protein immobilisation.

### 2.4.3.2 Binding affinity assays with Tec SH3

To investigate the degree of off-site binding of the current ligands to GST in GST-Tec SH3 fusion proteins, the ligands were assayed against Tec SH3 protein. Favourably, both **18a** and **18b** displayed

comparable binding affinities for both the Tec SH3 domain and GST-Tec SH3 fusion protein (Table 2.9), and exhibited similar binding kinetics through fast on-off rates in the obtained sensorgrams (Figure 2.24).

Table 2.9: Comparison of binding affinities for control ligands **18a** and **18b** to GST-Tec SH3 and Tec SH3 proteins.

Compound	Structure	GST-Tec SH3 $K_d \pm SD$ ( $\mu\text{M}$ )	Tec SH3 $K_d \pm SD$ ( $\mu\text{M}$ )
<b>18a</b>		$5.5 \pm 0.9$	$6.6 \pm 0.6$
<b>18b</b>		$3.0 \pm 0.7$	$4.3 \pm 0.4$

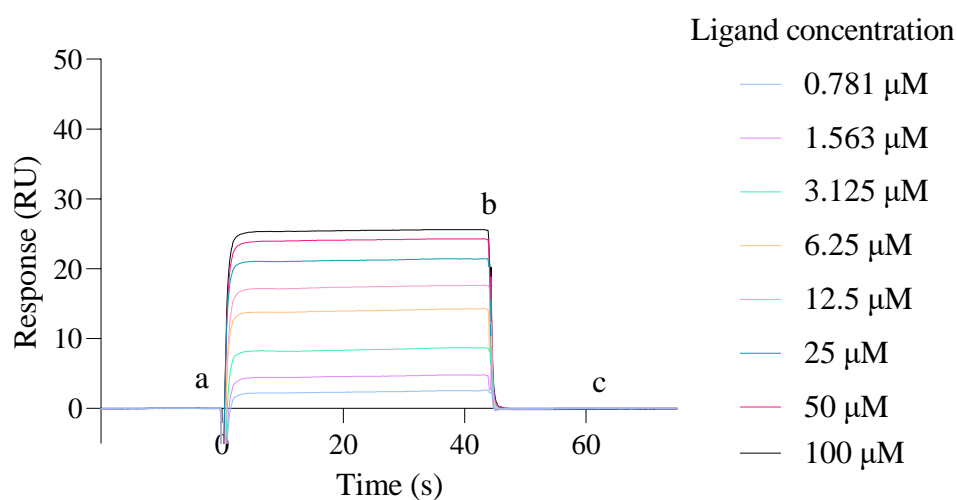


Figure 2.24: SPR Sensorgrams for binding of **18a** to Tec SH3. 'a' indicates ligand injection, 'b' indicates the end of ligand injection, and 'c' indicates the approximate return of response to baseline following ligand injection.

Interestingly, while the derived binding affinities ( $K_d$ ) values are comparable, there were some discrepancies in the relative change in response (RU) upon ligand binding to the sensor chip surface. In an attempt to investigate this further, a method was sought and consequently developed to normalise and compare the changes in RU ( $\Delta\text{RU}$ ) between different SPR experiments – normalisation of  $\Delta\text{RU}$  values is imperative for this approach, due to the relativity of  $\Delta\text{RU}$  to  $\text{RU}_{\text{max}(\text{theor.})}$ , which is dependent on the identity and amount of immobilised protein for a particular SPR experiment.

## 2.4. SPR BINDING ASSAY VALIDATION

---

From Equation 2.2 above (Section 2.4.1.1),  $RU_{\max(\text{theor.})}$  can be determined; for each SPR assay, a maximum RU value is recorded ( $RU_{\max}$ ), and  $\Delta RU$  can be calculated (Equation 2.3, below). Following this,  $\Delta RU$  can be normalised to a percentage, as per Equation 2.4 below. For a validated SPR assay,  $\Delta RU$  values  $\leq 0$  would indicate that the measured amount of ligand binding to the protein immobilised to the chip surface is consistent with a 1:1 ligand-protein binding model, and therefore  $\Delta RU$  (normalised) values  $\approx 0\%$  are expected. In addition, if  $\Delta RU$  (normalised) values  $\leq 0\%$  are observed, this would be considered acceptable — as the immobilised protein for all SPR assays in this thesis was attached using amine coupling chemistry, it is possible that the ligand binding site for some immobilised protein molecules is inaccessible, which would translate to  $\Delta RU < 0$ .<sup>67,73</sup> However, if  $\Delta RU$  and  $\Delta RU$  (normalised) values are  $> 0$ , it may suggest that the ligand-protein binding interaction does not follow a 1:1 binding model, and would warrant further investigation, or potentially assay optimisation.<sup>65,67,73</sup>

$$\Delta RU = RU_{\max} - RU_{\max(\text{theor.})} \quad (2.3)$$

$$\Delta RU \text{ (normalised)} = \frac{\Delta RU}{RU_{\max(\text{theor.})}} \times 100 \quad (2.4)$$

The  $\Delta RU$  (normalised) values for **18a** and **18b** binding to both GST-Tec SH3 and Tec SH3 were calculated, and the distribution of  $\Delta RU$  (normalised) values displayed in a violin plot (Figure 2.25). From Figure 2.25, the  $RU_{\max}$  value for both **18a** and **18b** was typically 30% greater than the  $RU_{\max(\text{theor.})}$  value for binding to Tec SH3, while binding to GST-Tec SH3 showed acceptable  $RU_{\max}$  values  $\sim 10\%$  lower than the  $RU_{\max(\text{theor.})}$  value.

As discussed above,  $RU_{\max}$  is generally greater than  $RU_{\max(\text{theor.})}$  when the ligand-protein binding stoichiometry is not 1:1. However, SPR binding studies with GST-Tec SH3 D196A indicated binding of **18a** and **18b** was consistent with the proposed ligand-binding model, which occurs in a 1:1 stoichiometry.<sup>46,47,54</sup> Furthermore, the shapes of the obtained sensorgrams and derived binding isotherms were consistent with a 1:1 binding model, rather than a multi-site ligand-protein binding model (Figure 2.7). Therefore, a non-1:1 ligand-protein binding stoichiometry was not anticipated to be a significant factor for binding of **18a** and **18b** to the Tec SH3 domain.

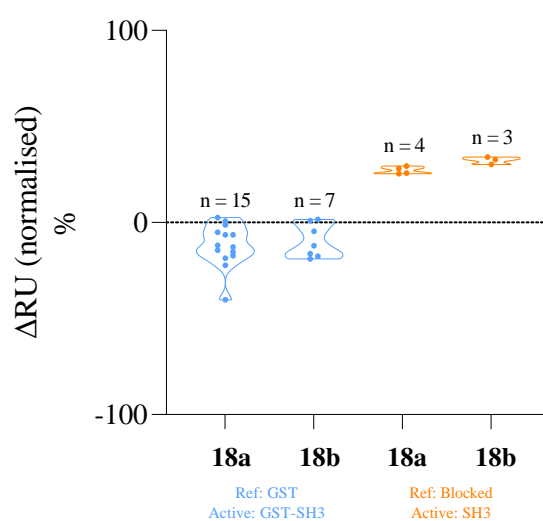


Figure 2.25: Violin plot comparison of normalised  $\Delta$ RU values for **18a** and **18b** binding to either GST-Tec SH3 or Tec SH3 proteins. Protein immobilised to reference cell indicated by ‘Ref’, where GST indicates GST protein, and ‘blocked’ indicates the chip surface was activated with NHS/EDC, then blocked with ethanolamine. Plots extend to the maximum and minimum calculated  $\Delta$ RU values (i.e., no extrapolation). Violin plots calculated using GraphPad Prism version 9.0.0 for Windows.<sup>51</sup>

A second possibility is that **18a** and **18b** are binding the Tec SH3 domain following 1:1 stoichiometry, however the ligands may be aggregating during this interaction, therefore increasing the relative mass increase upon ligand binding, and recording a larger RU value increase. While this is a possibility, non-specific aggregation of ligands would be expected to produce continually increasing sensorgrams as aggregation of the ligands proceeded during the ligand injection, similar to Figure 2.7. However, this was not observed — in each case the obtained sensorgrams achieved steady-state binding, as indicated by a plateaued response, consistent with Figure 2.24.

A third possibility is that a poorly-selected reference protein to detect for non-specific binding interactions may implicate  $RU_{\max}$  values, relative to  $RU_{\max(\text{theor.})}$ . The ligands investigated in these assays are quite hydrophobic (predicted  $\log P$ : 3.38-3.50),<sup>61</sup> so it would not be unreasonable to expect the ligands to associate non-specifically with hydrophobic regions on the proteins surface. Analysis of Tec SH3 protein hydrophobicity was initially conducted via sequence analysis (ProtScale by Expasy)<sup>76</sup> which appeared to indicate the Tec SH3 domain was mostly hydrophilic (Figure 2.26). Hydrophobicity analysis of surface residues of the Tec SH3 domain was then conducted using the Kyte-Doolittle scale<sup>79</sup> which revealed some substantially hydrophobic regions on the protein surface (not located near the proposed ligand-protein binding site), despite initial sequence analysis suggesting a predominantly hydrophilic structure (Figure 2.27).

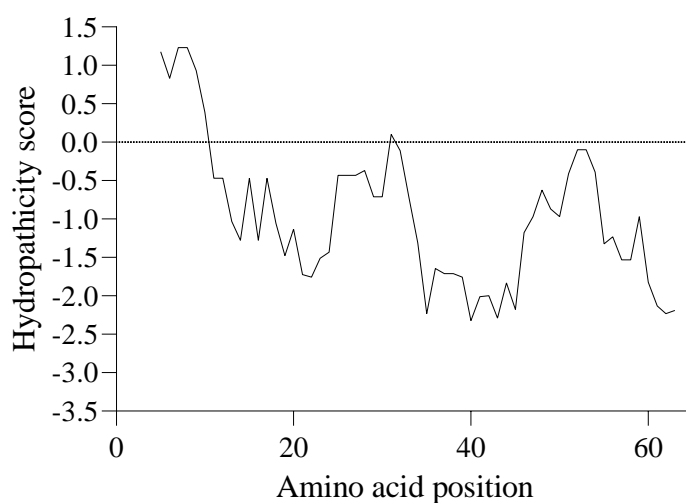


Figure 2.26: Hydropathicity analysis of Tec SH3 protein sequence, as determined by ProtScale by ExPASy. Hydropathicity score refers to hydrophobicity, where hydrophobic residues have a more positive score. First 5 amino acid residues omitted from analysis due to flexibility considerations.<sup>76</sup>

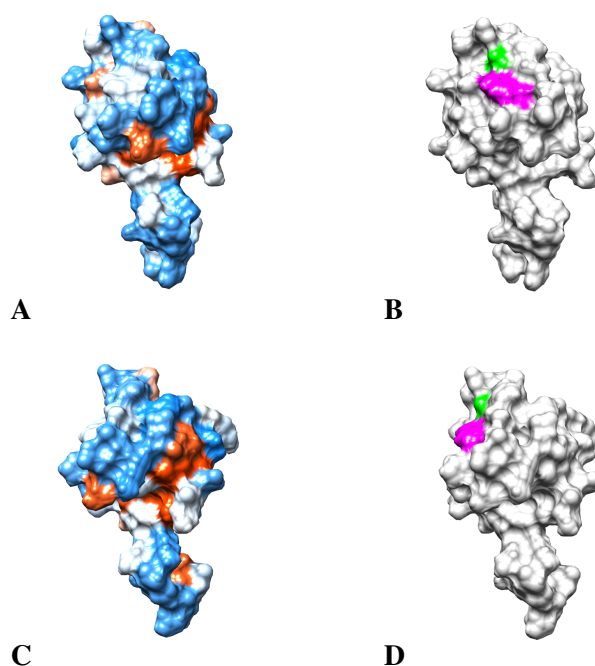


Figure 2.27: Hydrophobicity surface analysis of Tec SH3 protein. (A) and (C) indicate hydrophobic (red), neutral (white) and hydrophilic (blue) regions on the protein surface. (B) and (D) indicate the position of key residues D196 (green) and W215 (pink) within the proposed ligand-protein binding site, relative to protein structures (A) and (C), respectively. Poses (A) and (B) are rotated 40° relative to poses (C) and (D).<sup>52</sup>

As a point of comparison, the hydrophobicity of GST-Tec SH3 protein sequence was also investigated via ProtScale by ExPASy.<sup>76</sup> Interestingly, analysis of the resulting hydropathicity plot (Figure 2.28) indicated GST-Tec SH3 contains a large number of neutral-hydrophobic residues,

therefore is likely to contain hydrophobic regions amenable to non-specific hydrophobic interactions.

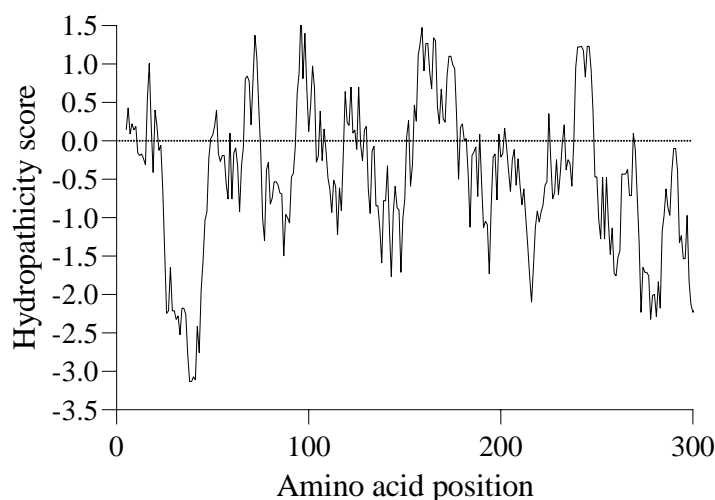


Figure 2.28: Hydrophobicity analysis of GST-Tec SH3 fusion protein sequence, as determined by ProtScale by ExPASy. Hydropathicity score refers to hydrophobicity, where hydrophobic residues have a more positive score. First 5 amino acid residues omitted from analysis due to flexibility considerations.<sup>76</sup>

As the GST tag is fused to the N-terminus of the Tec SH3 domain, from Figure 2.28 it is apparent that many of the hydrophobic residues (and regions) of GST-Tec SH3 are located within the GST tag. Unfortunately, as the structure of GST-Tec SH3 has not been solved, an analysis of protein surface residue hydrophobicity could not be undertaken to validate this. However, as a consequence of the GST tag of GST-Tec SH3 containing a number of hydrophobic regions, it is expected that non-specific hydrophobic interactions would be occurring between ligands and the GST tag during SPR binding assays. For the currently reported GST-Tec SH3 SPR assay protocol, these non-specific hydrophobic interactions with the GST tag would not be observed due to immobilisation of GST to the reference flow channel, therefore any measured non-specific hydrophobic interaction responses would be removed during post-run processing. However, if GST was not immobilised to the reference flow channel, it is possible the responses from these non-specific hydrophobic interactions may be observed. Therefore, an additional binding assay with GST-Tec SH3 fusion protein was conducted, except the reference channel was activated with NHS/EDC, then blocked with ethanolamine. The obtained  $K_d$  values were loosely consistent with those determined previously (Table 2.10) but interestingly the  $RU_{max}$  values were also greater than  $RU_{max(\text{theor.})}$ , generally by more than that reported for binding to Tec SH3 (Figure 2.29).



## 2.4. SPR BINDING ASSAY VALIDATION

Table 2.10: Comparison of determined binding affinities of **18a** and **18b** for various Tec SH3 domain-containing proteins, indicating the protein immobilised in the reference flow cell channel.

Compound	Reference flow cell: GST	Reference flow cell: activated, blocked (ethanolamine)	
	GST-Tec SH3 $K_d \pm SD$ ( $\mu\text{M}$ )	GST-Tec SH3 $K_d \pm SD$ ( $\mu\text{M}$ )	Tec SH3 $K_d \pm SD$ ( $\mu\text{M}$ )
<b>18a</b>	$5.5 \pm 0.9$	$8.2 \pm 1.7$	$6.6 \pm 0.6$
<b>18b</b>	$3.0 \pm 0.7$	$10.2 \pm 2.7$	$4.3 \pm 0.4$

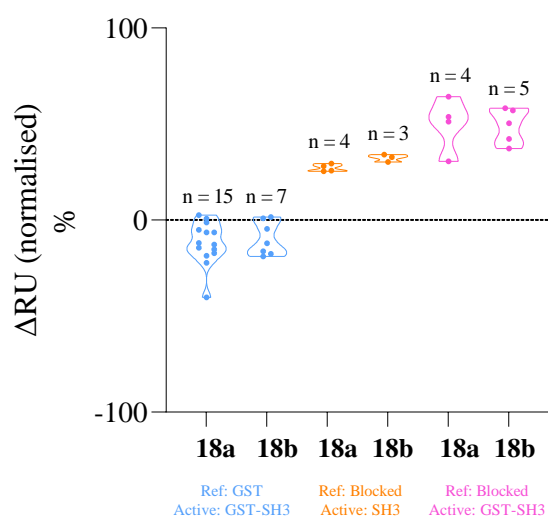


Figure 2.29: Violin plot comparison of normalised  $\Delta\text{RU}$  values for **18a** and **18b** binding to either GST-Tec SH3 or Tec SH3 proteins. Protein immobilised to reference cell indicated by ‘Ref’: GST indicates GST protein; ‘blocked’ indicates the chip surface was activated with NHS/EDC, then blocked with ethanolamine. Sample sizes listed above respective violin plot, with each plot extending to the maximum and minimum calculated  $\Delta\text{RU}$  values (i.e., no extrapolation). Violin plots calculated using GraphPad Prism version 9.0.0 for Windows.<sup>51</sup>

From Figure 2.29, the  $\text{RU}_{\text{max}}$  value for **18a** and **18b** was generally 50% greater than the  $\text{RU}_{\text{max}(\text{theor.})}$  value for binding to GST-Tec SH3, when the reference flow channel is activated and blocked. Interestingly, this is greater than the  $\Delta\text{RU}$  (normalised) value for **18a** and **18b** binding to both Tec SH3 ( $\sim 30\%$ ), and GST-Tec SH3 when GST is immobilised to the reference channel ( $\sim -10\%$ ). Importantly, the  $\Delta\text{RU}$  (normalised) value derived for **18a** and **18b** binding to GST-Tec SH3 increased when the reference flow channel is activated and blocked, which is consistent with the hypothesis of non-specific hydrophobic interactions occurring at the GST tag of GST-Tec SH3.

Despite the proposed non-specific hydrophobic interactions of ligands with both GST-Tec SH3 and Tec SH3 proteins, these non-specific interactions are considered to be minor, as the derived

isotherms and calculated  $K_d$  values were generally consistent. Therefore, due to the similar  $K_d$  values obtained from binding to GST-Tec SH3 and Tec SH3 proteins, it was determined that the  $K_d$  values were representative of binding to the proposed ligand-protein binding site on Tec SH3.

## **2.5 Protein structure determination: X-ray crystallography**

### **2.5.1 Introduction to protein crystallography in rational drug design**

Effective structure-based drug design is substantially improved if an appropriate protein and/or ligand-bound protein structure is available. The solution NMR structure of the Tec SH3 domain has been reported previously,<sup>3</sup> however a ligand-bound protein structure of the Tec SH3 domain is not currently available. Previous attempts to investigate the relationship between experimentally-determined ligand binding affinities and predicted ligand binding orientations *in silico* were undertaken, but were not successful in producing a suitably predictive model (Stojkoski, C., unpublished work), likely due to the dynamic nature of the proposed ligand-protein binding site (i.e., at a PPI site, rather than an enzyme pocket). To better guide ligand design, it would be ideal to obtain a ligand-bound protein structure. It was envisaged that this might be most readily achievable through crystallisation of the Tec SH3 domain, and subsequent ligand co-crystallisation or crystal soaking methods. For this project, crystallisation of either GST-Tec SH3, or Tec SH3 would be suitable, as ligand-protein binding assays have been conducted with each of these proteins.

### **2.5.2 Introduction to crystallisation of GST-containing proteins**

Literature crystallisation conditions for both GST and GST-containing fusion proteins were investigated to help guide screening condition selection for GST-Tec SH3 protein crystallisation. A search of the Protein Data Bank (PDB) for GST-tagged proteins (search terms: “GST-SH3”, “GST SH3”) yielded no results. Some papers have reported the crystallisation of proteins containing a large tag (such as GST) being quite challenging due to their reduced ability to form well-ordered crystals, likely caused by poor homogeneity of the flexible linker region between the large GST tag and protein of interest.<sup>80,81</sup> There have been reports of inter-domain linker sequence modification being a suitable solution to flexibility-induced heterogeneity, to afford greater rigidity within the protein structure,<sup>80</sup> however protein sequence modifications were deemed beyond the scope of work described in this thesis. Interestingly, crystallisation and x-ray diffraction of the GST-tagged DNA

## 2.5. PROTEIN STRUCTURE DETERMINATION: X-RAY CRYSTALLOGRAPHY

replication-related element-binding factor (GST-DREF) has been reported to 2.5-3.0 Å,<sup>82</sup> however the obtained crystals were small (“microcrystals”), and no subsequent structure has been deposited into the PDB at this time. Conversely, there are numerous reports in the PDB of crystallisation conditions for formation of x-ray diffraction quality GST protein crystals (Table 2.11).

Table 2.11: Examples of crystallisation conditions for GST proteins reported in the Protein Data Bank.<sup>43</sup>

<b>PDB ID</b>	<b>Crystallisation method</b>	<b>Crystallisation conditions</b>	<b>Resolution (Å)</b>
1AQW <sup>83,84</sup>	Vapour diffusion	Protein solution: 20 mg/mL in PBS (pH 7.0), with glutathione to final conc. of 5 mM. Reservoir solution: 30% PEG, 100 mM MES-NaOH (pH 6.5), 200 mM NaAc. Precipitant: PEG 8000	1.80
1M9A <sup>85,86</sup>	Hanging drop	Protein solution: 10-20 mg/mL in 20mM Tris-HCl (pH 7.5), 10 mM threalose, 0.02% (w/v) NaN <sub>3</sub> , 10 mM DTT, with glutathione sulfonate. Reservoir solution: 48-50% sat. (NH <sub>4</sub> ) <sub>2</sub> SO <sub>4</sub> , 225 mM NaAc (pH 5.6), %2 (v/v) EtOH.	2.10
1GNW <sup>87</sup>	Sitting drop	Protein solution: 20 mg/mL in 10 mM HEPES-NaOH, (pH 7.0), 0.02% (w/v) NaN <sub>3</sub> , with 30 mM S-hexylglutathione in 10 mM HEPES-NaOH (pH 7.0), 0.02% (w/v) Na <sub>3</sub> N. Reservoir solution: 2.8 M (NH <sub>4</sub> ) <sub>2</sub> SO <sub>4</sub> , 0.2% PEG 4000, in 0.2 M HEPES-NaOH, 0.02% (w/v) Na <sub>3</sub> N.	2.20
1PKZ <sup>88,89</sup>	Hanging drop	Protein solution: 10 mg/mL in 20 mM NaH <sub>2</sub> PO <sub>4</sub> (pH 7.0), 0.02% (w/v) Na <sub>3</sub> N, 0.2 M NaCl. Reservoir solution: 0.1 M Tris-HCl (pH 8.5), 19% methyl PEG 2000, 30 mM NaAc (pH 4.6) and 1% 2-mercaptoethanol.	2.10

From analysis of the crystallisation conditions in Table 2.11, it was deemed that crystallisation of GST was quite tolerant of several different protein solutions, generally with a minimum protein concentration of 10 mg/mL. Furthermore, GST protein crystals were reported to form in the presence and absence of both native ligands (glutathione) and reducing agents (DTT, 2-mercaptoethanol).

Therefore, crystallisation screens covering a broad range of conditions were deemed a suitable starting point for GST-Tec SH3 crystallisation studies.

### 2.5.3 Attempted crystallisation of GST-Tec SH3

Due to the relatively high protein yields obtained for GST-Tec SH3 protein, a series of crystallography screens were plated, in an attempt to identify suitable conditions for optimisation of protein crystallisation. After consideration of previously reported conditions for crystallisation of both GST-containing proteins and SH3 domains, purified GST-Tec SH3 protein in TBS (20 mg/mL) was screened against Hampton Research crystallisation screens Crystal Screen HT (HR2-130), Index (HR2-144), PEG/Ion HT (HR2-139) and Grid Screen Ammonium Sulfate (HR2-211), plated in a 1:1 drop ratio and stored at 16 °C. Unfortunately, no protein crystals were observed after 9 months, with most drops remaining clear. Although it is possible that the protein solution was too dilute, the lack of crystallisation activity was predicted to be caused by the inherent entropic penalty associated with the GST-Tec SH3 fusion protein containing two distinct, separate subunits. Therefore, further attempts to crystallise the fusion protein were not undertaken, and efforts were directed towards crystallisation of the Tec SH3 domain.

### 2.5.4 Introduction to crystallisation of SH3 domains

Similarly to Section 2.5.2, literature crystallisation conditions for SH3 domain proteins were investigated in the PDB, to guide screening condition selection for Tec SH3 protein crystallisation. A basic search for “SH3” in the PDB revealed 7000 reported structures containing a SH3 domain, 4826 of which were derived by x-ray diffraction.<sup>43</sup> In an attempt to identify relevant SH3 structures only (i.e., exclude SH3 dimers, multi-domain proteins containing a SH3 domain), searches for SH3 domains in Src, Abl and Tec tyrosine kinase family proteins were conducted. Following protein sequence alignment with Tec SH3 by BLAST,<sup>59</sup> a small number of relevant SH3 protein crystallisation reports were identified, as indicated in Table 2.12. The SH3 proteins listed in Table 2.12 share between 37.0 - 44.1% sequence similarity with the Tec SH3 domain.

## 2.5. PROTEIN STRUCTURE DETERMINATION: X-RAY CRYSTALLOGRAPHY

Table 2.12: Examples of crystallisation conditions for SH3 proteins reported in the Protein Data Bank.<sup>43 a</sup> indicates the resultant crystals were microseeded to grow larger crystals suitable for structure determination by x-ray diffraction.

PDB ID	SH3 protein	Crystallisation method	Crystallisation conditions	Resolution (Å)
6MNW <sup>90</sup>	Lyn	Hanging drop	Protein solution: 10 mg/mL in 20 mM Tris (pH 7.5). Reservoir solution: 0.1 M Na citrate (pH 3.5) and 3.2 M NaCl.	1.20
5NP3 <sup>91</sup>	Abl2	Hanging drop	Protein solution: ~5 mg/mL in 20 mM Tris-HCl, 150 mM NaCl, 3 mM NaN <sub>3</sub> , 0.5 mM TCEP (pH 7.6). Reservoir solution: 1.8 M disodium DL-malate (pH 7.0).	2.00
6IPY <sup>92</sup>	Fyn	Sitting drop	Protein solution: 5-8 mg/mL in 20 mM Tris (pH 8.0), 150 mM NaCl, 1 mM EGTA. Reservoir solution: 0.1 M citric acid (pH 3.5), 25% (w/v) PEG 3350.	1.34
6SDF <sup>93</sup>	Grb2	Hanging drop <sup>a</sup>	Protein solution: 7 mg/mL in 20 mM HEPES, 0.01% (w/v) NaN <sub>3</sub> (pH 7.2). Reservoir solution: 55% MPD, 0.1 M HEPES (pH 7.5).	2.50

From Table 2.12, the reported SH3 proteins were generally amenable to crystallisation from protein solutions containing Tris, both in the presence and absence of NaCl. The reservoir solutions were variable in pH and components, but citrate-based salts appear to be common crystallisation agents. Notably, there were no reducing agents reported. Consequently, crystallisation screens covering a range of pH levels and citrate salts were considered a suitable starting point for crystallisation of the Tec SH3 domain.

### 2.5.5 Attempted crystallisation of Tec SH3

In an effort to overcome the entropic penalties associated with crystallisation of fusion proteins, crystallisation of the cleaved Tec SH3 protein was investigated. As SH3 domains had previously been reported to crystallise in Tris-containing buffers, in both the presence and absence of salt, the

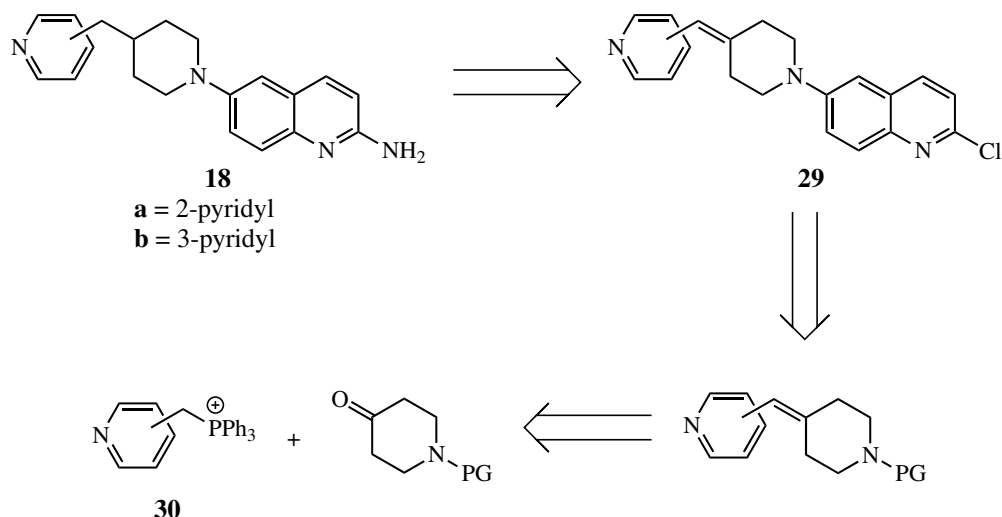
purified Tec SH3 protein was used as a stock in TBS (6 mg/mL). No reducing agents were added to the protein stock, as the Tec SH3 protein does not contain any cysteine residues.

The initial crystallisation screens, Hampton Research Crystal Screen HT (HR2-130), Index (HR2-144) and PEG/Ion HT (HR2-139), were selected to encompass a broad range of conditions. After ~1 month of storage at 16 °C, most drops remained clear, suggesting the protein may be too dilute. Interestingly, those conditions which contained citric acid often resulted in precipitation of protein. This was not unexpected, as analysis of literature SH3 domain crystallisation conditions indicated that typical conditions generally included a citrate salt, and low pH values (~3.5-4.5). Consequently, the Tec SH3 protein was concentrated to 11 mg/mL, and plated against a Molecular Dimensions ProPlex HT-96 (MD1-42) screen, and an optimisation tray based on citric acid, with variable pH and PEG 3350 concentrations was plated, and stored at 16 °C. In an attempt to increase the relative protein concentration in the optimisation tray, the protein was mixed with the crystallisation buffers at a range of drop ratios. While less clear drops were observed, protein crystals were not obtained for any of the more concentrated Tec SH3 protein trays after 9 months. Interestingly, protein precipitation was observed generally across the citric acid optimisation tray, but reduction of precipitant/PEG concentration was insufficient to induce protein crystallisation. No further attempts at protein crystallisation were attempted.

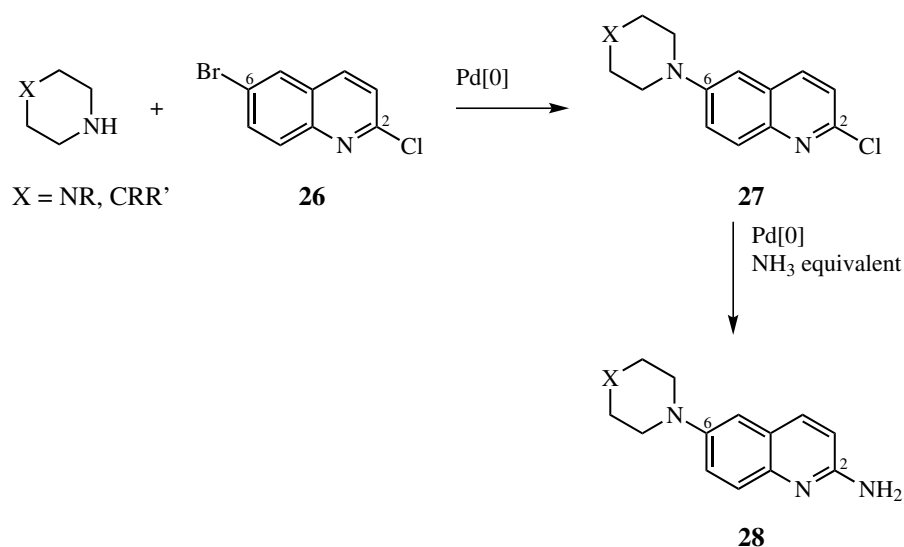
## 2.6 Preparation of control ligands: general synthetic pathway

The proposed synthesis of **18a** and **18b** was consistent with previously reported methods, and is shown in Scheme 2.1.<sup>56</sup> A protocol for the synthesis of 6-substituted heterocyclic 2-aminoquinoline derivatives has been identified and optimised after thorough investigation in previous work, utilising two key sequential palladium-catalysed Buchwald-Hartwig coupling reactions (Scheme 2.2).<sup>47,60</sup> Conditions for the selective coupling of piperidine derivatives at the 6-position of 6-bromo-2-chloroquinoline **26** were identified to afford the corresponding 2-chloroquinoline derivatives **27**, impressively in the presence of an activated aryl chloride in the 2-position. Following this, a second amine source can couple at the activated aryl chloride to yield the desired 2-aminoquinoline compounds **28**.

## 2.6. PREPARATION OF CONTROL LIGANDS: GENERAL SYNTHETIC PATHWAY



Scheme 2.1: Proposed general retrosynthetic plan for the synthesis of control ligands **18a** and **18b**.



Scheme 2.2: General workflow of sequential Buchwald-Hartwig coupling reactions from **26** and the appropriate heterocyclic amine to afford the desired 6-substituted 2-chloroquinoline **27** and 6-substituted 2-aminoquinoline **28**.

Initial investigations into selective coupling conditions for the first Buchwald-Hartwig reaction yielded a range of side products, in varying quantities (Figure 2.30).<sup>47,60</sup> Generally, the desired 6-substituted 2-chloroquinoline derivative **27** was isolated as the main product, followed by the 2-substituted-6-bromoquinoline product **31**. It is anticipated that the latter would be likely to form via direct nucleophilic aromatic substitution at the 2-position aryl chloride, which is activated by the adjacent quinolinyl nitrogen. Additionally, utilising metal *tert*-butoxide bases in Buchwald-Hartwig coupling reactions afford the possibility of alternative substitution with *tert*-butoxide at the activated aryl chloride in the 2-position, as for **32** and **33**. In some instances, reduction of the 6-position aryl bromide was also observed as for **34**, likely due to the reaction conditions (elevated temperature

and pressures in a sealed tube system) required for the desired transformation. After thorough investigation of several components of the Buchwald-Hartwig coupling system (including phosphine ligand, base, solvent, mechanism of heating, copper co-catalysts and halogen-substitution), the reaction conditions were optimised to consistently yield the desired 6-substituted-2-chloroquinoline derivative as the predominant product.<sup>47,60</sup>

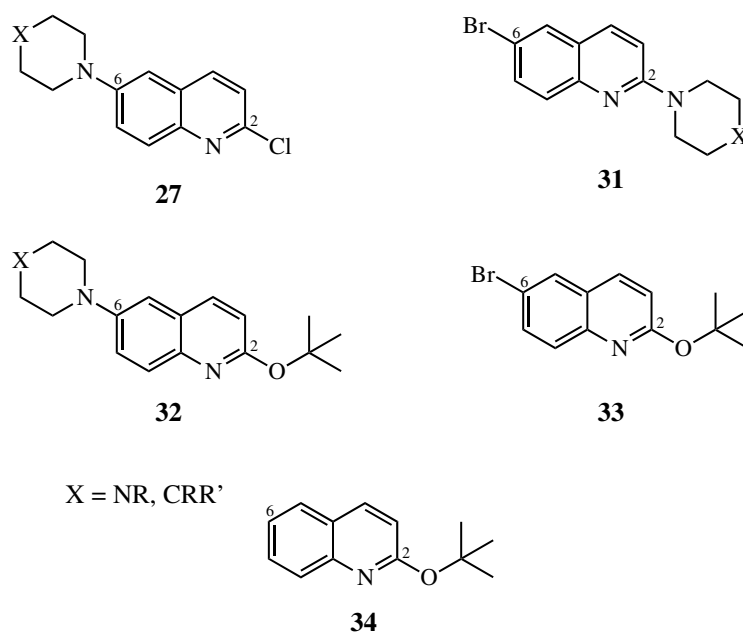


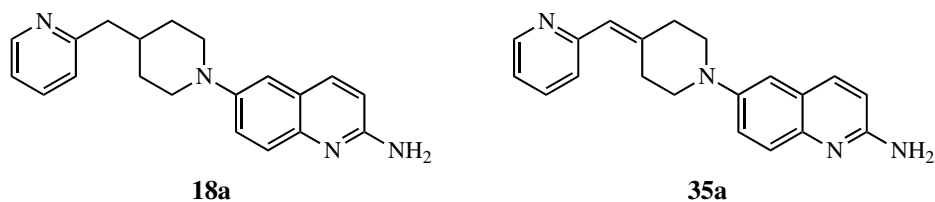
Figure 2.30: General structures of possible products from Buchwald-Hartwig coupling of heterocyclic amines and **26**, as reported previously.<sup>47,60</sup>

Introduction of the amine functionality at the 2-position of 6-substituted-2-chloroquinoline derivatives was also investigated previously. Implementation of a second Buchwald-Hartwig coupling reaction reported by Buchwald *et al.*, utilising  $Pd(dba)_2$ , lithium bis(trimethylsilyl)amine (LiHMDS) as both an ammonia equivalent and base, with a phosphine ligand, was shown to be effective for the desired transformation of 2-chloroquinoline derivatives, affording the corresponding 2-aminoquinoline derivatives in high yields.<sup>47</sup>

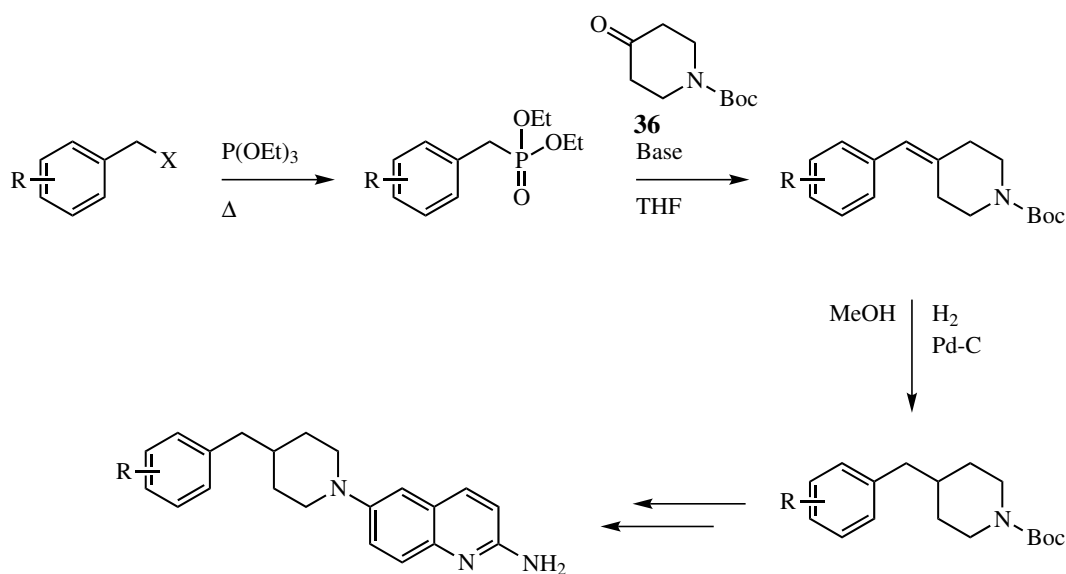
Using these sequential Buchwald-Hartwig coupling reactions with **26**, the desired 2-aminoquinolines **18a** and **18b** could be successfully synthesised following literature methods. In addition, synthesis of an additional novel ligand for testing **35a** could be possible, as a precursor to the target ligand **18a**, whereby the alkene bond is not reduced.



## 2.6. PREPARATION OF CONTROL LIGANDS: GENERAL SYNTHETIC PATHWAY



Previous reports have investigated the synthesis of simple benzylpiperidinyll intermediates, intended for the synthesis of 6-benzylpiperidinyll-2-aminoquinoline ligands.<sup>56</sup> Synthesis of the benzylpiperidinyll components was achieved via conversion of the appropriate benzyl halide derivative to the corresponding benzyl phosphonate derivative via a Michaelis-Arbuzov reaction, followed by a Horner-Emmons reaction with *N*-Boc-4-piperidone **36** to afford the desired benzylidenepiperidinyll derivative (Scheme 2.3). This intermediate was then reduced under standard hydrogenations conditions, and subsequently deprotected before sequential Buchwald-Hartwig coupling reactions to afford the desired 6-benzylpiperidinyll-2-aminoquinoline ligands.<sup>56</sup>

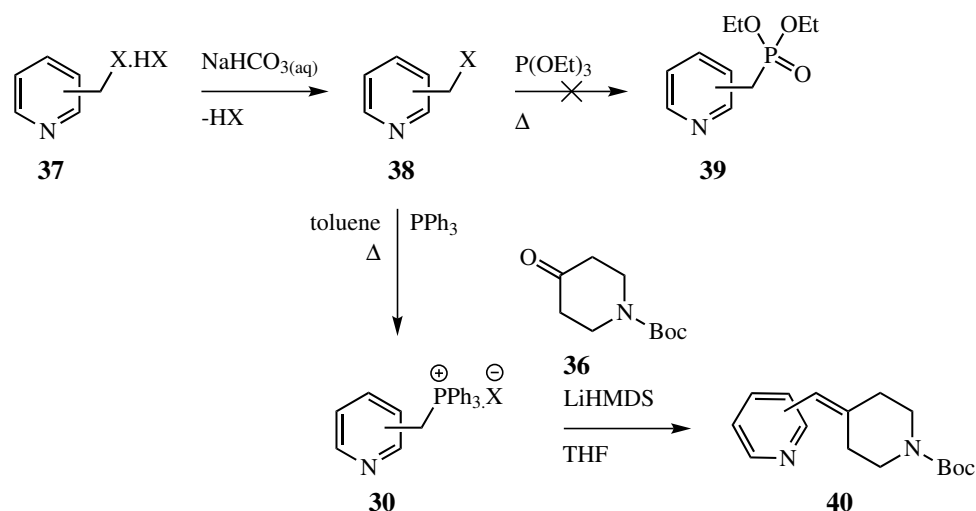


Scheme 2.3: General synthetic pathway for the synthesis of 6-benzylpiperidinyll 2-aminoquinoline ligands.<sup>56</sup>

However, when the same methodology was applied for the synthesis of pyridylmethylene piperidinyll derivatives, conversion of the pyridylmethyl halide to the corresponding pyridylmethyl phosphonate were reported in extremely poor yields, likely due to volatility of the pyridylmethyl halide (which was liberated from the appropriate hydrohalide salt).<sup>56</sup> Consequently, alternative precursors for an alkene-forming reaction were sought, with the intention to utilise either mild reaction conditions, or possessing the capacity to “trap” the desired compound as a non-volatile salt. It was reported that the pyridylmethyl halide derivatives could be converted into the corresponding phosphonium salts

## 2.7. SYNTHESIS OF CONTROL 2-AMINOQUINOLINE LIGANDS WITH A PYRIDYL SUBSTITUENT

in comparatively good yields, and subsequent conversion into the corresponding pyridylmethylene piperidinyll derivative via Wittig reaction with **36** was successful (Scheme 2.4). Favourably, the alkylidene product could generally be separated from the triphenylphosphine oxide by-product. Hence, for the synthesis of **18a** and **18b** in this work, formation of the appropriate pyridylmethylene piperidinyll derivatives will be investigated via Wittig reaction.



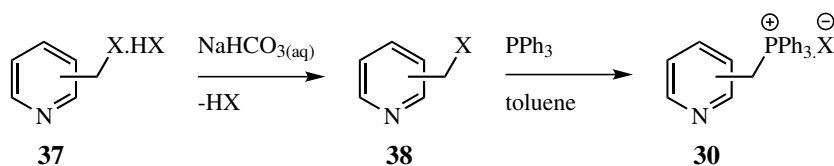
Scheme 2.4: Literature attempts towards the synthesis of pyridylmethylene piperidinyll derivatives **40** via Michaelis-Arbuzov and Horner Emmons reactions, or phosphonium salt formation and subsequent reaction.<sup>56</sup>

## 2.7 Synthesis of control 2-aminoquinoline ligands with a pyridyl substituent

### 2.7.1 Synthesis of arylmethyl piperidine derivatives

It was envisaged that the desired ligands **18a**, **18b** and **35a** would be synthesised via pyridylmethylene piperidinyll intermediates, and previous work indicated that these intermediates were most readily synthesised via Wittig reactions with **36** (Scheme 2.4). Therefore, synthesis of the appropriate pyridylmethyl phosphonium salts **30** was required. Using commercially available halomethyl pyridine salts **37**, the halomethyl pyridine **38** was carefully liberated via treatment with saturated  $\text{NaHCO}_3(\text{aq})$ . Crude **38** was then immediately added to  $\text{PPh}_3$  in toluene, and heated at reflux to form the desired pyridylmethyl phosphonium salt **30** (Scheme 2.5).

## 2.7. SYNTHESIS OF CONTROL 2-AMINOQUINOLINE LIGANDS WITH A PYRIDYL SUBSTITUENT



Scheme 2.5: Synthesis of pyridylmethyl phosphonium salts **30** following literature methods.<sup>56</sup>

Table 2.13: Yields for phosphonium salt **30** formation from **37** derivatives (Scheme 2.5).

Compound	Pyridyl substitution	Halogen (X = )	Yield (%)
<b>30a</b>	2	Br	78
<b>30b</b>	3	Cl	32

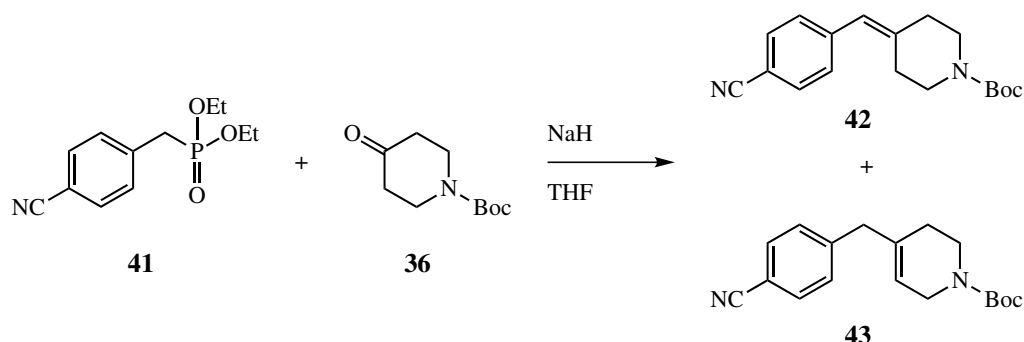
Formation of **30** derivatives was determined primarily via NMR analysis; the presence of an additional aromatic multiplet in  $^1\text{H}$  NMR spectra integrating to 15H was observed for both derivatives, consistent with the introduction of the triphenylphosphine group. Furthermore, the signal consistent with the 2H methylene group appeared as a doublet, due to coupling to phosphorous. This heteroatom coupling was also observed in  $^{13}\text{C}$  NMR, and in all cases, the obtained spectra were consistent with those reported previously.<sup>56,66</sup> Notably, the obtained yields for **30a** and **30b** are also consistent with those obtained previously (Table 2.13);<sup>56,66</sup> it is anticipated that for the pyridylmethyl halide derivatives, the bromide derivative **38a** is more reactive than the chloride derivative **38b**, thus forms the desired **30a** derivative more readily. Conversely, the lower reactivity of **38b** could allow for a substantial amount of the volatile reagent to be lost via evaporation, before it is trapped as the non-volatile phosphonium salt **30b**, causing a lower yield to be obtained.

### Synthesis of pyridylmethylenepiperidine derivatives via Wittig reaction

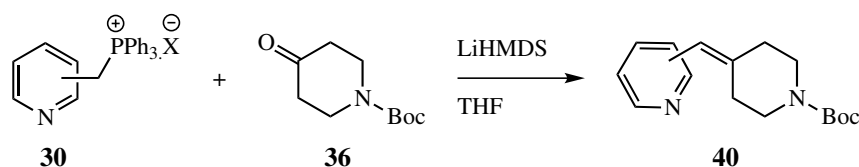
In order to introduce the piperidine ring functionality, the Wittig reactions with **30** derivatives were completed with **36**. Interestingly, previous work identified that for derivatives containing an electron-deficient aromatic group (e.g., **41**, which has a nitrile substituent), conducting the analogous Horner-Emmons reaction using bases containing hydroxide ions (e.g., KOH) or bases which were amenable to hydroxide formation (e.g., NaH) catalysed the isomerisation of the exocyclic alkene bond in the desired product **42** to the less stable endocyclic tetrahydropyridine product **43** (Scheme 2.6). Furthermore, treatment of pure **42** with NaH in THF facilitated alkene isomerisation to **43**, suggesting the isomerisation process was occurring independently to the Horner-Emmons reaction pathway,<sup>56</sup> and it was anticipated that the electron-deficient pyridyl groups would behave in a similar manner. To maximise formation of the desired **40** derivatives, LiHMDS was employed

## 2.7. SYNTHESIS OF CONTROL 2-AMINOQUINOLINE LIGANDS WITH A PYRIDYL SUBSTITUENT

as the base in the Wittig reaction (Scheme 2.7), to potentially avoid isomerisation to the tetrahydropyridine compounds — both **40** derivatives were synthesised in good yields (Table 2.14).



Scheme 2.6: Previously attempted synthesis of electron-deficient benzylpiperidinyll derivatives via Horner Emmons reaction, resulting in the formation of the corresponding tetrahydropyridine isomer **43**.<sup>56</sup>



Scheme 2.7: Synthesis of pyridylmethylene Boc-protected piperidine derivatives (**40**) via Wittig reaction.

Table 2.14: Yields for pyridylmethylene Boc-protected piperidine (**40**) formation from **30** derivatives via Wittig reaction (Scheme 2.7), including diagnostic <sup>1</sup>H NMR chemical shift for alkene H. \* indicates the isolated product contained triphenylphosphine oxide impurity

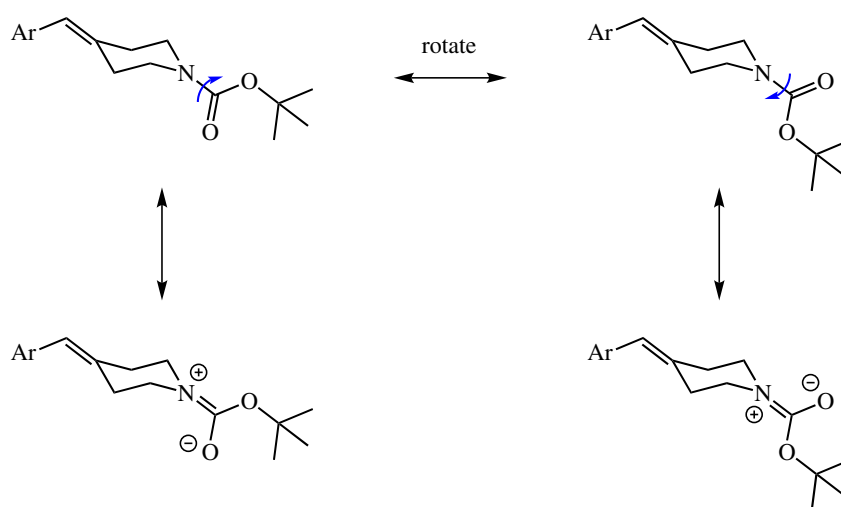
Compound	Pyridyl substitution	Halogen (X = )	Yield (%)	$\delta_{\text{H}}$ alkene (ppm)
<b>40a</b>	2	Br	63	6.37
<b>40b</b>	3	Cl	62*	6.30

In each case, successful formation of the desired product was observed following analysis of HRMS and <sup>1</sup>H NMR spectra; detected product masses of *m/z* 219.1133 and 275.1754 were observed for **40a** and **40b** respectively, which are consistent with either the desired product (expected for **40b** *m/z*: 275.1754), or the Boc-fragmented product (expected for **40a** *m/z*: 219.1128), which is not surprising due to the nature of the labile *tert*-butyl group. Analysis of <sup>1</sup>H NMR spectra of both **40a** and **40b** revealed the presence of a singlet at approximately 6.30 ppm integrating to 1H, which was diagnostic for the presence of the newly-formed alkene. Furthermore, the introduction of a singlet at approximately 1.48 ppm (integrating to 9H), and the emergence of four broadened triplet signals integrating to 2H each, suggested the successful appendage of a Boc-protected piperidine group. Interestingly, while each of the piperidine signals integrated to 2H, [<sup>1</sup>H, <sup>13</sup>C] HSQC spectra indicated that each 2H signal corresponded to a single carbon signal (i.e., was a CH<sub>2</sub> group), suggesting that each piperidine signal was unique. This is not surprising, as the lack of symmetry

## 2.7. SYNTHESIS OF CONTROL 2-AMINOQUINOLINE LIGANDS WITH A PYRIDYL SUBSTITUENT

---

about the piperidine ring would afford four 2H signals, rather than two 4H signals. Furthermore, a 4-substituted piperidine ring would typically be expected to adopt a chair-like conformation, where each hydrogen would exhibit distinct  $^1\text{H}$  NMR signals for either an axial or equatorial geometry. However, **40** derivatives contain substantially planarised piperidine rings, flanked by an alkene at the 4-position, and the Boc-protecting group, which contains double-bond character (Scheme 2.8). Consequently, the planarised piperidine ring would have less-defined axial and equatorial hydrogen environments, hence they may not be distinguishable in NMR spectra obtained at room temperature, as for **40** derivatives (and for most related compounds described in this thesis).



Scheme 2.8: Representation of Boc-protecting group partial double bond character in benzyl piperidinyl derivatives, where Ar = aryl. Rotated bonds indicated by blue arrows. Adapted from Jayne.<sup>56</sup>

In addition, the piperidine ring signals in both  $^1\text{H}$  and  $^{13}\text{C}$  NMR are broadened, likely due to the restricted rotation of the carbamate bond in the Boc protecting group. The partial double bond character exhibited by the Boc protecting group would cause slower bond rotation of the carbonyl group on the NMR timescale, therefore the adjacent piperidinyl H and C are affected differentially by the Boc carbonyl group on the NMR timescale, and their  $^{13}\text{C}$  and  $^1\text{H}$  signals broadened. For each unique chemical environment, if the piperidine ring conformation was unhindered and allowed to ring-flip freely, a sharp, single signal would be expected in the NMR spectra. Conversely, if ring-flipping of the piperidine ring were significantly hindered (sterically or energetically), two distinct chemical environments for each ring-flipped state would be observed in NMR spectra (i.e., axial and equatorial). As the conformation of the piperidine ring is affected by the substituents to varying degrees, the ability to resolve these distinct ring-flipped chemical environments exists on a spectrum; if the conformation of the piperidine ring is partially restricted, complete resolution of

distinct chemical environments between ring-flipped states may not be possible. Compounded with slow bond rotation of flanking substituents, this may result in significantly broadened signals, as observed for **40** derivatives in both  $^1\text{H}$  and  $^{13}\text{C}$  NMR spectra (Figure 2.31).

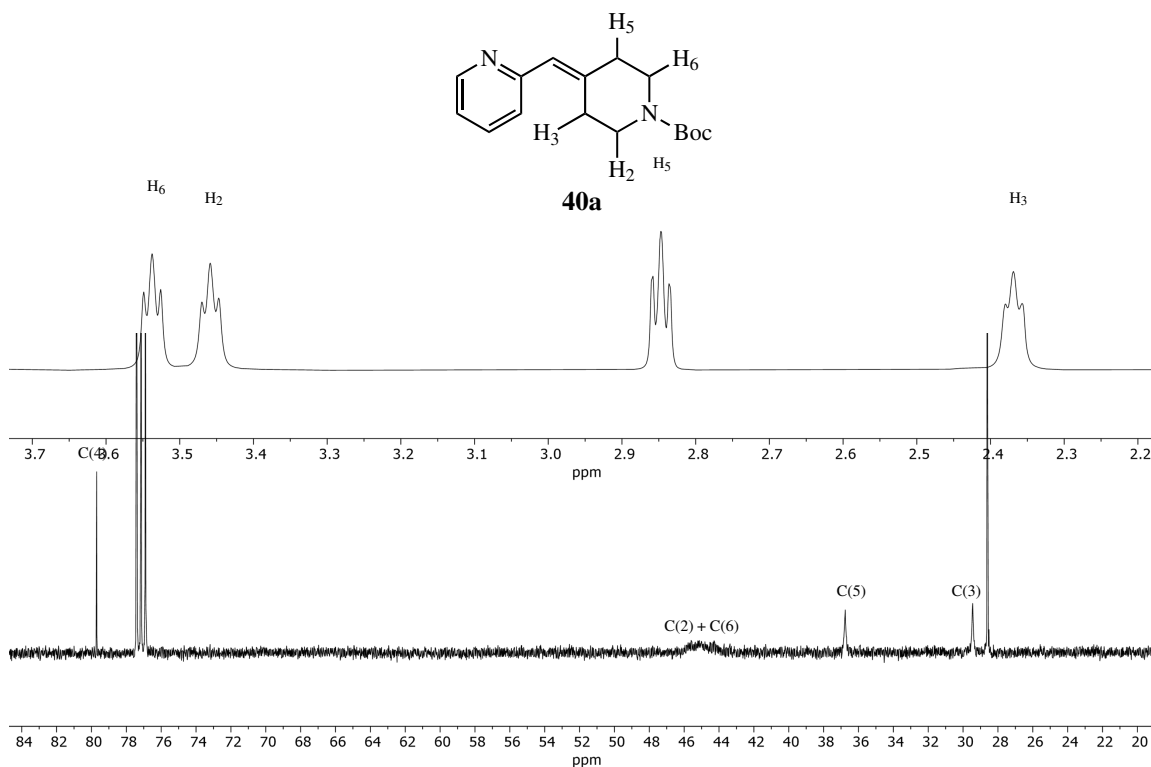


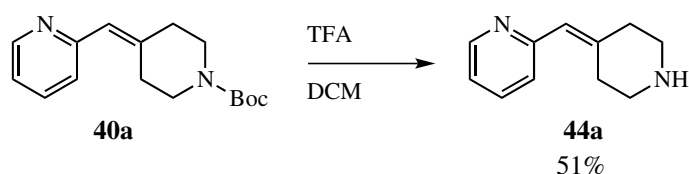
Figure 2.31: Excerpts of  $^1\text{H}$  and  $^{13}\text{C}$  NMR spectra ( $\delta_{\text{H}}$ : 2.2-3.7 ppm;  $\delta_{\text{C}}$ : 20-84 ppm) of **40a** in  $\text{CDCl}_3$ , indicating broadened signals due to restricted conformation of the piperidiny ring and slow rotation of the Boc protecting group. Signals were assigned by HSQC and HMBC 2D NMR spectra.

Again, the obtained spectra were consistent with those reported previously, supporting that the desired products had been obtained.<sup>56,66</sup> For the 3-pyridyl derivative **40b**, the product was unable to be completely separated from the triphenylphosphine oxide by-product that formed during the Wittig reaction. However,  $^1\text{H}$  NMR integration revealed that this impurity was a minor product in comparison to **40b**; it was envisaged that the impurity would be removed at a later stage of the synthetic pathway through successive column chromatography, so was carried forward.

In order to synthesise ligand **35a**, it was imperative that the alkene bond in **40a** be retained, and be reduced later in the synthetic pathway to afford synthesis of **18a**. Therefore, Boc group deprotection of **40a** was achieved using trifluoroacetic acid in DCM to afford the desired product **44a** (Scheme 2.9).

## 2.7. SYNTHESIS OF CONTROL 2-AMINOQUINOLINE LIGANDS WITH A PYRIDYL SUBSTITUENT

---



Scheme 2.9: Synthesis of **44a** via Boc-deprotection of **40a**.

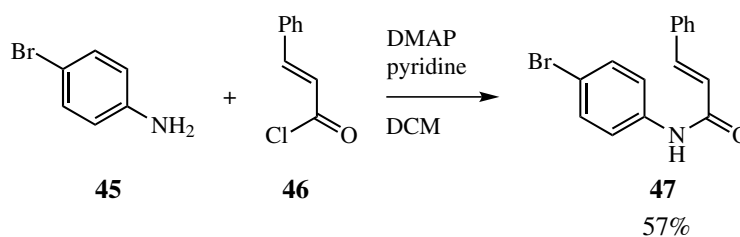
Successful removal of the Boc protecting group was again supported by both HRMS and NMR spectra; a mass product of  $m/z$  175.1232 was detected, consistent with the desired product (expected  $m/z$ : 175.1230). The most diagnostic changes were observed in the  $^1\text{H}$  NMR spectra as the disappearance of the 9H *tert*-butyl singlet at 1.48 ppm, and the appearance of a broad 1H singlet at 4.49 ppm, which were consistent with the liberation of a secondary amine. However, as the alkene bond was retained in the 4-position of the piperidine ring, the ring was still substantially planarised, and distinct axial and equatorial signals were not observed.

### 2.7.2 Synthesis of 6-position substituted 2-chloroquinolines via selective Buchwald-Hartwig coupling

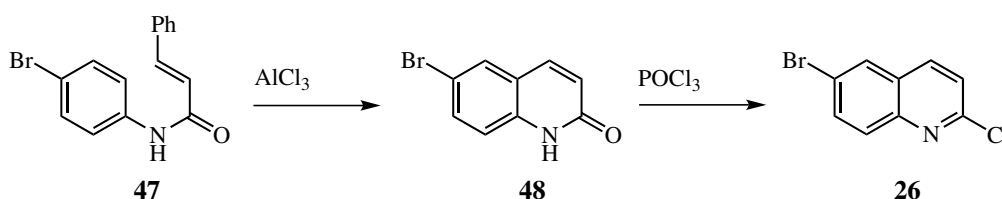
#### Synthesis of 6-bromo-2-chloroquinoline

To synthesise the desired ligands **18a**, **18b** and **35a**, the key intermediate 6-bromo-2-chloroquinoline **26** was required, as the different halide groups permit the required scaffold for sequential amine coupling. A three-step synthesis of **26** has been reported in the literature using commercially-available starting materials in acceptable yields,<sup>47,94,95</sup> and would be undertaken in this work.

Following the reported literature method, 4-bromoaniline **45** and cinnamoyl chloride **46** were combined to afford the desired cinnamanilide **47** in moderate yield (Scheme 2.10). Formation of the desired product was supported primarily by HRMS and NMR spectra, as well as melting point comparison to literature. Mass products of  $m/z$  302.0176 and 304.0157 were observed in  $\sim 1:1$  ratio, consistent with the desired product (expected  $m/z$ : 302.0175 [ $^{79}\text{Br}$ ] / 304.0157 [ $^{81}\text{Br}$ ]). From  $^1\text{H}$  NMR analysis, the diagnostic *trans* alkene coupling was observed ( $J = 15.5$  Hz), as well as a para-substituted phenyl ring, as consistent with that reported previously.<sup>47</sup> Lastly, the melting point obtained (190-192 °C) was consistent with that reported in the literature (lit. 193-194 °C).<sup>94</sup> While the yield for this reaction was moderate, an alternative synthesis of **47** has since been reported, suggesting that the reaction can be optimised.<sup>55</sup>

Scheme 2.10: Synthesis of **47** via literature conditions.<sup>47,94</sup>

From **47**, it was anticipated that the desired 2-chloroquinoline **26** could be synthesised via a quinolone intermediate **48** as indicated in Scheme 2.11.

Scheme 2.11: Proposed synthesis of 2-chloroquinoline **26** following literature methods.<sup>47,94,95</sup>

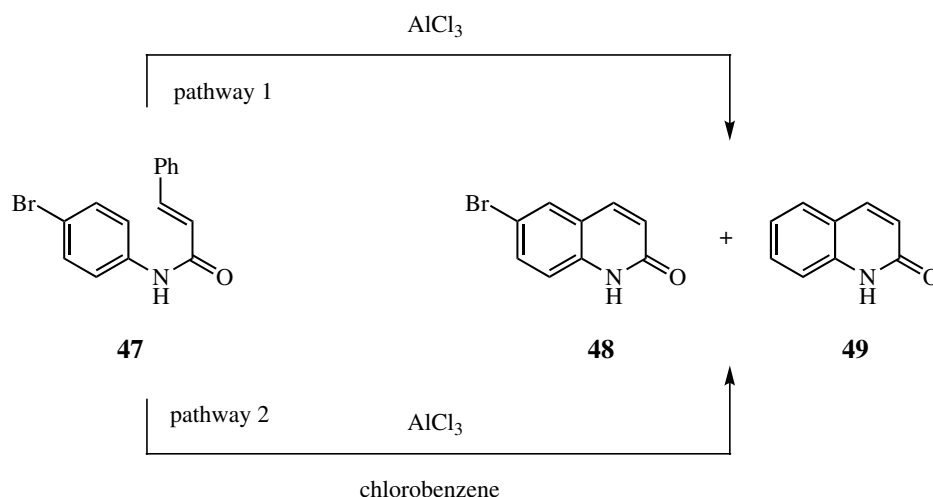
The ring-closing step involves an interesting Friedel-Crafts type reaction, in the form of a melt reaction to form **48**; subsequent chlorination with phosphorous oxychloride ( $\text{POCl}_3$ ) affords the desired 2-chloroquinoline **26**.<sup>47,94,95</sup> In this work, formation of the desired quinolone **48** was determined by analysis of HRMS and NMR spectra. Mass products of  $m/z$  223.9270 and 225.9683 were detected in a  $\sim 1:1$  ratio, consistent with the desired product (expected  $m/z$ : 223.9706 [ $^{79}\text{Br}$ ] / 225.9685 [ $^{81}\text{Br}$ ]). Notably, loss of the 5H aromatic multiplet (consistent with loss of benzene), and the emergence of a *cis* alkene 1H doublet in  $^1\text{H}$  NMR ( $J = 9.5$  Hz) were observed. Unfortunately, formation of an unbrominated side product **49** was also observed, and supported via detection of the mass product  $m/z$  146.0598 (expected  $m/z$ : 146.0600) in HRMS spectra, and comparison of  $^1\text{H}$  NMR signals with previously reported data.<sup>56</sup> Due to the formation of **49**, the yield of **48** from the melt reaction with  $\text{AlCl}_3$  was found to be quite variable, and was dependent upon both the homogeneity of heat distribution during the melt reaction, and the quality of  $\text{AlCl}_3$ , as consistent with previous work.<sup>56</sup> Conducting the melt reaction at higher temperatures, reducing the homogeneity of heating of the reaction mixture (not quantified) or using older, partially hydrolysed samples of  $\text{AlCl}_3$  (not quantified) appeared to increase the formation of the undesired reduced side-product **49**. Therefore, it is hypothesised that formation of the unbrominated side product **49** might be occurring through a reduction reaction caused by uneven heating — maintaining a consistent heat gradient across the reaction mixture (with a heat gun) during the initial stages of the melt reaction is quite difficult;



## 2.7. SYNTHESIS OF CONTROL 2-AMINOQUINOLINE LIGANDS WITH A PYRIDYL SUBSTITUENT

inconsistent heating may cause reduction of the labile C-Br bond in **47**. Furthermore, inconsistent heating may cause condensation of atmospheric water in concentrated pockets within the reaction mixture, leading to unwanted hydrolysis of  $\text{AlCl}_3$ .

Due to the unwanted formation of **49**, conditions were sought to improve selectivity of the ring-closing reactions, and an alternative synthetic procedure was tested, whereby the reaction was completed by refluxing in chlorobenzene, rather than as a melt reaction (Scheme 2.12).<sup>94</sup> While the ratio of brominated:unbrominated product wasn't ideal at  $\sim 5:2$  (Table 2.15), this reaction was shown to be reproducible, and the product was generally safer to work up as the suspension could be pipetted into ice water. In all cases, resolution of the quinolone mixture was challenging, so the resulting precipitate was carried through to the next step as an inseparable mixture.



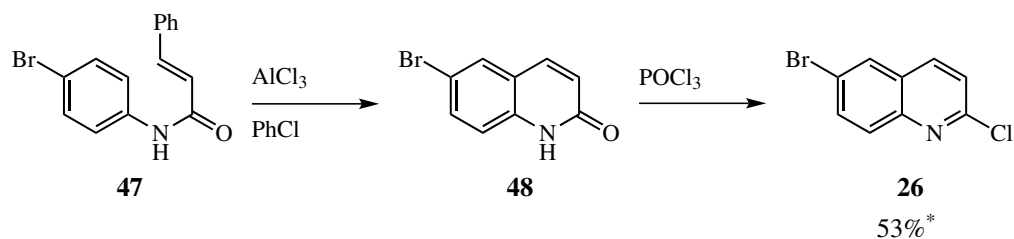
Scheme 2.12: Explored literature pathways for the synthesis of quinolone intermediate **48**, and side product **49**.<sup>94</sup>

Table 2.15: Observed product distributions from employing various literature procedures for the synthesis of **48** (see Scheme 2.12).

Pathway	Temperature (°C)	Product distribution (48:49)
1	110	1:1
1	150	2:9
2	132	5:2

The final step from the literature procedure involved a chlorination reaction with the crude mixture of quinolones **48** and **49** using  $\text{POCl}_3$ , where the desired product **26** was isolated by precipitation before further purification. As the reaction was conducted using a mixture of quinolone reagents, the yields were recorded over two steps, as indicated in Scheme 2.13. While the literature procedure suggested purification of **26** via recrystallisation, it was observed that the isolated product yield was

generally low (data not shown). Alternatively, **26** could be purified via short path vacuum column chromatography, with generally improved yields. Although a minor, coloured impurity remained in the product following chromatography, it did not appear to impact subsequent reactions. As chromatographic purification generally resulted in improved product mass recovery compared to recrystallisation, this was the preferred method of purification.



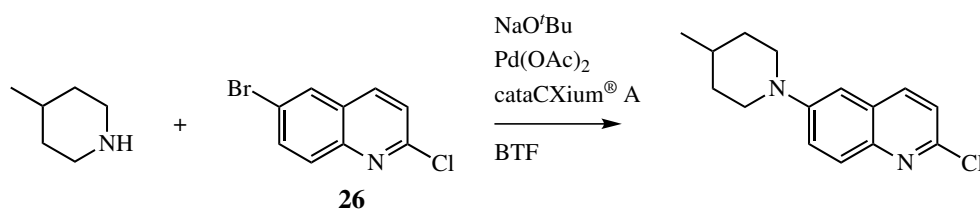
Scheme 2.13: Optimised synthesis of 2-chloroquinoline **26**. PhCl indicates chlorobenzene. \* indicates yield over two steps.

Formation and isolation of the desired product was determined primarily by analysis of HRMS and NMR spectra; mass products of  $m/z$  241.9367, 243.3945 and 245.9319 were observed in  $\sim 7:9:2$  ratio, as consistent with the Cl and Br isotope distributions (expected  $m/z$ : 241.9367 [ $^{79}\text{Br}$ ,  $^{35}\text{Cl}$ ], 243.9337 [ $^{79}\text{Br}$ ,  $^{37}\text{Cl}$ ], 243.9346 [ $^{81}\text{Br}$ ,  $^{35}\text{Cl}$ ], 245.9317 [ $^{81}\text{Br}$ ,  $^{37}\text{Cl}$ ]). In the  $^1\text{H}$  NMR spectrum, absence of the 1H amide signal, and the upfield shift for C(3)H of the quinoline ring (due to *ortho/para* shielding by resonance from the chlorine atom) were diagnostic for formation of the desired product. Each of the obtained spectra were consistent with literature,<sup>47</sup> supporting that **26** had successfully been synthesised.

The next step in the synthesis of **18a** and **35a** required the selective coupling of the corresponding alkene-containing amine, **44a** and **26**. Previous work had extensively investigated the application of a Buchwald-Hartwig coupling reaction to selectively couple heterocyclic amines at the 6-position of **26**. As part of this prior work, general conditions were identified for the selective coupling of amines including substituted piperidinyl and piperazinyl rings (Scheme 2.14),<sup>47,60</sup> and it was envisaged that these conditions could similarly be applied for the work in this thesis.

## 2.7. SYNTHESIS OF CONTROL 2-AMINOQUINOLINE LIGANDS WITH A PYRIDYL SUBSTITUENT

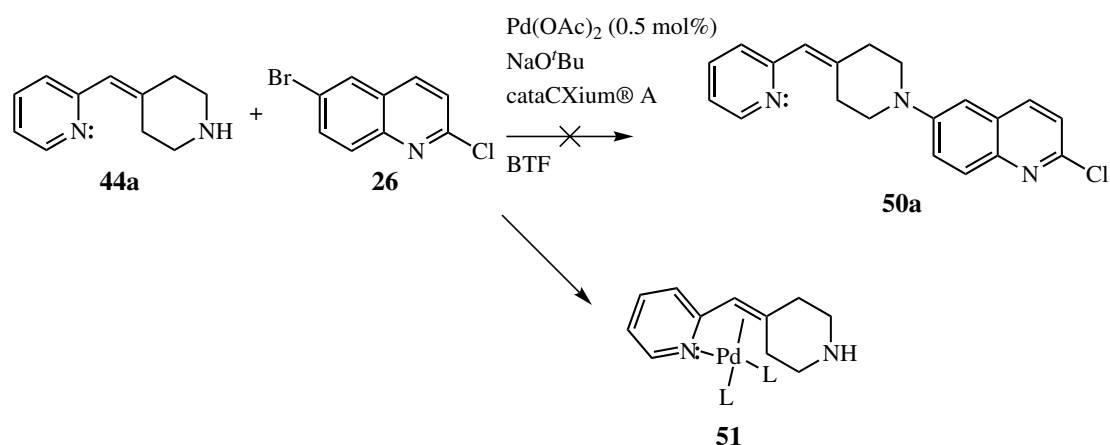
---



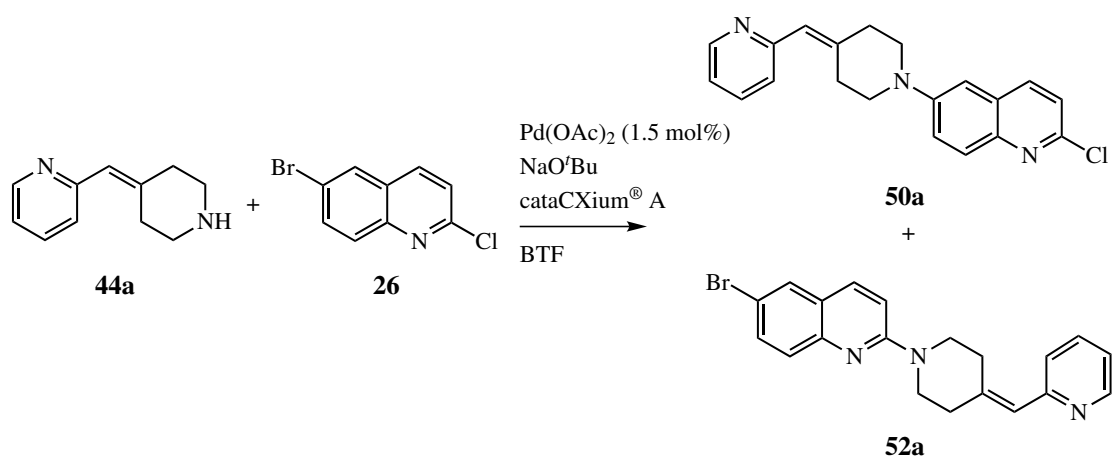
Scheme 2.14: Previously optimised Buchwald-Hartwig reaction conditions for the selective coupling of heterocyclic amines at the 6-position of **26**.<sup>47,60</sup>

Conditions for Buchwald-Hartwig coupling reactions are generally substrate specific, which can be complicated if chemoselectivity or regioselectivity is desired; the coupling reaction is dependent upon several variables including solvent, base, catalyst system (including associated ligands), temperature and pressure.<sup>47,96</sup> Previous work had identified a catalyst system comprised of Pd(OAc)<sub>2</sub> and the phosphine ligand cataCXium<sup>®</sup> A that generally afforded the desired coupling product with minimal formation of undesired side products. Furthermore, when NaOtBu was employed as the base, the desired coupling product was the major product generally across a range of solvent systems. Initially, toluene was identified as the ideal solvent for facilitating formation of the desired coupling product under thermal conditions (in a sealed tube); upon investigation of the mechanism of heating, the toluene derivative benzotrifluoride (BTF) was tested as a solvent due to its high prevalence in microwave-assisted reactions, stemming from its unique polarisability.<sup>97</sup> In general, it was established that for both thermal and microwave-assisted Buchwald-Hartwig coupling reactions, utilising BTF as the solvent afforded the desired coupling product as the major product. Although microwave-assisted reactions typically have shorter reaction times compared to thermal reactions, only thermal reactions were conducted in this research due to the available facilities. Thus, using these previously optimised conditions, **44a** was reacted with **26** in an attempt to synthesise the desired 2-chloroquinoline, **50a**. The previously optimised conditions required a catalyst loading of only 0.5 mol %, however separate work had identified that attempted synthesis of **50a** using this catalyst loading did not afford any of the desired coupling product.<sup>66</sup> This apparent lack of reactivity is potentially due to sequestration of the Pd species, which could coordinate to the pyridyl nitrogen and alkene  $\pi$  bond simultaneously as **51** (Scheme 2.15), thus removing it from the catalytic cycle. Hence, the catalyst loading for this reaction was increased to 1.5 mol % to compensate for this hypothesised Pd sequestration, to afford the desired product **50a** as the major product (Scheme 2.16, Table 2.16).

2.7. SYNTHESIS OF CONTROL 2-AMINOQUINOLINE LIGANDS WITH A PYRIDYL SUBSTITUENT



Scheme 2.15: Reported attempted coupling of **44a** and **26** via previously optimised Buchwald-Hartwig reaction conditions,<sup>47</sup> and proposed catalyst sequestration intermediate, **51**. “L” indicates coordinate ligands.<sup>66</sup>



Scheme 2.16: Selective coupling of **44a** and **26** via previously optimised Buchwald-Hartwig reaction conditions<sup>47</sup> with increased catalyst loading.

Table 2.16: Observed products and yields from selective Buchwald-Hartwig coupling reaction between **44a** & **26**. <sup>a</sup> indicates product was observed in crude <sup>1</sup>H NMR and partially purified, but yield not calculated.

Compound	Yield (%)	$\delta_{\text{H}}$ C(3)H (ppm)	$\delta_{\text{H}}$ C(5)H (ppm)
<b>50a</b>	19	7.28	7.02
<b>52a</b>	<sup>a</sup>	7.03	7.72

## 2.7. SYNTHESIS OF CONTROL 2-AMINOQUINOLINE LIGANDS WITH A PYRIDYL SUBSTITUENT

To confirm the desired coupling had occurred at the 6-position of the quinoline ring, analysis of NMR and HRMS spectra was conducted, and compared to the reagents for the reaction. Analysis of HRMS spectra showed detection of the corresponding mass product, including the expected chlorine or bromine isotope distributions. Analysis of NMR spectra (both 1D and 2D) provided insights into the structure of the isolated compound. For the desired 6-substituted quinoline product **50a**, the  $^1\text{H}$  NMR spectra displayed significant upfield shifts of C(5)H and C(7)H, as consistent with coupling of an amine, imparting a greater *ortho/para* shielding effect by resonance, than a bromine atom. Conversely, the  $^1\text{H}$  NMR of the side product, **52a** displayed a significant upfield shift of C(3)H, due to coupling of the electron-donating amine at the 2-position. Extended structural insights were obtained from both [ $^1\text{H}$ ,  $^{13}\text{C}$ ] HMBC and ROESY spectra; the former was utilised to trace connectivity between piperidinyll hydrogens and either C(6) or C(2) of the quinoline ring, while the latter was used to determine proximity of piperidinyll hydrogens and either C(5)H & C(7)H, or C(3)H, for **50a** and **52a** respectively (Figure 2.32 & Figure 2.33).

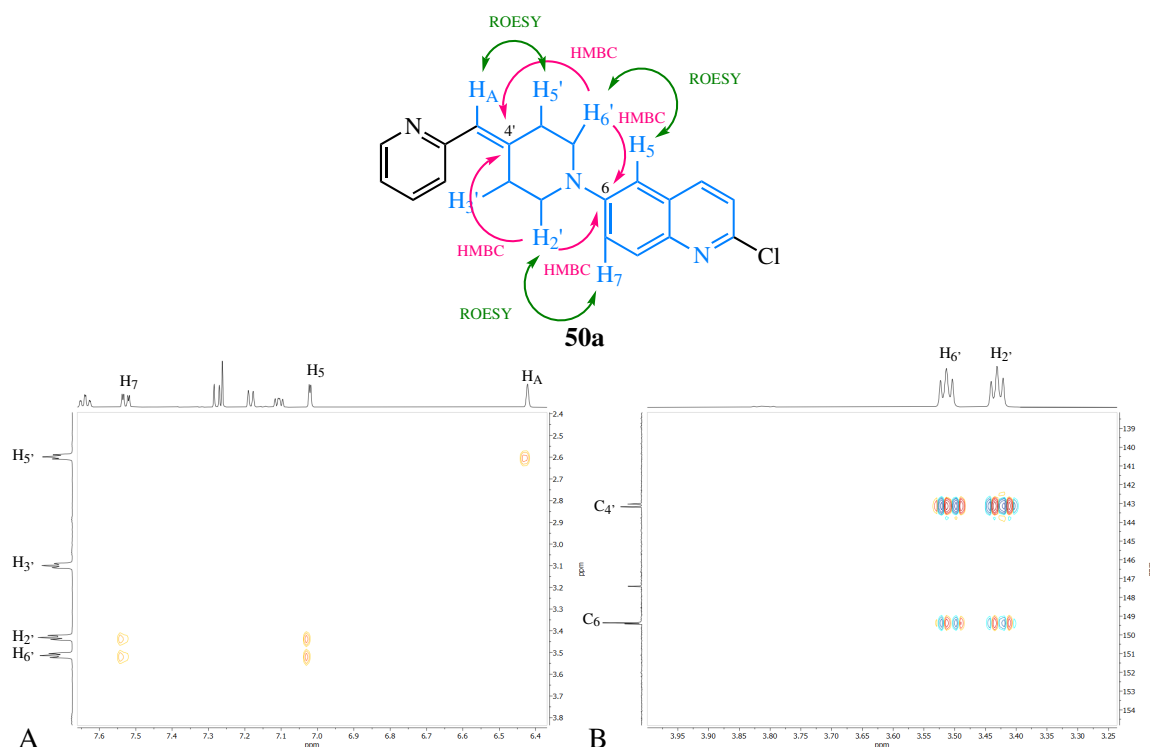


Figure 2.32: Structural analysis of **50a** via 2D NMR spectra, with (A) ROESY correlations shown in green, and (B) HMBC correlations shown in pink. Structural components of interest indicated in blue.

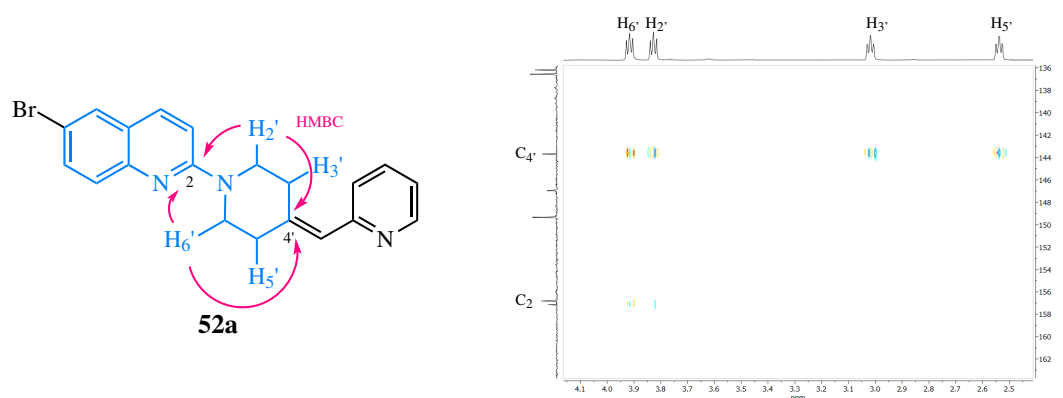


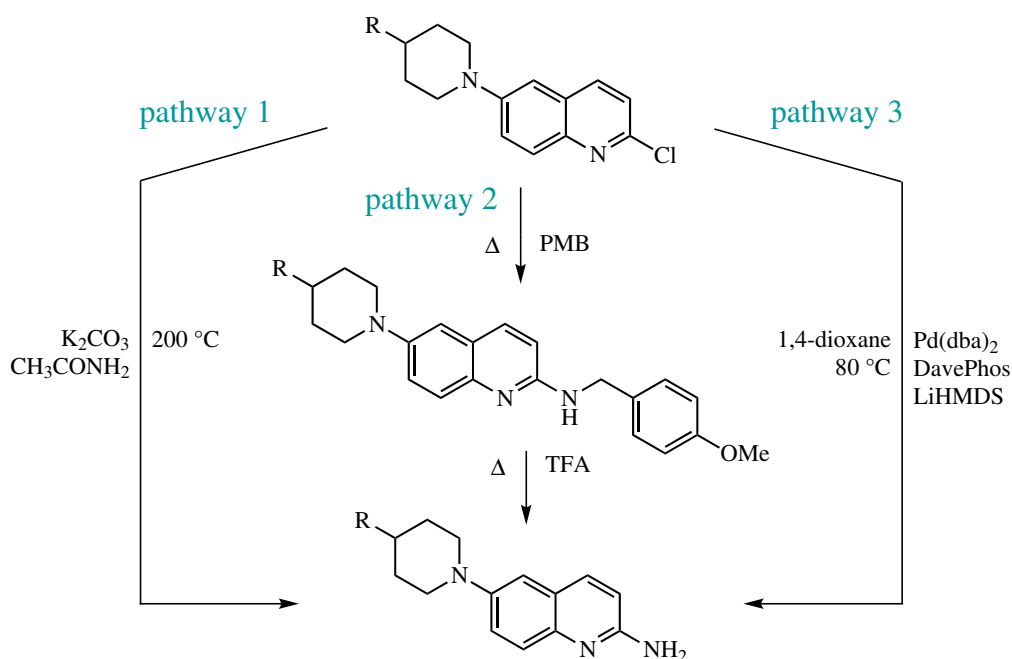
Figure 2.33: Structural analysis of **52a** via 2D [ $^1\text{H}$ , $^{13}\text{C}$ ] HMBC NMR spectra, with HMBC correlations shown in pink. Structural components of interest indicated in blue.

While the desired product was isolated in low yield, there was sufficient material to continue the synthesis, so subsequent amination at the 2-position to form **35a** was attempted.

### 2.7.3 Synthesis of 6-position substituted 2-aminoquinolines via Buchwald-Hartwig coupling

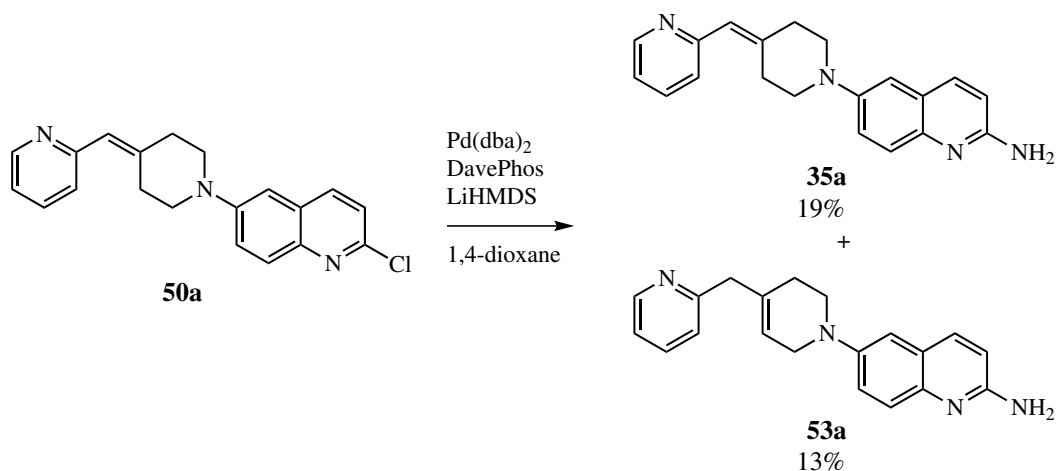
Previous work has investigated a variety of methods to achieve the synthesis of 2-aminoquinolines from the corresponding 2-chloroquinoline derivatives. The majority of early work utilised the method reported by Kóródi to introduce amine functionality at the 2-position, however these conditions required high temperatures for the reaction to occur, and the yields were quite variable, ranging from low to moderate (4-64%, pathway 1, Scheme 2.17).<sup>46,47,98</sup> Another previously utilised method involved a simple nucleophilic aromatic substitution reaction with *para*-methoxybenzylamine (pathway 2, Scheme 2.17).<sup>48</sup> The reaction conditions for introduction of the amine functionality were considerably milder compared to that of the Kóródi method, however an additional deprotection step was required for liberation of the desired 2-aminoquinoline ligand.<sup>48</sup> Favourably, a second (and therefore sequential) Buchwald-Hartwig coupling reaction was identified as an effective method for the transformation of 2-chloroquinolines to 2-aminoquinoline derivatives (pathway 3, Scheme 2.17).<sup>47</sup> Comparative studies between Buchwald-Hartwig coupling and Kóródi conditions for the amination of heterocycle-extended 2-chloroquinolines reported consistently higher yields for the former method over the latter (88-98%, c.f. 4-46%). Additionally, the Buchwald-Hartwig method generally afforded only minor (<5%) impurities, while the Kóródi method was reported to yield a complex mixture of products.<sup>47</sup>

## 2.7. SYNTHESIS OF CONTROL 2-AMINOQUINOLINE LIGANDS WITH A PYRIDYL SUBSTITUENT



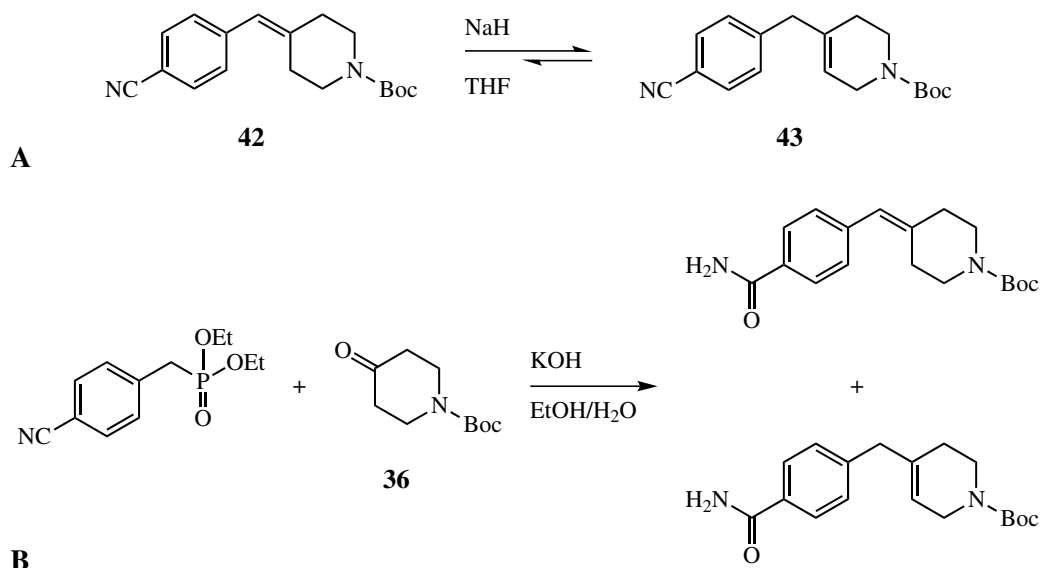
Scheme 2.17: Previously reported reaction conditions for the introduction of the 2-amine functionality for 6-substituted 2-chloroquinoline derivatives. Pathway 1 indicates the method reported by Kőródi.<sup>46,47,98</sup> Pathway 2 indicates a *para*-methoxybenzylamine protection and deprotection strategy.<sup>48</sup> Pathway 3 indicates a Buchwald-Hartwig coupling reaction, using LiHMDS as both the base and an ammonia equivalent.<sup>47,60</sup>

Although previous work has reported that the isolated 2-aminoquinoline products may be photosensitive,<sup>56</sup> it is unlikely that this large discrepancy in observed yields from each method is due to light-accelerated product degradation alone. Therefore, due to the general reliability of the Buchwald-Hartwig coupling reaction for introduction of the amine functionality,<sup>47,56,60</sup> these conditions were also employed for the transformation of **50a** to **35a** (Scheme 2.18).



Scheme 2.18: Synthesis of **35a** and corresponding THP isomer **53a** via Buchwald-Hartwig coupling reaction.

Successful amination was supported by both NMR and HRMS spectra; analysis of HRMS spectra indicated the presence of the desired mass product (detected  $m/z$  317.1761, required  $m/z$  317.1761). In addition, analysis of  $^1\text{H}$  and  $^{13}\text{C}$  NMR spectra revealed both C(3)H and C(3) were substantially shielded relative to those signals for **50a**, consistent with the introduction of an amine substituent at the 2-position, which is strongly *ortho/para* shielding by resonance (compared to Cl). Furthermore, a broad singlet integrating to 2H was observed in the  $^1\text{H}$  NMR spectrum, consistent with a primary amine. Interestingly, formation of the corresponding tetrahydropyridine (THP) isomer **53a** (Scheme 2.18) was also observed. From NMR spectra, indicative  $^1\text{H}$  NMR signals for tetrahydropyridine hydrogens were observed which were consistent with those reported in the literature.<sup>56</sup> Formation of THP isomers has been investigated previously, where it was hypothesised their isomerism is catalysed by hydroxide-containing bases (e.g., KOH, LiOH), or bases prone to hydroxide formation (e.g., NaH) (Scheme 2.19, and Scheme 2.6 in Section 2.7.1).<sup>56</sup> If an older supply of LiHMDS solution was used in the reaction, the seal on the bottle would have been punctured previously, so slow hydrolysis of the LiHMDS to LiOH within the bottle could reasonably occur, and introduce a hydroxide-containing base to catalyse THP isomerisation. A similar effect would be observed if the reaction solvent was not sufficiently dried, however this was not investigated. The combined yields of **35a** and **53a** indicated the reaction had occurred in moderate yield (32%).



Scheme 2.19: Previously reported reactions with hydroxide-containing or hydroxide-producing bases to afford THP formation. (A) Isomerisation of a methylenepiperidine derivative using NaH (and consequently NaOH) to afford the corresponding THP isomer. (B) Concurrent nitrile hydrolysis and alkene synthesis via Horner-Emmons-like conditions to afford the methylenepiperidine derivative and THP isomer.<sup>56</sup>

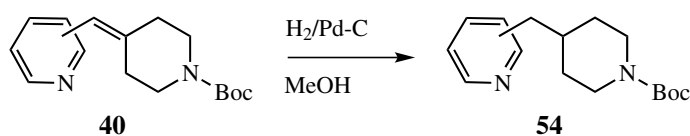


## 2.7. SYNTHESIS OF CONTROL 2-AMINOQUINOLINE LIGANDS WITH A PYRIDYL SUBSTITUENT

Notably, THP isomers for similar compounds have been reported, and in each case separation of each isomer had been very difficult by chromatographic methods due to the isomers exhibiting similar retention factors. While some separation of isomers was obtained for **35a** and **53a**, the isolated ligand masses were insufficient for biological binding assay investigation. Due to the formation of generally inseparable isomers, and reduced yields through hypothesised Pd complexation in the first Buchwald-Hartwig coupling reaction, it was envisaged that the desired ligand **18a** might be more accessible from an earlier, reduced intermediate. Thus, optimisation for the synthesis of **35a** was not pursued further.

### Synthesis of reduced pyridylmethyl piperidine derivatives

In an attempt to synthesise the desired ligands **18a** and **18b** it was envisaged that early reduction of the alkene bond may help overcome some of the previously identified challenges encountered during amine-quinoline coupling reactions. Early reduction of the alkene bond would prevent synthesis of **35a**, as the common precursor **50a** would not be readily accessible. While it would be desirable to test the binding affinity of the novel ligand **35a**, the primary aim of this chapter was to synthesise control ligands with known activity for binding assay validation and optimisation. Therefore, the priority was for synthesis of **18a** and **18b**, with the revised synthetic pathway analogous to that suggested in Scheme 2.3; reduction of the alkene bond in **40** derivatives was achieved using canonical catalytic hydrogenation conditions, in moderate-high yields (Scheme 2.20, Table 2.17).



Scheme 2.20: Synthesis of pyridylmethyl Boc-protected piperidine derivatives **54** via hydrogenation.<sup>56</sup>

Table 2.17: Yields for pyridylmethyl Boc-protected piperidine **54** formation from **40** derivatives via hydrogenation reaction (Scheme 2.20). \* indicates residual triphenylphosphine oxide was present in starting material from previous reactions, so reported yield is a theoretical minimum.

Compound	Pyridyl substitution	Yield (%)
<b>54a</b>	2	96
<b>54b</b>	3	66*

Successful reduction of the alkene bond was supported by analysis of HRMS spectra; for **54b**, a mass product with  $m/z$  277.1908 was detected (expected  $m/z$ : 277.1911). The  $^1\text{H}$  NMR spectra was further diagnostic for the desired reduction; for both **54a** and **54b**, the  $^1\text{H}$  alkene signal was absent.

Additionally, the piperidinyl  $^1\text{H}$  signals were more complex than those of the precursors, **40a** and **40b** (Figure 2.34). This would be consistent with the desired hydrogenation products; reduction of the alkene bond would afford reduced planarisation about the piperidine ring, allowing it to adopt a more chair-like conformation. Due to this decreased planarisation, ring-flipping of piperidine ring is anticipated to be slower on the NMR timescale (i.e., **54** c.f. **40**), and therefore would produce distinct chemical environments for axial and equatorial hydrogens, although some broadness still remained as the Boc-protecting group was retained. Again, some of the triphenylphosphine oxide impurity was carried through during the synthesis of **54b**, but as no thorough chromatographic purification was undertaken in this step, its retention is not surprising.

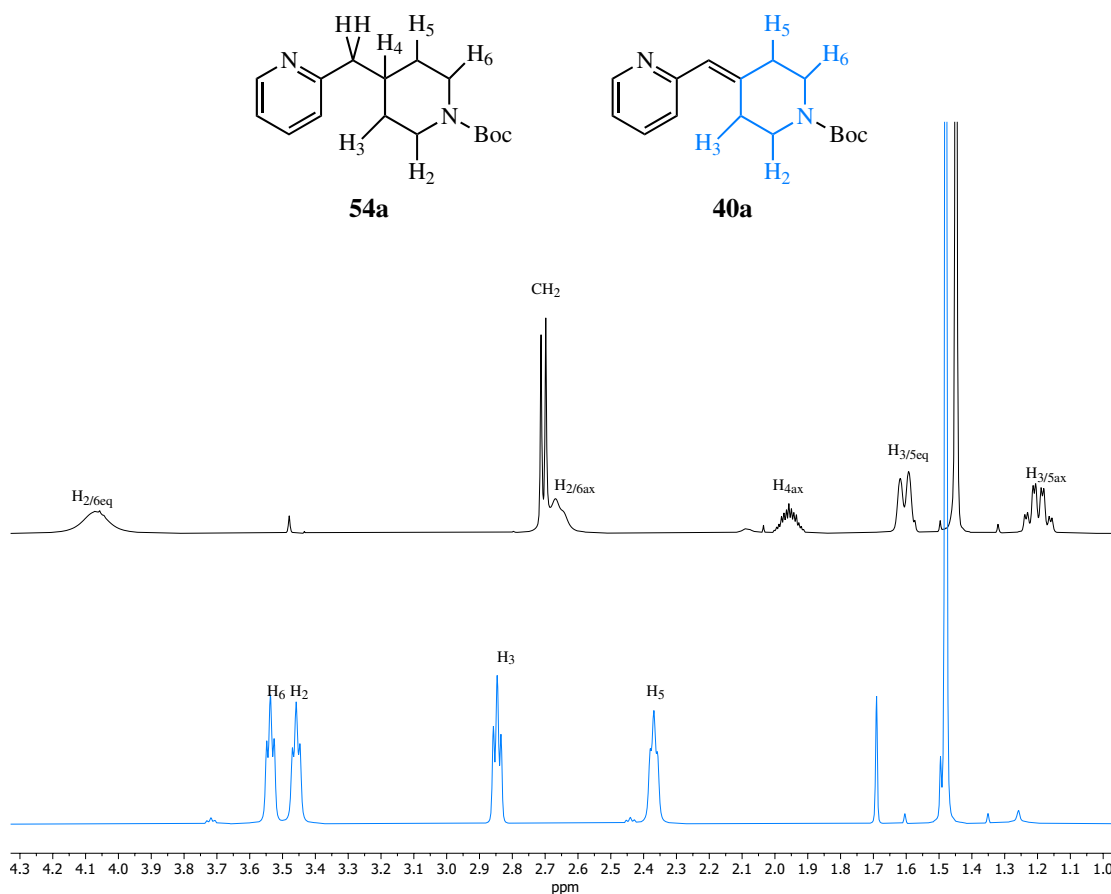
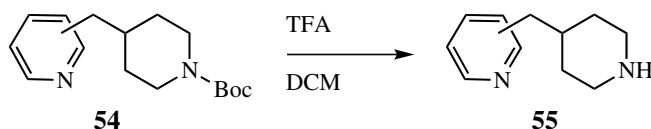


Figure 2.34: Comparison of  $^1\text{H}$  NMR spectra ( $\delta_{\text{H}}$ : 1.0 - 4.3 ppm) of **40a** (black) and **54a** (blue), indicating increased piperidinyl ring signal complexity upon alkene bond reduction by hydrogenation. Integrations shown in green.

## 2.7. SYNTHESIS OF CONTROL 2-AMINOQUINOLINE LIGANDS WITH A PYRIDYL SUBSTITUENT

---

Liberation of the free amine **55** was again undertaken via TFA-mediated deprotection of the Boc-protected **54** derivatives, in moderate-high yields (Scheme 2.21, Table 2.18). In this case, the yields were considered acceptable; for both derivatives, the workup involved a liquid-liquid extraction from NaHCO<sub>3(aq)</sub> into either DCM or 3:1 CHCl<sub>3</sub>:isopropanol, it is therefore likely that some reduction in yield occurred due to product partitioning into the aqueous phase.



Scheme 2.21: Synthesis of pyridylmethyl piperidines **55** via Boc deprotection.

Table 2.18: Yields for pyridylmethyl piperidine **55** liberation from **54** derivatives via Boc deprotection (Scheme 2.21). \* indicates yield over two steps ^ indicates residual triphenylphosphine oxide was present in starting material from previous reactions, so reported yield is a theoretical minimum.

Compound	Pyridyl substitution	Yield (%)
<b>55a</b>	2	74*
<b>55b</b>	3	62^

Successful deprotection to liberate the amine derivatives **55** was identified by both HRMS and more significantly, NMR spectra. Analysis of HRMS spectra indicated the presence of the desired mass product for each derivative (detected  $m/z$  of 177.1388 and 199.1211, required  $m/z$  of 177.1386 and 199.1211 for protonated and Na adducts respectively). Significantly, analysis of <sup>1</sup>H NMR spectra revealed loss of the Boc group by absence of the 9H singlet corresponding to the *tert*-butyl group. Successful product formation also evidenced by the resolution of the 2H piperidine ring signals; loss of the bulky Boc group would remove the fluxional limitations imposed at the piperidinyl nitrogen in **54** derivative. Loss of the slow-rotating carbamate bond of the Boc group is exemplified by piperidinyl H signal resolution in <sup>1</sup>H NMR, particularly for comparison of **54** and **55** derivatives. This would suggest that of the arylmethyl piperidinyl derivatives discussed so far in this thesis, **55** is expected to have the least sterically-hindered, most-chair-like conformation, resulting in distinct, more resolved 2H piperidinyl signals in <sup>1</sup>H NMR spectra, as consistent with Figure 2.35. Similar trends were observed in <sup>13</sup>C NMR spectra following Boc group removal from **54**, where broad piperidinyl ring signals were substantially resolved to characteristically sharp <sup>13</sup>C signals (data not shown).

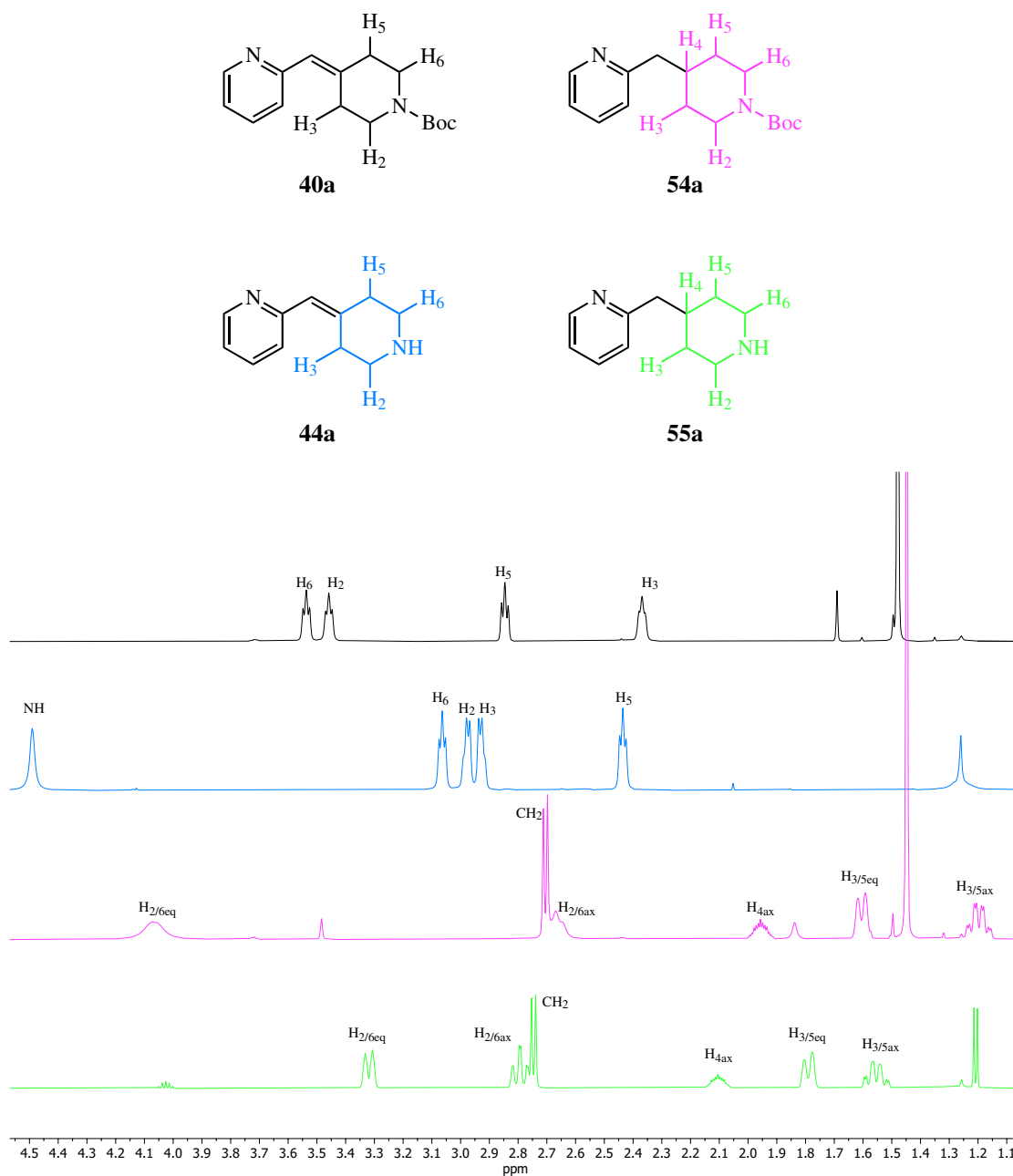
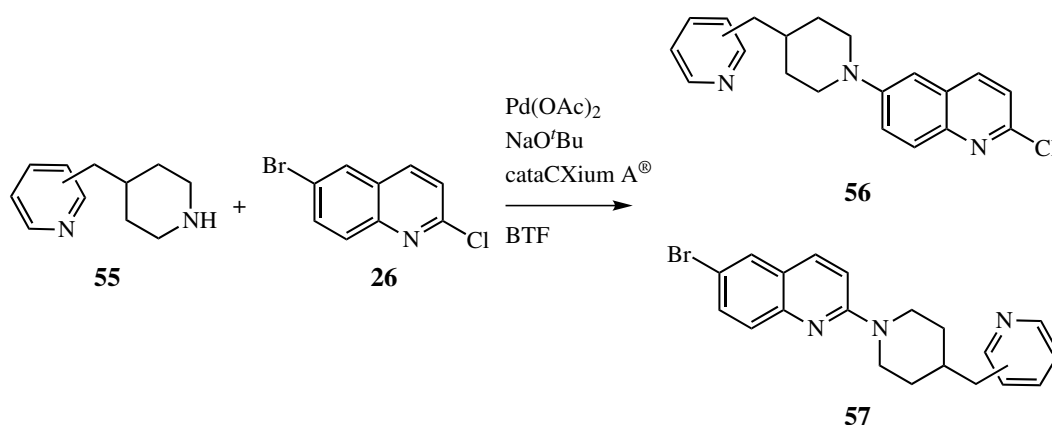


Figure 2.35: Comparison of  $^1\text{H}$  NMR spectra ( $\delta_{\text{H}}$ : 1.1 - 4.5 ppm) of differentially substituted piperidine derivatives, demonstrating the effects of steric bulk, altered ring-flipping and chair-like structure on signal resolution. Derivatives include **40a** (black), **44a** (blue), **54a** (pink), and **55a** (green).

### 2.7.4 Synthesis of reduced 6-position substituted 2-aminoquinolines via Buchwald-Hartwig coupling

It was envisaged that synthesis of the key intermediate 6-substituted 2-chloroquinoline derivatives **56** could be achieved through selective Buchwald-Hartwig coupling with **26**. Therefore, those conditions that were previously optimised for selective 6-position coupling of **26** (Scheme 2.14) were applied with **55** derivatives for the synthesis of **56** derivatives (Scheme 2.22 and Table 2.19).



Scheme 2.22: Synthesis of pyridylmethyl piperidine-substituted quinolines **56** and **57** via Buchwald Hartwig coupling reaction.<sup>47,56</sup>

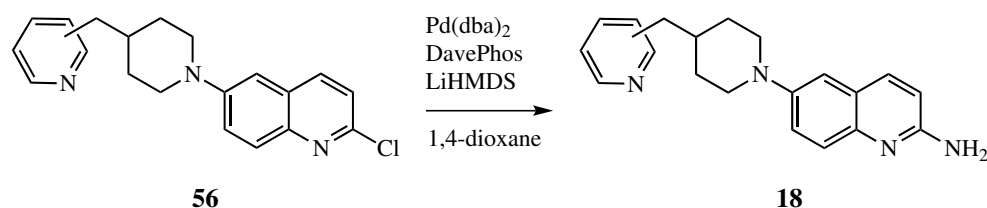
Table 2.19: Yields for synthesis of pyridylmethyl piperidine-substituted quinolines from **55** derivatives via Buchwald Hartwig coupling reaction (Scheme 2.22). <sup>a</sup> indicates **57a** was observed in crude <sup>1</sup>H NMR spectra; a small amount of **57a** was isolated for characterisation, but an isolated yield was not obtained. <sup>b</sup> indicates trace amounts of **57b** were observed in crude <sup>1</sup>H NMR spectra, but product was not isolated. <sup>^</sup> indicates residual triphenylphosphine oxide was present in starting material from previous reactions, so reported yield is a theoretical minimum.

Amine	Pyridyl substitution	Yield <b>56</b> (%)	Yield <b>57</b> (%)
<b>55a</b>	2	11	<sup>a</sup>
<b>55b</b>	3	26 <sup>^</sup>	<sup>b</sup>

Formation of the desired products was again supported by analysis of HRMS and NMR spectra. The desired mass products in the expected chlorine isotope distributions were observed for both **56a** and **56b**, and similarly for the side product **57a** the expected mass products in the expected bromine isotope distribution. Successful coupling at the 6-position was again identified by upfield shifts of quinolinyl C(5)H in <sup>1</sup>H NMR spectra due to electron donation by resonance from the piperidinyl nitrogen. Similarly, formation of the 2-substituted side-product **57a** was identified by upfield shifts of quinolinyl C(3)H in <sup>1</sup>H NMR spectra due to electron donation by resonance from the piperidinyl nitrogen, and HMBC correlations between piperidinyl C(2'/6')H and quinolinyl C(2). It is noted

that the yield obtained for **56a** is lower than that reported previously,<sup>56</sup> and also slightly lower than that reported for formation of **50a**; it is not immediately clear why this is the case, but it is possible that if an older sample of sodium *tert*-butoxide was used, then it may have been substantially hydrolysed to NaOH, therefore less of the desired active base would be present to participate in the catalytic cycle, thus reducing the yield. Again for **56b**, some triphenylphosphine oxide was carried through from previous reactions, so only a minimum yield could be calculated. Regardless, despite the slightly lower yields, sufficient material was obtained in both cases to progress to the final synthetic step.

The final step in the synthesis of **18** ligands required a second sequential Buchwald-Hartwig coupling reaction. This was achieved using chloroquinoline derivatives **56a** and **56b**, and previously optimised conditions, including the use of LiHMDS as both a base and ammonia equivalent, to introduce the amine functionality at the 2-position of the quinoline ring as shown in Scheme 2.23, in low to moderate yields (Table 2.20).



Scheme 2.23: Synthesis of pyridylmethyl piperidine-substituted 2-aminoquinolines **18** via Buchwald Hartwig coupling reaction.<sup>47,56</sup>

Table 2.20: Yields for synthesis of pyridylmethyl piperidine-substituted 2-aminoquinoline **18** from **56** derivatives via Buchwald Hartwig coupling reaction (Scheme 2.23). \* indicates residual triphenylphosphine oxide was present in starting material from previous reactions, so reported yield is a theoretical minimum.

Compound	Pyridyl substitution	Yield (%)
<b>18a</b>	2	44
<b>18b</b>	3	19*

Successful synthesis of the target ligands **18a** and **18b** was supported primarily by HRMS and NMR spectra. In both instances, analysis of HRMS spectra revealed mass products consistent with that of the desired product ( $m/z$  required 319.1917; found 319.1918 & 319.1926 for **18a** and **18b** respectively). Furthermore, analysis of <sup>1</sup>H NMR spectra revealed a characteristic upfield shift for C(3)H of the quinolinyl ring, consistent with the introduction of an amine as an electron-donating by resonance group. The presence of a broad singlet near  $\delta_{\text{H}}$  4.90-5.00 ppm, integrating to approximately 2H, was also indicative of the presence of a primary amine (Figure 2.36). The yield for

## 2.7. SYNTHESIS OF CONTROL 2-AMINOQUINOLINE LIGANDS WITH A PYRIDYL SUBSTITUENT

formation of **18a** is generally consistent with that reported previously;<sup>56</sup> while the yield for **18b** is lower,<sup>66</sup> it has been recorded as a minimum due to the presence of triphenylphosphine oxide in the chloroquinoline reagent, **56b** (Table 2.20). Importantly, the triphenylphosphine oxide impurity was removed during chromatography, therefore both ligands **18a** and **18b** were sufficiently pure for SPR assays (Figure 2.36).

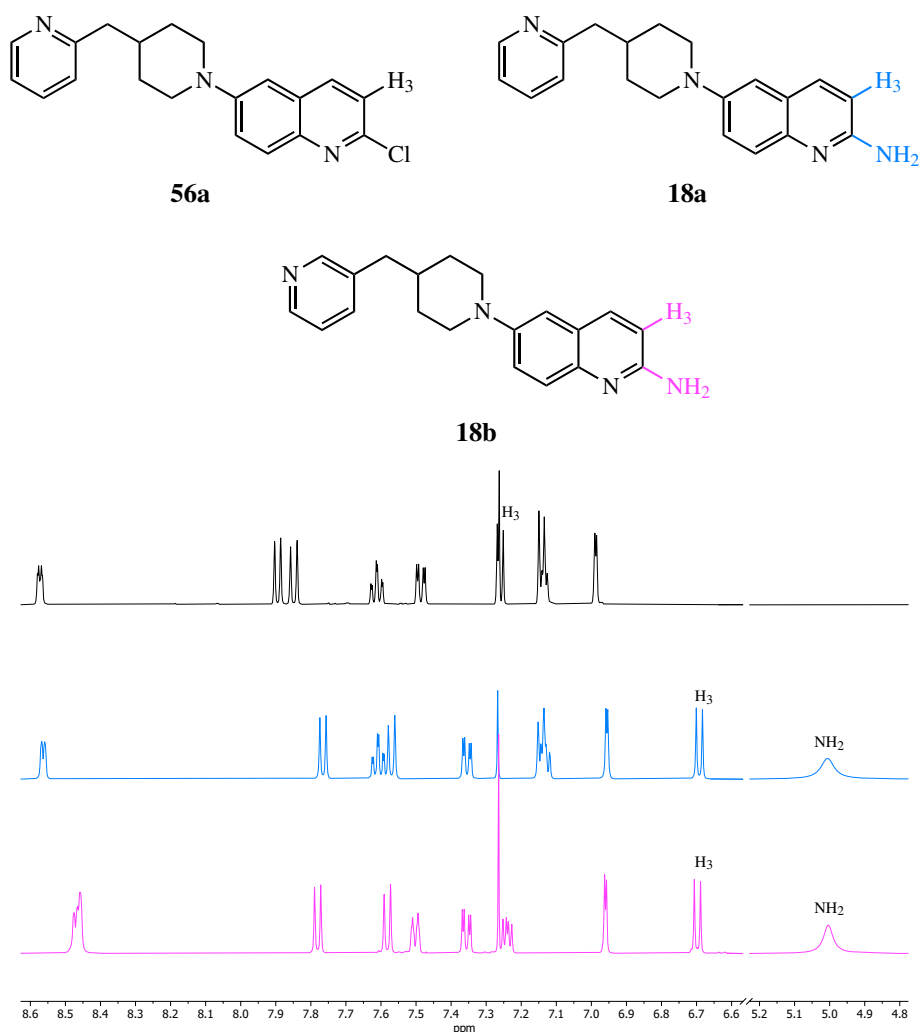


Figure 2.36: Comparison of truncated <sup>1</sup>H NMR spectra ( $\delta_{\text{H}}$ : 4.8 - 8.6 ppm) of **56a** (black), **18a** (blue), and **18b** (pink), indicating different chemical shifts for C(3)H and emergence of amine signal.

## 3 | Synthesis of simple 6-position substituted 2-aminoquinoline ligands

### 3.1 Introduction

Previous investigations into the development of ligands for the Tec SH3 domain revealed that 6-position heterocyclic substituted 2-aminoquinolines with a piperidine substituent had improved binding affinity relative to the previous hit compound **2**.<sup>47</sup> Furthermore, modification of the ligand through including either an electron-deficient substituent, an electron-withdrawing by resonance substituent, biaryl benzyl substituents, or increasing rigidity (i.e., reduced number of rotatable bonds) resulted in further improved binding affinity, to afford some of the strongest identified ligands to date (**18a**, **18b**, **19**, **20**, **23**, **24**, **25**, **35b** and **58**, Table 3.1).<sup>56,66</sup>

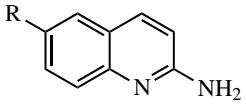
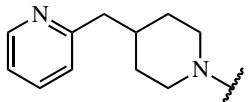
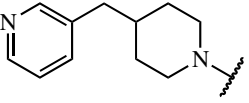
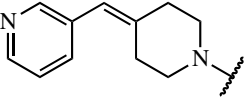
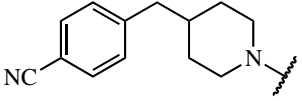
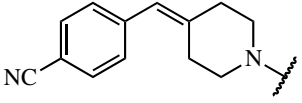
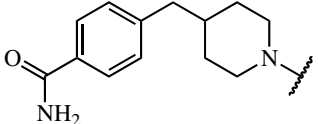
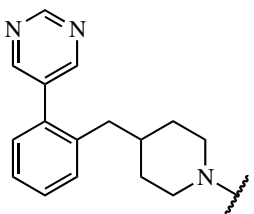
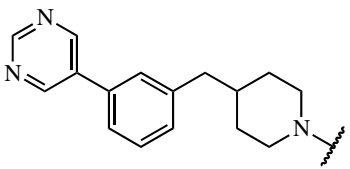
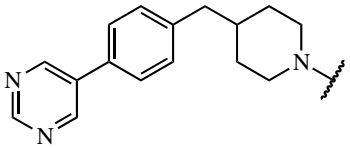
Further work is required to investigate the nature of the binding interaction of these ligands on the protein surface, and to rationally develop ligands based upon the general structure **15** with improved binding affinity. Previous attempts to elucidate the structure of the 3D protein-ligand complex have generally been unsuccessful, likely due to insufficiently strong binding affinity of the ligands available. Consequently, in the absence of a solved ligand-bound protein crystal structure, exploration of the binding surface would be most informative through SAR studies with a series of structurally similar compounds derived from the **15** skeleton against the Tec SH3 domain.

During previous ligand binding assays, the binding affinity of many synthesised ligands could not be determined as the ligands were insoluble under biologically relevant assay conditions.<sup>56</sup> This is not surprising; the surface of the Tec SH3 domain (like many PPI interfaces) is quite hydrophobic, therefore for a ligand to bind to the protein surface, it too must have a comparable degree of hydrophobicity. Interestingly, of the strongest ligands identified for the Tec SH3 domain thus far, the binding affinities tended to increase as the solubility of the ligands under assay conditions also increased. While these solubilities were not quantified, qualitative trends emerged, where solubility was improved for ligands with *clogP* values <5 (and were generally consistent with Lipinski's Rule of 5).<sup>32</sup> Therefore, it was proposed that a range of extended 6-heterocyclic 2-aminoquinoline compounds with a benzylpiperazine-derived substituent would have improved solubility under as-



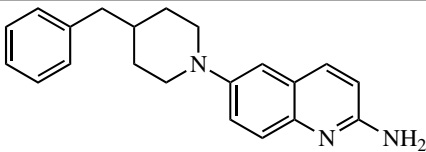
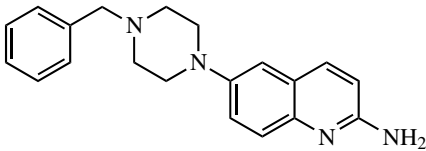
### 3.1. INTRODUCTION

Table 3.1: Binding affinities of previously reported 6-heterocycle substituted 2-aminoquinoline derivatives, with high binding affinity for the Tec SH3 domain (determined by SPR assays)<sup>56,66</sup> and calculated *logP* (*clogP*) values.<sup>61</sup>

			
Compound	R =	<i>K<sub>d</sub></i> (μM)	<i>clogP</i>
18a		5 ± 1	3.38
18b		3.0 ± 0.7	3.50
35b		1.9 ± 0.1	3.18
19		2.0 ± 0.5	4.58
58		2.2 ± 0.7	3.25
20		2.0 ± 0.1	3.57
23		7 ± 1	4.44
24		4.1 ± 0.7	4.44
25		2.4 ± 0.2	4.44

say conditions relative to the parent compound **15** (Table 3.2), and could be used to investigate the binding interaction of such ligands with the Tec SH3 domain. This may lead to identification of a strong-binding ligand for the Tec SH3 domain, which could aid the determination of the structure of the 3D protein-ligand complex.

Table 3.2: Binding affinities of previously reported 6-heterocycle substituted 2-aminoquinoline derivatives (determined by 2D NMR chemical shift perturbation assays) and calculated  $\log P$  ( $clogP$ ) values.<sup>61</sup>

Compound	Structure	$K_d$ ( $\mu\text{M}$ )	$clogP$
<b>15</b>		$9 \pm 1$	4.72
<b>17a</b>		$28 \pm 8$	3.58

While the binding affinity of **17a** for the Tec SH3 domain is weaker than for **15** (Table 3.2), it is anticipated that investigating SAR studies of structurally-similar **17a** derivatives will help identify ligands with improved binding affinity.

The range of derivatives investigated in this chapter (Figure 3.1) were proposed to improve ligand solubility under biologically-relevant assay conditions, and also to investigate the effect upon binding affinity of altering the geometry about the methylene group in the benzyl substituent, through flattening of the piperazinyl ring (relative to a piperidinyl ring) (**17** and **59**), or flattening of the piperazinyl ring, with restricted rotation about the methylene group in the benzyl substituent via substitution for an amide bond (**60** and **61**).

The derivatives within these families were chosen to investigate the effects of adding simple substituents to the benzyl group; they include simple hydrophobic (methyl) groups (**b-c**), electron-withdrawing by induction/electron-donating by resonance fluoro groups (**d-e**) and methoxy groups (**f-g**), and electron-withdrawing by resonance nitrile derivatives (**h-k**). Previous studies revealed that ligands with *meta*- and *para*-substituted benzyl groups had improved binding affinities relative to ligands with *ortho*-substituted benzyl groups, likely due to steric hindrance of the *ortho* substituent with the benzylpiperidinyl group. Hence, only ligands with *meta*- and *para*-substituted

### 3.2. GENERAL SYNTHETIC PATHWAY

---

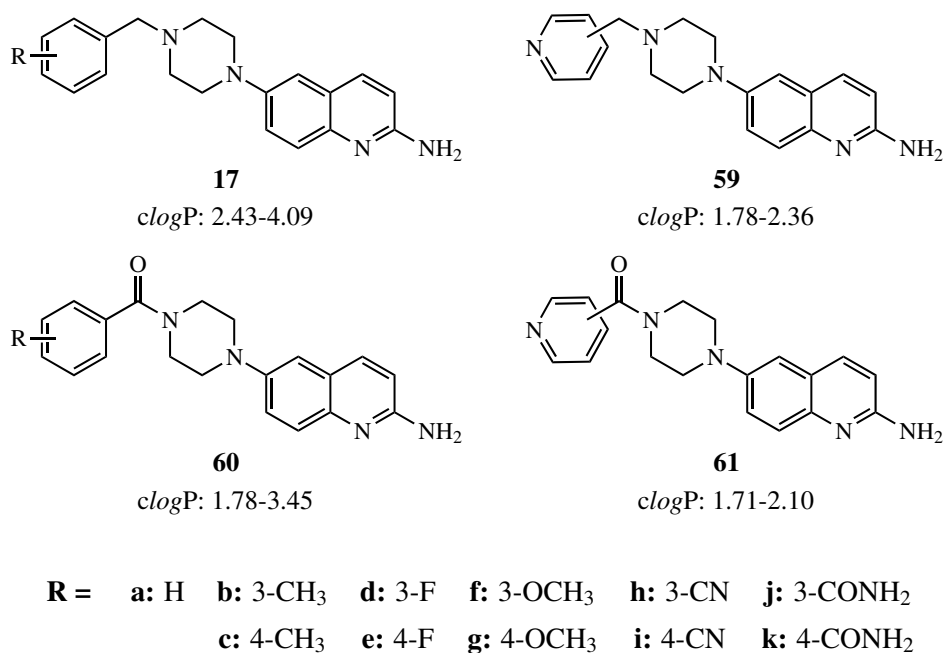
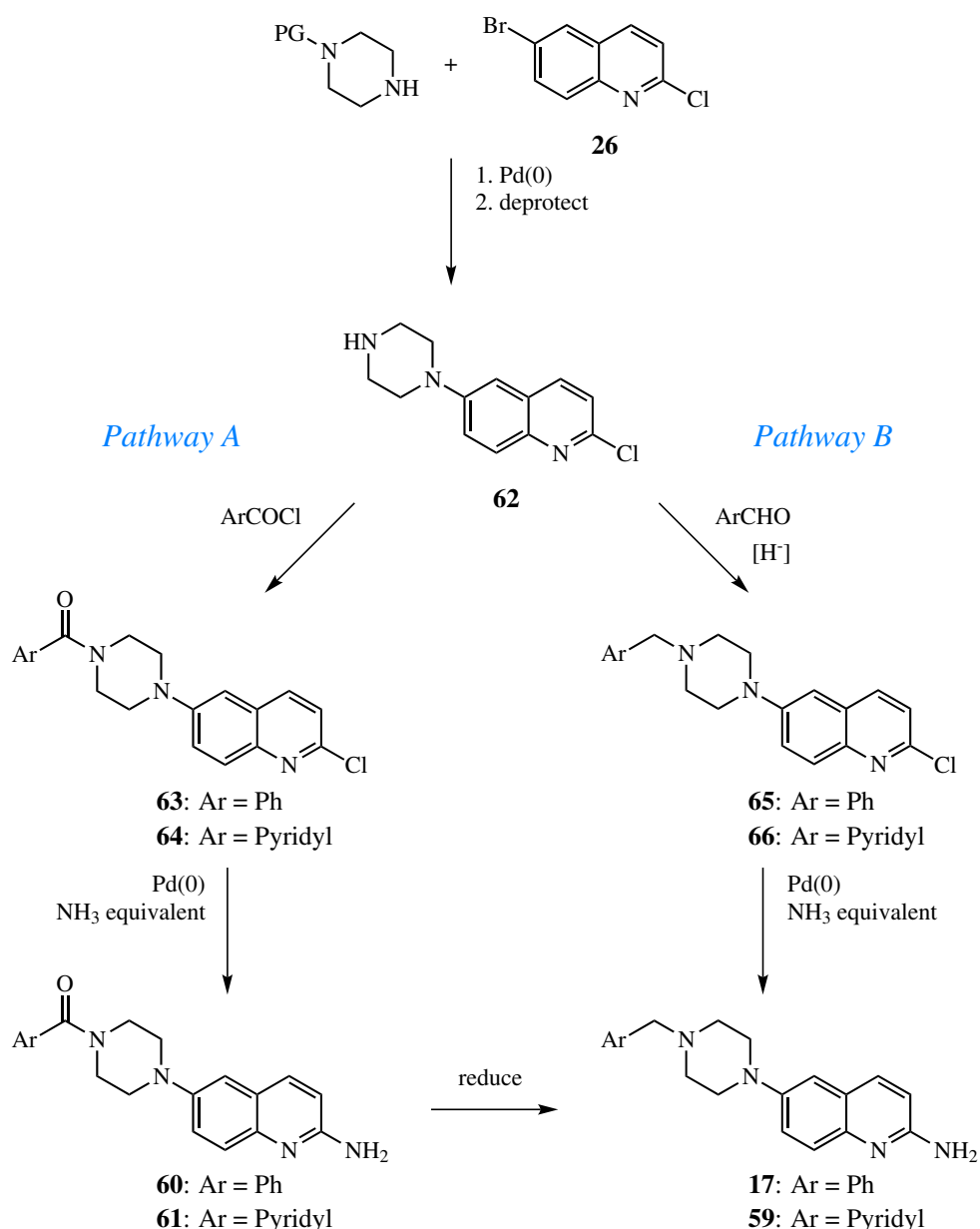


Figure 3.1: Proposed 6-position substituted 2-aminoquinoline ligand families with calculated *logP* values to investigate a more hydrophilic benzylpiperidinyloxy derivative. *LogP* (*clogP*) values calculated using Marvin by ChemAxon.<sup>61</sup>

benzyl groups will be investigated in this project. A range of pyridyl derivatives are also proposed, to further investigate how reduced electron density in the aromatic ring affects the binding interaction.

### 3.2 General synthetic pathway

The proposed ligand derivatives to be investigated in this chapter (**17**, **59**, **60** and **61**) have not been reported previously in the literature (with the exception of **17a**), therefore development of synthetic pathways was required. Due to the number of derivatives proposed for each ligand family, it was desirable to develop generally applicable synthetic routes; in particular, it would be beneficial to introduce ligand derivatisation as late as possible throughout the synthetic pathway, as this would provide an opportunity for efficient large-batch synthesis and purification of common intermediate compounds. Furthermore, as ligand families **60** and **61** differ from **17** and **59** ligand families by the substitution of a tertiary amide for a tertiary amine, in principle it would be possible to derive **17** and **59** from **60** and **61** respectively via amide reduction. The general proposed synthetic pathways for the synthesis of ligand families **17**, **59**, **60** and **61** is shown in Scheme 3.1.



Scheme 3.1: Proposed general synthetic pathways for the synthesis of benzylpiperazinyl-derived ligand families, **17**, **59**, **60** and **61**. Ar = aryl, PG = protecting group.

With reference to Scheme 3.1, both proposed synthetic pathways share the same starting materials (mono-protected piperazine and **26**), and subsequent reactions to form an advanced common intermediate, **62**. Formation of **62** is anticipated by a selective Buchwald-Hartwig coupling reaction between mono-protected piperazine and **26**, and subsequent by removal of the piperazinyl amine protecting group. Following purification of **62**, the desired ligand families **17**, **59**, **60** and **61** could be synthesised by Pathway A or Pathway B. Pathway A suggests derivatisation of **62** via amidation with the appropriate acyl chloride derivative, followed by amine coupling at the 2-position on the quinoline ring via a second Buchwald-Hartwig coupling reaction, to afford the ligand families **60**

and **61**. The remaining ligand families **17** and **59** could be accessed from **60** and **61** via amide reduction. Alternatively, Pathway B suggests derivatisation of **62** via reductive amination with the corresponding aryl aldehyde derivative, followed by a Buchwald-Hartwig coupling reaction to afford the ligand families **17** and **59**.

Importantly, both Pathways A and B introduce derivatisation from acyl chlorides (for **60** and **61** ligands) and aldehydes (for **17** and **59** ligands), which are readily synthesised from the appropriate commercially-available carboxylic acid derivatives. However, ligand synthesis following Pathway A provides an opportunity for derivatisation of the amide group, and therefore more efficient synthesis of **17** and **59** from **60** and **61**. Conversely, ligand synthesis following Pathway B is comparatively linear. Overall, synthesis of **17**, **59**, **60** and **61** ligand families via Pathway A was deemed more attractive and was therefore undertaken.

## 3.3 Synthesis of simple 6-arylamidopiperazinyl-2-aminoquinolines

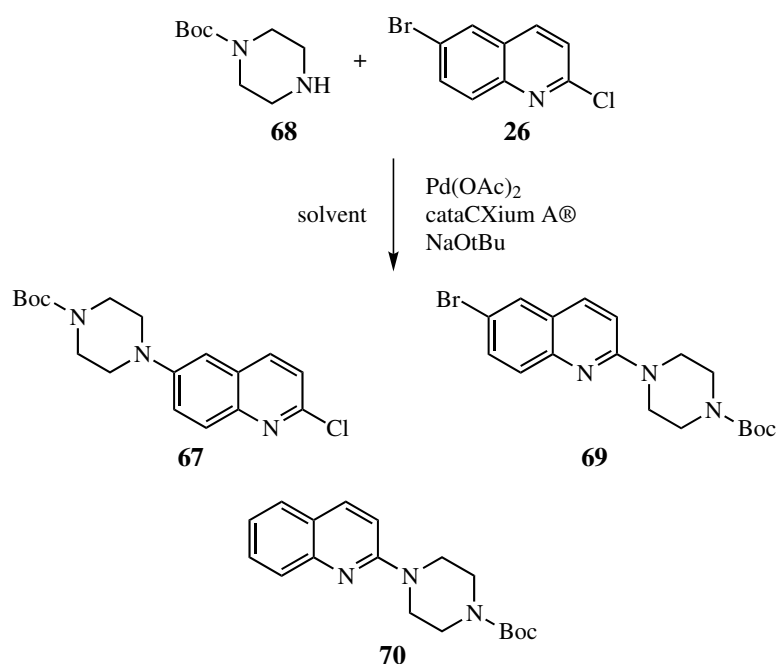
### 3.3.1 Synthesis of 6-position substituted 2-chloroquinoline derivatives

As described in Chapter 2, general reaction conditions for the selective Buchwald-Hartwig coupling of heterocyclic amines at the 6-position of **26** have been reported previously.<sup>47</sup> From analysis of relevant literature, identification of successful reaction conditions for Buchwald-Hartwig couplings (and particularly generally-applicable reaction conditions) is quite challenging, and typically requires extensive optimisation of each variable of the catalytic cycle.<sup>99,100</sup> Even upon optimisation of (general) reaction conditions, the yields of desired products can vary substantially between seemingly similar substrates,<sup>47,100</sup> so it is not surprising to see yields which would normally be classified as 'poor' being considered 'acceptable' in the context of Buchwald-Hartwig coupling reactions. Conditions for synthesis of the desired intermediate **67** have been reported previously, indicating high selectivity for the desired 6-position coupling in good yields,<sup>47,60</sup> therefore there was little incentive to conduct an in-depth investigation into further optimisation of reaction yield.

Reaction conditions for synthesis of 2-chloroquinoline compounds similar to **67** by selective Buchwald-Hartwig coupling reaction utilised the same catalytic system as reported previously,<sup>47,60</sup> but differed in choice of solvent. Previous synthesis of **67** reported toluene as the reaction solvent,<sup>47</sup> while synthesis of comparable intermediates for historical ligands **18a** and **18b** reported either tri-

### 3.3. SYNTHESIS OF SIMPLE 6-ARYLAMIDOPIPERAZINYL-2-AMINOQUINOLINES

fluorotoluene (BTF) or 1,4-dioxane as the reaction solvent.<sup>56,66</sup> Generally, BTF or 1,4-dioxane were utilised to ensure suitable reagent solubility, but in some cases differing chemoselectivity for amine coupling at the Br, rather than Cl in **26** was reported. There are reports describing the more efficient heating of BTF as a reaction solvent (compared to toluene), resulting in a faster reaction.<sup>97</sup> Therefore, despite published conditions for the synthesis of **67**,<sup>47</sup> attempts to optimise the desired product yield through solvent substitution were undertaken (Scheme 3.2, Table 3.3).



Scheme 3.2: Obtained products from various Buchwald-Hartwig coupling reactions with **26** and **68**, where the reaction is completed in a sealed tube.

Table 3.3: Effect of reaction solvent upon isolated yields of products from Buchwald-Hartwig coupling reactions between **68** and **26** (see Scheme 3.2). <sup>a</sup> indicates only 50% conversion of limiting reagent was observed in <sup>1</sup>H NMR spectra of the crude product. N/A indicates characteristic <sup>1</sup>H NMR signals for the compound were not observed during analysis of <sup>1</sup>H NMR of the crude product.

Solvent	Reaction period (hrs)	Yield (%)		
		<b>67</b>	<b>69</b>	<b>70</b>
toluene	20	69	5	0
BTF	17	<50 <sup>a</sup>	N/A	N/A
1,4-dioxane	18	9	0	4

From Table 3.3, the reported reaction conditions using toluene as a solvent yielded good selectivity for the desired 6-position coupled product **67**; relatively poor conversion was observed for the reaction conducted in BTF, while substantially poorer yields were observed for the reaction conducted in 1,4-dioxane. This suggests that the reagents may not be soluble in BTF and 1,4-dioxane under the reaction conditions, leading to poorer product conversion. Furthermore, the reaction conducted in

### 3.3. SYNTHESIS OF SIMPLE 6-ARYLAMIDOPIPERAZINYL-2-AMINOQUINOLINES

1,4-dioxane displayed worse chemoselectivity than the reaction in toluene, due to the formation of the reduced product **70**. The period of the reaction was also important; synthesis of control ligands **18a** and **18b** (from Chapter 2) for the analogous quinoline-coupling reaction were complete within 16 hrs, however coupling of **68** and **26** was incomplete after 16 hrs, with some recovery of starting material; generally, successful formation of **67** was only observed after a period of 20 hrs (data not shown). In this case, there were no observable benefits of using alternative solvents to toluene for the selective coupling of **68** with **26** via Buchwald-Hartwig reaction, despite use of these solvents for similar derivatives in the same coupling reaction.<sup>47,56</sup>

Formation of **67** was determined by analysis of HRMS and NMR spectra, and comparison to literature. From HRMS experiments, the expected mass product was observed, including the corresponding mass products at the expected abundances for naturally-occurring Cl isotopes. Analysis of <sup>1</sup>H NMR spectra supported successful coupling of **68** at the 6-position of **26**, by characteristic chemical shifts for C(3)H and C(5)H of the quinolinyl ring, as described previously for **56a** (Figure 3.2). Furthermore, coupling through the piperazinyl nitrogen exerts an *ortho/para* shielding effect on the quinolinyl ring, causing C(5)H to be significantly shielded in comparison to C(3)H.<sup>47</sup>

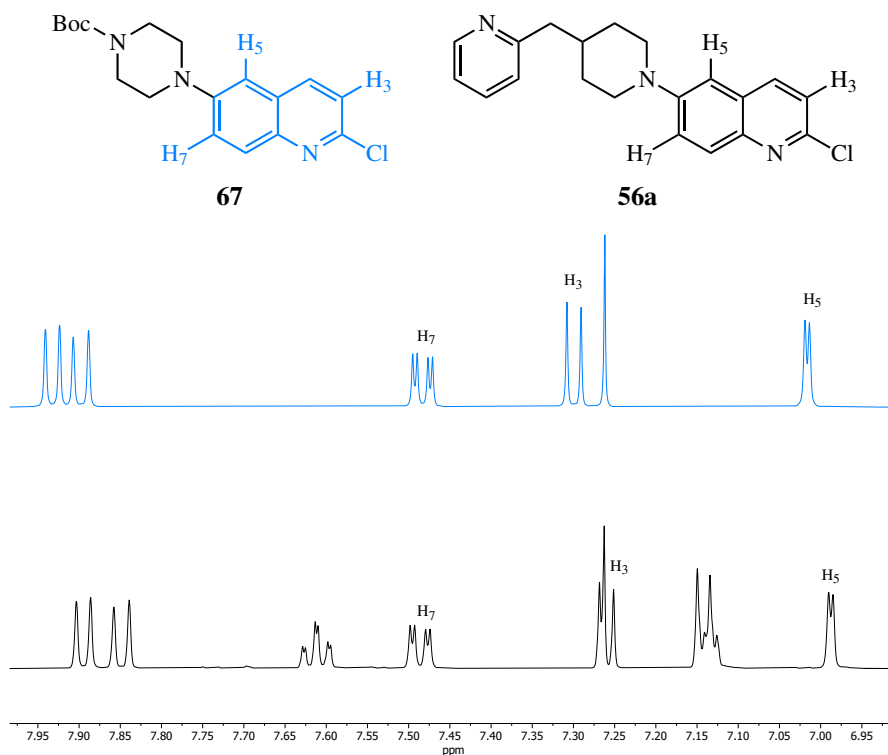
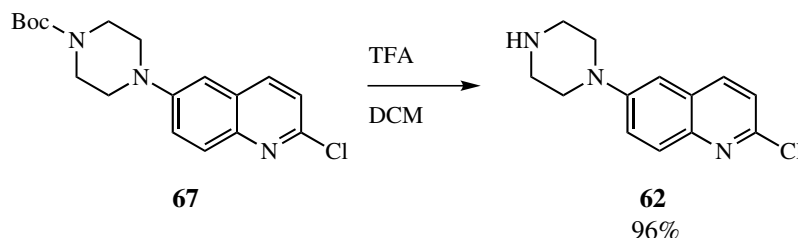


Figure 3.2: Comparison of <sup>1</sup>H NMR spectra (CDCl<sub>3</sub>, δ<sub>H</sub>: 6.95 - 7.95 ppm) of **67** (blue) and **56a** (black). Comparable chemical shifts observed for C(3)H, C(5)H and C(7)H of the quinoline ring indicates similar chemical structures and therefore successful coupling of **68** at the 6-position of **26**.

### 3.3. SYNTHESIS OF SIMPLE 6-ARYLAMIDOPIPERAZINYL-2-AMINOQUINOLINES

In preparation for ligand derivatisation, the second piperazinyl nitrogen needed to be exposed, therefore the next step was amine deprotection of **67**. Removal of the Boc protecting group was completed using trifluoroacetic acid, to afford the free amine **62** in high yields (Scheme 3.3).

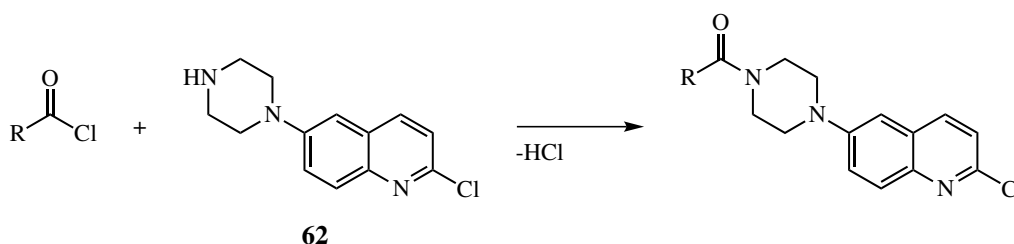


Scheme 3.3: Reaction scheme for Boc deprotection of **67**

Successful removal of the Boc protecting group was supported by analysis of HRMS, IR and NMR spectra; mass products of  $m/z$  248.0956 and 250.0915 were detected at a ratio of  $\sim 3:1$ , consistent with the desired product (expected  $m/z$ : 248.0949 [ $^{35}\text{Cl}$ ] / 250.0920 [ $^{37}\text{Cl}$ ]). Comparison of the IR spectra between **67** and **62** revealed loss of a sharp absorbance stretch at  $1681\text{ cm}^{-1}$  (C=O), and emergence of a broad absorbance stretch at  $3269\text{ cm}^{-1}$  (N-H) following Boc deprotection. Lastly, analysis of  $^1\text{H}$  NMR spectra for **62** revealed a diagnostic loss of the 9H singlet at 1.50 ppm (observed in **67**), consistent with removal of the Boc protecting group.

#### Synthesis of amidopiperazinyl 2-chloroquinoline derivatives

In order to synthesise the desired intermediates **63** and **64**, the next step of the synthetic pathway required derivatisation of **62**. It was envisaged that the most efficient route would involve amidation of **62** with the appropriate acid chloride derivative, as indicated in Scheme 3.4. This approach was considered favourable due to the high reactivity of acid chlorides (and therefore shortened reaction times), the ease of accessibility of acid chlorides (either commercially, or from the corresponding benzoic acid precursors), and the abundance of literature investigating amidations with acid chlorides.

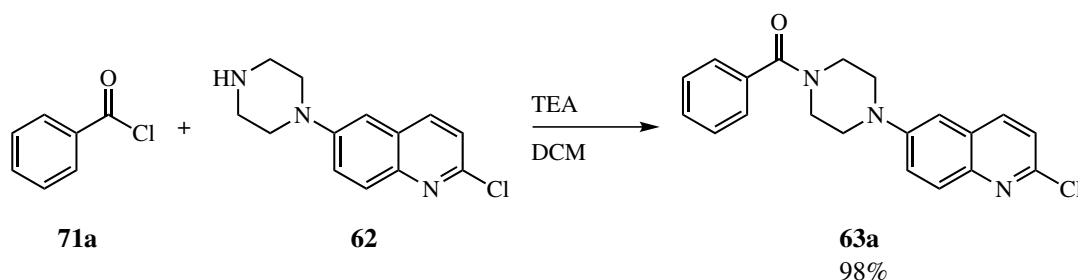


Scheme 3.4: General scheme for amidation of **62** with acid chlorides.



### 3.3. SYNTHESIS OF SIMPLE 6-ARYLAMIDOPIPERAZINYL-2-AMINOQUINOLINES

In the first instance, a proof-of-concept amidation reaction with a commercially available acid chloride was sought. Therefore, the proof-of-concept reaction was conducted with **62** and benzoyl chloride **71a**, using triethylamine as the base (Scheme 3.5) — this led to the formation of **63a** in an excellent yield.



Scheme 3.5: Proof-of-concept reaction for general amidation conditions with **71a**.

Formation of the desired amide product **63a** was observed through several techniques; the desired mass products were detected by HRMS, displaying the diagnostic chlorine isotope distribution of 3:1 (required  $m/z$  352.1211 / 354.1185; found  $m/z$  352.1213 [ $^{35}\text{Cl}$ ] / 354.1186 [ $^{37}\text{Cl}$ ]). The most interesting evidence was obtained from NMR spectra; amidation of **62** with **71a** gave rise to the formation of a tertiary amide. Compared to previous benzylpiperidinyl-containing ligands, the piperazinyl ring is significantly more planarised, and thus energetic barriers for ring flipping are lower than for piperidinyl rings (and ligands). The presence of a tertiary amide and N-C<sub>sp2</sub> group (with C(6) of the quinoline ring), each with partial double bond character at distal piperazinyl nitrogens, further flattens the piperazinyl ring in comparison to **62**, therefore there is no differentiation of distinct axial and equatorial chemical environments for piperazinyl ring H in  $^1\text{H}$  NMR. However, rotation of the newly-attached phenylamido group in **63a** would be substantially restricted by the partial-double bond character about the tertiary amide, and potentially implicate the rate of piperazinyl ring-flipping (ring inversion) on the NMR timescale. Consequently, piperazinyl H signals could be broadened due to slower piperazinyl ring flipping and slow rotation of the phenylamido group, as shown in Figure 3.3. Furthermore, the altered rate of ring-flipping may reduce symmetry about piperazinyl ring H, as seen in the difference in observed chemical environments for C(3')H and C(5')H in  $^1\text{H}$  NMR spectra; while the chemical environments for C(2')H and C(6')H of the piperazinyl ring were not completely resolved in  $^1\text{H}$  NMR spectra, the broadened C(2')H/C(6')H signal could be readily assigned due to ROESY correlations with C(5)H and C(7)H of the quinoline ring (Figure 3.4).

### 3.3. SYNTHESIS OF SIMPLE 6-ARYLAMIDOPIPERAZINYL-2-AMINOQUINOLINES

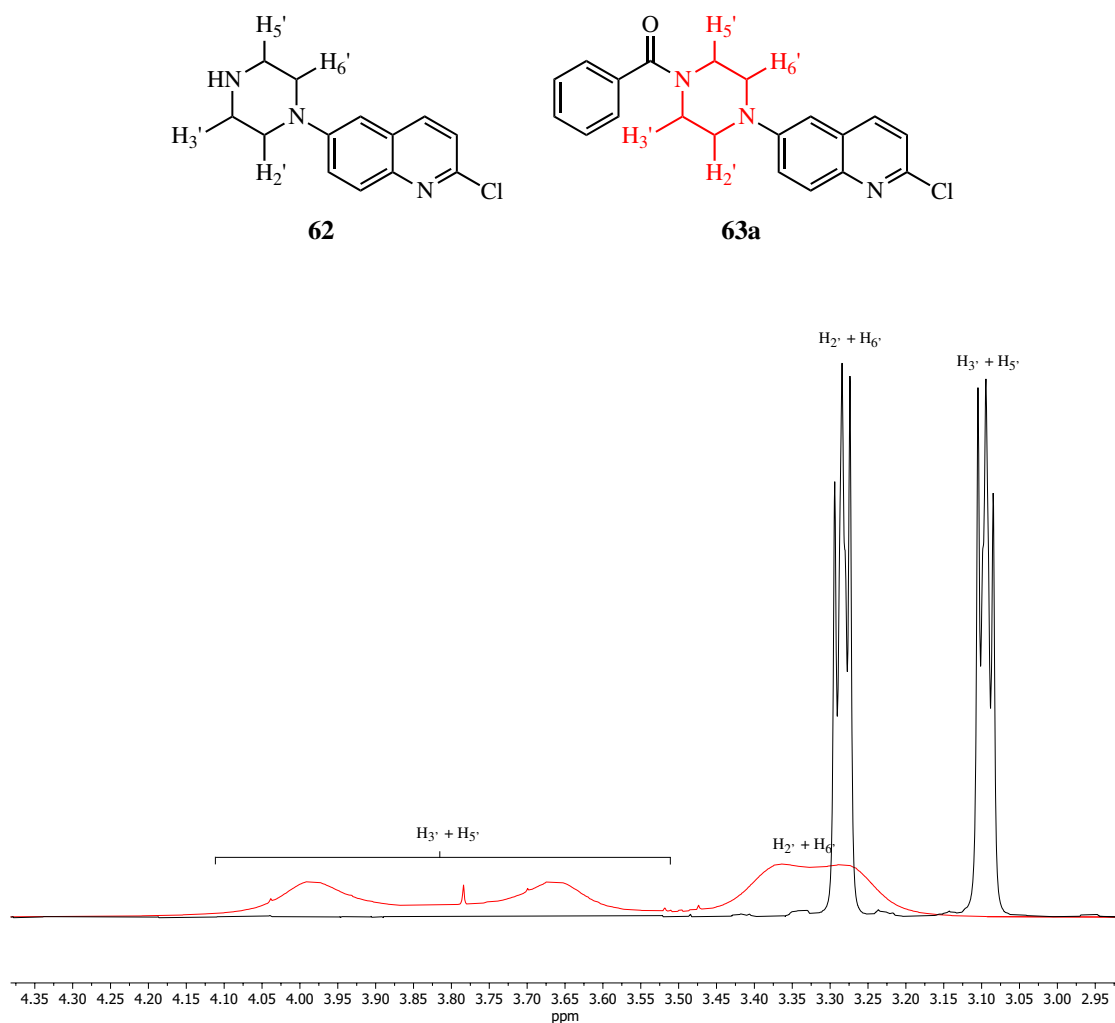


Figure 3.3: Normalised and overlaid  $^1\text{H}$  NMR spectra ( $\delta_{\text{H}}$ : 2.95 - 4.35 ppm) of **62** (black) and **63a** (red), indicating deshielding and substantial broadening of piperazinyll H signals upon amide formation.

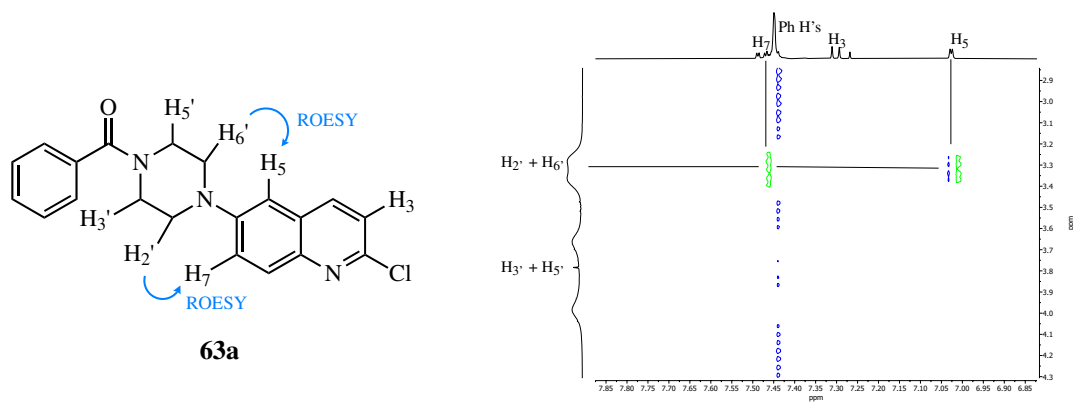
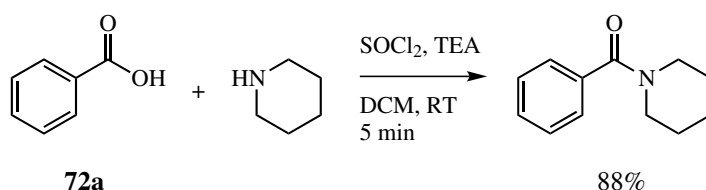


Figure 3.4: ROESY correlations (green) between piperazinyll ring hydrogens ( $\text{C}(2'/6')\text{H}$ ) and quinolinyll ring hydrogens ( $\text{C}(5)\text{H}$ ,  $\text{C}(7)\text{H}$ ), indicating successful formation of the amidopiperazinyll-substituted 2-chloroquinoline **63a**.

### 3.3. SYNTHESIS OF SIMPLE 6-ARYLAMIDOPIPERAZINYL-2-AMINOQUINOLINES

Due to the successful synthesis of **63a**, it was proposed that synthesis of the remaining **63** derivatives would be achieved with the corresponding acid chloride derivatives **71**. However, while some of the acid chloride derivatives were readily available, many derivatives were more accessible as the corresponding benzoic acids. Therefore, a general synthetic approach was required to convert the appropriate benzoic acid derivatives to acid chlorides **71**.

Acid chloride formation from benzoic acids has been well documented in the literature,<sup>101–104</sup> so it was likely that a suitable synthetic method could be identified which would be tolerant to a wide range of functional groups, and could be generally applied for the synthesis of **63** derivatives. The first synthetic method that was identified was a recent report by Leggio *et al.*, detailing a one-pot synthesis of amides from carboxylic acids **72**, which are activated using thionyl chloride to form acid chlorides *in situ*.<sup>101</sup> This method was investigated primarily due to the reported tolerability of a range of carboxylic acids (including some with acid-sensitive functional groups) and a rapid reaction time (5–20 mins), as indicated in Scheme 3.6. The synthesis of several **63** derivatives following this one-pot synthetic method were attempted, as reported in Table 3.4.

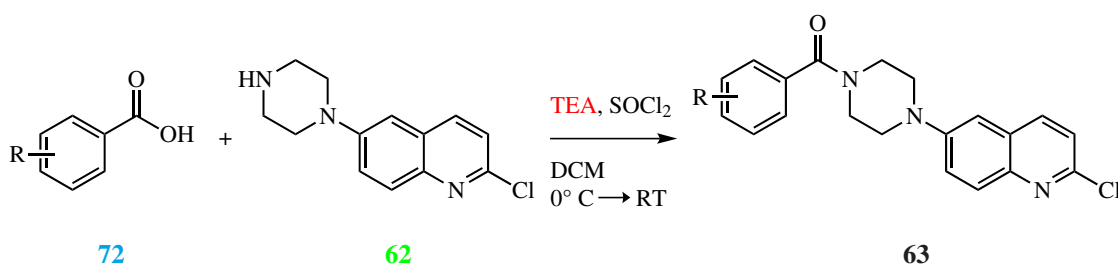


Scheme 3.6: Literature synthesis of tertiary amides via *in situ* acid chloride formation.<sup>101</sup>

Unfortunately, synthesis of **63** derivatives via one-pot synthesis from benzoic acid derivatives **72** was unsuccessful (Table 3.4) and generally resulted in a complex mixture of degradation/oxidation products, typically indicated by the reaction mixture rapidly changing colour from pale yellow to dark brown/black. With reference to Table 3.4, Entry 1 was undertaken as an initial proof-of-concept reaction following the reported literature conditions,<sup>101</sup> except the acid chloride was added to the reaction mixture at 0° C instead of room temperature, and the reaction was allowed to proceed for longer than 20 minutes to ensure product formation. From analysis of <sup>1</sup>H NMR of the crude reaction mixture, the characteristically broad piperazinyll signals observed for **63a** were not observed, therefore the desired product **63b** was not present. To investigate whether this may be a feature of the 3-Me derivative, reactivity of the 4-Me derivative was investigated, as reported in Entry 2. Unfortunately, analysis of the crude reaction mixture by <sup>1</sup>H NMR again revealed the desired product **63c** had not been synthesised. Given the lack of reactivity and/or degradation

## 3.3. SYNTHESIS OF SIMPLE 6-ARYLAMIDOPIPERAZINYL-2-AMINOQUINOLINES

Table 3.4: Attempted syntheses of **63** derivatives via *in situ* acid chloride formation, based upon the method reported by Leggio *et al.*<sup>101</sup> Each entry indicates order of addition (and molar equivalents) of reagents. In all cases, the reaction mixture was cooled to 0°C immediately prior to SOCl<sub>2</sub> addition, then warmed to RT following complete addition of SOCl<sub>2</sub>. Reaction time refers to the time allowed for amide formation following the addition of all reagents. N.D. = not determined. TEA = triethylamine. <sup>a</sup> indicates no product detected in crude <sup>1</sup>H NMR spectra. <sup>b</sup> indicates product detected in crude <sup>1</sup>H NMR spectra, but not purified.



Entry	R =	Sequence of reagent addition (molar equivalents)	Amide formation time (hr)	Product	Yield (%)
1	3-Me	<b>62</b> (1.0 eq.), <b>72b</b> (1.1 eq.), <b>TEA</b> (3.1 eq.), SOCl <sub>2</sub> (1.1 eq.).	1.5	<b>63b</b>	N.D. <sup>a</sup>
2	4-Me	<b>62</b> (1.1 eq.), <b>72c</b> (1.1 eq.), <b>TEA</b> (3.1 eq.), SOCl <sub>2</sub> (1 eq.).	2	<b>63c</b>	N.D. <sup>a</sup>
3	4-Me	<b>72c</b> (1.0 eq.), SOCl <sub>2</sub> (1.3 eq.), <b>TEA</b> (3.3 eq.), <b>62</b> (1.1 eq.).	18	<b>63c</b>	N.D. <sup>b</sup>
4	3-OMe	<b>72f</b> (1.0 eq.), SOCl <sub>2</sub> (1.4 eq.), <b>TEA</b> (3.2 eq.), <b>62</b> (1.2 eq.).	19	<b>63f</b>	16
5	4-OMe	<b>72g</b> (1.0 eq.), SOCl <sub>2</sub> (1.3 eq.), <b>TEA</b> (3.2 eq.), <b>62</b> (1.2 eq.).	19	<b>63g</b>	7

### 3.3. SYNTHESIS OF SIMPLE 6-ARYLAMIDOPIPERAZINYL-2-AMINOQUINOLINES

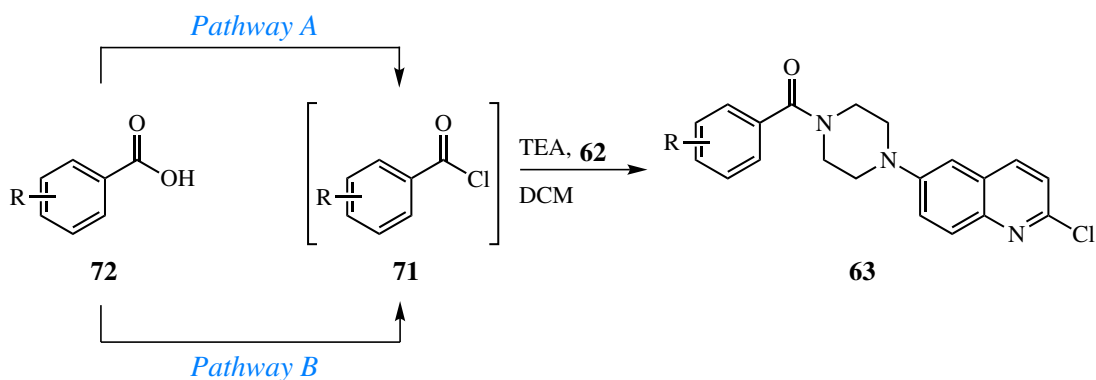
---

appeared to be indiscriminate to the position of the functional group of **72**, it as proposed that perhaps the late addition of  $\text{SOCl}_2$  to the reaction mixture containing **62** and **72** was providing the opportunity for  $\text{SOCl}_2$  to react with **62** before acid chloride formation from **72** could occur, therefore causing reagent (amine) degradation. Consequently, the sequence of reagent addition and reaction period was amended in an effort to facilitate initial acid chloride **71** formation, followed by addition of triethylamine (TEA) and **62** to allow amide formation through **63** synthesis, as indicated in Entry 3. Again, analysis of  $^1\text{H}$  NMR spectra of the crude reaction mixture revealed a complex mixture which could not be purified, however some signals were observed which were consistent with the broad piperazinyl  $^1\text{H}$  NMR signals reported for **63a**, suggesting that the desired product **63c** may have formed, albeit in small quantities. This small success prompted investigation of a different derivative under the same reaction conditions, as reported in Entry 4; a complex reaction mixture was obtained, but favourably a small amount of the desired product **63f** was isolated. Similarly, this could be replicated for the 4-OMe derivative, albeit in very low yield (Entry 5).

While the one-pot synthetic pathway reported by Leggio *et al.*<sup>101</sup> was initially attractive, it required further optimisation as the desired product could only be obtained in very low yields after a substantially longer reaction time (19 hr, c.f. 20 mins<sup>101</sup>). Therefore, an alternative general synthetic procedure for acid chloride synthesis was sought. Two alternative synthetic pathways were identified, each involving stepwise formation of the acid chloride derivative **71**, before reaction with **62** to form the desired product **63**. The first synthetic pathway (Pathway A) involved the use of oxalyl chloride ( $(\text{COCl})_2$ ) with catalytic DMF in DCM to synthesise the acid chloride **71** from the benzoic acid derivative **72**, and uses the acid chloride **71** without purification.<sup>102</sup> Alternatively, the second synthetic pathway (Pathway B) involved conversion of the benzoic acid **72** to the acid chloride **71** by refluxing in  $\text{SOCl}_2$ , then distillation of excess  $\text{SOCl}_2$ , followed by dilution of the crude product with dry toluene, and subsequent azeotropic distillation of  $\text{SOCl}_2$ /toluene,<sup>103,104</sup> and finally dilution of the acid chloride **71** with dry DCM before reaction with **62**. Each synthetic pathway had advantages: Pathway A was a comparably gentle method, and involved the use of more environmentally-friendly reagents. Alternatively, Pathway B was expected to have shorter reaction times, and has been reported many times in the literature. A select number of **72** derivatives were reacted following both Pathways A and B; the results are summarised in Table 3.5.

### 3.3. SYNTHESIS OF SIMPLE 6-ARYLAMIDOPIPERAZINYL-2-AMINOQUINOLINES

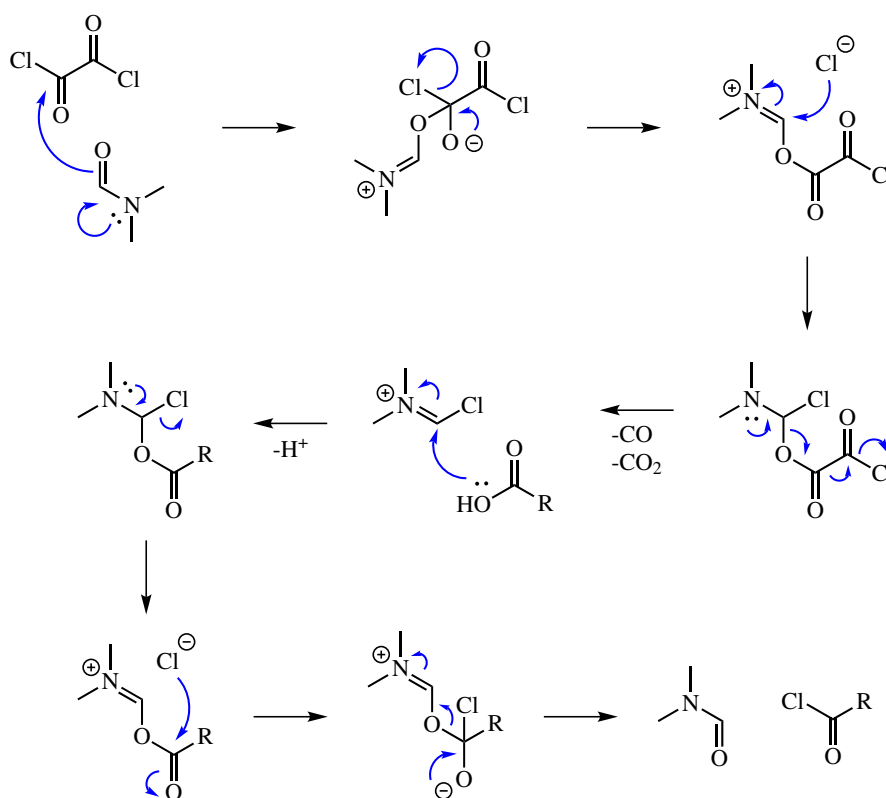
Table 3.5: Syntheses of **63** derivatives via stepwise acid chloride formation and amidation. Pathway A conditions: **72** (1.0 eq.), (COCl)<sub>2</sub> (1.1 eq.), DMF (1 mol %), RT, 16 hr.<sup>102</sup> Pathway B conditions: **72** (1.0 eq.), SOCl<sub>2</sub> (60-100 eq.), reflux, 2 hr.<sup>103,104</sup>



Entry	Product	R =	Pathway	Yield (% over two steps)
1	<b>63b</b>	3-Me	A	19
2	<b>63b</b>	3-Me	B	88
3	<b>63c</b>	4-Me	A	44
4	<b>63c</b>	4-Me	B	85
5	<b>63e</b>	4-F	A	11
6	<b>63e</b>	4-F	B	67

From comparison of the yields reported for each **72** derivative both between derivatives (Entries 1 v.s. 2, 3 v.s. 4, 5 v.s. 6), and between synthetic pathways (Entries 1, 3, & 5 v.s. 2, 4 & 6) in Table 3.5, the yields for Pathway B are substantially greater than those for Pathway A. There are several hypotheses for the lower yields associated with reactions following Pathway A: firstly, (COCl)<sub>2</sub> and SOCl<sub>2</sub> both react in the presence of water, therefore all reagents and solvents used in the reaction must be anhydrous prior to use. Pathway A requires the use of catalytic DMF which is hygroscopic; if the DMF was not sufficiently dry, it may cause hydrolysis of (COCl)<sub>2</sub>, and reduce the amount of (COCl)<sub>2</sub> available for acid chloride formation; secondly, the proposed mechanism for acid chloride formation following Pathway A is quite long, and involves many intermediates (Scheme 3.7), any of which could react with impurities carried over from the DMF bottle or **72** derivatives, which were used as received; lastly, there is no removal of excess (COCl)<sub>2</sub> or DMF prior to reaction with **62** and TEA, therefore any excess (COCl)<sub>2</sub> or dissolved HCl (from (COCl)<sub>2</sub> hydrolysis) may neutralise the TEA, reducing the TEA available to drive amide formation.

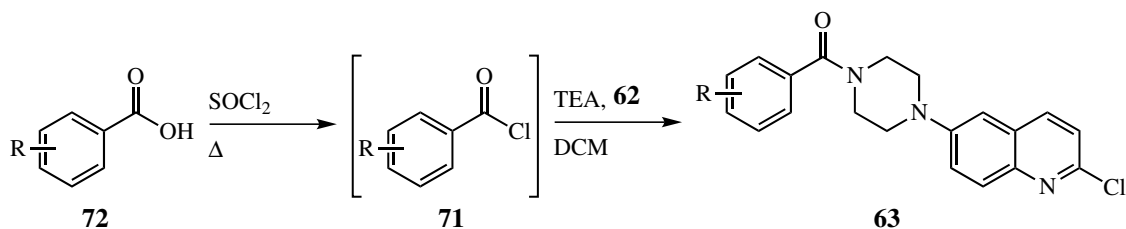
### 3.3. SYNTHESIS OF SIMPLE 6-ARYLAMIDOPIPERAZINYL-2-AMINOQUINOLINES



Scheme 3.7: Proposed mechanism for acid chloride synthesis from benzoic acids following synthetic Pathway A, with  $(\text{COCl})_2$  and catalytic DMF.<sup>105</sup> Mechanism arrows indicated in blue.

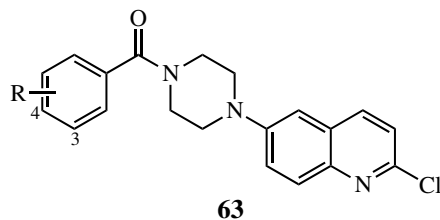
Alternatively, following Pathway B, removal of excess  $\text{SOCl}_2$  would minimise any neutralisation of TEA during the amidation reaction, therefore a higher yield would be expected. Consequently, Pathway B (illustrated in Scheme 3.8) was chosen as the general synthetic method of choice for the synthesis of **63** derivatives due to the faster reaction time and consistently higher yields compared to Pathway A; the yields for each derivative are listed in Table 3.6. In addition to the proposed **63** derivatives, the biphenyl derivative **73** was also synthesised, as [1,1'-biphenyl]-4-carbonyl chloride was available. From Table 3.6, the yield for formation of **73** is considerably lower than for **63** derivatives — this is attributed to the old sample of [1,1'-biphenyl]-4-carbonyl chloride which was used in the reaction; it is very likely the sample was substantially hydrolysed, therefore the reagent contained a large proportion of [1,1'-biphenyl]-4-carboxylic acid, which would not be reactive under the reaction conditions.

### 3.3. SYNTHESIS OF SIMPLE 6-ARYLAMIDOPIPERAZINYL-2-AMINOQUINOLINES



Scheme 3.8: General reaction conditions for the synthesis of amidopiperazinyl-substituted 2-chloroquinoline derivatives **63** from benzoic acids **72** and **62**.

Table 3.6: Results of stepwise acid chloride formation from benzoic acid derivatives **72** and subsequent amidation with **62** to afford amidopiperazinyl-substituted 2-chloroquinolines derivatives **63**, as per Scheme 3.8. <sup>a</sup> indicates a commercially available acid chloride was used, reported yield over 1 step.

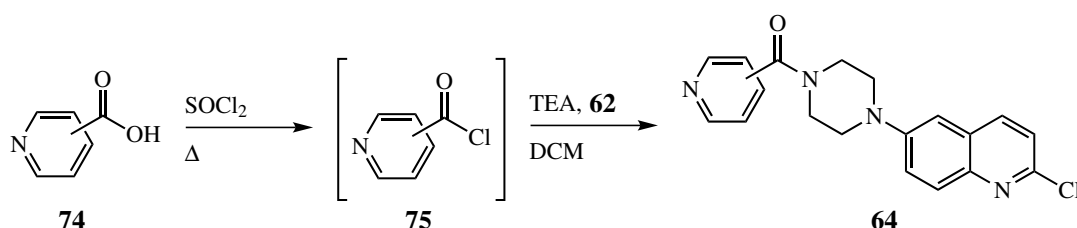


Compound	R =	Yield (% over two steps)
<b>63a</b>	H	98 <sup>a</sup>
<b>63b</b>	3-Me	88
<b>63c</b>	4-Me	85
<b>63d</b>	3-F	44
<b>63e</b>	4-F	67
<b>63f</b>	3-OMe	48
<b>63g</b>	4-OMe	39
<b>63h</b>	3-CN	78
<b>63i</b>	4-CN	75
<b>73</b>	4-Ph	11 <sup>a</sup>



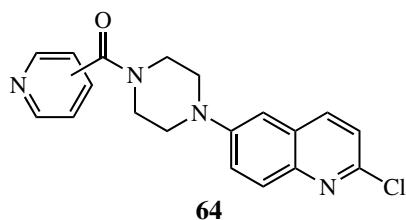
### 3.3. SYNTHESIS OF SIMPLE 6-ARYLAMIDOPIPERAZINYL-2-AMINOQUINOLINES

Due to the success of Pathway B (Table 3.6) for the synthesis of **63** derivatives, the same conditions were also utilised for the synthesis of the pyridyl analogues **64** from the corresponding pyridyl carboxylic acids **74** as indicated in Scheme 3.9. From Table 3.7, the desired **64** derivatives were synthesised in moderate-good yields, and successful synthesis of the desired products was again supported by HRMS and NMR spectra. Additionally, analysis of IR spectra obtained for **64** derivatives revealed the emergence of a sharp absorbance stretch around  $1619\text{ cm}^{-1}$ , consistent with a C=O stretch from a tertiary amide.



Scheme 3.9: General reaction conditions for the synthesis of pyridyl amidopiperazinyl-substituted 2-chloroquinoline derivatives **64** from pyridyl carboxylic acids **74** and **62**.

Table 3.7: Results of stepwise acid chloride formation from pyridyl carboxylic acid derivatives **74** and subsequent amidation with **62** to afford pyridyl amidopiperazinyl-substituted 2-chloroquinolines derivatives **64**, as per Scheme 3.9.



Compound	Pyridyl substitution	Yield (% over two steps)
<b>64a</b>	2	55
<b>64b</b>	3	64
<b>64c</b>	4	46

Interestingly, the observed piperazinyl ring H signals in  $^1\text{H}$  NMR for **64a** and **64c** were much more resolved than for **63a** (to differing degrees, as shown in Figure 3.5), while the piperazinyl ring H signals for **64b** were not as resolved, and exhibited broadness consistent with **63a**.

The stacked NMR spectra in Figure 3.5 tends to suggest that the position of the nitrogen in the pyridyl ring has some influence on the dynamics of the piperazinyl ring. While the potential factors implicating piperidinyl ring conformations were discussed previously in Chapter 2, additional fac-

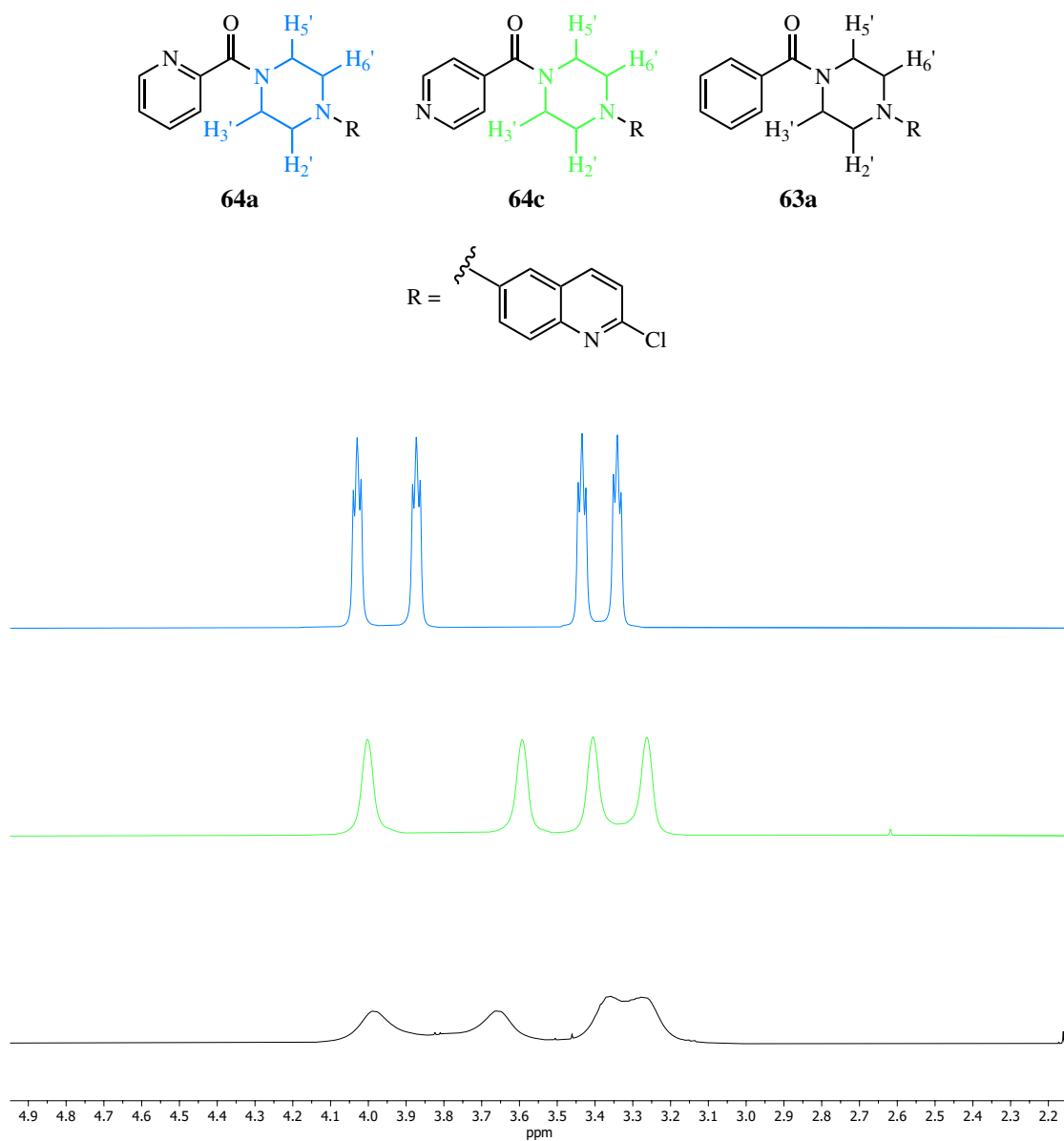


Figure 3.5: Stacked comparison of normalised  $^1\text{H}$  NMR spectra ( $\delta_{\text{H}}$ : 2.2 - 4.9 ppm) of pyridyl **64a** (blue), **64c** (green); and parent derivative **63a** (black) highlighting differences in shape, chemical shift and coalescence of piperazinyl ring signals.

### 3.3. SYNTHESIS OF SIMPLE 6-ARYLAMIDOPIPERAZINYL-2-AMINOQUINOLINES

tors must be considered for piperazinyll rings (in the context of **63** and **64** derivatives) due to their increased complexity (and flatness) relative to piperidinyl rings: firstly, amide-functionalised piperazinyll rings will experience hindered rotation of the amide C-N bond due to partial double-bond character (Figure 3.6); restricted rotation of the amide bond will mean that two different rotamers are accessible, and therefore the chemical environment at C(3')H and C(5')H of the piperazinyll ring will differ between each rotamer; secondly, similarly to piperidinyl rings, the piperazinyll ring can also undergo changes in ring conformation between chair- and boat-like conformers (ring inversion); and lastly, the nitrogen atoms within the piperazinyll ring can undergo pyramidal inversion, changing the conformation about the amine or amide group (for **63** and **64** derivatives). However, there is supporting evidence in the literature which indicates that pyramidal inversion of the nitrogens in the piperazinyll ring is likely to have a relatively indifferent effect on ring dynamics, compared to restricted amide bond rotation and piperazinyll ring inversion,<sup>106,107</sup> therefore nitrogen pyramidal inversion will not be considered further in this thesis.

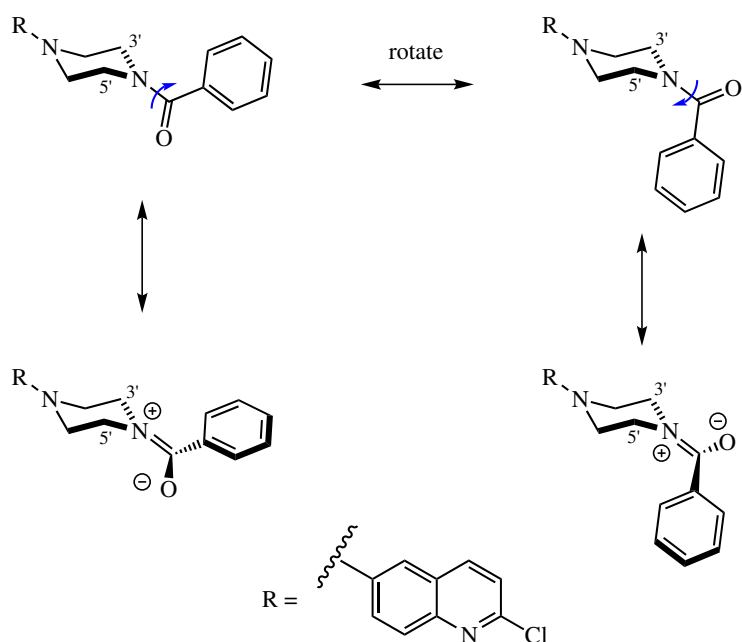


Figure 3.6: Representation of rotamers accessible through amide group rotation, highlighting amide group partial double bond character in amide-substituted piperazinyll rings (using **63a** as an exemplar). Rotated bonds indicated by blue arrows. Piperazinyll carbons (and therefore hydrogens) which are likely to experience different chemical environments for each rotamer in NMR are labelled. Adapted from Jayne.<sup>56</sup>

Recently, Wodtke *et al.* reported the conformational behaviours of acyl-functionalised piperazines (i.e., amidopiperazines) in solution by <sup>1</sup>H NMR spectroscopy, including both mono-*N*-benzoylated, and unsymmetrically *N,N'*-substituted piperazinyll derivatives.<sup>107</sup> In particular, they investigated the relative effects of both restricted rotation of the amide double bond and piperazine ring inversion on

piperazinyl ring conformational behaviour, and calculated the coalescence points (i.e., the temperature at which chemically equivalent piperazinyl ring H signals coalesce to a single signal due to unrestricted dynamics,  $T_C$ ) and resultant activation energy barriers ( $\Delta G^\ddagger$ ) for both of these effects. Interestingly, for most of the amidopiperazine derivatives investigated, the  $T_C$  and  $\Delta G^\ddagger$  values for amide bond rotation were typically higher than the  $T_C$  and  $\Delta G^\ddagger$  values for piperazine ring inversion. Furthermore, they compared the  $\Delta G^\ddagger$  values for each amidopiperazine derivative to the corresponding Hammett constants ( $\sigma$ ) to elucidate any relationships between the electronic nature of the benzoyl substituent and energetic barrier to coalescence in  $^1\text{H}$  NMR spectra, and reported a positive relationship between  $\sigma$  and  $\Delta G^\ddagger$  values, suggesting that benzoyl substituents containing a strongly electron-withdrawing group would have a higher activation energy barrier for amide bond rotation, likely through stabilisation of the zwitterionic amide forms illustrated in Figure 3.6.<sup>107</sup>

As the NMR spectra obtained for **63** and **64** derivatives have only been obtained at room temperature, it is not possible to derive  $T_C$ , and therefore  $\Delta G^\ddagger$  values to compare the energetic barrier for amide bond rotation against corresponding  $\sigma$  values for each **63** and **64** derivative. However, a qualitative analysis can be undertaken, through comparison of the shape and number of the observed piperazinyl ring signals in  $^1\text{H}$  NMR spectra. For a **63** or **64** derivative experiencing very slow amide bond rotation, the appearance of 4 distinct piperazinyl ring H signals would be expected in  $^1\text{H}$  NMR spectra; slow rotation of the amide bond on the NMR timescale would mean that C(3')H & C(5')H of the piperazinyl ring (see Figure 3.6), and consequently C(2')H & C(6')H, are impacted differentially by the adjacent phenylamido group, to the extent that they may be observed in separate chemical environments in NMR spectra. However, for those **63** and **64** derivatives which exhibit fast (unhindered) amide bond rotation on the NMR timescale, it is possible that 2 distinct piperazinyl ring signals H may be observed in  $^1\text{H}$  NMR spectra; C(3')H & C(5')H of the piperazinyl ring (and consequently C(2')H & C(6')H) may experience the same chemical environment (induced by amide bond rotation), therefore they may be observed in a single chemical environments in NMR spectra. Alternatively, if the amide bond in **63** and **64** derivatives is rotating at an intermediate rate (on the NMR timescale), the piperazinyl ring H signals may be significantly broadened, as they may not have achieved coalescence (compared to the expected  $^1\text{H}$  NMR spectra for **63** and **64** derivatives with unhindered amide bond rotation).

### 3.3. SYNTHESIS OF SIMPLE 6-ARYLAMIDOPIPERAZINYL-2-AMINOQUINOLINES

While Wodtke's previous work suggested that piperazinyll ring chemical environments in amidopiperazinyll derivatives are dictated primarily by amide bond rotation (through containing higher  $T_C$  and  $\Delta G^\ddagger$  values for amide bond rotation than those for piperazinyll ring inversion), the structures of **63** and **64** derivatives differ slightly from those used in Wodtke's experiments.<sup>107</sup> Therefore, it is crucial to determine whether the differential chemical environments integrating to 2H in  $^1\text{H}$  NMR spectra are representative of chemical environments induced primarily by amide bond rotation (as  $4 \times \text{CH}_2$ , i.e., as described above and per Wodtke *et al.*),<sup>107</sup> or piperazinyll ring inversion (as  $4 \times (2 \times \text{CH})$ , i.e., different chemical environments based on pseudo-axial and -equatorial piperazinyll ring Hs). Following analysis of [ $^1\text{H}$ ,  $^{13}\text{C}$ ] HSQC 2D NMR spectra in Figure 3.7, each 2H piperazinyll ring signal corresponds to a unique carbon signal, therefore the  $^1\text{H}$  NMR spectra for **63** and **64** represents  $4 \times \text{CH}_2$  piperazinyll ring signals, where the chemical environment of each H is controlled primarily by amide bond rotation, and is consistent with literature.<sup>107</sup>

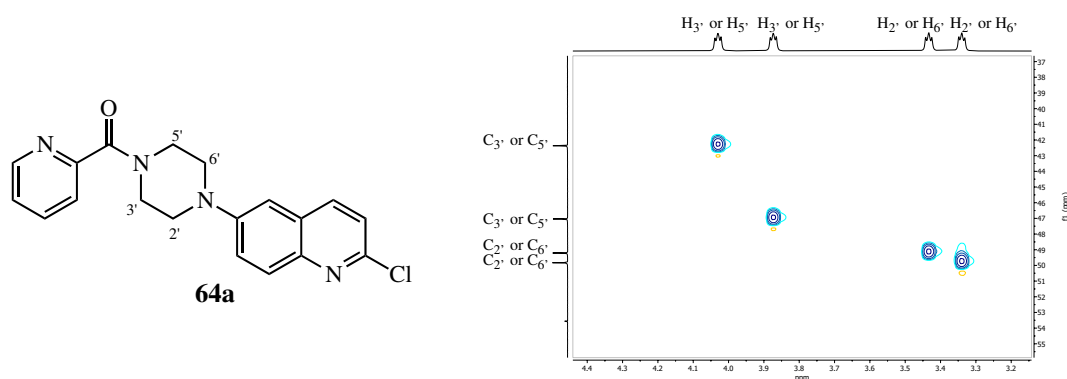


Figure 3.7: HSQC correlations (blue) between piperazinyll ring hydrogens and corresponding carbons in **64a**, displaying 4 distinct chemical environments for each piperazinyll ring  $\text{CH}_2$  group.

As the piperazinyll ring chemical environments in NMR spectra are suggested to be primarily controlled by amide bond rotation (as per Figure 3.7), an analysis of amide bond rotation (through the resolution and number of distinct piperazinyll ring H signals observed in  $^1\text{H}$  NMR spectra at room temperature) and  $\sigma$  values can be undertaken, as shown in Figure 3.8.

### 3.3. SYNTHESIS OF SIMPLE 6-ARYLAMIDOPIPERAZINYL-2-AMINOQUINOLINES

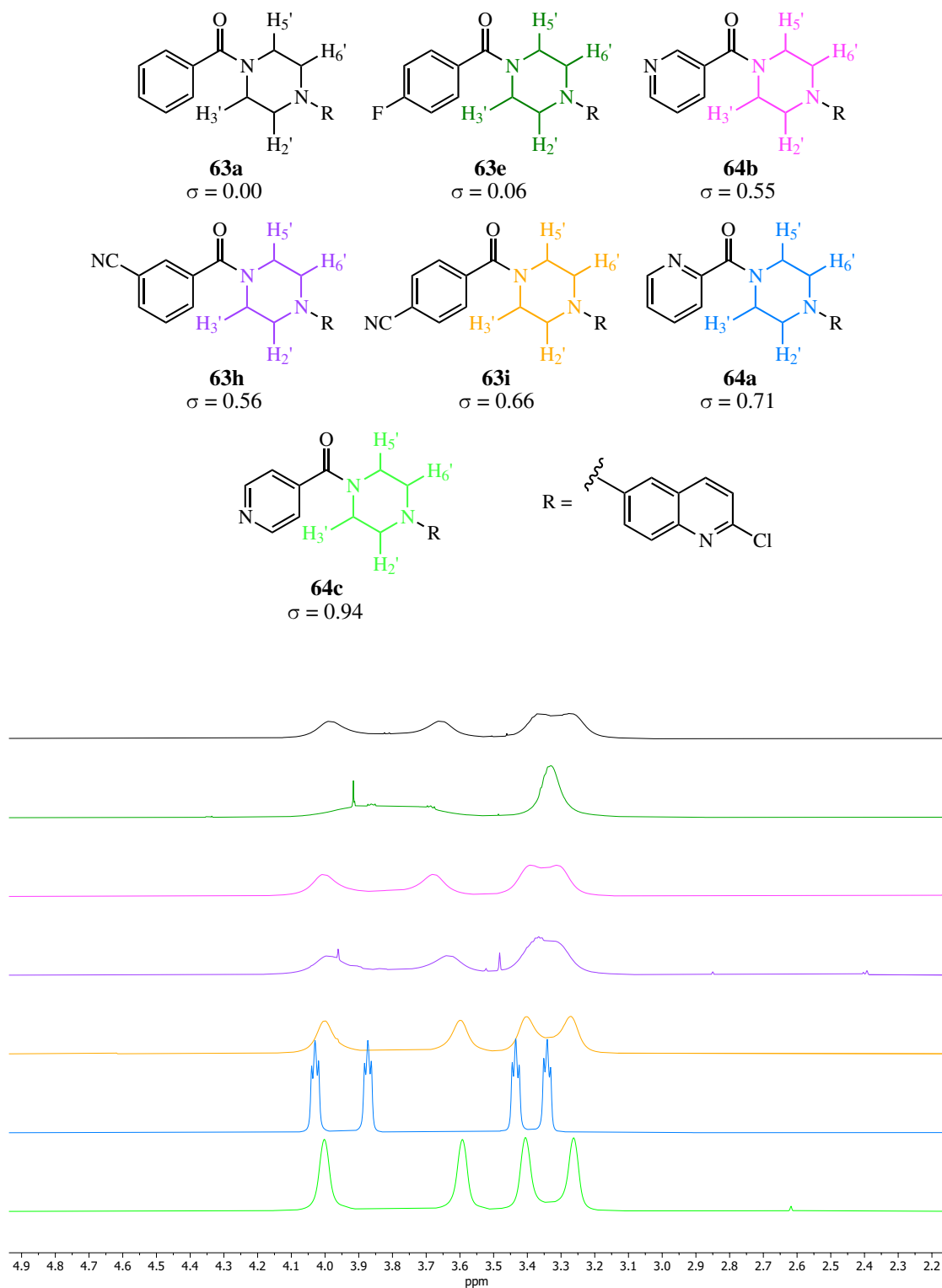


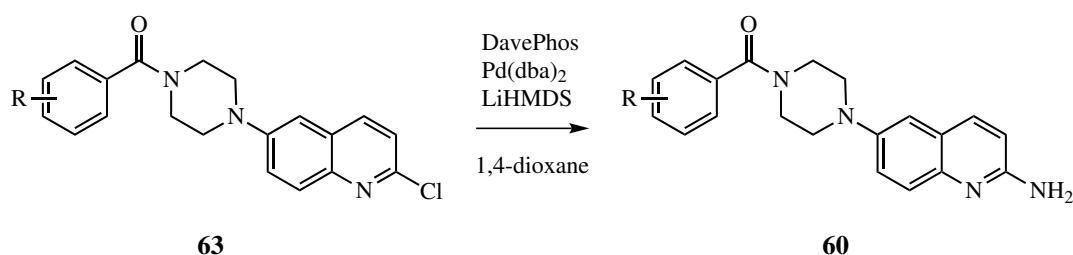
Figure 3.8: Stacked comparison of normalised  $^1\text{H}$  NMR spectra ( $\delta_{\text{H}}$ : 2.2 - 4.9 ppm) of select **63** and **64** derivatives, from lowest to highest value Hammett constants ( $\sigma$ ) for phenyl ring substituents given below each structure.<sup>108–110</sup> Compounds include: **63a** (black), pyridyl derivatives **64a** (blue); **64b** (pink); **64c** (light green), and electron-poor phenyl derivatives **63e** (dark green); **63h** (purple); and **63i** (orange), with NMR spectra highlighting differences in shape, chemical shift and coalescence of piperaziny ring signals.

### 3.3. SYNTHESIS OF SIMPLE 6-ARYLAMIDOPIPERAZINYL-2-AMINOQUINOLINES

From Figure 3.8, it appears that **63** and **64** derivatives which have a higher  $\sigma$  value (i.e., are more strongly electron-withdrawing) generally have 4 distinct chemical environments for piperazinyl ring H in  $^1\text{H}$  NMR spectra, and therefore rotation of the amide bond must be slow, which is consistent with literature.<sup>107</sup> While it would be interesting to determine the coalescence points for the piperazinyl ring signals of **63** and **64** derivatives in  $^1\text{H}$  NMR spectra, they do not currently have any bearing on how these **63** and **64** intermediates may perform as Tec SH3 domain ligands, therefore it is beyond the scope of this thesis to further investigate piperazinyl ring conformational changes in this context.

#### 3.3.2 Synthesis of amidopiperazinyl 2-aminoquinoline derivatives

The final step in the synthesis of **60** and **61** ligand families required amination of the corresponding 2-chloroquinoline derivatives **63** and **64**. Due to the number of compounds under investigation, ligand production would be more efficient if a general synthetic method was undertaken with 2-chloroquinoline derivatives. Consequently, literature-reported conditions for amine formation via Buchwald-Hartwig coupling reaction were applied, using previously optimised conditions with LiHMDS as both a base and ammonia equivalent (Scheme 3.10).<sup>47</sup> Favourably, for all but one derivative, synthesis of the desired **60** ligands was achieved (Table 3.8).

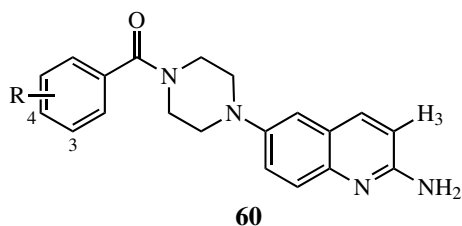


Scheme 3.10: General Buchwald-Hartwig reaction conditions for amination of **63** derivatives, using LiHMDS as an ammonia equivalent to synthesise amidopiperazinyl-substituted 2-aminoquinoline derivatives **60**.

Formation of the desired **60** derivatives was supported by a combination of spectra including HRMS, IR and NMR spectra. Using the parent derivative **60a** as an example: successful coupling of the ammonia equivalent at the 2-position of **63a** was supported by the presence of the corresponding mass product in HRMS spectra ( $m/z$  required 333.1710, found 333.1712). In addition, analysis of IR spectra revealed the emergence of two broad stretches at 3389 & 3166  $\text{cm}^{-1}$ , consistent with the symmetric and asymmetric stretches of a primary amine, and a strong stretch at 1602  $\text{cm}^{-1}$ , suggesting retention of the amide carbonyl group. Analysis of  $^1\text{H}$  NMR revealed a characteristic

### 3.3. SYNTHESIS OF SIMPLE 6-ARYLAMIDOPIPERAZINYL-2-AMINOQUINOLINES

Table 3.8: Results of Buchwald-Hartwig amination of **63** derivatives using LiHMDS as an ammonia equivalent, to successfully synthesise amidopiperazinyl-substituted 2-aminoquinoline derivatives (**60**). N/A indicates not applicable.



Compound	R =	Yield (%)	$\delta_{\text{H}}$ H <sub>3</sub> (ppm)
<b>60a</b>	H	31	6.70
<b>60b</b>	3-Me	62	6.70
<b>60c</b>	4-Me	63	6.72
<b>60d</b>	3-F	14	6.71
<b>60e</b>	4-F	14	6.70
<b>60f</b>	3-OMe	61	6.69
<b>60g</b>	4-OMe	14	6.70
<b>60h</b>	3-CN	0	N/A
<b>60i</b>	4-CN	11	6.73
<b>76</b>	4-Ph	66	6.70

upfield shift for C(3)H to 6.70 ppm (compared to 7.28 ppm in **63a**), which is anticipated due to shielding by resonance from the newly-introduced 2-amino group in **60a** (described previously; see Section 2.7.4 of Chapter 2), and lastly, emergence of a broad 2H singlet at 4.70 ppm, which would be consistent with a primary amine. Unsurprisingly, the broad piperazinyl ring H signals did not resolve following conversion of **63** to **60**, as no changes were expected about the amidopiperazinyl group. For each synthesised **60** derivative, the corresponding spectra were obtained and following analysis supported formation of the desired product, which is exemplified by the reported <sup>1</sup>H NMR chemical shifts for C(3)H in each **60** derivative (Table 3.8).

To investigate whether the broad piperazinyl ring signals in <sup>1</sup>H and <sup>13</sup>C NMR spectra were caused by slow amide bond rotation on the NMR timescale (where restricted amide bond rotation is the predominant factor in controlling piperazinyl ring dynamics for amidopiperazine derivatives on the NMR timescale,<sup>107</sup> see Figure 3.6 & Figure 3.8, and related discussions in Section 3.3.1), additional <sup>13</sup>C NMR spectra for **60c** were obtained at a higher temperature (Figure 3.9); if the broad signals in <sup>13</sup>C NMR spectra were caused by slower amide bond rotation on the NMR timescale, then increasing the ambient temperature (during spectra acquisition) would facilitate faster amide



### 3.3. SYNTHESIS OF SIMPLE 6-ARYLAMIDOPIPERAZINYL-2-AMINOQUINOLINES

bond rotation relative to that observed at room temperature, resulting in coalescence (and hence resolution) of signals in NMR spectra. From Figure 3.9, partial resolution in  $^{13}\text{C}$  NMR spectra for **60c** was observed when the spectra was obtained at 35 °C, due to the convergence of the C(2'/6') signal upon heating (blue). Interestingly, the signals corresponding to C(3'/5') are significantly broadened upon heating, which is not unexpected for amide bond rotation occurring at an intermediate rate on the NMR timescale (see Section 3.3.1). Therefore, the variable temperature NMR experiments with **60c** support the theory that the observed piperazinyl ring signal broadness in NMR spectra is due to slow amide bond rotation on the NMR timescale.

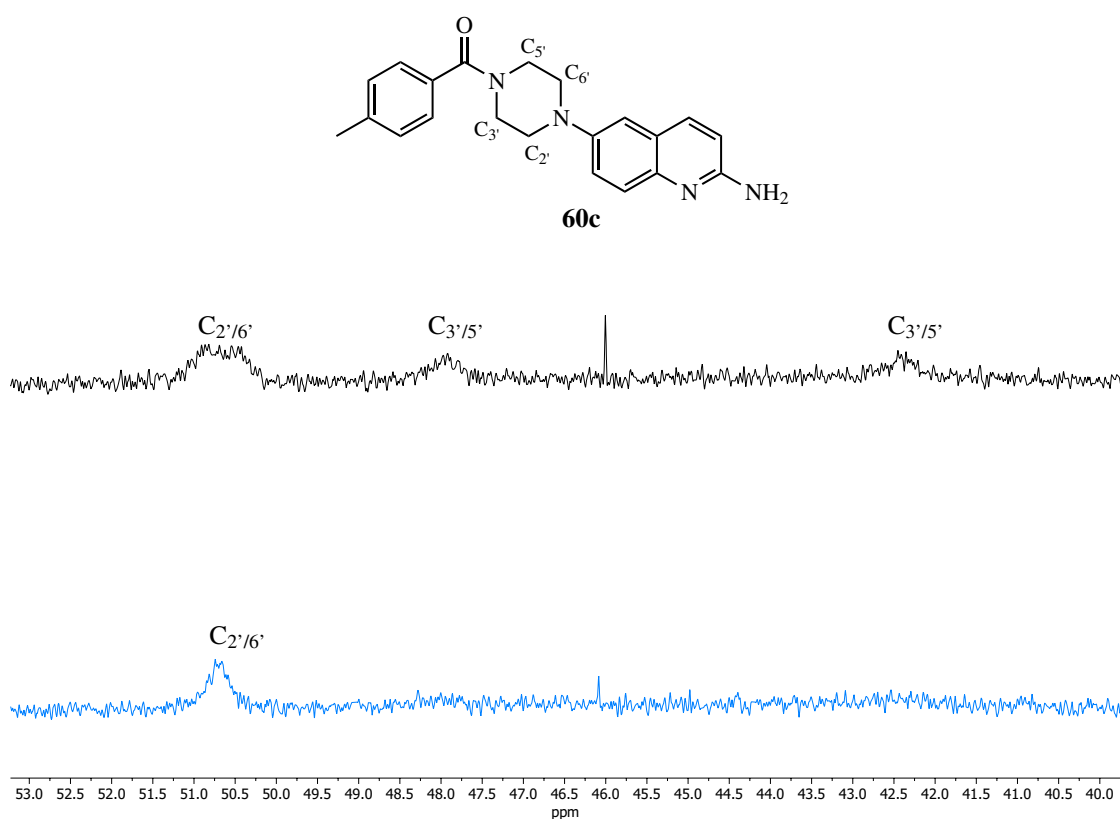


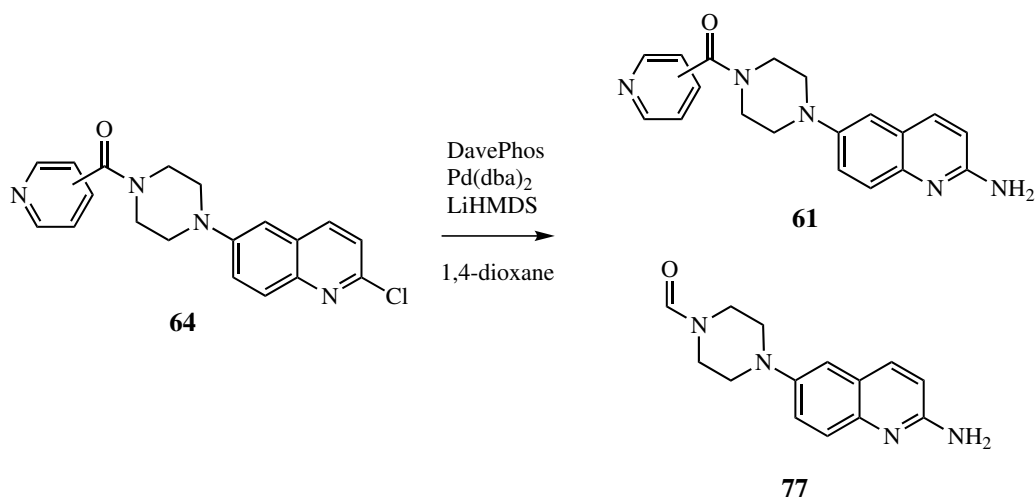
Figure 3.9: Stacked & normalised  $^{13}\text{C}$  NMR spectra ( $\delta_{\text{C}}$ : 40.0 - 53.0 ppm) of **60c** obtained at 25 °C (black) and 35 °C (blue).

While previous reports indicate that these reaction conditions were generally applicable across a broad range of 6-piperidinyl-2-chloroquinoline derivatives,<sup>47,56,66</sup> it appears that **63** derivative behaviour is more variable under these reaction conditions, as indicated by the low-moderate reported yields in Table 3.8. Analysis of the yields in Table 3.8 tends to suggest that for the given Buchwald-Hartwig coupling conditions, **63** derivatives with an electron-withdrawing substituent are less reactive, or are less amenable to partaking in the Buchwald-Hartwig catalytic cycle. This could potentially be resolved by conducting a phosphine ligand and/or Pd catalyst screen to iden-

### 3.3. SYNTHESIS OF SIMPLE 6-ARYLAMIDOPIPERAZINYL-2-AMINOQUINOLINES

tify more suitable Buchwald-Hartwig reaction conditions for **63** derivatives, however at this point a full ligand and catalyst screen was considered beyond the scope of work described in this thesis, as the affinity (and therefore value) of the synthesised **60** ligands was not known. Interestingly, the 3-nitrile derivative **60h** could not be synthesised via literature Buchwald-Hartwig coupling conditions with **63h**, leading to recovery of starting material only. In an additional effort to conduct the Buchwald-Hartwig coupling reaction between **63h** and LiHMDS (as an ammonia equivalent), both the Pd and phosphine ligand concentrations were increased (from 1.6 mol % and 1.4 mol %, to 3.1 mol % and 3.0 mol % respectively), with the aim to increase the relative concentration of Pd species available to facilitate the coupling reaction. However, this did not yield any desired product — as no difference in product conversion was observed upon (approximately) doubling Pd and phosphine ligand concentrations, it is unlikely that the lack of reactivity is due to Pd sequestration. It is not immediately clear why **63h** does not react under the conditions described in Scheme 3.10, as the only difference between **63h** and other **63** derivatives is the nature and position of the nitrile group, which is expected to be spatially distant from the reaction site (i.e., the 2-chloro substituent of the quinoline ring). No further efforts towards synthesis of **60h** were undertaken in the absence of any ligand binding affinity data, as it was likely significant optimisation of the synthetic pathway would be required, which may not afford a ligand of value.

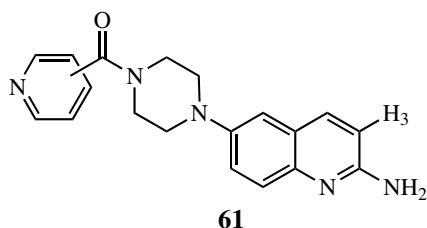
Following synthesis of **60** derivatives, the analogous transformation was undertaken for synthesis of pyridyl-containing ligands **61** from the corresponding **64** 2-chloroquinoline compounds, as indicated in Scheme 3.11 and Table 3.9.



Scheme 3.11: General Buchwald-Hartwig reaction conditions for amination of **64** derivatives, using LiHMDS as an ammonia equivalent to synthesise pyridinyl amidopiperazinyl-substituted 2-aminoquinoline derivatives, **60** and proposed aldehyde side product **77**.

### 3.3. SYNTHESIS OF SIMPLE 6-ARYLAMIDOPIPERAZINYL-2-AMINOQUINOLINES

Table 3.9: Results of Buchwald-Hartwig amination of **64** derivatives using LiHMDS as an ammonia equivalent, to successfully synthesise pyridyl amidopiperazinyl-substituted 2-aminoquinoline derivatives (**60**) and proposed side product **77**. <sup>a</sup> yield of a 4:1 mixture of **61a** and **77**.



Compound	Pyridyl substitution	Yield (%)	$\delta_{\text{H}}$ H <sub>3</sub> (ppm)
<b>61a</b>	2	26 <sup>a</sup>	6.71
<b>61b</b>	3	14	6.70
<b>61c</b>	4	46	6.74

As the pyridyl ring is an electron-deficient substituent, the lower yields described in Table 3.9 are not surprising. Furthermore, the pyridyl substrates **64** may be amenable to Pd coordination and sequestration in the catalytic cycle (Figure 3.10), which may help to explain the lower yields.

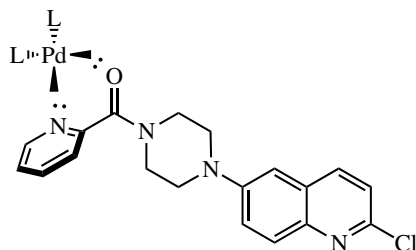


Figure 3.10: Proposed mechanism of Pd sequestration during attempted Buchwald-Hartwig coupling reaction with **64a**, indicating undesired coordination of the Pd species. “L” indicates coordinate ligands.

In each case, synthesis of the desired **61** derivative was supported by the presence of the desired mass product in HRMS spectra, the emergence of broad amine absorbance stretches in IR spectra, and characteristic shielding of C(3)H in <sup>1</sup>H NMR spectra.

Surprisingly, during the synthesis of **61a**, a side-product was present, which could not be separated from the desired product (4:1 mixture of **61a** and side product). From analysis of <sup>1</sup>H NMR spectra, this impurity had a general structure consistent with the 6-piperazinyl-2-aminoquinoline core, however did not contain the 2-pyridyl aromatic ring. Interestingly, a singlet at 8.12 ppm integrating to 1H had emerged, which may be consistent with an aldehyde <sup>1</sup>H signal, as highlighted in Figure 3.11.

Comparison of  $^1\text{H}$  NMR spectra of other **60** and **63** derivatives in Figure 3.11 supports the general 6-piperaziny-2-aminoquinoline structure, and further analysis of HRMS spectra revealed a second mass product with  $m/z$  256.1327, which may be consistent with the proposed formamide-containing product **77** ( $m/z$  requires 256.1319) (Scheme 3.11). Unfortunately, analysis of IR spectra of the **61a** and side product mixture did not reveal any distinguishing IR stretches for a formamide functional group, likely because the presence of characteristic C=O or CHO stretches could be masked by the amide C=O and amine NH stretches in **61a**. It is not immediately clear how this proposed side-product **77** may have formed, as formation of the formamide would generally be considered unlikely from the more stable tertiary amide in **61a**. Furthermore, formation of **77** was not observed for any other **60** or **61** derivatives. A deeper investigation into the exact structure and mechanism of formation of the formamide side product **77** is required, however as it could not be isolated from the desired ligand **61a**, further investigations were not undertaken. Consequently, any binding assays conducted with **61a** in this thesis are acknowledged to be undertaken as a 4:1 mixture of **61a** and a side product, proposed to be **77**.

While sufficient quantities of **60** and **61** ligands were synthesised for SPR ligand binding assays, unfortunately the low yields obtained from the second Buchwald-Hartwig coupling reaction precluded further derivatisation of **60** and **61**, towards the synthesis of the benzylpiperazine ligand families **17** and **59**. Rather than repeating synthesis of **60** and **61** derivatives (including optimisation of the second Buchwald-Hartwig coupling reaction), it was considered more efficient to develop an alternative synthetic pathway for the synthesis of **17** and **59** ligands, which will be described in further detail in Section 3.5.

### 3.3. SYNTHESIS OF SIMPLE 6-ARYLAMIDOPIPERAZINYL-2-AMINOQUINOLINES

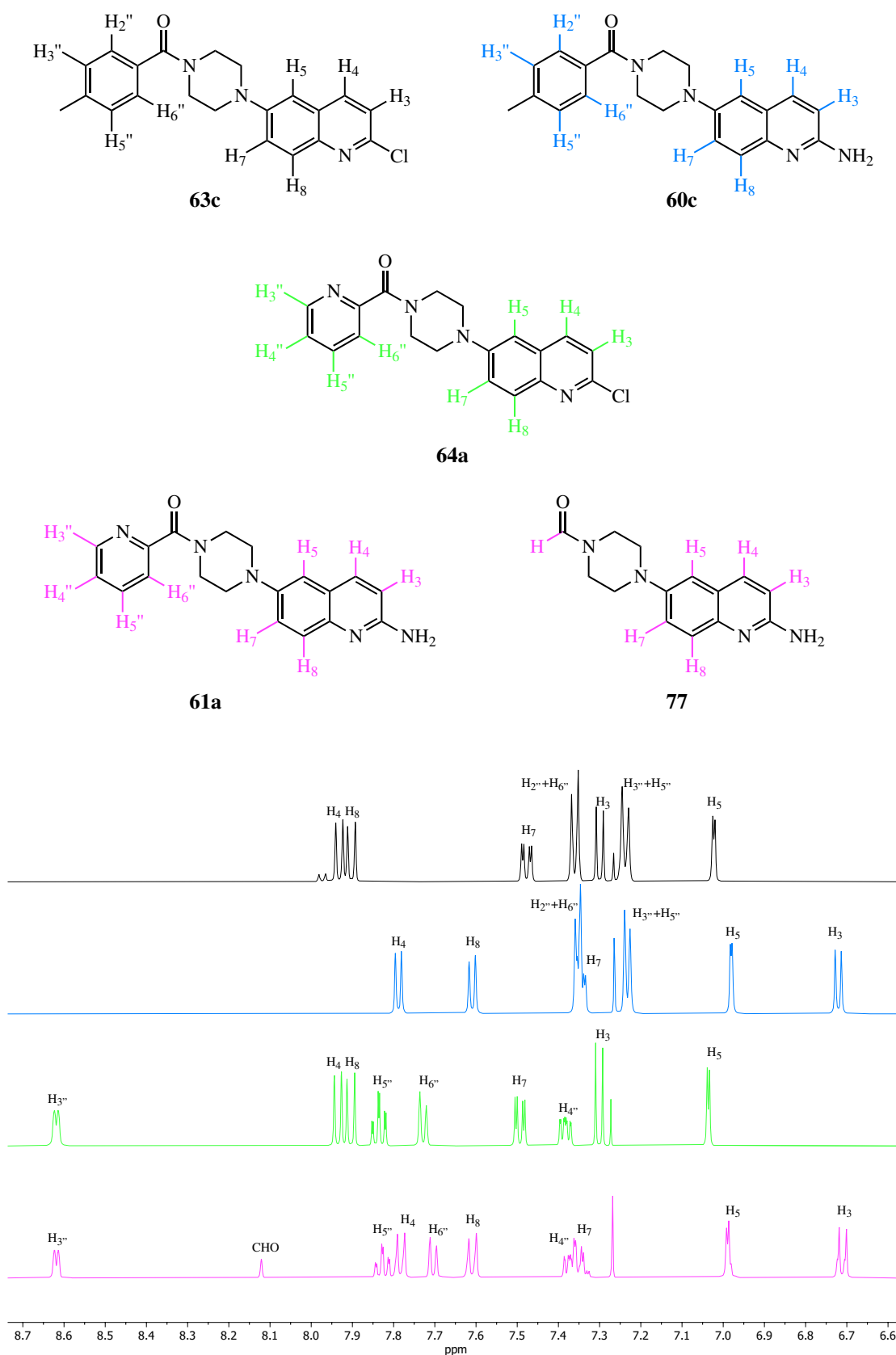


Figure 3.11: Stacked & normalised <sup>1</sup>H NMR spectra ( $\delta_{\text{H}}$ : 6.6 - 8.7 ppm) of various **60**, **61**, **63** and **64** derivatives, indicating key signals for product formation (upfield shift of H<sub>3</sub> upon amination), and signals indicating side-product formation. Spectra shown for **63c** (black); **60c** (blue); **64a** (green); and a 4:1 mixture of **61a** and **77** (pink).

### 3.4 SPR binding studies of 6-arylamidopiperaziny-2-aminoquinoline derivatives

#### 3.4.1 SPR binding assay aims

In order to determine the binding affinities of the newly-synthesised 6-arylamidopiperaziny-2-aminoquinoline ligand families **60** and **61** for the Tec SH3 domain, it was determined that the affinities would be screened and calculated by SPR assays. In the first instance, the ligand binding affinities would be determined by conducting binding assays against GST-Tec SH3 protein, as this target has previously been validated for testing binding affinities against the Tec SH3 domain (see Chapter 2).<sup>46,54</sup> Furthermore, to expand the data set for validation of GST-Tec SH3 as a suitable surrogate for Tec SH3 binding, a second set of binding assays for **60** and **61** against Tec SH3 was undertaken, and compared to the binding assay results obtained for SPR assays with GST-Tec SH3. Lastly, as **60** and **61** ligands have not been assayed against the Tec SH3 domain previously, it was important to ascertain that the location of ligand binding was consistent with the proposed ligand-protein binding model.<sup>46,47</sup> Therefore, a third set of ligand binding assays was conducted with the mutant protein GST-Tec SH3 D196A, to investigate whether **60** and **61** ligands are binding at the proposed ligand-protein binding site. Each of these SPR ligand binding assays were prepared and conducted as previously described in Chapter 2.

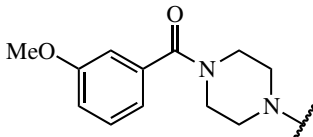
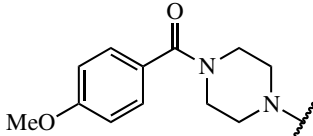
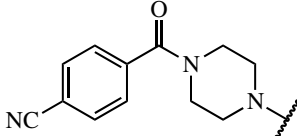
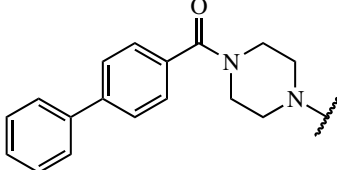
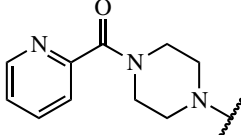
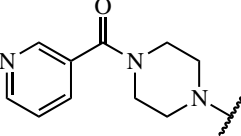
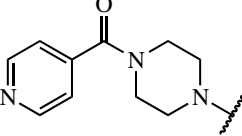
## 3.4.2 Results of SPR binding assays with GST-Tec SH3 and Tec SH3

The affinities of **60** and **61** ligands for the Tec SH3 domain were determined by SPR binding assays against both GST-Tec SH3 (Section 2.4.1, Chapter 2) and Tec SH3 (Section 2.4.3, Chapter 2), and the results reported in Table 3.10.

Table 3.10: Binding affinities of **60**, **61** and **76** ligands determined by SPR for binding GST-tagged- and naked Tec SH3.  $K_d$  values were obtained from assays completed in triplicate across separate runs, and the average  $K_d$  value (and standard deviation) reported.  $\log P$  values ( $clogP$ ) were calculated using Marvin by ChemAxon.<sup>61</sup> N.D. denotes not determined as the ligand was not soluble under assay conditions. <sup>a</sup> indicates assays (in triplicate) were completed within a single run.

Compound	R =	$clogP^{61}$	GST-SH3	SH3
			$K_d \pm SD$ ( $\mu M$ )	$K_d \pm SD$ ( $\mu M$ )
<b>60a</b>		2.93	$8.2 \pm 0.5$	$10.1 \pm 0.3$
<b>60b</b>		3.45	N.D.	N.D.
<b>60c</b>		3.45	$5.3 \pm 0.6$	$8.2 \pm 0.4$
<b>60d</b>		3.08	$6.6 \pm 0.7$	$8.3 \pm 0.3$
<b>60e</b>		3.08	$7.2 \pm 0.5$	$9.0 \pm 0.5$

3.4. SPR BINDING STUDIES OF 6-ARYLAMIDOPIPERAZINYL-2-AMINOQUINOLINE DERIVATIVES

<b>60f</b>		2.77	$7.8 \pm 0.2$	$11.1 \pm 0.8$
<b>60g</b>		2.77	$5.4 \pm 0.2$	$8.7 \pm 0.3$
<b>60i</b>		2.79	$10.3 \pm 0.8$	$11.6 \pm 1.0$
<b>76</b>		4.58	N.D.	N.D.
<b>61a</b>		2.10	$7.8 \pm 0.2^a$	$11.5 \pm 1.7^a$
<b>61b</b>		1.71	$8.6 \pm 0.4$	$7.4 \pm 0.3$
<b>61c</b>		1.71	$8.6 \pm 0.6$	$9.5 \pm 0.8$



### 3.4. SPR BINDING STUDIES OF 6-ARYLAMIDOPIPERAZINYL-2-AMINOQUINOLINE DERIVATIVES

---

With the exception of the 4-nitrile derivative **60i**, the **60** derivatives generally exhibited improved binding affinity to GST-Tec SH3 relative to their previously reported benzylpiperidinyl counterparts ( $K_d$  values typically 9.1 - 23.7  $\mu\text{M}$ ).<sup>56</sup> Unfortunately, each **61** derivative had reduced binding affinities relative to **18a** and **18b** ( $K_d$  values 5.0 and 3.0  $\mu\text{M}$ , respectively — see Table 3.1).<sup>56,66</sup> Favourably, for each **60** and **61** ligand assayed, the binding affinities calculated for binding to both GST-Tec SH3 and SH3 were quite consistent (Table 3.10). This indicates that the calculated binding affinities are representative of ligand binding to Tec SH3, rather than the GST-tag of GST-Tec SH3, and is consistent with the data reported in Section 2.4.3 (Chapter 2).

In addition, the previously reported ligands displayed fast binding kinetics (i.e., fast on/fast off) during binding to GST-Tec SH3, illustrated by the resultant box-shaped sensorgrams in Figure 2.5 of Chapter 2.<sup>56,66</sup> The majority of **60** and **61** ligands assayed also displayed similar rapid binding kinetics upon binding and dissociation, with the exception of the 2-pyridyl derivative **61a**. It is noted that **61a** displayed substantially slower association and dissociation during the binding interaction compared to the previously reported ligands, to the extent that during SPR binding assays for **61a**, the ligand injection time was increased to 120 sec (c.f., 45 sec in Figure 2.5, Chapter 2) to ensure steady-state binding (shown as sensorgram plateau) was achieved (Figure 3.12). Typically, slower associations would indicate a longer period is required to occupy the available ligand binding sites on the protein surface — this is not surprising given presence of **77** in the **61a** sample, which may be interfering with **61a**-GST-Tec SH3 binding. Conversely, slower dissociations typically suggest that the ligand is experiencing a stronger binding interaction with the protein surface (see Chapter 1, Equations 1.3, 1.4 and 1.5), and therefore has an increased residence time. While **61a** appeared to exhibit slower association and dissociation compared to other **60** and **61** derivatives (Chapter 2, Figure 2.5), the sensorgrams shown in Figure 3.12 are still relatively box-shaped, so kinetic data analysis was not undertaken as the resultant rate constants would likely be close to the limit of measurement for the instrument.<sup>65</sup> Regardless, high-level qualitative analysis indicates that the binding interaction of **61a** is likely to differ from the previously assayed ligands, including **60** and **61** derivatives.

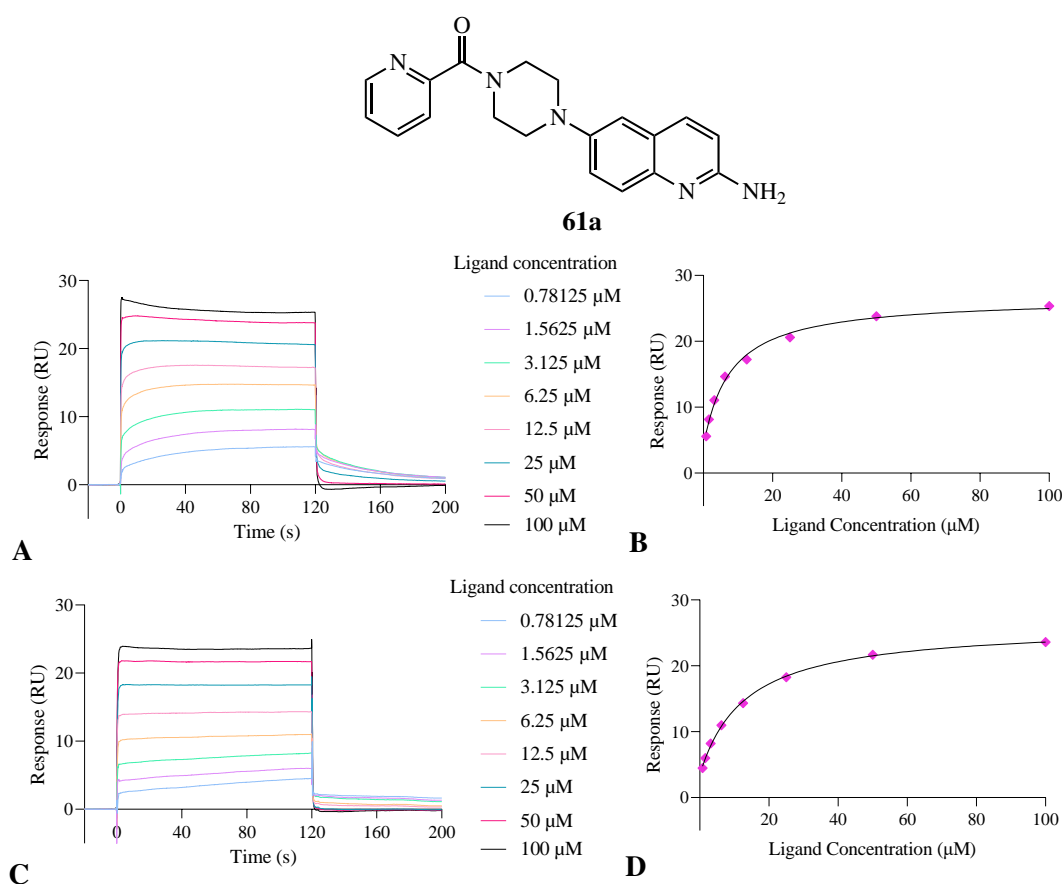


Figure 3.12: SPR sensorgrams and derived isotherms for binding of **61a** to GST-Tec SH3 or Tec SH3. (A) Reference-subtracted and corrected sensorgrams for binding of **61a** to GST-Tec SH3. (B) Derived isotherm for binding of **61a** to GST-Tec SH3. (C) Reference-subtracted and corrected sensorgrams for binding of **61a** to Tec SH3. (D) Derived isotherm for binding of **61a** to Tec SH3.

Upon comparison to the previously reported lead ligands in Table 3.1,<sup>56,66</sup> none of the **60** and **61** derivatives in Table 3.10 displayed a stronger binding affinity for the Tec SH3 domain. This suggests that further flattening of the piperazinyl ring (relative to a piperidinyl ring) does not appear to substantially influence binding affinity. Furthermore, the introduction of the tertiary amide as a potential H-bond acceptor does not appear to improve ligand binding affinity relative to the previously reported benzylpiperidinyl ligands, and therefore does not appear to be making an additional favourable bonding interaction. However, all but two ligands were soluble under the SPR assay conditions, suggesting the reduced *clogP* values translated well to improved aqueous solubility. Overall, while a significant gain in ligand binding affinity was not achieved for **60** and **61** derivatives, the physicochemical properties and predicted drug-like character of these ligands was improved, without significantly compromising ligand binding affinity.

### 3.4.3 Analysis of trends in SPR binding assay data with GST-Tec SH3

In an attempt to identify any trends in **60** and **61** ligand family binding affinity for the Tec SH3 domain, it was envisaged that analysis of certain variables via Hansch plots could be beneficial. Given the range of functional groups in the **60** and **61** ligands tested, the most prominent variables were expected to be electronic character (as Hammett constants,  $\sigma$ ),<sup>108–110</sup> volume (as molar refractivity constants)<sup>111</sup> and overall hydrophobicity (as *clogP* values).<sup>61,112</sup> Therefore, using the available Hammett & molar refractivity constant tables in the literature,<sup>108–111</sup> and *clogP* values<sup>61</sup> the binding affinities (where available) were plotted (Figure 3.13).

For simplicity, analysis of each Hansch plot in Figure 3.13 will be conducted separately. In advance of any data interpretation, it is noted that the sample size for the **60** and **61** ligands is quite small ( $n = 10$  ligands). In addition, the substituents are generally quite small and simple, therefore the range and diversity of constants is limited in some cases, so any conclusions should be considered with these factors in mind. Ligands containing functional groups which are preferable will display a higher activity ( $1/\log K_d$ ) value, while ligands containing functional groups which are not favoured will display a lower activity value. Given the current  $K_d$  values recorded in Table 3.10, a 10-fold difference in binding affinity corresponds to an activity difference of  $\sim 0.03$ . Where indicated, GraphPad Prism v 9.0.0(121) was used to calculate a line-of-best-fit by simple linear regression.<sup>51</sup>

With regard to the relationship between binding activity of **60** and **61** ligand substituents and electronic effects (Figure 3.13A), the plotted data appears to follow an approximately horizontal trend-line (slope  $\approx -0.006$  Activity/ $\sigma$ ,  $R^2 = 0.5546$ , see Figure B.1A in Appendix), indicating that there does not appear to be any strong correlation between  $\sigma$  values and ligand activities. Due to the small number and limited diversity of ligands tested, it would be wise to synthesise and test the binding affinity of additional **60** and **61** ligands containing a wider range of  $\sigma$  values, including those which are more strongly electron-withdrawing (e.g.,  $\text{CONH}_2$ , as **60j** and **60k**) or electron-donating (e.g.,  $\text{NH}_2$ ), to probe whether any potential relationships may require more extreme  $\sigma$  values in order to become apparent.

From Figure 3.13B, the binding activities for all **60** and **61** ligands appears to be quite consistent, with no clear influence by molar refractivity constant upon data point distribution (slope  $\approx 0.0003$

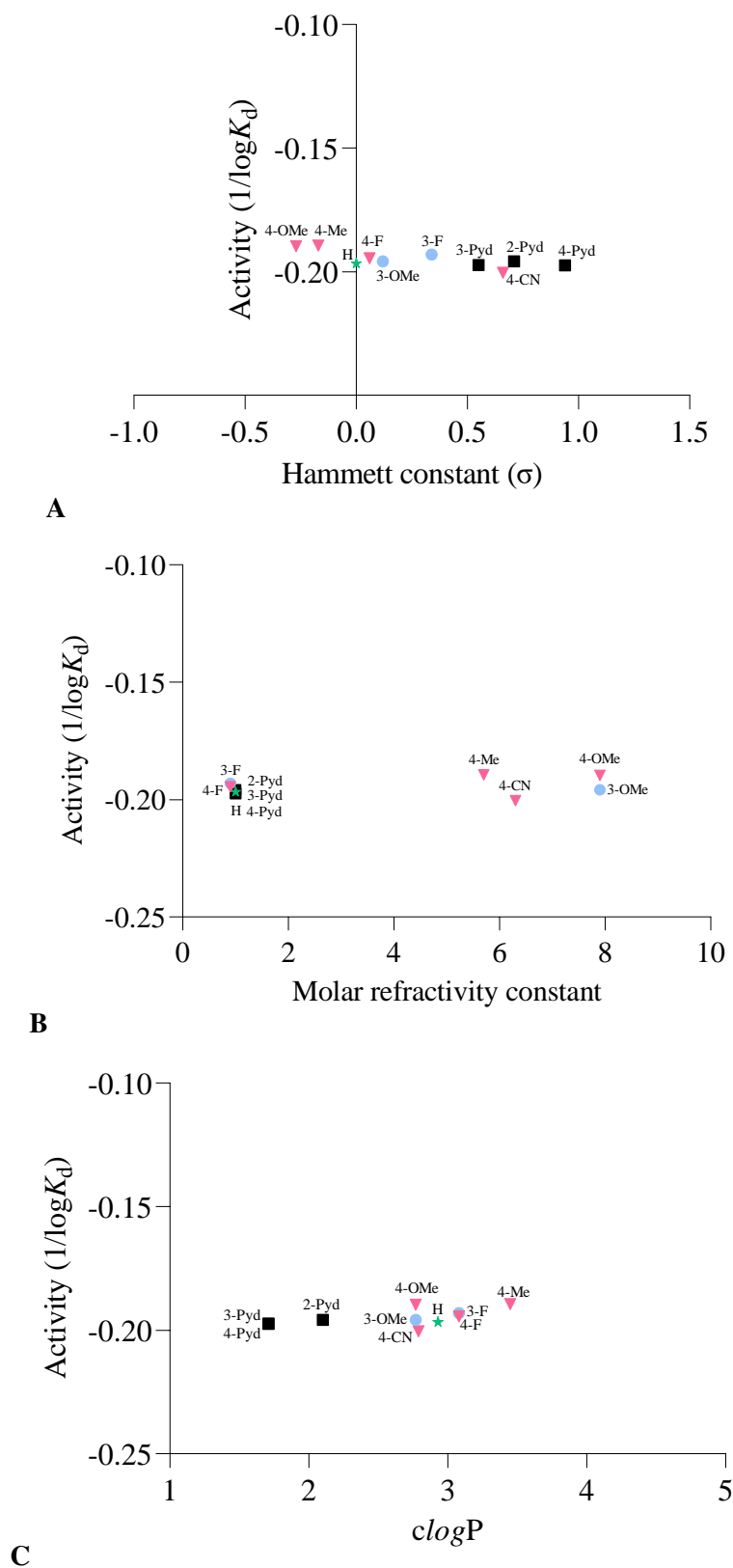


Figure 3.13: Hansch plots displaying relationship between binding activity of **60** and **61** ligands and the: (A) electronic nature of substituent (as Hammett constant,  $\sigma$ );<sup>108–110</sup> (B) volume of substituent (as molar refractivity constant);<sup>111</sup> or (C) hydrophobicity of substituent (as *clogP* value).<sup>61,112</sup> The number indicates the position of the substituent on the phenyl ring, or the position of the nitrogen in the pyridyl ring (denoted 'Pyd').

Activity/molar refractivity constant,  $R^2 = 0.0847$ , see Figure B.1B in Appendix). This suggests that for each of the small substituents in **60** and **61** ligands reported in Figure 3.13B, there does not appear to be any significant steric contributions upon ligand-protein binding. To investigate this further, it would be desirable to expand the sample size, to include **60** and **61** ligands with bulkier substituents in different positions.

Lastly, when investigating **60** and **61** ligand hydrophobicity (Figure 3.13C), again there does not appear to be any significant influence by overall hydrophobicity upon ligand binding activity; determination of a line-of-best-fit by simple linear regression revealed a slightly increasing trend (slope  $\approx 0.003$  Activity/*clogP*,  $R^2 = 0.2775$ , see Figure B.1C in Appendix). However, the sample of ligands tested is biased, as each of the **60** and **61** ligands were designed to have lower *clogP* values (typically  $<4$ ) in line with Lipinski's Rules.<sup>32</sup> Therefore, in order to truly consider relationships between **60** and **61** ligands and overall hydrophobicity, the sample size should be expanded to include a greater diversity of **60** ligands with more hydrophilic and hydrophobic substituents.

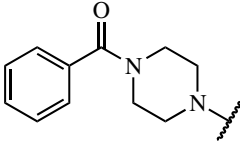
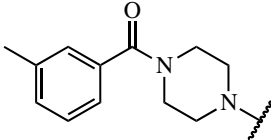
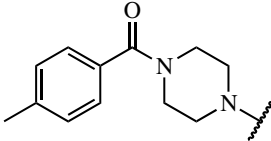
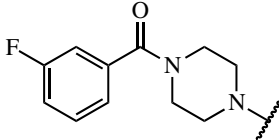
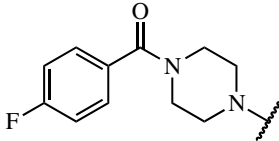
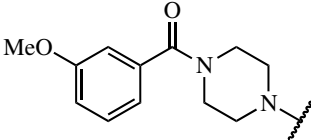
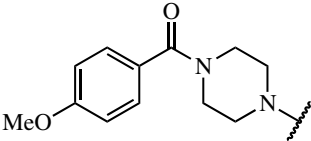
Overall, the analysis of **60** and **61** ligand binding activity via Hansch plots was limited by the small sample size and the diversity of phenyl ring substituents. Initial Hansch plot analyses suggest there are no clear contributions by phenyl ring substituent  $\sigma$  values, substituent size/steric bulk (as volume, described by molar refractivity) or hydrophobicity to the ligand binding activity of **60** and **61**.

#### 3.4.4 Results of SPR binding assays with GST-Tec SH3 D196A mutant

The reported binding affinities for **60** and **61** derivatives give an indication of the strength of the binding interaction between each ligand and the Tec SH3 domain, however does not reveal any insights into the location of the ligand-protein binding interaction. To investigate this, a series of SPR binding assays against GST-Tec SH3 D196A mutant protein were undertaken, as described in Chapter 2, Section 2.4.2. If the ligand binding mode is consistent with the previously proposed ligand-protein binding model, which relies upon key interactions with W215 and D196 side chain residues on the protein surface,<sup>46,47</sup> then no binding interaction should be observed following ligand injection. The results of the SPR binding assays with **60** and **61** derivatives are reported in Table 3.11, with exemplar sensorgrams and the resultant isotherm for **60a** shown in Figure 3.14.

### 3.4. SPR BINDING STUDIES OF 6-ARYLAMIDOPIPERAZINYL-2-AMINOQUINOLINE DERIVATIVES

Table 3.11: Binding affinities of 6-arylamidopiperazinyl-2-aminoquinoline ligands for GST-Tec SH3 D196A mutant protein, as determined by SPR. N.D. denotes not determined as the ligand was not soluble under assay conditions.

Compound	R =	GST-Tec SH3 D196A
		$K_d \pm SD$ ( $\mu\text{M}$ )
60a		no binding
60b		N.D.
60c		no binding
60d		no binding
60e		no binding
60f		no binding
60g		no binding

### 3.4. SPR BINDING STUDIES OF 6-ARYLAMIDOPIPERAZINYL-2-AMINOQUINOLINE DERIVATIVES

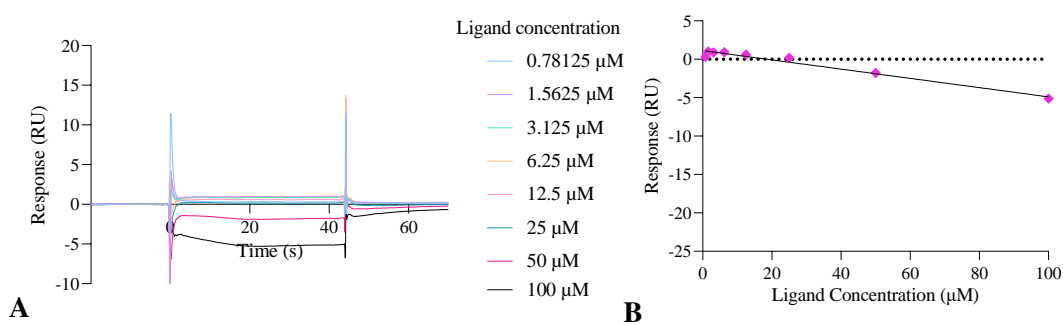
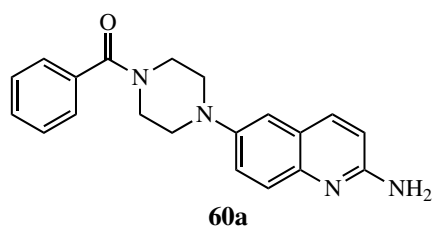
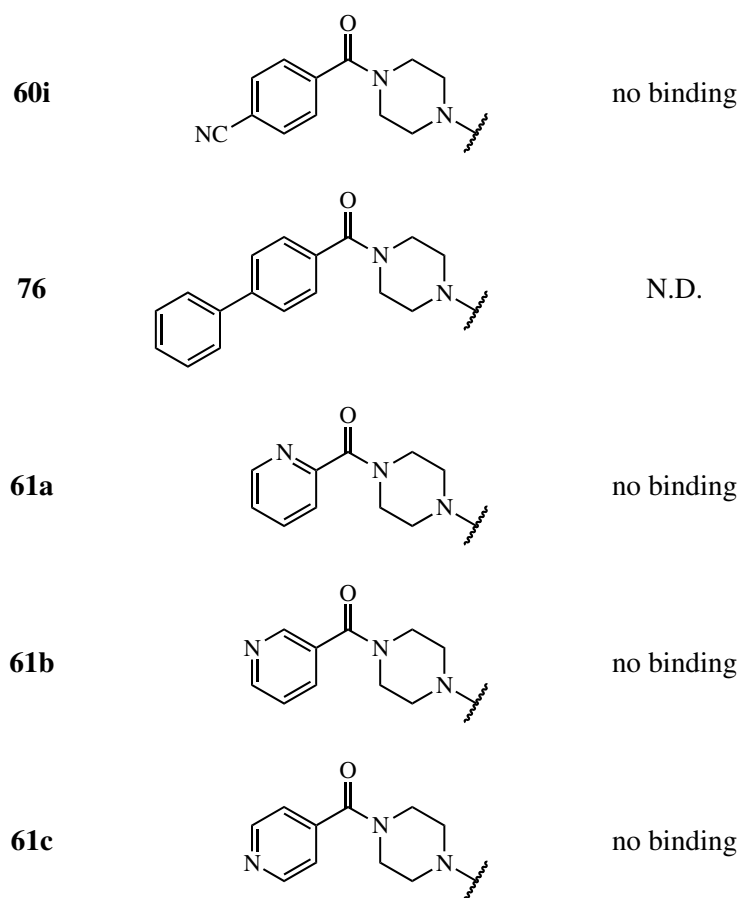


Figure 3.14: SPR sensorgrams and derived isotherm for binding of **60a** to GST-Tec SH3 D196A mutant. (A) Reference-subtracted and corrected sensorgrams for binding of **60a** to GST-Tec SH3 D196A mutant. (B) Derived isotherm for binding of **60a** to GST-Tec SH3 D196A mutant.

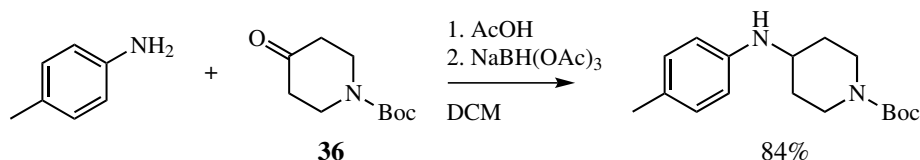
Pleasingly, none of the **60** and **61** ligands displayed any binding to GST-Tec SH3 D196A mutant in SPR binding assays; the SPR sensorgrams for each derivative were similar to Figure 3.14, which are consistent with those in Figure 2.20 (Chapter 2), illustrating no ligand binding. Taken together, this suggests that each of the **60** and **61** derivatives are binding to the Tec SH3 domain in a manner consistent with the previously proposed ligand-protein binding model, and importantly, we can describe the location of the binding interaction being measured by SPR with greater confidence.

### 3.5 Synthesis of simple 6-benzylpiperazinyl-2-aminoquinolines

#### 3.5.1 Synthesis of 6-position substituted 2-chloroquinoline derivatives

It was originally proposed that **17** and **59** derivatives could be synthesised by amide reduction of **60** and **61** derivatives (see Pathway A, Scheme 3.1). However, the unexpectedly low yields obtained during the synthesis of **60** and **61** derivatives meant there was insufficient material available to complete the desired transformations, so an alternative approach was required for the synthesis of **17** and **59** derivatives. As the early-stage intermediates **62** and **67** from Pathway A (Scheme 3.1) were generally isolated in high yields, Pathway B (Scheme 3.1) was investigated as a possible route for the synthesis of **17** and **59** derivatives.

From Scheme 3.1 and using **62** as a starting material, the first proposed step required introduction of benzyl group derivatisation via reductive amination with the corresponding benzaldehyde derivative. Earlier work investigating the synthesis of 4-(phenylamino)piperidinyl derivatives reported general conditions for successful reductive aminations between aniline derivatives and **36** (Scheme 3.12);<sup>113</sup> due to broad reported substrate scope, these conditions were also investigated for the synthesis of **65** derivatives through undertaking an initial proof-of-concept reaction with benzaldehyde and **62** (Scheme 3.13).



Scheme 3.12: Previously reported reaction conditions for the synthesis of 4-(phenylamino)piperidinyl derivatives via reductive amination with aniline derivatives and **36**.<sup>113,114</sup>

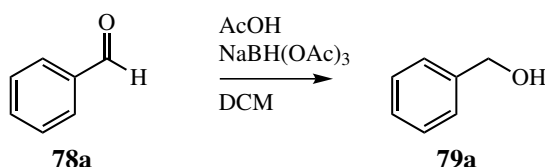
Successful synthesis of the desired compound **65a** was supported by analysis of HRMS and NMR spectra; mass products of  $m/z$  338.1418 / 340.1395 were detected in a ratio of  $\sim 3:1$ , consistent with





### 3.5. SYNTHESIS OF SIMPLE 6-BENZYLPIPERAZINYL-2-AMINOQUINOLINES

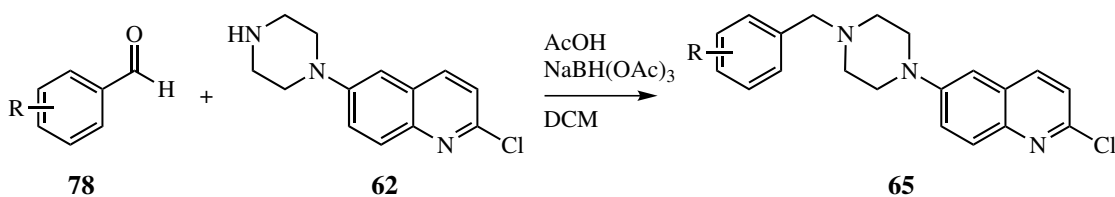
Importantly, the data supported synthesis of the desired product **65a**, and was consistent with literature.<sup>47</sup> While the yield reported in Scheme 3.13 is low at 17%, it is noted that this refers to the isolated yield; analysis of <sup>1</sup>H NMR analysis of crude **65a** revealed the reaction had gone to completion, however as benzaldehyde **78a** and the reducing agent NaBH(OAc)<sub>3</sub> were used in excess, some reduction of **78a** to the corresponding benzyl alcohol **79a** was observed (Scheme 3.14).



Scheme 3.14: Reaction scheme showing formation of reduced benzyl alcohol product **79a** following treatment of **78a** under reductive amination conditions.

There were some difficulties in isolating the desired product **65a** chromatographically from **79a** when a mixture of MeOH/DCM was used as the eluant. However, it was anticipated that an alternative eluant system with reduced polarity (e.g., EtOAc/hexanes) may allow for more effective chromatographic product separation.

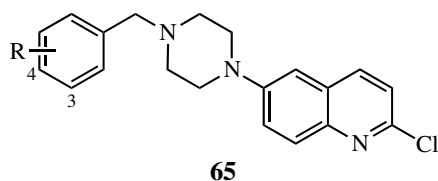
Overall, the reductive amination conditions shown in Scheme 3.13 for the synthesis of **65a** were deemed to be successful and therefore could be applied generally for synthesis of the remaining **65** derivatives, as shown in Scheme 3.15; the yields and corresponding benzyl CH<sub>2</sub> chemical shifts are shown in Table 3.12, indicating successful transformations were achieved for the synthesis of all **65** derivatives.



Scheme 3.15: General reaction conditions for the synthesis of benzylpiperazinyl-substituted 2-chloroquinoline derivatives **65** via reductive amination with benzaldehyde derivatives **78**, and **62**.

### 3.5. SYNTHESIS OF SIMPLE 6-BENZYLPIPERAZINYL-2-AMINOQUINOLINES

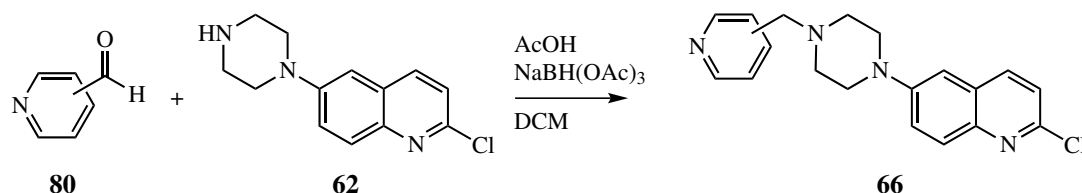
Table 3.12: Yields from synthesis of benzylpiperazinyl-substituted 2-chloroquinoline derivatives **65** via reductive amination. Successful synthesis of each **65** derivative supported by the presence of characteristic benzyl CH<sub>2</sub> signals in <sup>1</sup>H NMR spectra.



Compound	R =	Yield (%)	$\delta_{\text{H}}$ benzyl CH <sub>2</sub> (ppm)
<b>65a</b>	H	17	3.59
<b>65b</b>	3-Me	49	3.56
<b>65c</b>	4-Me	43	3.55
<b>65d</b>	3-F	50	3.57
<b>65e</b>	4-F	39	3.55
<b>65f</b>	3-OMe	55	3.56
<b>65g</b>	4-OMe	28	3.53
<b>65h</b>	3-CN	56	3.61
<b>65i</b>	4-CN	67	3.64

From Table 3.12, the desired **65** derivatives were generally synthesised in moderate-good yields, and their successful synthesis was supported by analysis of both HRMS (where the desired mass products were observed for each **65** derivative) and NMR spectra (where characteristic chemical shifts for incorporation of the corresponding benzyl substituent were observed for each **65** derivative). Notably, the chemical shifts of the benzyl CH<sub>2</sub> signals for each derivative in <sup>1</sup>H NMR spectra were consistently observed at ~3.57 ppm.

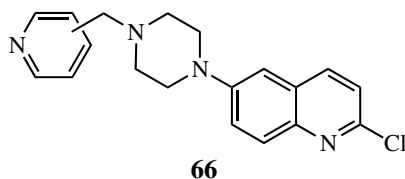
Based upon the successful synthesis of **65** derivatives reported in Table 3.12, the same reductive amination conditions were applied towards the synthesis of **66** derivatives (Scheme 3.16), and the resultant yields and chemical shifts for each pyridylmethyl CH<sub>2</sub> group reported in Table 3.13.



Scheme 3.16: General reaction conditions for the synthesis of pyridylmethyl piperazinyl-substituted 2-chloroquinoline derivatives **66** via reductive amination with pyridinecarboxaldehyde derivatives **80**, and **62**.

### 3.5. SYNTHESIS OF SIMPLE 6-BENZYLPIPERAZINYL-2-AMINOQUINOLINES

Table 3.13: Yields from reductive amination of pyridinecarboxaldehyde derivatives **80** and **62**, to successfully synthesise pyridylmethyl piperazinyl-substituted 2-chloroquinoline derivatives **66**. Successful synthesis of each **66** derivative supported by the presence of characteristic pyridylmethyl CH<sub>2</sub> signals in <sup>1</sup>H NMR spectra.



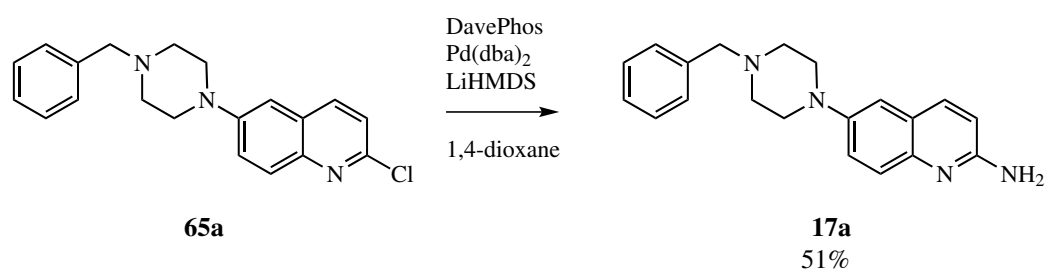
Compound	Pyridyl substitution	Yield (%)	$\delta_{\text{H}}$ pyridylmethyl CH <sub>2</sub> (ppm)
<b>66a</b>	2	51	3.75
<b>66b</b>	3	72	3.60
<b>66c</b>	4	73	3.60

Again, the successful synthesis of **66** derivatives reported in Table 3.13 was supported by analysis of HRMS and NMR spectra — for each **66** derivative, the observed major mass products in mass spectra displayed  $m/z$  consistent with the desired products; similarly in NMR spectra, signals were observed which were consistent with the incorporation of a pyridylmethyl group. When comparing the chemical shifts in <sup>1</sup>H NMR spectra for benzyl CH<sub>2</sub> group signals in **65** derivatives to the pyridylmethyl CH<sub>2</sub> signals in **66** derivatives, the pyridylmethyl CH<sub>2</sub> signals are slightly deshielded relative to the parent **65a** derivative, likely due to the electron-deficient nature of the pyridyl ring (average CH<sub>2</sub> chemical shift ~3.65 ppm, c.f. 3.57 ppm). Overall, each **65** and **66** derivative had been synthesised in sufficient yields to support continuation to the next synthetic step.

#### 3.5.2 Synthesis of 6-position substituted 2-aminoquinoline derivatives

Similarly to the synthesis of **60** and **61** derivatives, the final step in the synthesis of **17** and **59** ligand families required amination of the 2-chloroquinoline **65** and **66** derivatives. A generally-applicable synthetic method was desired, and as reported previously (in the literature<sup>47,56,66</sup> and in this thesis), a second Buchwald-Hartwig reaction using LiHMDS as both a base and an ammonia equivalent was considered. While this approach previously afforded **60** and **61** ligands in lower yields (presumably due to Pd coordination and sequestration), it was hypothesised that Pd coordination would be less likely for the synthesis of **17** and **59** derivatives, due to the absence of the tertiary amide. To test the applicability of this approach, a proof-of-concept reaction was undertaken towards the synthesis of **17a** as shown in Scheme 3.17.

### 3.5. SYNTHESIS OF SIMPLE 6-BENZYLPIPERAZINYL-2-AMINOQUINOLINES



Scheme 3.17: Proof-of-concept Buchwald-Hartwig reaction conditions for amination of **65a**, using LiHMDS as an ammonia equivalent to synthesise the benzylpiperazinyl-substituted 2-aminoquinoline derivatives **17a**.

Successful formation of **17a** was supported by analysis of HRMS and NMR spectra; a major mass product with  $m/z$  consistent with **17a** was observed (observed  $m/z$  319.1921; required  $m/z$  319.1917). Furthermore, analysis of  $^1\text{H}$  NMR spectra revealed a characteristic upfield shift of C(3)H to 6.69 ppm in **17a**, consistent with *ortho* shielding from the newly introduced amino group (Figure 3.16).

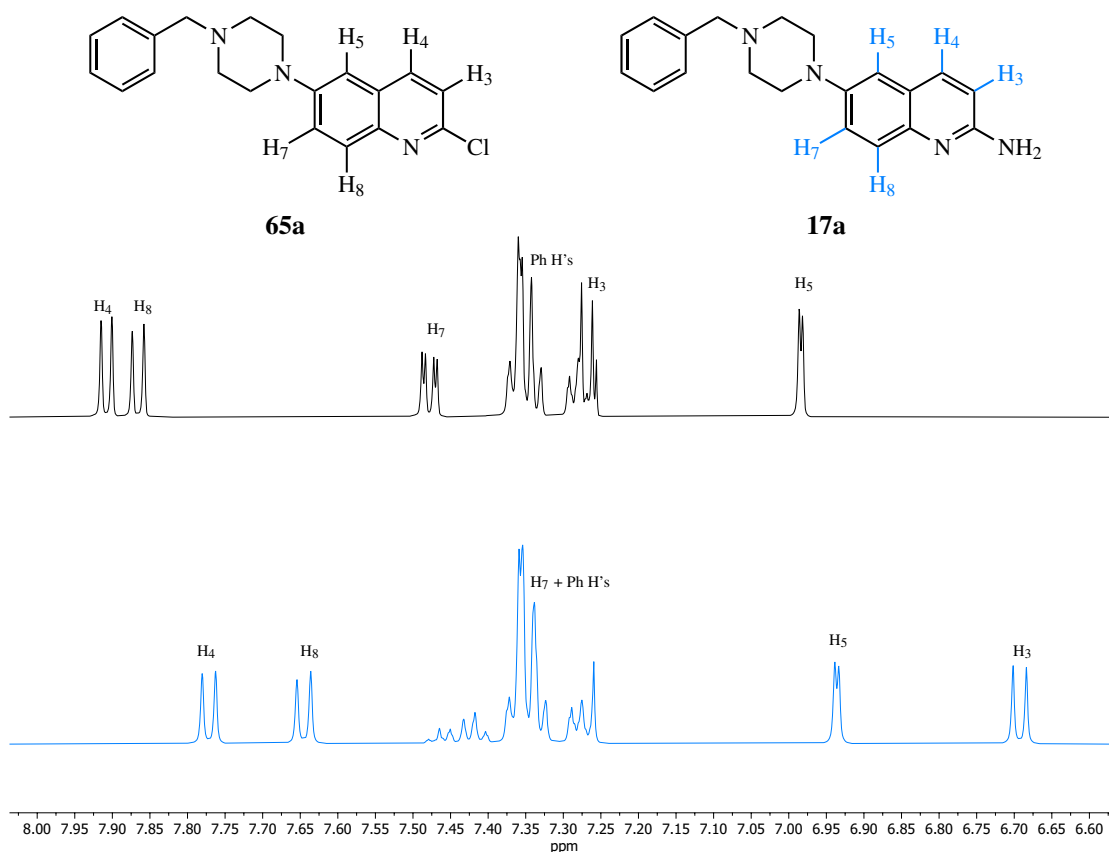
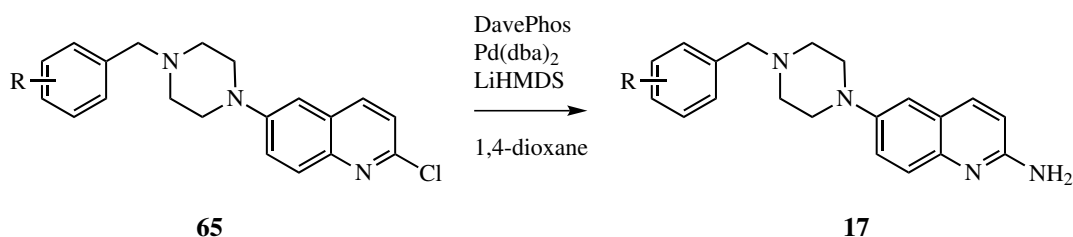


Figure 3.16: Stacked comparison of normalised  $^1\text{H}$  NMR spectra ( $\delta_{\text{H}}$ : 6.60 - 8.00 ppm) of **65a** (black) and **17a** (blue), displaying upfield shift of C(3)H signal in **17a**

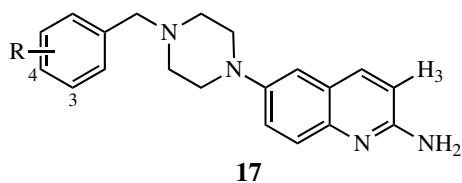
### 3.5. SYNTHESIS OF SIMPLE 6-BENZYLPIPERAZINYL-2-AMINOQUINOLINES

The observed chemical shifts in  $^1\text{H}$  NMR spectra for **17a** were consistent with literature,<sup>47</sup> indicating the product had been successfully synthesised. Additionally, the obtained yield was quite good for a Buchwald-Hartwig coupling reaction which had not been optimised for this specific substrate (i.e., **65a**), therefore it was hypothesised that the reaction conditions would be suitable for the formation of other **17** derivatives. The synthesis of **17** derivatives was undertaken as shown in Scheme 3.18, and the results reported in Table 3.14.



Scheme 3.18: General Buchwald-Hartwig reaction conditions for amination of **65** derivatives, using LiHMDS as an ammonia equivalent to synthesise benzylpiperazinyl-substituted 2-aminoquinoline derivatives, **17**.

Table 3.14: Results of Buchwald-Hartwig amination of **65** derivatives using LiHMDS as an ammonia equivalent, to successfully synthesise benzylpiperazinyl-substituted 2-aminoquinoline derivatives **17**. <sup>a</sup> indicates the product contained trace amounts of benzyl alcohol.



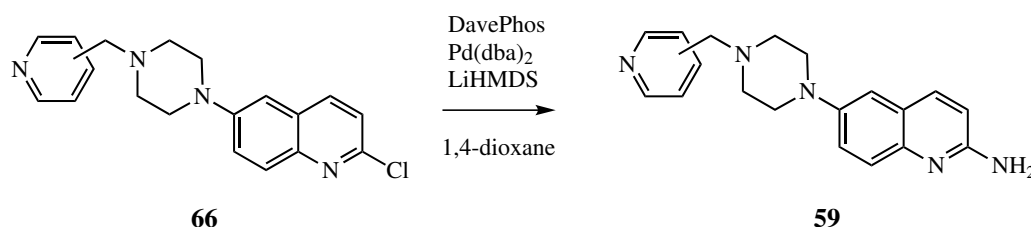
Compound	R =	Yield (%)	$\delta_{\text{H}}$ H <sub>3</sub> (ppm)
<b>17a</b>	H	51 <sup>a</sup>	6.69
<b>17b</b>	3-Me	56	6.68
<b>17c</b>	4-Me	41	6.69
<b>17d</b>	3-F	64	6.67
<b>17e</b>	4-F	55	6.70
<b>17f</b>	3-OMe	47	6.68
<b>17g</b>	4-OMe	67	6.68
<b>17h</b>	3-CN	35	6.70
<b>17i</b>	4-CN	28	6.69

For each of the ligands reported in Table 3.14, successful synthesis of each **17** derivative was supported by analysis of HRMS and NMR spectra as reported previously. For each **17** derivative, the characteristic upfield shift of C(3)H was observed in  $^1\text{H}$  NMR spectra (to  $\sim 6.70$  ppm), indicating successful introduction of the amino group in the 2-position of the quinoline ring. Interestingly,

### 3.5. SYNTHESIS OF SIMPLE 6-BENZYLPIPERAZINYL-2-AMINOQUINOLINES

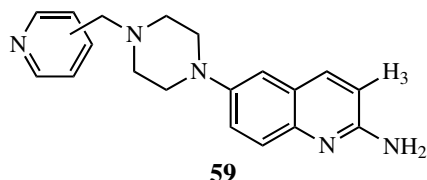
the yields for synthesis of **60** and **61** ligands were typically quite poor (Table 3.8, Table 3.9), while the yields for synthesis of **17** ligands were generally better (moderate-good yields). Therefore, the yields for the desired conversion of the substituted 2-chloroquinoline derivative to the substituted 2-aminoquinoline ligand is generally improved when the tertiary amide group (in **60** and **61** ligands) is absent, suggesting that the tertiary amide may be responsible for the poor conversions observed in the synthesis of **60** and **61** ligands via Buchwald-Hartwig coupling reaction.

Following the successful synthesis of **17** derivatives (and therefore ligands) via Buchwald-Hartwig coupling reaction, the same reaction conditions were utilised for the synthesis of **59** derivatives, as shown in Scheme 3.19, and the results reported in Table 3.15.



Scheme 3.19: General Buchwald-Hartwig coupling reaction conditions for amination of **66** derivatives, using LiHMDS as an ammonia equivalent to synthesise pyridylmethyl piperazinyl-substituted 2-aminoquinoline derivatives, **59**.

Table 3.15: Results of Buchwald-Hartwig amination of **66** derivatives using LiHMDS as an ammonia equivalent, to successfully synthesise pyridylmethylpiperazinyl-substituted 2-aminoquinoline derivatives **59**.



Compound	Pyridyl substitution	Yield (%)	$\delta_{\text{H H}_3}$ (ppm)
<b>59a</b>	2	11	6.71
<b>59b</b>	3	71	6.68
<b>59c</b>	4	51	6.72

Again, successful synthesis of each **59** derivative was supported by analysis of HRMS and NMR spectra; in each case, the desired mass product was observed in mass spectra, and each derivative exhibited the characteristic upfield shift of C(3)H in <sup>1</sup>H NMR spectra, to ~6.70 ppm, which is diagnostic for the introduction of the 2-amino group at the quinoline ring (Table 3.15). It is noted that the yield for the 2-pyridyl derivative **59a** is substantially lower than for either **59b** and **59c** (11%

v.s., 71% & 51%) — it is hypothesised that the reduced yield for **59a** may also be due to Pd sequestration from the catalytic cycle, as the positioning of the 2-pyridyl ring adjacent the piperazinyl ring may be amenable to coordination of Pd, as indicated in Figure 3.17. Despite the lower yield observed for synthesis of **59a**, sufficient material for all **17** and **59** ligands had been synthesised to proceed with SPR binding studies.

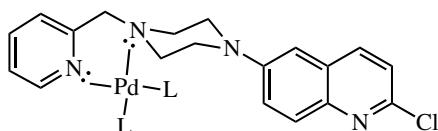


Figure 3.17: Proposed mechanism of Pd sequestration during synthesis of **59a**, indicating undesired coordination of the Pd species. “L” indicates coordinate ligands.”

### 3.5.3 Derivatisation of nitrile-containing 2-aminoquinoline ligands

In an effort to investigate a wider variety of electron-deficient 2-aminoquinoline ligands, and to obtain more comparable data to previously reported lead compounds (including **20**) for targeting the Tec SH3 domain,<sup>56</sup> it was desirable to synthesise the amide-substituted derivatives **17j**, **17k**, **60j** and **60k** (Figure 3.18).

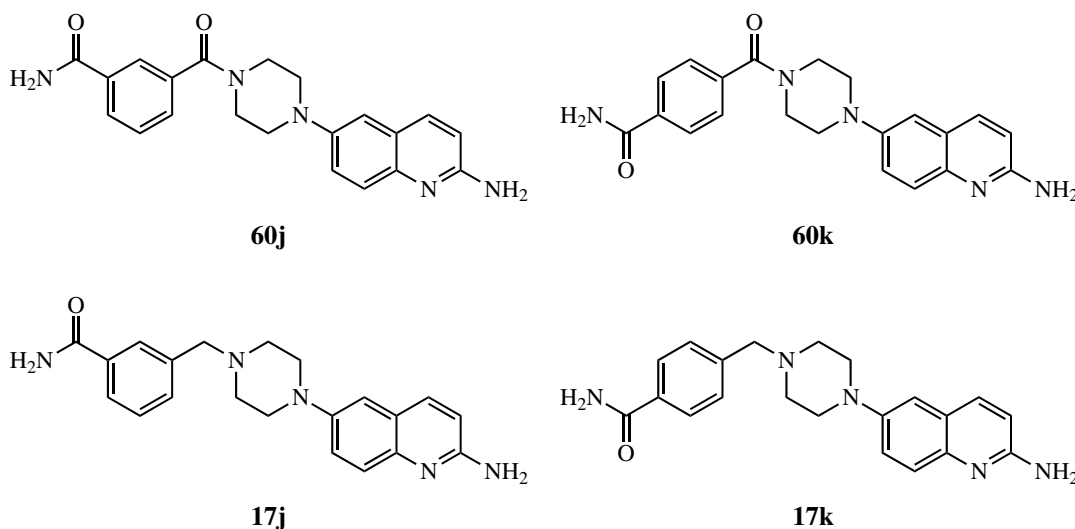


Figure 3.18: Structures of proposed amide-substituted 2-aminoquinoline ligands, **17j**, **17k**, **60j** and **60k**

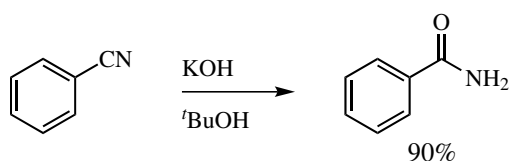
It was envisaged that the corresponding nitrile substituted ligands **17h**, **17i**, **60h** and **60i** would be suitable reagents for synthesis of **17j**, **17k**, **60j** and **60k**, as the nitrile group could be selectively hydrolysed to the corresponding amide by following previously reported methods.<sup>56,66</sup> Unfortunately, due to low yields obtained in the previous Buchwald-Hartwig coupling reaction for **60** derivatives, there were insufficient quantities of **60h** and **60i** to proceed with nitrile hydrolysis. However, the



### 3.5. SYNTHESIS OF SIMPLE 6-BENZYLPIPERAZINYL-2-AMINOQUINOLINES

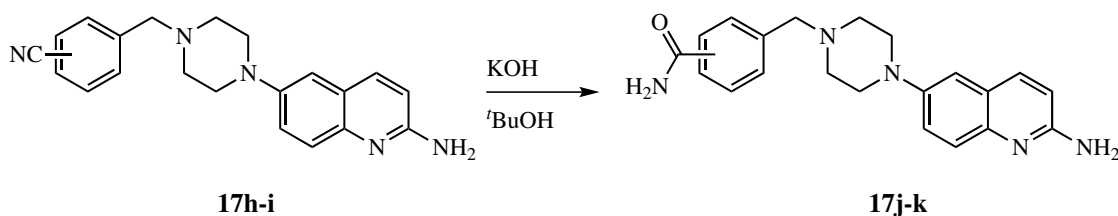
yields obtained for synthesis of **17h** and **17i** were comparably higher, to the extent that sufficient material was available to attempt nitrile hydrolysis for the synthesis of amide-substituted ligands **17j** and **17k**.

An interesting literature procedure reported the selective hydrolysis of benzonitrile to benzamide, and not benzoic acid (Scheme 3.20).<sup>115</sup> Typically, nitrile hydrolysis occurs by heating the nitrile in a weakly basic medium in the presence of hydrogen peroxide.<sup>116</sup> However, Hall and Gisler noted that when benzamide was refluxed in *tert*-butanol with potassium hydroxide, it was not hydrolysed to benzoic acid. Following this, when benzonitrile was treated under analogous reaction conditions, it was hydrolysed to benzamide only, and not benzoic acid; Hall and Gisler proposed that hydrolysis stops upon benzamide formation due to formation of the potassium salt of the amide, which is insoluble and therefore cannot undergo further nucleophilic attack to facilitate hydrolysis to the carboxylic acid.<sup>115</sup>



Scheme 3.20: Literature synthesis of benzamide by selective hydrolysis of benzonitrile.<sup>115</sup>

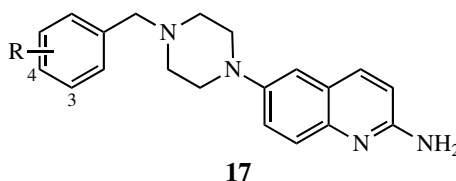
As we were only interested in synthesising the amide-containing derivatives **17j** and **17k**, the method reported by Hall and Gisler<sup>115</sup> was attractive, and had been validated for similar substituted 2-aminoquinoline compounds previously.<sup>66</sup> Therefore, hydrolysis of **17h** and **17i** was undertaken using the conditions reported by Hall and Gisler,<sup>115</sup> with minor adaptations for reaction scale (Scheme 3.21); the yields for this hydrolysis are reported in Table 3.16.



Scheme 3.21: General reaction conditions for hydrolysis of nitrile-containing 2-aminoquinoline derivatives, **17h** and **17i** to synthesise amide-containing 2-aminoquinoline ligands, **17j** and **17k**, respectively.<sup>66,115</sup>

### 3.5. SYNTHESIS OF SIMPLE 6-BENZYLPIPERAZINYL-2-AMINOQUINOLINES

Table 3.16: Results and yields of nitrile hydrolysis of **17** derivatives using potassium hydroxide in *tert*-butanol, to successfully synthesise amide-containing 2-aminoquinoline ligands.



Compound	R =	Yield (%)
<b>17j</b>	3-CONH <sub>2</sub>	53
<b>17k</b>	4-CONH <sub>2</sub>	43

Successful synthesis of the desired amide-containing ligands **17j** and **17k** was supported by analysis of HRMS, IR and NMR spectra. For both **17j** and **17k**, analysis of mass spectra revealed major mass product with  $m/z$  values of 362.1973 and 362.1976 respectively (expected  $m/z$ : 362.1975). In addition, each of **17j** and **17k** exhibited a strong IR stretch at  $\sim 1604\text{ cm}^{-1}$  (C=O) and medium IR stretches at  $\sim 3347$  and  $\sim 3204\text{ cm}^{-1}$  (N-H), which may be consistent with a conjugated amide (however it is noted the latter N-H stretches may be overlapping with N-H stretches from 2-aminoquinoline group). Importantly, for both **17j** and **17k**, there were no IR stretches observed in the region around  $2226\text{ cm}^{-1}$ , indicating the nitrile group was no longer present. In addition, analysis of <sup>1</sup>H NMR spectra for both **17j** and **17k** revealed the emergence of two distinct broad amide N-H signals (Figure 3.19), consistent with the formation of a primary amide.

While the yields for synthesis of **17j** and **17k** are moderate, it is noted that the reactions had gone to completion via TLC. It is possible that some material may have been lost during reaction workup and product purification, despite concerted efforts to maximise product recovery. During the liquid-liquid extraction stage of workup, the reaction mixtures were extracted several times with a 3:1 mixture of CHCl<sub>3</sub>/*i*PrOH, in an attempt to remove the polar **17j** or **17k** from the aqueous phase. Furthermore, the products were purified by column chromatography on silica gel, and during purification a dark band was observed at the top of the silica column — while this was not investigated, it is possible that some product may have oxidised, and could not be eluted from the silica. Overall, despite the moderate yields obtained during nitrile hydrolysis, sufficient quantities of **17j** and **17k** were obtained to proceed with SPR ligand binding studies.

### 3.5. SYNTHESIS OF SIMPLE 6-BENZYLPIPERAZINYL-2-AMINOQUINOLINES

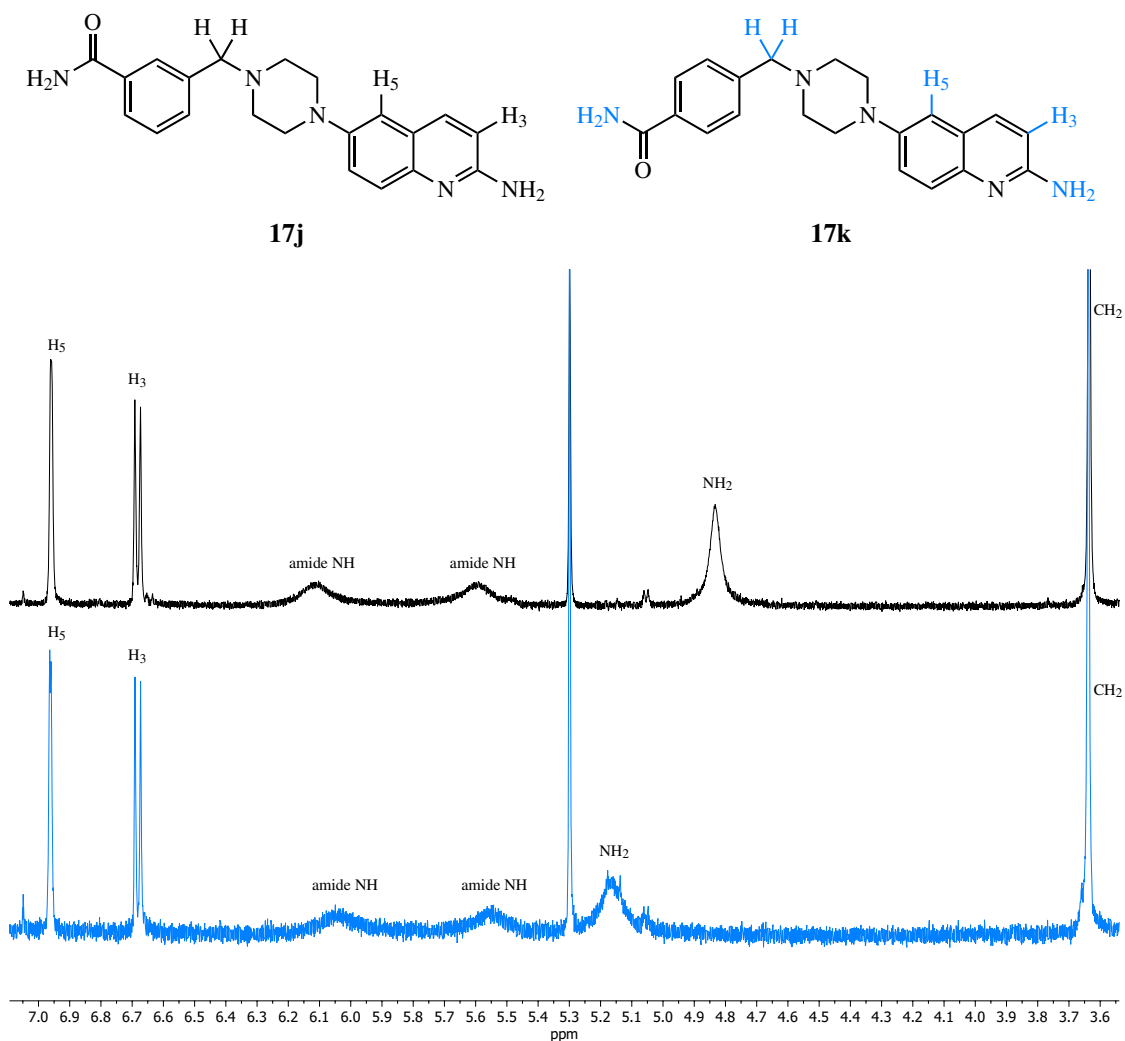


Figure 3.19: Stacked comparison of normalised <sup>1</sup>H NMR spectra (δ<sub>H</sub>: 3.6 - 7.0 ppm) of **17j** (black) and **17k** (blue), displaying formation of two distinct, broad amine NH signals following nitrile hydrolysis of **17h** and **17i**, respectively. Residual DCM peak present at 5.30 ppm.

## **3.6 SPR binding studies of 6-benzylpiperazinyl-2-aminoquinoline derivatives**

### **3.6.1 SPR binding assay aims**

To determine the binding affinities of the 6-benzylpiperazinyl 2-aminoquinoline ligand families **17** and **59** for the Tec SH3 domain, it was decided that the binding affinities would again be screened and calculated by SPR assays. The ligand binding affinities for the Tec SH3 domain would be determined by conducting SPR binding assays against GST-Tec SH3 protein, using the assay method validated previously (see Chapter 2).<sup>56,66</sup> In addition, it was also desirable to ensure that the newly synthesised **17** and **59** ligands were binding the Tec SH3 domain in a manner consistent with the proposed ligand-protein binding model.<sup>46,47</sup> Therefore, a second set of ligand binding assays were conducted with the mutant protein GST-Tec SH3 D196A, to investigate whether **17** and **59** ligands are making key binding interactions with amino acid residues W215 and D196 of the Tec SH3 domain surface. Both of these SPR ligand binding assays were prepared and conducted as previously described in Chapter 2, and the results described in the following sections.

### **3.6.2 Results of SPR binding assays with GST-Tec SH3**

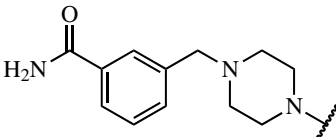
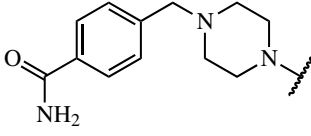
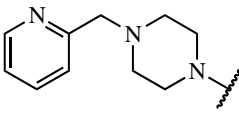
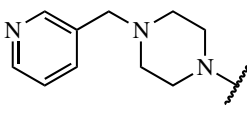
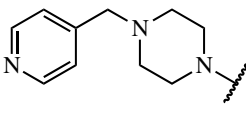
The binding affinities of **17** and **59** ligands for the Tec SH3 domain were determined by SPR binding assays against GST-Tec SH3 (as described in Section 2.4.1 of Chapter 2), and the results reported below in Table 3.17.

### 3.6. SPR BINDING STUDIES OF 6-BENZYLPIPERAZINYL-2-AMINOQUINOLINE DERIVATIVES

Table 3.17: Binding affinities of **17** and **59** ligands determined by SPR for binding GST-Tec SH3.  $K_d$  values were obtained from assays completed in triplicate across separate runs, and the average  $K_d$  value (and standard deviation) reported. <sup>a</sup> indicates only a screening  $K_d$  value was obtained. <sup>b</sup> indicates binding isotherms had not reached plateau, as the ligand showed precipitation at high concentrations, therefore the data point was removed. <sup>c</sup> indicates ligand exhibited some off-site binding to reference channel protein. <sup>d</sup> indicates assays (in triplicate) were completed within a single run.

Compound	R =	GST-SH3
		$K_d \pm SD$ ( $\mu\text{M}$ )
<b>17a</b>		$9.2 \pm 0.6$
<b>17b</b>		$27.4^a$
<b>17c</b>		$4.1 \pm 0.6^{b,c}$
<b>17d</b>		$18.9 \pm 2.5$
<b>17e</b>		$10.6 \pm 1.9$
<b>17f</b>		$11.1 \pm 3.6^b$
<b>17g</b>		$6.7 \pm 0.5$
<b>17h</b>		$13.0 \pm 1.4$
<b>17i</b>		$29.9^a$

---

<b>17j</b>		$9.2 \pm 0.4$
<b>17k</b>		$6.8 \pm 0.1$
<b>59a</b>		$5.2 \pm 0.9^d$
<b>59b</b>		$10.6 \pm 0.7$
<b>59c</b>		$11.6 \pm 1.3$

---

The **17** derivatives reported in Table 3.17 typically displayed different binding affinities compared to their **60** equivalents reported in Table 3.10. While the **60** derivatives typically displayed consistent binding affinities of  $K_d \approx 10 \mu\text{M}$ , the binding affinities for **17** derivatives showed more variability, particularly between 3- and 4-substituted derivatives with the same functional group; 3-position substituted **17** derivatives typically displayed weaker binding affinities than their 4-position substituted counterparts. It is currently unclear whether this differentiation in ligand binding affinity between 3- and 4-position substituted **17** derivatives is due to electronic or steric effects, however the (almost) consistently reduced binding affinity for 3-position substituted **17** derivatives tends to suggest substitution at the 3-position is not sterically favourable. The exception to this is the nitrile substituted derivatives **17h** and **17i**. Interestingly, the 4-amido substituted derivative **17k** exhibits a 4-fold gain in binding affinity over **17i**, suggesting the amide group may be making an additional favourable contact with the Tec SH3 domain. This also suggests that the improvement in binding affinity typically observed for electron-deficient ligands<sup>56,66</sup> may not be solely attributed to the electron-deficient character of the phenyl group, but rather through formation of a non-covalent binding interaction. Importantly, the reported binding affinity of **17a** ( $K_d = 9.2 \pm 0.6 \mu\text{M}$ ) is not

### 3.6. SPR BINDING STUDIES OF 6-BENZYLPIPERAZINYL-2-AMINOQUINOLINE DERIVATIVES

overly different from that reported in the literature ( $K_d = 28 \pm 8 \mu\text{M}$ ),<sup>47</sup> particularly when considering comparison of  $K_d$  values between different techniques (SPR & NMR), using different concentrations of DMSO to aid ligand solubilisation. This alignment of current binding affinity data with literature values further supports the applicability of SPR for screening ligands against the Tec SH3 domain, and comparing their affinity values to those reported previously.

Regarding the pyridyl-containing **59** ligands, none of the newly-synthesised derivatives displayed improved binding affinity over either **61** ligands, or the previously-reported lead ligands in Table 3.1. However, the 2-pyridyl derivative **59a** displayed comparable binding affinity to **18a** and **61a** ( $K_d = 5.2 \mu\text{M}$ , c.f.  $5.0$  &  $7.8 \mu\text{M}$ , respectively). Similarly to **61a**, **59a** also exhibited slower association to and dissociation from the sensor chip surface, requiring extended association and dissociation times of 400 sec as shown in Figure 3.20.

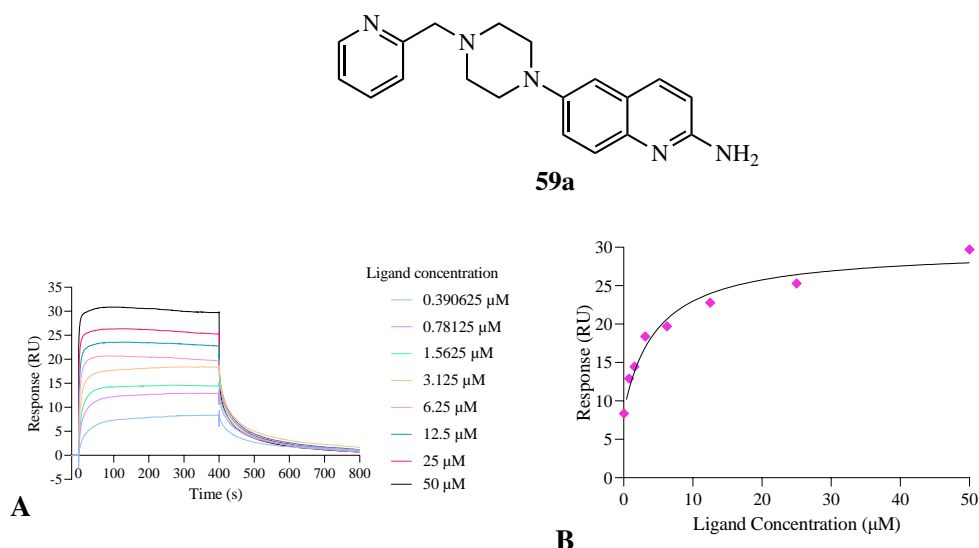


Figure 3.20: SPR sensorgrams and derived isotherm for binding of **59a** binding to GST-Tec SH3. (A) Reference subtracted and corrected sensorgrams for binding of **59a** binding to GST-Tec SH3. Sensor chip surface was washed with 50% DMSO following ligand dissociation phase, and response returned to baseline (not shown). (B) Derived isotherm for the binding of **59a** binding to GST-Tec SH3.

Due to the relatively slower off-rate of **59a** compared to the other **17**, **18**, **59**, **60** and **61** ligands, it would be ideal to investigate the validity of the **59a** data for undertaking kinetic analyses (in addition to affinity analyses). However, from Figure 3.20A, the obtained sensorgrams for **59a** are still quite box-shaped (i.e., have a “square-wave” appearance) and therefore display relatively fast ligand association and dissociation; typically for kinetic analyses of SPR sensorgrams, the sensorgrams should contain sufficient curvature during the association and dissociation phases to enable reliable evaluation of kinetic information (see Figure 3.21).

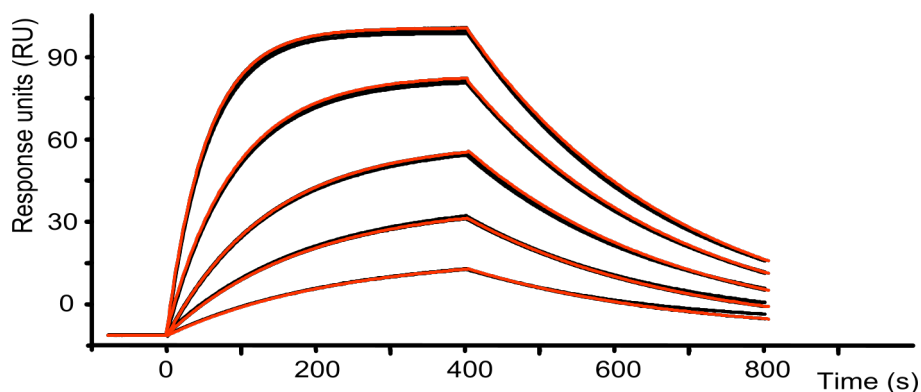


Figure 3.21: Example sensorgrams (black) with sufficient curvature for kinetic model fitting (following a 1:1 interaction model, red). Taken from SPRPages.<sup>117</sup>

Despite **59a** displaying relatively box-shaped sensorgrams (Figure 3.20), 1:1 kinetic model fitting was attempted, with the hope of elucidating kinetic information from the **59a**-GST-Tec SH3 binding interaction; the overlaid **59a** sensorgrams and 1:1 kinetic model are shown in Figure 3.22, and the residuals for the fitted 1:1 kinetic model (i.e., the difference in RU between the sensorgrams and fitted model) are shown in Figure 3.23.

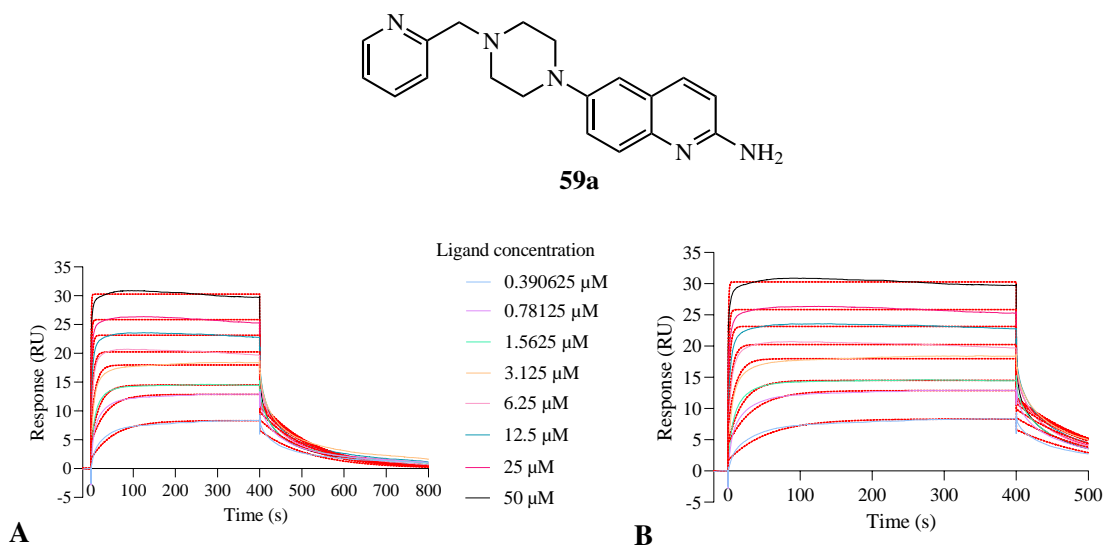


Figure 3.22: Overlaid sensorgrams and fitted 1:1 kinetic model (red dashed lines) for binding of **59a** to GST-Tec SH3. (A) shows full sensorgram and fitted kinetic model. (B) shows truncated sensorgram and kinetic model.



### 3.6. SPR BINDING STUDIES OF 6-BENZYLPIPERAZINYL-2-AMINOQUINOLINE DERIVATIVES

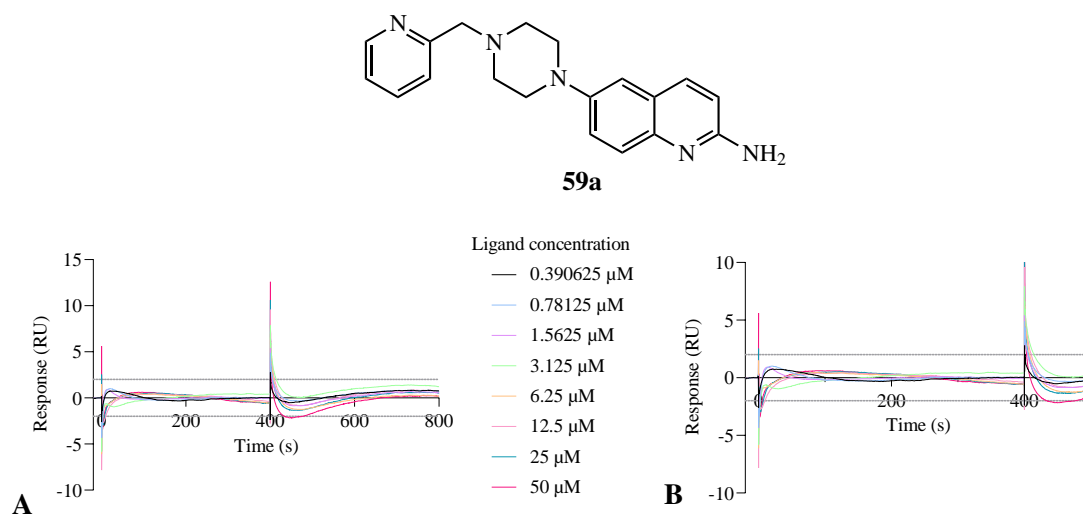


Figure 3.23: Residuals plot of fitted 1:1 kinetics model for binding of **59a** to GST-Tec SH3. Acceptable boundaries for variations in RU ( $0 \pm 2$  RU) shown as grey dashed lines. Full residuals plot shown in (A), truncated and expanded residuals plot shown in (B).

From Figure 3.22, there is some clear deviation between the **59a** sensorgrams and the fitted 1:1 kinetic model, particularly during the association and dissociation phases of the sensorgram. Typically, the goodness-of-fit of a model derived from SPR sensorgram data can be indicated by the chi-square ( $\chi^2$ ) value, where this value is a measure of the average squared residual (i.e., the difference between experimental data and a fitted curve), therefore a lower  $\chi^2$  value suggests the model fits the experimental data closely — for reference, a  $\chi^2$  value should typically be  $<2$  RU.<sup>65</sup> Given the substantial variation of the **59a** sensorgrams from the fitted kinetic model in Figure 3.22 and Figure 3.23, the resultant  $\chi^2$  value was quite high at 11.9. Furthermore, for a well-fitting kinetic model, the residuals should be randomly scattered about 0 (values of  $0 \pm 2$  RU are acceptable),<sup>65</sup> however from Figure 3.23, the distribution of the residuals has a definite pattern, and is well beyond the recommended acceptable limits during the critical phases of ligand interaction for determining association and dissociation rates constants (at  $\sim 0$  sec and  $\sim 400$  sec, respectively). Notably, upon fitting of the kinetic model, the subsequent report generated by the model-fitting software (Biacore S200 Evaluation Software v1.0, GE Healthcare) reported that “high bulk contributions (RI) (i.e., bulk refractive index shifts) were found” in the data, despite reference-channel & blank sample subtractions, and solvent corrections of the raw sensorgrams as described in Section 2.1.1 of Chapter 2. However, it is not unusual for 1:1 kinetic models fitted to sensorgrams that have been correctly processed (to minimise effects from bulk refractive index shifts), but which display rapid ligand association and dissociation, to report “high bulk contributions (RI) were found”, and this has been well-documented previously;<sup>65,117</sup> typically, the model fitting software may incorrectly interpret

rapid interaction events as bulk refractive index shifts.<sup>65,117</sup> Therefore, while the kinetics of **59a** are relatively slower than for other **17**, **18**, **59**, **60** and **61** ligands reported so far in this thesis, **59a** still displays relatively rapid association and dissociation compared to SPR sensorgram literature (see Figure 3.21), so kinetic analyses for **59a** cannot be reliably interpreted at this point. Favourably, as all sensorgrams for **59a** have achieved steady-state and therefore equilibrium binding (Figure 3.20), binding affinity analyses (as  $K_d$  values) are still considered reliable.<sup>65</sup>

Unfortunately, none of the **17** ligands tested displayed improved binding affinity over the previously reported lead compounds reported in Table 3.1. However, there were several instances of ligands exhibiting comparable binding affinity with those reported in Table 3.1 (e.g., **17k** and **59a**), indicating that ligands had been identified with improved physicochemical properties (with regard to predicted oral bioavailability), without compromising binding affinity.

### 3.6.3 Analysis of trends in SPR binding assay data with GST-Tec SH3

Due to the differences in observed binding affinities for **17** and **59** ligands (compared to their **60** and **61** counterparts), investigations into ligand binding activity relationships was again undertaken by Hansch plot analysis. As consistent with Section 3.4.3, the properties investigated for each ligand were electronic character (as Hammett constants,  $\sigma$ ),<sup>108–110</sup> volume (as molar refractivity constants)<sup>111</sup> and overall hydrophobicity (as *clogP* values),<sup>61,112</sup> and the results illustrated in Figure 3.24. Similarly to the Hansch plots utilised for analysis of **60** and **61** ligands, due to the recorded  $K_d$  values for **17** and **59** ligands (Table 3.17), a 10-fold difference in ligand binding affinity is consistent with an activity difference of  $\sim 0.03$ .

For simplicity, analysis of each Hansch plot in Figure 3.24 will be conducted separately. It is noted that **17c** has been excluded from Hansch plot analyses, due to exhibiting some off-site binding to the reference channel protein in SPR assays (Table 3.17), therefore interpretation of binding activity trends using this datapoint would be misleading.

### 3.6. SPR BINDING STUDIES OF 6-BENZYLPIPERAZINYL-2-AMINOQUINOLINE DERIVATIVES

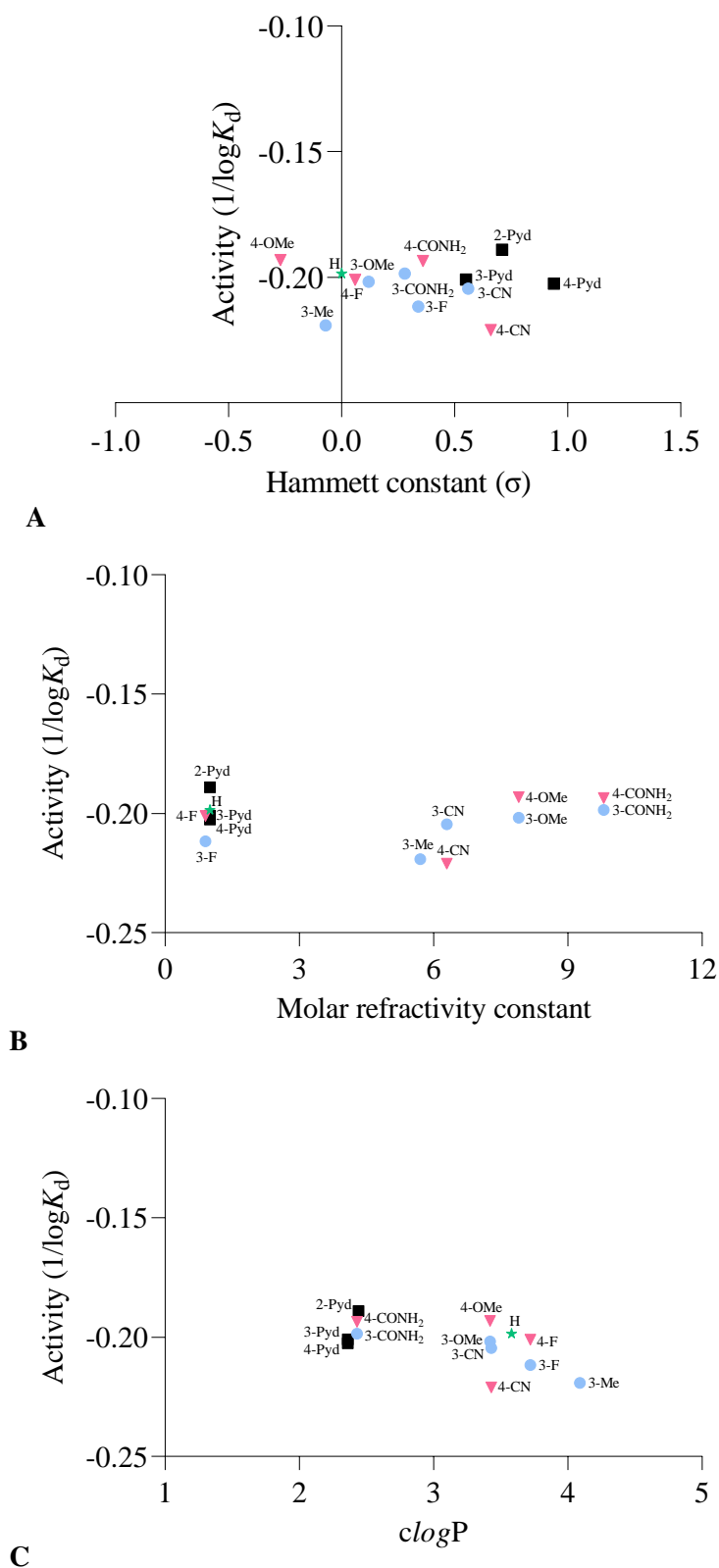


Figure 3.24: Hansch plots displaying relationship between binding activity of **17** and **59** ligands and the: (A) electronic nature of substituent (as Hammett constant,  $\sigma$ );<sup>108–110</sup> (B) volume of substituent (as molar refractivity constant);<sup>111</sup> or (C) hydrophobicity of substituent (as  $c\log P$  value).<sup>61,112</sup> The number indicates the position of the substituent on the phenyl ring, or the position of the nitrogen in the pyridyl ring (denoted ‘Pyd’).

From Figure 3.24A, there does not appear to be any clear contributions by the electronic substituent effects towards **17** and **59** ligand binding activity (Figure 3.24) when **17** and **59** ligands are analysed together (slope  $\approx -0.006$  Activity/ $\sigma$ ,  $R^2 = 0.04230$ , see Figure B.2A in Appendix). However, if the ligands are separated into groups based on phenyl ring substituent position, some weak trends begin to emerge; for **17** ligands with a substituent in the 3-position, the ligand binding activity appears to increase with an increasing  $\sigma$  value (i.e., as the substituent becomes more electron-withdrawing). Conversely, there does not appear to be a clear contribution between  $\sigma$  value and binding activity of **17** ligands with a substituent in the 4-position of the phenyl ring; with the exception of the 4-nitrile derivative (**17i**), the binding activities for 4-position substituted **17** ligands are quite consistent, suggesting that there may be more complex interactions besides  $\sigma$  value implicating binding affinity of **17** ligands. These conclusions should be interpreted with a degree of caution, as grouping the **17** ligands for analysis based on substituent position reduces the sample size substantially.

With regard to Figure 3.24B, again there does not appear to be any clear steric contributions by substituent volume towards **17** and **59** ligand binding activity (slope  $\approx 0.0002$  Activity/molar refractivity constant,  $R^2 = 0.003069$ , see Figure B.2B in Appendix). Furthermore, separating the **17** ligands into groups based upon their substituent position does not elucidate any clear relationships. Similar to **60** and **61** ligands, this suggests that for **17** and **59** ligands with small, simple substituents (consistent with those in Figure 3.24B), there does not appear to be any significant steric effects induced by phenyl substituent size.

When investigating **17** and **59** ligand hydrophobicity (as shown in Figure 3.24C), there did not appear to be any substantial contributions by overall hydrophobicity towards **17** and **59** ligand binding activity (slope  $\approx -0.005$  Activity/ $\log P$ ,  $R^2 = 0.08954$ , see Figure B.2C in Appendix). Again, it is noted that the sample of ligands tested is biased, as each of the **17** and **59** ligands were designed to have lower  $clogP$  values (typically  $<4$ ) in line with Lipinski's Rules,<sup>32</sup> therefore a more diverse sample of ligands may be required to elucidate any significant contributions by overall hydrophobicity on ligand binding activity.

While analysis of **17** and **59** ligand binding activity via Hansch plots did not reveal any clear contributions by phenyl ring substituent  $\sigma$  values, substituent size/steric bulk (as volume, described by molar refractivity) or hydrophobicity to the ligand binding activity of **17** and **59** ligands, it did provide some insights into favourable features which may guide future ligand development — when

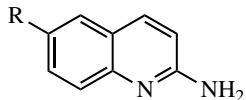
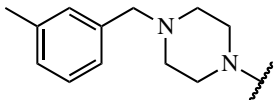
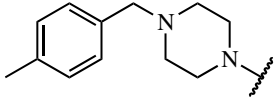
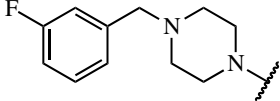
### 3.6. SPR BINDING STUDIES OF 6-BENZYLPIPERAZINYL-2-AMINOQUINOLINE DERIVATIVES

considering substituent volume (Figure 3.24B), there did not appear to be any restrictions to the size or position of the phenyl ring substituents for the **17** and **59** ligands tested, suggesting some tolerability; this could be investigated further.

#### 3.6.4 Results of SPR binding assays with GST-Tec SH3 D196A mutant

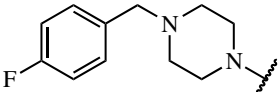
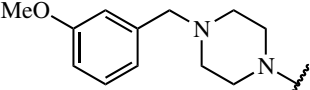
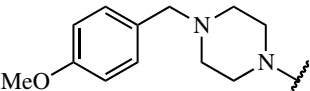
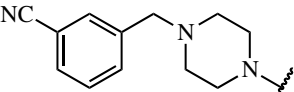
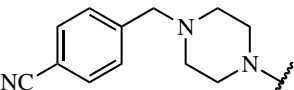
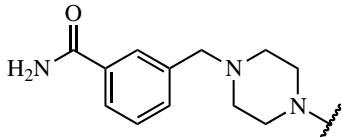
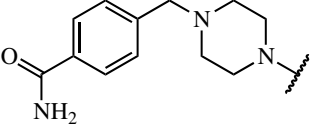
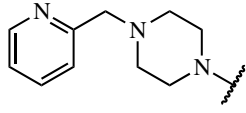
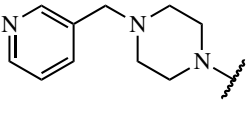
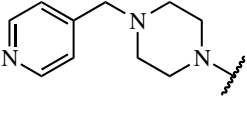
To investigate the location of **17** and **59** ligand family binding to the Tec SH3 domain, and to determine whether their binding mode was consistent with the proposed ligand-protein binding model,<sup>46,47</sup> a series of SPR binding assays against GST-Tec SH3 D196A mutant protein were undertaken as described in Section 2.4.2 of Chapter 2. As discussed previously, if the ligand interaction is consistent with the proposed ligand-protein binding model, then the ligands will not display any binding to the GST-Tec SH3 D196A mutant due to an inability to form the crucial salt-bridge with the D196 side chain residue.<sup>46,47</sup> The results of the SPR binding assays with **17** and **59** ligands are shown in Table 3.18, with exemplar sensorgrams and isotherm for **17a** shown in Figure 3.25.

Table 3.18: Binding affinities of **17** and **59** ligands determined by SPR for binding GST-Tec SH3 D196A mutant protein.

Compound	R =	GST-Tec SH3 D196A
		$K_d \pm SD$ ( $\mu\text{M}$ )
<b>17a</b>		no binding
<b>17b</b>		no binding
<b>17c</b>		no binding
<b>17d</b>		no binding

3.6. SPR BINDING STUDIES OF 6-BENZYLPIPERAZINYL-2-AMINOQUINOLINE  
DERIVATIVES

---

17e		no binding
17f		no binding
17g		no binding
17h		no binding
17i		no binding
17j		no binding
17k		no binding
59a		no binding
59b		no binding
59c		no binding

---

### 3.6. SPR BINDING STUDIES OF 6-BENZYLPIPERAZINYL-2-AMINOQUINOLINE DERIVATIVES

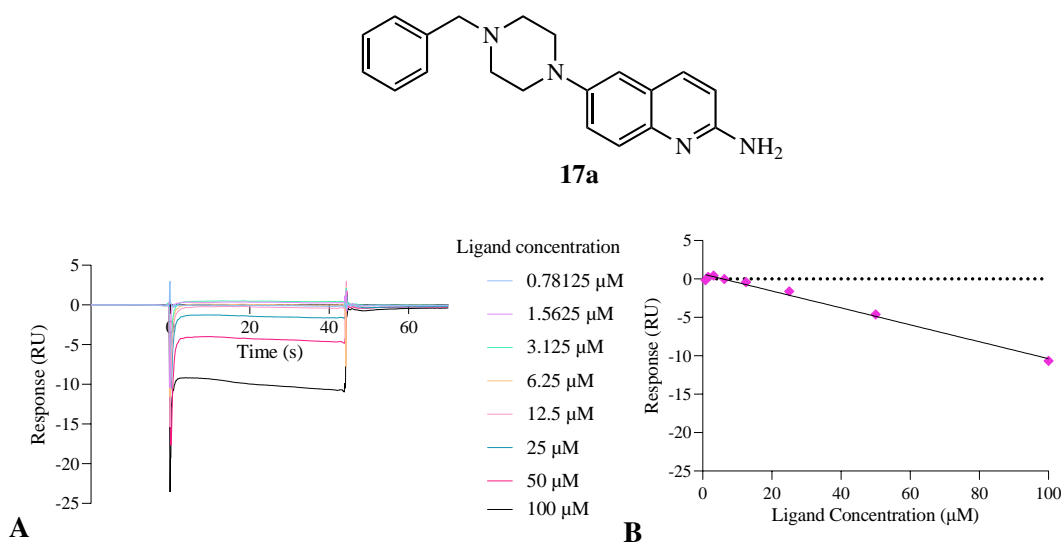


Figure 3.25: SPR sensorgrams and derived isotherms for binding of **17a** to GST-Tec SH3 D196A mutant. (A) Reference-subtracted and corrected sensorgrams for binding of **17a** to GST-Tec SH3 D196A mutant. (B) Derived isotherm for binding of **17a** to GST-Tec SH3 D196A mutant.

None of the **17** and **59** ligands exhibited any binding to GST-Tec SH3 D196A mutant in SPR binding assays; the SPR sensorgrams for each derivative were similar to Figure 3.25, which are consistent with the **60** and **61** ligands, and also those in Figure 2.20 of Chapter 2, indicating no ligand binding. This suggests that each of the **60** and **61** ligands are binding the Tec SH3 domain in a mode consistent with the proposed ligand-protein binding model, and specifically at amino acid residues D196 and W215 on the protein surface.

#### 3.6.5 Summary - Results of SPR binding assays and insights into binding model

Investigation of the piperazinyl-containing ligand families **17**, **59**, **60** and **61** did not lead to the identification of ligands with improved binding affinity for the Tec SH3 domain over the previously reported lead compounds (Table 3.1). However, several novel piperazinyl-containing ligands were identified which had comparable binding affinities to those reported in Table 3.1, whilst also containing improved physicochemical features, through lower *clogP* values and therefore better predicted oral bioavailability, as shown in Figure 3.26. From conducting SPR binding assays with GST-Tec SH3 D196A mutant protein, it was shown that all of the **17**, **59**, **60** and **61** ligands investigated bound the Tec SH3 domain in a mode consistent with the previously proposed ligand-protein binding model; this information about the ligand-protein binding site is invaluable, and can be exploited to infer further ligand development in combination with previously reported data.<sup>46,47</sup>

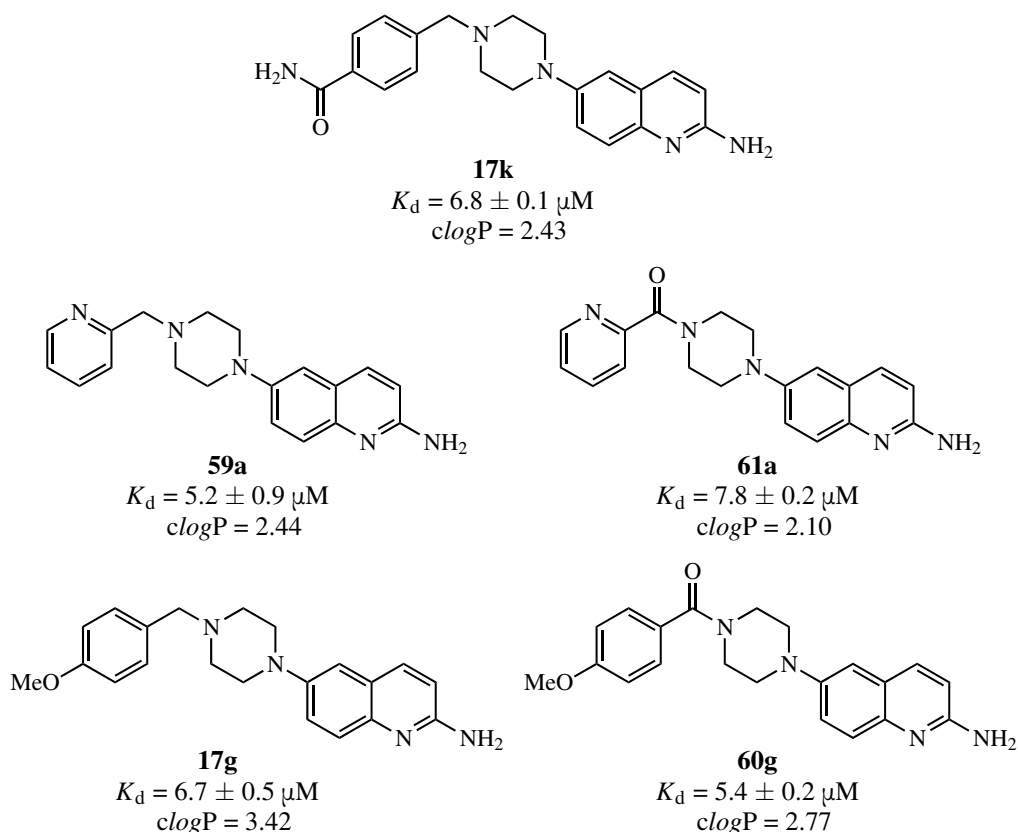


Figure 3.26: Structures of strongest binding piperazinyl 2-aminoquinoline ligands for the Tec SH3 domain, as determined by SPR assays.  $\text{LogP}$  values ( $clogP$ ) calculated using Marvin by ChemAxon.<sup>61</sup>

In an attempt to identify trends in ligand binding affinity, Hansch plots were investigated in the hope of elucidating relationships between **17**, **59**, **60** and **61** ligand binding activity and phenyl substituent features, including electronic characteristics (as Hammett constants), size/volume (as molar refractivity constants), and overall hydrophobicity (as  $clogP$  values). The limited sample size and poor diversity of tested **60** and **61** ligands precluded the reporting of any meaningful relationships; preliminary data did not reveal any clear trends for contributions by  $\sigma$  values upon ligand binding activity, however none of the tested **60** and **61** ligands displayed any reductions in binding affinity upon increasing substituent size, suggesting good steric tolerability in the ligand-protein binding site for a range of small substituents. Regarding **17** and **59** ligands, no clear trends were observed upon analysis of the entire **17** and **59** ligand dataset, however separation of **17** and **59** ligands into groups for analysis based upon phenyl ring substituent position revealed a weak trend showing improved binding activity for **17** ligands containing an electron-withdrawing substituent in the 3-position of the phenyl ring; analysis of **17** ligands with a phenyl ring substituent in the 4-position did not reveal any clear contributions to binding affinity based upon  $\sigma$  values, but instead suggested that the ligand-protein binding interaction was likely complex, and could not be rationalised solely

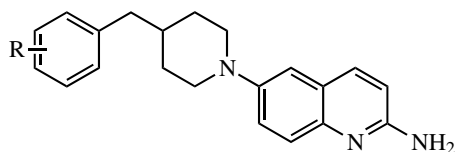


### 3.6. SPR BINDING STUDIES OF 6-BENZYLPIPERAZINYL-2-AMINOQUINOLINE DERIVATIVES

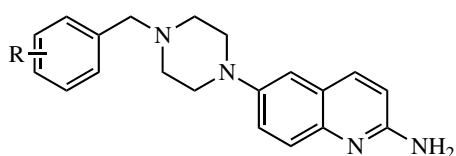
---

by analysis of  $\sigma$  values. Similarly to **60** and **61** ligands, no steric penalties upon ligand binding were observed for any **17** and **59** ligands, suggesting steric tolerability of all substituents tested, and provides an opportunity for future ligand development by extension from the phenyl ring.

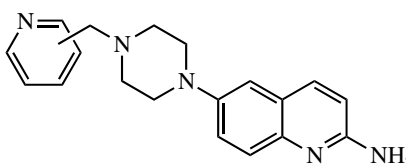
Given the inherent challenges in the synthesis of **60** and **61** ligands, the lack of improvement in binding affinity, and insufficient quantity of SAR data extrapolated from Hansch plot analysis (in the absence of any ligand-bound protein structure to suggest otherwise), it is likely not favourable to pursue further ligand development based on the **60** and **61** structures. Conversely, synthesis and purification of the **17** and **59** ligands were comparably more successful, and the insightful SAR data extrapolated from Hansch plots suggested more promising avenues for future ligand development. Due to the reduced (or comparable) binding affinities for **17** and **59** ligands (with reference to previously reported lead compounds in Table 3.1), it is proposed that future ligand development for targeting the Tec SH3 domain is based upon general ligand structures **15**, **17** and **59**.



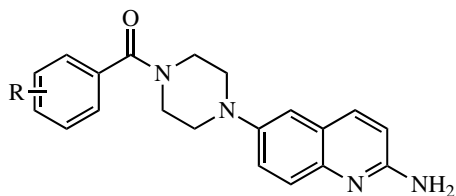
**15**



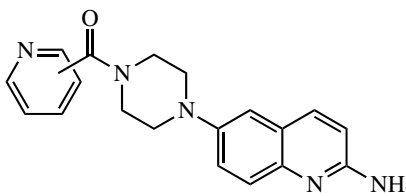
**17**



**59**



**60**



**61**

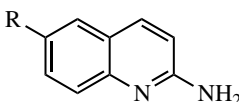
## 4 | Synthesis of complex 6-position substituted 2-aminoquinoline ligands

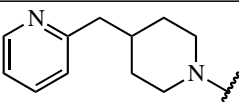
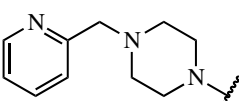
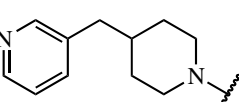
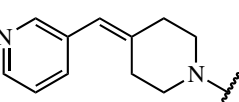
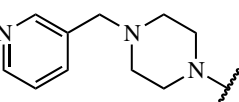
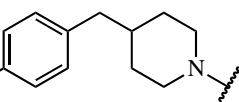
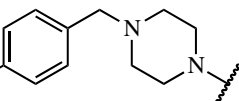
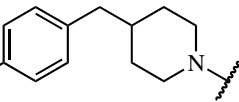
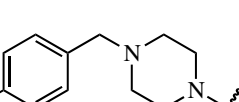
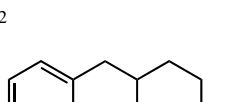
### 4.1 Introduction

The strongest ligands reported to date for binding the Tec SH3 domain (see Table 3.1 in Chapter 3 and Table 4.1) have contained a benzylpiperidinyl or arylmethylpiperidinyl substituent at the 6-position of 2-aminoquinoline. While the previously proposed ligand-protein binding model provides a good indication of the orientation and position of 2-aminoquinoline binding on the Tec SH3 domain surface,<sup>46,47</sup> the binding orientation of the benzylpiperidinyl or arylmethylpiperidinyl substituent is not currently known. Despite this lack of 3-dimensional structural binding information about the benzylpiperidinyl group, previous studies have reported that the nature and position of the substituents on the phenyl ring of the benzylpiperidinyl group can significantly impact ligand binding affinity,<sup>56</sup> therefore some SAR data has been derived. The current SAR data for the strongest Tec SH3 domain small molecule ligands to date indicate that benzylpiperidinyl-substituted 2-aminoquinoline ligands containing either a nitrile or amido group in the 4-position of the phenyl ring, or a single 2,5-pyrimidinyl group at any position around the phenyl ring were well tolerated (Table 3.1 in Chapter 3 and Table 4.1). Furthermore, arylmethylpiperidinyl-substituted 2-aminoquinoline ligands **18a** and **18b** with reduced electron density in the aryl ring also had stronger binding affinity. Therefore, in an attempt to identify an improved small molecule ligand for the Tec SH3 domain, and in the absence of any experimentally-determined structural information (except SAR studies) to describe the benzylpiperidinyl substituent binding interaction, it would be valuable to investigate whether combining each of these favourable benzylpiperidinyl substituents within a single ligand would afford improved binding affinity for the Tec SH3 domain.

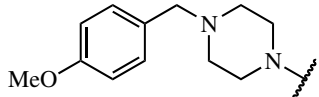
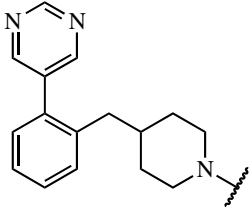
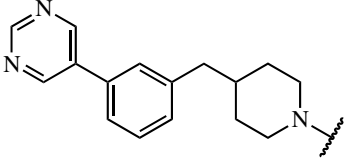
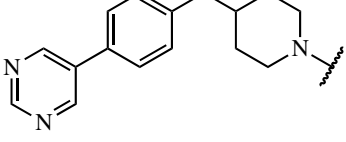
## 4.1. INTRODUCTION

Table 4.1: Binding affinities of 6-heterocycle piperidinyl and piperazinyl substituted 2-aminoquinoline derivatives, with high binding affinity for the Tec SH3 domain (determined by SPR assays)<sup>56,66</sup> and *clogP* values.<sup>61</sup> <sup>a</sup> indicates highest concentration datapoint removed due to precipitation or aggregation of compound under assay conditions. <sup>b</sup> indicates Response-concentration curve not at plateau; saturation binding not achieved.



Compound	Structure	$K_d$ ( $\mu\text{M}$ )	<i>clogP</i>
18a		$5 \pm 1^{56}$	3.38
59a		$5.2 \pm 0.9$	2.44
18b		$3.0 \pm 0.7^{66}$	3.50
35b		$1.9 \pm 0.1^{56}$	3.18
59b		$10.6 \pm 0.7$	2.36
19		$2.0 \pm 0.5^{a56}$	4.58
17i		29.9	3.43
20		$2.0 \pm 0.1^{a56}$	3.57
17k		$6.8 \pm 0.1$	2.43
81		$15.4^{b56}$	4.56

---

<b>17g</b>		$6.7 \pm 0.5$	3.42
<b>23</b>		$7 \pm 1^{56}$	4.44
<b>24</b>		$4.1 \pm 0.7^{56}$	4.44
<b>25</b>		$2.4 \pm 0.2^{56}$	4.44

---

A previously noted limitation of the current lead ligands was the increased hydrophobicity of the parent benzylpiperidinyl-substituted 2-aminoquinoline structure, which would present limited opportunities for further derivatisation (as ligand activity assays are conducted under biologically-relevant conditions). However, the work described in Chapter 3 of this thesis revealed identification of benzylpiperazinyl derivative-containing ligands **17** and **59**, with generally comparable binding affinities to their benzylpiperidinyl counterparts, but with improved predicted oral bioavailability (*clogP* values, Table 4.1), and therefore more favourable physicochemical properties. Importantly, the lower *logP* values for these benzylpiperazinyl-containing structures are likely to provide more scope for ligand derivatisation, whilst also maintaining favourable ligand solubility under biologically-relevant conditions. Considering the improved *clogP* values for **17** and **59** ligands (and therefore greater scope for derivatisation) and generally comparable binding affinities, it was envisaged that combining favourable benzylpiperazinyl substituents within a single ligand would also be worthwhile to investigate.

From the phenyl ring substituents and aryl groups of the strongest binding ligands listed in Table 4.1, it was determined that there were three key phenyl ring substituents or aryl groups (i.e.,

## 4.1. INTRODUCTION

---

three key features) which typically afforded improved binding affinity in both benzylpiperidinyl and benzylpiperazinyl-containing ligands; these key phenyl ring substituents and aryl groups are identified as:

1. A 2,5-pyrimidinyl substituent, at any position around the phenyl or aryl ring;
2. An amido substituent, at the 4-position of the phenyl or aryl ring; and
3. A 2-pyridyl ring as the aryl group.

Given that the three key features listed above are not necessarily mutually exclusive (with regard to substituent position), it would be ideal to investigate the synthesis and subsequent binding activity of complex ligands containing a combination of these three key features, in an attempt to identify a ligand with improved binding affinity for the Tec SH3 domain. However, as an experimentally-determined ligand-bound protein structure is not available for any of the ligands listed in Table 4.1, it would be rash to immediately combine all three key features in one “ultimate” ligand; if the binding affinity data for this “ultimate” ligand was poor, there would be insufficient SAR data to elucidate which functional group is responsible for the reduced binding affinity. Therefore, it was proposed that sequential combinations of the three key features above to form complex ligands should be undertaken (i.e., combine features 1 & 2 in one ligand, combine features 2 & 3 in another ligand, and combine features 1 & 3 in another ligand) — this should provide sufficient SAR information to infer any positive or negative interactions caused by the combination of each of the three key features. Potentially, the binding affinity data from these complex ligands may also provide a strong rationale for or against the development of an “ultimate” ligand containing all three key functional features in future.

For design of the potential complex ligands, there appeared to be some flexibility regarding the positioning of the 2,5-pyrimidinyl group — from Table 4.1, the binding affinities for **23**, **24** and **25** were comparable. Conversely, the position of the amido group around the phenyl ring was important; ligand binding affinity was substantially improved when the amido group was located in the 4-position of the phenyl ring (in **17k** and **20**), rather than the 3-position (**17j**  $K_d = 9.2 \mu\text{M}$  (see Chapter 3, Table 3.17), and previously reported ligands).<sup>66</sup> Lastly, while the binding affinities of some 3-pyridyl derivatives (**18b** and **35b**) indicate strong binding, the consistent binding affinities of 2-pyridyl derivatives across both benzylpiperidinyl- and benzylpiperazinyl-substituted ligands (**18a**

and **59a**, respectively) could provide better opportunities for development of potential ligands with more ideal drug-like character (through reduced *clogP* values). Furthermore, the slower rates of 2-pyridyl ligand interactions with the Tec SH3 domain in SPR binding assays (particularly the slower binding dissociation rate of **59a**) may be indicative of more favourable ligand binding kinetics, so ligands containing a 2-pyridyl aryl group should be considered. Therefore, various combinations of the position and nature of these key ligand features were investigated, and some general, more complex (relative to those reported in Chapters 2 & 3) ligands are proposed (Figure 4.1).

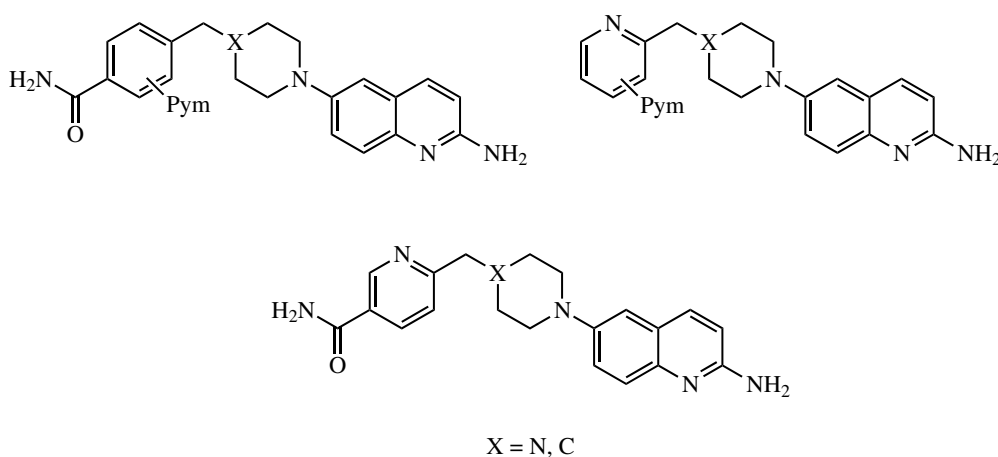


Figure 4.1: Proposed general structures for complex 2-aminoquinoline ligands. Pym = 2,5-pyrimidine.

It was hypothesised that at least some of the key features (2,5-pyrimidinyl-, 4-amido-, or 2-pyridyl groups) may combine synergistically within a single structure (suggested in Figure 4.1), to potentially allow identification of a small molecule ligand for the Tec SH3 domain with improved binding affinity, whilst maintaining (predicted) oral bioavailability. Consequently, routes towards the synthesis of the more complex ligands proposed in Figure 4.1 were required.

## 4.2 Proposed ligands and general synthetic pathways

To synthesise the more complex ligands proposed in Figure 4.1, it would be ideal to develop general synthetic pathways for both benzylpiperidinyl- and benzylpiperazinyl-substituted ligands; the synthesis of each of these ligand families are proposed to be undertaken via the general synthetic pathways shown in Figure 4.2 and Figure 4.3. The synthetic pathway shown in Figure 4.2 is consistent with the methods utilised in Chapter 2, and those reported previously,<sup>56,66</sup> while the general synthetic pathway shown in Figure 4.3 is based upon the methods utilised in Chapter 3 towards the synthesis of **17** and **59** ligands.

## 4.2. PROPOSED LIGANDS AND GENERAL SYNTHETIC PATHWAYS

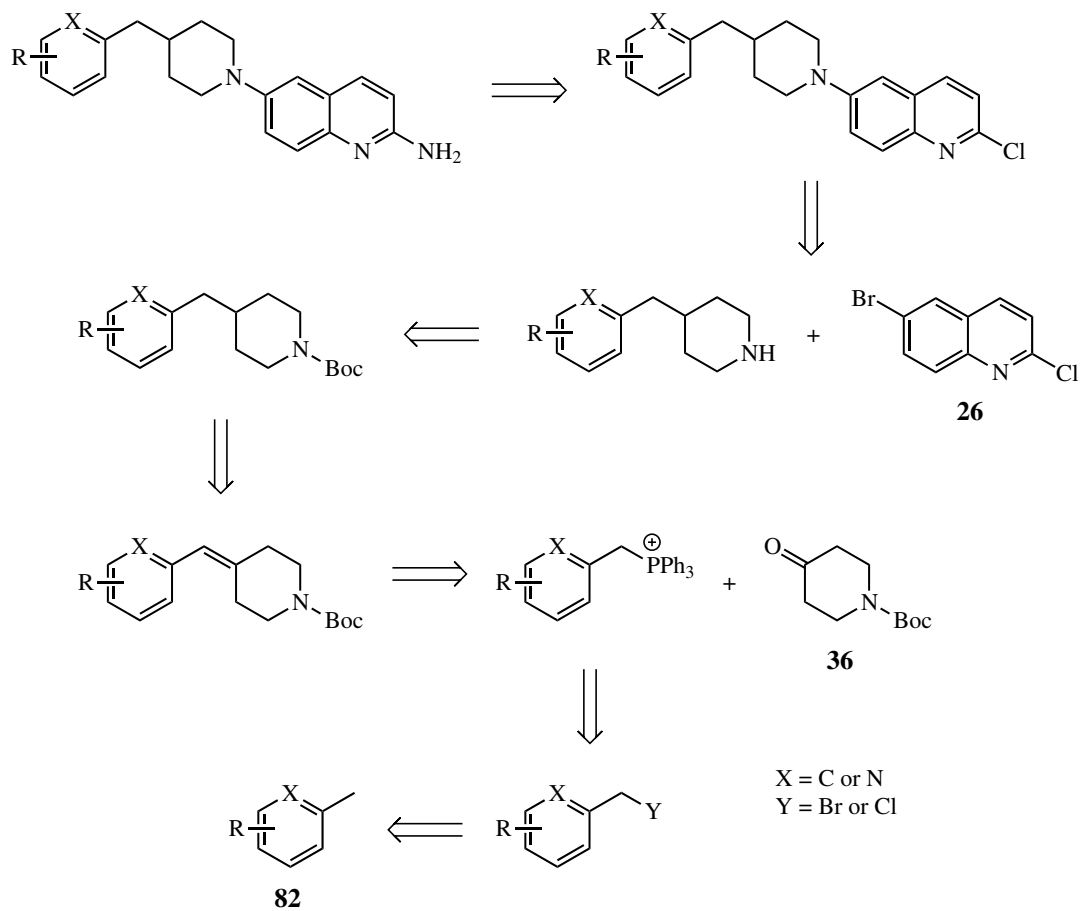


Figure 4.2: Proposed general retrosynthesis for substituted benzylpiperidinyl 2-aminoquinoline ligands. X = C or N, Y = Br or Cl.

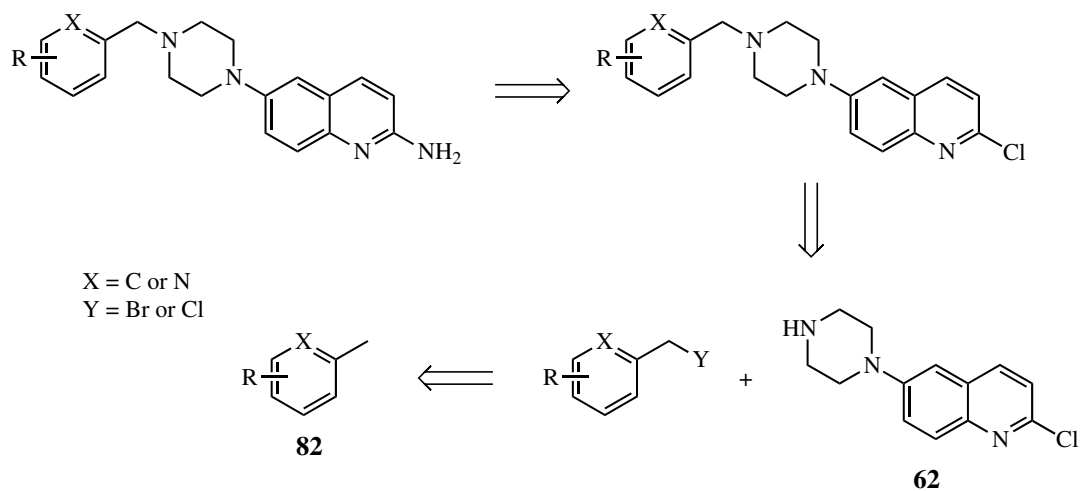


Figure 4.3: Proposed general retrosynthesis for substituted benzylpiperazinyl 2-aminoquinoline ligands. X = C or N, Y = Br or Cl.

The general synthetic pathways shown in Figure 4.2 & Figure 4.3 display a number of common features — they both require the synthesis of **26**, which has been described previously in Chapter 2. Furthermore, they each utilise two Buchwald-Hartwig coupling reactions, firstly for selective coupling of a heterocyclic amine at the 6-position of **26**, and secondly to convert 2-chloroquinoline derivatives into the corresponding 2-aminoquinoline derivatives. Importantly, the general synthetic pathways shown in Figure 4.2 & Figure 4.3 indicate that both benzylpiperidinyl- and benzylpiperazinyl-substituted 2-aminoquinoline ligands might be synthesised from the same substituted tolyl derivatives, with the general structure represented as **82**. Given **82** is common starting material, it was necessary that the proposed general complex ligands shown in Figure 4.1 could theoretically be synthesised from suitable **82** derivatives, which should be commercially available — the appropriate **82** derivatives (i.e., **83**, **84** and **85**, Figure 4.4) were identified for the synthesis of complex 2-aminoquinoline ligands (Table 4.2), where ligands **86** & **87** could be synthesised from **83**, ligands **88** & **89** could be synthesised from **84**, and ligands **90** & **91** could be synthesised from **85**.

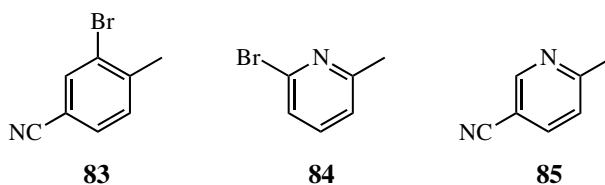


Figure 4.4: Commercially-available starting materials for the synthesis of complex 2-aminoquinoline ligands.

For each of the ligands proposed in Table 4.2, the synthesis of each pair of benzylpiperidinyl and benzylpiperazinyl ligands (i.e., synthesis of: **86** & **87** ligands from **83**; **88** & **89** ligands from **84**; and **90** & **91** ligands from **85**) will be discussed separately in the following sections.



## 4.2. PROPOSED LIGANDS AND GENERAL SYNTHETIC PATHWAYS

Table 4.2: Structures of target complex ligands for synthesis. *LogP* values calculated using Marvin by ChemAxon (*clogP*).<sup>61</sup>

Compound	Structure	<i>clogP</i>
86		3.29
87		2.15
88		3.45
89		2.55
90		2.23
91		1.29

## 4.3 Synthesis of complex ligands containing biaryl and 4-amido functional groups

### 4.3.1 Proposed synthetic pathways of complex ligands containing biaryl and 4-amido functional groups

While the general synthetic methods towards the synthesis of combinatorial ligands are displayed in Figure 4.2 and Figure 4.3, more detailed pathways are required for the synthesis of each specific ligand — for combinatorial ligands **86** and **87** containing 4-amido and 2,5-pyrimidinyl substituents, the proposed synthetic pathways are shown in Figure 4.5 and Figure 4.6.

Favourably, both Figure 4.5 and Figure 4.6 begin with the common substituted tolyl derivative **83**, however the more advanced derivative **92** is also a common intermediate, which would be accessible following an aryl (Suzuki) cross-coupling reaction and radical bromination from **83**. For synthesis of the benzylpiperidinyl ligand **86**, the advanced substituted benzyl bromide derivative **92** can be used as a precursor to the corresponding phosphonium salt **93**, in preparation for formation of **94** formation via Wittig reaction with **36**. The Boc-protected amine in **94** could then be liberated to **95**, in preparation for a selective Buchwald-Hartwig coupling reaction with **26** to form **96**. A second, sequential Buchwald-Hartwig coupling reaction can then be undertaken with **96**, using LiHMDS as an ammonia equivalent to form the corresponding 2-aminoquinoline derivative **97**, which can then undergo nitrile hydrolysis and alkene reduction to form the desired ligand **86**. It is noted that the proposed sequence describing late-stage nitrile hydrolysis and alkene reduction is intentional; previous studies reported that early stage nitrile hydrolysis of Boc-protected methylenepiperidinyl derivatives (to the corresponding amide) led to difficulties in subsequent Buchwald-Hartwig coupling reactions, likely due to the presence of the amide group which could coordinate Pd.<sup>56</sup> Furthermore, previous attempts to conduct alkene reductions of Boc-protected methylenepiperidinyl derivatives resulted in poor conversion to the desired product due to the formation of nitrile-reduction side products.<sup>56</sup> Lastly, for the methylenepiperidinyl derivatives, alkene isomerisation to the corresponding tetrahydro-pyridine isomer is likely under nitrile hydrolysis conditions (as described previously in Chapter 2, see Scheme 2.19 and associated text),<sup>56,66</sup> therefore to minimise the number of steps containing a complex product mixture, it would be ideal to conduct the nitrile hydrolysis, followed immediately by alkene reduction at the end of the synthetic route.

#### 4.3. SYNTHESIS OF COMPLEX LIGANDS CONTAINING BIARYL AND 4-AMIDO FUNCTIONAL GROUPS

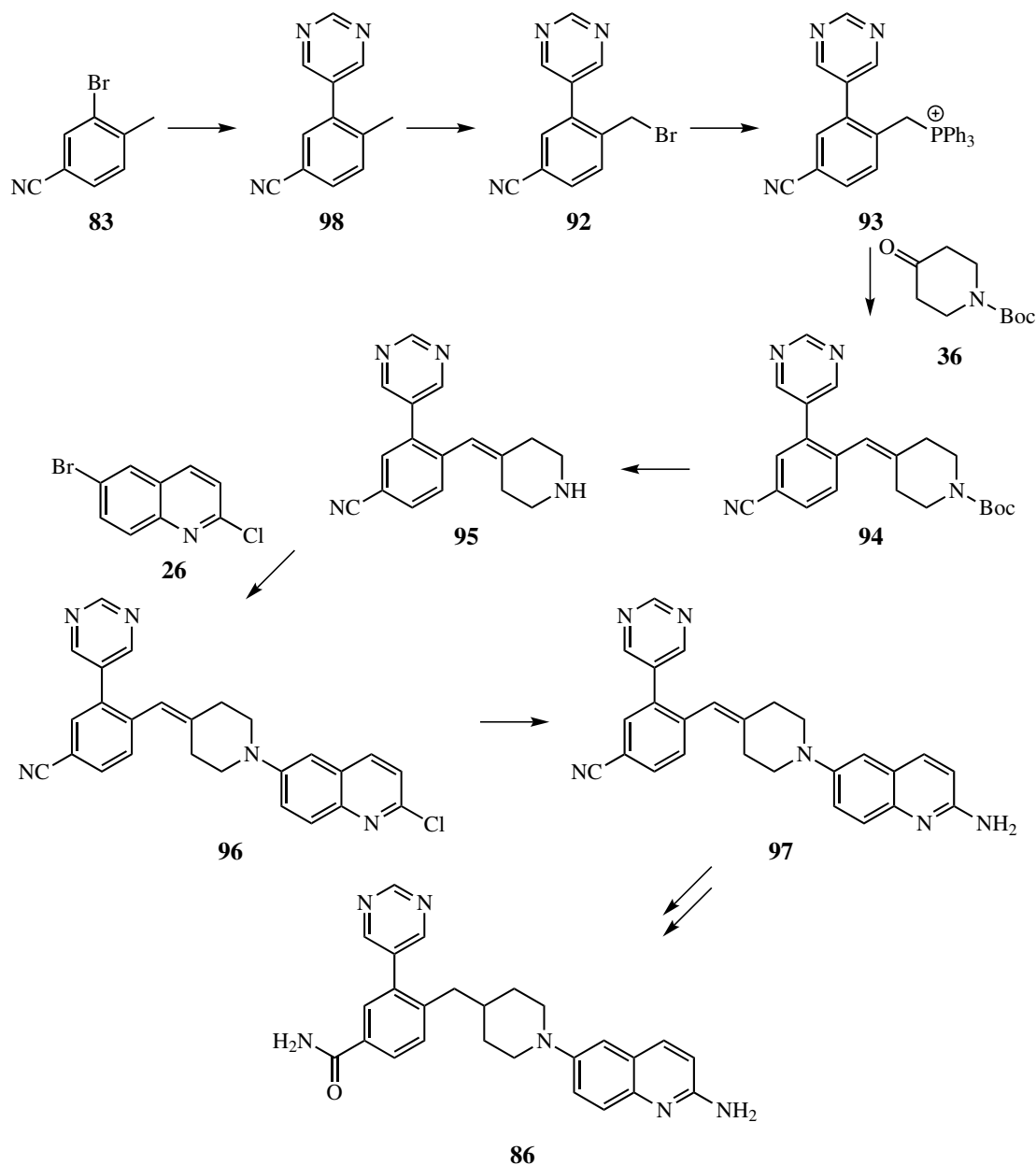


Figure 4.5: Proposed synthetic pathway for synthesis of a complex ligand **86**, which contains 4-amido and biaryl substituents.

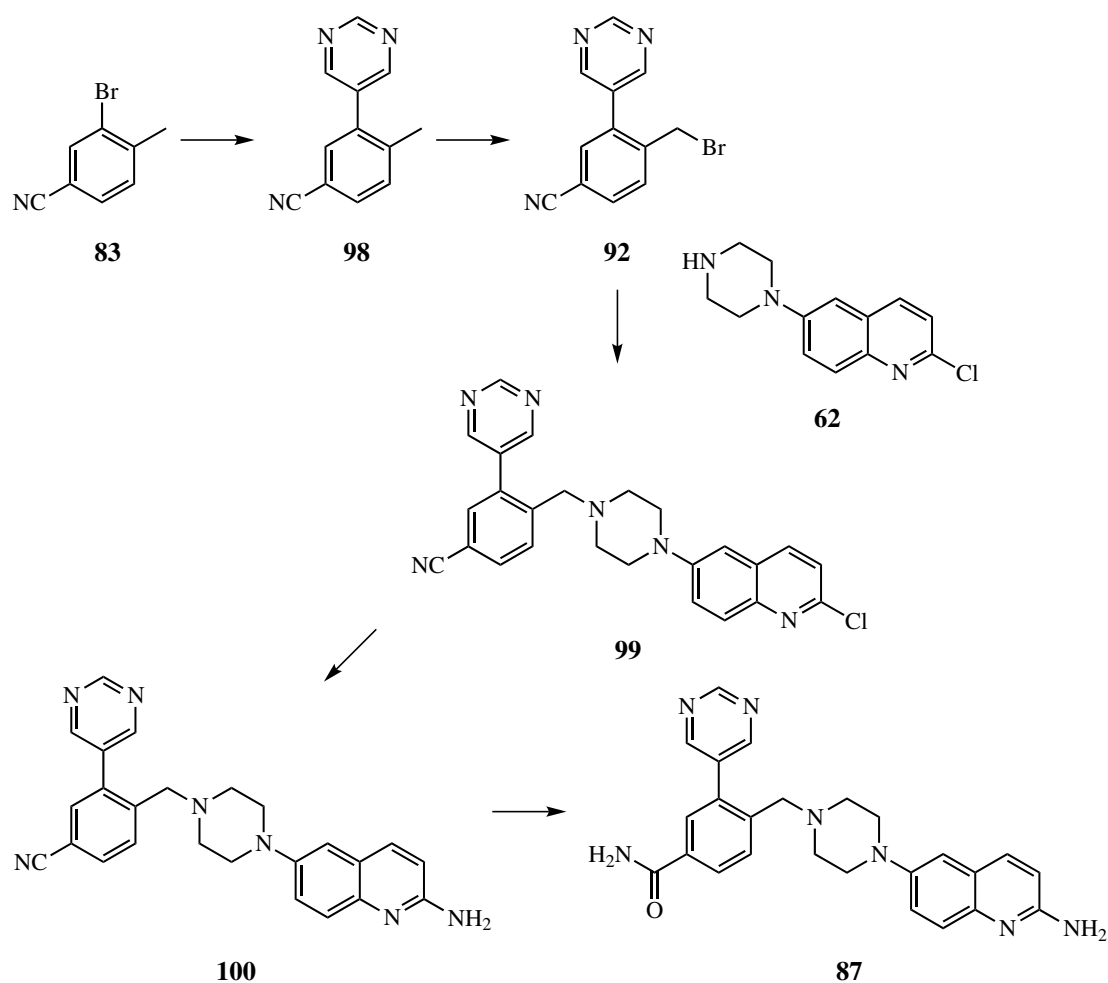


Figure 4.6: Proposed synthetic pathway for synthesis of the complex ligand **87**, which contains 4-amido and biaryl substituents.

Conversely, synthesis of the ligand **87** is proposed to occur following the shorter synthetic method shown in Figure 4.6. From the advanced common intermediate **92**, an alkylation with **62** could be undertaken to form the 2-chloroquinoline derivative **99**, followed by a Buchwald-Hartwig coupling reaction, using LiHMDS as an ammonia equivalent to afford the corresponding 2-aminoquinoline derivative **100**. Lastly, late stage derivatisation via nitrile hydrolysis should then produce the desired ligand **87**. One of the key limitations of the proposed synthetic pathway in Figure 4.6 is the potential for reduced yield due to polyalkylation during the reaction between **92** and **62** to form **99**. To account for this, an alternative synthetic route towards **99** could entail conversion of **92** to the corresponding alcohol, followed by selective oxidation to the corresponding aldehyde and subsequent reductive amination with **62** (Figure 4.7), as shown previously in Scheme 3.15 (Chapter 3).

#### 4.3. SYNTHESIS OF COMPLEX LIGANDS CONTAINING BIARYL AND 4-AMIDO FUNCTIONAL GROUPS

---

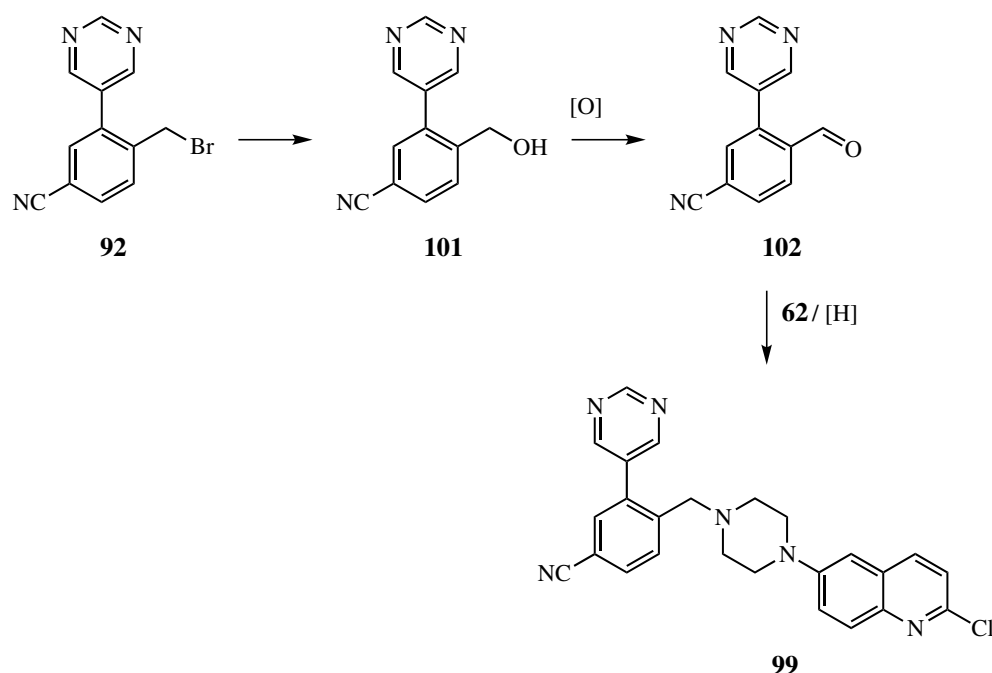


Figure 4.7: Proposed alternative synthetic pathway for the synthesis of chloroquinoline **99** to prevent polyalkylation of **92** and **62**.

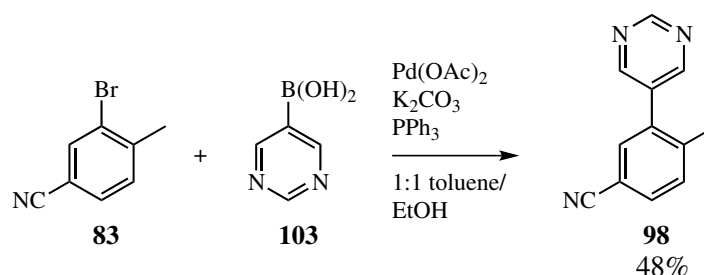
It was proposed that synthesis of the benzylpiperidinyl-containing ligand **86** would be undertaken in the first instance; this is described in the following section. Due to the proposed 9-step pathway proposed in Figure 4.5, it was vital that the early steps of the synthetic pathway be optimised for sufficient yields in order to carry enough material through the entire procedure.

#### 4.3.2 Synthesis of methylenepiperidinyl derivatives containing biaryl and 4-nitrile functional groups

To synthesise the desired ligand **86**, the first step from Figure 4.5 involved introduction of the 2,5-pyrimidinyl ring to the substituted tolyl derivative **83**. Previous studies investigating the synthesis of 2-aminoquinoline derivatives for the Tec SH3 domain reported general Suzuki cross-coupling conditions for the synthesis of biaryl-containing intermediates, including 2,5-pyrimidinyl derivatives.<sup>56</sup> It was envisaged that these conditions would be a suitable starting point for introduction of the 2,5-pyrimidinyl group towards the synthesis of **98**; this is shown in Scheme 4.1.

Successful coupling of the 2,5-pyrimidine ring was supported by analysis of HRMS and NMR spectra; a mass product of  $m/z$  196.0871 was observed (expected  $m/z$ : 196.0869). Analysis of  $^1\text{H}$  NMR spectra revealed the emergence of a 2H singlet at 8.73 ppm and a 1H singlet at 9.28 ppm — given the electron-deficient nature of the 2,5-pyrimidine ring and particularly the strongly-deshielded en-

### 4.3. SYNTHESIS OF COMPLEX LIGANDS CONTAINING BIARYL AND 4-AMIDO FUNCTIONAL GROUPS



Scheme 4.1: Reaction conditions and yield for synthesis of **98** by Suzuki coupling of **83** and **103**, based on literature methods.<sup>56</sup>

environment about C(4')H due to electron-withdrawing by induction of each N, these observed signals are consistent with the successful formation of **98** (Figure 4.8). The yield was acceptable at 48%, as sufficient material had been obtained to proceed to the next synthetic step.

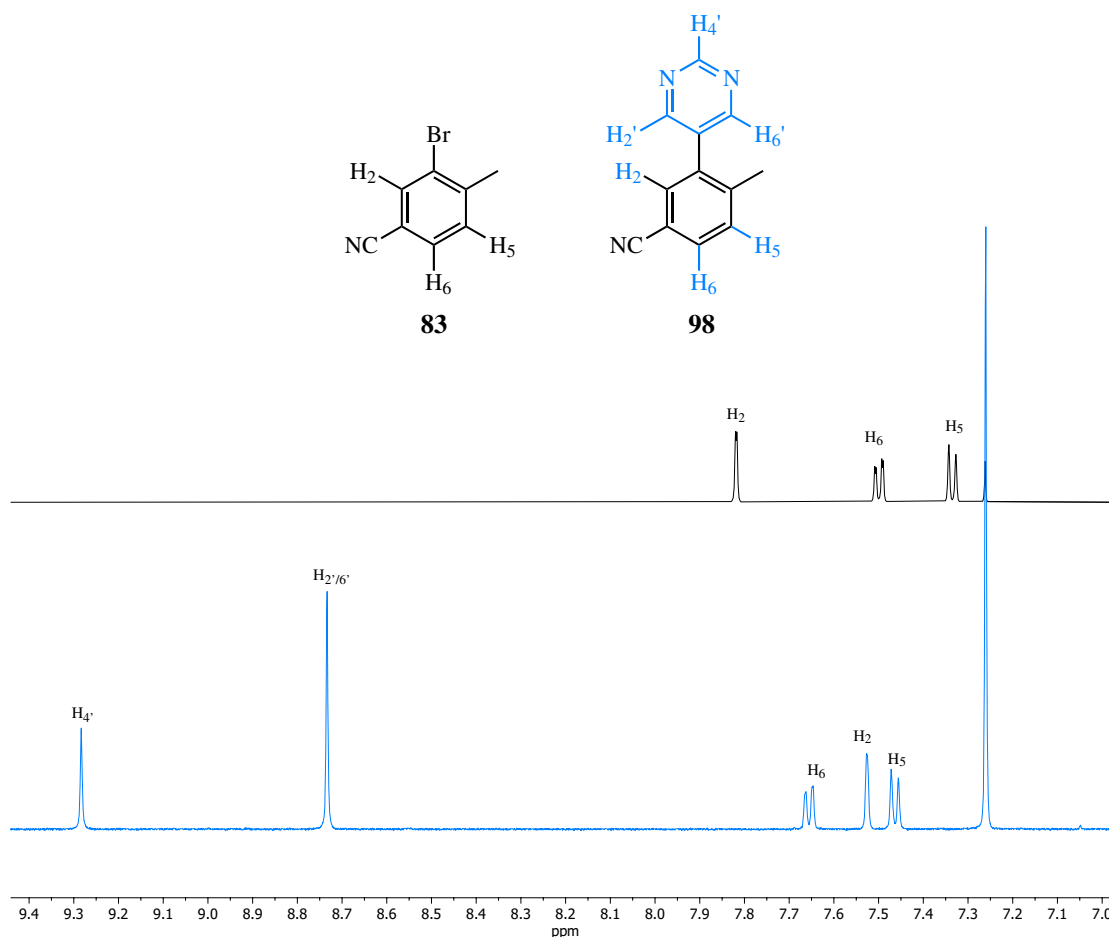
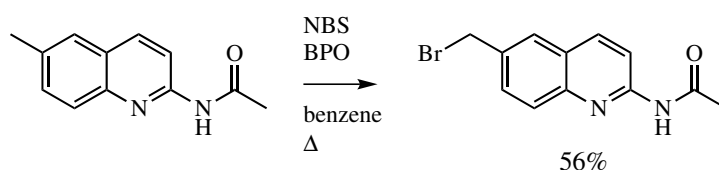


Figure 4.8: Comparison of stacked and normalised <sup>1</sup>H NMR ( $\delta_{\text{H}}$ : 7.0 - 9.4 ppm) of **83** (black) and **98** (blue), indicating successful incorporation of the 2,5-pyrimidinyl ring.

### 4.3. SYNTHESIS OF COMPLEX LIGANDS CONTAINING BIARYL AND 4-AMIDO FUNCTIONAL GROUPS

---

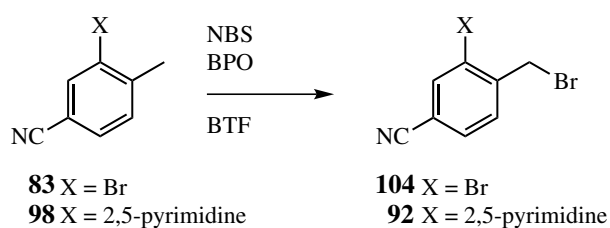
The next step of the synthetic pathway was conversion of **98** to the corresponding aryl halide, ideally as the aryl bromide **92**. Formation of the aryl bromide over other aryl halides (aryl chlorides, for example) would provide a more reactive substrate for subsequent phosphonium salt synthesis given the weaker C-Br bond (c.f., C-Cl), therefore would be more likely to facilitate higher yields in later synthetic steps. It was anticipated that **92** might be synthesised via radical bromination; a literature procedure from Inglis *et al.* reported the synthesis of 6-bromomethyl quinoliny derivatives via radical bromination, as indicated in Scheme 4.2.



Scheme 4.2: Literature radical bromination conditions for the synthesis of bromomethyl quinoliny derivatives. NBS = *N*-bromosuccinimide, BPO = benzoyl peroxide.<sup>47,58</sup>

While the proposed synthesis of **92** does not involve structures containing a quinoliny ring, it was thought that the literature conditions<sup>58</sup> shown in Scheme 4.2 might be a suitable starting point for the synthesis of **92**, as there would likely be some functional group tolerability. In addition, radical bromination of **83** could also be investigated (Scheme 4.3) to determine if the presence of the 2,5-pyrimidinyl ring in **98** might have some effect on the accessibility of the methyl group for bromination. Therefore, radical bromination reaction conditions consistent with those reported previously<sup>58</sup> were investigated for the synthesis of **92** and **104**, as shown in Scheme 4.3 and Table 4.3, albeit with some variations. An alternative solvent to benzene was desired due to its inherent toxicity;<sup>118</sup> while CCl<sub>4</sub> is historically the canonical solvent for radical brominations, it too has similar toxicity issues.<sup>118</sup> Typically, toluene is substituted for benzene in many chemical reactions,<sup>119</sup> however the methyl group of toluene has been reported to react readily under radical bromination conditions to produce benzyl bromide.<sup>120</sup> Conversely, BTF has previously been recommended as a substitute to benzene for use as a solvent in radical reactions,<sup>118</sup> therefore was selected as an alternative solvent due to its high boiling point, reduced toxicity (relative to benzene and CCl<sub>4</sub>), and lack of accessible sites for undesired alkyl radical brominations.

### 4.3. SYNTHESIS OF COMPLEX LIGANDS CONTAINING BIARYL AND 4-AMIDO FUNCTIONAL GROUPS



Scheme 4.3: General proposed conditions for synthesis of benzyl bromide derivatives via radical bromination with *N*-bromosuccinimide (NBS) and benzoyl peroxide (BPO) in BTF.

Table 4.3: Results of radical bromination of substituted tolyl derivatives **83** and **98** containing a nitrile substituent, as shown in Scheme 4.3. <sup>a</sup> indicates the yield represents a partially purified 5:6 mixture of **92** and **98**.

Compound	R =	Yield (%)
<b>104</b>	Br	53
<b>92</b>	2,5-pyrimidine	15 <sup>a</sup>

From Table 4.3, radical bromination of both **83** and **98** using adapted literature conditions<sup>58</sup> resulted in the formation of both **92** and **104**, but unfortunately the corresponding di-brominated side products **105** and **106** were observed (Figure 4.9) in differing quantities; **105** was observed in crude <sup>1</sup>H NMR spectra but was not purified, while **106** was purified in trace amounts (<1% yield).

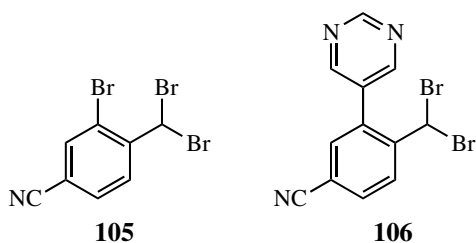


Figure 4.9: Structures of di-brominated side products **105** and **106** detected following synthesis of **104** and **92**, respectively.

For those radical bromination products which were purified, compound identification was supported by analysis of a combination of relevant HRMS and NMR spectra: for **92** and **106**, mass products with the expected *m/z* values and intensities (based upon natural bromine isotope abundances) were detected. For each of **104**, **92** and **106**, analysis of <sup>1</sup>H NMR revealed the emergence of either a 2H (for **104** and **92**) or 1H singlet (for **106**), as exemplified in Figure 4.10. A diagnostic dibromomethyl CH singlet at 6.44 ppm was also observed in the <sup>1</sup>H NMR spectra for crude **104**, indicating the presence of **105** prior to purification (data not shown).



### 4.3. SYNTHESIS OF COMPLEX LIGANDS CONTAINING BIARYL AND 4-AMIDO FUNCTIONAL GROUPS

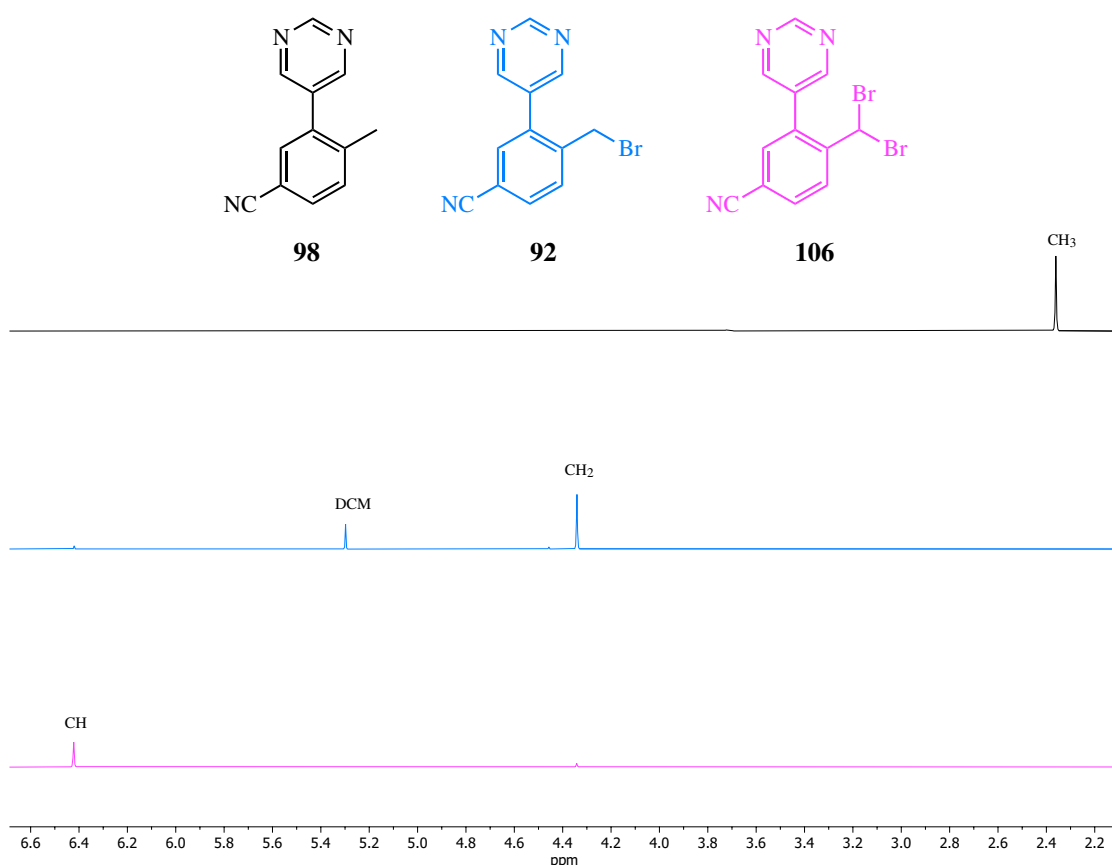


Figure 4.10: Comparison of normalised and overlaid  $^1\text{H}$  NMR spectra ( $\delta_{\text{H}}$ : 2.2 - 6.6 ppm) of **98** (black), **92** (blue) and **106** (pink), showing disappearance of methyl 3H singlet and emergence of downfield 2H or 1H singlet in **92** and **106** spectra, respectively. DCM = dichloromethane.

From 2D NMR spectra, the HMBC correlations between the 2H singlet at 4.58 ppm in  $^1\text{H}$  NMR, and C(3), C(4) and C(5) of the phenyl ring in **104** support that the desired transformation has occurred (Figure 4.11), and similar HMBC correlations were observed for **92** and **106**.

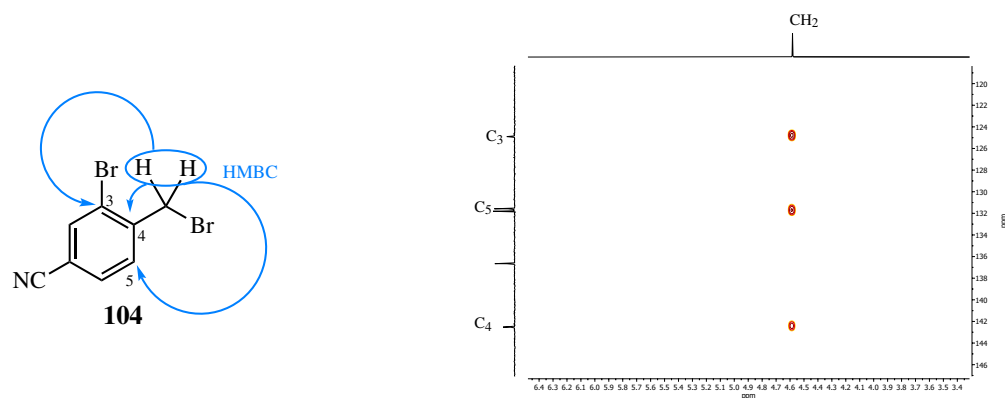
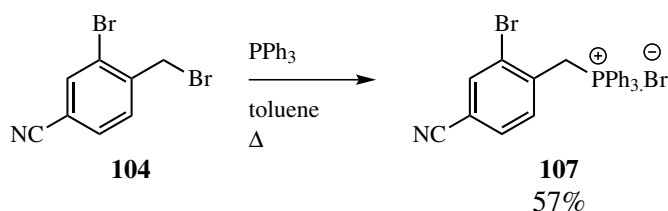


Figure 4.11: HMBC correlations (red) between methyl group hydrogens ( $\text{CH}_2$ ) and phenyl ring carbons C(3), C(4) and C(5), indicating successful formation of **104**.

Taken together, this data indicates that the desired radical bromination transformations were successful, albeit to varying degrees considering the yields reported in Table 4.3. Given the high selectivity for the mono-brominated product in all cases, no further optimisation of reaction conditions was undertaken. In addition, due to the relatively higher yield obtained for synthesis of **104**, it was determined that **104**, and not **92**, was more favourable to carry forward through the synthetic pathway for the benzylpiperidinyl-substituted ligand **86**, as the 2,5-pyrimidine ring could be introduced at a later stage.

Following synthesis of **104**, the next synthetic step required transformation of **104** into a phosphonium salt, in preparation for a Wittig reaction with **36**. Following the method described previously in Section 2.7.1 of Chapter 2, synthesis of the desired phosphonium salt **107** was successfully achieved (Scheme 4.4).

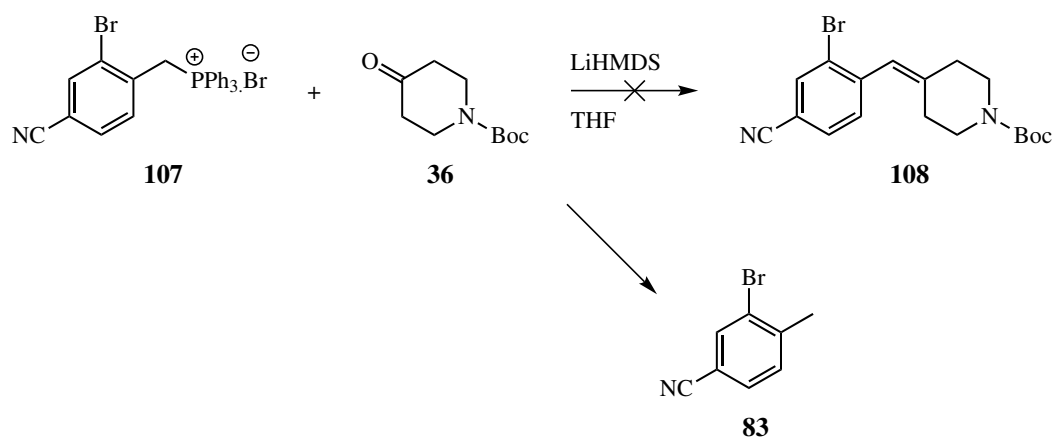


Scheme 4.4: Reaction conditions and yield for synthesis of phosphonium salt **107** from benzyl bromide derivative **104**.

Again, formation of **107** was determined primarily by <sup>1</sup>H NMR analysis; the presence of an additional aromatic multiplet in <sup>1</sup>H NMR spectra integrating to 15H was diagnostic for supporting the introduction of the triphenylphosphine group. Furthermore, the methylene CH<sub>2</sub> signal, which was previously a singlet in <sup>1</sup>H NMR spectra for **104**, was observed as a doublet in the <sup>1</sup>H NMR spectra for **107** due to coupling with phosphorous. Similarly, all signals in <sup>13</sup>C NMR for **107** appeared as doublets, as expected for C-P coupling.

In order to introduce the piperidine ring functionality, a Wittig reaction was attempted between **36** and **107**, as described previously in Section 2.7.1 of Chapter 2 (Scheme 4.5). Unfortunately, upon working up the reaction mixture, the desired product **108** was only observed in trace quantities in the crude reaction mixture (from analysis of <sup>1</sup>H NMR spectra).

### 4.3. SYNTHESIS OF COMPLEX LIGANDS CONTAINING BIARYL AND 4-AMIDO FUNCTIONAL GROUPS



Scheme 4.5: Reaction conditions for attempted synthesis of **108** via Wittig reaction with **36** and **107**.

To rationalise the lack of reagent conversion of **107** to **108**, attention was returned to the  $^1\text{H}$  NMR spectra of the crude reaction mixture. Upon further analysis, it was apparent that substantial quantities of both triphenylphosphine oxide **109** and the earlier starting material **83** were present in the crude product mixture (Figure 4.12).

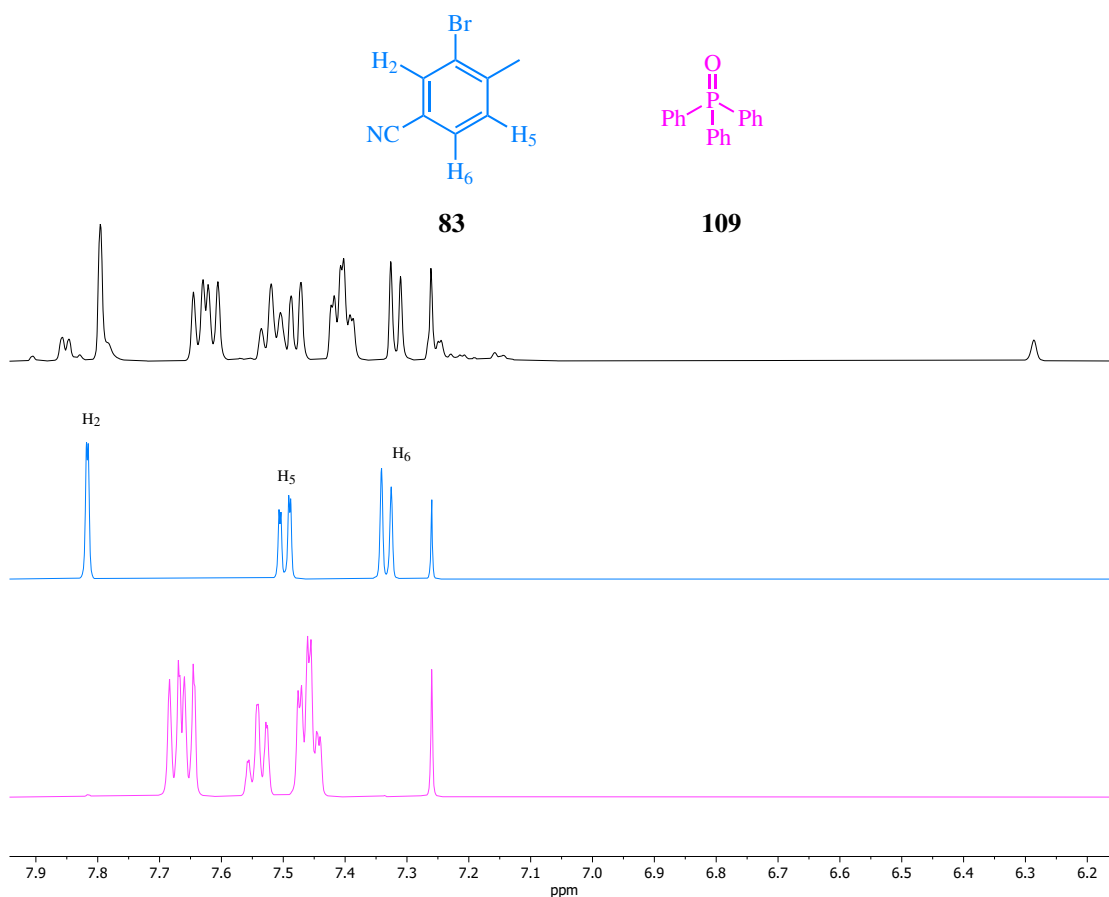


Figure 4.12: Stacked and normalised  $^1\text{H}$  NMR spectra ( $\delta_{\text{H}}$ : 6.3 - 7.9 ppm) of crude reaction mixture from attempted synthesis of **108** (black), starting material **83** (blue) and **109** (pink), indicating presence of **83** and **109** in the crude reaction mixture.

The presence of triphenylphosphine oxide in the crude reaction mixture suggests that the phosphonium salt is being deprotonated to form the ylide intermediate, but is not reacting further with **36** to form **108**. This lack of ylide reactivity is not surprising; there are several reports in the literature of electron-deficient ylides exhibiting reduced nucleophilic character in Wittig reactions through stabilisation of the ylide intermediate.<sup>121</sup> Therefore, the presence of the nitrile group in **107** (which forms an extended conjugated system in the corresponding ylide) could stabilise the ylide as suggested in Figure 4.13, to the extent that it reduces the reactivity of the ylide towards the ketone in **36**. Furthermore, if the reaction mixture was quenched prematurely (e.g., with water or MeOH during workup), then it is possible that the ylide could be reduced to the starting material **83** via the proposed mechanism in Figure 4.14. It is noted that the proposed mechanism is intended to be general, and not strictly represented as a concerted reaction — an interesting study by Byrne *et al.* reported certain trends for concerted v.s. stepwise addition of an ylide and water/alcohol to form the phosphorane, where lower ylide  $pK_a$  values typically followed a concerted mechanism for phosphorane formation.<sup>122</sup> As the  $pK_a$  value was not determined for the ylide of **107**, the exact mechanism may differ from that suggested in Figure 4.14.

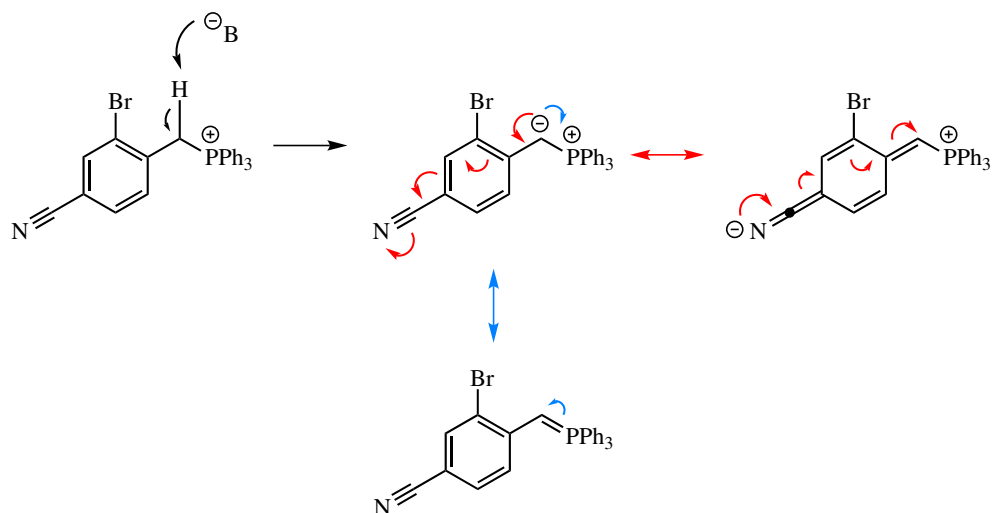


Figure 4.13: Proposed mechanisms for stabilisation of ylide formed from deprotonation of **107** by a base ( $B$ ). Resonance forms following blue arrows indicate a possible pathway for stabilisation by delocalisation of negative charge. Resonance forms following red arrows indicate improved stabilisation by delocalisation of negative charge across a more extended conjugated system.

#### 4.3. SYNTHESIS OF COMPLEX LIGANDS CONTAINING BIARYL AND 4-AMIDO FUNCTIONAL GROUPS

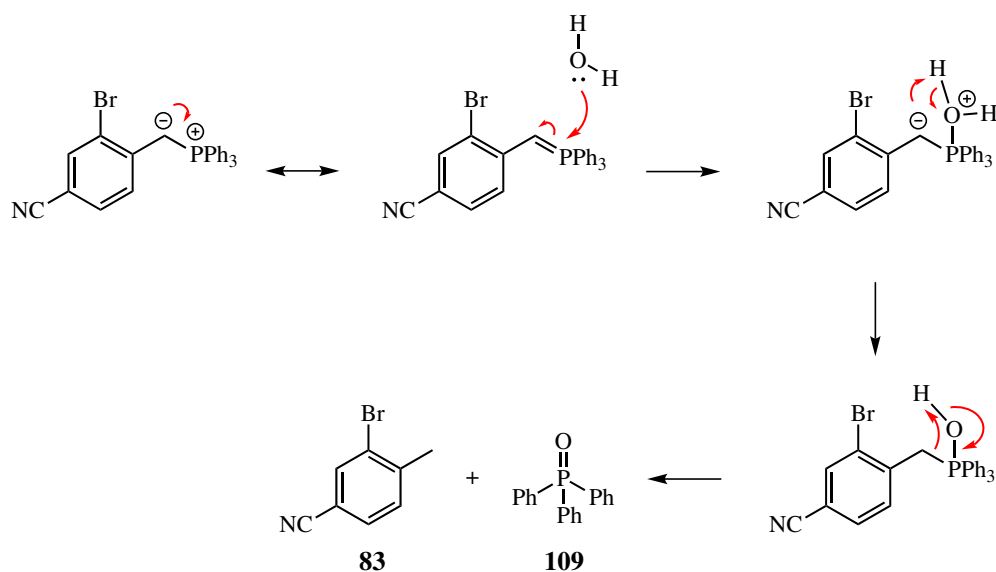
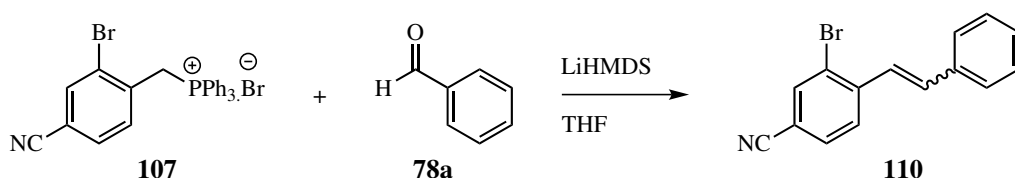


Figure 4.14: Proposed mechanism for quenching of ylide of **107** by water, to afford triphenylphosphine oxide **109** and the substituted tolyl starting material **83**.

To test whether the poor conversion to **108** in Scheme 4.5 was due to reduced reactivity of the ylide of **107** towards **36**, the Wittig reaction was repeated, except benzaldehyde **78a** was used as the electrophile rather than **36**. It was anticipated that if the ylide of **107** was being formed, then a Wittig reaction with **107** should afford the alkene product **110** due to the increased electrophilic character of **78a** (aldehyde) compared to **36** (ketone) — this reaction is indicated in Scheme 4.6.



Scheme 4.6: Reaction conditions for synthesis of **110** via Wittig reaction with **78a** and **107**.

From analysis of the <sup>1</sup>H NMR spectrum of the crude product, approximately 75% of the limiting reagent (**78a**) had been converted to the desired product **110**; formation of **110** was indicated by formation of key vicinal alkene CH doublets at ~6.58 & 6.84 ppm with coupling constants of *J* = 12.1 Hz (Figure 4.15). Interestingly, from Figure 4.15 a smaller, second pair of vicinal key alkene doublets at ~6.61 & 6.78 ppm (also with coupling constants of *J* = 12.1 Hz) are present; it is plausible that these might correspond to the reduced (i.e., de-brominated) equivalent of **110**. Further characterisation by HRMS would be beneficial to investigate this hypothesis, but unfortunately this analysis was not possible at the time. In any case, the formation of diagnostic alkene doublets of **110** or its de-brominated equivalent indicated that the Wittig reaction was successful.

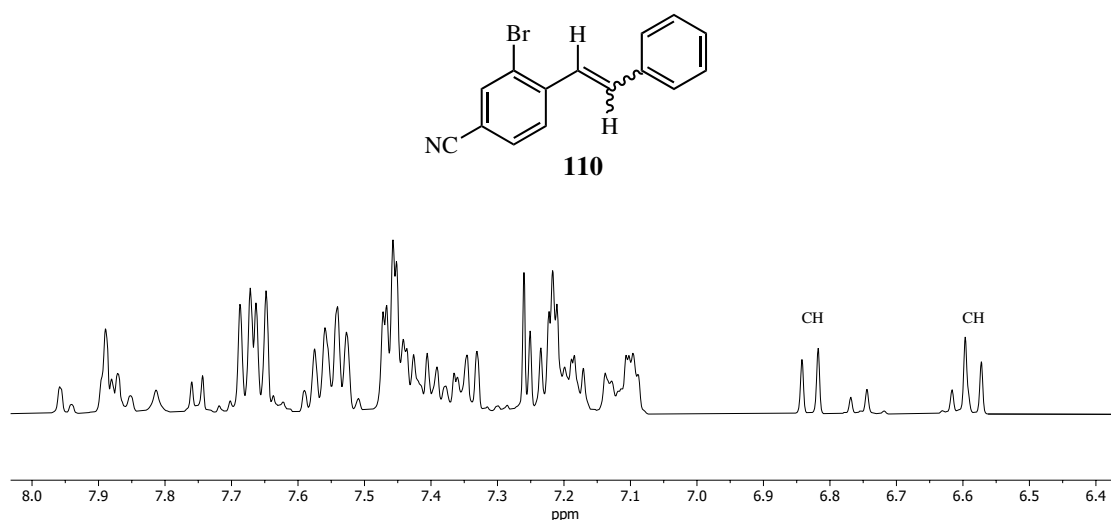
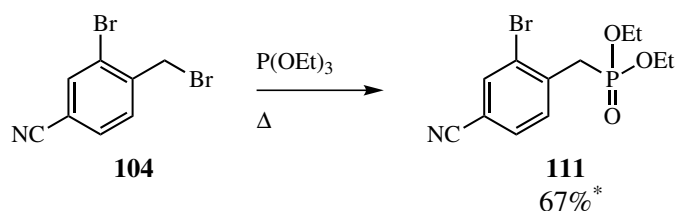


Figure 4.15:  $^1\text{H}$  NMR Spectra ( $\delta_{\text{H}}$ : 6.4 - 8.0 ppm) indicating successful Wittig reaction between **107** and **78a** to form **110** (black, crude) via emergence of alkene CH doublet signals.

In addition, no substituted tolyl starting material **83** was observed in the crude product  $^1\text{H}$  NMR spectra, indicating that the ylide was sufficiently reactive when the substrate had more electrophilic character (i.e., reacting with an aldehyde, rather than a ketone). Therefore, the reduced conversion of **107** to **108** is likely due a combination of the increased stability (and therefore reduced nucleophilicity) of the corresponding ylide, and the reduced electrophilic character of the ketone in **36**.

In order to synthesise the desired intermediate **108**, an alternative method to the Wittig reaction was sought; it was envisaged that **108** might be accessible via Horner-Emmons reaction with the corresponding benzyl phosphonate, as described earlier in Scheme 2.3 of Chapter 2 and in previous work.<sup>56,66</sup> This approach required synthesis of the benzyl phosphonate derivative **111** via Michaelis-Arbuzov rearrangement, as shown in Scheme 4.7.



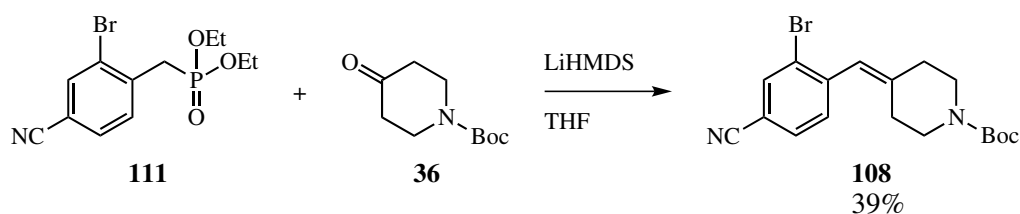
Scheme 4.7: Reaction conditions and synthesis of phosphonate **111** from benzyl bromide derivative **104** via Michaelis-Arbuzov rearrangement. \* indicates **111** was isolated with some impurities, so the true yield is slightly lower.

#### 4.3. SYNTHESIS OF COMPLEX LIGANDS CONTAINING BIARYL AND 4-AMIDO FUNCTIONAL GROUPS

---

Formation of the desired benzyl phosphonate **111** was supported via analysis of  $^1\text{H}$  NMR spectra; similarly as for **107**, splitting of the distinctive methylene  $\text{CH}_2$  signal from a singlet to a doublet (due to H-P) coupling was observed. Furthermore, all signals in  $^{13}\text{C}$  NMR spectra for **111** appeared as doublets due to C-P coupling. It is noted that **111** could not be completely isolated from some impurities (residual triethylphosphite and some unidentified side products), however it was expected that these impurities could be readily removed during subsequent reactions and purification steps.

Following synthesis of **111**, the next step involved a Horner-Emmons reaction with **36** using previously reported conditions,<sup>56,66</sup> as indicated in Scheme 4.8.



Scheme 4.8: Reaction conditions for synthesis of **108** via Horner-Emmons reaction with **36** and **111**.

The desired product **108** was synthesised by Horner-Emmons reaction, and successful formation was supported by analysis of both HRMS and NMR spectra; mass products with  $m/z$  of 321.0232 & 323.0213 were observed in a ratio of  $\sim 1:1$ , as expected for a bromine-containing structure (expected  $m/z$ : 321.0233 [ $^{79}\text{Br}$ ] / 323.0213 [ $^{81}\text{Br}$ ]). Furthermore, analysis of  $^1\text{H}$  NMR spectra revealed emergence of piperidine ring signals (including a characteristic 9H singlet representative of the Boc protecting group at 1.48 ppm), and a distinctive 1H singlet at 6.31 ppm, consistent with formation of an alkene. Finally, analysis of 2D NMR (particularly HMBC and ROESY) spectra revealed successful alkene formation, as shown in Figure 4.16. While the yield was not ideal at 39%, this was attributed to slow formation of the desired product; after 24 hrs, the reaction had still not gone to completion (monitoring by TLC). However, sufficient material had been obtained to proceed to the next step, so further optimisation of Horner-Emmons reaction conditions was not undertaken.

### 4.3. SYNTHESIS OF COMPLEX LIGANDS CONTAINING BIARYL AND 4-AMIDO FUNCTIONAL GROUPS

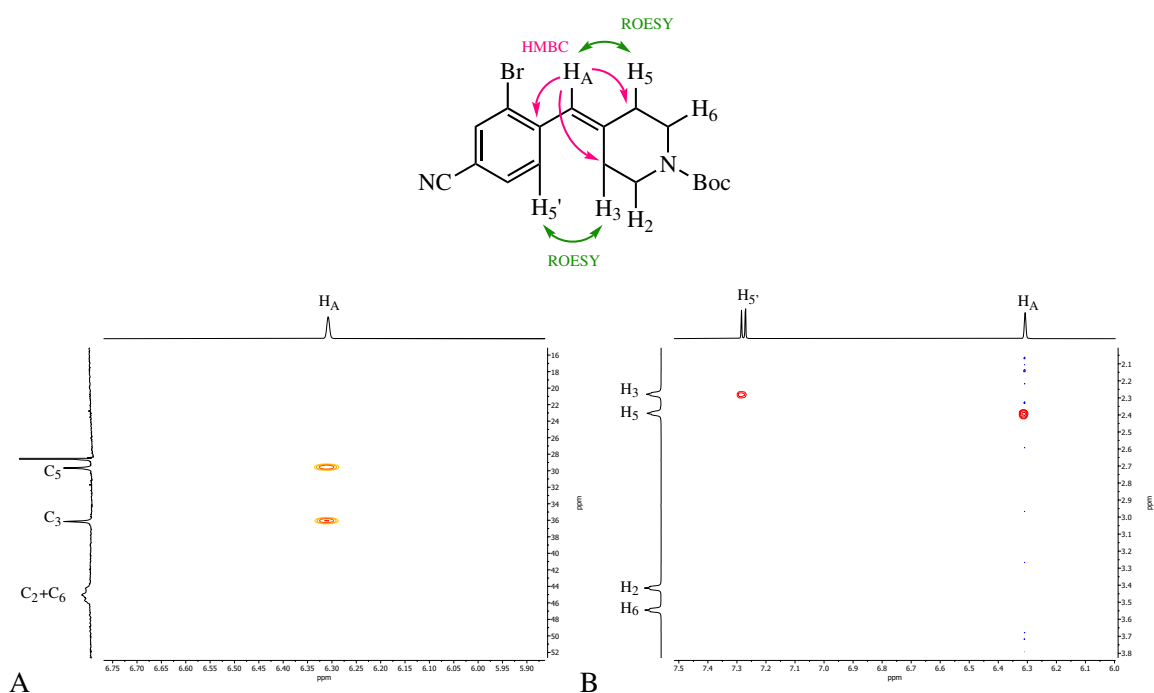
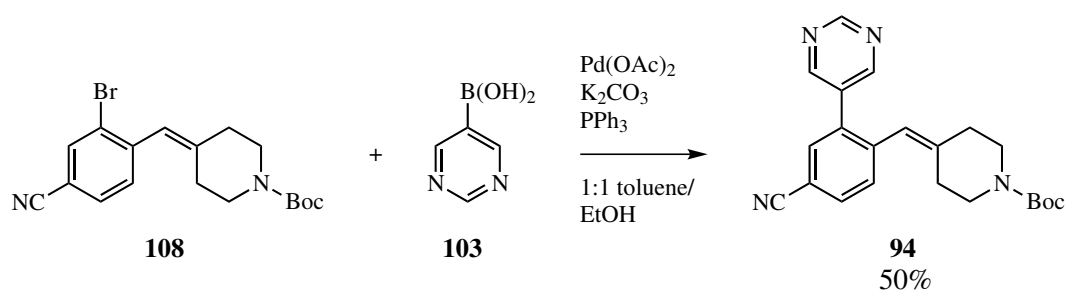


Figure 4.16: Structural analysis of **108** via 2D NMR spectra, with (A) HMBC correlations indicated by pink arrows, and (B) ROESY correlations indicated by green arrows.

With reference to Figure 4.5, it was necessary to introduce the 2,5-pyrimidinyl ring prior to any Buchwald-Hartwig coupling reactions with **26** to prevent any undesired cross-coupling (polymerisation) reactions between amine molecules. Consequently, the next synthetic step required aryl coupling of 2,5-pyrimidine with **108**; Suzuki cross-coupling conditions analogous to those described previously (in Scheme 4.1)<sup>56</sup> were utilised, and the results shown in Scheme 4.9.



Scheme 4.9: Reaction conditions and yield for synthesis of **94** by Suzuki coupling of **108** and **103**, based on literature methods.<sup>56</sup>

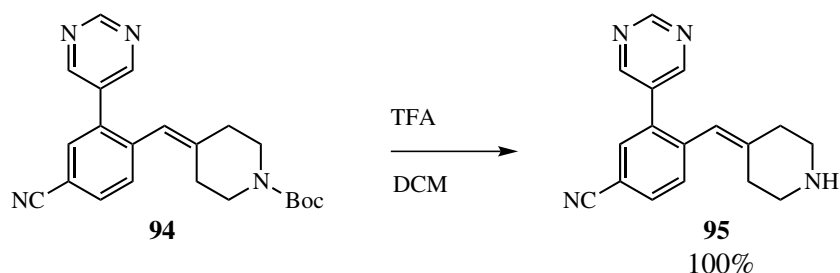


#### 4.3. SYNTHESIS OF COMPLEX LIGANDS CONTAINING BIARYL AND 4-AMIDO FUNCTIONAL GROUPS

---

Again, successful aryl coupling to form **94** was supported by analysis of HRMS and NMR spectra; a major mass product of  $m/z$  377.1981 was observed in HRMS spectra (expected  $m/z$ : 377.1972). Furthermore, successful coupling of the 2,5-pyrimidinyl ring was clearly observed in  $^1\text{H}$  NMR spectra through the emergence of 2,5-pyrimidinyl ring H signals, consistent with those described earlier in Figure 4.8. The yield was consistent with that reported in Scheme 4.1, therefore sufficient material had been obtained to continue synthesis towards the desired ligand **86**.

In preparation for synthesis of the 2-chloroquinoline intermediate **96**, it was necessary to liberate the amine **95** prior to Buchwald-Hartwig coupling with **26**. The Boc-protected amine **94** was therefore treated with TFA as described in Chapters 2 and 3, in an attempt to afford the free amine **95** (Scheme 4.10).



Scheme 4.10: Reaction conditions and yield for synthesis of **95** via Boc deprotection of **94**.

Successful removal of the Boc protecting group was supported by analysis of NMR and HRMS spectra. From  $^1\text{H}$  NMR spectra, a diagnostic loss of the 9H singlet was observed (previously appearing at 1.48 ppm), consistent with removal of the *tert*-butyl group component of the Boc protecting group (Figure 4.17). In addition, loss of the Boc protecting group allowed some resolution of piperidiny ring H signals, due to removal of the slowly-rotating carbamate bond in the Boc protecting group (on the NMR timescale, see Figure 2.35 in Chapter 2 and related text for further discussion). Analysis of HRMS spectra revealed a major mass product with a  $m/z$  of 277.1442, consistent with that expected for **95** (expected  $m/z$  277.1448). Pleasingly, the yield was quantitative, so sufficient material was obtained to proceed to the next synthetic step.

### 4.3. SYNTHESIS OF COMPLEX LIGANDS CONTAINING BIARYL AND 4-AMIDO FUNCTIONAL GROUPS

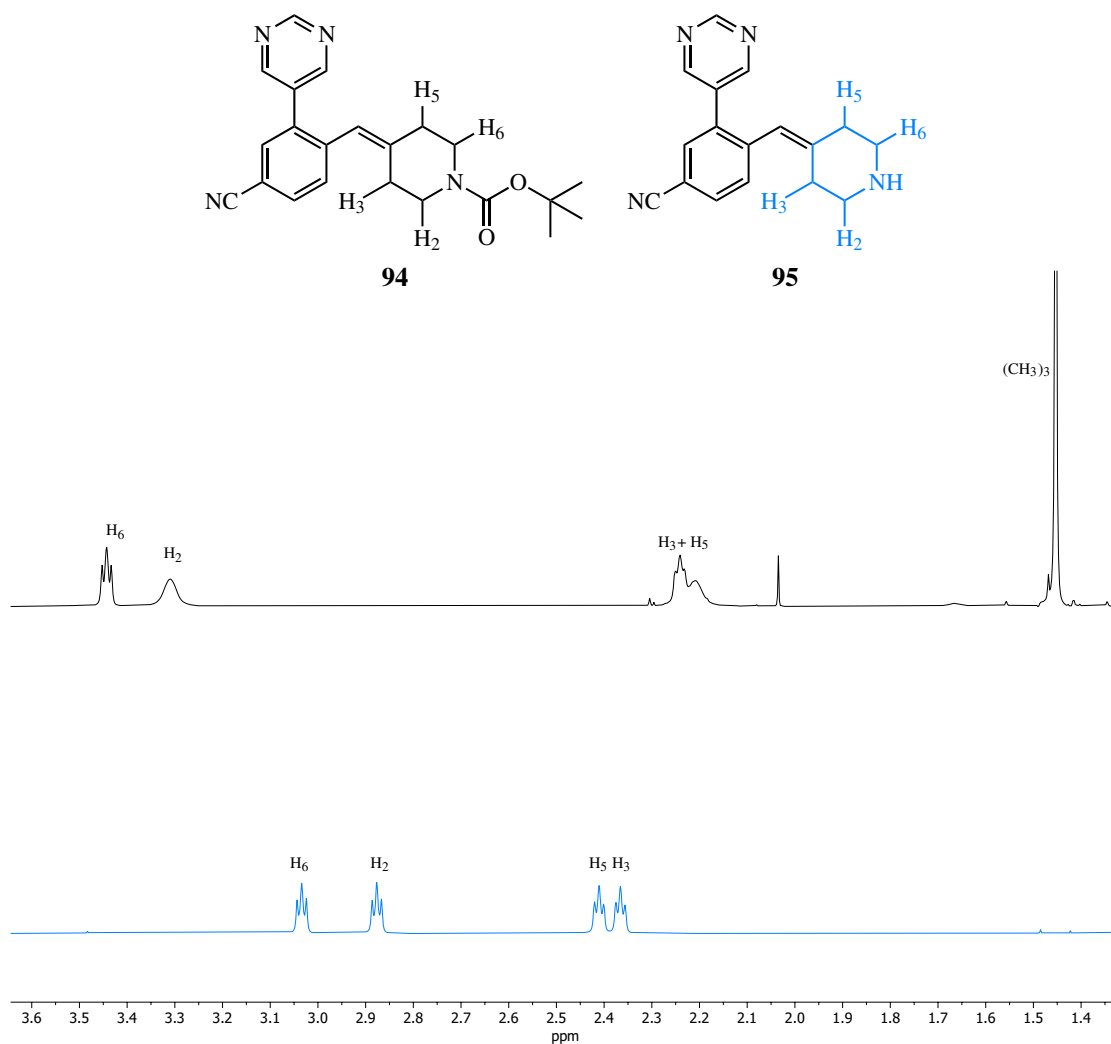
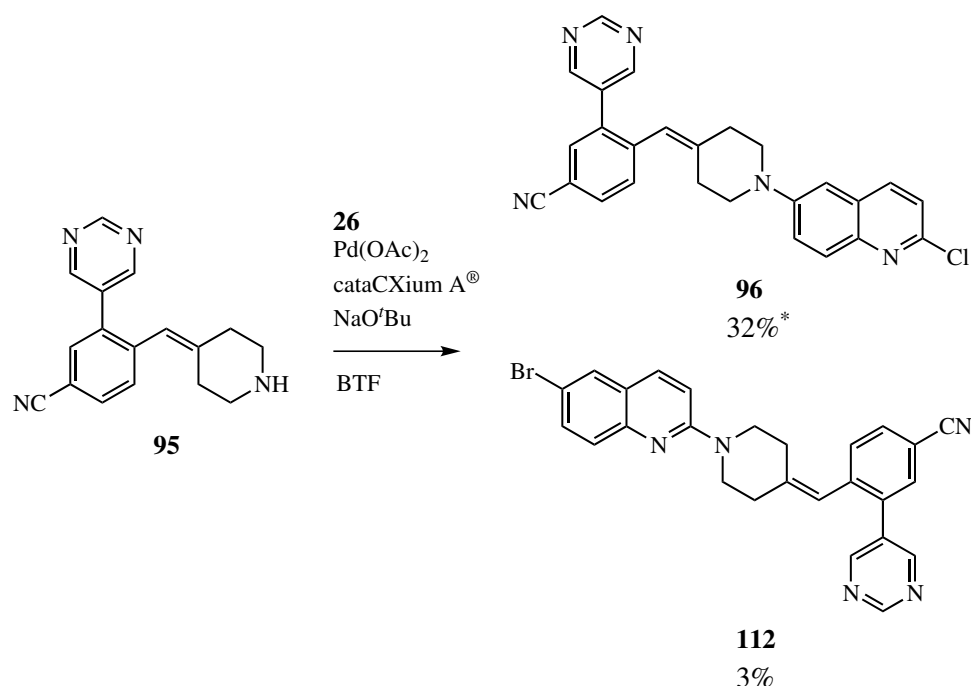


Figure 4.17: Stacked and normalised <sup>1</sup>H NMR spectra ( $\delta_{\text{H}}$ : 1.4 - 3.6 ppm), indicating successful removal of the Boc protecting group in **94** (black) to afford **95** (blue), and partial resolution of piperidiny ring H signals in **95**.

### 4.3.3 Synthesis of methylenepiperidiny-substituted quinoline derivatives containing biaryl and 4-nitrile functional groups

It was envisaged that the key 2-chloroquinoline derivative **96** could be synthesised via Buchwald-Hartwig coupling reaction between **95** and **26**, using reaction conditions optimised for coupling at the 6-position of **26**, as described in Chapters 2 & 3 and reported previously;<sup>47,60</sup> the results from employing these optimised reaction conditions are reported in Scheme 4.11.



Scheme 4.11: Reaction conditions and yield for synthesis of piperidine-coupled 2-chloroquinoline derivative **96** and side-product **112** via Buchwald-Hartwig coupling of **26** and **95**, based on literature methods.<sup>47,56</sup> \* indicates yield represents mixture of **96** and corresponding tetrahydropyridine isomer.

From Scheme 4.11, selectivity for coupling at the 6-position of **26** was observed, with the corresponding 2-substituted side product **112** isolated in minor quantities. Identification of both the desired product **96** and side product **112** were supported by analysis of HRMS and NMR spectra. From mass spectra, mass products with  $m/z$  values consistent with  $[\text{M}+\text{H}]^+$  for each of **96** and **112** were observed, in the expected halogen isotope distributions ( $\sim 3:1$  for  $^{35}\text{Cl}$  /  $^{37}\text{Cl}$  in **96**;  $\sim 1:1$  for  $^{79}\text{Br}$  /  $^{81}\text{Br}$  in **112**). From  $^1\text{H}$  NMR analysis, successful coupling at the 6-position to afford **96** was supported by an upfield shift of the quinolinyl C(5)H due to electron donation by resonance from the piperidiny nitrogen (Figure 4.18). Similarly, formation of the 2-substituted side product **112** was indicated by upfield shifts of the quinolinyl C(3)H in  $^1\text{H}$  NMR spectra due to electron donation by resonance from the piperidiny nitrogen.

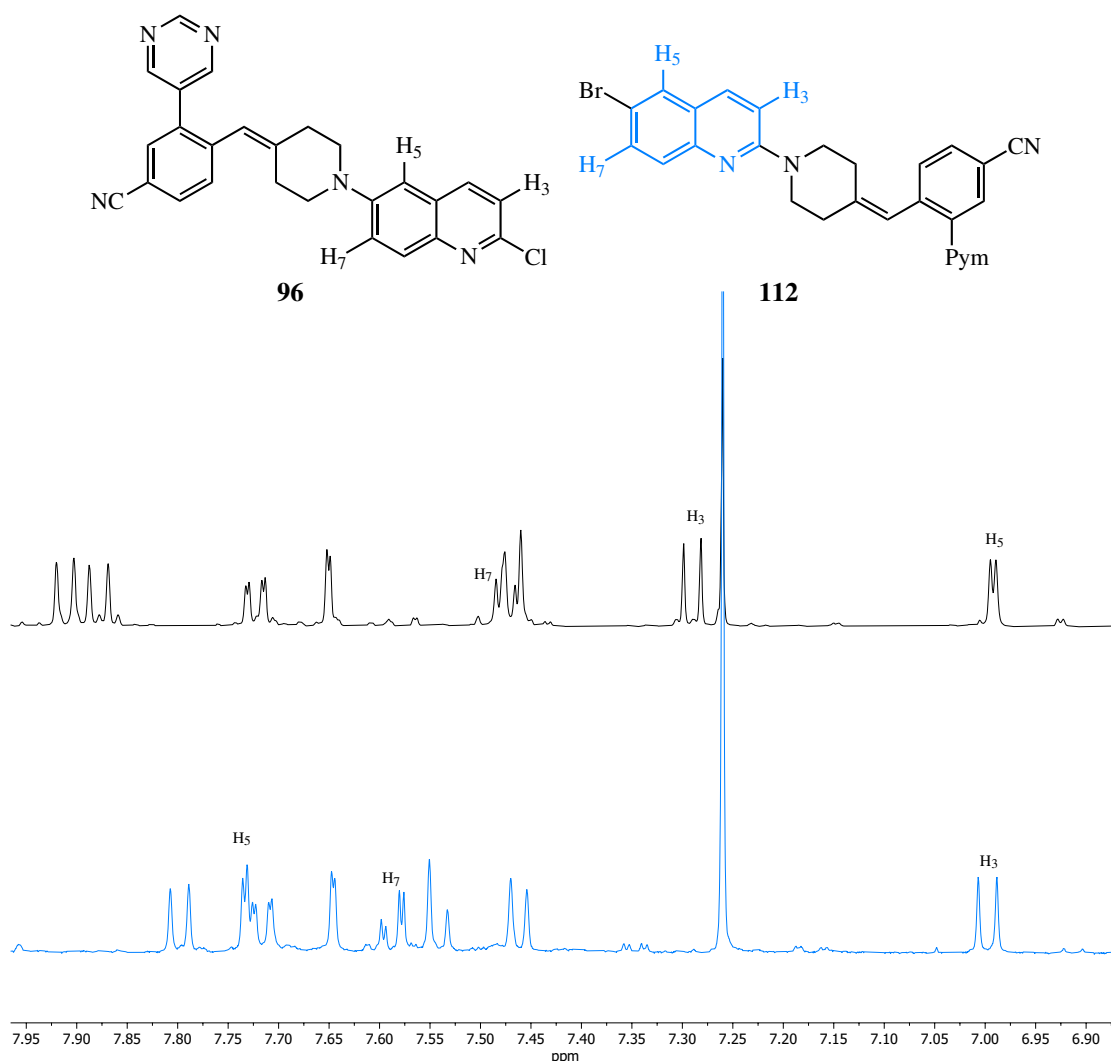


Figure 4.18: Comparison of stacked and normalised  $^1\text{H}$  NMR spectra ( $\delta_{\text{H}}$ : 6.90 - 7.95 ppm) of **96** (black) and **112** (blue), indicating different chemical shifts C(3)H, C(5)H and C(7)H. “Pym” indicates 2,5-pyrimidine.

For **96**, piperidinyl-quinoline connectivity was also supported by 2D NMR spectra, including HMBC and ROESY correlations (Figure 4.19).

The applied reaction conditions were optimised for the selective coupling of heterocyclic amines at the 6-position of **26**,<sup>47</sup> therefore were not strictly optimised for **95**. Considering the previously reported substrate-sensitivity in Buchwald-Hartwig coupling reactions,<sup>47,100</sup> a yield of 32% for **96** was acceptable for the purpose of initial ligand synthesis. Furthermore, the yield of 32% represents an inseparable 7:3 mixture of **96** and the corresponding THP isomer **113**; presence of the THP isomer was indicated by the emergence of  $^1\text{H}$  NMR signals for THP hydrogens, which are consistent with those reported previously for similar derivatives (Figure 4.20).<sup>56</sup>

### 4.3. SYNTHESIS OF COMPLEX LIGANDS CONTAINING BIARYL AND 4-AMIDO FUNCTIONAL GROUPS

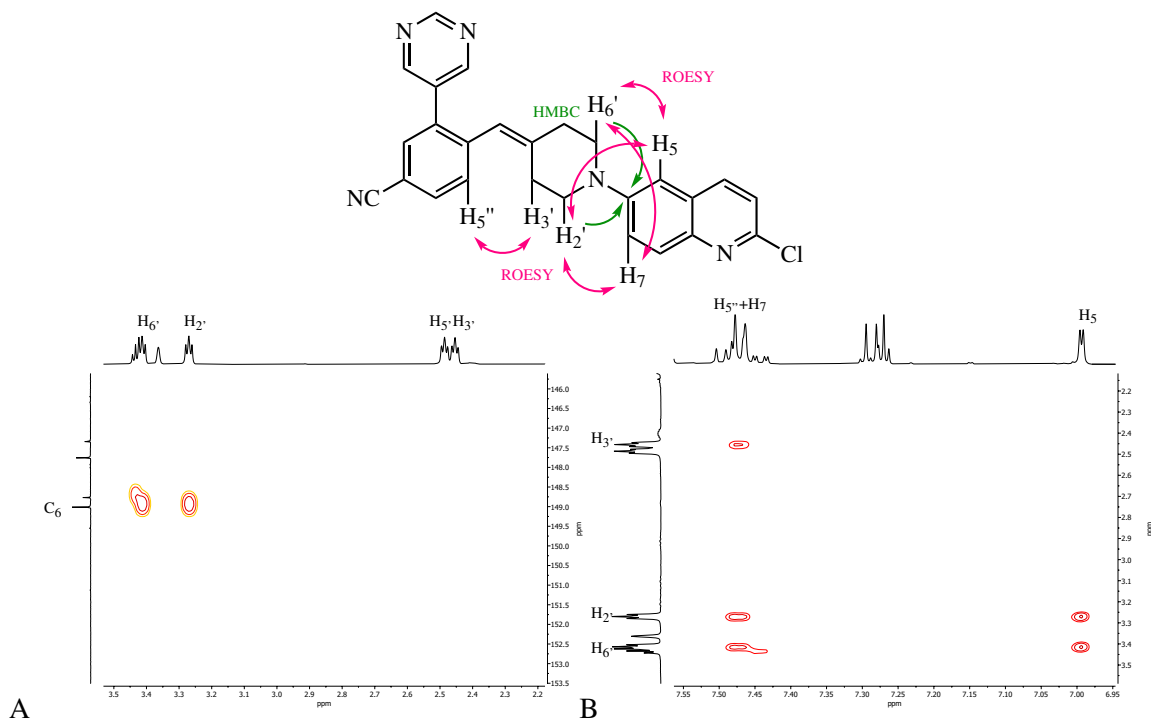


Figure 4.19: Structural analysis of **96** via 2D NMR spectra, with (A) HMBC correlations indicated by green arrows, and (B) ROESY correlations indicated by pink arrows.

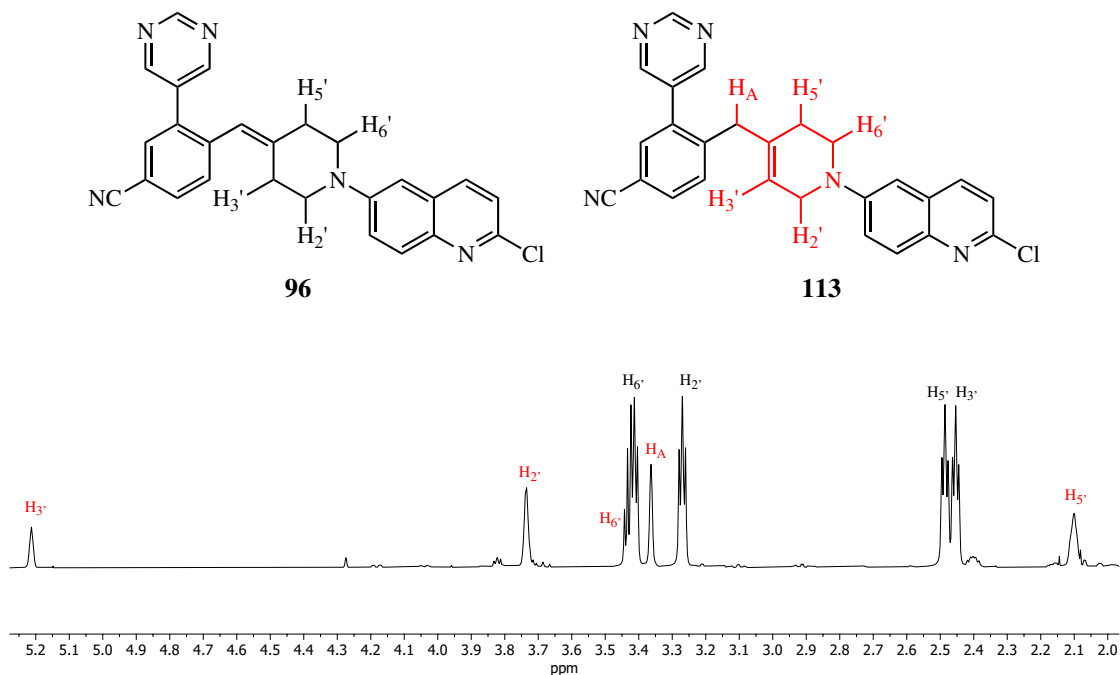
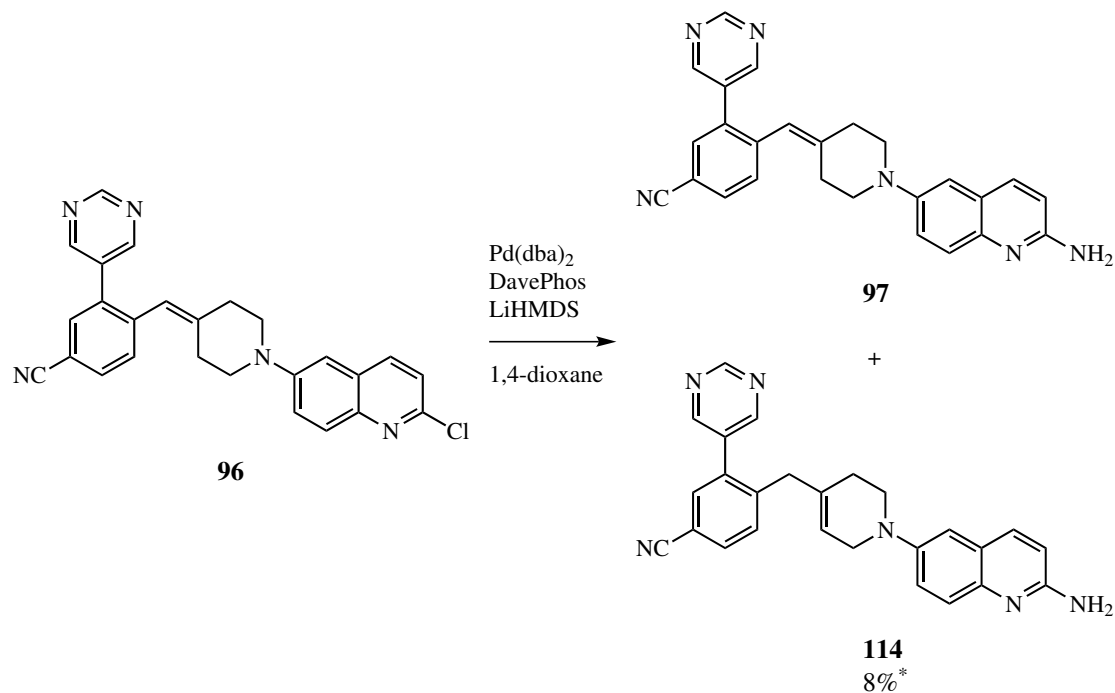


Figure 4.20:  $^1\text{H}$  NMR spectra ( $\delta_{\text{H}}$ : 2.0 - 5.2 ppm) containing methylene piperidinyll derivative **96** and the corresponding tetrahydropyridine (THP) isomer **113**, indicating distinctive THP ring signals in red, as consistent with previous studies.<sup>56</sup>

Isomerisation of **96** to the THP isomer **113** is not unexpected given the nature of the reagents used in the Buchwald-Hartwig coupling reaction, as a slight excess of base (NaO<sup>t</sup>Bu) was used (1.3 molar eq. c.f., 1.2 molar eq.). Noting that NaO<sup>t</sup>Bu is susceptible to hydrolysis (to NaOH), and isomerisation of methylene piperidinyl derivatives appeared to be mediated by hydroxide-containing bases (Scheme 2.19 in Chapter 2 and associated text),<sup>56</sup> it is not surprising that some isomerisation of **96** to the THP isomer **113** was observed, particularly as an older sample of NaO<sup>t</sup>Bu was used. It is also possible that the O<sup>t</sup>Bu anion may be facilitating isomerisation of **96** to the THP isomer **113**. Favourably, it was anticipated that the presence of the THP isomer was not a cause for concern, as it should undergo the same transformations in following synthetic steps, and could (in theory) be reduced to form the desired ligand **86**.

#### Synthesis of methylenepiperidinyl-substituted 2-aminoquinoline derivatives

Following successful synthesis of the 2-chloroquinoline derivative **96**, the next step required conversion of **96** to the corresponding 2-aminoquinoline derivative **97**. Again, it was expected that synthesis of **97** could be achieved via Buchwald-Hartwig coupling reaction, using LiHMDS as both a base and an ammonia equivalent under previously optimised reaction conditions;<sup>47,56</sup> this is shown in Scheme 4.12.



Scheme 4.12: Reaction conditions for synthesis of 2-aminoquinoline derivative **97** and side-product **114** via Buchwald-Hartwig amination with **96**, based on literature methods.<sup>47,56</sup> \* indicates the yield represents a 6:1 mixture of **97** & **114**

### 4.3. SYNTHESIS OF COMPLEX LIGANDS CONTAINING BIARYL AND 4-AMIDO FUNCTIONAL GROUPS

Formation of the desired product **97** was supported by analysis of HRMS and NMR spectra; a major mass product with  $m/z$  value of 419.1981 was observed (expected  $m/z$  419.4179) in HRMS spectra. From  $^1\text{H}$  NMR spectra, a distinct upfield shift of C(3)H of the quinolinyl ring was observed, consistent with *ortho/para* shielding via resonance from the introduced amine group in the 2-position of the quinoline ring Figure 4.21.

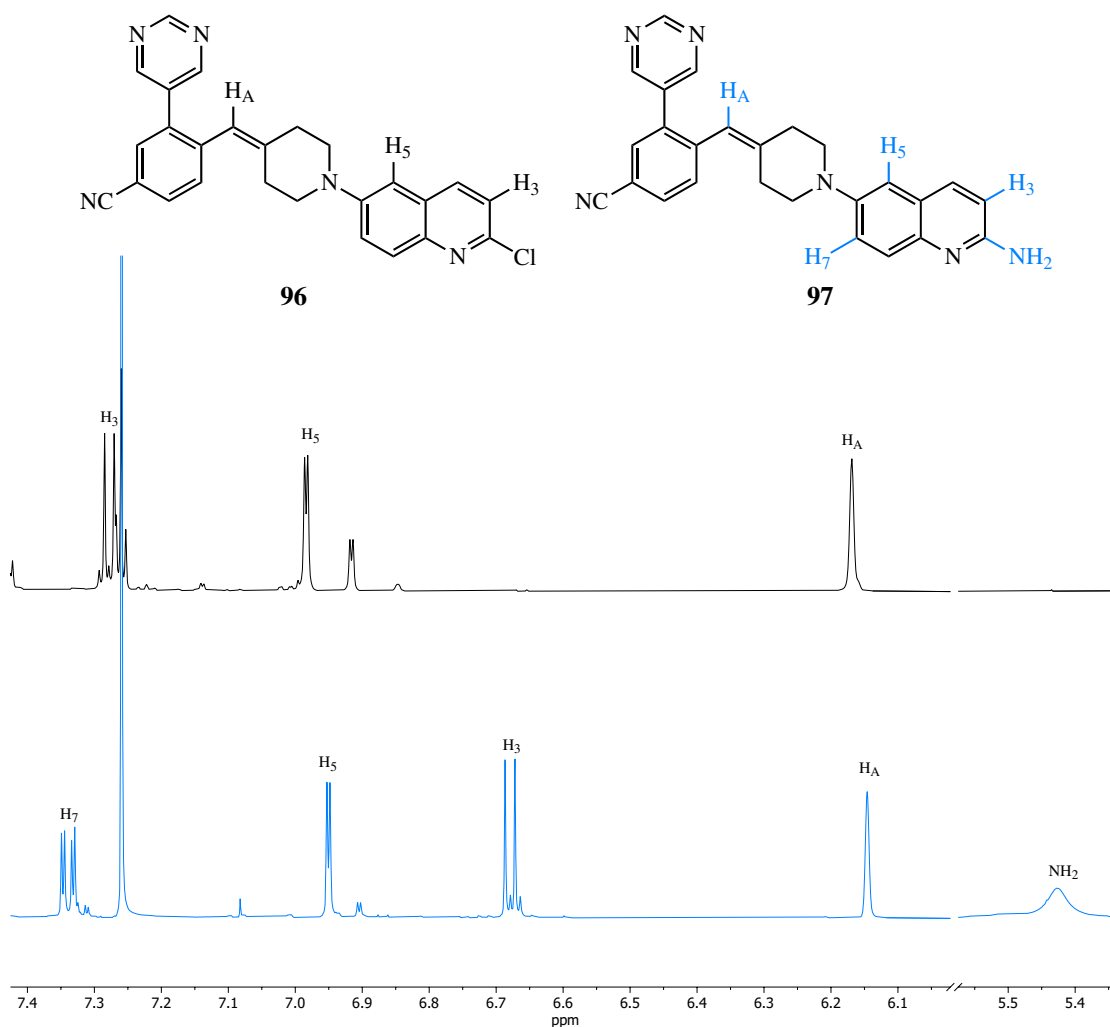


Figure 4.21: Stacked comparison of truncated and normalised  $^1\text{H}$  NMR spectra ( $\delta_{\text{H}}$ : 5.4 - 7.4 ppm) of **96** (black) and **97** (blue), indicating the change in chemical shifts for C(3)H, and the emergence of an amine signal. Note: spectra for **96** comprises a 7:3 mixture of **96** and **113**; spectra for **97** comprises a 6:1 mixture of **97** and **114**.

While the desired product **97** was obtained, it was purified as an inseparable 6:1 mixture with the corresponding THP isomer **114**; the presence of the THP isomer was supported by analysis of  $^1\text{H}$  NMR spectra, which revealed signals consistent with a THP ring.<sup>56</sup> It is not clear whether the THP isomer was carried through from the starting material (which was comprised of a 7:3 mixture of **96** and **113**), or if additional isomerisation to the THP isomer occurred during the Buchwald-

Hartwig coupling reaction (potentially mediated by LiHMDS, which could have partially hydrolysed to LiOH if an old LiHMDS aliquot or non-anhydrous reaction solvent was used). Furthermore, the overall yield for this reaction was poor at 8% (combined yield of **97** & **114**), yielding a combined mass of 3.7 mg (from ~50 mg scale), which was not sufficient to carry through the remaining synthetic steps for synthesis of the desired ligand **86**. In an attempt to increase the amount of **97** available for use in further reactions, the Buchwald-Hartwig reaction was repeated, but the concentrations of Pd catalyst, phosphine ligand and base were increased from 1 mol %, 1.2 mol% and 2.2 molar equivalents, to 3.1 mol %, 5.7 mol % and 3.1 molar equivalents, respectively. From this repeated reaction, **97** was purified in an improved yield of at 20%, however due to the reaction scale the quantity of product was quite low (4 mg), precluding further derivatisation of **97**.

As described previously in Chapter 3, optimising the Buchwald-Hartwig coupling reaction conditions for a particular ligand was not considered viable at this point, given the value of the desired ligand **86** was not yet known. As **97** and **114** (in the 6:1 mixture of **97** & **114**) each contain the core 2-aminoquinoline structures, it was concluded that **97** & **114** would be suitable ligands for investigation of binding affinity for the Tec SH3 domain by SPR, in lieu of the desired ligand **86**. Furthermore, given a small quantity of **97** had been purified, the ability to compare binding affinities between the methylene piperidinyl derivative **97** and THP isomer **114** would provide valuable SAR information about how the shape of the piperidinyl ring influences ligand binding activity, which has not been investigated previously. Given the numerous challenges with synthesis encountered up to this point, no further attempts to prepare the ligand **86** were undertaken.

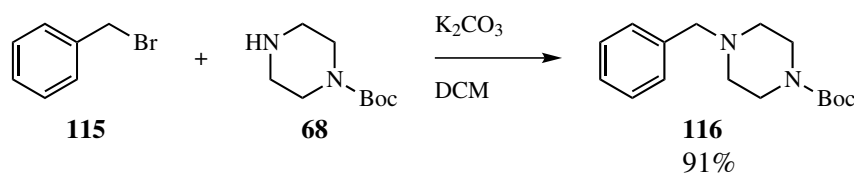
#### **4.3.4 Synthesis of benzylpiperazinyl derivatives containing biaryl and 4-nitrile functional groups**

To complement the obtained benzylpiperidinyl-derived ligand **97**, synthesis of the benzylpiperazinyl-derived ligand **87** was also desired. From Figure 4.6, it envisaged that **86** could be synthesised from the substituted tolyl derivative **83**, or preferably, from the advanced intermediate **92**. Based upon Figure 4.6, the first synthetic step involved a nucleophilic substitution reaction between **92** and **62**. A key concern associated with this synthetic approach was the potential for polyalkylation of the amine, therefore reducing the yield of the desired intermediate **99**. However, following a search



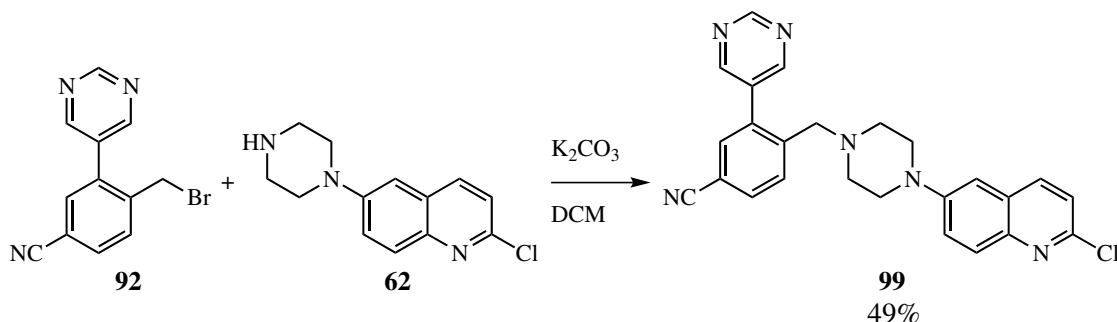
#### 4.3. SYNTHESIS OF COMPLEX LIGANDS CONTAINING BIARYL AND 4-AMIDO FUNCTIONAL GROUPS

of relevant literature, conditions were identified which reported the synthesis of benzylpiperazinyl derivatives via nucleophilic substitution with benzyl bromide (Scheme 4.13).<sup>123</sup>



Scheme 4.13: Literature conditions for the synthesis of benzyl piperazine derivative **116** by nucleophilic substitution with **68** and **115**.<sup>123</sup>

As there was a precedent in the literature for similar nucleophilic reactions affording the desired tertiary amine (rather than the polyalkylated product),<sup>123</sup> it was decided that the conditions reported in Scheme 4.13 were a suitable starting point for the synthesis of **99**, with the results reported in Scheme 4.14. It is noted that the starting material **92** was not pure and was contaminated with residual substituted tolyl derivative **98** — this was not expected to be problematic, as only **92** should react under the nucleophilic substitution reaction conditions described in Scheme 4.14. In order to facilitate more accurate yield calculations for synthesis of **99**, the mixture of **92** and **98** was added to the reaction in excess, so that **62** would be the limiting reagent.



Scheme 4.14: Reaction conditions for yield and synthesis of benzylpiperazine derivative **99** by nucleophilic substitution with **62** and **92**, based on literature methods.<sup>123</sup>

The desired product **99** was synthesised and purified in sufficient yield (49%) for further derivatisation. Evidence to support that **99** had been isolated was observed in HRMS and NMR spectra — mass products with  $m/z$  values consistent with **99** were observed in a 3:1 ratio, consistent with the natural chlorine isotope abundance. Furthermore, the emergence of a characteristic benzyl  $CH_2$  singlet at 3.45 ppm indicated successful attachment of the benzyl substituent, and the expected HMBC and ROESY correlations with phenyl and piperazinyl ring atoms and benzyl  $CH_2$  group were also observed (Figure 4.22).

### 4.3. SYNTHESIS OF COMPLEX LIGANDS CONTAINING BIARYL AND 4-AMIDO FUNCTIONAL GROUPS

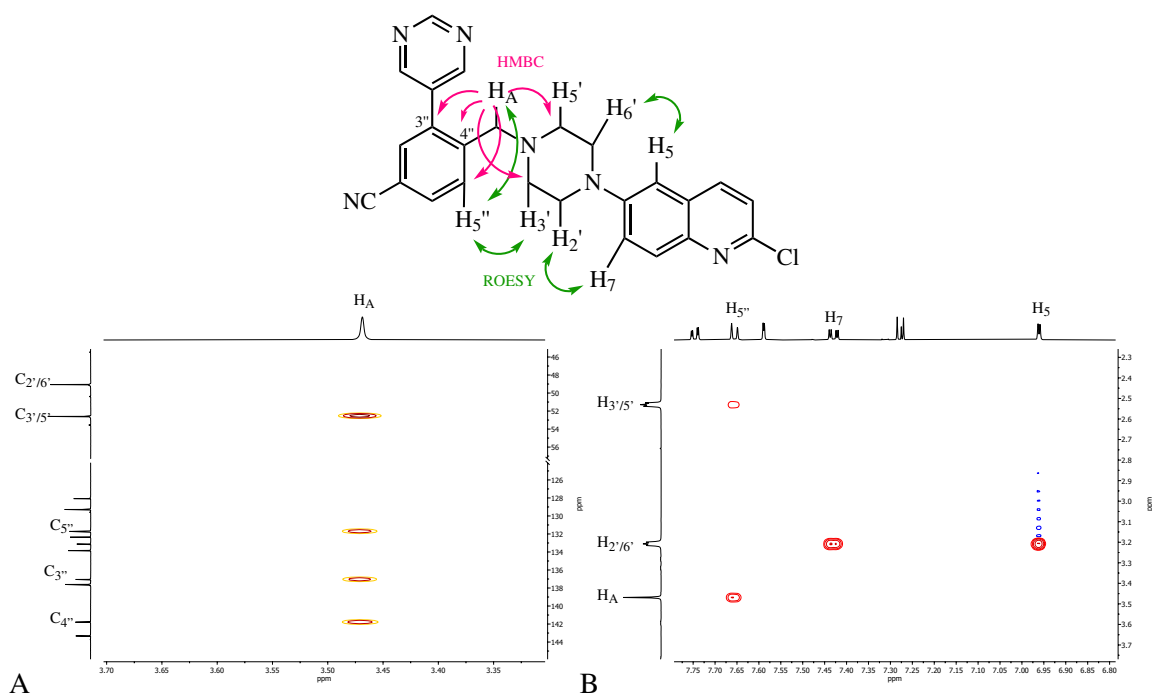
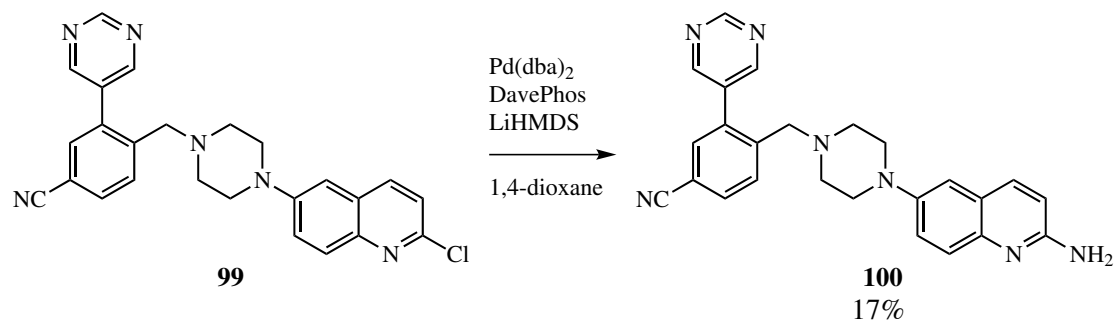


Figure 4.22: Structural analysis of **99** via 2D NMR spectra, with (A) HMBC correlations indicated by green arrows, and (B) ROESY correlations indicated by pink arrows.

For the conversion of **99** to the 2-aminoquinoline derivative **100**, it was expected that this transformation could be achieved via Buchwald-Hartwig coupling reaction, using LiHMDS as both a base and an ammonia equivalent as described previously;<sup>47,56</sup> these results are shown in Scheme 4.15.



Scheme 4.15: Reaction conditions for synthesis of 2-aminoquinoline derivative **100** via Buchwald-Hartwig amination with **99**, based on literature methods.<sup>47,56</sup>

Analysis of both HRMS and NMR spectra supported that the desired product **100** had been synthesised — a major mass product with a  $m/z$  value of 422.2090 was observed (expected  $m/z$ : 422.2088). From  $^1\text{H}$  NMR spectra, a characteristic upfield shift of the quinolinyl C(3)H signal was observed, which would be consistent with the introduction of the 2-amino group (Figure 4.23).

#### 4.3. SYNTHESIS OF COMPLEX LIGANDS CONTAINING BIARYL AND 4-AMIDO FUNCTIONAL GROUPS

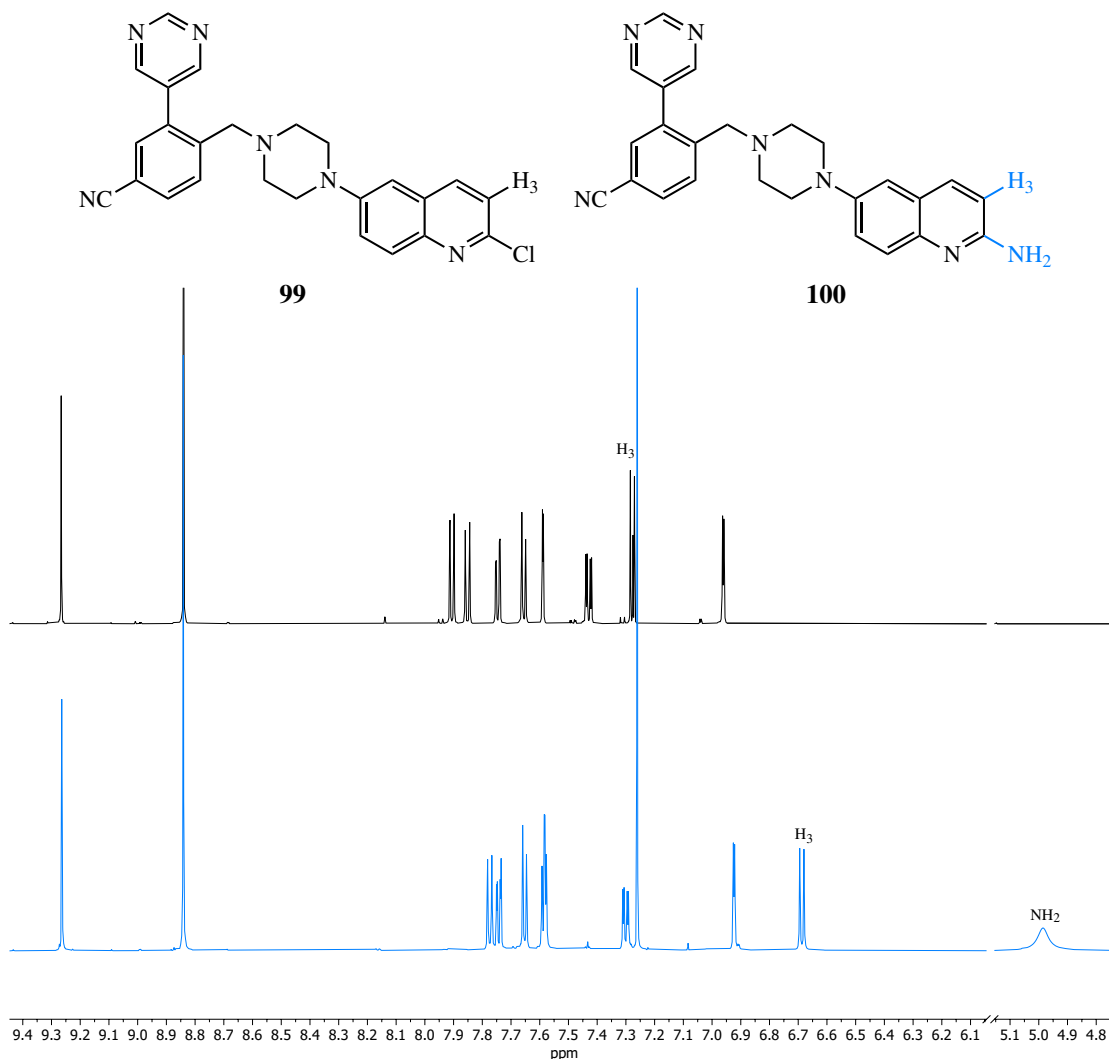
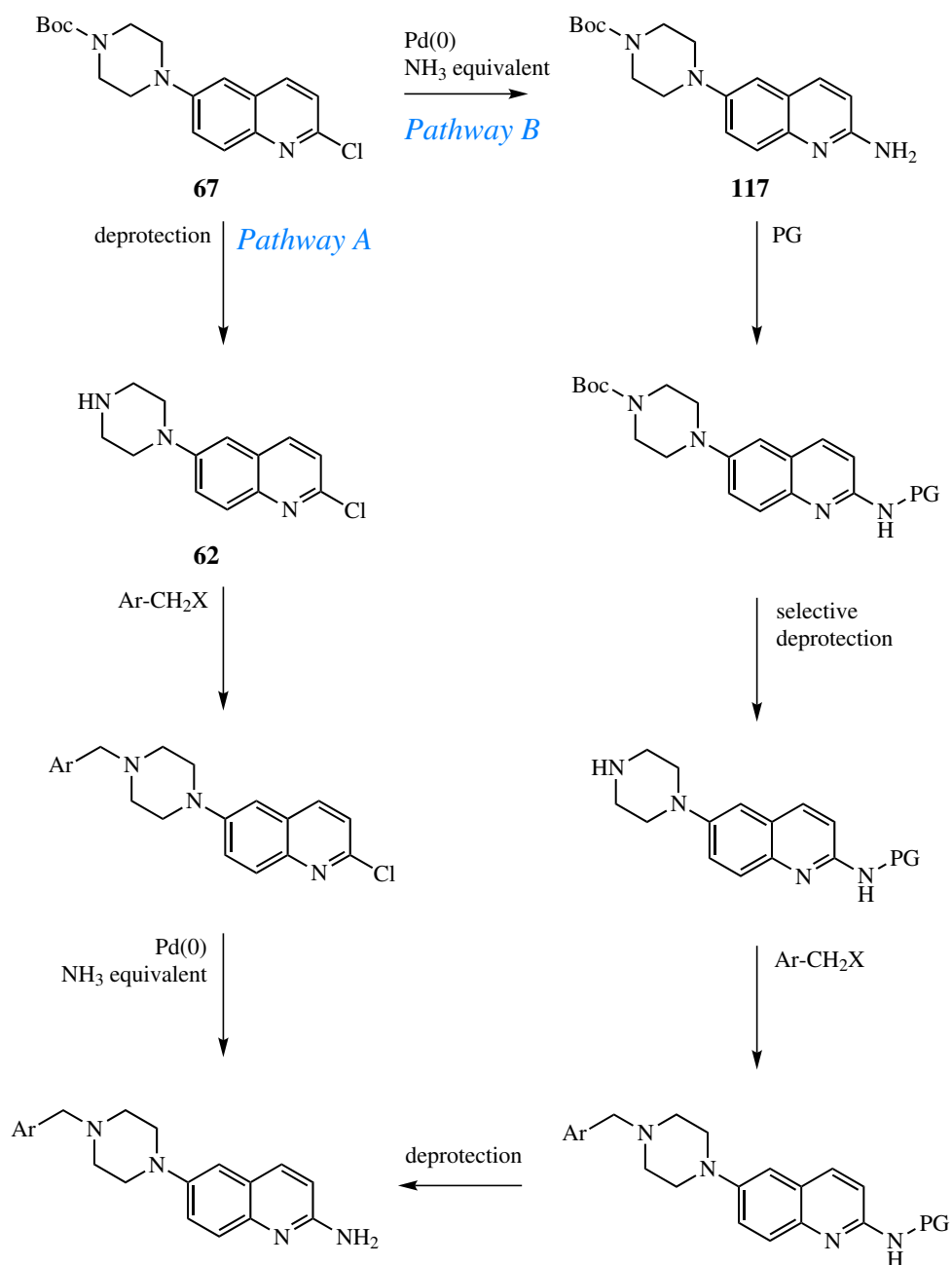


Figure 4.23: Stacked comparison of truncated and normalised  $^1\text{H}$  NMR spectra ( $\delta_{\text{H}}$ : 4.8 - 9.4 ppm) of **99** (black) and **100** (blue), indicating the change in chemical shifts for C(3)H, and the emergence of an amine signal.

As **100** was only synthesised in a low yield (17%, Scheme 4.15), insufficient material was available to attempt the final nitrile hydrolysis step for synthesis of the desired ligand **87**. Several repeat attempts to synthesise **100** via Buchwald-Hartwig coupling were undertaken, but the resulting yields were dismal. Given the numerous low yields obtained from using Buchwald-Hartwig coupling reactions with LiHMDS as both a base and an ammonia equivalent to introduce the 2-amino functionality into the quinoline ring, an alternative synthetic pathway to afford quinoline ring amination was sought. In lieu of optimising the late-stage Buchwald-Hartwig coupling reaction (Pathway A in Scheme 4.16), an alternative synthetic pathway for synthesis of benzylpiperazinyl-containing 2-aminoquinoline derivatives was proposed, as shown in Scheme 4.16 (Pathway B).

### 4.3. SYNTHESIS OF COMPLEX LIGANDS CONTAINING BIARYL AND 4-AMIDO FUNCTIONAL GROUPS



Scheme 4.16: Proposed synthetic pathways for the synthesis of arylmethylpiperazinyl 2-aminoquinoline ligands from common intermediate **67**. Pathway A indicates late-stage introduction of the 2-amino functional group. Pathway B indicates early introduction of 2-amino functional group, and exploits differing reactivities of multiple amine protecting groups. Ar = aryl. PG = protecting group. X = Br or Cl.

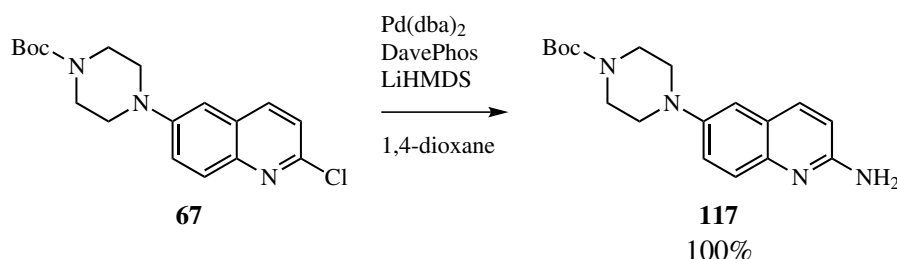
### 4.3. SYNTHESIS OF COMPLEX LIGANDS CONTAINING BIARYL AND 4-AMIDO FUNCTIONAL GROUPS

---

The key difference between Pathways A and B in Scheme 4.16 is the point of introduction of the 2-amino functionality to the quinoline ring; in Pathway A, the amine group is introduced late in the synthetic pathway, while in Pathway B, the amine is introduced early in **117**, and subsequently protected during the following synthetic steps before a late-stage deprotection to liberate the free amine. A major consideration for Pathway B is the choice of amine protecting group; due to the presence of the Boc protecting group on the piperazinyl nitrogen, it would be ideal to select an amine protecting group that could be selectively attached and removed in the presence of a Boc protecting group (e.g., acetamide, trifluoroacetamide protecting groups). As Pathway B was only 2 steps longer than the previously attempted Pathway A, it would be reasonable to attempt synthesis of benzylpiperazinyl-containing 2-aminoquinoline derivatives via Pathway B.

#### 4.3.4.1 Synthesis of benzylpiperazinyl derivatives containing biaryl and 4-nitrile functional groups via alternative protecting group strategy

The first step of Pathway B in Scheme 4.16 involves a Buchwald-Hartwig coupling reaction, again using LiHMDS as both a base and an ammonia equivalent. Reaction conditions analogous to those optimised previously were implemented;<sup>47</sup> the results are shown in Scheme 4.17.

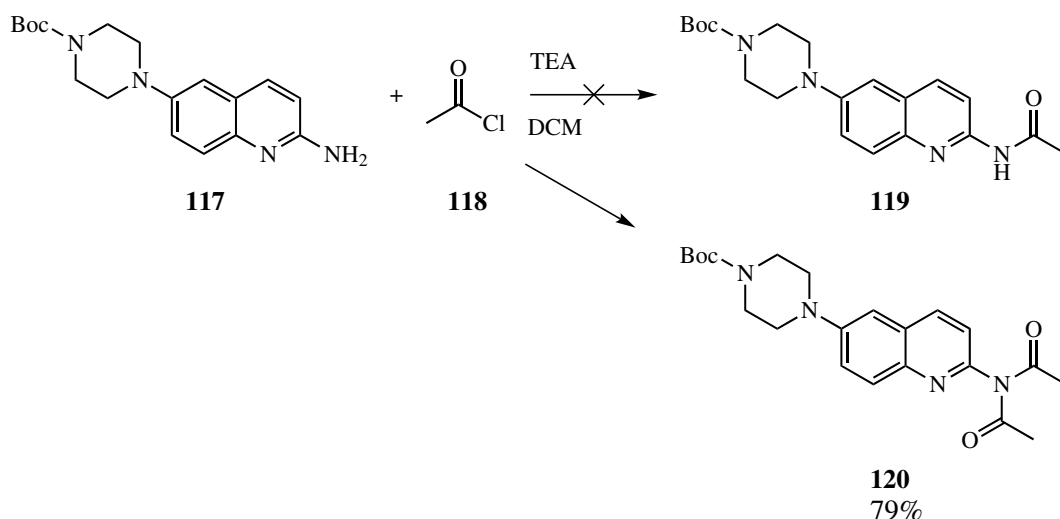


Scheme 4.17: Reaction conditions for synthesis of 2-aminoquinoline derivative **117** via Buchwald-Hartwig amination with **67**, based on literature methods.<sup>47,56</sup>

Formation of the desired 2-aminoquinoline derivative **117** was supported by analysis of HRMS and NMR spectra, and comparison to literature;<sup>47</sup> a major mass product with a  $m/z$  value of 329.1974 was observed in HRMS spectra (expected  $m/z$ : 329.1972). In addition, analysis of <sup>1</sup>H NMR spectra revealed the diagnostic upfield shift of the quinolinyl C(3)H due to *ortho/para* shielding by resonance from the introduced 2-amino group. Furthermore, the 9H singlet corresponding to the *tert*-butyl group in the Boc protecting group was present in <sup>1</sup>H NMR spectra for **117**, indicating the Boc protecting group was not removed under the reaction conditions. Importantly, the observed chemical shifts in NMR spectra were consistent with those reported in the literature, suggesting

the desired product had been formed.<sup>47</sup> The desired product **117** was isolated in quantitative yield; this is demonstrative of the attainable yields when Buchwald-Hartwig reaction conditions are optimised for a specific substrate. The conditions used for the reaction in Scheme 4.17 were previously optimised for 6-substituted 2-chloroquinoline substrates containing simple piperidinyl substituents (e.g., 4-methylpiperidine)<sup>60</sup> which bear substantial structural similarity to **67** (compared to other 2-chloroquinoline derivatives reported in this thesis).

The next step required protection of the newly-introduced amino group in **117**. To facilitate selective removal of the Boc protecting group in subsequent reactions, it was important that the selected amine protecting group to be attached to the quinolinyl amine would be stable under (non-aqueous) acidic conditions at room temperature, as these are the conditions typically required for efficient Boc protecting group removal.<sup>124</sup> It was envisaged that protection of the amine as an acetamide would be suitable, as attachment of the corresponding acetyl group can occur under mildly basic conditions (with acetyl chloride), which is not expected to affect the Boc protecting group. Furthermore, removal of an acetyl protecting group typically occurs under (aqueous) acidic conditions at higher temperatures,<sup>124</sup> therefore a Boc protecting group can selectively be removed in the presence of an acetamide. Consequently, the acetyl protecting group was introduced to **117** utilising the reaction conditions reported earlier in Chapter 3 for synthesis of amidopiperazine derivatives, as shown in Scheme 4.18.



Scheme 4.18: Reaction conditions for attempted synthesis of acetyl-protected 2-aminoquinoline derivative **119** via amide formation between **117** and acetyl chloride **118**.

#### 4.3. SYNTHESIS OF COMPLEX LIGANDS CONTAINING BIARYL AND 4-AMIDO FUNCTIONAL GROUPS

While the anticipated product from the acetyl protection of **117** was expected to be the monoacetylated product **119**, following analysis of HRMS and NMR spectra, it appeared that the diacetylated product **120** had been synthesised; the mass spectra revealed a major mass product with a  $m/z$  value of 413.2184 (which is consistent with a the diacetylated product), while the monoacetylated product was only detected ( $m/z$ : 371.2075) at comparatively very low abundance. Furthermore, from analysis of  $^1\text{H}$  NMR spectra, a distinctive downfield shift of the quinoliny C(3)H was observed, as expected for deshielding by anisotropy from the adjacent carbonyls in the acetyl groups (Figure 4.24). It is noted that the acetyl  $\text{CH}_3$  groups are observed as a single 6H singlet in NMR spectra (Figure 4.24), which suggests that each  $\text{CH}_3$  group is in the same chemical environment. Given there is no symmetry about the diacetyl-quinoline group, it is possible that the acetamide group is rotating sufficiently fast on the NMR timescale, such that the acetyl  $\text{CH}_3$  groups appear to share the same chemical environment.

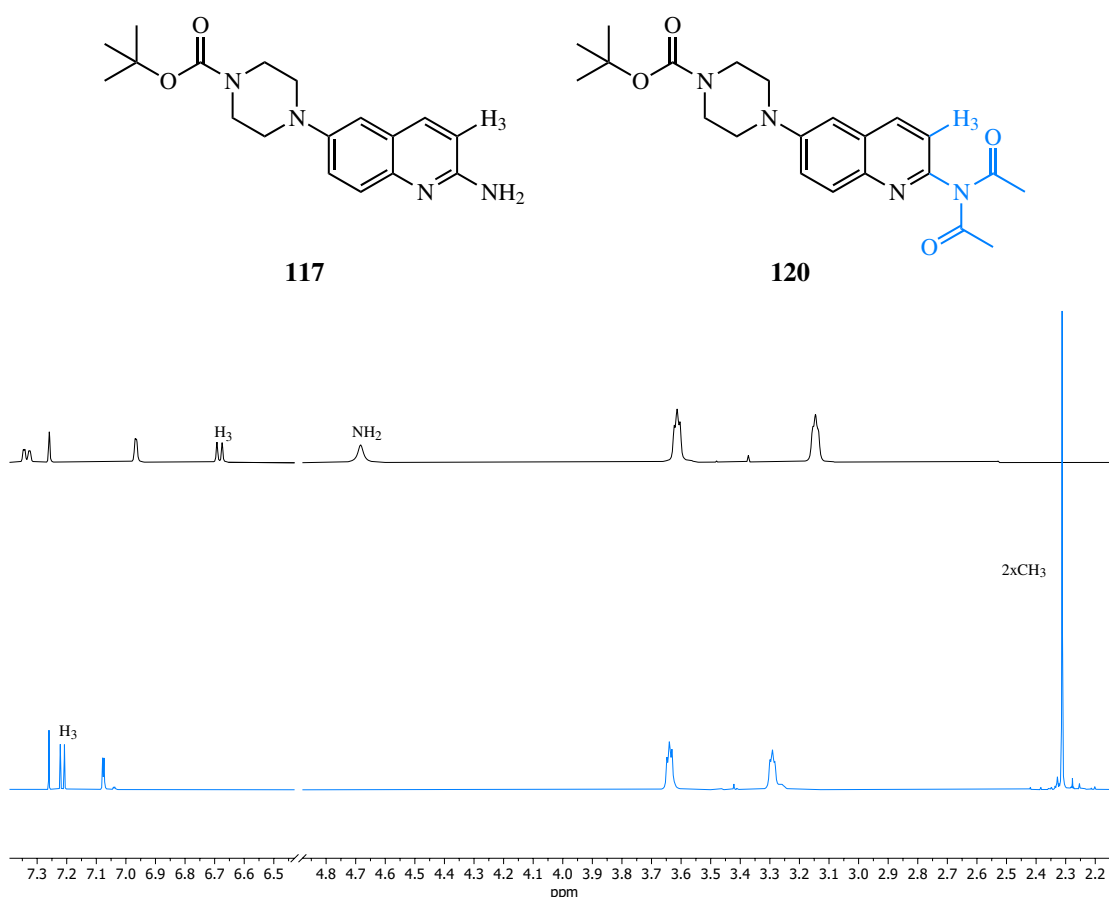


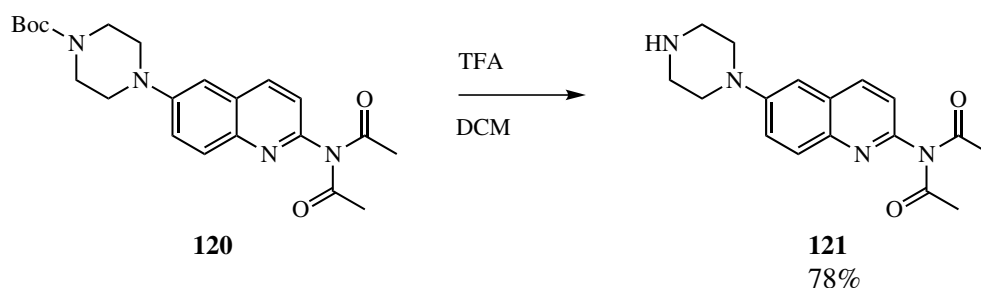
Figure 4.24: Stacked comparison of truncated and normalised  $^1\text{H}$  NMR spectra ( $\delta_{\text{H}}$ : 2.2 - 7.3 ppm) of **117** (black) and **120** (blue), indicating the downfield change in chemical shifts for C(3)H, and the emergence of a 2x $\text{CH}_3$  singlet.

### 4.3. SYNTHESIS OF COMPLEX LIGANDS CONTAINING BIARYL AND 4-AMIDO FUNCTIONAL GROUPS

---

As the acetylation reaction was conducted on a small scale (~70 mg), using a disposable syringe for measuring the volume of acetyl chloride, it is not unlikely that an excess of acetyl chloride was added during the reaction (given the limited precision for measuring liquids using disposable syringes), resulting in formation of the diacetylated product **120**. Formation of the diacetylated product was not anticipated to be an issue; the main purpose of the acetamide formation step was to minimise the chemoselectivity risks in subsequent synthetic steps, which is achieved in the diacetylated product. Furthermore, deprotection of each acetyl group should theoretically occur under the same reaction conditions — if anything, the acetyl deprotection reaction may need to proceed for a longer period of time, to ensure complete removal of both acetyl protecting groups.

Following synthesis of **120**, the next step required the selective removal of the Boc protecting group; reaction conditions consistent with those described earlier in this thesis were implemented, as shown in Scheme 4.19.



Scheme 4.19: Reaction conditions and yield for synthesis of **121** via Boc deprotection of **119**.

Selective removal of the Boc protecting group from **120** was supported by analysis of HRMS and NMR spectra; a major mass product with a  $m/z$  value of 313.1656 was observed in HRMS spectra, as well as a minor mass product with a  $m/z$  value of 271.1556 (consistent with the expected  $m/z$  values for diacetylated product **121** and monoacetylated product **122** respectively). However, analysis of  $^1\text{H}$  NMR spectra suggested the presence of the diacetylated product **121** only, due to the presence two distinct singlets integrating to 3H (at 2.17 and 2.24 ppm). Therefore, it is possible that the monoacetylated product **122** may simply be observed in HRMS spectra due to the harsh ionisation conditions applied during data acquisition. Importantly, from analysis of  $^1\text{H}$  NMR spectra, a diagnostic loss of the 9H singlet at ~1.48 ppm was observed, suggesting the desired selective removal of the Boc protecting group had been achieved (data not shown).

It is interesting to note the signal broadening and distinct chemical environments observed for the acetyl  $\text{CH}_3$  group in **121**, compared to the single acetyl  $\text{CH}_3$  chemical environment in **120** (Fig-



#### 4.3. SYNTHESIS OF COMPLEX LIGANDS CONTAINING BIARYL AND 4-AMIDO FUNCTIONAL GROUPS

ure 4.24); this resolution of the CH<sub>3</sub> signals into separate chemical environments suggests that rotation of the acetamide bond is slower on the NMR timescale for **121** than for **120** (Figure 4.25). In addition, the quinolinyl C(3)H signal was also shifted downfield significantly to 8.35 ppm (from 7.22 ppm), and is substantially broadened in <sup>1</sup>H NMR spectra for **121**, which would be consistent with experiencing different chemical environments due to slower rotation of the acetamide bond on the NMR timescale. As the only difference between the structures of **120** and **121** is removal of the Boc protecting group (i.e., there is no obvious change in the character of the acetamide group), it is hypothesised that the Boc protecting group must be impacting the speed of rotation of the acetamide bond. However, given the distance between the Boc and acetyl protecting groups in the molecules, it is not clear how Boc group removal to form **121** would implicate rotation of the acetamide bond, and subsequently the observed ~1 ppm downfield shift of C(3)H of the quinolinyl ring.

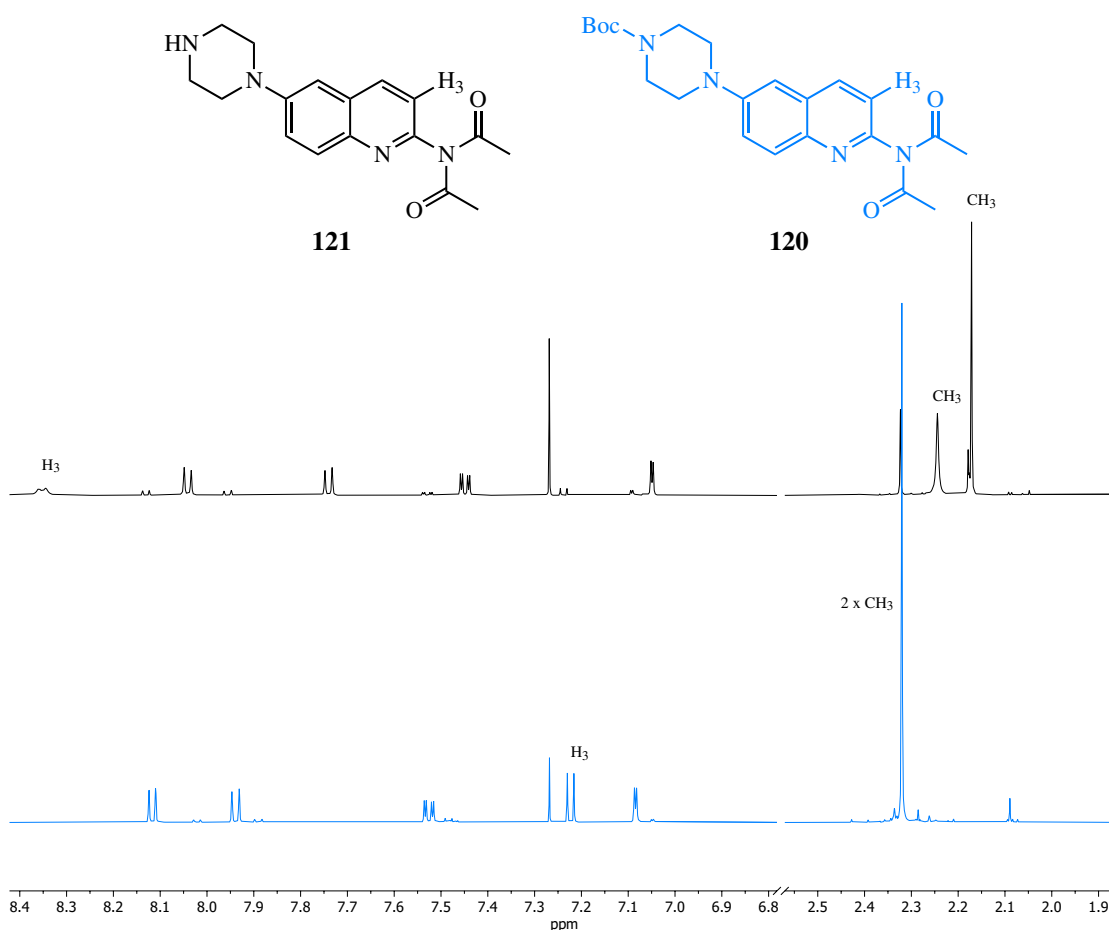
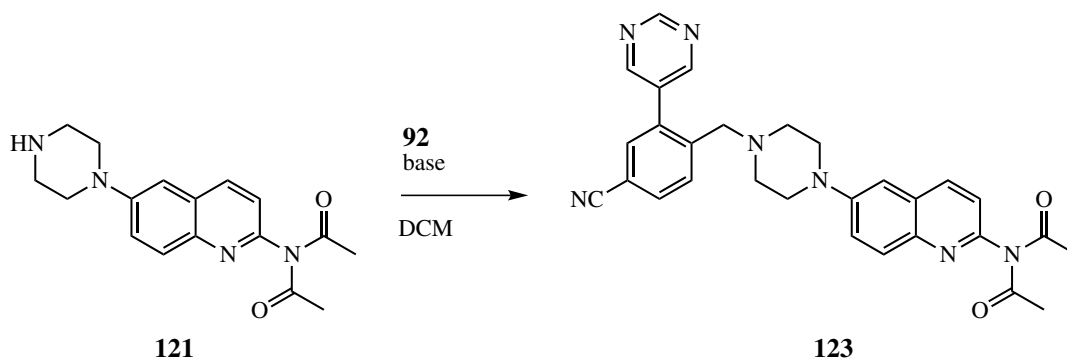


Figure 4.25: Stacked comparison of truncated and normalised <sup>1</sup>H NMR spectra ( $\delta_{\text{H}}$ : 1.9 - 8.4 ppm) of **121** (black) and **120** (blue), indicating resolution of acetyl CH<sub>3</sub> signals, and the corresponding downfield chemical shifts and signal broadening for C(3)H of the quinolinyl ring following Boc group removal.

### 4.3. SYNTHESIS OF COMPLEX LIGANDS CONTAINING BIARYL AND 4-AMIDO FUNCTIONAL GROUPS

The next step required derivatisation of **121**; from Scheme 4.16, it was envisaged that a nucleophilic substitution reaction with the appropriate benzyl halide derivative would be a suitable approach to achieve the desired transformation. Therefore, nucleophilic substitution reactions were attempted between **121** and **92**, as shown in Table 4.4.

Table 4.4: Attempted syntheses of acetyl-protected 2-aminoquinoline derivative **123** via alkylation of **121** and **92**, using various bases. <sup>a</sup> indicates only trace amounts of **123** were observed in crude <sup>1</sup>H NMR spectra, but could not be isolated.



Entry	Base (molar equivalents)	Reaction time (hr)	Temperature (°C)	Yield <b>123</b> (%)
1	K <sub>2</sub> CO <sub>3</sub> (1.2)	23	R.T.	<sup>a</sup>
2	TEA (1.4)	23	R.T.	0

From Entry 1 in Table 4.4, unfortunately there was only minimal conversion of **121** and **92** to the desired product **123** (Figure 4.26). This was quite interesting; when these nucleophilic substitution reaction conditions had been applied previously (see Scheme 4.14), the desired product had been isolated in moderate yields.

During the reaction between **121** and **92**, it was noted that both **121** and the base (K<sub>2</sub>CO<sub>3</sub>) had quite poor solubility in the reaction solvent (DCM). While it would be ideal to change the reaction solvent to a more polar solvent (e.g., DMF), there were concerns that extracting the desired product from DMF could be quite challenging, and result in low yields. Therefore, rather than changing the reaction solvent, an alternative approach was to identify and utilise a base with a comparable pK<sub>a</sub> to K<sub>2</sub>CO<sub>3</sub>, but with improved solubility under the reaction conditions; if a higher proportion of base was soluble under the reaction conditions, then perhaps there would be sufficient base available to facilitate the desired nucleophilic substitution reaction. Subsequently, the reaction was attempted again, instead using triethylamine as the base (Entry 2, Table 4.4). Unfortunately, this did not yield any product, and also led to consumption of the benzyl bromide derivative **92**. Further investigation

#### 4.3. SYNTHESIS OF COMPLEX LIGANDS CONTAINING BIARYL AND 4-AMIDO FUNCTIONAL GROUPS

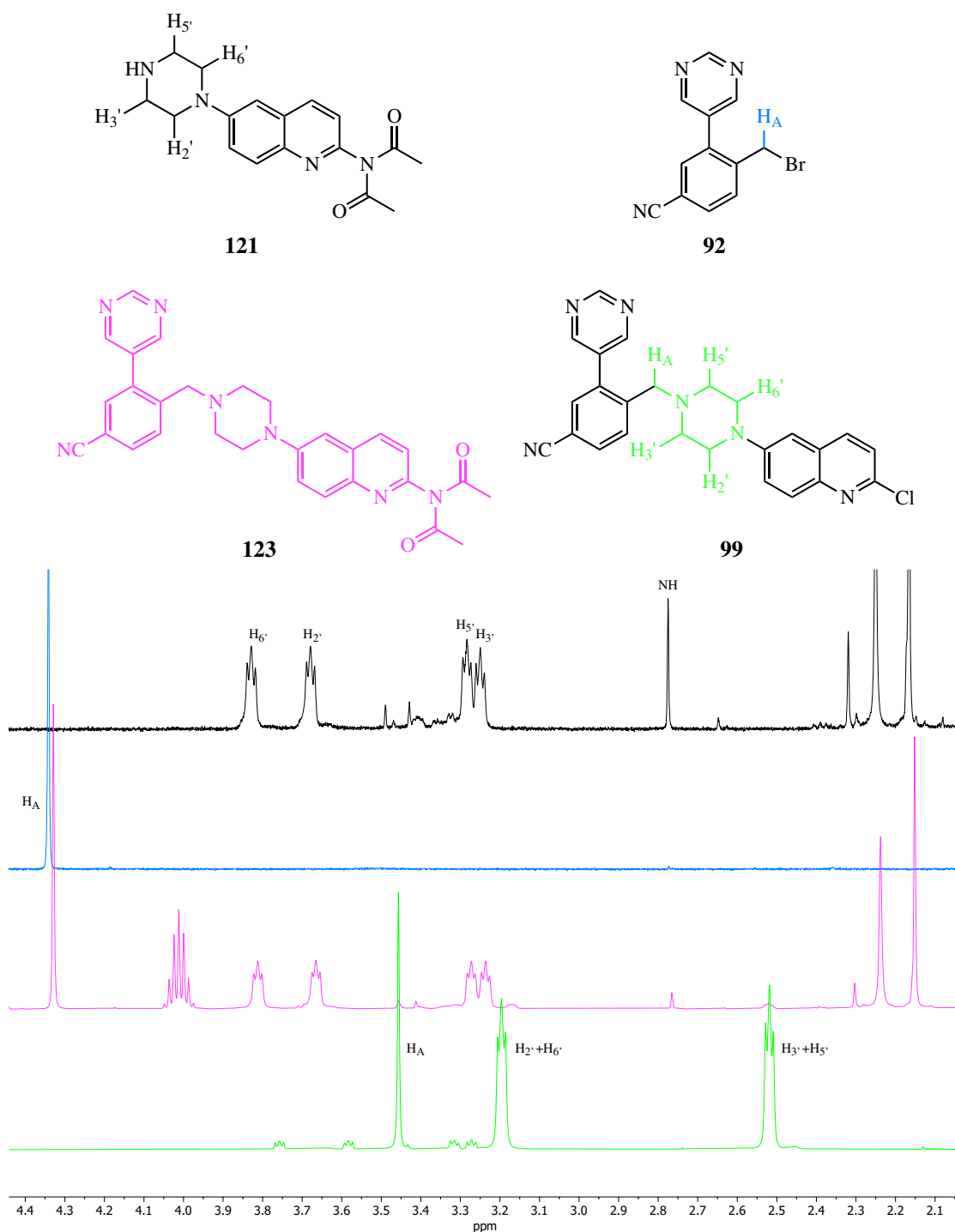
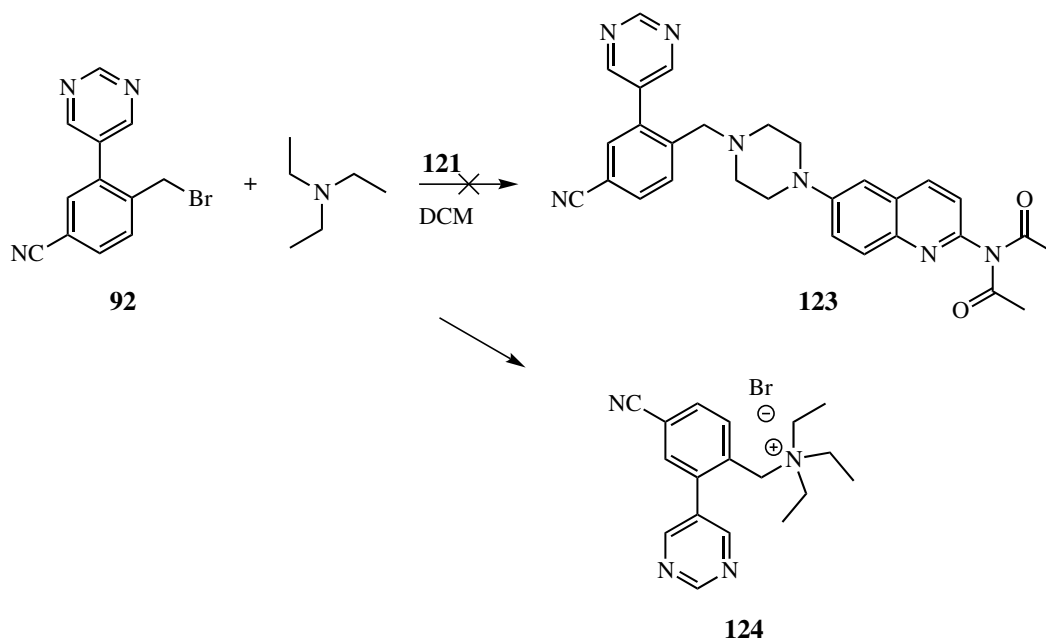


Figure 4.26: Stacked comparison of normalised  $^1\text{H}$  NMR spectra ( $\delta_{\text{H}}$ : 2.1 - 4.4 ppm) of **121** (black), **92** (blue), worked up reaction mixture from attempted synthesis of **123** using  $\text{K}_2\text{CO}_3$  as the base (pink), and **99** (green), indicating presence of starting materials **121** and **92** following attempted synthesis of **123**. Comparison of piperazinyl ring signals between spectra for attempted synthesis of **123** and **99** ( $\sim 2.52$  &  $3.20$  ppm) indicate trace amounts of the **123** may be present.

into the literature indicated that the reaction conditions described in Entry 2 of Table 4.4 were ideal reaction conditions for facilitating a Menshutkin reaction,<sup>125</sup> whereby a tertiary amine reacts with an alkyl halide to form a quaternary ammonium salt. Given the presence of both triethylamine and **92** in the reaction mixture in Table 4.4 (Entry 2), it is highly likely that a Menshutkin reaction had occurred to form the quaternary ammonium salt **124**, leading to consumption of **92** and no formation of the desired product **123** (Scheme 4.20).



Scheme 4.20: Proposed explanation for consumption of the benzyl bromide derivative **92** in an attempted nucleophilic substitution reaction with **121**, via Menshutkin reaction with TEA to form the quaternary ammonium salt **124**.

It was clear that substantial optimisation would be required to facilitate the nucleophilic substitution reaction; given that the reaction would be consuming late stage intermediates (i.e., **121** and **92**), these optimisation attempts would be quite expensive from a materials consumption standpoint. Furthermore, in the absence of any binding activity data, the value of the desired ligand **87** was not known, therefore any extensive attempts to optimise the nucleophilic substitution reaction would be considered risky. Subsequently, no further attempts to synthesise **123** or optimise Pathway B in Scheme 4.16 as an alternative synthetic strategy to synthesise benzylpiperazinyl-substituted 2-aminoquinoline derivatives were undertaken.

## 4.4 Synthesis of complex ligands containing biaryl and 2-pyridyl functional groups

### 4.4.1 Proposed synthetic pathways of complex ligands containing biaryl and 2-pyridyl functional groups

Following synthesis of ligands **97** (both purified, and as a mixture with its THP isomer **114**) and **100**, the next pair of complex ligands to be synthesised (**88** and **89**) were to contain 2-pyridyl and biaryl substituents, where the biaryl substituent would preferably be 2,5-pyrimidine. Considering the general synthetic methods proposed in Figure 4.2 and Figure 4.3, more detailed pathways were required for the synthesis of ligands **88** and **89**, and are proposed in Figure 4.27 and Figure 4.28.

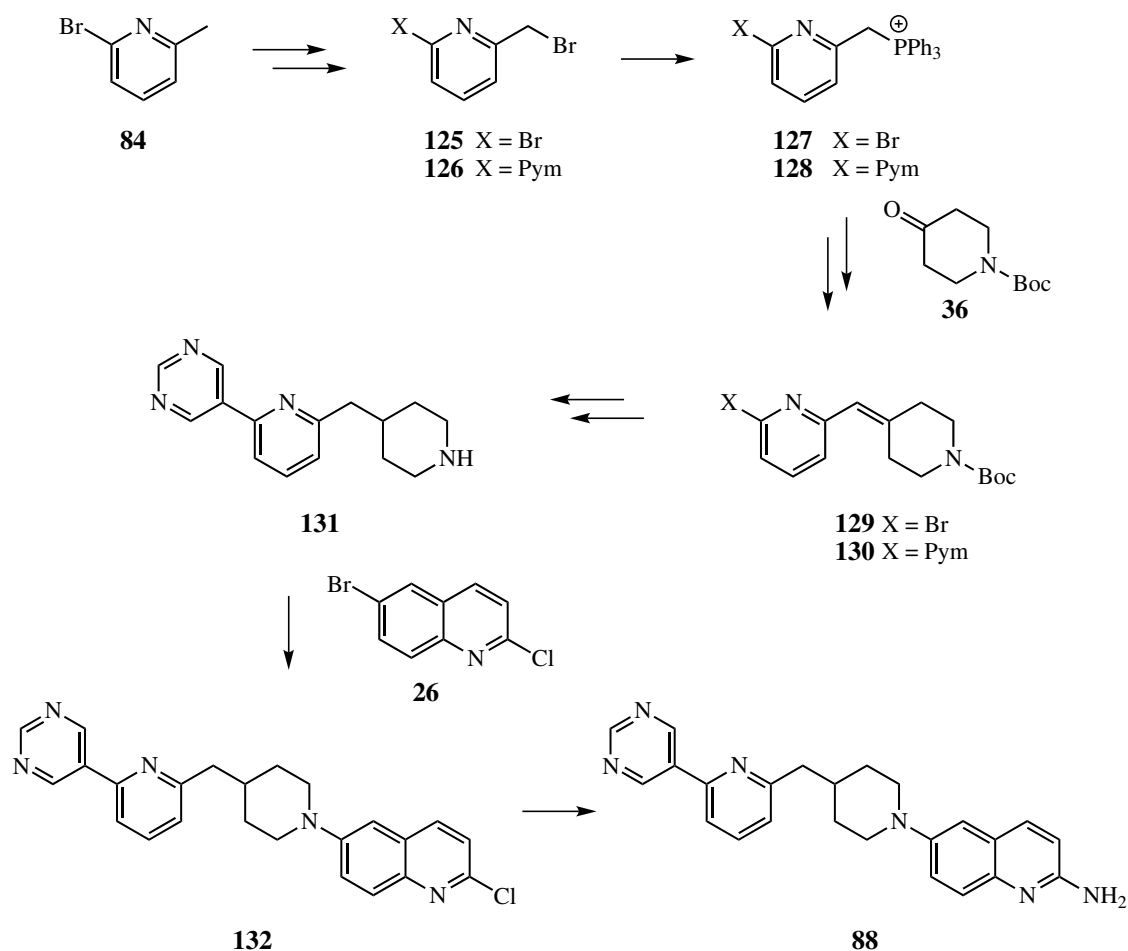


Figure 4.27: Proposed synthetic pathway for synthesis of complex ligand **88**, which contains 2-pyridyl and biaryl substituents. “Pym” indicates 2,5-pyrimidinyl.

Again, both Figure 4.27 and Figure 4.28 suggest the common substituted tolyl (methylpyridine) derivative **84** as the initial starting material, however the more advanced intermediate **126** is also a shared intermediate, which would be accessible following aryl (Suzuki) cross-coupling reaction and radical bromination from **84**. In the context of synthesis of the benzylpiperidinyl ligand **88**, the pyridylmethyl bromide derivative (**125** or **126**) can be converted to the corresponding phosphonium salt, followed by a Wittig reaction with **36** to form the methylenepiperidine derivative **129** or **130**. Given the previous issues observed for attempted Wittig reactions (Scheme 4.5), it would be ideal to investigate a Wittig reaction with the more simple bromopyridyl derivative **127**, followed by a Suzuki cross-coupling reaction with **129** to form **130** in the first instance, as this approach would require fewer synthetic steps, and therefore any synthetic challenges would be identified sooner. It is noted that for synthesis of pyridylmethylene piperidinyl derivatives (including **129** and **130**), utilisation of the Wittig reaction to form the key methylene-piperidine bond is preferred over a Horner-Emmons reaction; pyridylmethyl halide derivatives are known for their volatility,<sup>56</sup> therefore synthesis of a (non-volatile) phosphonium salt (for a Wittig reaction, i.e., **127** and **128**) is anticipated to be higher yielding than synthesis of the corresponding phosphonates, which requires reflux at high temperatures.

From Figure 4.27, there is some flexibility regarding the point at which the 2,5-pyrimidine ring is coupled to the 2-pyridyl ring, where the latest possible point of introduction of the 2,5-pyrimidine ring (to prevent unwanted Br reduction or selectivity issues in subsequent Buchwald-Hartwig coupling reactions) would be a Suzuki cross-coupling with **129** and the appropriate boronic acid to form **130**. Upon synthesis of **130**, subsequent alkene bond reduction and Boc group deprotection would liberate the free amine **131**, which can undergo a selective Buchwald-Hartwig coupling reaction with **26** using previously optimised reaction conditions<sup>47</sup> to synthesise **132**. Followed this, a sequential Buchwald-Hartwig coupling reaction (using LiHMDS as both a base and an ammonia equivalent) can be undertaken to afford the desired 2-aminoquinoline ligand **88**. Favourably, early reduction of the alkene bond in the methylenepiperidine derivative **130** will prevent isomerisation to the corresponding THP isomer, which would simplify subsequent (Buchwald-Hartwig) reaction steps substantially.

#### 4.4. SYNTHESIS OF COMPLEX LIGANDS CONTAINING BIARYL AND 2-PYRIDYL FUNCTIONAL GROUPS

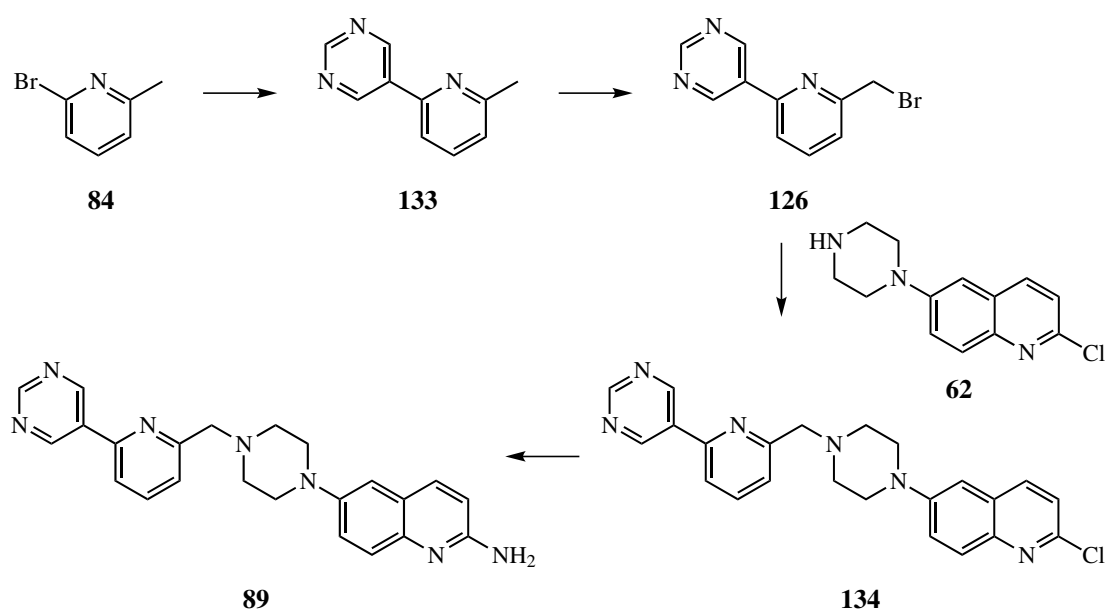
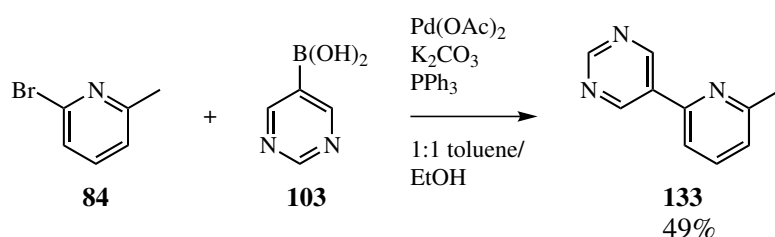


Figure 4.28: Proposed synthetic pathway for synthesis of the complex ligand **89**, which contains 2-pyridyl and biaryl substituents.

For synthesis of the benzylpiperazinyl-containing ligand **89**, from Figure 4.28 it was anticipated that **62** could be derivatised with the pyridylmethyl bromide **126** to afford synthesis of the 2-chloroquinoline **134** via nucleophilic substitution reaction. Following this, the desired ligand **89** could be synthesised by a Buchwald-Hartwig coupling reaction, using LiHMDS as both a base and an ammonia equivalent.

##### 4.4.1.1 Synthesis of methylene piperidinyl derivatives containing 2-pyridyl and biaryl functional groups

In order to synthesise the desired ligand **88**, the first step from Figure 4.27 required aryl coupling of a 2,5-pyrimidinyl ring; it was envisaged that this aryl group might be introduced via Suzuki cross-coupling with the pyridylmethyl derivative **84** and the appropriate boronic acid **103** using previously established conditions,<sup>56</sup> as shown in Scheme 4.21.



Scheme 4.21: Reaction conditions and yield for synthesis of **133** by Suzuki coupling of **84** and **103**, based on literature methods.<sup>56</sup>

Formation of the desired biaryl methylpyridine **133** was supported by analysis of HRMS and NMR spectra; a major mass product with a  $m/z$  value of 189.1128 was detected, consistent with an ammonium adduct of the desired product (expected  $m/z$  for  $[\mathbf{133}+\text{NH}_4]^+$ : 189.1135). In addition, successful incorporation of the 2,5-pyrimidine ring was observed in  $^1\text{H}$  NMR spectra, through the emergence of deshielded 2H and 1H singlets at 9.32 and 9.14 ppm. Furthermore, the desired connectivity of the 2,5-pyrimidine group was supported by correlations in 2D (HMBC) NMR spectra (Figure 4.29). While the yield for formation of **133** was moderate at 49%, due to the number of variables available for potential optimisation in the Suzuki cross-coupling reaction (solvent, Pd species, phosphine ligands, base, temperature etc., see Scheme 4.21), it was not considered beneficial to invest a substantial amount of time in yield optimisation at this point, particularly as sufficient material had been obtained to proceed to the next synthetic step.

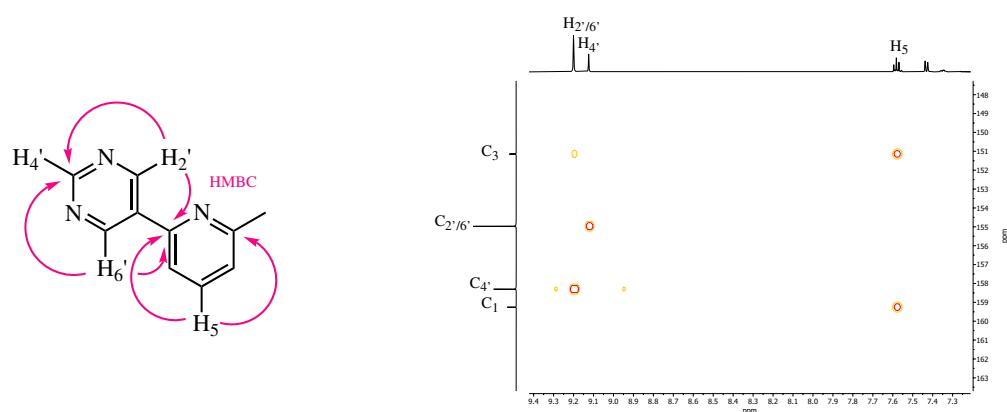
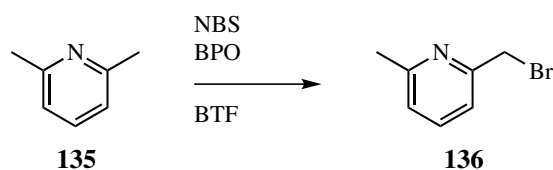


Figure 4.29: Structural analysis of **133** via HMBC 2D NMR spectra, with correlations indicated by pink arrows.

Following the successful synthesis of the biaryl intermediate **133**, the next step required radical bromination of the methylpyridine component, to afford the desired bromomethyl pyridine **126**. Due to the previously reported volatility of halomethyl pyridine compounds,<sup>56</sup> it was desirable to conduct a proof-of-concept reaction with a commercially available methylpyridine derivative, to avoid consumption of the valuable intermediate **133**. Subsequently, 2,6-lutidine **135** was selected as a suitable substrate to conduct a proof-of-concept radical bromination (employing the conditions reported earlier in Scheme 4.3), as shown in Scheme 4.22.



#### 4.4. SYNTHESIS OF COMPLEX LIGANDS CONTAINING BIARYL AND 2-PYRIDYL FUNCTIONAL GROUPS



Scheme 4.22: Proof-of-concept reaction for radical bromination of methylpyridine derivatives using **135** to form **136**. NBS = *N*-bromosuccinimide, BPO = benzoyl peroxide,

Formation of the desired bromomethyl pyridine was supported by analysis of crude product  $^1\text{H}$  NMR spectra; emergence of a characteristic 2H singlet at 4.57 ppm was observed, as consistent for similar benzyl bromide derivatives (Figure 4.30). In addition, from integration of key signals in crude **136**  $^1\text{H}$  NMR spectra, approximately 50% of the starting material had been converted to the desired product **136** (data not shown). Overall, this suggested that 2-methylpyridines (such as **135**, and therefore **133**) may be amenable to derivatisation via radical bromination reactions.

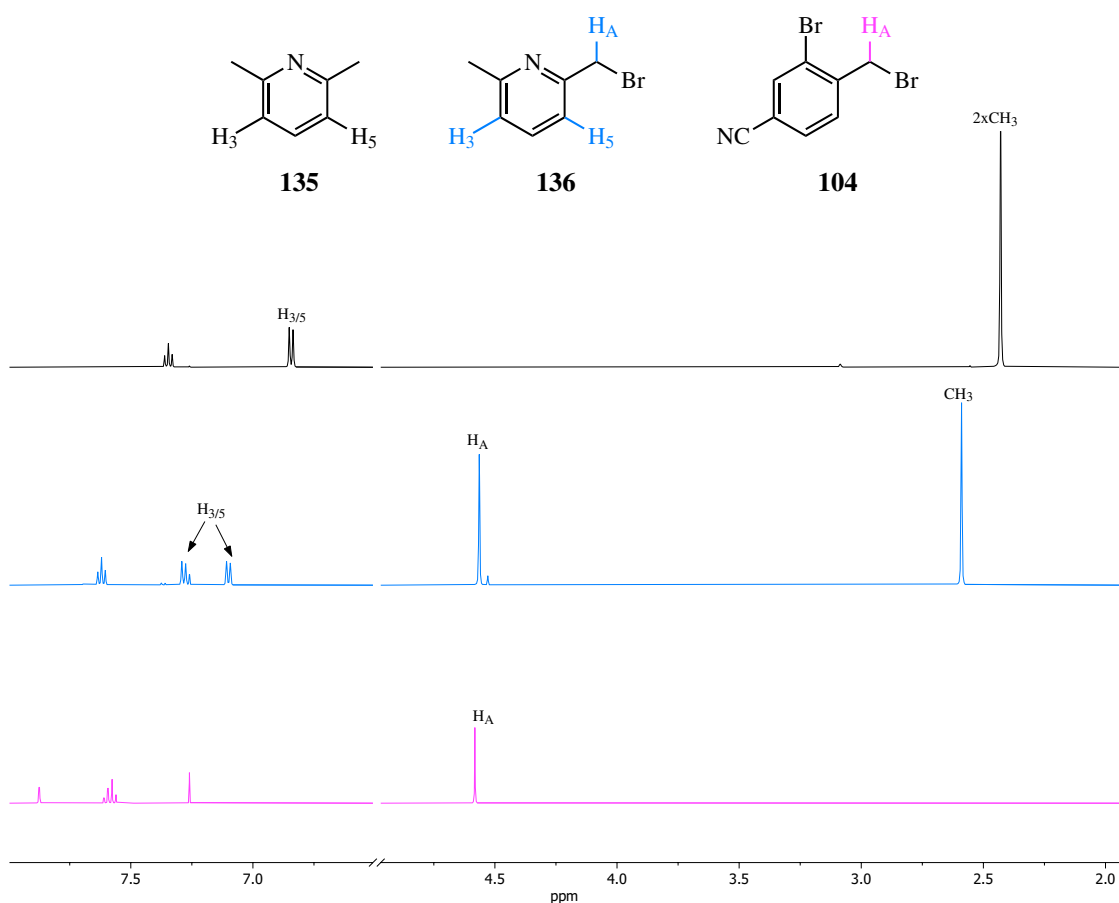
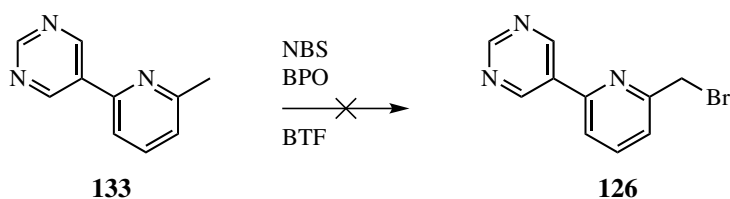


Figure 4.30: Stacked comparison of normalised and truncated  $^1\text{H}$  NMR spectra ( $\delta_{\text{H}}$ : 2.0 - 7.6 ppm) of **135** (black), **136** (blue) and **104** (pink), indicating emergence of bromomethyl  $\text{CH}_2$  singlet following radical bromination of **135**, and loss of symmetry about  $\text{H}_3$  and  $\text{H}_5$  in **136** due to introduction of bromomethyl group.

Given the favourable results from the proof-of-concept radical bromination reaction in Scheme 4.22, the reaction was attempted using the biaryl methylpyridine **133** as a substrate (Scheme 4.23).



Scheme 4.23: Reaction conditions for the attempted synthesis of **126** by radical bromination with **133**, *N*-bromosuccinimide (NBS) and benzoyl peroxide (BPO) in BTF.

The attempted synthesis of **126** via radical bromination was unsuccessful — during the course of the reaction, the reaction mixture turned a dark brown/black colour, which afforded a brown, oily solid following workup. Analysis of the crude product mixture by  $^1\text{H}$  NMR revealed that the crude product was comprised mostly of the starting material **133**, with only trace amounts of the desired product present. This suggests that either the desired product **126** or the preceding intermediates were unstable, and degrading during either the reaction (despite the reaction being conducted under an atmosphere of nitrogen) or workup. However, given the same workup was applied for purification of the similar benzyl bromide derivative **104**, it is unlikely that that **126** was degrading due to the workup procedure, therefore must it must be degrading during the reaction.

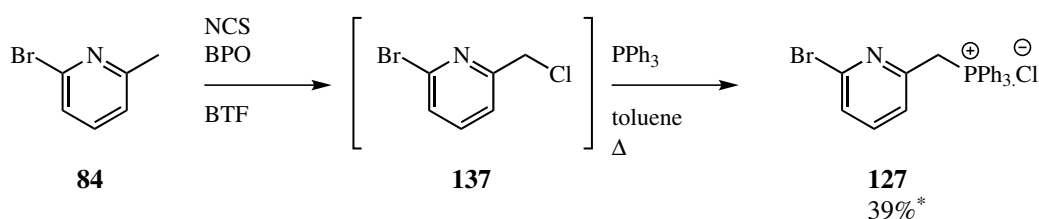
Investigations into the literature revealed limited reports of methylpyridine halogenation — on the few occasions where radical bromination was reported, despite using the resulting pyridylmethyl bromide derivative immediately without further purification, the reported yield was typically low (32%);<sup>126</sup> this is consistent with the previously reported volatility of pyridylmethyl halide derivatives.<sup>56</sup> Interestingly, a methodology paper published by Newkome *et al.* reported the synthesis of methyl chloride derivatives of various electron-poor heterocycles, including methylpyridines.<sup>127</sup> They also reported an “indirect but real relationship between the ease of chlorination and the electronic environment of the methyl substituent”, where chlorination of methyl substituents in an electron-rich environment was consistently more successful.<sup>127</sup> Furthermore, for each of the methylchloride derivatives synthesised, characterisation via melting or boiling point analysis was attempted — for those pyridylmethyl chloride derivatives which were synthesised and purified, the associated melting and boiling points (at 1 atm) were typically quite low (lowest b.p.: 39-42°C),<sup>127</sup> supporting the notion that pyridylmethyl halide derivatives are highly volatile.

Given the previously reported success of radical chlorinations for pyridylmethyl derivatives,<sup>127</sup> it was anticipated that synthesis of pyridylmethyl chloride derivatives could be a suitable alternative

#### 4.4. SYNTHESIS OF COMPLEX LIGANDS CONTAINING BIARYL AND 2-PYRIDYL FUNCTIONAL GROUPS

---

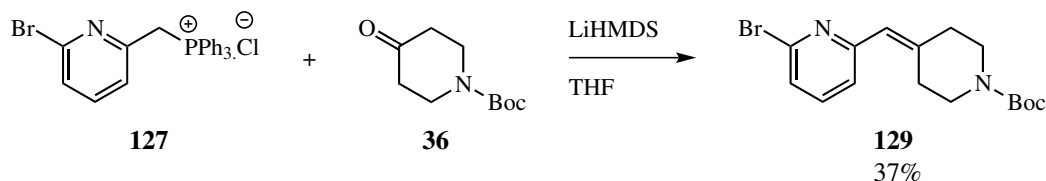
to pyridylmethyl bromide derivatives (**125** and **126**), as pyridylmethyl chloride derivatives would also be suitable substrates for either phosphonium salt formation (towards synthesis of ligand **88**) or as electrophiles in nucleophilic substitution reactions (towards synthesis of ligand **89**). In addition, given the relationship reported by Newkome *et al.* between the electronic nature of the heterocycle and ease of chlorination, it was envisaged that a radical chlorination reaction with **84** might be favourable (compared to **133**), due to the presence of the Br group (i.e., **84** should be more electron rich than **133**, as the Br group is electron-donating by resonance). Therefore, chlorination of **84** was attempted using almost analogous conditions to those used for radical brominations in Scheme 4.23, except NBS was replaced with *N*-chlorosuccinimide (NCS) as shown in Scheme 4.24. Due to the canonical volatility of pyridylmethyl halide derivatives,<sup>56,126,127</sup> the pyridylmethyl chloride derivative **137** was not isolated. Instead, the resultant succinimide (by-product from the radical chlorination reaction) was filtered from the reaction mixture, and crude **137** used without further purification — it was envisaged that immediate usage of crude **137** would minimise product loss due to volatility, particularly through trapping **137** as the insoluble phosphonium salt **127** (Scheme 4.24).



Scheme 4.24: Reaction conditions and yield for synthesis of **127** via radical chlorination with **84**, *N*-chlorosuccinimide (NCS) and benzoyl peroxide (BPO) in BTF, followed by conversion to the phosphonium salt. \* indicates yield over 2 steps.

Favourably, the desired phosphonium salt **127** was synthesised, indicating successful formation of the pyridylmethyl chloride intermediate **137**. Successful formation of **127** was supported by analysis of <sup>1</sup>H NMR spectra, which revealed the emergence of a 15H aromatic multiplet, consistent with the expected additional phenyl groups. In addition, splitting of all signals in both <sup>1</sup>H and <sup>13</sup>C NMR was observed due to H-P and C-P coupling respectively, which supported successful introduction of the triphenylphosphine group. Formation of **127** occurred in reasonable yield, considering the yield in Scheme 4.24 represents both radical chlorination and phosphonium salt synthesis steps. Furthermore, despite using crude **137** (likely containing a mixture of **137**, starting material **84**, succinimide and BPO), purification of the desired product **127** was straightforward, and achieved simply by vacuum filtration and washing with cold toluene.

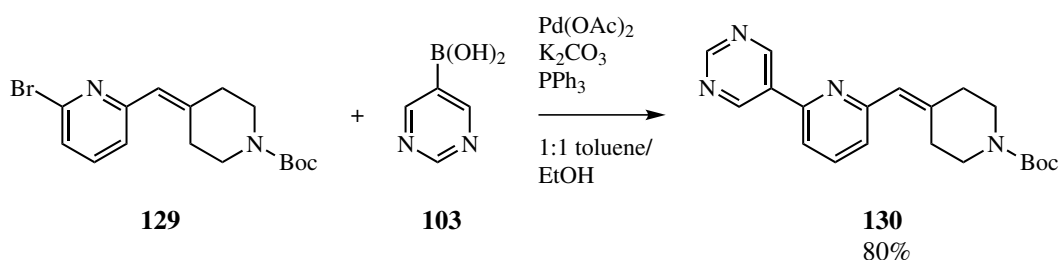
Following the successful synthesis of **127**, the next step required formation of the key methylene-piperidinyll bond with **36** via Wittig reaction, as shown in Scheme 4.25.



Scheme 4.25: Reaction conditions and yield for synthesis of **129** via Wittig reaction with **36** and **127**.

Successful synthesis of **129** was supported by analysis of HRMS and NMR spectra; the expected mass products were observed in a ~1:1 ratio, consistent with naturally occurring  $^{79}\text{Br} / ^{81}\text{Br}$  isotope abundances. From  $^1\text{H}$  NMR analysis, four separate  $\text{CH}_2$  signals were observed, consistent with the introduction of a piperidinyll ring. Furthermore, distinctive singlets integrating to 9H (at 1.48 ppm) and 1H (at 6.29 ppm) were observed, corresponding to the *tert*-butyl group within the Boc protecting group, and newly-formed alkene signal respectively. While the desired product was only synthesised in a yield of 37% (due to an incomplete reaction after 22 hr), sufficient material had been obtained to proceed to the next synthetic step, so further optimisation was not undertaken.

It was essential that the 2,5-pyrimidine ring be coupled to **129** prior to reduction of the alkene bond; said reduction was expected to be achieved via hydrogenation, but these reaction conditions have previously been reported to cause reduction of the C-Br bond.<sup>56</sup> Therefore, the next synthetic step required introduction of the 2,5-pyrimidinyl ring via Suzuki cross-coupling, as shown in Scheme 4.26.



Scheme 4.26: Reaction conditions and yield for synthesis of **130** by Suzuki coupling of **129** and **103**, based on literature methods.<sup>56</sup>

The desired product **130** was synthesised and purified in a sufficiently high yield (80%). Successful coupling of the 2,5-pyrimidine ring was supported by analysis of HRMS and NMR spectra; the major mass product had a  $m/z$  value of 353.1974, consistent with the expected  $m/z$  value of 353.1972. From  $^1\text{H}$  NMR spectra, 2H and 1H singlets corresponding to C(2''/6'')H (at 9.34 ppm) and C(4'')H

#### 4.4. SYNTHESIS OF COMPLEX LIGANDS CONTAINING BIARYL AND 2-PYRIDYL FUNCTIONAL GROUPS

(at 9.26 ppm) of the 2,5-pyrimidine ring were observed, as expected for an electron-deficient heterocyclic ring. Furthermore, the desired connectivity of **130** was supported by analysis of 2D NMR spectra, through the emergence of specific correlations in HMBC NMR spectra (i.e., C(2''/6'')H & C(3'), C(4')H & C(1''), Figure 4.31).

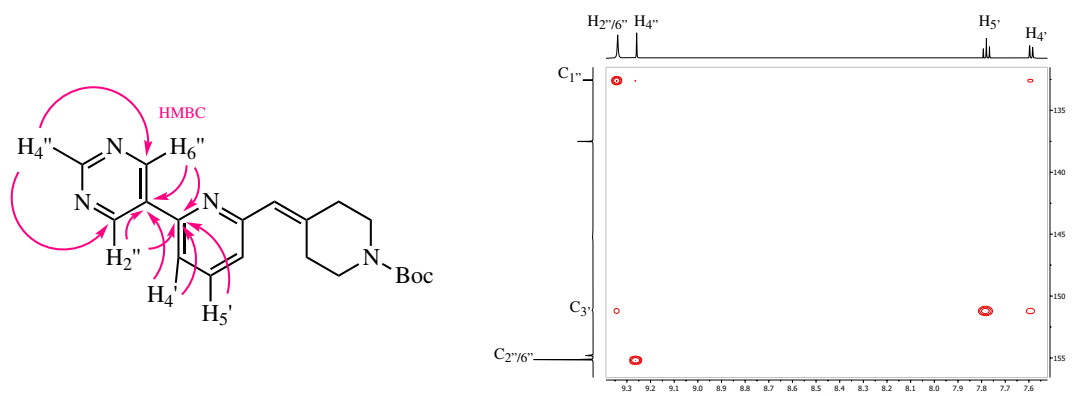
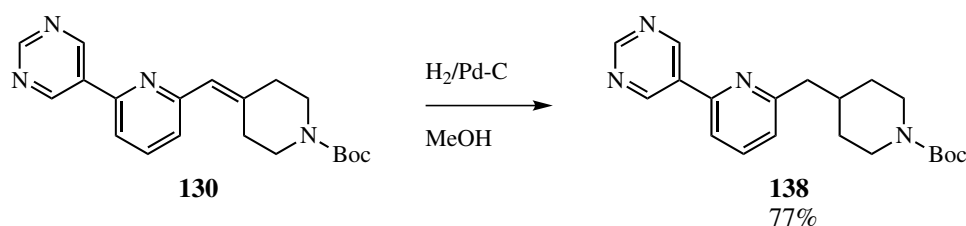


Figure 4.31: Structural analysis of **130** via HMBC 2D NMR spectra, with correlations indicated by pink arrows.

In order to prevent complications in subsequent Buchwald-Hartwig coupling reactions, it was desirable to reduce the alkene in **130** to prevent isomerisation to the THP isomer; the presence of multiple amine-containing species typically leads to reduced yields and purification challenges in Buchwald-Hartwig coupling reactions.<sup>56</sup> To achieve reduction of **130** to **138**, it was anticipated that standard Pd-C catalysed hydrogenation conditions could be applied (Scheme 4.27), as the liability of the reducible C-Br bond had been removed from the structure of **130**.



Scheme 4.27: Reaction conditions and yield for synthesis of **138** via reduction of **130**.

Formation of the desired methylpiperidinyl derivative **138** was achieved in good yield (77%), and was supported by analysis of HRMS and NMR spectra; a major mass product with a  $m/z$  value of 355.2127 was observed in HRMS spectra, which was consistent with the mass of the desired product (required  $m/z$ : 355.2129). Following alkene reduction (and therefore reduced planarisation of the piperidinyl ring), the piperazinyl ring would be expected to adopt a more chair-like conformation, and potentially allow differentiation of pseudo-axial and pseudo-equatorial piperidinyl ring H

environments — this was indeed observed, with clear differentiation of chemical environments (and multiplicities due to different dihedral angles between axial/equatorial H), as shown in Figure 4.32. As described previously in Chapter 2, the piperidiny ring signals still exhibit noticeable broadness due to reduced rotation about the carbamate bond in the Boc protecting group.

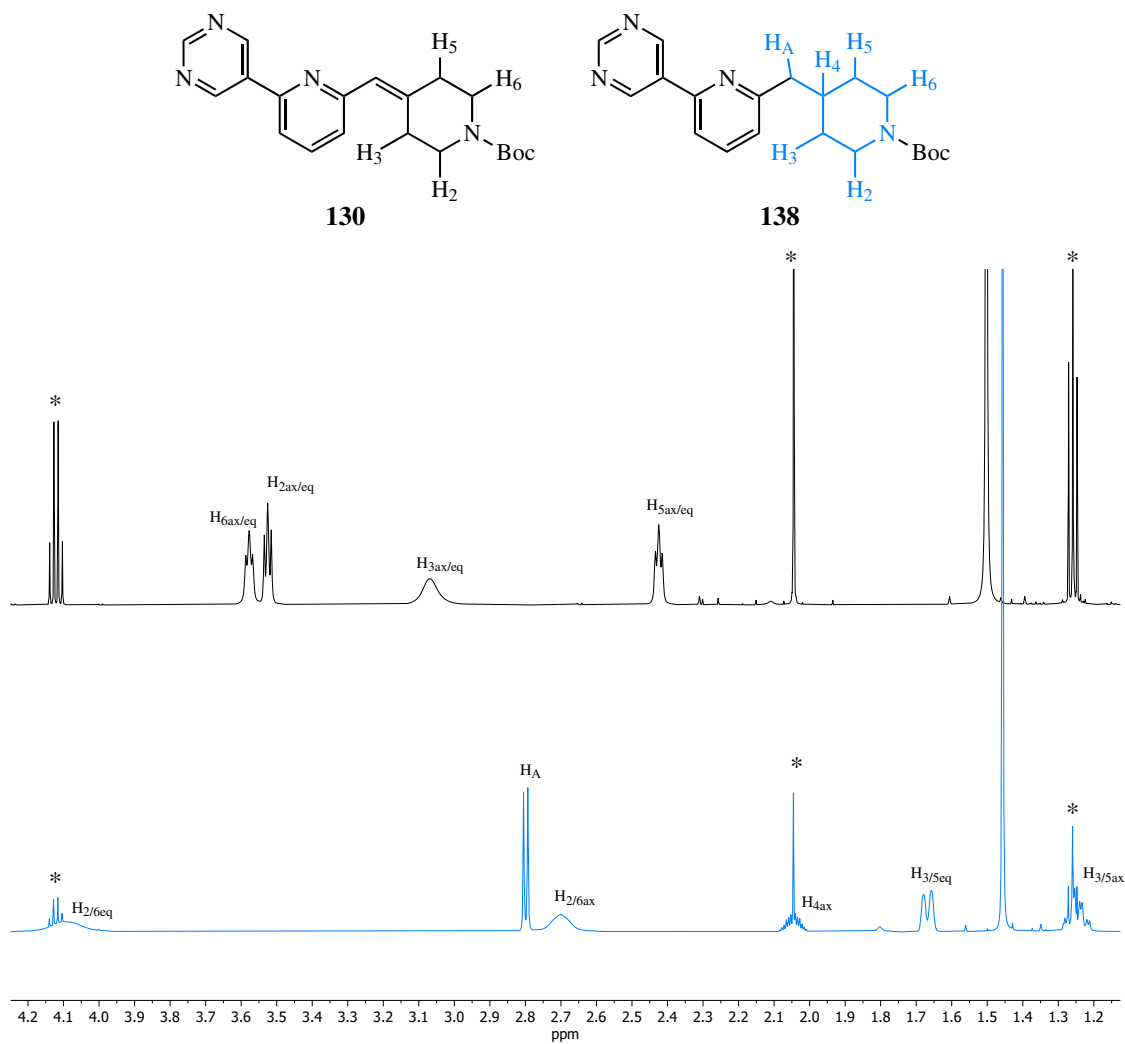
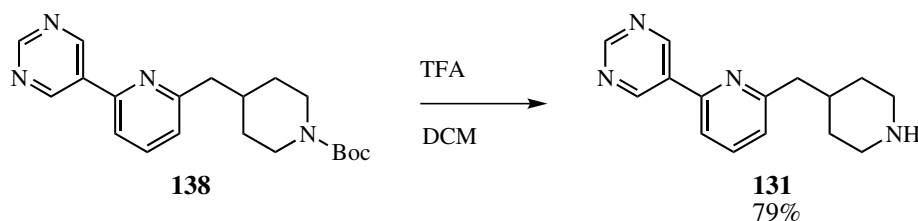


Figure 4.32: Stacked comparison of normalised  $^1\text{H}$  NMR spectra ( $\delta_{\text{H}}$ : 1.2 - 4.2 ppm) of **130** (black) and **138** (blue), indicating deconvolution of piperidiny ring signals into pseudo-axial and pseudo-equatorial chemical environments upon alkene bond reduction. \* indicates signals due to residual EtOAc.

#### 4.4. SYNTHESIS OF COMPLEX LIGANDS CONTAINING BIARYL AND 2-PYRIDYL FUNCTIONAL GROUPS

---

In preparation for synthesis of the 2-chloroquinoline intermediate **132**, liberation of the free amine **131** was required — the Boc protecting group was removed under standard deprotection reaction conditions in good yield (Scheme 4.28).



Scheme 4.28: Reaction conditions and yield for synthesis of **131** via Boc group deprotection of **138**.

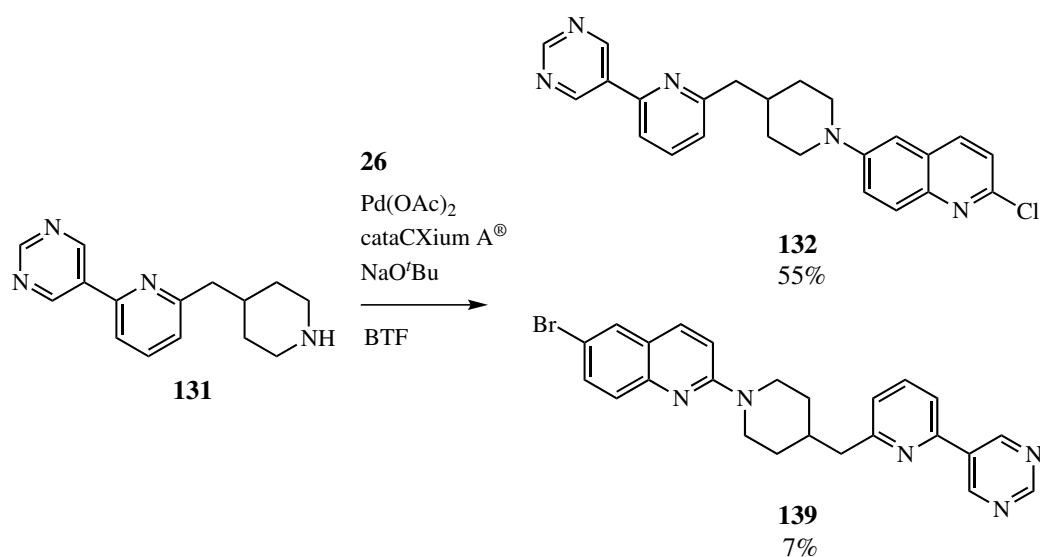
Isolation of the desired product was supported by analysis of HRMS and NMR spectra; the major mass product had a  $m/z$  value of 255.1604, which was consistent with **131** (required  $m/z$ : 255.1604). From  $^1\text{H}$  NMR, loss of the Boc protecting group was evidenced by disappearance of the 9H singlet at 1.48 ppm (indicating loss of the *tert*-butyl group within the Boc protecting group), and resolution of piperidinyll ring signals due to the absence of the carbamate group (see Figure 2.35 in Chapter 2 for exemplar and associated text).

##### 4.4.1.2 Synthesis of methylpiperidine-substituted quinoline derivatives containing 2-pyridyl and biaryl functional groups

Given the successful synthesis of **131**, the next transformation towards the target ligand **88** required a selective coupling reaction at the 6-position of **26** to form **132**. Consistent with previous sections in this thesis, it was envisaged that this selective coupling might be achieved by employing Buchwald-Hartwig coupling conditions which have been optimised previously for selective coupling at the 6-position of **26**,<sup>47</sup> as shown in Scheme 4.29.

The yield obtained for the desired product **132** was higher than for other 2-chloroquinolines reported in this chapter (Scheme 4.11); this is not surprising — the amine substrate **131** does not contain any functional groups that would typically be amenable to side reactions (e.g., nitrile groups, **95**), or any obvious geometries for unwanted Pd coordination (**66a**, see Figure 3.17 in Chapter 3). While some of the 2-position substituted product **139** had formed, it was only present in low yield, indicating chemoselectivity for coupling at the 6-position was retained in this catalytic system.

#### 4.4. SYNTHESIS OF COMPLEX LIGANDS CONTAINING BIARYL AND 2-PYRIDYL FUNCTIONAL GROUPS



Scheme 4.29: Reaction conditions and yield for synthesis of piperidine-coupled 2-chloroquinoline derivative **132** and side product **139** via Buchwald-Hartwig coupling reaction based on literature methods.<sup>47</sup>

Formation of the desired product **132** was supported following analysis of HRMS and NMR spectra; major mass products with  $m/z$  values of 417.1589 & 419.1569 were observed in a ratio of 3:1, as expected for **132** (required  $m/z$ : 417.1589 [<sup>35</sup>Cl] / 419.1560 [<sup>37</sup>Cl]). Analysis of <sup>1</sup>H NMR spectra revealed the emergence of quinoline ring signals, particularly the presence of a characteristic upfield <sup>1</sup>H doublet at 7.00 ppm, which representative of C(5)H of the quinolinyl ring. Importantly, the desired connectivity at the 6-position of the quinoline ring was supported by analysis of 2D NMR spectra, exemplified by the ROESY correlations shown in Figure 4.33.

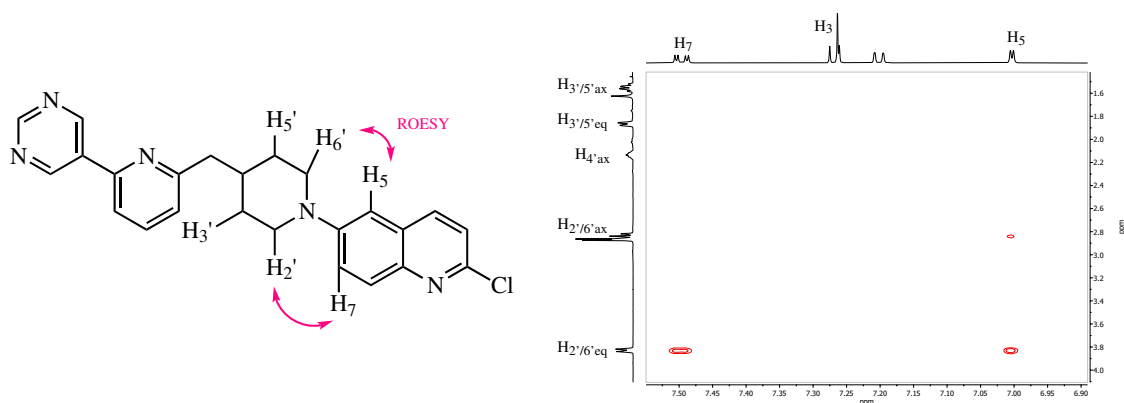


Figure 4.33: Structural analysis of **132** via 2D NMR spectra, with ROESY correlations indicated by pink arrows.

Similarly, formation of the 2-position substituted product **139** was supported by analysis of HRMS and NMR spectra — mass products with  $m/z$  values of 460.1126 & 462.1113 were observed in a ~1:1 ratio (expected  $m/z$  for **139**: 460.1131 [<sup>79</sup>Br] / 462.1113 [<sup>81</sup>Br]). Analysis of <sup>1</sup>H NMR spectra



#### 4.4. SYNTHESIS OF COMPLEX LIGANDS CONTAINING BIARYL AND 2-PYRIDYL FUNCTIONAL GROUPS

indicated the presence of a diagnostic upfield shift for C(3)H of the quinolinyl ring, consistent with the introduction of an amine group and consequent *ortho/para* shielding. Lastly, analysis of 2D NMR spectra revealed key HMBC and ROESY correlations to support coupling at the 2-position of the quinoline ring, as shown in Figure 4.34.

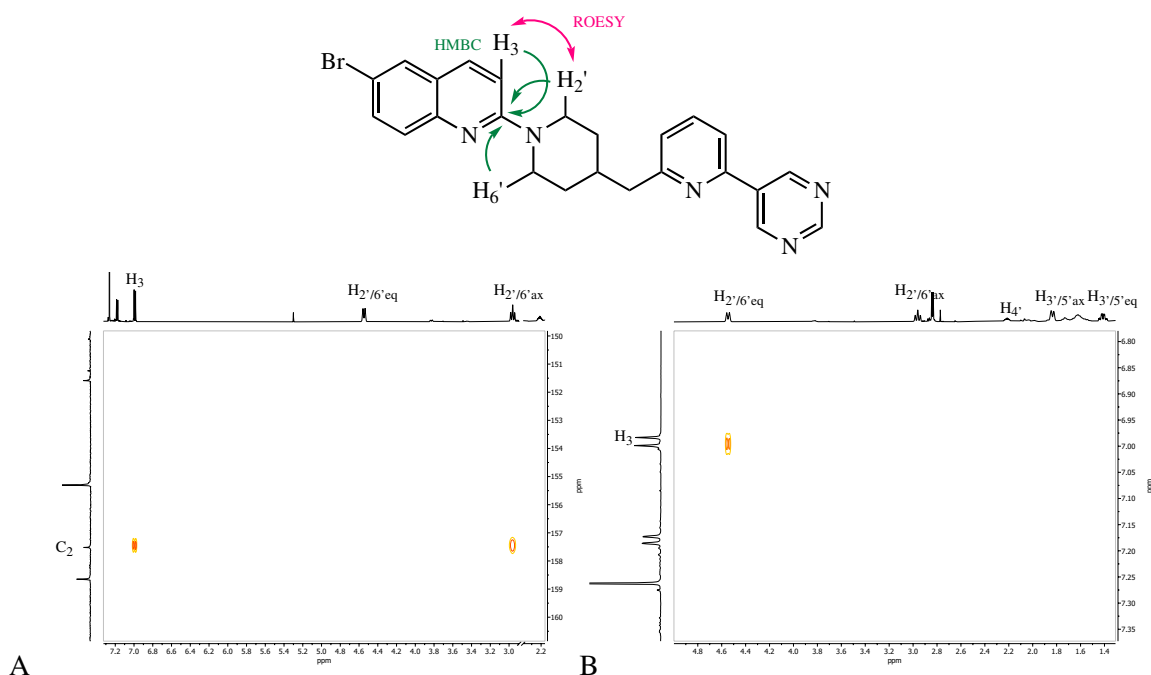
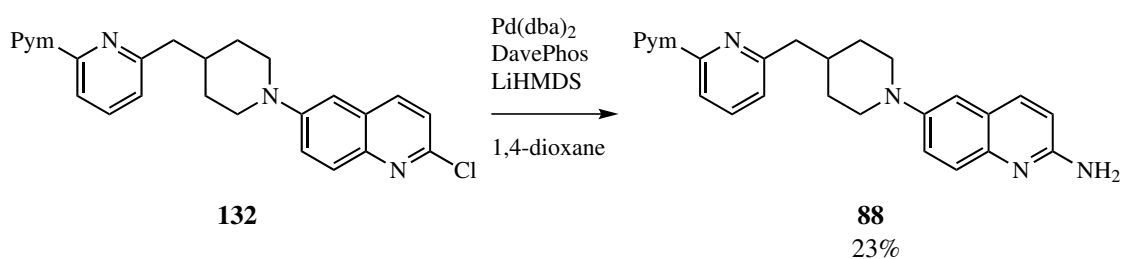


Figure 4.34: Structural analysis of **139** via 2D NMR spectra, with (A) HMBC correlations indicated by green arrows, and (B) ROESY correlations indicated by pink arrows.

The final step for synthesis of the target ligand **88** required introduction of the 2-amino functionality to **132**, and again it was envisaged that this might be achieved via Buchwald-Hartwig coupling reaction, using previously optimised conditions which include LiHMDS as both a base and an ammonia equivalent.<sup>47</sup> It was hypothesised that this second Buchwald-Hartwig coupling reaction might proceed in a higher yield than that reported for other complex ligands (i.e., **97**, yield = 8%, see Scheme 4.12), as **132** does not contain any potentially base-sensitive functional groups (i.e., nitrile, amide) which could be derivatised in an unwanted manner under the reaction conditions; the results of this transformation are shown in Scheme 4.30.

Successful formation of the desired ligand **88** was supported by analysis of HRMS and NMR spectra; a major mass product with a  $m/z$  value of 397.2142 was detected (required  $m/z$ : 397.2135). In addition, analysis of  $^1\text{H}$  NMR spectra revealed characteristic emergence of a broad  $\text{NH}_2$  singlet, and an upfield shift of C(3)H of the quinolinyl ring, due to *ortho/para* shielding by the newly-introduced 2-amino group (Figure 4.35). While the yield for this transformation was seemingly low

#### 4.4. SYNTHESIS OF COMPLEX LIGANDS CONTAINING BIARYL AND 2-PYRIDYL FUNCTIONAL GROUPS



Scheme 4.30: Reaction conditions and yield for synthesis of 2-aminoquinoline derivative **88** via Buchwald-Hartwig coupling reaction. “Pym” = 2,5-pyrimidinyl.

at 23%, it was substantially higher than that for other complex ligands (e.g., **97**, yield = 8%, see Scheme 4.12). In any case, a sufficient amount of the target ligand **88** had been synthesised in high purity (Figure 4.35), ready for use in SPR binding assays.

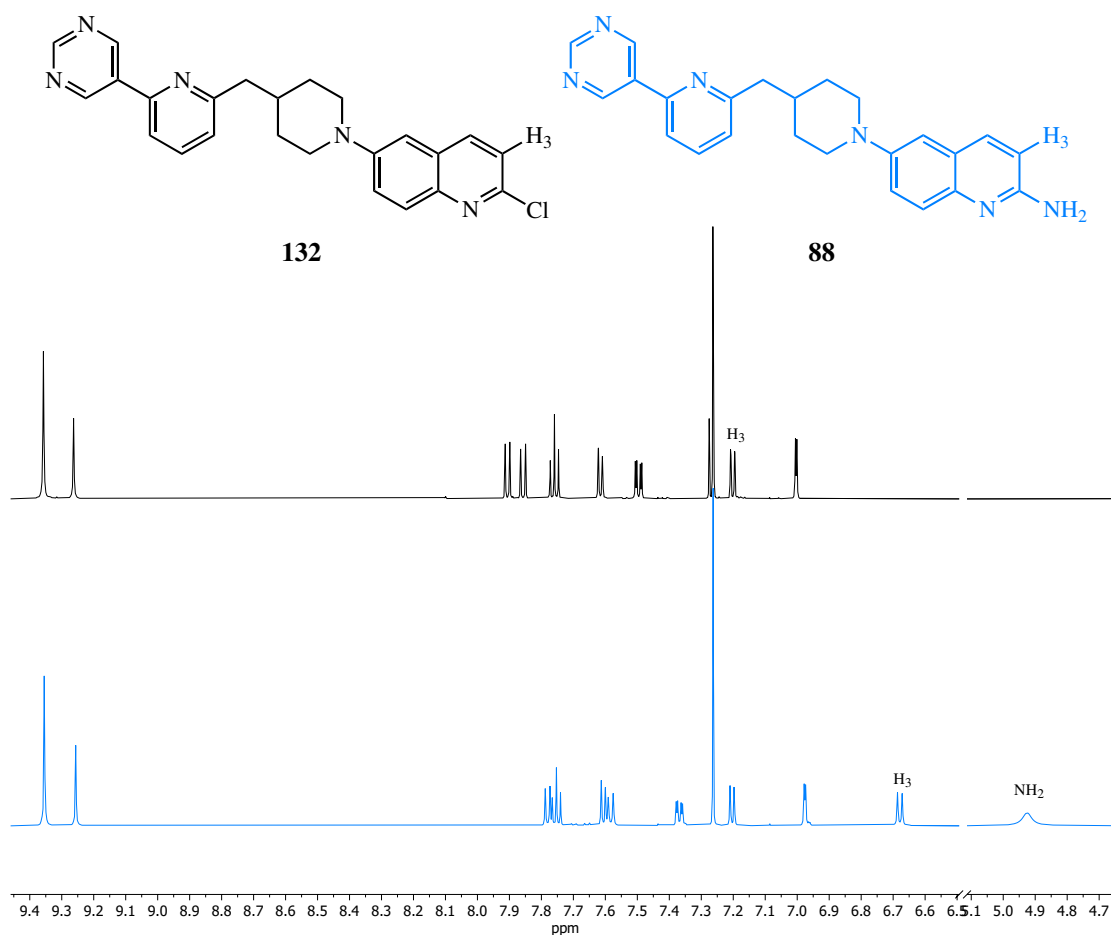
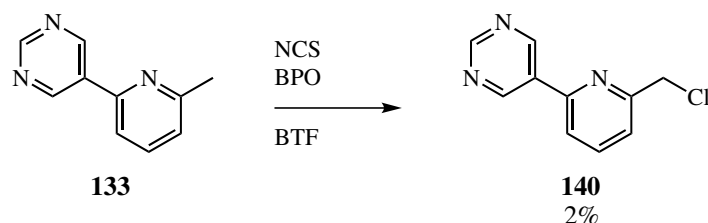


Figure 4.35: Comparison of truncated and normalised  $^1\text{H}$  NMR spectra ( $\delta_{\text{H}}$ : 4.7 - 9.4 ppm) of **132** (black) and **88** (blue), indicating different chemical shifts for C(3)H and emergence of an amine signal.

#### 4.4.1.3 Synthesis of methylpiperazine-substituted quinoline derivatives containing 2-pyridyl and biaryl functional groups

Following successful synthesis of the complex piperidiny-substituted ligand **88**, it was desirable to synthesise the analogous piperazinyl-substituted ligand **89** — it was expected that this could be achieved following the proposed synthetic pathway in Figure 4.28. However, given the synthetic challenges reported earlier regarding radical bromination of **133** (Scheme 4.23 and associated text), it was desirable to attempt synthesis of the pyridylmethyl chloride equivalent of **126**, as the pyridylmethyl chloride derivative should exhibit similar reactivity in a nucleophilic substitution reaction to **126**, albeit with reduced electrophilic character.

The first step required radical chlorination of a pyridylmethyl derivative, as either **84** or **133**. In order to prevent chemoselectivity issues in subsequent reactions (e.g., Buchwald-Hartwig couplings, Suzuki-cross-couplings), it was desirable to mask any aryl halogens early in the synthetic pathway. Therefore, it was ideal to conduct the radical chlorination with the biaryl pyridylmethyl derivative **133** rather than **84**; previously optimised radical chlorination conditions were applied for the synthesis of **140**, as shown in Scheme 4.31.



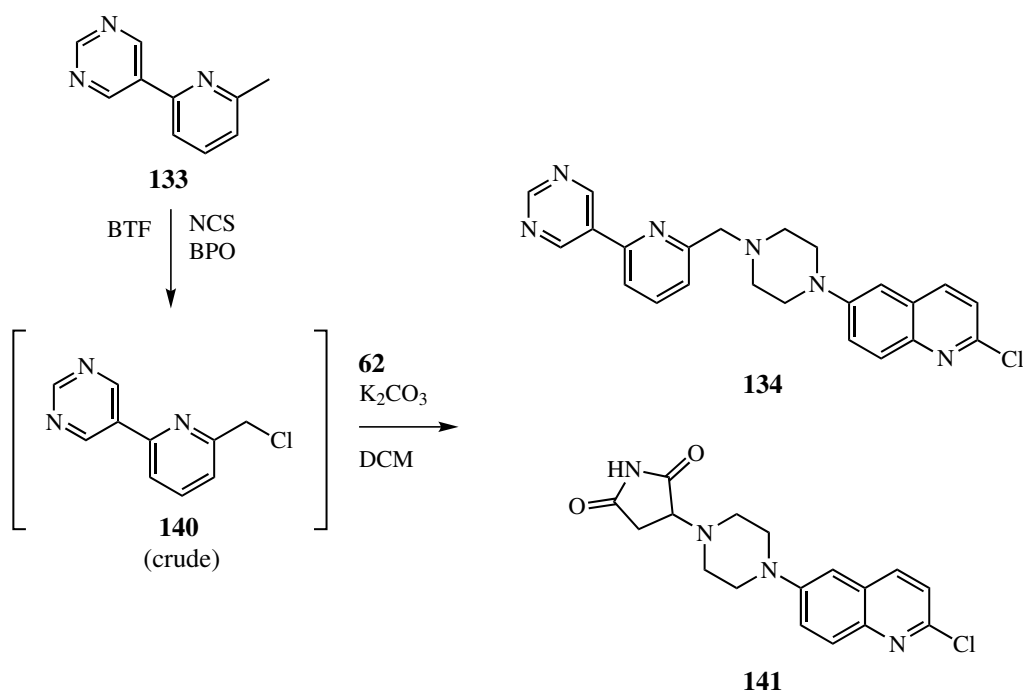
Scheme 4.31: Reaction conditions and yield for synthesis of **140** via radical chlorination with **133**, *N*-chlorosuccinimide (NCS) and benzoyl peroxide (BPO) in BTF. \* indicates the purified product was contaminated with residual succinimide.

The radical chlorination conditions in Scheme 4.31 afforded the desired product **140**; analysis of <sup>1</sup>H NMR spectra revealed the emergence of a diagnostic 2H singlet at 4.76 ppm, consistent with the CH<sub>2</sub> methyl chloride group. In addition, analysis of HRMS spectra revealed major mass products with *m/z* values of 206.0482 and 208.0453 in a 3:1 ratio, consistent with natural chlorine isotope abundances (expected *m/z*: 206.0480 [<sup>35</sup>Cl] / 208.0480 [<sup>37</sup>Cl]). While **140** was only purified in very low yields, it is noted that the crude product was dried, sealed with Parafilm® and stored at -20°C — the intention was to purify the product soon after formation to minimise time in storage, where it may be susceptible to degradation. However, due to unforeseen circumstances the crude

#### 4.4. SYNTHESIS OF COMPLEX LIGANDS CONTAINING BIARYL AND 2-PYRIDYL FUNCTIONAL GROUPS

product was stored at  $-20^{\circ}\text{C}$  for a period of  $\sim 4$  weeks before purification. In combination with the reported volatility of pyridylmethyl halides,<sup>56,127</sup> it is not surprising that the **140** had degraded during an extended period of storage before purification. Importantly, analysis of crude product  $^1\text{H}$  NMR spectra (taken before storage at  $-20^{\circ}\text{C}$ ) indicated a substantial formation of **140** had occurred (i.e., more than a 2% yield), suggesting the low yield was not due poor conversion during the reaction.

In light of the low yield recorded for synthesis of **140**, the reaction was repeated with some modifications; similarly to synthesis of **127**, it was envisaged that crude **140** could be used in the subsequent synthesis of the 2-chloroquinoline derivative **134**, therefore the pyridylmethyl chloride derivative **140** was not isolated before further reaction in a nucleophilic substitution reaction to form **134**, as shown in Scheme 4.32.



Scheme 4.32: Reaction conditions for attempted synthesis of **134** via radical chlorination of **133** and subsequent nucleophilic substitution reaction with crude **140**, and formation of the side product **141**. NCS = *N*-chlorosuccinimide, BPO = benzoyl peroxide.

While the desired product **134** was formed, unfortunately it was only partially purified as a 3:2 inseparable mixture with a side product, which is proposed to have the structure of **141**. Formation of the desired product **134** was supported by analysis of analysis of HRMS and NMR spectra; in the mixture of **134** and **141**, major mass products with  $m/z$  values of 417.1589 & 419.1569 were observed in a 3:1 ratio (consistent with natural chlorine isotope abundance, expected  $m/z$  for **134**:

417.1589 [ $^{35}\text{Cl}$ ] / 419.1560 [ $^{37}\text{Cl}$ ]). From analysis of  $^1\text{H}$  NMR spectra, attachment of the biaryl pyridylmethyl group to the piperazinyl-quinoline component was apparent due to the emergence of additional aromatic H signals, consistent with the 2,5-pyrimidine and di-substituted 2-pyridyl ring. Importantly, a characteristic  $\text{CH}_2$  singlet was observed at 3.85 ppm, as expected for the methyl group linking the pyridyl and piperazinyl rings, and consistent with other arylmethyl piperazinyl derivatives (e.g., **99**) described in this thesis.

With regard to the proposed by-product **141**, analysis of HRMS spectra (of the 3:2 mixture of **134** and **141**) revealed an additional mass product with  $m/z$  values of 345.1114 and 347.1095 in a 3:1 ratio (expected  $m/z$  for **141**: 345.1113 [ $^{35}\text{Cl}$ ] / 347.1084 [ $^{37}\text{Cl}$ ]). Importantly, given the distinctive 3:1 ratio of the mass product peaks, it suggests that the side product contains a chlorine atom. From analysis of  $^1\text{H}$  NMR spectra of the 3:2 mixture of **134** and **141**, only one set of 2,5-pyrimidine and 2-pyridyl ring signals were observed — these must be representative of **134**, therefore the side-product **141** does not contain the biaryl (2,5-pyrimidine + 2-pyridyl) group. In addition, two sets of piperazinyl ring signals were observed with approximately equal chemical shifts, suggesting **141** also contains a di-substituted piperazinyl ring. Similarly, two sets of 6-substituted 2-chloroquinoline signals were observed, again with approximately equal chemical shifts, indicating that the 2-chloroquinoline structure in **141** is essentially the same as in **134**. Interestingly, a broad singlet at 8.23 ppm was observed which may be consistent with the NH signal from a strongly deshielded secondary amide (such as a succinimide), this was supported by analysis of  $^{13}\text{C}$  NMR spectra, which revealed the emergence of signals at 174.4 ppm and 175.8 ppm, which may be consistent with two non-symmetric  $\text{C}=\text{O}$  groups. Further analysis of  $^1\text{H}$  NMR spectra revealed emergence of a series of additional alkyl signals, which did not exhibit multiplicities consistent with a piperazinyl ring (Figure 4.36). Lastly, analysis of 2D NMR revealed some interesting correlations between these additional alkyl signals (Figure 4.37), which in conjunction with the derived coupling constants (and considering the typical dihedral angles between each of the succinimide alkyl hydrogens (i.e.,  $\text{H}_\text{A}$ ,  $\text{H}_\text{B}$  in Figure 4.37), support the proposed structure of **141**.

4.4. SYNTHESIS OF COMPLEX LIGANDS CONTAINING BIARYL AND 2-PYRIDYL  
FUNCTIONAL GROUPS

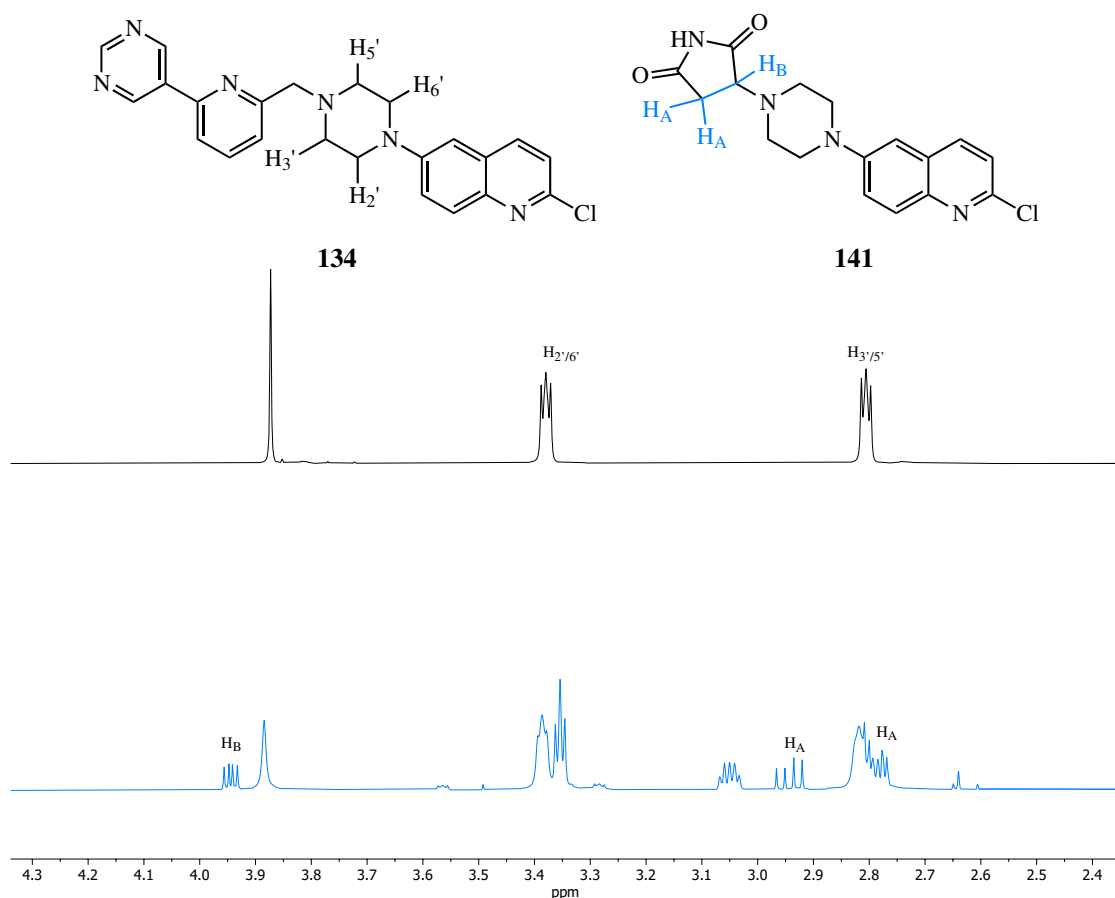


Figure 4.36: Stacked comparison of normalised  $^1\text{H}$  NMR spectra ( $\delta_{\text{H}}$ : 2.4 - 4.3 ppm) of a purified analytical sample of **134** (black) and a 3:2 mixture of **134** & **141** (blue), indicating the emergence of additional, non-piperazinyll alkyl signals for **141**.

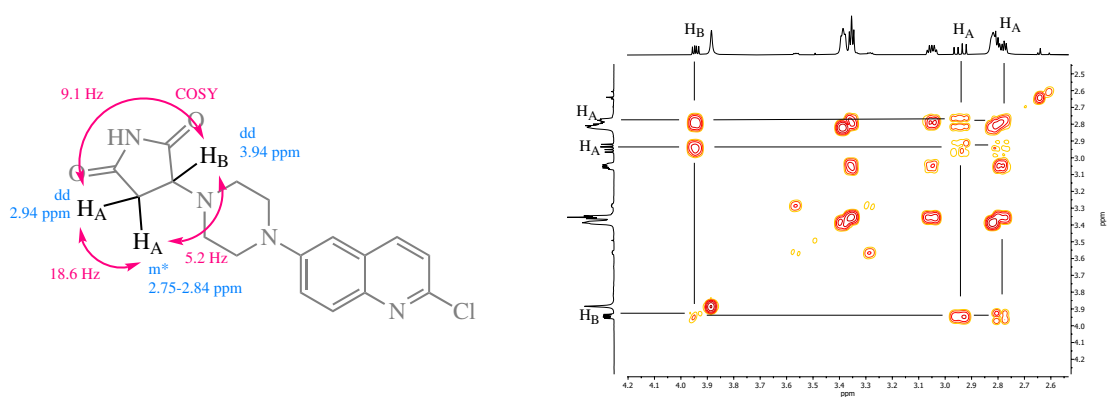


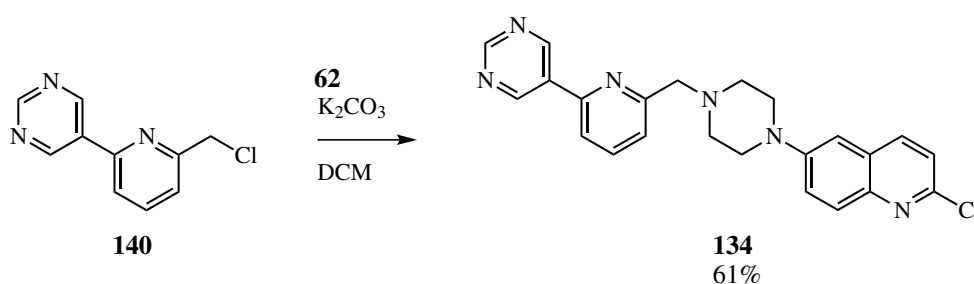
Figure 4.37: Structural analysis of proposed side product **141** via 2D NMR spectra, with COSY correlations indicated by pink arrows. Chemical shifts and multiplicities from corresponding  $^1\text{H}$  NMR spectra indicated in blue, where “dd” indicates a doublet of doublets, and “m\*” indicates a multiplet which was overlapping with another signal.

#### 4.4. SYNTHESIS OF COMPLEX LIGANDS CONTAINING BIARYL AND 2-PYRIDYL FUNCTIONAL GROUPS

---

It is not surprising that the side product **141** contains a succinimide functional group - as crude **140** was used in the nucleophilic substitution reaction, it is likely that residual succinimide by-product from the radical chlorination was carried through in the crude product (despite attempts to remove succinimide by-product by vacuum filtration of crude **140**). What is not clear is the mechanism by which **141** could have formed — the hydrogens in the succinimide group are expected to be acidic due to the adjacent carbonyl groups; if anything, the resultant succinimide enolate (following acidic hydrogen abstraction) component should be nucleophilic.

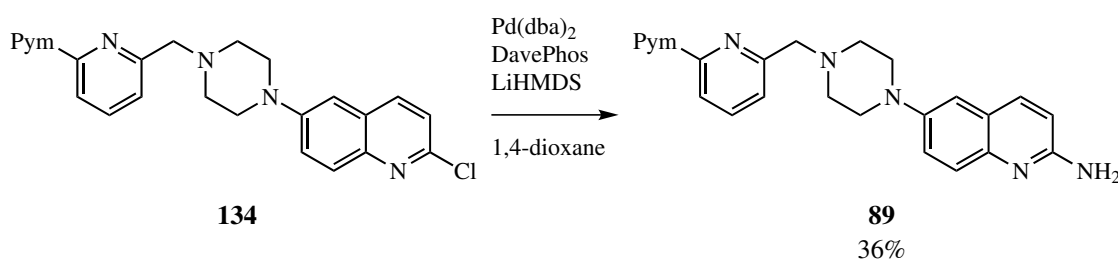
The presence of **141** in the inseparable mixture with **134** was problematic — the next synthetic step required conversion of **134** to the corresponding 2-aminoquinoline derivative **89** via Buchwald-Hartwig coupling reaction, using LiHMDS as both a base and an ammonia equivalent. However, **141** would also be a suitable substrate for transformation to the corresponding 2-aminoquinoline derivative under the previously reported Buchwald-Hartwig reaction conditions.<sup>47</sup> Furthermore, it was anticipated that chromatographic separation of the corresponding 2-aminoquinoline derivatives (with reference to **134** & **141**) would be difficult. Therefore, it was desirable to repeat the nucleophilic substitution reaction, but instead using purified **140** to prevent formation of the undesired side product **141**. Conveniently, during purification of the crude reaction mixture following nucleophilic substitution reaction in Scheme 4.32, some unreacted **140** was recovered in sufficient quantity to repeat the nucleophilic substitution reaction, and is shown in (Scheme 4.33).



Scheme 4.33: Reaction conditions and yield for synthesis of pyridylmethyl piperazine derivative **134** via nucleophilic substitution with **140** and **62**.

Pleasingly, when the nucleophilic substitution reaction was repeated with purified **140**, only the desired product **134** was formed, suggesting that formation of the side product **141** was dependent upon components of the crude **140**-containing product mixture (such as succinimide) from the radical chlorination reaction. Importantly, the yield for **134** was sufficiently high to afford a suitable amount of material for further derivatisation.

Following synthesis of **134**, the final step involved conversion to the 2-aminoquinoline ligand **89** via Buchwald-Hartwig coupling reaction, as shown in Scheme 4.34.



Scheme 4.34: Reaction conditions and yield for synthesis of 2-aminoquinoline derivative **89** via Buchwald-Hartwig coupling reaction. “Pym” = 2,5-pyrimidinyl.

Successful synthesis and purification of the ligand **89** was supported by analysis of HRMS and NMR spectra; a major mass product with an  $m/z$  value of 398.2085 was observed in HRMS spectra, consistent with the expected mass for **89** (required  $m/z$ : 398.2088). From analysis of <sup>1</sup>H NMR spectra, a characteristic upfield shift of C(3)H of the quinolinyl ring was observed for **89**, due to the *ortho/para* shielding effects of the 2-amino group. In addition, a broad singlet integrating to 2H had emerged, consistent with the newly-introduced amine group. Lastly, from Figure 4.38, the desired ligand **89** was isolated in high purity, and was suitable for use in SPR binding assays.

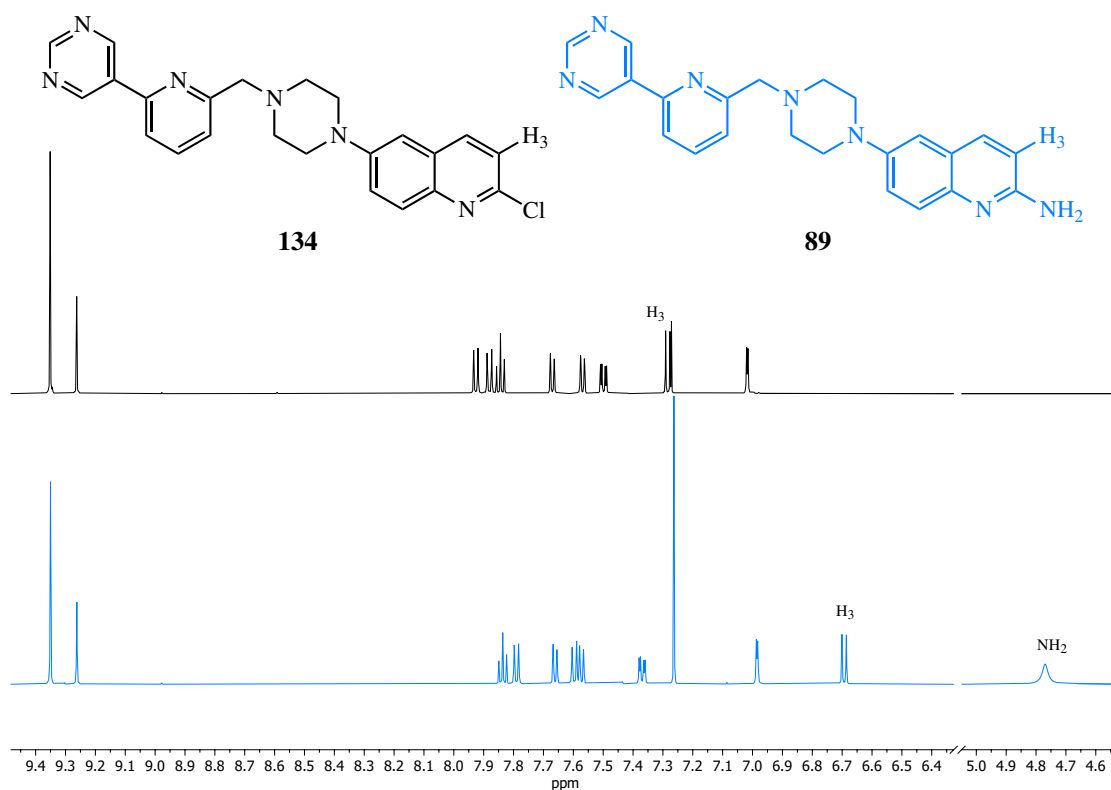


Figure 4.38: Comparison of truncated and normalised <sup>1</sup>H NMR spectra (δ<sub>H</sub>: 4.6 - 9.4 ppm) of **134** (black) and **89** (blue), indicating different chemical shifts for C(3)H and emergence of an amine signal.



## 4.5 Synthesis of complex ligands containing 2-pyridyl and 4-amido functional groups

### 4.5.1 Proposed synthetic pathways of complex ligands containing 2-pyridyl and 4-amido functional groups

Considering the proposed target complex ligands in Table 4.2 and the previous sections in this chapter, the last pair of ligands to be synthesised were **90** and **91**. While the general synthetic pathways for ligands **90** and **91** are described in Section 4.2, the exact sequence of transformations must be interrogated to minimise off-site and undesired cross-reactivity; more prescriptive synthetic pathways for ligands **90** and **91** are shown in Figure 4.39 and Figure 4.40, respectively.

Figure 4.39 and Figure 4.40 suggest the common substituted methylpyridine derivative **85** as the starting material; they also identify the more advanced pyridylmethyl chloride derivative **142** as a common intermediate. Given the previously-reported volatility of pyridylmethyl halides,<sup>56,127</sup> it was desirable to synthesise the pyridylmethyl chloride derivatives, rather than the pyridylmethyl bromides (see Scheme 4.23 and associated text). In the context of synthesis of the arylmethyl piperidinyl ligand **90** (Figure 4.39), the pyridylmethyl chloride derivative can be converted into the phosphonium salt **143**, in preparation for a Wittig reaction with **36** to form the corresponding methylene piperidine derivative **144**. Following amine deprotection, the free base **145** can undergo a selective Buchwald-Hartwig coupling reaction<sup>47</sup> with **26** to afford the 2-chloroquinoline derivative **146**. Given the reported challenges of using 2-pyridyl methylenepiperidine derivatives in Buchwald-Hartwig coupling reactions (Chapter 2, Scheme 2.15), it would be desirable to reduce the methylene alkene bond to prevent unfavourable Pd-coordination and subsequently reduced yields, but an early-stage reduction was not considered beneficial for the synthesis of **90**. There were concerns that alkene reduction in the presence of a nitrile group could lead to partial reduction of the nitrile group,<sup>56</sup> leading to purification challenges and reduced homogeneity of the amine substrate for Buchwald-Hartwig coupling reactions, ultimately lowering product yields. To mitigate concerns of 2-pyridylmethylene piperidinyl-Pd coordination in Buchwald-Hartwig coupling reactions, it was envisaged that increasing the relative concentrations of Pd catalyst and phosphine ligands would avail sufficient Pd to facilitate the catalytic cycle in the Buchwald-Hartwig coupling reaction and afford product formation, as shown previously (Chapter 2, Scheme 2.16 and Table 2.16).

4.5. SYNTHESIS OF COMPLEX LIGANDS CONTAINING 2-PYRIDYL AND 4-AMIDO  
FUNCTIONAL GROUPS

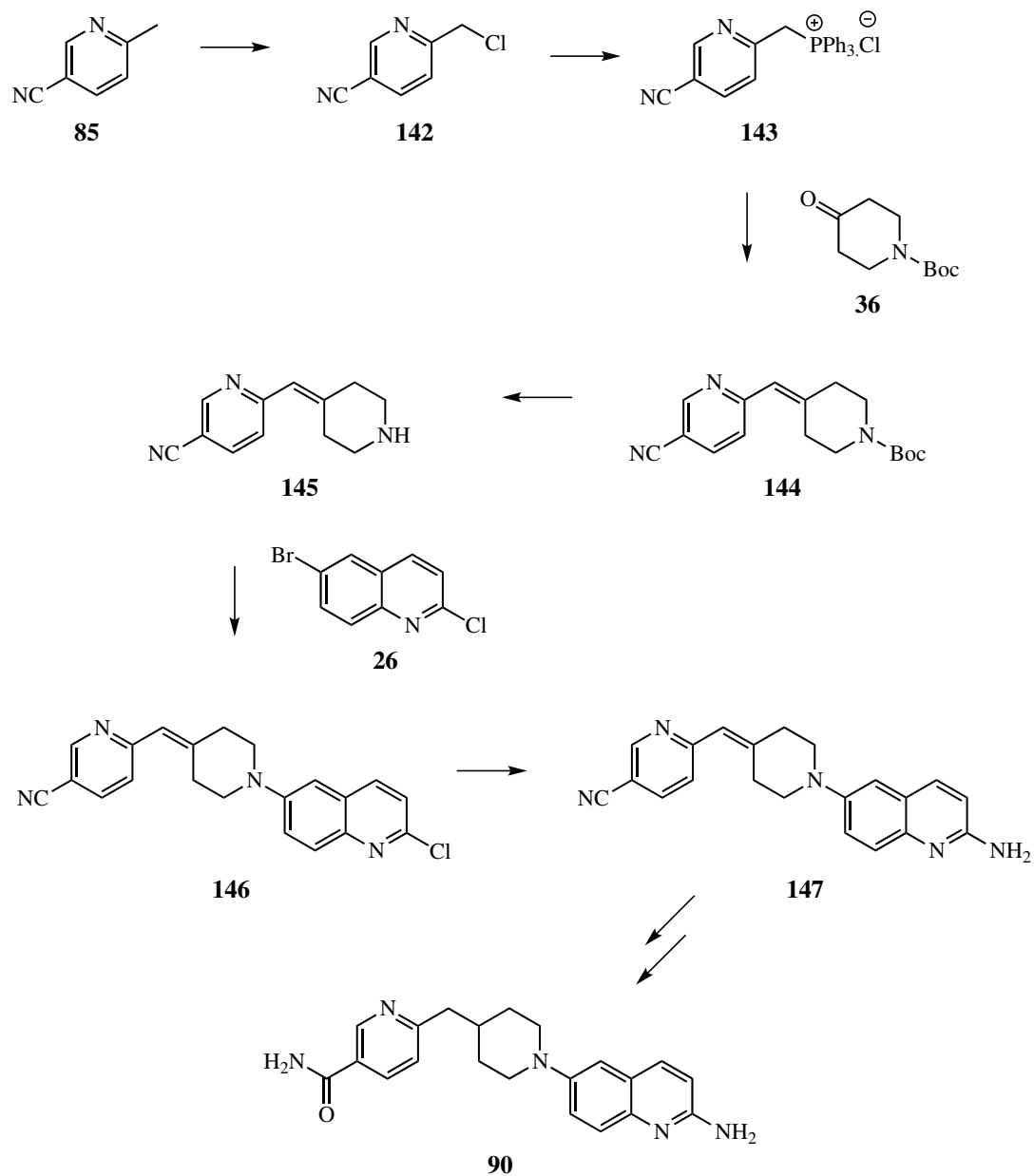


Figure 4.39: Proposed synthetic pathway for the synthesis of complex ligand **90**, which contains 2-pyridyl and 4-amido substituents.

#### 4.5. SYNTHESIS OF COMPLEX LIGANDS CONTAINING 2-PYRIDYL AND 4-AMIDO FUNCTIONAL GROUPS

Following synthesis of the 2-chloroquinoline derivative **146**, the 2-amino functionality can be introduced via sequential Buchwald-Hartwig coupling reaction using LiHMDS as both a base and an ammonia equivalent;<sup>47</sup> subsequent nitrile hydrolysis and alkene reduction could then afford the desired ligand **90**.

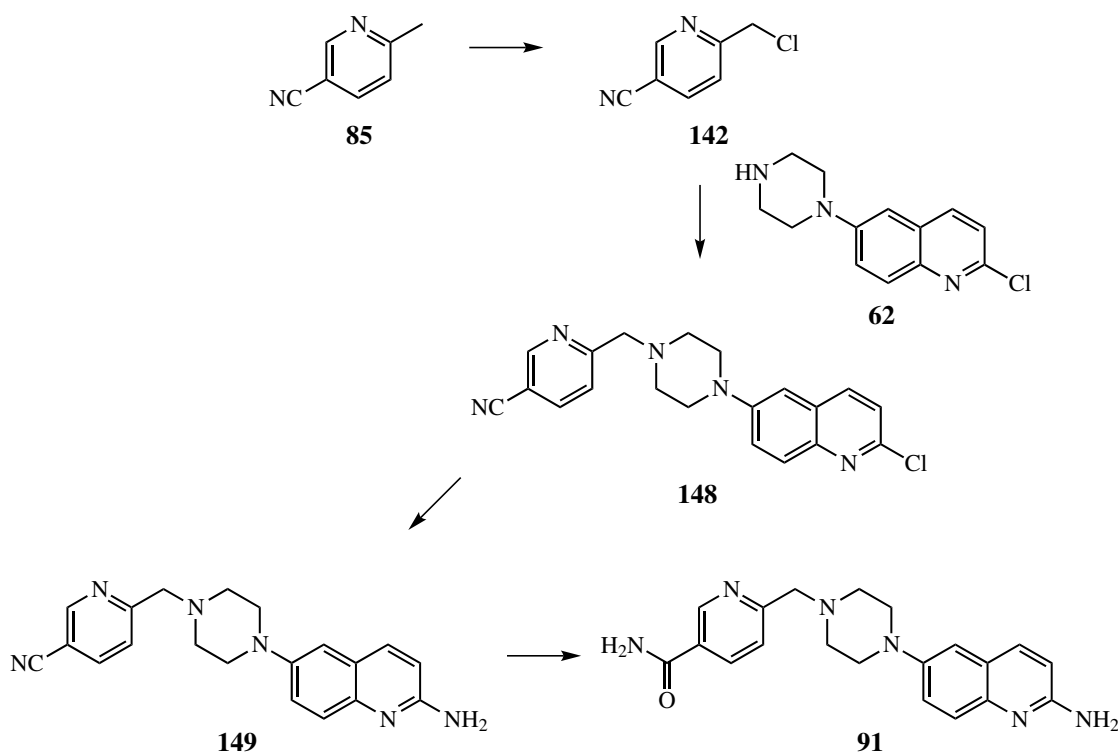
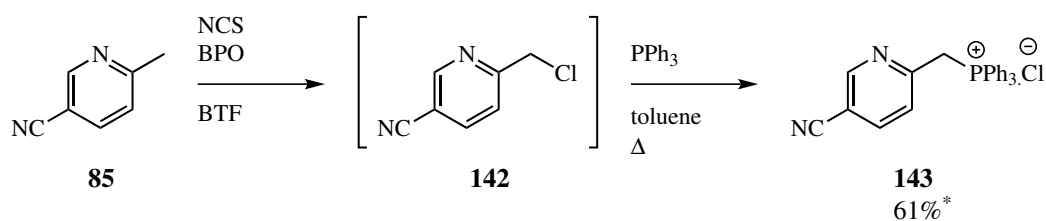


Figure 4.40: Proposed synthetic pathway for the synthesis of complex ligand **91**, which contains 2-pyridyl and 4-amido substituents.

From Figure 4.40, synthesis of the arylmethyl piperazinyl-containing ligand **91** was anticipated to be achieved via nucleophilic substitution reaction between **142** and **62**. The resultant 2-chloroquinoline derivative **148** could then undergo a Buchwald-Hartwig coupling reaction, followed by nitrile hydrolysis to afford the desired target ligand **91**. Again, given the low yields reported previously for Buchwald-Hartwig coupling reactions with electron-deficient benzylpiperazine derivatives (including 4-nitrile and 2-pyridyl, Table 3.14 and Table 3.15, Chapter 3), it was anticipated that synthesis of the 2-aminoquinoline derivative **149** may only occur in low yield. In order to increase the desired product yield, it was proposed that increasing the relative Pd and phosphine ligand concentrations would be appropriate to afford sufficient product formation.

#### 4.5.1.1 Synthesis of methylene piperidinyl derivatives containing 2-pyridyl and 4-nitrile functional groups

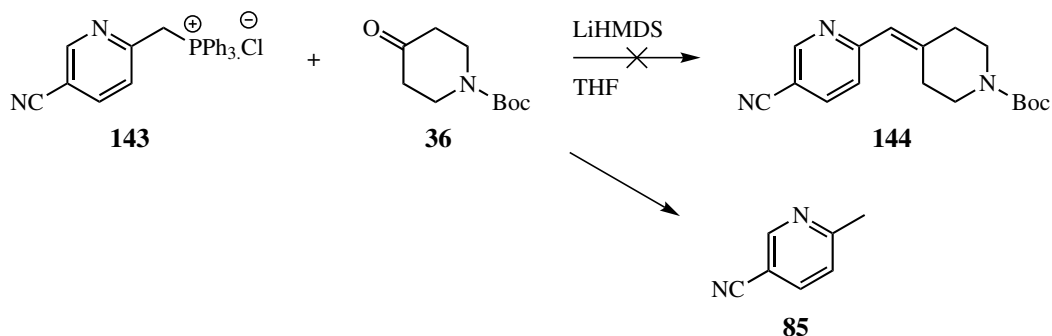
To synthesise the target ligand **90**, the first step from Figure 4.39 required synthesis of the pyridyl-methyl chloride derivative **142**. Due to the previously reported pyridylmethyl halide volatility<sup>56,127</sup> and synthetic challenges for pyridylmethyl bromides (Scheme 4.23), it was desirable to minimise the time available for **142** to undergo unwanted side-reactions. Following radical chlorination of **85** with NCS, the crude product **142** was filtered from the succinimide by-product, and used immediately without further purification to afford the phosphonium salt **143** (Scheme 4.35).



Scheme 4.35: Reaction conditions and yield for synthesis of **143** via radical chlorination with **85**, *N*-chlorosuccinimide (NCS) and benzoyl peroxide (BPO) in BTF, followed by conversion to the phosphonium salt. \* indicates yield over 2 steps.

Formation of **142** was inferred by the synthesis of **143**, as **85** alone would not be a suitable substrate for phosphonium salt synthesis. Successful formation of **143** was supported by analysis of NMR spectra; in both <sup>1</sup>H and <sup>13</sup>C NMR spectra all signals displayed splitting due to H-P or C-P coupling. In addition, introduction of the triphenylphosphine group was supported by the emergence of aryl multiplets integrating to 15H. Pleasingly, the phosphonium salt **143** was formed in a good yield (over two steps), particularly when compared to Scheme 4.24.

Following synthesis of **143**, the next step required formation of the methylene piperidine derivative **144** — this was attempted via Wittig reaction, as shown in Scheme 4.36.



Scheme 4.36: Reaction conditions for attempted synthesis of **144** via Wittig reaction with **143** and **36**.

#### 4.5. SYNTHESIS OF COMPLEX LIGANDS CONTAINING 2-PYRIDYL AND 4-AMIDO FUNCTIONAL GROUPS

---

Unfortunately, the attempted Wittig reaction to form **144** from **143** and **36** was unsuccessful. From analysis of crude product  $^1\text{H}$  NMR spectra, a significant amount of triphenylphosphine oxide **109** was observed, as well reduction to the substituted tolyl derivative **85** (Figure 4.41), similarly to that described earlier for the 4-nitrile 2-bromophenyl derivative (see Scheme 4.5 and associated text). In addition, some other aromatic signals consistent with a di-substituted 2-pyridyl derivative were observed in crude product  $^1\text{H}$  NMR spectra (Figure 4.41), suggesting the presence of some minor side (or degradation) products which could not be further identified.

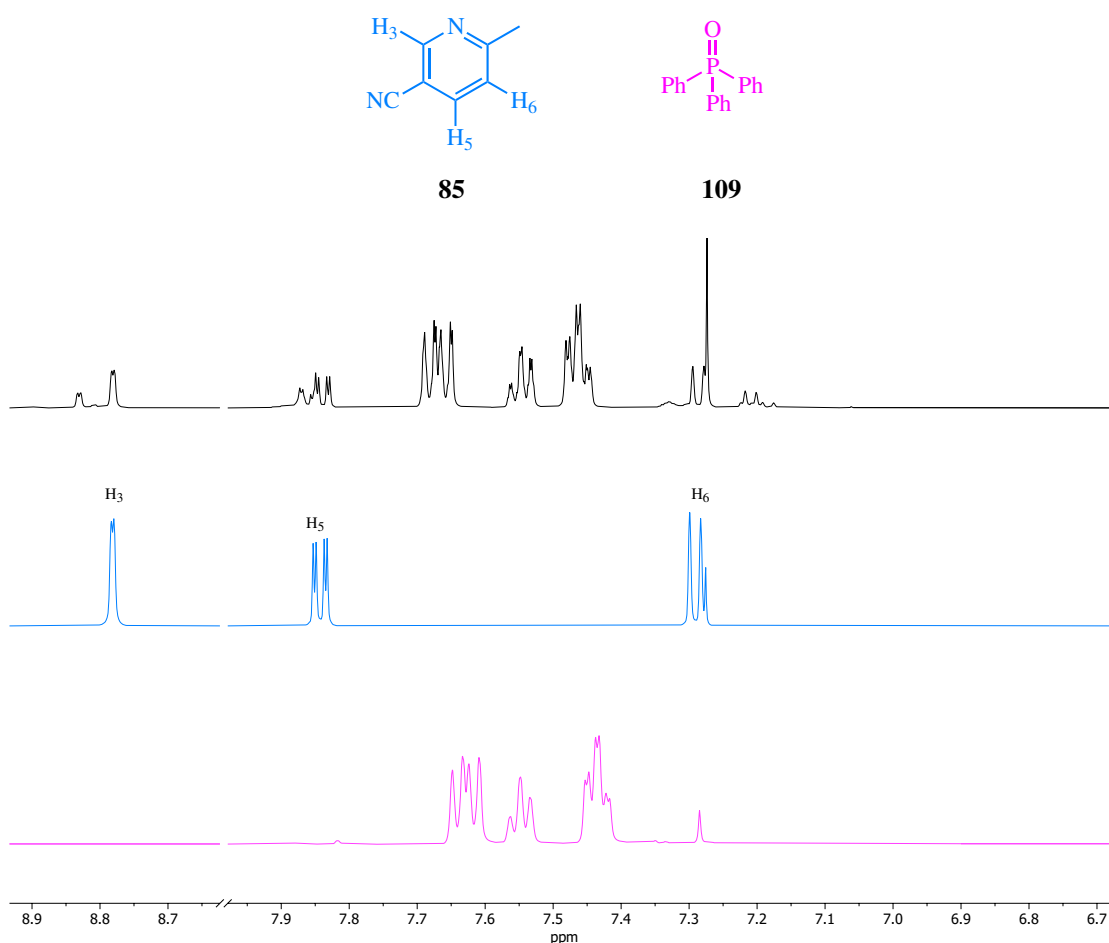
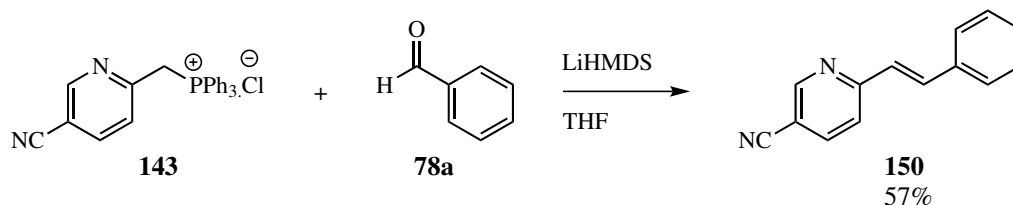


Figure 4.41: Stacked and truncated  $^1\text{H}$  NMR spectra ( $\delta_{\text{H}}$ : 6.7 - 8.9 ppm) of crude reaction mixture from attempted synthesis of **144** (black), starting material **85** (blue) and **109** (pink), indicating presence of **85** and **109** in the crude reaction mixture.

As both **143** and **107** contain nitrile groups (electron-withdrawing by resonance), each of their corresponding ylides are expected to be stabilised in a manner consistent with Figure 4.13. Therefore, similarly to **107**, it is likely that the stabilised ylide of **143** is not sufficiently nucleophilic to react with the ketone in **36**, which would be a poor electrophile (relative to an aldehyde). To test this hypothesis, the Wittig reaction with **143** was repeated, but instead using the aldehyde **78a** as the

electrophile — if the reduced reactivity in Scheme 4.36 is due to a combination of the reduced nucleophilic character of the ylide of **143** and the poor electrophilic character of **36**, then theoretically reacting **143** with a better electrophile (such as **78a**) should facilitate the desired transformation; this is shown in Scheme 4.37.



Scheme 4.37: Reaction conditions and yield for synthesis of **150** via Wittig reaction with **78a** and **143**.

Similarly to Scheme 4.6, when the Wittig reaction was undertaken with a better electrophile (i.e., **78a**), the desired product formed, as shown in Scheme 4.37. Successful synthesis of **150** was supported by analysis of NMR spectra; in  $^1\text{H}$  NMR spectra, the emergence of several aromatic multiplets integrating to a total of 5H were indicative of successful attachment of the phenyl ring in **78a**. In addition, two separate 1H doublets with coupling constants of 16.0 Hz were observed at 7.16 ppm and 7.80 ppm, consistent with the introduction of a *trans*-substituted alkene; while these chemical shifts appear quite deshielded for an alkene H signal, they can be justified by the potential resonance contributors indicated in Figure 4.42, and also due to anisotropic deshielding from the adjacent aryl groups. Finally, the desired connectivity for **150** was supported by analysis of 2D NMR spectra (Figure 4.43).

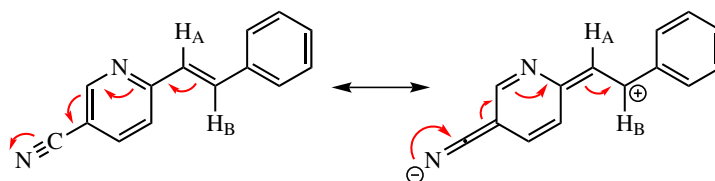


Figure 4.42: Possible resonance contributors for **150**, indicating deshielding of alkene chemical environments through electron delocalisation across the nitrile group.

#### 4.5. SYNTHESIS OF COMPLEX LIGANDS CONTAINING 2-PYRIDYL AND 4-AMIDO FUNCTIONAL GROUPS

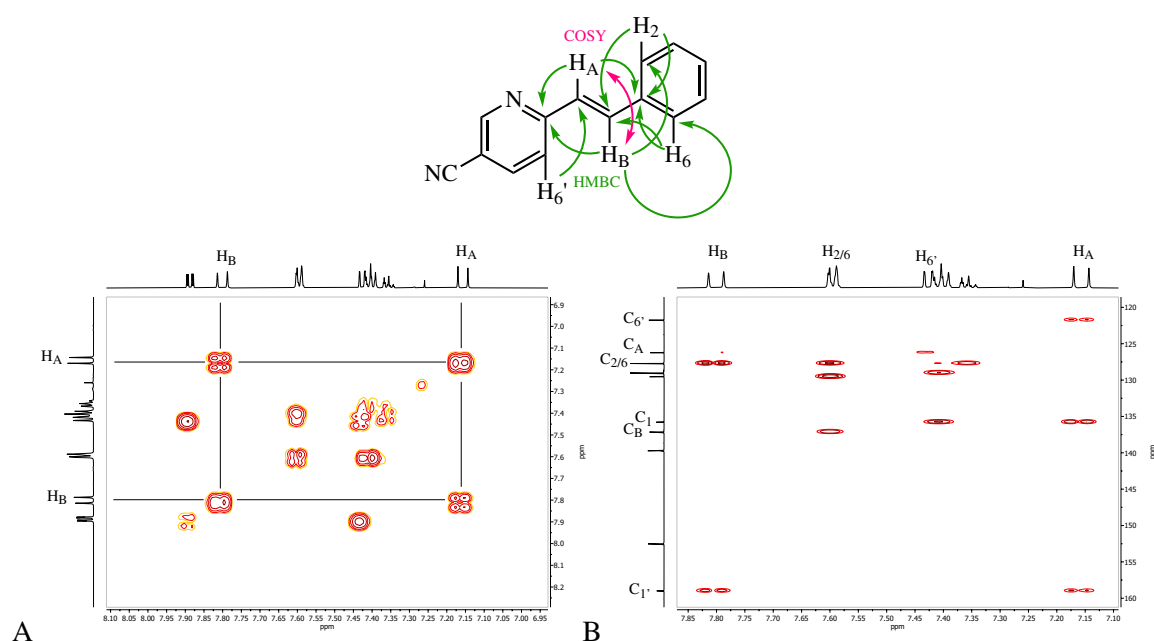


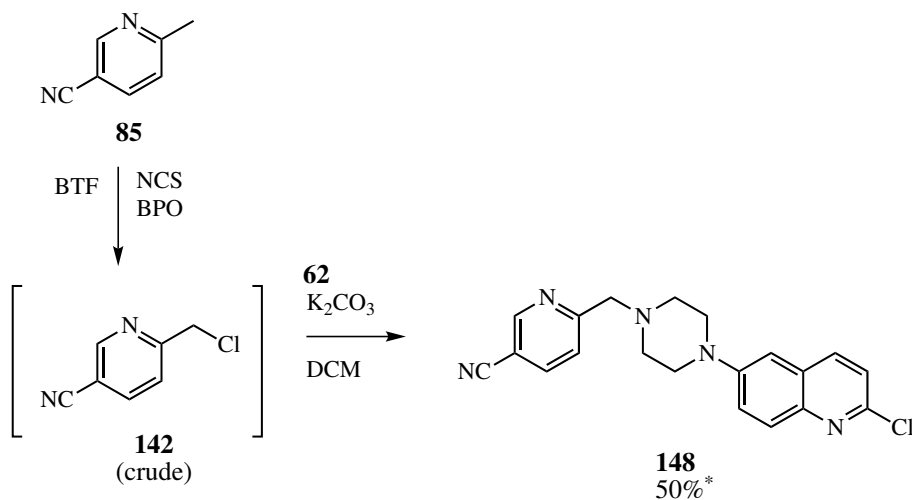
Figure 4.43: Structural analysis of **150** via 2D NMR spectra, with (A) COSY correlations indicated by pink arrows, and (B) HMBC correlations indicated by green arrows.

Given the successful synthesis of **150**, it was clear that the ylide of **143** was sufficiently stabilised, to the extent that it was not sufficiently nucleophilic to react with the ketone of **36** (i.e., a poor electrophile). Therefore, in order to facilitate formation of **144**, an alternative synthetic pathway was required, whereby the nucleophilic equivalent of **142** is sufficiently strong to react with the poor electrophile, **36**. For previous transformations, this was achieved with the appropriate benzyl phosphonate derivative in a Horner-Emmons reaction, as the benzyl phosphonate is typically more nucleophilic when the phosphonate is stabilised (by an electron-withdrawing group). However, this was not a viable option for synthesis of **144** — given the volatility of pyridylmethyl halide derivatives,<sup>56,127</sup> it was anticipated that synthesis of a pyridylmethyl phosphonate derivative would be prohibitively low-yielding, as phosphonate synthesis typically requires synthesis at high temperatures (Scheme 4.7). At this point, significant optimisation of either the Wittig reaction (through identification of a suitable adjuvant to facilitate ylide reactivity with **36** as a weak electrophile) or pyridylmethyl phosphonate synthesis would be required for synthesis of **144**. It was apparent that additional efforts towards synthesis of **144**, and ultimately the ligand **90** would require a significant investment of time and resources, which could not be justified in the absence of any compelling SAR information. Therefore, no further attempts to produce the ligand **90** were undertaken.

#### 4.5.1.2 Synthesis of methyloperazine-substituted derivatives containing 2-pyridyl and 4-nitrile functional groups

Following the attempted synthesis of **90**, it was desirable to synthesise the target ligand **91**. The first step required synthesis of the pyridylmethyl chloride derivative **142**, followed by nucleophilic substitution reaction with **62** to afford the 2-chloroquinoline intermediate **148** (Figure 4.40).

Due to the previously reported volatility of pyridylmethyl halide derivatives, it was desirable to attempt synthesis of **148** using crude **142**. However, there were concerns that the succinimide-coupled side product **141** may also form if crude **142** was used in the nucleophilic substitution reaction. Both factors were considered, but ultimately the potential volatility issues of **142** were deemed to be of greater importance — if the side product **141** did form, it was possible that the polarities of **141** and **148** might be sufficiently different to allow for separation using chromatographic methods. Conversely, mitigation of **142** volatility was likely to be challenging — while it would typically be reasonable to convert the pyridylmethyl chloride derivative to the corresponding hydrochloride salt, this was not a suitable approach for **142** as it would be extremely difficult to separate the hydrochloride salt of **142** from precipitated succinimide by-product following the radical chlorination reaction. Furthermore, **142** would need to be liberated from its hydrochloride salt prior to nucleophilic substitution reaction; this process of liberation (indicated in Chapter 2, Scheme 2.5) would provide an additional opportunity for product loss by evaporation. Therefore, the nucleophilic substitution reaction to synthesise **148** was undertaken with crude **142** (Scheme 4.38).



Scheme 4.38: Reaction conditions and yield for synthesis of **148** via radical chlorination of **85** and subsequent nucleophilic substitution reaction with crude **142**. NCS = *N*-chlorosuccinimide, BPO = benzoyl peroxide. \* indicates yield calculated over two steps.



#### 4.5. SYNTHESIS OF COMPLEX LIGANDS CONTAINING 2-PYRIDYL AND 4-AMIDO FUNCTIONAL GROUPS

Analysis of crude **148**  $^1\text{H}$  NMR spectra fortunately did not reveal any signals indicative of the succinimide-coupled by-product **141**. Formation and purification of the desired 2-chloroquinoline derivative **148** was achieved in good yield, and was supported by analysis of HRMS and NMR spectra; mass products with  $m/z$  values of 364.1325 and 366.1303 were observed in  $\sim 2:1$  ratio in mass spectra, consistent with natural chlorine isotope abundance (**148**  $[\text{M}+\text{H}]^+$   $m/z$  requires 364.1313 [ $^{35}\text{Cl}$ ] / 366.1294 [ $^{37}\text{Cl}$ ]). Analysis of  $^1\text{H}$  NMR spectra revealed the emergence of aromatic signals consistent with successful incorporation of a 6-position substituted 2-chloroquinoline component, as well as two characteristic 4H piperazinyl ring H signals, and a 2H singlet at 3.83 ppm, indicating formation of the pyridylmethyl-piperazine bond. Importantly, successful attachment of the pyridylmethyl component was supported by analysis of 2D NMR spectra, with displayed correlations consistent with those expected for **148** (Figure 4.44).

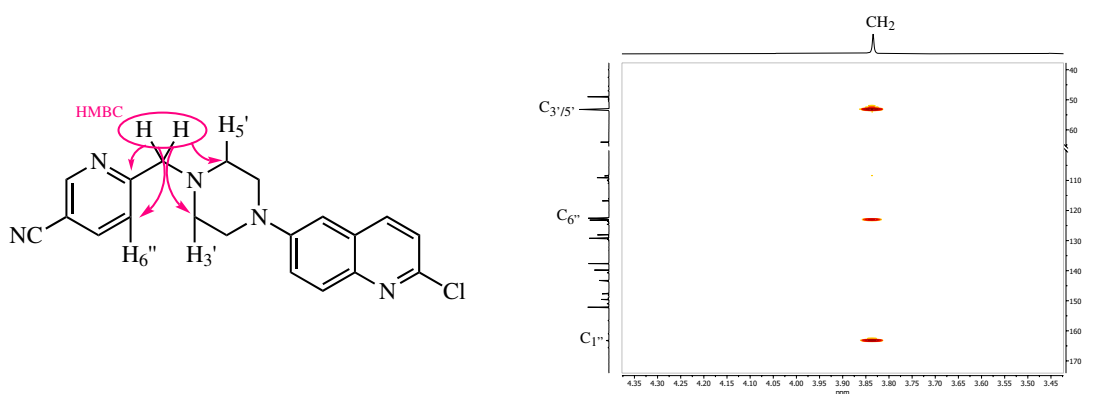
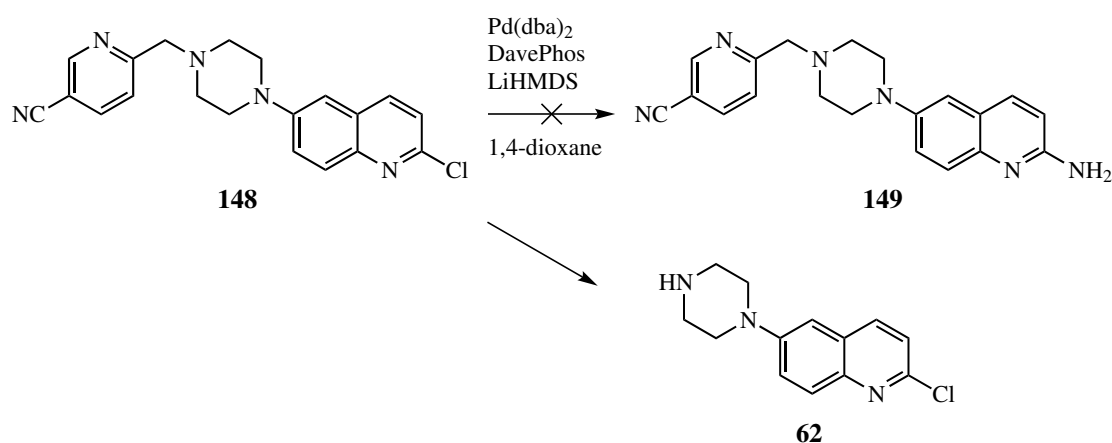


Figure 4.44: Structural analysis of **148** via 2D NMR spectra, with HMBC correlations indicated by pink arrows.

Following successful synthesis of **148**, the next step required introduction of the 2-amino functionality in **149**. It was anticipated that this could be achieved via Buchwald-Hartwig coupling reaction with LiHMDS as both a base and an ammonia equivalent, using previously optimised conditions;<sup>47</sup> the results are shown in Scheme 4.39.



Scheme 4.39: Attempted synthesis of 2-aminoquinoline derivative **149** via Buchwald-Hartwig coupling reaction with **148**, using LiHMDS as both a base and an ammonia equivalent.

Unfortunately, analysis of <sup>1</sup>H NMR spectra of the crude product mixture indicated the desired product **149** had not formed, but appeared to contain some type of 2-chloroquinoline derivative; subsequent analysis of the crude product mixture by HRMS revealed a mass product with an *m/z* value consistent with that expected for **149**, but only in very low abundance. An attempt was made to purify the crude product mixture using chromatographic methods, in the hope to obtain at least an analytical sample of **149**, but this too was unsuccessful. Interestingly, during purification a side product was isolated; from analysis of <sup>1</sup>H NMR spectra, this side product appeared to contain a 6-piperazinyl 2-chloroquinoline structure, but no pyridyl component. Upon overlaying the spectra of this side product with that of **62**, there was close correspondence between chemical shifts, with the exception of some slight differences in the piperazinyl ring signals (Figure 4.45) — this could be attributed due to potential differences in chemical environment about the piperazinyl free amine (the obtained side product from the Buchwald-Hartwig reaction was dark orange, while the overlaid NMR spectra for **62** was obtained for purified **62**, which is typically dark yellow).

#### 4.5. SYNTHESIS OF COMPLEX LIGANDS CONTAINING 2-PYRIDYL AND 4-AMIDO FUNCTIONAL GROUPS

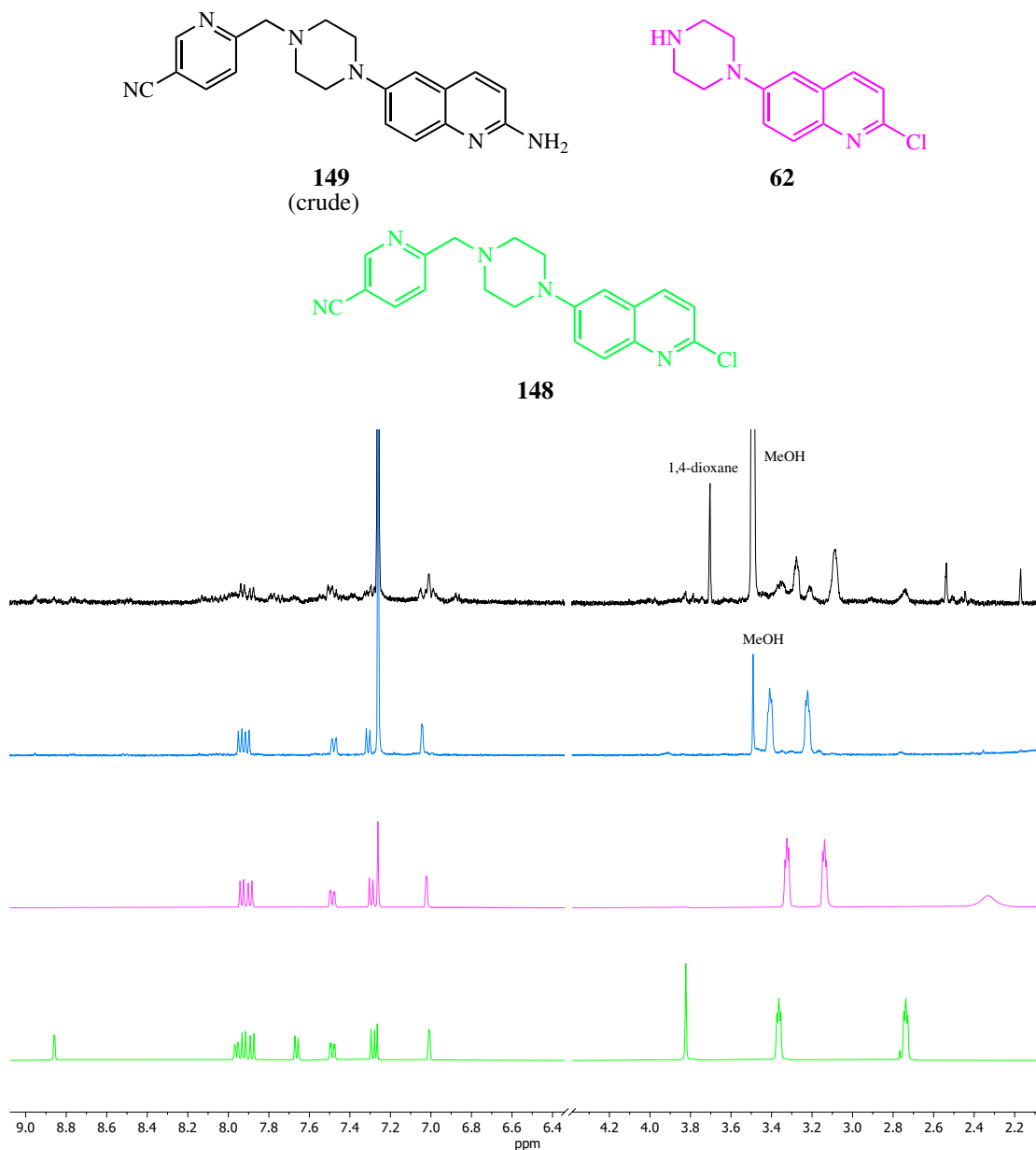


Figure 4.45: Stacked comparison of truncated and normalised <sup>1</sup>H NMR spectra ( $\delta_{\text{H}}$ : 2.2 - 9.0 ppm) of the crude product mixture from attempted synthesis of **149** via Buchwald-Hartwig coupling reaction (Scheme 4.39, black), purified 2-chloroquinoline side product from the same Buchwald-Hartwig coupling reaction (blue), **62** (pink) and starting material **148** (green), indicating that signals from side product are consistent with **62**.

Following this, the crude product mass spectra was re-analysed, and mass products with  $m/z$  values consistent with those expected for **62** (in the expected 3:1 ratio for natural chlorine isotope abundance) were observed. Together, this indicates that the 2-chloroquinoline side-product which formed during the attempted synthesis of **149** was **62**; while the 2-pyridyl 4-nitrile component from **148** could not be identified in any of the crude product HRMS or NMR spectra, it is possible that this may have degraded during the reaction (which is conducted in a sealed system at high pressure and temperature). Potentially, **62** may have formed during the attempted Buchwald-Hartwig coupling reaction in Scheme 4.39 if the pyridylmethyl component of **148** was functioning as a “decorated” benzyl protecting group for the piperazinyl nitrogen — given benzyl protecting groups can be removed under basic conditions at room temperature,<sup>124</sup> this would not be unreasonable under the reaction conditions (Scheme 4.39).

It is interesting that formation of **62** was not detected during the synthesis of any other benzylpiperazine substituted 2-aminoquinolines in this thesis, and two hypotheses are presented for this: firstly, of all the compounds investigated in this thesis, the pyridylmethyl group in **148** (i.e., the benzylamine derivative) is anticipated to be the most electron-deficient benzylamine derivative, so perhaps this functional group lability relies upon an electron deficient system; secondly, it is recognised that **62** as a side product was only isolated in trace quantities, and it was only isolated as concerted efforts were being undertaken while seeking to purify **149**, which was only present in low abundance by HRMS — it is possible that some **62** liberation was occurring in other Buchwald-Hartwig coupling reactions with benzylpiperazinyl 2-chloroquinoline derivatives, however **62** may not have been identified due to low abundance relative to the desired 2-aminoquinoline products (or being indistinguishable from baseline noise in HRMS spectra).

Formation of **62** under the Buchwald-Hartwig coupling reaction conditions shown in Scheme 4.39 was quite disappointing. For synthesis of the ligand **91**, it was clear that a comprehensive optimisation of Buchwald-Hartwig coupling reaction conditions would be required. Given the number of ligands already synthesised, optimisation of the Buchwald-Hartwig coupling reaction for synthesis of **91** (when the value of **91** was unknown) was considered beyond the scope of this thesis, therefore no further attempts to produce the target ligand **91** were undertaken.

## **4.6 SPR binding studies of complex 6-position substituted 2-aminoquinoline ligands**

### **4.6.1 SPR binding assay aims**

To determine the binding affinities of the complex 2-aminoquinoline ligands synthesised in this section (**88**, **89**, **97** and **114**) and to ensure comparability of SAR data with the ligands reported in Chapters 2 and 3 of this thesis, the ligand affinities for the Tec SH3 domain were screened and calculated by SPR assays against GST-Tec SH3 protein, using the assay method validated in Chapter 2 (2.4.1). As the location of the ligand binding site on the Tec SH3 protein surface had been previously interrogated with **17**, **18**, **59**, **60** and **61** ligand families, it was reasonable to infer that sufficient data had been obtained to support that each of the synthesised complex ligands described in this chapter would be binding the Tec SH3 domain surface in a similar manner to those reported previously, therefore no SPR assays with mutant GST-Tec SH3 D196A or Tec SH3 were conducted. Consequently, the results of the SPR binding assays with the complex ligands and GST-Tec SH3 will be described in the following sections. It is noted that binding activity investigations by Hansch plot analysis will not be undertaken for the complex ligands — it would be an oversimplification to represent the combinations of multiple substituents in each of the complex ligands by the sum of either the  $\sigma$  or molar refractivity constants, therefore the results (as  $K_d$  values) will only be discussed qualitatively.

### **4.6.2 Results of SPR binding assays with GST-Tec SH3 and insights into binding model**

The binding affinities of complex ligands **88**, **89**, **97** and **114** for the Tec SH3 domain were determined by SPR binding assays against GST-Tec SH3 (as described in Chapter 2, 2.4.1), and the results reported in Table 4.5.

4.6. SPR BINDING STUDIES OF COMPLEX 6-POSITION SUBSTITUTED 2-AMINOQUINOLINE LIGANDS

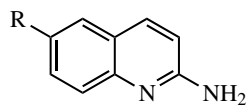


Table 4.5: Binding affinities of compounds determined by SPR for binding GST-Tec SH3.

Compound	R =	GST-SH3 $K_d \pm SD$ ( $\mu\text{M}$ )
97		$8.4 \pm 1.2$
97 & 114 (3:1)		$8.3 \pm 1.5$
100		$20.6 \pm 3.4$
88		$7.3 \pm 1.0$
89		$18.1 \pm 1.3$

#### 4.6. SPR BINDING STUDIES OF COMPLEX 6-POSITION SUBSTITUTED 2-AMINOQUINOLINE LIGANDS

---

Disappointingly, none of the ligands in Table 4.5 displayed improved binding affinities relative to the current lead ligands listed in Table 4.1. In spite of this, some interesting trends were observed, which may help guide further ligand development. Firstly, from comparison of the methylene piperidine-containing ligands **97** and **114** (where **114** was tested as a 3:1 mixture of **97** and **114**), there was a negligible difference in  $K_d$  value — this suggests that there is no gain in binding affinity upon exchange of the methylene piperidine group with a THP ring. Conversely, when each piperidinyl/piperazinyl ligand pair was analysed (i.e., **97** & **100**, and **88** & **89**), in each case the piperazinyl derivatives exhibited lower binding affinities. Taken together, this suggests that minor modifications of a piperidinyl (and possibly a methylene piperidinyl) ring are tolerated in the ligand-protein binding site, but an isosteric substitution of C(4) in the piperidine ring for a nitrogen (as in the piperazinyl ring) is not preferred. In the absence of a ligand-bound protein structure, a hypothesis to support these observations could be based upon the shape of the heterocycle — the piperazinyl ring is expected to have a “flatter” chair-like structure compared to a piperidinyl ring due to containing a pair of distal nitrogens; if a key binding interaction with the protein surface involved a hydrophobic interaction with the heterocyclic ring, then it is possible the “flatter” piperazinyl ring might not have sufficient depth across the heterocycle to form a key hydrophobic interaction. The presence and position of the additional nitrogen atom on the piperazinyl ring may also be detrimental to a potential hydrophobic interaction.

A second trend was observed in relation to the binding affinities of each of the piperidinyl biaryl structures (**88**, **97** and **114**). The 2- and 3-position substituted biaryl lead ligands (**23** & **24**) in Table 4.1 had  $K_d$  values of 7 and 4.1  $\mu\text{M}$  respectively; from Table 4.5, there is minimal difference in the binding affinities of the complex ligands **88**, **97** and **114** compared to those for **23** & **24**. Therefore, there is no apparent gain in binding affinity observed following combination of an additional aryl substituent (i.e., the 2,5-pyrimidine ring), and either a 2-pyridyl group (as for **88**), or a 4-nitrile group (as for **97** and **114**); it appears that these biaryl-containing ligands hit a “binding affinity floor”. It is possible that the ligand binding orientation required to facilitate a favourable interaction between the (ligand) biaryl structure and protein surface may not be conducive to additional interactions which might occur between either the 2-pyridyl or 4-nitrile groups, therefore no significant gain in binding affinity (relative to the lead biaryl ligands **23** and **24**) are observed. To investigate this hypothesis, a ligand-bound protein structure would be required to determine the favourable ligand orientations upon biaryl ligand binding. A key limitation of the complex ligands tested in Table 4.5

is the absence of any ligand with a 4-amido substituent. Given the observed trend within the biaryl ligands, it would be interesting to investigate whether the combination of a 4-amido substituent is compatible with a biaryl group within a single ligand (as for the proposed complex ligand **86**) is tolerated, and if it translates to a stronger-binding ligand.

Lastly, the 2-pyridylmethyl piperazinyl ligand **59a** tested in Chapter 3 displayed slower binding kinetics relative to the 2-pyridylmethyl piperidinyl ligand **18a** — interestingly, **89** did not display slower binding kinetics, but instead exhibited “box-shaped” sensorgrams consistent with **18a**. This is not surprising, as the calculated  $K_d$  value for **89** is higher than that for **59a**, the binding interactions between **89** and GST-Tec SH3 would be weaker (relative to **59a** and GST-Tec SH3), allowing the ligand to dissociate faster from the protein surface. The only structural difference between ligands **89** and **59a** is the presence of the 2,5-pyrimidinyl ring — this suggests that the 2,5-pyrimidinyl ring in **89** is interacting unfavourably with the Tec SH3 domain surface, to the extent that **89** dissociates faster from the protein surface during SPR binding assays. It is noted that the binding affinity of **88** ( $K_d = 7.3 \mu\text{M}$ ) is comparable to that of the lead biaryl ligand **24** ( $K_d = 4.1 \mu\text{M}$ ).<sup>56</sup> Given that the 2,5-pyrimidine ring is tolerated in a pyridylmethyl piperidine ligand (**88**) but not a pyridylmethyl piperazine ligand (**89**), this suggests that the reduced binding affinity and faster binding kinetics of **89** are due to the unfavourable combination of a 2,5-pyrimidine ring in an arylmethyl piperazine-containing ligand; this may be caused by an undesirable interaction between the biaryl (2,5-pyrimidine) group, and the flatter piperazinyl ring (compared to piperidine).



## 5 | Conclusions and Future Directions

### 5.1 SPR ligand binding assay

Through the synthesis and subsequent binding affinity analysis of control ligands **18a** and **18b** with various derivatives of the Tec SH3 domain, sufficient data was obtained to validate the ligand-protein binding interaction measured by SPR, and ligand binding affinities reported previously.<sup>56</sup>

Experiments investigating the binding affinity of **18a** and **18b** against GST-Tec SH3 by SPR (using GST as a reference protein) produced comparable values to those reported previously,<sup>56</sup> indicating reproducibility in the assay method and results. Subsequent investigation of the binding activities of **18a** and **18b** with the GST-Tec SH3 D196A mutant protein revealed no ligand binding activity, consistent with previous reports.<sup>54</sup> This indicates the binding interaction between control ligands **18a** and **18b** and Tec SH3 measured by SPR is consistent with the previously proposed ligand-protein binding model,<sup>46,54</sup> therefore the binding interaction with **18a** and **18b** is likely occurring at the same site on the protein surface.

The significance of off-site binding to the GST tag of GST-Tec SH3 was investigated, through binding affinity analysis of **18a** and **18b** with Tec SH3 — SPR assays with Tec SH3 removed the opportunity for any off-site binding interactions between ligands and the GST tag. Pleasingly, the obtained binding affinities were consistent with those obtained for **18a** and **18b** binding to GST-Tec SH3, suggesting that any off-site binding interactions with the GST tag did not have a significant impact on the derived binding affinities — ligand binding affinity for GST-Tec SH3 was therefore representative of ligand binding affinity for Tec SH3.

Given the reproducibility of SPR ligand binding assays with the Tec SH3 domain, and the insights into the location of the ligand-protein binding interaction being measured by SPR, there is sufficient data to suggest the SPR ligand binding assay has been successfully validated for investigating the proposed ligand-protein binding model with the Tec SH3 domain.<sup>46</sup> The secondary aim of this thesis was therefore achieved.

## 5.2 Protein crystallisation

To aid the identification of suitable ligands in structure-based drug design, it is desirable to obtain a ligand-bound protein structure which can inform binding geometries and facilitate confident predictions of ligand-protein contacts. Crystallisation of both GST-Tec SH3 fusion protein and the Tec SH3 domain were attempted.

Whilst GST-Tec fusion protein was plated with several crystallisation conditions, very few protein precipitation events were observed, with none yielding protein crystals amenable to x-ray diffraction. This lack of protein precipitation was likely due to the entropic penalty of a fusion protein containing two distinct subunits, and not a dilute protein stock.

More concentrated efforts were applied in an attempt to facilitate crystallisation of the Tec SH3 domain. While more precipitation events were observed (indicated by fewer clear drops), no protein crystals suitable for analysis by x-ray diffraction were observed; only some general conditions facilitating protein precipitation (but not degradation) were identified.

Despite best efforts, the absence of a Tec SH3 domain-containing protein crystal did not allow for the identification of an experimentally-derived bound ligand-protein structure, therefore the proposed ligand-protein binding model was not conclusively substantiated. The subsidiary aim of this thesis was therefore not achieved.

## 5.3 Simple 6-substituted 2-aminoquinoline ligands containing a piperazine component

A range of 6-position extended 2-aminoquinoline derivatives containing a piperazinyl ring were synthesised and their binding affinities for the Tec SH3 domain investigated by SPR binding assays. The piperazinyl-containing 2-aminoquinoline derivatives were designed based on the benzylpiperidinyl ligands reported previously,<sup>56</sup> in an attempt to identify a more hydrophilic (i.e., more drug-like) ligand scaffold with potentially improved binding affinity for the Tec SH3 domain. The ligand scaffolds investigated varied in their hydrophilicity (measured as *clogP* value),<sup>61</sup> and also in the geometry about the piperazinyl ring. In addition, the ligand substituents varied in electronic nature, size, position and hydrophilicity. General synthetic pathways were developed and afforded

### 5.3. SIMPLE 6-SUBSTITUTED 2-AMINOQUINOLINE LIGANDS CONTAINING A PIPERAZINE COMPONENT

access to most of the desired target ligands, indicating wide applicability and functional group tolerance of the developed synthetic methods.

In SPR binding assays, all of the simple 6-substituted 2-aminoquinoline ligands containing a piperazine component displayed binding to GST-Tec SH3 and Tec SH3 (where tested), but not to GST-Tec SH3 D196A. Therefore, all of the tested ligands exhibited binding to the Tec SH3 domain in a manner consistent with the previously proposed ligand-protein binding model.<sup>46</sup> From Hansch plot analyses, there did not appear to be any significant impact of ligand substituent size, electronic nature (represented as Hammett constant,  $\sigma$  value)<sup>108</sup> or overall hydrophilicity on ligand binding activity, suggesting a degree of substituent tolerability at the ligand binding site. Unfortunately, none of the synthesised ligands displayed improved binding affinity for the Tec SH3 domain compared to previously reported ligands.<sup>56</sup> However, several ligands displayed comparable binding affinities to the previous lead compounds,<sup>56</sup> whilst containing a lower *clogP* value,<sup>61</sup> and therefore improved predicted bioavailability (Figure 5.1).

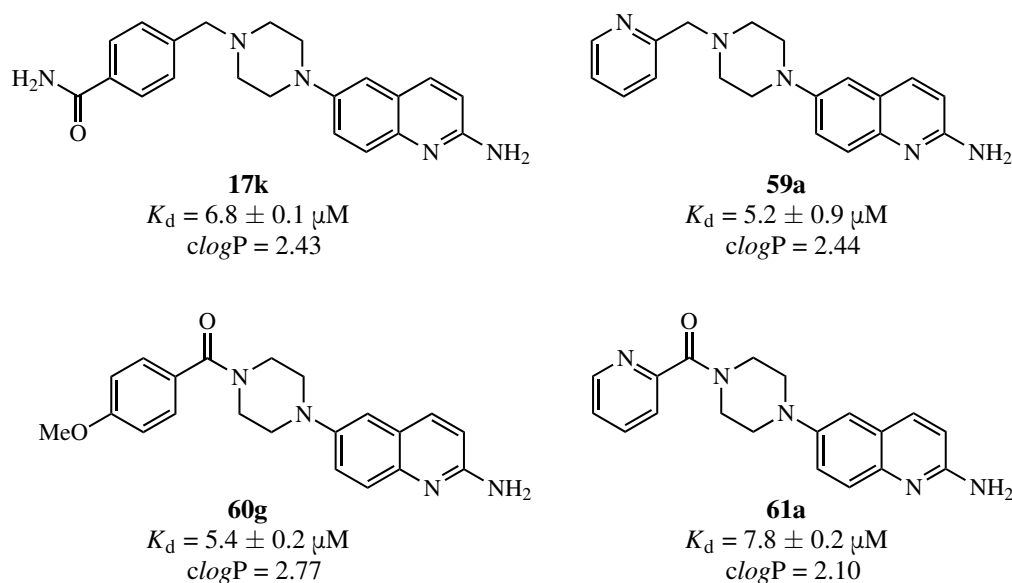


Figure 5.1: Structures of strongest binding simple 6-substituted piperazinyl 2-aminoquinoline ligands for the Tec SH3 domain (determined by SPR assays) for work in this thesis. *LogP* values (*clogP*) calculated using Marvin by ChemAxon.<sup>61</sup>

Previous work reported that the presence of an electron-poor aromatic ring typically afforded a ligand with improved binding affinity, through either a comparatively electron-poor pyridine ring, or the presence of an electron-withdrawing (by resonance) functional group. This was also observed for most of the strongest ligands in this work, as for **17k**, **59a** and **61a**, but not for **60g**, which contained an electron-donating (by resonance) methoxy group. The 2-pyridyl containing ligands

**59a** and **61a** also exhibited slower binding kinetics during the measured SPR assay binding event compared to other **17**, **59**, **60** and **61** ligands, and those ligands reported previously.<sup>56</sup> While the binding kinetics of **59a** and **61a** were not sufficiently slow to allow reliable derivation of unique kinetic constants,<sup>65</sup> the relatively slower binding kinetics for **59a** and **61a** may be indicative of a slower ligand dissociation, and therefore a more favourable binding interaction which requires more energy to disrupt.

## 5.4 Complex 6-substituted 2-aminoquinoline ligands

A small number of more complex 6-substituted 2-aminoquinoline ligands were designed, synthesised, then their binding affinities for the Tec SH3 domain were investigated by SPR binding assays. The structures of these complex ligands were inspired by the favourable features of previously reported ligands<sup>56</sup> (including those in Figure 5.1), in line with the primary aim of this work, to identify a small molecule ligand with improved binding affinity and drug-like character for binding the Tec SH3 domain. Three specific structural features were identified as favourable (a 2,5-pyrimidinyl substituent, an amide substituent, and 2-pyridyl ring as the aryl group), and various combinations of these substituents within a single ligand were considered. A total of six theoretically accessible ligands were identified, with each ligand requiring a tailored synthetic pathway of between 4-9 synthetic steps. Two of these target ligands were successfully synthesised, along with three other 2-aminoquinoline ligand intermediates with similar structures to the target ligands.

None of the five complex ligands tested exhibited improved binding affinity for the Tec SH3 domain compared to the previously reported lead compounds,<sup>56</sup> however some valuable insights to the ligand-protein binding interaction were derived from the obtained SPR assay results. For the assayed ligands containing a biaryl substituent (Figure 5.2), those containing a piperidinyl ring (**88**, **97** and **114**) displayed improved binding affinities compared to those with a piperazinyl ring (**89** and **100**), suggesting either the relative flatness or the additional nitrogen in the piperazinyl ring is not preferred at the ligand binding site. Furthermore, the differing geometries between a methylenepiperidine-containing ligand (**97**) and a tetrahydropyridine-containing ligand (**114**) did not appear to significantly alter ligand binding affinity. Lastly, for each of the biaryl-containing piperidinyl ligands (**88**, **97** and **114**), the binding affinity was comparable to the lead biaryl ligands reported previously,<sup>56</sup> suggesting the binding geometries of the biaryl-containing ligands may

## 5.5. PROPOSED FUTURE WORK

---

preclude formation of favourable contacts necessary for either the 2-pyridyl or 4-nitrile (in lieu of 4-amido) substituents, resulting in a “binding affinity floor”.

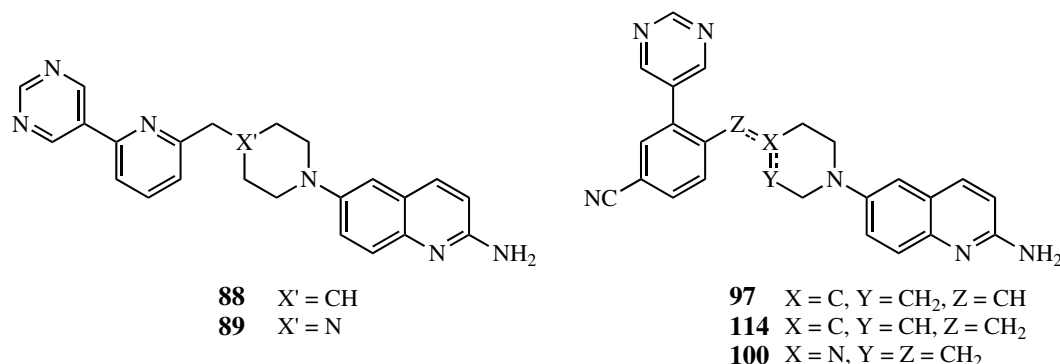


Figure 5.2: Structures of complex 6-substituted 2-aminoquinoline ligands which were successfully synthesised for testing in SPR ligand binding assays.

In the absence of an experimentally-determined bound ligand-protein structure, an extensive range of ligand SAR studies were undertaken with the aim of identifying a more hydrophilic ligand scaffold for inhibitor translation towards preclinical use. While novel small molecule ligands with improved *clogP* values (and therefore predicted bioavailability) were identified in this work, their binding affinities were comparable, but not improved compared to the previously reported lead compounds,<sup>56</sup> so the primary aim of this work was only partially achieved. This indicates that alternative structural modifications to piperazinyl ring implementation are likely required to achieve a significant gain in ligand binding affinity.

## 5.5 Proposed future work

### 5.5.1 Optimisation of Tec SH3 protein yields

A key limitation identified in this work was the lack of access to larger quantities of Tec SH3 protein — this particularly impacted crystallisation attempts of Tec SH3 protein (with the overall goal of determining the ligand-protein bound structure). Given the small quantities of available Tec SH3 protein (4 ml, 0.9 mg/mL), only a narrow range of sparse-matrix crystallisation screens could be tested, which unfortunately were unsuccessful in producing diffraction-quality protein crystals. To allow access to larger quantities of Tec SH3 protein for various experiments (including investigations of the ligand-protein binding model and ligand binding assays), it would be desirable to increase the protein yields.

From Chapter 2, expression and purification of the GST-Tec SH3 protein was generally successful, however protein yields for Tec SH3 were substantially reduced following thrombin-mediated cleavage of the GST tag. The GST cleavage conditions reported in Chapter 2 involved extended digestion periods and subsequent formation of insoluble (assumed) protein precipitate, potentially due to non-specific cleavage.<sup>128</sup> It would be reasonable to investigate optimisation of thrombin cleavage conditions, noting that this has been attempted previously with limited success.<sup>50,129</sup>

Alternatively, a longer linker containing the thrombin cleavage sequence (LVPR/GS)<sup>130</sup> could be inserted between the GST tag and SH3 domain. As both GST and Tec SH3 are globular proteins, increasing the length of the linker sequence may improve steric accessibility of thrombin to the cleavage site, therefore shortening the digest period and potentially reducing non-specific protease cleavage due to prolonged incubation. An extended linker sequence may also drive protein insolubility by aggregation, so it would be preferable to investigate iterative linker sequences to mitigate potential solubility issues. It would also be possible to insert a different cleavage sequence between the GST tag and SH3 domain, to allow cleavage by a different (more efficient and selective) protease, such as Tobacco Etch Virus (TEV) protease, which recognises the cleavage sequence of ENLYFQ/G.<sup>130</sup> TEV Protease has several advantages:<sup>130</sup> it has high cleavage specificity with minimal off-site activity, its cleavage conditions (including activity at different pH) have been well-characterised, and is commercially available as tagged isoforms (His<sub>6</sub>, GST), allowing for easy removal of TEV protease from the substrate. Extending the linker sequence or changing the protease cleavage site in the GST-Tec SH3 protein would require a new plasmid construct; this would involve preparation of the appropriate plasmids via restriction enzyme-mediated DNA digest, insertion of the desired sequence, and transformation of these plasmids into competent bacterial cells prior to protein expression.

### **5.5.2 Elucidation of the ligand-protein binding model**

Given the lack of improvements towards ligand binding affinity (compared to the current lead compounds)<sup>56</sup> in this work, it is abundantly clear that a determination of a ligand-bound protein structure should be prioritised to guide further ligand development. There are several methods which could facilitate this — it would be ideal to obtain a Tec SH3 protein crystal structure, as attempted in this thesis. Assuming reproducible crystallisation conditions are identified, it should then be possible to either co-crystallise different small molecule ligands with the protein, or soak

## 5.5. PROPOSED FUTURE WORK

---

the protein crystals with various ligand solutions; crystallisation of either GST-Tec SH3 or Tec SH3 protein would be suitable. For crystallisation of GST-Tec SH3, it would be logical to investigate whether the addition of glutathione, as the native ligand for the GST tag, will help to stabilise the protein structure and encourage crystallisation. It may also be beneficial to consider mutation of the amino acid sequence between the GST tag and Tec SH3 domain to confer more rigidity in the structure (i.e., reducing the entropic penalty through reduced linker sequence flexibility).<sup>131</sup> For crystallisation of Tec SH3, it would be ideal to conduct crystallisation screens with a higher concentration of protein (ideally ~15-20 mg/mL) and test a broader range of crystallisation conditions, not focussed primarily on citrate-containing screens.

The ligand-bound protein structure could also be investigated by NMR spectroscopy, providing a sufficiently strongly-binding ligand was identified (i.e., binds the Tec SH3 domain in slow exchange on the NMR timescale). Of the 2-aminoquinoline ligands investigated by 2D [<sup>1</sup>H, <sup>15</sup>N] HSQC NMR chemical shift perturbation assays to date, the strongest binding ligands ( $K_d \approx 10 \mu\text{M}$ ) have only bound the Tec SH3 domain in intermediate exchange on the NMR timescale.<sup>47</sup> As the strongest ligands reported in this work typically exhibited  $K_d$  values of ~5-10  $\mu\text{M}$ , it is possible that the ligands reported in this thesis would also bind the Tec SH3 domain in intermediate exchange, but possibly in slow exchange on the NMR timescale — this can only be determined by conducting 2D [<sup>1</sup>H, <sup>15</sup>N] HSQC NMR chemical shift perturbation assays with <sup>15</sup>N-labelled Tec SH3 protein. Regardless, it may be possible to force a ligand-protein complex from intermediate exchange into slow exchange on the NMR timescale, by either increasing the field strength of the NMR spectrometer used, or reducing the temperature of the sample during spectra acquisition (noting that the ligand-protein samples would typically contain 10% d<sub>6</sub>-DMSO, so a substantial temperature reduction may not be possible).

Theoretically, it would also be possible to generate a docked *in silico* ligand-bound protein model, as the solution NMR structure of the Tec SH3 domain is published.<sup>3,44</sup> This was attempted previously, but subsequent validation of predicted ligand binding affinities with experimentally determined values was not achieved (Stojkoski 2007, unpublished data). At the time, it was hypothesised that the inconsistency between predicted and experimental  $K_d$  values was due to the nature of the ligand-protein binding site — as a PPI inhibitor, the ligand is binding the Tec SH3 domain on the surface, and not in an active site or well-defined pocket. Given that PPIs have only gained

traction as suitable “druggable” targets over recent years,<sup>29,132,133</sup> it is unlikely that the ligand-protein docking software available at the time was developed with the intent of modelling PPIs, therefore many assumptions made by the software during analysis were likely misguided. However, as interest in PPIs as therapeutic targets across both academia and industry has increased, the intent of ligand-protein docking software has since been updated to reflect this paradigm shift, and should be reconsidered for investigation of a ligand-bound protein structure.

### 5.5.3 SPR binding assay optimisation

While the SPR binding assay was successfully validated, there are some aspects of the assay which could be further optimised. In particular, the importance of selecting an appropriate reference protein to generally correct for non-specific binding interactions to the protein surface was identified; binding affinity assays conducted without a reference protein (i.e., with only an activated and ethanolamine-blocked flow channel) displayed aberrant  $RU_{\max(\text{act.})}$  values, which were hypothesised to be caused by weak, non-specific hydrophobic interactions between **18a** or **18b**, and hydrophobic regions on the protein surface. However, analysis of the relative variation in  $RU_{\max(\text{act.})}$  for **18a** and **18b** revealed that this effect was consistent between ligands, therefore treated as a systematic error, and not considered to impact significantly on the derived binding affinities.

It would be useful to investigate the binding affinities of ligands to GST-Tec SH3, using GST-Tec SH3 D196A (or a similar mutant protein) as a reference protein. Not only would the MW of the active and reference proteins be suitably close, but the total number of hydrophobic regions on the protein surface should be similar, therefore any non-specific hydrophobic binding interactions should theoretically be removed following reference protein binding subtraction. Extending from this, it would also be ideal to conduct a similar assay to investigate the binding affinities of ligands to Tec SH3, using Tec SH3 D196A as a reference protein, as this should provide the most accurate estimation of ligand binding affinity for the Tec SH3 domain by SPR. The latter proposed endeavour would likely require optimisation of Tec SH3 protein yields (as described in Section 5.5.1) to avail sufficient quantities of protein for SPR assay development and optimisation.

In addition, it would be useful to consider alternative protein capture or immobilisation methods, such as antibody-capture (e.g., with an anti-GST antibody) or biotin-streptavidin capture. This would allow attachment of the Tec SH3 protein to the chip in a more controlled manner (relative



to the currently used amine coupling method), and therefore ensure consistent accessibility of the ligand binding site on the protein surface.

#### 5.5.4 Synthesis of additional complex 6-substituted 2-aminoquinoline ligands

A number of functional groups and structures were identified in this work which appeared to improve ligand binding affinity for the Tec SH3 domain. In the absence of a ligand-bound protein structure, the main aim of Chapter 4 was to combine only some of these components within a single ligand, to investigate combination of these components in a step-wise manner — if all components were immediately combined into a single ligand, it would be impossible to determine the complementarity and necessity of each group in the ligand structure.

While some of the target ligands identified in Chapter 4 were synthesised, there were a number that could not be synthesised due to limiting yields or unsuccessful reactions, namely the combination of a 2-pyridyl ring with a 4-amido group within a single ligand. This combination is of great interest, as all of the complex ligands tested in Chapter 4 contained a biaryl component, and appeared to hit a “binding affinity floor” consistent with current lead biaryl compounds — investigating the binding affinity of either **90** or **91** would provide some insights into whether the biaryl component is responsible for this observation.

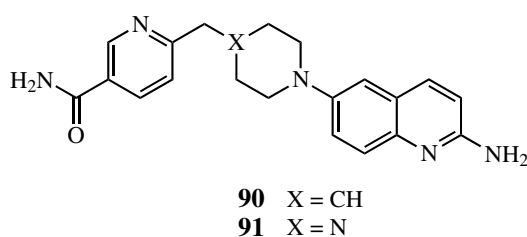


Figure 5.3: Structures of complex ligands of interest, **90** and **91**.

To synthesise **90**, it would be necessary to optimise the Wittig reaction with *N*-Boc-4-piperidone (**36**), to increase the reactivity of the ylide towards the ketone in **36** (Pathway A, Figure 5.4). Investigations into the synthesis of a pyridylmethyl phosphonate derivative could also be undertaken in preparation for pyridylmethylene piperidine synthesis via Horner-Emmons reaction (Pathway B, Figure 5.4), however this too would require optimisation to overcome challenges associated with halomethyl pyridine volatility and the expected low product yields.

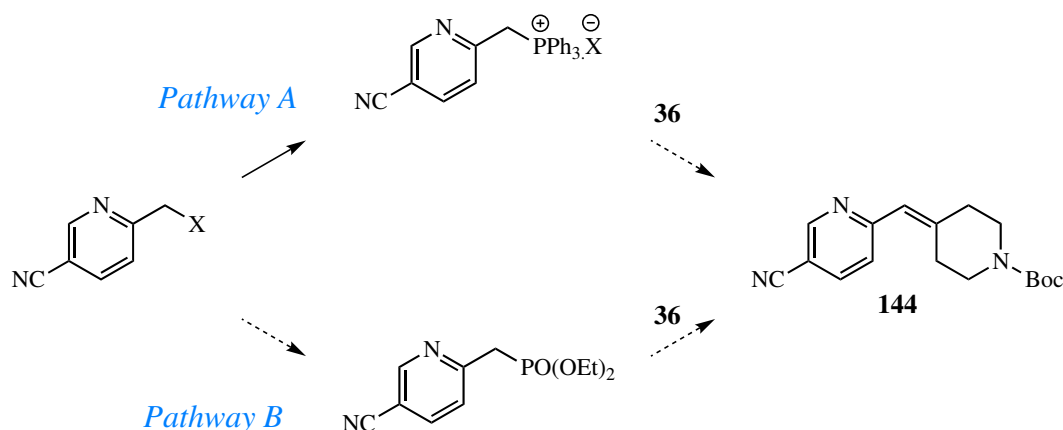


Figure 5.4: Possible synthetic pathways for synthesis of a pyridylmethylene piperidine derivative containing a nitrile substituent. Pathway A involves synthesis of a phosphonium salt followed by Wittig reaction with **36**. Pathway B involves synthesis of a pyridylmethyl phosphonate derivative via Michaelis-Arbusov reaction, followed by Horner-Emmons reaction with **36**. X = Br or Cl.

The Buchwald-Hartwig reaction conditions employed in Chapter 4 were reported as optimised coupling conditions in previous work.<sup>47</sup> However, the substrate used for optimisation of that system<sup>47</sup> was smaller and simpler compared to the structures utilised in the same Buchwald-Hartwig system in Chapter 4, therefore the lower yields observed for synthesis of the complex ligands in Chapter 4 are not surprising. Given the high degree of substrate specificity typically observed in Buchwald-Hartwig coupling reactions,<sup>47,99,100</sup> it is likely that re-optimisation of the Buchwald-Hartwig coupling reaction conditions would be required for synthesis of ligands **90** and **91**, particularly when introducing the 2-amino functionality in the quinoline ring.

In general, synthetic pathways proposed for each of the complex ligands in Chapter 4 involve many synthetic steps which naturally lead to lower overall product yields; rather than attempting to optimise a 9-step synthesis, it may be efficacious to invest in the development of a shorter synthetic pathway to produce each of the complex ligands. While this approach would still likely require optimisation of multiple reaction conditions, this uncertainty can be balanced by the expected increase in overall product yield due to a shorter synthetic pathway and improved stepwise economy.

### 5.5.5 Synthesis of ligands with variable heterocycle geometry

An interesting finding from the complex 6-substituted 2-aminoquinoline ligands in this work was the reduced binding affinities of the benzylpiperazinyl containing ligands (**89** and **100**, compared to the benzylpiperidinyl containing ligands (**88** and **97**). In addition, the methylenepiperidine-containing ligand **97** and its THP isomer **114** exhibited comparable binding affinities for the Tec

## 5.5. PROPOSED FUTURE WORK

---

SH3 domain, suggesting that the slight differences in geometry about the methylenepiperidine and THP rings did not significantly impact the binding interaction. Conversely, it is possible that the reduced binding affinity observed for the benzylpiperazine-containing ligands may be caused by the flatter piperazinyl ring (compared to a piperidine ring), which may not be positioned correctly to facilitate favourable interactions with the protein surface. As PPI surfaces are typically quite flat compared to enzyme active sites, it is possible that the nuances in chair-like geometry of the heterocycles may be substantial with regard to forming favourable interactions with the PPI surface. This provides a strong impetus to investigate the SARs of the cyclic linker group attached to the 6-position of the 2-aminoquinoline ring, as indicated in Figure 5.5.

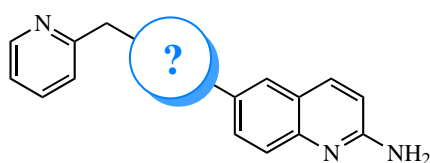


Figure 5.5: General proposed structure indicating the cycloalkyl group to be investigated in 6-substituted 2-aminoquinoline ligands.

To investigate how the planarity of the cycloalkyl group implicates ligand binding to Tec SH3, it would be interesting in the first instance to synthesise and test the binding interaction of ligands such as **151** and **152** (Figure 5.6). These ligands would adopt a more chair-like geometry about the cyclohexane ring compared to piperidine- (**24** and **88**) and piperazine- (**89**) containing ligands.

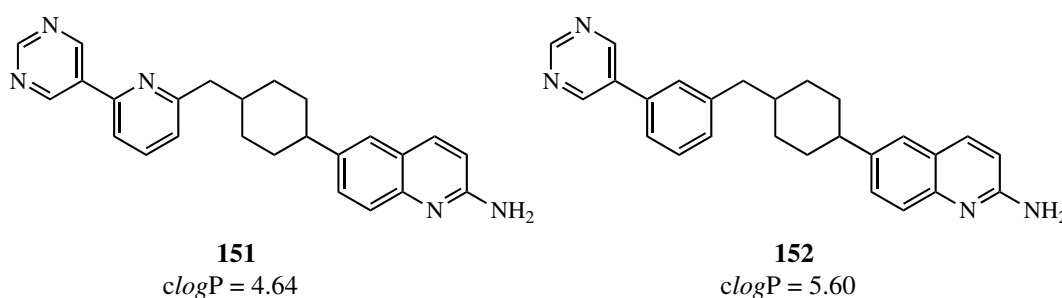


Figure 5.6: Proposed structures of cyclohexane-containing ligands for investigating how chair-like geometry impacts ligand binding affinity for Tec SH3 domain.  $LogP$  values ( $clogP$ ) calculated using Marvin.<sup>61</sup>

The ligands proposed in Figure 5.6 have higher  $clogP$  values compared to similar ligands reported in this thesis, therefore are expected to be more hydrophobic and have reduced (predicted) bioavailability. Given this, **151** and **152** are unlikely to be translated into developable scaffolds, however there is still merit in investigating these ligands as an intellectual endeavour to derive SAR information for the binding interaction.

To complement investigations of planarity, it may be valuable to investigate substitution of the cyclic linker group for a cubane group in 2-aminoquinoline ligands. Cubane has previously been identified as a benzene bioisostere,<sup>134,135</sup> whilst conferring relatively lower *clogP* values compared to benzene in the context of 2-aminoquinoline ligands (Figure 5.7).<sup>61</sup>

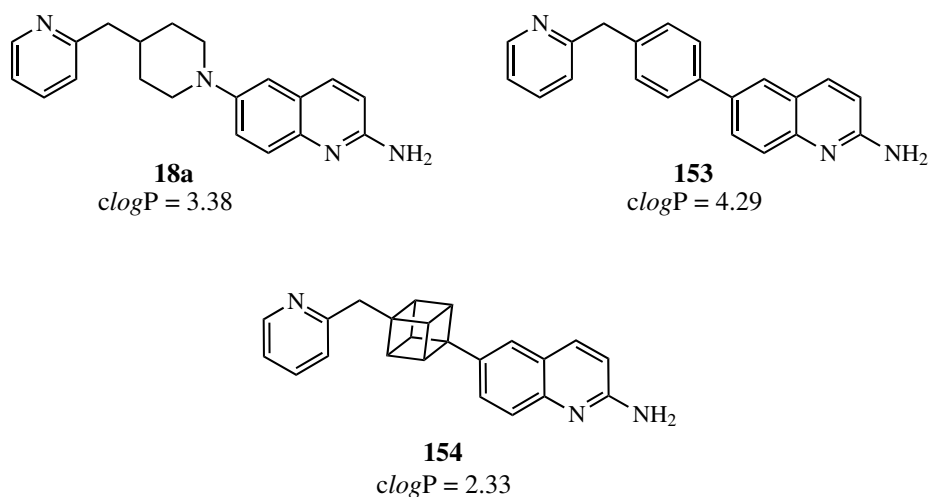


Figure 5.7: Comparison of *clogP* values for 2-aminoquinoline ligands containing variable 6-position substituents. *cLogP* calculated using Marvin.<sup>61</sup>

From a translational perspective, the rigidity of cubane affords a structure which is only slowly metabolised by cytochrome P450s,<sup>134</sup> whilst also providing a unique ligand scaffold to access 3-dimensional space.<sup>135,136</sup> Compared to those ligands shown in Figure 5.6, cubane-containing ligands such as **154** have a much better (predicted) physicochemical profile, and therefore may be suitable, developable scaffolds as small molecule ligands for the Tec SH3 domain.

## 6 | Experimental

### 6.1 General procedures - chemistry

All commercially available reagents and reagent grade solvents were used without further purification, unless otherwise stated. Prior to use, THF and toluene were dried and stored over 4Å molecular sieves, while DCM was dried and stored over 3Å molecular sieves. Triethylamine (TEA) was distilled and stored over 4Å molecular sieves prior to use. Commercially available lithium bis(trimethylsilyl)amide (LiHMDS) was used as a 1.0 M solution in THF. *N*-Bromosuccinimide was recrystallised from water (10 g/100 mL) prior to use.<sup>137</sup> *N*-Chlorosuccinimide was recrystallised from glacial acetic acid prior to use.<sup>138</sup> Pressure tubes (Ace Glass Inc. Vineland USA, cat. no. 8648-04 and 8648-07) were purchased from Sigma-Aldrich.

Reactions progress (where possible) was monitored by thin layer chromatography, using MERCK aluminium-backed silica gel 60 F<sub>254</sub> plates, which were visualised under UV light at 254 nm before staining with KMnO<sub>4</sub> and heating. Flash column chromatography was performed with Kieselgel 60 (40-63 µm) grade silica gel. Where indicated, silica gel was conditioned by addition of 1-2 drops of TEA to the mobile phase prior to product purification by flash column chromatography.

For all substituted 2-aminoquinoline derivatives, CDCl<sub>3</sub> was filtered through basic alumina prior to preparing NMR samples. All NMR spectra were obtained using either an Agilent DD2 NMR spectrometer at 26°C (<sup>1</sup>H NMR [499.818 MHz] and <sup>13</sup>C NMR [125.692 MHz]), or an Agilent DD2 NMR spectrometer (with cryoprobe) at 25°C (<sup>1</sup>H NMR [599.842 MHz] and <sup>13</sup>C NMR [150.842 MHz]) using VnmrR v.4.2 revision A. Spectra of samples were recorded in solutions of CDCl<sub>3</sub> using tetramethylsilane (0.03% v/v) as an internal standard. NMR spectra were processed using MestReNova v.14.0.0-23239 (Mestrelab Research S.L.). The following notations for multiplicities were applied: s (singlet), d (doublet), t (triplet), q (quartet), br (broad), † (unresolved coupling) and ^ (overlapping signals). <sup>1</sup>H and <sup>13</sup>C signals for previously unreported compounds were assigned with the assistance of gCOSY, HSQCAD, gHMQC, gHMBCAD and ROESYAD 2D NMR experiments, where required. Analysis of these combined spectra allowed for the assignment of all signals for compounds with the same general structure. Where required, processing techniques including zero-filling and apodization were applied to aid interpretation of NMR spectra.

HRMS (ESI, positive ion mode) of samples dissolved in acetonitrile or methanol were obtained using an Agilent Series 6230 TOF LC/MS spectrometer, using MassHunter Workstation LC/MS Data Acquisition for 6200 series TOF/6500 series Q-TOF, v. 10.1, build 10.1.48 (Agilent technologies). Mass spectra were processed using MassHunter Workstation Software - Qualitative Analysis v.B.07.00 (Agilent Technologies).

All infrared spectra were obtained using either a Perkin Elmer FT-IR or Shimadzu IR Spirit FT-IR spectrometer. Melting point determinations were conducted using a Stanley Research Systems Digimelt MPA161, at a ramp rate of either 2 or 5 °C/min.

## 6.2 General synthetic methods

### General Method 1: Synthesis of pyridylmethyl triphenylphosphonium salts<sup>56</sup>

The halomethylpyridine hydrohalide derivative (1 eq.) was suspended in toluene (10 mL/1 g reagent). Saturated aqueous NaHCO<sub>3</sub> solution (10 mL/1 g reagent) was carefully added and left until visible signs of the reaction had ceased. The aqueous layer was extracted with toluene (2 x 30 mL), and the combined organic extracts were dried over MgSO<sub>4</sub>, then filtered. Triphenylphosphine (1.5 eq.) was added to the filtrate, and the reaction mixture was heated at reflux for the specified time. The reaction mixture was cooled to 0 °C, then the resulting precipitate was collected by vacuum filtration and used without further purification.

### General Method 2: Synthesis of arylvinyl Boc-protected piperidines via Wittig reaction<sup>56</sup>

The triphenylphosphonium salt (1.4 eq.) was suspended in anhydrous THF and stirred under an atmosphere of nitrogen. The suspension was cooled to 0°C, and LiHMDS (1.0 M in THF, 2 eq.) was added dropwise. The reaction mixture was then warmed to room temperature, and stirred for 15 mins before a solution of *N*-Boc-4-piperidone (1 eq.) in anhydrous THF was added dropwise. The reaction mixture was stirred for the specified time before quenching with MeOH (30 mL), then concentrated under reduced pressure. The resulting residue was suspended in EtOAc/hexanes (2:3, 40 mL) and filtered. The filtrate was concentrated under reduced pressure, then the resulting residue purified by flash column chromatography on silica gel with the specified eluant.

### **General Method 3: Alkene reduction by hydrogenation reaction**

The alkene was dissolved in MeOH and stirred for the specified time under an atmosphere of hydrogen with a catalytic amount of 5% or 10% palladium on carbon catalyst. The reaction mixture was filtered through Celite<sup>®</sup>, washed with MeOH, and the filtrate concentrated under reduced pressure to afford the crude product.

### **General Method 4: TFA-mediated deprotection of Boc-protected amines**

A solution of the Boc-protected amine in DCM (3 mL/100 mg amine) was treated with trifluoroacetic acid (1 mL/100 mg amine) and stirred at room temperature for the specified time. The reaction mixture was cooled to 0°C, partially neutralised with sat. NaHCO<sub>3(aq)</sub> (15 mL), then completely neutralised by addition of NaHCO<sub>3(s)</sub>, followed by extraction with DCM (3 x 20 mL). The combined organic phases were dried over MgSO<sub>4</sub>, filtered, then concentrated under reduced pressure to afford the free amine, used without further purification.

### **General Method 5: Synthesis of 6-substituted-2-chloroquinoline derivatives via selective Buchwald-Hartwig coupling reaction<sup>47</sup>**

A pressure tube was loaded with Pd(OAc)<sub>2</sub> (0.5 mol %), cataCXium<sup>®</sup> A (1 mol %), sodium *tert*-butoxide (1.2 eq.), **26** (1 eq.) and the amine derivative (1.2 eq.). The specified solvent was added, and the pressure tube sealed before heating at 120°C for the specified time. The reaction mixture was cooled to room temperature before opening the pressure tube, then diluting with MeOH and filtering through Celite<sup>®</sup>, washing with MeOH. The filtrate was concentrated under reduced pressure before purification by flash column chromatography on silica gel with the specified eluant.

### **General Method 6: Synthesis of 6-substituted-2-aminoquinoline derivatives via Buchwald-Hartwig amination reaction<sup>47</sup>**

A pressure tube was loaded with Pd(dba)<sub>2</sub> (1 mol %), DavePhos ligand (1.2 mol %) and the 2-chloroquinoline derivative (1 eq.). 1,4-Dioxane was added, followed by LiHMDS solution (1.0 M in THF, 2.2 eq.). The pressure tube was sealed, and the reaction mixture heated for the specified time at 120 °C. The reaction mixture was cooled to room temperature before opening the pressure

tube, then diluting with MeOH and filtering through Celite<sup>®</sup>, washing with MeOH. The filtrate was concentrated under reduced pressure before purification by flash column chromatography on silica gel with the specified eluant.

**General Method 7: Synthesis of aryl(piperazin-1-yl)methanone derivatives via amidation with acyl chlorides**

Under an atmosphere of nitrogen, triethylamine (1.25 eq.) was added to a stirring solution of the amine (1.1 eq.) in anhydrous DCM at room temperature. The reaction mixture was cooled to 0 °C, and the acyl chloride (1 eq.) was added dropwise to the reaction mixture. The reaction mixture was warmed to room temperature, then stirred for the specified time before dilution with DCM. The reaction mixture was washed with 1 N HCl (10 mL) and the organic products extracted with DCM (3 x 10 mL). The combined organic phases were dried over MgSO<sub>4</sub>, filtered, then concentrated under reduced pressure before purification by flash column chromatography on silica gel with the specified eluant.

**General Method 8: Synthesis of phenyl(piperazin-1-yl)methanone derivatives via one-pot amidation from carboxylic acids<sup>101</sup>**

Under an atmosphere of nitrogen, the carboxylic acid (1 eq.) was added to a stirring mixture of the amine (1 eq.) and triethylamine (3 eq. in anhydrous DCM at room temperature. Thionyl chloride (1 eq.) was added dropwise, and the reaction mixture was stirred at room temperature for the specified time. The reaction mixture was diluted with DCM, washed with 1 N HCl followed by 1 N NaOH, then the organic products were extracted with DCM. The combined organic phases were dried over MgSO<sub>4</sub>, filtered, then concentrated under reduced pressure. The resulting residue was purified by flash column chromatography on silica gel with the specified eluant.

**General Method 9: Synthesis of acyl chloride derivatives using oxalyl chloride<sup>102</sup>**

Under an atmosphere of nitrogen, oxalyl chloride (1.1 eq.) was added dropwise to a stirring solution of the carboxylic acid (1 eq.) in anhydrous DCM. A solution of anhydrous DMF (1 mol %) in anhydrous DCM was added dropwise, and the reaction mixture was then stirred at room temperature for the specified time. The crude product was then used without further purification.



### **General Method 10: Synthesis of acyl chloride derivatives using thionyl chloride<sup>104</sup>**

Under an atmosphere of nitrogen, a solution of the carboxylic acid (1 eq.) in  $\text{SOCl}_2$  ( $> 1.5$  eq.) was heated at reflux for the specified time. Excess thionyl chloride was removed via distillation, then  $\sim 1$  mL anhydrous toluene was added to the reaction mixture. The reaction mixture was partially purified by azeotropic distillation with anhydrous toluene, then the crude product was suspended in anhydrous DCM, and used without further purification.

### **General Method 11: Synthesis of phenyl(piperazin-1-yl)methanone derivatives via inverse-addition with acyl chlorides**

Under an atmosphere of nitrogen, a mixture of triethylamine (1.25 eq.) and amine derivative (1.1 eq.) in anhydrous DCM were added dropwise to the acyl chloride (1 eq.) in anhydrous DCM, at  $0^\circ\text{C}$ . The reaction mixture was warmed to room temperature, then stirred for the specified time before dilution with DCM. The reaction mixture was washed with 1 N HCl (10 mL) and extracted with DCM (3 x 10 mL). The organic phases were dried over  $\text{MgSO}_4$ , filtered, then concentrated under reduced pressure before purification by flash column chromatography on silica gel with the specified eluant.

### **General Method 12: Synthesis of phenyl(piperazin-1-yl)methanone derivatives via one-pot sequential amidation from carboxylic acids**

Under an atmosphere of nitrogen,  $\text{SOCl}_2$  (1.5 eq.) was added to the carboxylic acid derivative (1 eq.) suspended in anhydrous DCM at  $0^\circ\text{C}$ . The reaction mixture was warmed to room temperature and stirred for the specified time. Triethylamine (3 eq.) was added to the reaction mixture, followed by a solution of the amine (1.2 eq.) in anhydrous DCM. The reaction mixture was stirred at room temperature for 1 hr, then washed with water (10 mL) and the organic products were extracted with DCM (2 x 15 mL). The organic phases were combined, dried over  $\text{MgSO}_4$ , filtered, then concentrated under reduced pressure. The product was purified by flash column chromatography on silica gel with the specified eluant.

**General Method 13: Synthesis of arylmethyl piperazin-1-yl derivatives via reductive amination**<sup>113,114</sup>

Under an atmosphere of nitrogen, the amine (1 eq.) and aldehyde derivative (1.1 eq.) were dissolved in anhydrous DCM. Glacial acetic acid (1.2-2.0 eq.) was added, and the reaction mixture was then stirred at room temperature for 1 hr. The reaction mixture was cooled to 0 ° C, before sodium triacetoxyborohydride (~1.5 eq.) was added. The reaction mixture was warmed to room temperature, and the reaction progress was monitored by TLC. The reaction mixture was washed with sat. NH<sub>4</sub>Cl<sub>(aq)</sub> and the organic products were extracted with DCM. The organic phases were combined, dried over MgSO<sub>4</sub>, filtered, then concentrated under reduced pressure. The product was purified by flash column chromatography on silica gel with the specified eluant.

**General Method 14: Synthesis of benzylpiperazinyl-2-chloroquinoline derivatives via alkylation**<sup>123</sup>

Under an atmosphere of nitrogen, a solution of the piperazine derivative (1 eq.) was added to anhydrous potassium carbonate (1.2 eq.) in anhydrous DCM. The reaction mixture was cooled to 0° C, and the arylmethyl halide derivative (1.2 eq.) was added dropwise. The reaction mixture was warmed to room temperature, then stirred for the specified period before quenching with sat. NaHCO<sub>3(aq)</sub>. The organic products were extracted with DCM (3 x 20 mL), then the combined organic phases were dried over MgSO<sub>4</sub>, filtered, and concentrated under reduced pressure. The product was purified by flash column chromatography on silica gel with the specified eluant.

**General Method 15: Synthesis of amide derivatives via nitrile hydrolysis**<sup>115</sup>

The nitrile derivative (1 eq.) was suspended in *t*-butanol, and stirred at room temperature. Finely crushed potassium hydroxide (~4 eq.) was then added to the nitrile suspension, and the reaction mixture was heated at reflux, monitoring by TLC. Once the nitrile had been consumed, the reaction mixture was cooled to room temperature, then poured into brine (10 mL). The amide-containing organic products were extracted with 3:1 chloroform/isopropanol (3 x 20 mL), then the combined organic phases were dried over MgSO<sub>4</sub>, filtered then concentrated under reduced pressure. The product was purified by column chromatography on silica gel with the specified eluant.

### **General Method 16: Synthesis of benzyltriphenylphosphonium salts**

Triphenylphosphine (1.2 eq.) was added to a solution of benzyl halide derivative (1 eq.) in toluene. The reaction mixture was heated at reflux for the specified time, then cooled to room temperature. The reaction mixture was further cooled to 0 °C, and the resulting precipitate was collected by vacuum filtration to afford the benzyltriphenylphosphonium salt, which was used without further purification.

### **General Method 17: Synthesis of biaryl benzylidene Boc-protected piperidines via Suzuki coupling reaction<sup>56</sup>**

The aryl halide derivative (1 eq.), boronic acid derivative (1.2 eq.), potassium carbonate (1.5 eq.), Pd(OAc)<sub>2</sub> (3 mol %) and triphenylphosphine (5 mol %) were combined in a pressure tube. The reactants were dissolved in the specified solvent, and the pressure tube was sealed before heating at 120°C for the specified time. The reaction mixture was then cooled to room temperature before opening the pressure tube, diluting with MeOH, and filtering through Celite<sup>®</sup>, washing with MeOH. The filtrate was concentrated under reduced pressure, and the product purified by flash column chromatography on silica gel with the specified eluant.

### **General Method 18: Synthesis of arylmethyl bromide derivatives via radical bromination**

Under an atmosphere of nitrogen, the tolyl derivative (1 eq.), *N*-bromosuccinimide (1.1 eq.) and benzoyl peroxide (variable mol %) in anhydrous BTF were stirred at the specified temperature for the specified period. The reaction mixture was cooled to room temperature, diluted with DCM, washed with sat. NaHCO<sub>3(aq.)</sub> (8 mL) the organic products were extracted with DCM (2 x 15 mL). The combined organic phases were dried over MgSO<sub>4</sub>, filtered, then concentrated under reduced pressure. The product was purified by flash column chromatography on silica gel with the specified eluant.

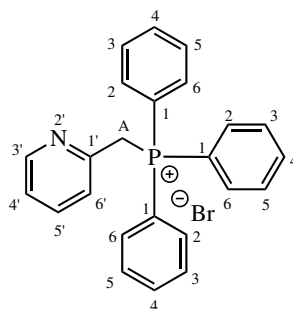
### **General Method 19: Synthesis of arylmethyl chloride derivatives via radical chlorination**

Under an atmosphere of nitrogen, the tolyl derivative (1 eq.), *N*-chlorosuccinimide (1.1 eq.) and benzoyl peroxide (5 mol %) in anhydrous BTF were stirred at the specified temperature for the specified period. The reaction mixture was cooled to room temperature, then filtered.

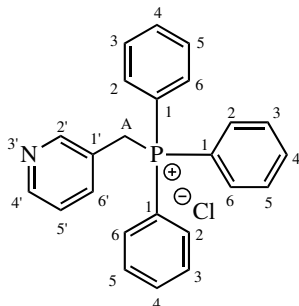
## 6.3 Synthesis of control ligands

### 6.3.1 Synthesis of arylmethyl and arylmethylene piperidine derivatives

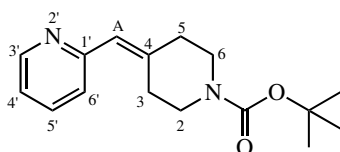
#### Triphenyl(pyridin-2-ylmethyl)phosphonium bromide (30a)<sup>56,66</sup>



2-(Bromomethyl)pyridine hydrobromide (2.52 g, 9.97 mmol) and triphenylphosphine (3.18 g, 12.1 mmol) in toluene (65 mL) were reacted using General Method 1 for 3 hrs to afford the title compound as an off-white solid (3.37 g, 78%). <sup>1</sup>H NMR (CDCl<sub>3</sub>, 500 MHz); δ<sub>H</sub>: 5.72 [2H, d, *J*<sub>H,P</sub> = 14.5 Hz, C(A)H], 7.10 [1H, dd, *J*<sub>4',5'</sub> = 7.6 Hz; *J*<sub>4',3'</sub> = 5.1 Hz, C(4')H], 7.57 [1H, t, *J*<sub>5',6'</sub> = *J*<sub>5',4'</sub> = 7.7 Hz, C(5')H], 7.61 [6H, td, *J*<sub>3,4/5,4</sub> = *J*<sub>3,2/5,6</sub> = 7.7 Hz; *J*<sub>H,P</sub> = 3.5 Hz, C(3/5)H], 7.70-7.76 [3H, m, C(4)H], 7.85 [6H, dd, *J*<sub>2,3/6,5</sub> = 7.7 Hz; *J*<sub>H,P</sub> = 13.5 Hz, C(2/6)H], 8.00 [1H, dd, *J*<sub>6',5'</sub> = 7.7 Hz; *J*<sub>H,P</sub> = 1.5 Hz, C(6')H], 8.23 [1H, dd, *J*<sub>3',4'</sub> = 5.1 Hz; *J*<sub>H,P</sub> = 1.8 Hz, C(3')H]. <sup>13</sup>C NMR (CDCl<sub>3</sub>, 125 MHz); δ<sub>C</sub>: 33.1 [d, *J*<sub>C,P</sub> = 51.7 Hz, C(A)], 119.2 [d, *J*<sub>C,P</sub> = 87.3 Hz, C(1)], 123.0 [d, *J*<sub>C,P</sub> = 2.2 Hz, C(4')], 127.4 [d, *J*<sub>C,P</sub> = 7.6 Hz, C(5')], 130.0 [d, *J*<sub>C,P</sub> = 12.8 Hz, C(3/5)], 134.5 [d, *J*<sub>C,P</sub> = 10.0 Hz, C(2/6)], 134.7 [d, *J*<sub>C,P</sub> = 3.0 Hz, C(4)], 137.5 [br s<sup>†</sup>, C(6')], 148.7 [d, *J*<sub>C,P</sub> = 1.9 Hz, C(3')], 150.0 [d, *J*<sub>C,P</sub> = 8.7 Hz, C(1')].

**Triphenyl(pyridin-3-ylmethyl)phosphonium chloride (30b)**<sup>56,66</sup>

3-(Chloromethyl)pyridine hydrochloride (3.03 g, 18.5 mmol) and triphenylphosphine (7.21 g, 27.5 mmol) in toluene (90 mL) were reacted using General Method 1 for 19 hrs to afford the title compound as a pale pink solid (2.29 g, 32%). <sup>1</sup>H NMR (CDCl<sub>3</sub>, 500 MHz); δ<sub>H</sub>: 5.82 [2H, d,  $J_{\text{H,P}} = 14.5$  Hz, C(A)H], 7.09 [1H, dd,  $J_{5',6'} = 7.9$  Hz;  $J_{5',4'} = 4.6$  Hz, C(5')H], 7.63 [6H, td,  $J_{3,4/5,4} = J_{3,2/5,6} = 7.8$  Hz;  $J_{\text{H,P}} = 3.5$  Hz, C(3/5)H], 7.73-7.79 [3H, m<sup>†</sup>, C(4)H], 7.79-7.87 [6H, m<sup>†</sup>, C(2/6)H], 7.93 [1H, dq,  $J_{6,5'} = 7.9$  Hz;  $J_{6',4'} = J_{6',2'} = J_{\text{H,P}} = 2.1$  Hz, C(6')H], 8.10 [1H, m<sup>†</sup>, C(2')H], 8.42 [1H, dt,  $J_{4',5'} = 4.6$  Hz;  $J_{4',2'} = J_{4',6'} = 2.1$  Hz, C(4')H]. <sup>13</sup>C NMR (CDCl<sub>3</sub>, 125 MHz); δ<sub>C</sub>: 28.0 [d,  $J_{\text{C,P}} = 47.5$  Hz, C(A)], 117.8 [d,  $J_{\text{C,P}} = 85.9$  Hz, C(1)], 123.9 [d,  $J_{\text{C,P}} = 3.0$  Hz, C(5')], 124.8 [d,  $J_{\text{C,P}} = 8.4$  Hz, C(1')], 130.4 [d,  $J_{\text{C,P}} = 12.6$  Hz, C(3/5)], 134.6 [d,  $J_{\text{C,P}} = 10.0$  Hz, C(2/6)], 135.2 [d,  $J_{\text{C,P}} = 3.1$  Hz, C(4)], 140.2 [d,  $J_{\text{C,P}} = 5.5$  Hz, C(6')], 149.4 [d,  $J_{\text{C,P}} = 4.3$  Hz, C(4')], 151.4 [d,  $J_{\text{C,P}} = 5.6$  Hz, C(2')].

**tert-Butyl 4-(pyridin-2-ylmethylene)piperidine-1-carboxylate (40a)**<sup>56,66</sup>

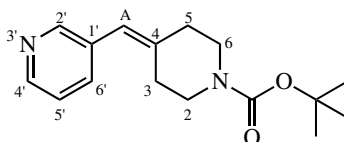
**30a** (1.00 g, 2.30 mmol), LiHMDS (1.0 M in THF) (3.4 mL, 3.4 mmol) and *N*-Boc-4-piperidone (0.337 g, 1.69 mmol) in anhydrous THF (10 mL) were reacted using General Method 2 for 4 hrs at room temperature. The crude product was purified by flash column chromatography on silica gel, eluting with 20% EtOAc in hexanes to afford the title compound as a white powder (0.291 g, 63%\*). HRMS: C<sub>16</sub>H<sub>22</sub>N<sub>2</sub>O<sub>2</sub> [M+H]<sup>+</sup>-C(CH<sub>3</sub>)<sub>3</sub> requires 219.1128; found 219.1133. <sup>1</sup>H NMR (CDCl<sub>3</sub>, 500 MHz); δ<sub>H</sub>: 1.48 [9H, s, C(CH<sub>3</sub>)<sub>3</sub>], 2.33-2.40 [2H, m<sup>†</sup>, C(3)H<sub>ax/eq</sub>], 2.81-2.88 [2H, m<sup>†</sup>, C(5)H<sub>ax/eq</sub>], 3.42-3.50 [2H, m<sup>†</sup>, C(2)H<sub>ax/eq</sub>], 3.51-3.58 [2H, m<sup>†</sup>, C(6)H<sub>ax/eq</sub>], 6.37 [1H, s, H(A)], 7.07 [1H, dd,  $J_{4',5'} = 7.7$  Hz;  $J_{4',3'} = 4.8$  Hz, C(4')H], 7.14 [1H, d,  $J_{6',5'} = 7.7$  Hz, C(6')H], 7.62

[1H, t,  $J_{5',4'} = J_{5',6'} = 7.7$  Hz, C(5')H], 8.57 [1H, d,  $J_{3',4'} = 4.8$  Hz, C(3')H].  $^{13}\text{C}$  NMR ( $\text{CDCl}_3$ , 125 MHz);  $\delta_{\text{C}}$ : 28.6 [CH<sub>3</sub>], 29.5 [C(3)], 36.8 [C(5)], 43.3-46.9 [br m, C(2); C(6)], 79.7 [ $\underline{\text{C}}(\text{CH}_3)_3$ ], 121.1 [C(4')], 124.2 [C(A); C(6')\*\*], 136.2 [C(5')], 143.3 [C(4)], 149.3 [C(2')], 154.9 [C=O], 156.7 [C(1')].

\* <2% *N*-Boc-4-piperidone present by  $^1\text{H}$  NMR analysis.

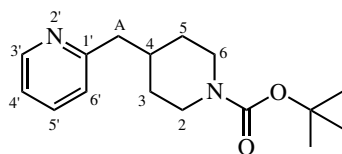
\*\* denotes overlapping signals in  $^{13}\text{C}$  NMR.

***tert*-Butyl 4-(pyridin-3-ylmethylene)piperidine-1-carboxylate (40b)**<sup>56,66</sup>



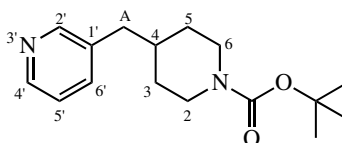
**30b** (0.892 g, 2.29 mmol), LiHMDS (1.0 M in THF) (3.4 mL, 3.40 mmol) and *N*-Boc-4-piperidone (0.335 g, 1.68 mmol) in anhydrous THF (10 mL) were reacted using General Method 2 for 15 hrs at room temperature. The crude product was purified by flash column chromatography on silica gel, eluting with 40% EtOAc/hexanes to afford the title compound as a yellow oil (0.288 g, 62%\*). HRMS: C<sub>16</sub>H<sub>22</sub>N<sub>2</sub>O<sub>2</sub> [M+H]<sup>+</sup> requires 275.1754; found 275.1754.  $^1\text{H}$  NMR ( $\text{CDCl}_3$ , 500 MHz);  $\delta_{\text{H}}$ : 1.48 [9H, s, C(CH<sub>3</sub>)<sub>3</sub>], 2.36 [2H, t<sup>†</sup>,  $J_{3\text{ax},3\text{eq}} = J_{3\text{ax}/3\text{eq},2\text{ax}/2\text{eq}} = 5.9$  Hz, C(3)H<sub>ax/eq</sub>], 2.43 [2H, t<sup>†</sup>,  $J_{5\text{ax},5\text{eq}} = J_{5\text{ax}/5\text{eq},6\text{ax}/6\text{eq}} = 5.9$  Hz, C(5)H<sub>ax/eq</sub>], 3.42 [2H, t<sup>†</sup>,  $J_{2\text{ax},2\text{eq}} = J_{2\text{ax}/2\text{eq},3\text{ax}/3\text{eq}} = 5.9$  Hz, C(2)H<sub>ax/eq</sub>], 3.52 [2H, t<sup>†</sup>,  $J_{6\text{ax},6\text{eq}} = J_{6\text{ax}/6\text{eq},5\text{ax}/5\text{eq}} = 5.9$  Hz, C(6)H<sub>ax/eq</sub>], 6.30 [1H, s, C(A)H], 7.25 [1H, ddd,  $J_{5',6'} = 7.9$  Hz;  $J_{5',4'} = 4.8$  Hz;  $J_{5',2'} = 0.9$  Hz, C(5')H], 7.49 [1H, dt,  $J_{6',5'} = 7.9$  Hz;  $J_{6',4'} = J_{6',2'} = 1.9$  Hz, C(6')H], 8.43-8.49 [2H, m<sup>^</sup>, C(2')H; C(4')H].  $^{13}\text{C}$  NMR ( $\text{CDCl}_3$ , 125 MHz);  $\delta_{\text{C}}$ : 28.6 [CH<sub>3</sub>], 29.5 [C(3)], 36.3 [C(5)], 43.3-46.4 [br m<sup>^</sup>, C(2); C(6)], 79.8 [ $\underline{\text{C}}(\text{CH}_3)_3$ ], 121.0 [C(A)], 123.2 [C(5')], 133.2 [C(1')], 136.1 [C(6')], 141.3 [C(4)], 147.6 [C(4')], 150.1 [C(2')], 154.8 [C=O].

\*Some triphenylphosphine oxide byproduct was present by  $^1\text{H}$  NMR analysis.

**tert-Butyl 4-(pyridin-2-ylmethyl)piperidine-1-carboxylate (54a)**

A catalytic amount of 5% Pd on carbon was added to **40a** (291 mg, 106  $\mu\text{mol}$ ) in MeOH (10 mL), and reacted via General Method 3 for 3 hrs to afford the title compound as an orange oil, which was used without further purification (281 mg, 96%). HRMS:  $\text{C}_{16}\text{H}_{24}\text{N}_2\text{O}_2$   $[\text{M}+\text{H}]^+$  requires 277.1911; found 277.1910.  $^1\text{H}$  NMR ( $\text{CDCl}_3$ , 500 MHz);  $\delta_{\text{H}}$ : 1.20 [2H, qd,  $J_{3/5\text{ax},3/5\text{eq}} = J_{3/5\text{ax},2/6\text{ax}} = J_{3/5\text{ax},4\text{ax}} = 12.6$  Hz;  $J_{3/5\text{ax},2/6\text{eq}} = 4.4$  Hz, C(3/5) $\text{H}_{\text{ax}}$ ], 1.45 [9H, s, C(CH<sub>3</sub>)<sub>3</sub>], 1.60 [2H, d<sup>†</sup>,  $J_{3/5\text{eq},3/5\text{ax}} = 12.6$  Hz, C(3/5) $\text{H}_{\text{eq}}$ ], 1.89-1.99 [1H, m<sup>†</sup>, C(4) $\text{H}_{\text{ax}}$ ], 2.69-2.75 [2H, m<sup>†</sup>, C(2/6) $\text{H}_{\text{ax}}$ ], 2.71 [2H, d,  $J_{\text{A},4\text{ax}} = 7.2$  Hz, CH<sub>2</sub>], 3.95-4.16 [2H, br s<sup>†</sup>, C(2/6) $\text{H}_{\text{eq}}$ ], 7.07-7.15 [2H, m<sup>^</sup>, C(4')H; C(6')H], 7.60 [1H, td,  $J_{5',4'} = 7.7$  Hz;  $J_{5',3'} = 1.7$  Hz, C(5')H], 8.53 [1H, d<sup>†</sup>,  $J_{3',4'} = 4.8$  Hz, C(3')H].  $^{13}\text{C}$  NMR ( $\text{CDCl}_3$ , 125 MHz);  $\delta_{\text{C}}$ : 28.5 [CH<sub>3</sub>], 32.1 [C(3/5)], 36.9 [C(4)], 42.8-45.0 [br s, C(2/6)], 45.3 [C(A)], 79.4 [C(CH<sub>3</sub>)<sub>3</sub>], 121.3 [C(4')\*/C(6')\*], 123.8 [C(4')\*/C(6')\*], 136.4 [C(5')], 149.4 [C(3')], 15.0 [C=O], 160.3 [C(1')].

\* denotes that overlapping signals in  $^1\text{H}$  NMR precluded unambiguous signal assignment in 2D NMR spectra.

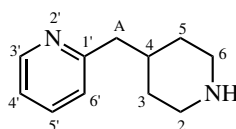
**tert-Butyl 4-(pyridin-3-ylmethyl)piperidine-1-carboxylate (54b)**

A catalytic amount of 5% Pd on carbon was added to **40b** (271 mg, <988  $\mu\text{mol}^*$ ) in MeOH (10 mL), and reacted via General Method 3 for 2 hrs to afford the title compound as an orange oil, used without further purification (181 mg, >66%<sup>\*</sup>). HRMS:  $\text{C}_{16}\text{H}_{24}\text{N}_2\text{O}_2$   $[\text{M}+\text{H}]^+$  requires 277.1911; found 277.1908.  $^1\text{H}$  NMR ( $\text{CDCl}_3$ , 500 MHz);  $\delta_{\text{H}}$ : 1.16 [2H, qd,  $J_{3/5\text{ax},3/5\text{eq}} = J_{3/5\text{ax},2/6\text{ax}} = J_{3/5\text{ax},4\text{ax}} = 12.3$  Hz;  $J_{3/5\text{ax},2/6\text{eq}} = 4.3$  Hz, C(3/5) $\text{H}_{\text{ax}}$ ], 1.45 [9H, s, C(CH<sub>3</sub>)<sub>3</sub>], 1.60-1.72 [3H, m<sup>^</sup>, C(3/5) $\text{H}_{\text{eq}}$ ; C(4) $\text{H}_{\text{ax}}$ ], 2.54 [2H, d,  $J_{4\text{ax},\text{A}} = 7.1$  Hz, C(A)H], 2.64 [2H, br t<sup>†</sup>,  $J_{2/6\text{ax},2/6\text{eq}} = J_{2/6\text{ax},3/5\text{ax}} = 12.3$  Hz, C(2/6) $\text{H}_{\text{ax}}$ ], 3.95-4.16 [2H, br s<sup>†</sup>, C(2/6) $\text{H}_{\text{eq}}$ ], 7.22 [1H, dd,  $J_{5',6'} = 7.6$  Hz;  $J_{5',4'} = 4.5$  Hz, C(5')H], 7.43-7.50 [1H, m<sup>†</sup>, C(6')H], 8.41 [1H, s<sup>†</sup>, C(2')H], 8.45 [1H, d,  $J_{4',5'} = 4.5$  Hz, C(4')H].  $^{13}\text{C}$

NMR (CDCl<sub>3</sub>, 125 MHz);  $\delta_C$ : 28.5 [CH<sub>3</sub>], 31.9 [C(3/5)], 38.0 [C(4)], 40.2 [C(A)], 44.0 [C(2/6)], 79.4 [C(CH<sub>3</sub>)<sub>3</sub>], 123.3 [C(5')], 135.5 [C(1')], 136.6 [C(6')], 147.6 [C(4')], 150.5 [C(2')], 154.9 [C=O].

\* indicates residual triphenylphosphine oxide was present in starting material from previous reactions; calculated yield is a theoretical minimum.

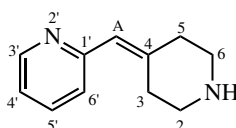
### 2-(Piperidin-4-ylmethyl)pyridine (55a)



Trifluoroacetic acid (1.4 mL, 18.3 mmol) and **54a** (148.2 mg, 53.6  $\mu$ mol) in DCM (4 mL) were reacted via General Method 4 for 1 hr, to afford the title compound as an orange oil (67.3 mg, 74% over two steps). HRMS: C<sub>11</sub>H<sub>6</sub>N<sub>2</sub> [M+H]<sup>+</sup> requires 177.1386; found 177.1388. <sup>1</sup>H NMR (CDCl<sub>3</sub>, 500 MHz);  $\delta_H$ : 1.55 [2H, qd,  $J_{3/5ax,3/5eq} = J_{3/5ax,2/6ax} = J_{3/5ax,4ax} = 13.0$  Hz;  $J_{3/5ax,2/6eq} = 4.1$  Hz, C(3/5)H<sub>ax</sub>], 1.79 [2H, d<sup>†</sup>,  $J_{3/5eq,3/5ax} = 13.0$  Hz, C(3/5)H<sub>eq</sub>], 2.06-2.16 [1H, m, C(4)H<sub>ax</sub>], 2.75 [2H, d,  $J_{A,4ax} = 7.2$  Hz, CH<sub>2</sub>], 2.79 [2H, dt,  $J_{2/6ax,2/6eq} = J_{2/6ax,3/5ax} = 13.0$  Hz;  $J_{2/6ax,4ax} = 2.9$  Hz, C(2/6)H<sub>ax</sub>], 3.32 [2H, br d<sup>†</sup>,  $J_{2/6eq,3/5eq} = 13.0$  Hz, C(2/6)H<sub>eq</sub>], 4.72-5.51 [1H, br s, NH], 7.10 [1H, d,  $J_{6',5'} = 7.7$  Hz, C(6')H], 7.13 [1H, dd,  $J_{4',5'} = 7.7$  Hz;  $J_{4',3'} = 5.0$  Hz, C(4')H], 7.60 [1H, dt,  $J_{5',6'} = J_{5',4'} = 7.7$  Hz;  $J_{5',3'} = 1.8$  Hz, C(5')H], 8.54 [1H, d<sup>†</sup>,  $J_{3',4'} = 5.0$  Hz, C(3')H]. <sup>13</sup>C NMR (CDCl<sub>3</sub>, 125 MHz);  $\delta_C$ : 29.5 [C(3/5)], 35.0 [C(4)], 44.6 [C(2/6)], 44.7 [C(A)], 121.6 [C(4'')\*/C(6'')\*], 124.0 [C(4')\*/C(6')\*], 136.5 [C(5')], 144.9 [C(3')], 159.3 [C(1')].

\* denotes that overlapping signals in <sup>1</sup>H NMR precluded unambiguous signal assignment in 2D NMR spectra.

### 2-(Piperidin-4-ylidenemethyl)pyridine (44a)<sup>66</sup>



Trifluoroacetic acid (1.6 mL, 20.9 mmol) and **40a** (176.9 mg, 64.5  $\mu$ mol) in DCM (4 mL) were reacted via General Method 4 for 2 hr, to afford the title compound as a yellow oil, which was used without further purification (57.2 mg, 51%). HRMS: C<sub>11</sub>H<sub>14</sub>N<sub>2</sub> [M+H]<sup>+</sup> requires 175.1230; found

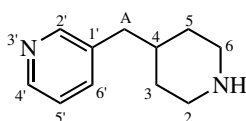


### 6.3. SYNTHESIS OF CONTROL LIGANDS

---

175.1232.  $^1\text{H}$  NMR ( $\text{CDCl}_3$ , 500 MHz);  $\delta_{\text{H}}$ : 2.40-2.48 [2H, m $^\dagger$ , C(5) $\text{H}_{\text{ax/eq}}$ ], 2.90-2.96 [2H, m $^\dagger$ , C(3) $\text{H}_{\text{ax/eq}}$ ], 2.96-3.02 [2H, m $^\dagger$ , C(2) $\text{H}_{\text{ax/eq}}$ ], 3.04-3.09 [2H, m $^\dagger$ , C(6) $\text{H}_{\text{ax/eq}}$ ], 4.49 [1H, br s, NH], 6.32 [1H, s, C(A)H], 7.08 [1H, dd,  $J_{4',5'} = 7.6$  Hz;  $J_{4',3'} = 5.0$  Hz, C(4')H], 7.14 [1H, d,  $J_{6,5'} = 7.6$  Hz, C(6')H], 7.61 [1H, t,  $J_{5',6'} = J_{5',4'} = 7.6$  Hz, C(5')H], 8.56 [1H, d,  $J_{3',4'} = 5.0$  Hz, C(3')H].  $^{13}\text{C}$  NMR ( $\text{CDCl}_3$ , 125 MHz);  $\delta_{\text{C}}$ : 29.8 [C(3)], 37.2 [C(5)], 46.9 [C(2)], 47.7 [C(6)], 121.0 [C(4')], 123.7 [C(A)], 124.1 [C(6')], 136.1 [C(5')], 142.8 [C(4)], 149.1 [C(3')], 156.5 [C(1')].

#### 3-(Piperidin-4-ylmethyl)pyridine (**55b**)

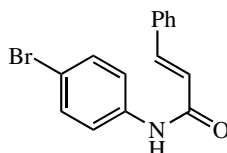


Trifluoroacetic acid (2 mL, 26.1 mmol) and **54b** (181 mg, <65.5  $\mu\text{mol}^*$ ) in DCM (4 mL) were reacted via General Method 4 for 2 hr, to afford the title compound as an orange oil (71.7 mg, >62% $^*$ ). HRMS:  $\text{C}_{11}\text{H}_{16}\text{N}_2$  [ $\text{M}+\text{Na}$ ] $^+$  requires 199.1201; found 199.1211.  $^1\text{H}$  NMR ( $\text{CDCl}_3$ , 500 MHz);  $\delta_{\text{H}}$ : 1.28-1.40 [2H, m $^\dagger$ , C(3/5) $\text{H}_{\text{ax}}$ ], 1.63-1.76 [3H, m $^\wedge$ , C(3/5) $\text{H}_{\text{eq}}$ ; C(4) $\text{H}_{\text{ax}}$ ], 2.55 [2H, d,  $J_{\text{A},4_{\text{ax}}} = 6.8$  Hz, C(A)H], 2.65 [2H, br t $^\dagger$ ,  $J_{2/6_{\text{ax}},2/6_{\text{eq}}} = J_{2/6_{\text{ax}},3/5_{\text{ax}}} = 12.5$  Hz, C(2/6) $\text{H}_{\text{ax}}$ ], 3.11-3.31 [3H, m $^\wedge$ , C(2/6) $\text{H}_{\text{eq}}$ ; NH], 7.22 [1H, dd,  $J_{5',6'} = 7.8$  Hz;  $J_{5',4'} = 4.8$  Hz, C(5')H], 7.43-7.50 [1H, m, C(6')H], 8.40 [1H, br d $^\dagger$ ,  $J_{2',6'} = 2.2$  Hz, C(2')H], 8.45 [1H, d,  $J_{4',5'} = 4.8$  Hz, C(4')H].  $^{13}\text{C}$  NMR ( $\text{CDCl}_3$ , 125 MHz);  $\delta_{\text{C}}$ : 31.3 [C(3/5)], 37.3 [C(4)], 40.3 [C(A)], 45.5 [C(2/6)], 123.4 [C(5')], 135.3 [C(1')], 136.7 [C(6')], 147.7 [C(4')], 150.4 [C(2')].

\* indicates residual triphenylphosphine oxide was present in starting material from previous reactions calculated yield is a theoretical minimum.

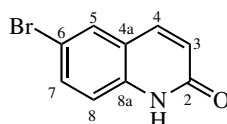
### 6.3.2 Synthesis of arylmethyl and arylmethylene piperidine 2-chloroquinoline derivatives

#### *N*-(4-Bromophenyl)cinnamamide (**47**)<sup>94</sup>



Cinnamoyl chloride (10.07 g, 60.4 mmol) in DCM was added dropwise to DMAP (0.734 g, 6.01 mmol), pyridine (4.8 mL, 59.6 mmol) and DCM at 0°C under an atmosphere of nitrogen. The reaction mixture was stirred for 15 mins before a solution of 4-bromoaniline (10.4 g, 60.5 mmol) in DCM was added dropwise. The reaction mixture was stirred for 15 minutes at 0°C, then stirred for a further 30 mins at room temperature. The resulting precipitate was collected via Buchner filtration and washed with DCM to afford the title compound as an off-white powder, m.p. 190-192 °C (lit.,<sup>94</sup> 193-194 °C), (10.26 g, 57%). HRMS: C<sub>15</sub>H<sub>12</sub>BrNO [M+H]<sup>+</sup> requires 302.0175 [<sup>79</sup>Br] / 304.0155 [<sup>81</sup>Br]; found 302.0176/304.0157. <sup>1</sup>H NMR (CDCl<sub>3</sub>, 500 MHz); δ<sub>H</sub>: 6.54 [1H, d, *J* = 15.5 Hz, =CH], 7.34-7.57 [10H, m, Ar H's; NH], 7.76 [1H, d, *J* = 15.5 Hz, =CH].

#### 6-Bromoquinolin-2(1*H*)-one (**48**)<sup>94</sup>



*Synthetic pathway A:* Aluminium chloride (14.4 g, 108 mmol) and **47** (10.01 g, 33.1 mmol) were ground together in a mortar and pestle to form an intimate mixture. The reaction mixture was transferred to a RBF and heated rapidly with a heat gun to melting, then maintained at 110°C for 1.5 hr. The reaction mixture was cooled to 0°C and quenched with ice water. The resulting precipitate was collected via Buchner filtration, washing with ice-cold water to afford a 1:1 mixture of **48** and **49** as a pink solid, which was used without further purification (9.02 g).

*Synthetic pathway B:* A suspension of aluminium chloride (19.5 g, 146 mmol) and **47** (7.11 g, 23.5 mmol) in chlorobenzene (50 mL) were heated at reflux for 1.5 hrs. The reaction mixture was cooled to room temperature, then the reaction mixture was carefully added to ice water. The precipitate

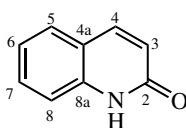
### 6.3. SYNTHESIS OF CONTROL LIGANDS

---

was collected via Buchner filtration and washed with water to afford a 5:2 mixture of **48** and **49** as a light brown solid, which was used without further purification (5.20 g).

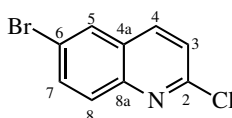
**48**: HRMS: C<sub>9</sub>H<sub>6</sub>BrNO [M+H]<sup>+</sup> requires 223.9706 [<sup>79</sup>Br] / 225.9685 [<sup>81</sup>Br]; found 223.9702 / 225.9683. <sup>1</sup>H NMR (CDCl<sub>3</sub>, 500 MHz); δ<sub>H</sub>: 6.73 [1H, d, J<sub>3,4</sub> = 9.6 Hz, C(3)H], 7.24-7.31 [1H, m<sup>^</sup>, C(8)H], 7.59 [1H, dd, J<sub>7,8</sub> = 8.8 Hz; J<sub>7,5</sub> = 2.2 Hz, C(7)H], 7.70-7.75 [1H, m<sup>^</sup>, C(5)H; C(4)H], 11.80 [1H, br s, NH].

#### Quinolin-2(1H)-one (**49**)



HRMS: C<sub>9</sub>H<sub>7</sub>NO<sub>2</sub> [M+H]<sup>+</sup> requires 146.0600; found 146.0598. <sup>1</sup>H NMR (CDCl<sub>3</sub>, 500 MHz); δ<sub>H</sub>: 6.70 [1H, d, J<sub>3,4</sub> = 9.6 Hz, C(3)H], 7.23 [1H, t, J<sub>6,5</sub> = J<sub>6,7</sub> = 7.9 Hz, C(6)H], 7.35 [1H, d, J<sub>8,7</sub> = 7.9 Hz, C(8)H], 7.52 [1H, t, J<sub>7,6</sub> = J<sub>7,8</sub> = 7.9 Hz, C(7)H], 7.57 [1H, d, J<sub>5,6</sub> = 7.9 Hz, C(5)H], 7.81 [1H, d, J<sub>4,3</sub> = 9.6 Hz, C(4)H], 11.30 [1H, br s, NH].

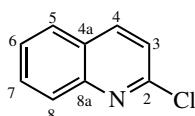
#### 6-Bromo-2-chloroquinoline (**26**)<sup>94,95</sup>



An impure mixture of **48** and **49** (5.20 g) and phosphorus oxychloride (20.0 mL, 215 mmol) were heated at reflux for 1 hr. The reaction mixture was cooled to room temperature, then slowly quenched with ice water. The resulting precipitate was collected via Buchner filtration\*, washing with ice water. The precipitate was purified by flash column chromatography on silica gel, eluting with 20% hexanes in DCM to afford the title compound as a pink powder, m.p. 158-160 °C (lit.,<sup>94</sup> 159-160 °C), (3.04 g, 53% over two steps). HRMS: C<sub>9</sub>H<sub>5</sub>BrClN [M+H]<sup>+</sup> requires 241.9367 [<sup>79</sup>Br, <sup>35</sup>Cl] / 243.9337 [<sup>79</sup>Br, <sup>37</sup>Cl] / 243.9346 [<sup>81</sup>Br, <sup>35</sup>Cl] / 245.9317 [<sup>81</sup>Br, <sup>37</sup>Cl]; found 241.9367 / 243.9345 / 243.3945 / 245.9319. <sup>1</sup>H NMR (CDCl<sub>3</sub>, 600 MHz); δ<sub>H</sub>: 7.42 [1H, d, J<sub>3,4</sub> = 8.6 Hz, C(3)H], 7.81 [1H, dd, J<sub>7,8</sub> = 9.0 Hz; J<sub>7,5</sub> = 2.2 Hz, C(7)H], 7.90 [1H, d, J<sub>8,7</sub> = 9.0 Hz, C(8)H], 7.99 [1H, d, J<sub>5,7</sub> = 2.2 Hz, C(5)H], 8.03 [1H, d, J<sub>4,3</sub> = 8.6 Hz, C(4)H].

\* The filtrate from the Buchner filtration was extracted with DCM (3 x 20 mL), then the organic phases were combined, dried over MgSO<sub>4</sub>, filtered and concentrated under reduced pressure to afford crude **155** with **49** as a yellow/brown solid.

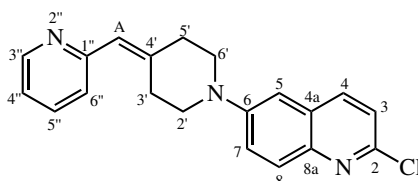
### 2-Chloroquinoline (**155**)



HRMS: C<sub>9</sub>H<sub>6</sub>ClN [M+H]<sup>+</sup> requires 164.0267 [<sup>35</sup>Cl] / 166.0238 [<sup>37</sup>Cl]; found 164.0263 / 166.0235.

<sup>1</sup>H NMR (CDCl<sub>3</sub>, 500 MHz); δ<sub>H</sub>: 7.39 [1H, d, J<sub>3,4</sub> = 8.6 Hz, C(3)H], 7.57 [1H, ddd, J<sub>6,5</sub> = 8.1 Hz; J<sub>6,7</sub> = 6.9 Hz; J<sub>6,8</sub> = 0.8 Hz, C(6)H], 7.75 [1H, ddd<sup>†</sup>, J<sub>7,8</sub> = 8.6 Hz; J<sub>7,6</sub> = 6.9 Hz; J<sub>7,5</sub> = 1.5 Hz, C(7)H], 7.82 [1H, dd<sup>†</sup>, J<sub>5,6</sub> = 8.1 Hz; J<sub>5,7</sub> = 1.5 Hz, C(5)H], 8.03 [1H, dq, J<sub>8,7</sub> = 8.6 Hz; J<sub>8,6</sub> = J<sub>8,5</sub> = J<sub>8,4</sub> = 0.8 Hz, C(8)H], 8.11 [1H, dd, J<sub>4,3</sub> = 8.6 Hz; J<sub>4,8</sub> = 0.8 Hz, C(4)H].

### 2-Chloro-6-(4-(pyridin-2-ylmethylene)piperidin-1-yl)quinoline (**50a**)



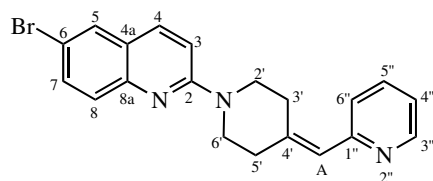
Sodium *tert*-butoxide (44.5 mg, 46.3 μmol), **44a** (57.2 mg, 32.8 μmol), **26** (99.7 mg, 41.1 μmol), cataCXium<sup>®</sup> A (2.5 mg, 6.97 μmol), Pd(OAc)<sub>2</sub> (1.1 mg, 4.90 μmol) and anhydrous BTF (3 mL) were reacted via General Method 5 for 16 hr. The crude product was purified by flash column chromatography on silica gel, eluting with 0.5 % MeOH in DCM to afford the title compound as a yellow oil (20.8 mg, 19%) and minor product **52a** as a yellow oil (not quantified).

**50a**: HRMS: C<sub>20</sub>H<sub>18</sub>ClN<sub>3</sub> [M+H]<sup>+</sup> requires 336.1262 [<sup>35</sup>Cl] / 338.1233 [<sup>37</sup>Cl]; found 334.1254 / 338.1240. <sup>1</sup>H NMR (CDCl<sub>3</sub>, 600 MHz); δ<sub>H</sub>: 2.57-2.63 [2H, m<sup>†</sup>, C(5')H<sub>ax/eq</sub>], 3.08-3.12 [2H, m<sup>†</sup>, C(3')H<sub>ax/eq</sub>], 3.41-3.46 [2H, m<sup>†</sup>, C(2')H<sub>ax/eq</sub>], 3.49-3.54 [2H, m<sup>†</sup>, C(6')H<sub>ax/eq</sub>], 6.42 [1H, s, C(A)H], 7.02 [1H, d, J<sub>5,7</sub> = 2.7 Hz, C(5)H], 7.11 [1H, d, J<sub>4'',5''</sub> = 7.7 Hz; J<sub>4'',3''</sub> = 4.9 Hz, C(4'')H], 7.18 [1H, d, J<sub>6'',5''</sub> = 7.7 Hz, C(6'')H], 7.28 [1H, d, J<sub>3,4</sub> = 8.6 Hz, C(3)H], 7.53 [1H, dd, J<sub>7,8</sub> = 9.3 Hz; J<sub>7,5</sub> = 2.7 Hz, C(7)H], 7.64 [1H, dt, J<sub>5'',6''</sub> = J<sub>5'',4''</sub> = 7.7 Hz; J<sub>5'',3''</sub> = 1.6 Hz, C(5'')H], 7.88 [1H, d, J<sub>8,7</sub> = 9.3 Hz, C(8)H], 7.91 [1H, d, J<sub>4,3</sub> = 8.6 Hz, C(4)H], 8.60 [1H, d<sup>†</sup>, J<sub>3'',4''</sub> = 4.9 Hz, C(3'')H]. <sup>13</sup>C NMR

### 6.3. SYNTHESIS OF CONTROL LIGANDS

(CDCl<sub>3</sub>, 150 MHz);  $\delta_{\text{C}}$ : 29.1 [C(3')], 36.4 [C(5')], 50.0 [C(2')], 51.0 [C(6')], 108.9 [C(5)], 121.2 [C(4'')], 122.5 [C(3)], 123.5 [C(7)], 123.9 [C(A)], 124.2 [C(6'')], 128.3 [C(4a)], 129.4 [C(8)], 136.2 [C(5'')], 137.5 [C(4)], 143.0 [C(8a)], 143.2 [C(4')], 147.4 [C(2)], 149.4 [C(3'')], 149.4 [C(6)], 156.8 [C(1'')].

#### 6-Bromo-2-(4-(pyridin-2-ylmethylene)piperidin-1-yl)quinoline (52a)

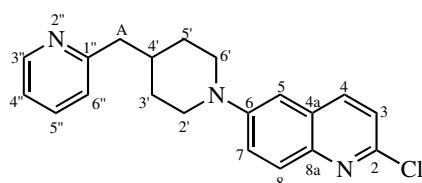


HRMS: C<sub>20</sub>H<sub>18</sub>BrN<sub>3</sub> [M+H]<sup>+</sup> requires 380.0757 [<sup>79</sup>Br] / 382.0736 [<sup>81</sup>Br]; found 380.0749/382.0738.

<sup>1</sup>H NMR (CDCl<sub>3</sub>, 500 MHz);  $\delta_{\text{H}}$ : 2.51-2.57 [2H, m<sup>†</sup>, C(5')H<sub>ax/eq</sub>], 2.99-3.05 [2H, m<sup>†</sup>, C(3')H<sub>ax/eq</sub>], 3.80-3.84 [2H, m<sup>†</sup>, C(2')H<sub>ax/eq</sub>], 3.89-3.95 [2H, m<sup>†</sup>, C(6')H<sub>ax/eq</sub>], 6.43 [1H, s, C(A)H], 7.03 [1H, d,  $J_{3,4} = 9.2$  Hz, C(3)H], 7.10 [1H, ddd,  $J_{4'',5''} = 7.7$  Hz;  $J_{4'',3''} = 4.8$  Hz;  $J_{4'',6''} = 1.0$  Hz, C(4'')H], 7.18 [1H, br d<sup>†</sup>,  $J_{6'',5''} = 7.7$  Hz, C(6'')H], 7.55 [1H, d,  $J_{8,7} = 8.9$  Hz, C(8)H], 7.57 [1H, dd,  $J_{7,8} = 8.9$  Hz;  $J_{7,5} = 1.9$  Hz, C(7)H], 7.63 [1H, td,  $J_{5'',4''} = J_{5'',6''} = 7.7$  Hz;  $J_{5'',3''} = 1.8$  Hz, C(5'')H], 7.72 [1H, d,  $J_{5,7} = 1.9$  Hz, C(5)H], 7.78 [1H, d,  $J_{4,3} = 9.2$  Hz, C(4)H], 8.59 [1H, d<sup>†</sup>,  $J_{3'',4''} = 4.8$  Hz, C(3'')H]. <sup>13</sup>C NMR (CDCl<sub>3</sub>, 125 MHz);  $\delta_{\text{C}}$ : 29.4 [C(3')], 36.5 [C(5')], 45.8 [C(2')], 46.8 [C(6')], 110.5 [C(3)], 115.0 [C(6)], 121.1 [C(4'')], 124.1 [C(A)\*C(6'')\*C(4a)\*], 124.2 [C(A)\*C(6'')\*C(4a)\*], 124.2 [C(A)\*C(6'')\*C(4a)\*], 128.4 [C(8)], 129.3 [C(5)], 132.7 [C(7)], 136.2 [C(5'')], 143.7 [C(4')], 147.0 [C(8a)], 149.4 [C(3'')], 156.8 [C(1'')], 157.2 [C(2)].

\* denotes that overlapping signals in <sup>13</sup>C NMR precluded unambiguous signal assignment in 2D NMR spectra.

#### 2-Chloro-6-(4-(pyridin-2-ylmethyl)piperidin-1-yl)quinoline (56a)

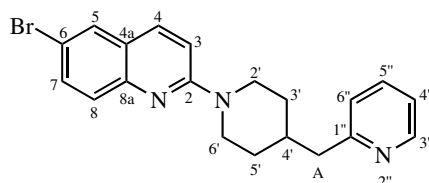


Sodium *tert*-butoxide (55.5 mg, 57.7  $\mu$ mol), **55a** (67.3 mg, 38.2  $\mu$ mol), **26** (115 mg, 47.6  $\mu$ mol), cataCXium<sup>®</sup> A (1.6 mg, 4.46  $\mu$ mol), Pd(OAc)<sub>2</sub> (0.6 mg, 2.67  $\mu$ mol) and anhydrous BTF (2 mL)

were reacted via General Method 5 for 16 hr. The crude product was purified by flash column chromatography on silica gel, eluting with 0.5% MeOH in DCM to afford the title compound as a yellow oil (13.8 mg, 11%) and minor product **57a** as a yellow oil.

**56a**: HRMS:  $C_{20}H_{20}ClN_3$   $[M+H]^+$  requires 338.1419 [ $^{35}Cl$ ] / 340.1389 [ $^{37}Cl$ ]; found 338.1412 / 340.1400.  $^1H$  NMR ( $CDCl_3$ , 500 MHz);  $\delta_H$ : 1.50 [2H, qd,  $J_{3'/5'_{ax},3'/5'_{eq}} = J_{3'/5'_{ax},2'/6'_{ax}} = J_{3'/5'_{ax},4'_{ax}} = 12.7$  Hz;  $J_{3'/5'_{ax},2'/6'_{eq}} = 4.0$  Hz,  $C(3'/5')$ H $_{ax}$ ], 1.80 [2H, br d $^\dagger$ ,  $J_{3'/5'_{eq},3'/5'_{ax}} = 12.7$  Hz,  $C(3'/5')$ H $_{eq}$ ], 1.99-2.09 [1H, m $^\dagger$ ,  $C(4')$ H $_{ax}$ ], 2.76-2.84 [4H, m $^\wedge$ , CH $_2$ ;  $C(2'/6')$ H $_{ax}$ ], 3.81 [2H, br d $^\dagger$ ,  $J_{2'/6'_{eq},3'/5'_{eq}} = 12.7$  Hz,  $C(2'/6')$ H $_{eq}$ ], 6.99 [1H, d,  $J_5 = 2.6$  Hz,  $C(5)$ H], 7.12-7.16 [2H, m $^\wedge$ ,  $C(4'')$ H;  $C(6'')$ H], 7.26 [1H, d,  $J_{3,4} = 8.6$  Hz,  $C(3)$ H], 7.49 [1H, dd,  $J_{7,8} = 9.3$  Hz;  $J_7 = 2.6$  Hz,  $C(7)$ H], 7.61 [1H, dt,  $J_{5'',6''} = J_{5'',4''} = 7.7$  Hz;  $J_{5'',3''} = 1.8$  Hz,  $C(5'')$ H], 7.85 [1H, d,  $J_{8,7} = 9.3$  Hz,  $C(8)$ H], 7.89 [1H, d,  $J_{4,3} = 8.6$  Hz,  $C(4)$ H], 8.56-8.59 [1H, m $^\dagger$ ,  $C(3'')$ H].  $^{13}C$  NMR ( $CDCl_3$ , 125 MHz);  $\delta_C$ : 32.0 [ $C(3'/5')$ ], 36.7 [ $C(4')$ ], 45.4 [ $C(A)$ ], 49.8 [ $C(2'/6')$ ], 109.0 [ $C(5)$ ], 121.3 [ $C(4'')$ ], 122.4 [ $C(3)$ ], 123.8 [ $C(7)$ ], 123.8 [ $C(6'')$ ], 128.3 [ $C(4a)$ ], 129.2 [ $C(8)$ ], 136.3 [ $C(5'')$ ], 137.5 [ $C(4)$ ], 143.1 [ $C(8a)$ ], 147.3 [ $C(2)$ ], 149.6 [ $C(3'')$ ], 150.2 [ $C(6)$ ], 160.4 [ $C(1'')$ ].

*6-Bromo-2-(4-(pyridin-2-ylmethyl)piperidin-1-yl)quinoline (57a)*:



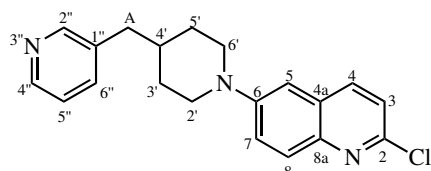
HRMS:  $C_{20}H_{20}BrN_3$   $[M+H]^+$  requires 382.0913 [ $^{79}Br$ ]/384.0893 [ $^{81}Br$ ]; found 382.0907/384.0892.  $^1H$  NMR ( $CDCl_3$ , 500 MHz);  $\delta_H$ : 1.36 [2H, qd,  $J_{3'/5'_{ax},3'/5'_{eq}} = J_{3'/5'_{ax},2'/6'_{ax}} = J_{3'/5'_{ax},4'_{ax}} = 12.9$  Hz;  $J_{3'/5'_{ax},2'/6'_{eq}} = 4.0$  Hz,  $C(3'/5')$ H $_{ax}$ ], 1.77 [2H, d $^\dagger$ ,  $J_{3'/5'_{eq},3'/5'_{ax}} = 12.9$  Hz,  $C(3'/5')$ H $_{eq}$ ], 2.06-2.19 [1H, m,  $C(4')$ H $_{ax}$ ], 2.74 [2H, d,  $J_{A,4'_{ax}} = 7.2$  Hz, CH $_2$ ], 2.92 [2H, dt,  $J_{2'/6'_{ax},2'/6'_{eq}} = J_{2'/6'_{ax},3'/5'_{ax}} = 12.9$  Hz;  $J_{2'/6'_{ax},4'_{ax}} = 2.3$  Hz,  $C(2'/6')$ H $_{ax}$ ], 4.52 [2H, d $^\dagger$ ,  $J_{2'/6'_{eq},3'/5'_{eq}} = 12.9$  Hz,  $C(2'/6')$ H $_{eq}$ ], 6.97 [1H, d,  $J_{3,4} = 9.2$  Hz,  $C(3)$ H], 7.08-7.16 [2H, m $^\wedge$ ,  $C(4'')$ H;  $C(6'')$ H], 7.52 [1H, d,  $J_{8,7} = 8.9$  Hz,  $C(8)$ H], 7.55 [1H, dd,  $J_{7,8} = 8.9$  Hz;  $J_{7,5} = 2.0$  Hz,  $C(7)$ H], 7.59 [1H, dt,  $J_{5'',6''} = J_{5'',4''} = 7.6$  Hz;  $J_{5'',3''} = 1.6$  Hz,  $C(5'')$ H], 7.69 [1H, d,  $J_{5,7} = 2.0$  Hz,  $C(5)$ ], 7.73 [1H, d,  $J_{4,3} = 9.2$  Hz,  $C(4)$ ], 8.57 [1H, d $^\dagger$ ,  $J_{3'',4''} = 4.8$  Hz,  $C(3'')$ H].  $^{13}C$  NMR ( $CDCl_3$ , 125 MHz);  $\delta_C$ : 32.1 [ $C(3'/5')$ ], 37.2 [ $C(4')$ ], 45.5 [ $C(A)$ ], 45.6 [ $C(2'/6')$ ], 110.7 [ $C(3)$ ], 114.8 [ $C(6)$ ], 121.3 [ $C(4'')$ ], 123.8 [ $C(6'')$ ],

### 6.3. SYNTHESIS OF CONTROL LIGANDS

---

124.1 [C(4a)], 128.4 [C(8)], 129.2 [C(5)], 132.6 [C(7)], 136.3 [C(5'')], 136.4 [C(4)], 147.0 [C(8a)], 149.6 [C(3'')], 157.6 [C(2)], 160.4 [C(1'')].

#### 2-Chloro-6-(4-(pyridin-3-ylmethyl)piperidin-1-yl)quinoline (56b)

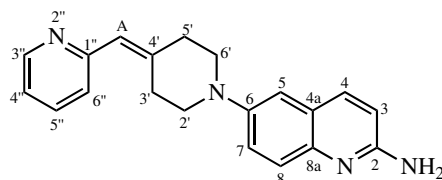


Sodium *tert*-butoxide (51.0 mg, 531  $\mu\text{mol}$ ), **156a** (71.7 mg, <407  $\mu\text{mol}^*$ ), **26** (117 mg, 484  $\mu\text{mol}$ ), cataCXium<sup>®</sup> A (20 mg, 5.58  $\mu\text{mol}$ ), Pd(OAc)<sub>2</sub> (12 mg, 5.35  $\mu\text{mol}$ ) and anhydrous BTF (2 mL) were reacted via General Method 5 for 16 hr. The crude product was purified by flash column chromatography on silica gel, eluting with 1% MeOH in DCM to afford the title compound as a yellow oil (36 mg, >26%<sup>\*</sup>) HRMS: C<sub>20</sub>H<sub>20</sub>ClN<sub>3</sub> [M+H]<sup>+</sup> requires 338.1419 [<sup>35</sup>Cl] /340.1389 [37Cl]; found 338.1413 / 340.1390. <sup>1</sup>H NMR (CDCl<sub>3</sub>, 500 MHz);  $\delta_{\text{H}}$ : 1.46 [2H, qd,  $J_{3'/5'\text{ax},3'/5'\text{eq}} = J_{3'/5'\text{ax},2'/6'\text{ax}} = J_{3'/5'\text{ax},4'\text{ax}} = 12.5$  Hz;  $J_{3'/5'\text{ax},2'/6'\text{eq}} = 4.1$  Hz, C(3'/5')H<sub>ax</sub>], 1.69-1.83 [3H, m<sup>^</sup>, C(3'/5')H<sub>eq</sub>; C(4')H<sub>ax</sub>], 2.61 [2H, d,  $J_{\text{A},4'\text{ax}} = 7.0$  Hz, CH<sub>2</sub>], 2.77 [2H, dt,  $J_{2'/6'\text{ax},2'/6'\text{eq}} = J_{2'/6'\text{ax},3'/5'\text{ax}} = 12.5$  Hz;  $J_{2'/6'\text{ax},4'\text{ax}} = 2.5$  Hz, C(2'/6')H<sub>ax</sub>], 3.82 [2H, d<sup>†</sup>,  $J_{2'/6'\text{eq},3'/5'\text{eq}} = 12.5$  Hz, C(2'/6')H<sub>eq</sub>], 6.99 [1H, d,  $J_{5,7} = 2.7$  Hz, C(5)H], 7.21-7.27 [1H, m, C(5'')H], 7.27 [1H, d,  $J_{3,4} = 8.6$  Hz, C(3)H], 7.44-7.50 [1H, m<sup>†</sup>, C(7)H], 7.86 [1H, d,  $J_{8,7} = 9.3$  Hz, C(8)H], 7.90 [1H, d,  $J_{4,3} = 8.6$  Hz, C(4)H], 8.44-8.55 [2H, m<sup>^</sup>, C(2'')H; C(4'')H].

\* indicates residual triphenylphosphine oxide was present in starting material from previous reactions calculated yield is a theoretical minimum.

### 6.3.3 Synthesis of arylmethyl and arylmethylene piperidine 2-aminoquinoline derivatives

#### 6-(4-(Pyridin-2-ylmethylene)piperidin-1-yl)quinolin-2-amine (35a)



DavePhos (0.8 mg, 2.03  $\mu\text{mol}$ ,  $\text{Pd}(\text{dba})_2$  (0.7 mg, 1.22  $\mu\text{mol}$ ), **50a** (20.8 mg, 61.9  $\mu\text{mol}$ ) and LiH-MDS solution (1.0 M in THF, 0.19 mL, 0.19 mmol) in 1,4-dioxane (2 mL) were reacted via General Method 6 for 16 hrs. The crude product was purified by flash column chromatography on silica gel, eluting with 10% MeOH in DCM to afford the title compound as a yellow oil (3.8 mg, 19%) and **53a** as a yellow oil (2.5 mg, 13%).

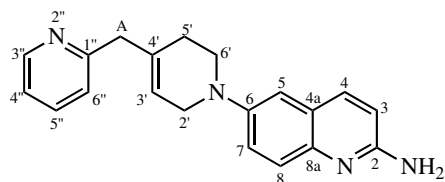
**35a**: HRMS:  $\text{C}_{20}\text{H}_{20}\text{N}_4$   $[\text{M}+\text{H}]^+$  requires 317.1761; found 317.1761.  $^1\text{H}$  NMR ( $\text{CDCl}_3$ , 500 MHz);  $\delta_{\text{H}}$ : 2.57-2.62 [2H, m $^\dagger$ , C(5'')H $_{\text{ax/eq}}$ ], 3.06-3.10 [2H, m $^\dagger$ , C(3'')H $_{\text{ax/eq}}$ ], 3.30-3.33 [2H, m $^\dagger$ , C(2'')H $_{\text{ax/eq}}$ ], 3.38-3.42 [2H, m $^\dagger$ , C(6'')H $_{\text{ax/eq}}$ ], 5.30 [2H, br s, NH $_2$ ], 6.41 [1H, s, C(A)H], 6.72 [1H, d,  $J_{3,4} = 8.9$  Hz, C(3)H], 6.99 [1H, d,  $J_{5,7} = 2.7$  Hz, C(5)H], 7.10 [1H, dd,  $J_{4'',5''} = 7.5$  Hz;  $J_{4'',3''} = 4.9$  Hz, C(4'')H], 7.18 [1H, d,  $J_{6'',5''} = 7.9$  Hz, C(6'')H], 7.40 [1H, dd,  $J_{7,8} = 9.2$  Hz;  $J_{7,5} = 2.7$  Hz, C(7)H], 7.61-7.66 [2H, m $^\wedge$ , C(8)H; C(5'')H], 7.80 [1H, d,  $J_{4,3} = 8.9$  Hz, C(4)H], 8.59 [1H, d,  $J_{3'',4''} = 4.9$  Hz, C(3'')H].  $^{13}\text{C}$  NMR ( $\text{CDCl}_3$ , 125 MHz);  $\delta_{\text{C}}$ : 29.3 [C(3')], 36.7 [C(5')], 51.2 [C(2')], 52.1 [C(6')], 111.5 [C(5)], 112.2 [C(3)], 121.1 [C(4'')], 123.7 [C(A)\*/C(7)\*], 123.7 [C(A)\*/C(7)\*] 123.8 [C(4a)], 124.2 [C(6'')], 125.4 [C(8)], 136.2 [C(5'')], 138.4 [C(4)], 140.3 [C(8a)], 143.6 [C(4')], 147.4 [C(6)], 149.4 [C(3'')], 155.1 [C(2)], 156.9 [C(1'')].

\* denotes that overlapping signals in  $^{13}\text{C}$  NMR precluded unambiguous signal assignment in 2D NMR spectra.



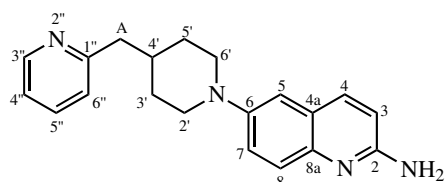
### 6.3. SYNTHESIS OF CONTROL LIGANDS

#### 6-(4-(Pyridin-2-ylmethyl)-5,6-dihydropyridin-1(2H)-yl)quinolin-2-amine (**53a**)



HRMS:  $C_{20}H_{20}N_4$   $[M+H]^+$  requires 317.1761; found 317.1763.  $^1H$  NMR ( $CDCl_3$ , 500 MHz);  $\delta_H$ : 2.25 [2H, br  $s^\dagger$ ,  $C(6')H_{ax/eq}$ ], 3.39 [2H, t,  $J_{5'ax/eq,6'ax/eq} = 5.7$  Hz,  $C(5')H_{ax/eq}$ ], 3.58 [2H, s,  $C(A)H$ ], 3.75 [2H, br  $s^\dagger$ ,  $C(2')H_{ax/eq}$ ], 5.30 [2H, br s,  $NH_2$ ], 5.62 [1H, br s,  $C(3')H$ ], 6.71 [1H, d,  $J_{3,4} = 8.9$  Hz,  $C(3)H$ ], 6.93 [1H, br  $s^\dagger$ ,  $C(5)H$ ], 7.10-7.17 [1H,  $m^\dagger$ ,  $C(4'')H$ ], 7.21 [1H, d,  $J_{6'',5''} = 7.7$  Hz,  $C(6'')H$ ], 7.36 [1H,  $d^\dagger$ ,  $J_{7,8} = 9.0$  Hz,  $C(7)H$ ], 7.60 [1H, d,  $J_{8,7} = 9.0$  Hz,  $C(8)H$ ], 7.63 [1H, t,  $J_{5'',4''} = J_{5'',6''} = 7.4$  Hz,  $C(5'')H$ ], 7.79 [1H, d,  $J_{4,3} = 8.9$  Hz,  $C(4)H$ ], 8.56 [1H, d,  $J_{3'',4''} = 4.9$  Hz,  $C(3'')H$ ].  $^{13}C$  NMR ( $CDCl_3$ , 125 MHz);  $\delta_C$ : 29.1 [ $C(5')$ ], 46.3 [ $C(A)$ ], 46.6 [ $C(6')$ ], 48.7 [ $C(2')$ ], 110.2 [ $C(5)$ ], 112.2 [ $C(3)$ ], 121.2 [ $C(3')$ ], 121.5 [ $C(4'')$ ], 122.5 [ $C(7)$ ], 123.4 [ $C(6'')$ ], 124.1 [ $C(4a)$ ], 125.7 [ $C(8)$ ], 135.2 [ $C(4')$ ], 136.6 [ $C(5'')$ ], 138.4 [ $C(4)$ ], 139.9 [ $C(8a)$ ], 147.6 [ $C(6)$ ], 154.9 [ $C(2)$ ], 159.9 [ $C(3'')$ ], 159.6 [ $C(1'')$ ].

#### 6-(4-(Pyridin-2-ylmethyl)piperidin-1-yl)quinolin-2-amine (**18a**)

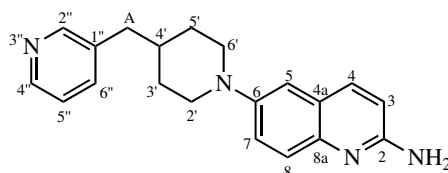


DavePhos (0.5 mg, 1.27  $\mu$ mol),  $Pd(dba)_2$  (0.5 mg, 0.87  $\mu$ mol), **56a** (13.8 mg, 40.8  $\mu$ mol) and LiH-MDS solution (1.0 M in THF, 0.12 mL, 0.12 mmol) in 1,4-dioxane (2 mL) were reacted via General Method 6 for 16 hrs. The crude product was purified by flash column chromatography on silica gel, eluting with 10% MeOH in DCM to afford the title compound as a yellow oily solid (5.7 mg, 44%). HRMS:  $C_{20}H_{22}N_4$   $[M+H]^+$  requires 319.1917; found 319.1918.  $^1H$  NMR ( $CDCl_3$ , 500 MHz);  $\delta_H$ : 1.52 [2H, qd,  $J_{3'/5'ax,3'/5'eq} = J_{3'/5'ax,2'/6'ax} = J_{3'/5'ax,4'ax} = 12.4$  Hz;  $J_{3'/5'ax,2'/6'eq} = 4.0$  Hz,  $C(3'/5')H_{ax}$ ], 1.80 [2H, br  $d^\dagger$ ,  $J_{3'/5'eq,3'/5'ax} = 12.4$  Hz,  $C(3'/5')H_{eq}$ ], 1.93-2.04 [1H,  $m^\dagger$ ,  $C(4')H_{ax}$ ], 2.71 [2H, dt,  $J_{2'ax/6'ax,2'eq/6'eq} = J_{2'ax/6'ax,3'ax/5'ax} = 12.4$  Hz;  $J_{2'ax/6'ax,4'ax} = 2.5$  Hz,  $C(2'/6')H_{ax}$ ], 2.78 [2H, d,  $J_{A,4'ax} = 7.1$  Hz,  $C(A)H$ ], 3.68 [2H, br  $d^\dagger$ ,  $J_{2'/6'eq,3'/5'eq} = 12.4$  Hz,  $C(2'/6')H_{eq}$ ], 4.90 [2H, br s,  $NH_2$ ], 6.69 [1H, d,  $J_{3,4} = 8.8$  Hz,  $C(3)H$ ], 6.96 [1H, d,  $J_{5,7} = 2.6$  Hz,  $C(5)H$ ], 7.10-

7.17 [2H, m<sup>^</sup>, C(4'')H; C(6'')H], 7.36 [1H, dd,  $J_{7,8} = 9.2$  Hz;  $J_{7,5} = 2.6$  Hz, C(7)H], 7.57 [1H, d,  $J_{8,7} = 9.2$  Hz, C(8)H], 7.61 [1H, td,  $J_{5'',4''} = J_{5'',6''} = 7.7$  Hz;  $J_{5'',3''} = 1.8$  Hz, C(5'')H], 7.78 [1H, d,  $J_{4,3} = 8.8$  Hz, C(4)H], 8.57 [1H, d<sup>†</sup>,  $J_{3'',4''} = 4.7$  Hz, C(3'')H]. <sup>13</sup>C NMR (CDCl<sub>3</sub>, 125 MHz); δ<sub>C</sub>: 32.3 [C(3'/5')], 36.7 [C(4')], 45.5 [C(A)], 50.8 [C(2'/6')], 111.4 [C(5)], 111.9 [C(3)], 121.3 [C(4'')], 123.9 [C(6'')\*C(7)\*], 123.9 [C(6'')\*C(7)\*], 124.2 [C(4a)], 126.0 [C(8)]. 136.3 [C(5'')], 137.9 [C(4)], 141.4 [C(8a)], 148.0 [C(6)], 149.6 [C(3'')], 155.2 [C(2)], 160.6 [C(1'')].

\* denotes that overlapping signals in <sup>1</sup>H NMR precluded unambiguous signal assignment in 2D NMR spectra.

### 6-(4-(Pyridin-3-ylmethyl)piperidin-1-yl)quinolin-2-amine (18b)



DavePhos (0.9 mg, 2.29 μmol), Pd(dba)<sub>2</sub> (0.9 mg, 1.57 μmol), **56b** (36 mg, <107 μmol<sup>\*</sup>) and LiH-MDS solution (1.0 M in THF, 0.3 mL, 0.3 mmol) in 1,4-dioxane (2 mL) were reacted via General Method 6 for 16 hrs. The crude product was purified by flash column chromatography on silica gel, eluting with 6% MeOH in DCM to afford the title compound as a yellow powder (6.3 mg, >19%<sup>\*§</sup>). HRMS: C<sub>20</sub>H<sub>22</sub>N<sub>4</sub> [M+H]<sup>+</sup> requires 319.1917; found 319.1926. <sup>1</sup>H NMR (CDCl<sub>3</sub>, 500 MHz); δ<sub>H</sub>: 1.48 [2H, qd,  $J_{3'/5'ax,3'/5'eq} = J_{3'/5'ax,2'/6'ax} = J_{3'/5'ax,4'ax} = 12.1$  Hz;  $J_{3'/5'ax,2'/6'eq} = 4.0$  Hz, C(3'/5')H<sub>ax</sub>], 1.70 [1H, m, C(4')H<sub>ax</sub>], 1.78 [2H, br d<sup>†</sup>,  $J_{3'/5'eq,3'/5'ax} = 12.1$  Hz, C(3'/5')H<sub>eq</sub>], 2.61 [2H, d,  $J_{A,4'ax} = 7.1$  Hz, C(A)H], 2.68 [2H, dt,  $J_{2'ax/6'ax,2'eq/6'eq} = J_{2'ax/6'ax,3'ax/5'ax} = 12.1$  Hz;  $J_{2'ax/6'ax,4'ax} = 2.5$  Hz, C(2'/6')H<sub>ax</sub>], 3.69 [2H, br d<sup>†</sup>,  $J_{2'/6'eq,3'/5'eq} = 12.1$  Hz, C(2'/6')H<sub>eq</sub>], 5.00 [2H, br s, NH<sub>2</sub>], 6.70 [1H, d,  $J_{3,4} = 8.8$  Hz, C(3)H], 6.96 [1H, d,  $J_{5,7} = 2.7$  Hz, C(5)H], 7.21-7.27 [1H, m<sup>†</sup>, C(5'')H], 7.36 [1H, dd,  $J_{7,8} = 9.2$  Hz;  $J_{7,5} = 2.7$  Hz, C(7)H], 7.50 [1H, dt,  $J_{6'',5''} = 7.8$  Hz;  $J_{6'',4''} = J_{6'',2''} = 2.7$  Hz, C(6'')H], 7.58 [1H, d,  $J_{8,7} = 9.2$  Hz, C(8)H], 7.78 [1H, d,  $J_{4,3} = 8.8$  Hz, C(4)H], 8.44-8.49 [2H, m<sup>^</sup>, C(2'')H; C(4'')H]. <sup>13</sup>C NMR (CDCl<sub>3</sub>, 125 MHz); δ<sub>C</sub>: 32.1 [C(3'/5')], 37.7 [C(4')], 40.3 [C(A)], 50.8 [C(2'/6')], 111.5 [C(5)], 112.0 [C(3)], 123.4 [C(5'')], 123.8 [C(7)], 124.2 [C(4a)], 125.9 [C(8)], 135.8 [C(1'')], 136.7 [C(6'')], 138.0 [C(4)], 141.2 [C(8a)], 147.7 [C(4'')], 147.8 [C(6)], 150.6 [C(2'')], 155.3 [C(2)].

## 6.4. SYNTHESIS OF SIMPLE 6-POSITION SUBSTITUTED 2-AMINOQUINOLINE LIGANDS

---

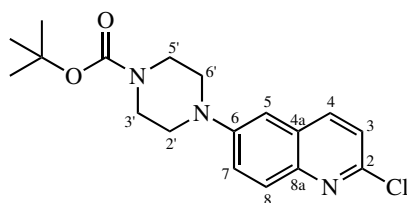
\* indicates residual triphenylphosphine oxide was present in starting material from previous reactions, so calculated yield is a theoretical minimum.

§ indicates **18b** was completely purified from residual triphenylphosphine oxide, as shown in Chapter 2, Figure 2.36.

### 6.4 Synthesis of simple 6-position substituted 2-aminoquinoline ligands

#### 6.4.1 Synthesis of simple 6-arylpiperazinyl-2-aminoquinoline derivatives

##### *tert*-Butyl 4-(2-chloroquinolin-6-yl)piperazine-1-carboxylate (**67**)



*Synthetic pathway A:* *N*-Boc-piperazine (374 mg, 2.01 mmol), **26** (398 mg, 1.64 mmol), sodium *tert*-butoxide (198 mg, 2.06 mmol), cataCXium<sup>®</sup> A (5.9 mg, 16.5  $\mu$ M), Pd(OAc)<sub>2</sub> (1.8 mg, 8.02  $\mu$ M) in anhydrous toluene (4.5 mL) were reacted via General Method 5 for 20 hr. The crude product was purified by flash column chromatography on silica gel conditioned with TEA, eluting with 5% EtOAc in DCM to afford the title compound as a pale yellow powder, m.p. 135-137 °C (396 mg, 69%\*). HRMS: C<sub>18</sub>H<sub>22</sub>ClN<sub>3</sub>O<sub>2</sub> [M+H]<sup>+</sup> requires 348.1473 [<sup>35</sup>Cl] / 350.1444 [<sup>37</sup>Cl]; found 348.1471 / 350.1451. IR (neat);  $\nu$ /cm<sup>-1</sup>: 1681, 1616, 1579, 1506, 1231, 1159, 822. <sup>1</sup>H NMR (CDCl<sub>3</sub>, 600 MHz);  $\delta$ <sub>H</sub>: 1.50 [9H, s, C(CH<sub>3</sub>)<sub>3</sub>], 3.23-3.29 [4H, m<sup>†</sup>, C(2'/6')H<sub>ax/eq</sub>], 3.61-3.66 [4H, m<sup>†</sup>, C(3'/5')H<sub>ax/eq</sub>], 7.01 [1H, d,  $J_{5,7}$  = 2.7 Hz, C(5)H], 7.29 [1H, d,  $J_{3,4}$  = 8.6 Hz, C(3)H], 7.48 [1H, dd,  $J_{7,5}$  = 2.7 Hz;  $J_{7,8}$  = 9.3 Hz, C(7)H], 7.89 [1H, d,  $J_{8,7}$  = 9.3 Hz, C(8)H], 7.93 [1H, d,  $J_{4,3}$  = 8.6 Hz, C(4)H]. <sup>13</sup>C NMR (CDCl<sub>3</sub>, 125 MHz);  $\delta$ <sub>C</sub>: 28.4 [CH<sub>3</sub>], 41.9-45.2 [br s, C(3'/5')], 49.2 [C(2'/6')], 80.1 [C(CH<sub>3</sub>)<sub>3</sub>], 109.5 [C(5)], 122.5 [C(3)], 123.5 [C(7)], 128.0 [C(4a)], 129.3 [C(8)], 137.5 [C(4)], 143.4 [C(8a)], 147.9 [C(2)], 149.6 [C(6)], 154.7 [C=O].

\*<5% **69** present by <sup>1</sup>H NMR.

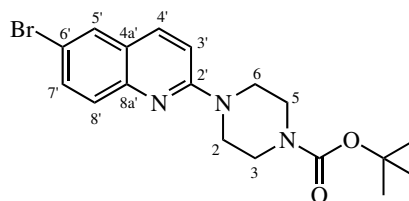
*Synthetic pathway B:* *N*-Boc-piperazine (90.6 mg, 0.486 mmol), **26** (95.8 mg, 0.395 mmol), sodium *tert*-butoxide (48.8 mg, 0.508 mmol), cataCXium<sup>®</sup> A (11.3 mg, 31.5  $\mu$ mol), Pd(OAc)<sub>2</sub> (0.8 mg, 3.56

$\mu\text{mol}$ ) in anhydrous BTF (2 mL) were reacted via General Method 5 for 17 hr. Analysis of the crude reaction mixture by  $^1\text{H}$  NMR revealed only 50% conversion of **26** had occurred.

*Synthetic pathway C:* *N*-Boc-piperazine (91.4 mg, 0.491 mmol), **26** (103.5 mg, 0.427 mmol), sodium *tert*-butoxide (58.4 mg, 0.608 mmol), cataCXium<sup>®</sup> A (18 mg, 5.02  $\mu\text{mol}$ ), Pd(OAc)<sub>2</sub> (0.6 mg, 2.67  $\mu\text{mol}$ ) in 1,4-dioxane (2 mL) were reacted via General Method 5 for 18 hr. The crude product was purified by flash column chromatography on silica gel, eluting with 5% EtOAc in DCM to afford the title compound as a pale yellow powder (12.7 mg, 9%, data as above), and **70** as a white-yellow powder (5.4 mg, 4%).

Small quantities of **69** and **70** were purified for analytical purposes, and are characterised below.

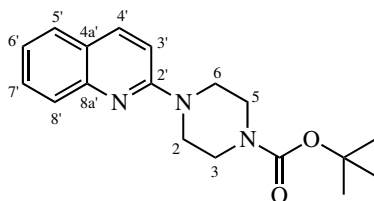
*tert*-Butyl 4-(6-bromoquinolin-2-yl)piperazine-1-carboxylate (**69**)



HRMS: C<sub>18</sub>H<sub>22</sub>BrN<sub>3</sub>O<sub>2</sub> [M+H]<sup>+</sup> requires 392.0968 [<sup>79</sup>Br] / 394.0948 [<sup>81</sup>Br]; found 392.0969 / 394.0950.  $^1\text{H}$  NMR (CDCl<sub>3</sub>, 500 MHz);  $\delta_{\text{H}}$ : 1.49 [9H, s, C(CH<sub>3</sub>)<sub>3</sub>], 3.55-3.60 [4H, m<sup>†</sup>, C(2/6)H<sub>ax/eq</sub>], 3.69-3.76 [4H, m<sup>†</sup>, C(3/5)H<sub>ax/eq</sub>], 6.98 [1H, d,  $J_{3',4'} = 9.1$  Hz, C(3')H], 7.56 [1H, d,  $J_{8',7'} = 8.9$  Hz, C(8')H], 7.59 [1H, dd,  $J_{7',8'} = 8.9$  Hz;  $J_{7',5'} = 2.1$  Hz, C(7')H], 7.74 [1H, d,  $J_{5',7'} = 2.1$  Hz, C(5')H], 7.81 [1H, d,  $J_{4',3'} = 9.1$  Hz, C(4')H].  $^{13}\text{C}$  NMR (CDCl<sub>3</sub>, 125 MHz);  $\delta_{\text{C}}$ : 28.4 [CH<sub>3</sub>], 42.7-44.2 [br s<sup>^</sup>, C(2/6); C(3/5)], 80.1 [C(CH<sub>3</sub>)<sub>3</sub>], 110.3 [C(3')], 115.4 [C(6')], 124.3 [C(4a')], 128.4 [C(8')], 129.2 [C(5')], 132.8 [C(7')], 136.6 [C(4')], 146.5 [C(8a')], 154.8 [C=O], 157.3 [C(2')].

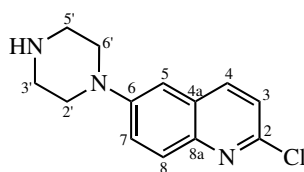
#### 6.4. SYNTHESIS OF SIMPLE 6-POSITION SUBSTITUTED 2-AMINOQUINOLINE LIGANDS

##### *tert*-Butyl 4-(quinolin-2-yl)piperazine-1-carboxylate (**70**)



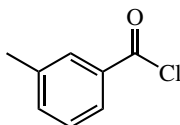
HRMS:  $C_{18}H_{23}N_3O_2$   $[M+H]^+$  requires 314.1863; found 314.1864.  $^1H$  NMR ( $CDCl_3$ , 500 MHz);  $\delta_H$ : 1.50 [9H, s,  $C(CH_3)_3$ ], 3.56-3.60 [4H, m $\dagger$ ,  $C(2/6)H_{ax/eq}$ ], 3.71-3.76 [4H, m $\dagger$ ,  $C(3/5)H_{ax/eq}$ ], 6.97 [1H, d,  $J_{3',4'} = 9.1$  Hz,  $C(3')H$ ], 7.21-7.27 [1H, m $\dagger$ ,  $C(6')H$ ], 7.52-7.57 [1H, m $\dagger$ ,  $C(7')H$ ], 7.61 [1H, dd,  $J_{5',6'} = 8.0$  Hz;  $J_{5',7'} = 1.0$  Hz,  $C(5')H$ ], 7.71 [1H, d,  $J_{8',7'} = 8.6$  Hz,  $C(8')H$ ], 7.91 [1H, d,  $J_{4',3'} = 9.1$  Hz,  $C(4')H$ ].  $^{13}C$  NMR ( $CDCl_3$ , 125 MHz);  $\delta_C$ : 28.5 [ $CH_3$ ], 42.4-44.7 [br s,  $C(2/6)$ ], 44.8-45.3 [br s,  $C(3/5)$ ], 80.0 [ $C(CH_3)_3$ ], 109.6 [ $C(3')$ ], 122.6 [ $C(6')$ ], 123.2 [ $C(4a')$ ], 126.7 [ $C(8')$ ], 127.2 [ $C(5')$ ], 129.6 [ $C(7')$ ], 137.6 [ $C(4')$ ], 147.8 [ $C(8a')$ ], 154.9 [ $C=O$ ], 157.3 [ $C(2')$ ].

##### 2-Chloro-6-(piperazin-1-yl)quinoline (**62**)



Trifluoroacetic acid (1.00 mL, 13.1 mmol) and **67** (99.7 mg, 0.287 mmol) in DCM (4 mL) were reacted for 1 hr via General Method 4, to afford the title compound as a yellow powder (68.5 g, 96%). HRMS:  $C_{13}H_{14}ClN_3$   $[M+H]^+$  requires 248.0949 [ $^{35}Cl$ ] / 250.0920 [ $^{37}Cl$ ]; found 248.0956 / 250.0915. IR (neat);  $\nu/cm^{-1}$ : 3269, 1616, 1573, 1502, 1230, 1097, 821.  $^1H$  NMR ( $CDCl_3$ , 500 MHz);  $\delta_H$ : 1.97 [1H, br s, NH], 3.05-3.10 [4H, m,  $C(3'/5')H_{ax/eq}$ ], 3.24-3.30 [4H, m,  $C(2'/6')H_{ax/eq}$ ], 6.99 [1H, d,  $J_{5,7} = 2.7$  Hz,  $C(5)H$ ], 7.27 [1H, d,  $J_{3,4} = 8.6$  Hz,  $C(3)H$ ], 7.48 [1H, dd,  $J_{7,8} = 9.3$  Hz;  $J_{7,5} = 2.7$  Hz,  $C(7)H$ ], 7.87 [1H, d,  $J_{8,7} = 9.3$  Hz,  $C(8)H$ ], 7.91 [1H, d,  $J_{4,3} = 8.6$  Hz,  $C(4)H$ ].  $^{13}C$  NMR ( $CDCl_3$ , 125 MHz);  $\delta_C$ : 45.9 [ $C(3'/5')$ ], 50.0 [ $C(2'/6')$ ], 108.8 [ $C(5)$ ], 122.3 [ $C(3)$ ], 123.1 [ $C(7)$ ], 129.0 [ $C(4a)$ ], 128.0 [ $C(3)$ ], 129.0 [ $C(8)$ ], 137.5 [ $C(4)$ ], 143.1 [ $C(8a)$ ], 147.4 [ $C(2)$ ], 150.0 [ $C(6)$ ].

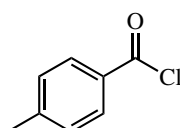
**3-Methylbenzoyl chloride (71b)**



*Synthetic pathway A:* Oxalyl chloride (0.04 mL, 0.466 mmol), 3-methylbenzoic acid (54.0 mg, 0.397 mmol) and DMF (0.21  $\mu$ L, 2.71  $\mu$ mol) in anhydrous DCM were reacted via General Method 9 for 15 hr. The crude product mixture was used without further purification.

*Synthetic pathway B:* Thionyl chloride (1.5 mL, 20.7 mmol) and 3-methylbenzoic acid (25.4 mg, 0.187 mmol) were reacted via General Method 10 for 1.5 hr. The crude product was used without further purification.

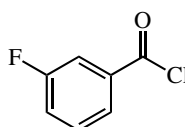
**4-Methylbenzoyl chloride (71c)**



*Synthetic pathway A:* Oxalyl chloride (0.01 mL, 0.116 mmol), 4-methylbenzoic acid (15.5 mg, 0.114 mmol) and DMF (86 nL, 1.10  $\mu$ M) in anhydrous DCM were reacted via General Method 9 for 22 hr. The crude product mixture was used without further purification.

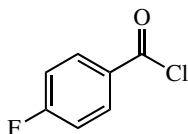
*Synthetic pathway B:* Thionyl chloride (1.5 mL, 20.7 mmol) and 4-methylbenzoic acid (29.6 mg, 0.217 mmol) were reacted via General Method 10 for 2 hr. The crude product was used without further purification.

**3-Fluorobenzoyl chloride (71d)**



Oxalyl chloride (0.02 mL, 0.233 mmol), 3-fluorobenzoic acid (37.7 mg, 0.271 mmol) and DMF (0.2  $\mu$ L, 2.58  $\mu$ M) in anhydrous DCM were reacted via General Method 9 for 15 hr. The crude product mixture was used without further purification.

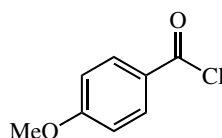
**4-Fluorobenzoyl chloride (71e)**



*Synthetic pathway A:* Oxalyl chloride (0.02 mL, 0.233 mmol), 4-fluorobenzoic acid (41.3 mg, 0.295 mmol) and DMF (0.2  $\mu$ L, 2.58  $\mu$ M) in anhydrous DCM were reacted via General Method 9 for 17 hr. The crude product mixture was used without further purification.

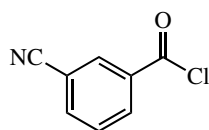
*Synthetic pathway B:* Thionyl chloride (1.5 mL, 20.7 mmol) and 4-fluorobenzoic acid (29.8 mg, 0.213 mmol) were reacted via General Method 10 for 1.5 hrs. The crude product was used without further purification.

**4-Methoxybenzoyl chloride (71g)**

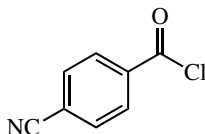


Thionyl chloride (1.5 mL, 20.7 mmol) and 4-methoxybenzoic acid (29.2 mg, 0.192 mmol) were reacted via General Method 10 for 2 hrs. The crude product was used without further purification.

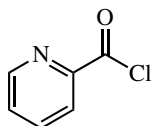
**3-Cyanobenzoyl chloride (71h)**



Thionyl chloride (1.5 mL, 20.7 mmol) and 3-cyanobenzoic acid (40.0 mg, 0.272 mmol) were reacted via General Method 10 for 2 hrs. The crude product was used without further purification.

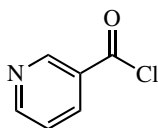
**4-Cyanobenzoyl chloride (71i)**

Thionyl chloride (1.5 mL, 20.7 mmol) and 4-cyanobenzoic acid (38.7 mg, 0.263 mmol) were reacted via General Method 10 for 2 hrs. The crude product was used without further purification.

**Picolinoyl chloride (75a)**

*Synthetic pathway A:* Oxalyl chloride (0.02 mL, 0.233 mmol), picolinic acid (33.5 mg, 0.256 mmol) and DMF (0.2  $\mu$ L, 2.58  $\mu$ M) in anhydrous DCM were reacted via General Method 9 for 17 hr. The crude product mixture was used without further purification.

*Synthetic pathway B:* Thionyl chloride (1 mL, 13.8 mmol) and picolinic acid (25.1 mg, 0.204 mmol) were reacted via General Method 10 for 2 hr. The crude product was used without further purification.

**Nicotinoyl chloride (75b)**

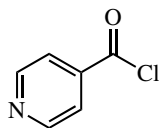
Thionyl chloride (1 mL, 13.8 mmol) and nicotinic acid (25.0 mg, 0.203 mmol) were reacted via General Method 10 for 2 hr. The crude product was used without further purification.



## 6.4. SYNTHESIS OF SIMPLE 6-POSITION SUBSTITUTED 2-AMINOQUINOLINE LIGANDS

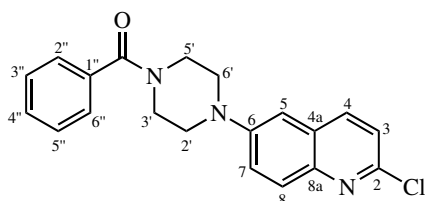
---

### Isonicotinoyl chloride (75c)



Thionyl chloride (0.5 mL, 6.93 mmol) and isonicotinic acid (25.4 mg, 0.206 mmol) were reacted via General Method 10 for 2 hr. The crude product was used without further purification.

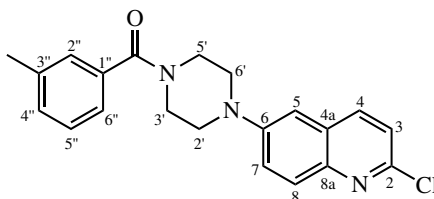
### (4-(2-Chloroquinolin-6-yl)piperazin-1-yl)(phenyl)methanone (63a)



Benzoyl chloride (0.02 mL, 0.172 mmol), **62** (48.3 mg, 0.195 mmol) and triethylamine (0.03 mL, 0.215 mmol) in anhydrous DCM (2.5 mL) were reacted via General Method 7 for 3 hr. The crude product was purified by flash column chromatography on silica gel conditioned with TEA, eluting with 2.5% MeOH in DCM to afford the title compound as a yellow-orange oil (66.7 mg, 97%). HRMS: C<sub>20</sub>H<sub>18</sub>N<sub>3</sub>OCl requires 352.1211 [<sup>35</sup>Cl] / 354.1182 [<sup>37</sup>Cl]; found 352.1213 / 354.1186. <sup>1</sup>H NMR (CDCl<sub>3</sub>, 500 MHz); δ<sub>H</sub>: 3.10-3.50 [4H, m<sup>†</sup>, C(2'/6')H<sub>ax/eq</sub>], 3.51-4.18 [4H, m, C(3'/5')H<sub>ax/eq</sub>], 7.02 [1H, d, J<sub>5,7</sub> = 2.7 Hz, C(5)H], 7.28 [1H, d, J<sub>3,4</sub> = 8.6 Hz, C(3)H], 7.40-7.49 [6H, m<sup>^</sup>, C(7)H; 5 x Ph H's], 7.90 [1H, d, J<sub>8,7</sub> = 9.4 Hz, C(8)H], 7.92 [1H, d, J<sub>4,3</sub> = 8.6 Hz, C(4)H]. <sup>13</sup>C NMR (CDCl<sub>3</sub>, 125 MHz); δ<sub>C</sub>: 41.4-42.5 [br s, C(3')\*/C(5')\*], 46.9-48.0 [br s, C(3')\*/C(5')\*], 48.6-50.3 [br m, C(2'/6')], 109.7 [C(5)], 122.6 [C(3)], 123.4 [C(7)], 127.1 [C(2''/6'')\*\*/C(4'')\*\*/C(3''/5'')\*\*], 127.9 [C(4a)], 128.6 [C(2''/6'')\*\*/C(4'')\*\*/C(3''/5'')\*\*], 129.3 [C(8)], 130.0 [C(2''/6'')\*\*/C(4'')\*\*/C(3''/5'')\*\*], 135.3 [C(1'')], 137.6 [C(4)], 143.4 [C(8a)], 148.0 [C(2)], 149.2 [C(6)], 170.5 [C=O].

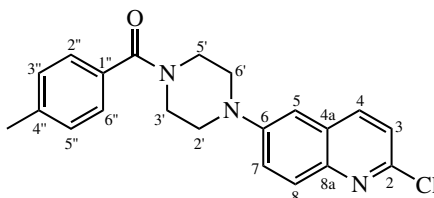
\* denotes signals which could not be unambiguously assigned due to dynamics-induced signal broadening on the NMR-timescale.

\*\* denotes overlapping signals in <sup>1</sup>H NMR precluded unambiguous signal assignment in 2D NMR spectra.

**(4-(2-Chloroquinolin-6-yl)piperazin-1-yl)(3-tolyl)methanone (63b)**

Triethylamine (0.04 mL, 0.287 mmol), **71b** (28.5 mg, 0.184 mmol) and **62** (47.0 mg, 0.190 mmol) in anhydrous DCM (2 mL) were reacted via General Method 7 for 1.5 hr. The crude product was purified by flash column chromatography on silica gel, eluting with 1.5% MeOH in DCM to afford the title compound as a yellow oil (60 mg, 88% over two steps). HRMS:  $C_{21}H_{20}ClN_3O$   $[M+H]^+$  requires 366.1368 [ $^{35}Cl$ ] / 368.1338 [ $^{37}Cl$ ]; found 366.1367 / 368.1348.  $^1H$  NMR ( $CDCl_3$ , 500 MHz);  $\delta_H$ : 2.39 [3H, s,  $CH_3$ ], 3.14-3.49 [4H,  $m^\dagger$ ,  $C(2'/6')$  $H_{ax/eq}$ ], 3.53-4.12 [4H,  $m^\dagger$ ,  $C(3'/5')$  $H_{ax/eq}$ ], 7.03 [1H, d,  $J_{5,7} = 2.6$  Hz,  $C(5)H$ ], 7.23 [1H, br d,  $J_{6'',5''} = 7.4$  Hz,  $C(6'')H$ ], 7.24-7.28 [2H,  $m^\wedge$ ,  $C(2'')H$ ;  $C(4'')H$ ], 7.30 [1H, d,  $J_{3,4} = 8.6$  Hz,  $C(3)H$ ], 7.31 [1H, t,  $J_{5'',4''} = J_{5'',6''} = 7.4$  Hz,  $C(5'')H$ ], 7.48 [1H, dd,  $J_{7,8} = 9.3$  Hz;  $J_{7,5} = 2.6$  Hz,  $C(7)H$ ], 7.91 [1H, d,  $J_{8,7} = 9.3$  Hz,  $C(8)H$ ], 7.93 [1H, d,  $J_{4,3} = 8.6$  Hz,  $C(4)H$ ].  $^{13}C$  NMR ( $CDCl_3$ , 125 MHz);  $\delta_C$ : 21.4 [ $CH_3$ ], 41.4-42.4 [br s,  $C(3')^*/C(5')^*$ ], 46.9-48.1 [br s,  $C(3'')^*/C(5'')^*$ ], 48.5-50.3 [br s,  $C(2'/6')$ ]. 109.7 [ $C(5)$ ], 122.6 [ $C(3)$ ], 123.4 [ $C(7)$ ], 124.0 [ $C(6'')$ ], 127.8 [ $C(2'')$ ], 127.9 [ $C(4a)$ ], 128.4 [ $C(5'')$ ], 129.4 [ $C(8)$ ], 130.7 [ $C(4'')$ ], 135.4 [ $C(1'')$ ], 137.6 [ $C(4)$ ], 138.6 [ $C(3'')$ ], 143.5 [ $C(8a)$ ], 148.0 [ $C(2)$ ], 149.3 [ $C(6)$ ], 170.7 [ $C=O$ ].

\* denotes signals which could not be unambiguously assigned due to dynamics-induced signal broadening on the NMR-timescale.

**(4-(2-Chloroquinolin-6-yl)piperazin-1-yl)(4-tolyl)methanone (63c)**

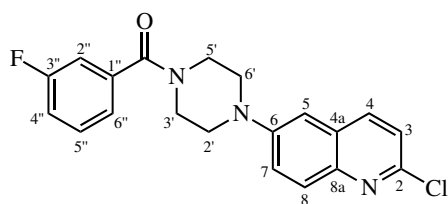
Triethylamine (0.05 mL, 0.359 mmol), **62** (61.0 mg, 0.246 mmol), and **71c** (33.6 mg, 0.217 mmol) in anhydrous DCM (3 mL) were reacted via General Method 7 for 1.5 hr. The crude product was purified by flash column chromatography on silica gel, eluting with 2% MeOH in DCM to afford the title compound as a yellow solid (67.6 mg, 85% over two steps). HRMS:  $C_{21}H_{20}ClN_3O$

#### 6.4. SYNTHESIS OF SIMPLE 6-POSITION SUBSTITUTED 2-AMINOQUINOLINE LIGANDS

[M+H]<sup>+</sup> requires 366.1368 [<sup>35</sup>Cl] / 368.1338 [<sup>37</sup>Cl]; found 366.1369 / 368.1347. IR (neat);  $\nu/\text{cm}^{-1}$ : 1618 (sh), 1580, 1502, 1451, 1101, 753. <sup>1</sup>H NMR (CDCl<sub>3</sub>, 500 MHz);  $\delta_{\text{H}}$ : 2.40 [3H, s, CH<sub>3</sub>], 3.15-3.47 [4H, br s<sup>†</sup>, C(2'/6')H<sub>ax/eq</sub>], 3.56-4.12 [4H, m<sup>†</sup>, C(3'/5')H<sub>ax/eq</sub>], 7.02 [1H, d,  $J_{5,7} = 2.6$  Hz, C(5)H], 7.21-7.26 [2H, m, C(3''/5'')H], 7.30 [1H, d,  $J_{3,4} = 8.6$  Hz, C(3)H], 7.34-7.38 [2H, m, C(2''/6'')H], 7.48 [1H, dd,  $J_{7,8} = 9.3$  Hz;  $J_{7,5} = 2.6$  Hz, C(7)H], 7.90 [1H, d,  $J_{8,7} = 9.3$  Hz, C(8)H], 7.93 [1H, d,  $J_{4,3} = 8.6$  Hz, C(4)H]. <sup>13</sup>C NMR (CDCl<sub>3</sub>, 125 MHz);  $\delta_{\text{C}}$ : 21.5 [CH<sub>3</sub>], 41.4-48.9 [br s, C(3')\*/C(5')\*], 46.7-48.9 [br s, C(3'')\*/C(5'')\*], 49.1-50.4 [br s, C(2'/6')], 109.8 [C(5)], 122.7 [C(3)], 123.5 [C(7)], 127.4 [C(2''/6'')], 128.0 [C(4a)], 129.3 [C(3'/5'')], 129.5 [C(8)], 132.5 [C(1'')], 137.7 [C(4)], 140.3 [C(4'')], 143.6 [C(8a)], 148.1 [C(2)], 149.4 [C(6)], 170.8 [C=O].

\* denotes signals which could not be unambiguously assigned due to dynamics-induced signal broadening on the NMR-timescale.

#### (4-(2-Chloroquinolin-6-yl)piperazin-1-yl)(3-fluorophenyl)methanone (63d)



Triethylamine (0.04 mL, 0.287 mmol), **71d** (42.7 mg, 0.241 mmol) and **62** (59.6 mg, 0.241 mmol) in anhydrous DCM (2 mL) were reacted via General Method 7 for 1 hr. The crude product was purified initially by micropipette column chromatography on silica gel, eluting with 1% MeOH in DCM, followed by flash column chromatography on silica gel, eluting with 55% EtOAc in hexanes to afford the title compound as a yellow oil (38.1 mg, 43% over two steps). HRMS: C<sub>20</sub>H<sub>17</sub>ClFN<sub>3</sub>O [M+H]<sup>+</sup> requires 370.1117 [<sup>35</sup>Cl] / 372.1087 [<sup>37</sup>Cl]; found 370.1117 / 372.1098. IR (neat);  $\nu/\text{cm}^{-1}$ : 1631, 1618, 1580, 1500, 1234, 1209, 1099 (sh), 747. <sup>1</sup>H NMR (CDCl<sub>3</sub>, 500 MHz);  $\delta_{\text{H}}$ : 3.18-3.51 [4H, br s<sup>†</sup>, C(2'/6')H<sub>ax/eq</sub>], 3.50-4.17 [4H, m<sup>†</sup>, C(3'/5')H<sub>ax/eq</sub>], 7.03 [1H, d,  $J_{5,7} = 2.7$  Hz, C(5)H], 7.12-7.19 [2H, m<sup>^</sup>, C(2'')H; C(4'')H], 7.21-7.25 [1H, m<sup>†</sup>, C(6'')H], 7.31 [1H, d,  $J_{3,4} = 8.6$  Hz, C(3)H], 7.39-7.45 [1H, m<sup>†</sup>, C(5'')H], 7.47 [1H, dd,  $J_{7,8} = 9.3$  Hz;  $J_{7,5} = 2.7$  Hz, C(7)H], 7.91 [1H, d,  $J_{8,7} = 9.3$  Hz, C(8)H], 7.93 [1H, d,  $J_{4,3} = 8.6$  Hz, C(4)H]. <sup>13</sup>C NMR (CDCl<sub>3</sub>, 125 MHz);  $\delta_{\text{C}}$ : 41.6-43.2 [br s, C(3')\*/C(5')\*], 46.8-48.2 [br s, C(3'')\*/C(5'')\*], 48.6-50.4 [br s, C(2'/6')], 109.5 [C(5)], 114.5 [d,  $J_{2''/4''}, \text{F}} = 22.7$  Hz, C(2'')\*\*/C(4'')\*\*], 117.1 [d,  $J_{2''/4''}, \text{F}} = 21.2$  Hz, C(2'')\*\*/C(4'')\*\*], 122.7 [C(3)], 122.8 [d,  $J_{6'', \text{F}} = 3.3$  Hz, C(6'')], 123.5 [C(7)], 127.9 [C(4a)], 129.4 [C(8)], 130.5 [d,  $J_{5'', \text{F}}$

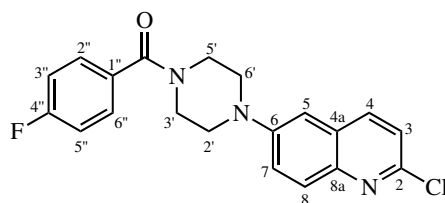
#### 6.4. SYNTHESIS OF SIMPLE 6-POSITION SUBSTITUTED 2-AMINOQUINOLINE LIGANDS

= 8.0 Hz, C(5''), 137.4 [d,  $J_{1'',F} = 7.0$  Hz, C(1'')], 137.6 [C(4)], 143.5 [C(8a)], 148.1 [C(2)], 149.1 [C(6)], 162.6 [d,  $J_{3'',F} = 248.5$  Hz, C(3'')], 169.0 [d,  $J_{C,F} = 2.3$  Hz, C=O].

\* denotes signals which could not be unambiguously assigned due to dynamics-induced signal broadening on the NMR-timescale.

\*\* denotes overlapping signals in  $^1\text{H}$  NMR precluded unambiguous signal assignment in 2D NMR spectra.

#### (4-(2-Chloroquinolin-6-yl)piperazin-1-yl)(4-fluorophenyl)methanone (63e)



*Synthetic pathway A:* Triethylamine (0.04 mL, 0.287 mmol), **71e** (34.9 mg, 0.226 mmol) and **62** (59.6 mg, 0.241 mmol) were reacted via General Method 11. The crude product was purified initially by micropipette column chromatography on silica gel, eluting with 2.5% MeOH in DCM, followed by flash column chromatography on silica gel, eluting with 55% EtOAc in hexanes to afford the title compound as a yellow oil (38.1 mg, 44% over two steps). HRMS:  $\text{C}_{20}\text{H}_{17}\text{ClFN}_3\text{O}$  [M+H]<sup>+</sup> requires 370.1117 [ $^{35}\text{Cl}$ ] / 372.1087 [ $^{37}\text{Cl}$ ]; found 370.1118 / 372.1094.  $^1\text{H}$  NMR ( $\text{CDCl}_3$ , 500 MHz);  $\delta_{\text{H}}$ : 3.18-3.45 [4H, br s<sup>†</sup>, C(2'/6')H<sub>ax/eq</sub>], 3.55-4.06 [4H, m<sup>†</sup>, C(3'/5')H<sub>ax/eq</sub>], 7.03 [1H, d,  $J_{5,7} = 2.7$  Hz, C(5)H], 7.10-7.16 [2H, m, C(3''/5'')H], 7.31 [1H, d,  $J_{3,4} = 8.6$  Hz, C(3)H], 7.45-7.50 [3H, m<sup>^</sup>, C(7)H; C(2''/6'')H], 7.91 [1H,  $J_{8,7} = 9.3$  Hz, C(8)H], 7.93 [1H,  $J_{4,3} = 8.6$  Hz, C(4)H].  $^{13}\text{C}$  NMR ( $\text{CDCl}_3$ , 125 MHz);  $\delta_{\text{C}}$ : 41.3-43.4 [br s, C(3')\*/C(5')\*], 46.5-48.3 [br s, C(3'')\*/C(5'')\*], 48.8-50.3 [br s, C(2'/6')], 109.8 [C(5)], 115.7 [d,  $J_{3''/5'',F} = 21.9$  Hz, C(3''/5'')], 122.7 [C(3)], 123.4 [C(7)], 127.9 [C(4a)], 129.5 [d,  $J_{2''/6'',F} = 8.8$  Hz, C(2''/6'')], 131.4 [d,  $J_{1'',F} = 3.5$  Hz, C(1'')], 137.6 [C(4)], 143.5 [C(8a)], 148.1 [C(2)], 149.2 [C(6)], 163.6 [d,  $J_{4'',F} = 250.4$  Hz, C(4'')], 169.6 [C=O].

\* denotes signals which could not be unambiguously assigned due to dynamics-induced signal broadening on the NMR-timescale.

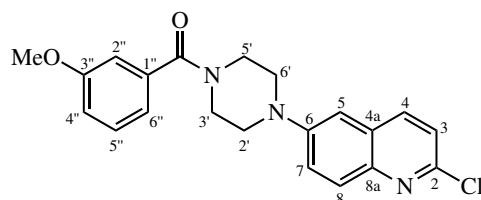
*Synthetic pathway B:* Triethylamine (0.04 mL, 0.287 mmol), **62** (56.1 mg, 0.226 mmol) and **71e** (33.7 mg, 0.213 mmol) in anhydrous DCM (6 mL) were reacted via General Method 7 for 2 hr.

#### 6.4. SYNTHESIS OF SIMPLE 6-POSITION SUBSTITUTED 2-AMINOQUINOLINE LIGANDS

---

The crude product was purified by flash column chromatography on silica gel, eluting with 0.5% MeOH in DCM to afford the title compound as a yellow oil (47.4 mg, 60% over two steps). Data as above.

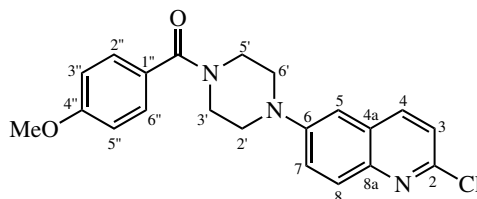
##### (4-(2-Chloroquinolin-6-yl)piperazin-1-yl)(3-methoxyphenyl)methanone (63f)



3-Methoxybenzoic acid (30.5 mg, 0.200 mmol),  $\text{SOCl}_2$  (0.02 mL, 0.275 mmol), triethylamine (0.09 mL, 0.646 mmol) and **62** (59.0 mg, 0.238 mmol) in anhydrous DCM (3 mL) were reacted via General Method 12 for 20 hr. The crude product was purified initially by micropipette column chromatography on silica gel, eluting with 2.5% MeOH in DCM, followed by flash column chromatography on silica gel, eluting with 60% EtOAc in hexanes, before micropipette column chromatography on silica gel, eluting in 1% MeOH in DCM to afford the title compound as a yellow oil (12.5 mg, 16% over two steps). HRMS:  $\text{C}_{21}\text{H}_{20}\text{ClN}_3\text{O}_2$   $[\text{M}+\text{H}]^+$  requires 382.1317 [ $^{35}\text{Cl}$ ] / 384.1287 [ $^{37}\text{Cl}$ ], found 382.1317 / 384.1294.  $^1\text{H}$  NMR ( $\text{CDCl}_3$ , 500 MHz);  $\delta_{\text{H}}$ : 3.12-3.50 [4H, m $^\dagger$ , C(2'/6') $\text{H}_{\text{ax/eq}}$ ], 3.56-4.10 [4H, m $^\dagger$ , C(3'/5') $\text{H}_{\text{ax/eq}}$ ], 3.84 [3H, s,  $\text{OCH}_3$ ], 6.96-7.02 [3H, m $^\wedge$ , C(2'')H; C(4'')H; C(6'')H], 7.03 [1H, d,  $J_{5,7} = 2.5$  Hz, C(5)H], 7.31 [1H, d,  $J_{3,4} = 8.6$  Hz, C(3)H], 7.32-7.37 [1H, m $^\dagger$ , C(5'')H], 7.48 [1H, dd,  $J_{7,8} = 9.3$  Hz;  $J_{7,5} = 2.5$  Hz, C(7)H], 7.91 [1H, d,  $J_{8,7} = 9.3$  Hz, C(8)H], 7.94 [1H, d,  $J_{4,3} = 8.6$  Hz, C(4)H].  $^{13}\text{C}$  NMR ( $\text{CDCl}_3$ , 125 MHz);  $\delta_{\text{C}}$ : 41.4-42.8 [br s, C(3'')\*/C(5'')\*], 46.8-48.2 [br s, C(3')\*/C(5')\*], 48.9-50.5 [br s, C(2'/6')], 55.5 [ $\text{OCH}_3$ ], 109.9 [C(5)], 112.7 [C(2'')\*\*/C(4'')\*\*/C(6'')\*\*], 115.9 [C(2'')\*\*/C(4'')\*\*/C(6'')\*\*], 119.3 [C(2'')\*\*/C(4'')\*\*/C(6'')\*\*], 122.8 [C(3)], 123.6 [C(7)], 128.0 [C(4a)], 129.6 [C(8)], 129.9 [C(5'')], 136.8 [C(1'')], 137.7 [C(4)], 143.6 [C(8a)], 148.2 [C(2)], 149.4 [C(6)], 159.9 [C(3'')], 170.3 [C=O].

\* denotes signals which could not be unambiguously assigned due to dynamics-induced signal broadening on the NMR-timescale.

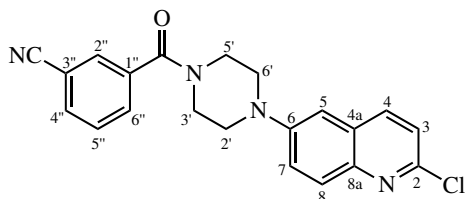
\*\* denotes overlapping signals in  $^1\text{H}$  NMR precluded unambiguous signal assignment in 2D NMR spectra.

**(4-(2-Chloroquinolin-6-yl)piperazin-1-yl)(4-methoxyphenyl)methanone (63g)**

*Synthetic pathway A:* 4-Methoxybenzoic acid (31.1 mg, 0.204 mmol),  $\text{SOCl}_2$  (0.02 mL, 0.275 mmol), triethylamine (0.09 mL, 0.646 mmol) and **62** (59.0 mg, 0.238 mmol) in anhydrous DCM (3 mL) were reacted via General Method 12 for 20 hr. The crude product was purified initially by micropipette column chromatography on silica gel, eluting with 2.5% MeOH in DCM, followed by flash column chromatography on silica gel, eluting with 60% EtOAc in hexanes, before micropipette column chromatography on silica gel, eluting in 1% MeOH in DCM to afford the title compound as an orange oil (5.5 mg, 7% over two steps). HRMS:  $\text{C}_{21}\text{H}_{20}\text{ClN}_3\text{O}_2$   $[\text{M}+\text{H}]^+$  requires 382.1317 [ $^{35}\text{Cl}$ ] / 384.1287 [ $^{37}\text{Cl}$ ], found 382.1318 / 384.1298. IR (neat);  $\nu/\text{cm}^{-1}$ : 1627, 1611, 1578, 1501, 1459, 1245, 1099, 762.  $^1\text{H}$  NMR ( $\text{CDCl}_3$ , 500 MHz);  $\delta_{\text{H}}$ : 3.26-3.38 [4H,  $\text{m}^\dagger$ , C(2'/6') $\text{H}_{\text{ax/eq}}$ ], 3.74-3.93 [4H,  $\text{m}^\dagger$ , C(3'/5') $\text{H}_{\text{ax/eq}}$ ], 3.84 [3H, s,  $\text{OCH}_3$ ], 6.92-6.97 [2H, m, C(3''/5'')H], 7.03 [1H, d,  $J_{5,7} = 2.7$  Hz, C(5)H], 7.31 [1H, d,  $J_{3,4} = 8.6$  Hz, C(3)H], 7.41-7.46 [2H, m, C(2''/6'')H], 7.49 [1H, dd,  $J_{7,8} = 9.3$  Hz;  $J_{7,5} = 2.7$  Hz, C(7)H], 7.91 [1H, d,  $J_{7,8} = 9.3$  Hz, C(8)H], 7.94 [1H, d,  $J_{4,3} = 8.6$  Hz, C(4)H].  $^{13}\text{C}$  NMR ( $\text{CDCl}_3$ , 125 MHz);  $\delta_{\text{C}}$ : 41.7-43.8 [br s, C(3')\*/C(5')\*], 45.7-47.4 [br s, C(3'')\*/C(5'')\*], 49.1-50.1 [br s, C(2'/6')], 55.6 [ $\text{OCH}_3$ ], 109.8 [C(5)], 114.0 [C(3''/5'')], 122.8 [C(3)], 123.6 [C(7)], 127.6 [C(1'')], 128.1 [C(4a)], 129.4 [C(2''/6'')], 129.6 [C(8)], 137.7 [C(4)], 143.6 [C(8a)], 148.2 [C(2)], 149.4 [C(6)], 161.2 [C(1'')], 170.6 [C=O].

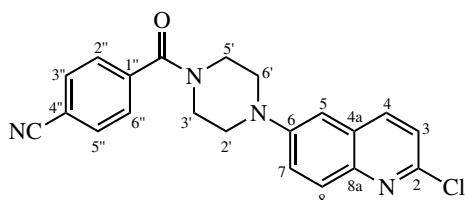
\* denotes signals which could not be unambiguously assigned due to dynamics-induced signal broadening on the NMR-timescale.

*Synthetic pathway B:* Triethylamine (0.04 mL, 0.287 mmol), **62** (45.8 mg, 0.185 mmol), and **71g** (32.7 mg, 192  $\mu\text{mol}$ ) in anhydrous DCM (3 mL) were reacted via General Method 7 for 1.5 hr. The crude product was purified by flash column chromatography on silica gel, eluting with 1% MeOH in DCM to afford the title compound as an orange oily solid (27.5 mg, 38% over two steps). Data as above.

**3-(4-(2-Chloroquinolin-6-yl)piperazine-1-carbonyl)benzonitrile (63h)**

Triethylamine (0.05 mL, 0.359 mmol), **71h** (45.0 mg, 0.272 mmol), and **62** (69.7 mg, 0.281 mmol) in anhydrous DCM (6 mL) were reacted via General Method 7 for 1.5 hr. The product was purified by flash column chromatography on silica gel, eluting with 0.5% MeOH in DCM to afford the title compound as an orange oil (79.5 mg, 78% over two steps). HRMS:  $C_{21}H_{17}ClN_4O$   $[M+H]^+$  requires 377.1164 [ $^{35}Cl$ ] / 379.1134 [ $^{37}Cl$ ]; found 377.1164 / 379.1142. IR (neat);  $\nu/cm^{-1}$ : 2229, 1633, 1618, 1579, 1501, 1233, 1100, 728.  $^1H$  NMR ( $CDCl_3$ , 500 MHz);  $\delta_H$ : 3.19-3.50 [4H, br s $^\dagger$ , C(2'/6)H $_{ax/eq}$ ], 3.53-4.12 [4H, m $^\dagger$ , C(3'/5')H $_{ax/eq}$ ], 7.04 [1H, d,  $J_{5,7} = 2.6$  Hz, C(5)H], 7.31 [1H, d,  $J_{3,4} = 8.6$  Hz, C(3)H], 7.48 [1H, dd,  $J_{7,8} = 9.3$  Hz;  $J_{7,5} = 2.6$  Hz, C(7)H], 7.59 [1H, t,  $J_{5'',6''} = J_{5'',4''} = 7.7$  Hz, C(5'')H], 7.71 [1H, d,  $J_{6'',5''} = 7.7$  Hz, C(6'')H], 7.75 [1H, d,  $J_{4'',5''} = 7.7$  Hz, C(4'')H], 7.76 [1H, s, C(2'')H], 7.91 [1H, d,  $J_{8,7} = 9.3$  Hz, C(8)H], 7.94 [1H, d,  $J_{4,3} = 8.6$  Hz, C(4)H].  $^{13}C$  NMR ( $CDCl_3$ , 125 MHz);  $\delta_C$ : 41.8-42.9 [br s, C(3')\*/C(5')\*], 47.0-48.2 [br s, C(3'')\*/C(5'')\*], 49.0-50.1 [br s, C(2'/6'')], 110.1 [C(5)], 113.2 [C(1'')], 119.0 [C $\equiv$ N], 122.8 [C(3)], 123.6 [C(7)], 128.0 [C(4a)], 129.6 [C(8)], 129.8 [C(5'')], 130.9 [C(2'')], 131.6 [C(6'')], 133.5 [C(4'')], 136.8 [C(3'')], 137.7 [C(4)], 143.7 [C(8a)], 148.3 [C(2)], 149.1 [C(6)], 168.1 [C=O].

\* denotes signals which could not be unambiguously assigned due to dynamics-induced signal broadening on the NMR-timescale.

**4-(4-(2-Chloroquinolin-6-yl)piperazine-1-carbonyl)benzonitrile (63i)**

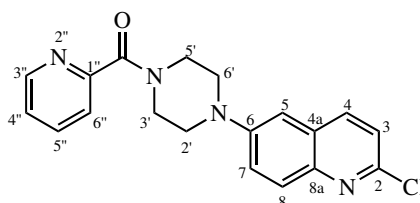
Triethylamine (0.05 mL, 0.359 mmol), **71i** (43.6 mg, 0.263 mmol), and **62** (69.9 mg, 0.282 mmol) in anhydrous DCM (6 mL) were reacted via General Method 7 for 1 hr. The product was purified by flash column chromatography on silica gel, eluting with 0.5% MeOH in DCM to afford the title

compound as an off-white, crystalline solid (74.2 mg, 75% over two steps). HRMS:  $C_{21}H_{17}ClN_4O$   $[M+H]^+$  requires 377.1164 [ $^{35}Cl$ ] / 379.1134 [ $^{37}Cl$ ]; found 377.1165 / 379.1146.  $^1H$  NMR ( $CDCl_3$ , 500 MHz);  $\delta_H$ : 3.19-3.48 [4H, m $^\dagger$ , C(2'')/6'') $H_{ax/eq}$ ], 3.50-3.70 [2H, m $^\dagger$ , C(3') $H_{ax/eq}$  or C(5') $H_{ax/eq}$ \*], 3.88-4.11 [2H, m $^\dagger$ , C(3') $H_{ax/eq}$  or C(5') $H_{ax/eq}$ \*], 7.03 [1H, d,  $J_{5,7} = 2.4$  Hz, C(5)H], 7.31 [1H, d,  $J_{3,4} = 8.6$  Hz, C(3)H], 7.47 [1H, dd,  $J_{7,8} = 9.3$  Hz;  $J_{7,5} = 2.4$  Hz, C(7)H], 7.54-7.59 [2H, m, C(2''/6'')H], 7.73-7.77 [2H, m, C(3''/5'')H], 7.90 [1H, d,  $J_{8,7} = 9.3$  Hz, C(8)H], 7.94 [1H, d,  $J_{4,3} = 8.6$  Hz, C(4)H].  $^{13}C$  NMR ( $CDCl_3$ , 125 MHz);  $\delta_C$ : 41.8-42.5 [br s, C(3'')\*/C(5'')\*], 47.2-47.8 [br s, C(3'')\*/C(5'')\*], 48.9-50.3 [br s, C(2''/6'')], 110.0 [C(5)], 113.9 [C(4'')], 118.1 [C $\equiv$ N], 122.8 [C(3)], 123.6 [C(7)], 128.0 [C(4a)\*\*; C(2''/6'')\*\*] 129.6 [C(8)], 132.6 [C(3''/5'')], 137.7 [C(4)], 139.8 [C(1'')], 143.7 [C(8a)], 148.3 [C(2)], 149.1 [C(6)], 168.4 [C=O].

\* denotes signals which could not be unambiguously assigned due to dynamics-induced signal broadening on the NMR timescale.

\*\* denotes overlapping signals in  $^{13}C$  NMR spectra.

**(4-(2-Chloroquinolin-6-yl)piperazin-1-yl)(pyridin-2-yl)methanone (64a)**



Triethylamine (0.07 mL, 0.502 mmol), **75a** (29.0 mg, 0.205 mmol) and **62** (53.6 mg, 0.216 mmol) in anhydrous DCM (3 mL) were reacted via General Method 7 for 1 hr. The product was purified by flash column chromatography on silica gel, eluting with 2% MeOH in DCM to afford the title compound as a yellow oil (31.7 mg, 44% over two steps). HRMS:  $C_{19}H_{17}ClN_4O$   $[M+H]^+$  requires 353.1164 [ $^{35}Cl$ ] / 355.1134 [ $^{37}Cl$ ]; found 353.1164 / 355.1158. IR (neat);  $\nu/cm^{-1}$ : 1629, 1617, 1578, 1501, 1231, 1100, 728.  $^1H$  NMR ( $CDCl_3$ , 600 MHz);  $\delta_H$ : 3.32-3.36 [2H, m $^\dagger$ , C(2') $H_{ax/eq}$ \*/C(6') $H_{ax/eq}$ \*], 3.40-3.46 [2H, m $^\dagger$ , C(2'') $H_{ax/eq}$ \*/C(6'') $H_{ax/eq}$ \*], 3.85-3.90 [2H, m $^\dagger$ , C(3') $H_{ax/eq}$ \*/C(5') $H_{ax/eq}$ \*], 4.01-4.06 [2H, m $^\dagger$ , C(3'') $H_{ax/eq}$ \*/C(5'') $H_{ax/eq}$ \*], 7.04 [1H, d,  $J_{5,7} = 2.7$  Hz, C(5)H], 7.30 [1H, d,  $J_{3,4} = 8.6$  Hz, C(3)H], 7.38 [1H, ddd,  $J_{4'',5''} = 7.7$  Hz;  $J_{4'',3''} = 4.9$  Hz;  $J_{4'',6''} = 1.1$  Hz, C(4'')H], 7.49 [1H, dd,  $J_{7,8} = 9.3$  Hz;  $J_{7,5} = 2.7$  Hz, C(7)H], 7.73 [1H, br d $^\dagger$ ,  $J_{6'',5''} = 7.7$  Hz, C(6'')H], 7.84 [1H, td,  $J_{5'',4''} = J_{5'',6''} = 7.7$  Hz;  $J_{5'',3''} = 1.7$  Hz, C(5'')H], 7.90 [1H, d,  $J_{8,7} = 9.3$  Hz,



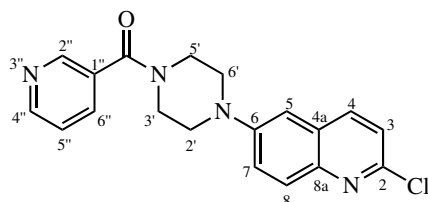
#### 6.4. SYNTHESIS OF SIMPLE 6-POSITION SUBSTITUTED 2-AMINOQUINOLINE LIGANDS

---

C(8)H], 7.94 [1H, d,  $J_{4,3} = 8.6$  Hz, C(4)H], 8.60-8.64 [1H, m<sup>†</sup>, C(3'')H]. <sup>13</sup>C NMR (CDCl<sub>3</sub>, 150 MHz); δ<sub>C</sub>: 42.4 [C(3')\*/C(5')\*], 47.0 [C(3')\*/C(5')\*], 49.2 [C(2')\*/C(6')\*], 49.8 [C(2')\*/C(6')\*], 109.8 [C(5)], 122.7 [C(3)], 123.5 [C(7)], 124.4 [C(6'')], 124.9 [C(4'')], 128.0 [C(4a)], 129.5 [C(8)], 137.3 [C(5'')], 137.7 [C(4)], 143.5 [C(8a)], 148.0 [C(2)], 148.4 [C(3'')], 149.4 [C(6)], 153.8 [C(1'')], 167.6 [C=O].

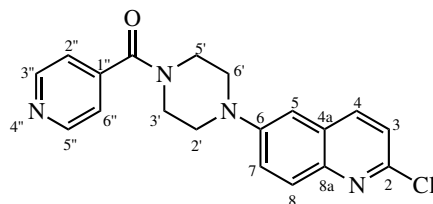
\* denotes signals which could not be unambiguously assigned due to dynamics-induced signal broadening on the NMR timescale.

#### (4-(2-Chloroquinolin-6-yl)piperazin-1-yl)(pyridin-3-yl)methanone (**64b**)



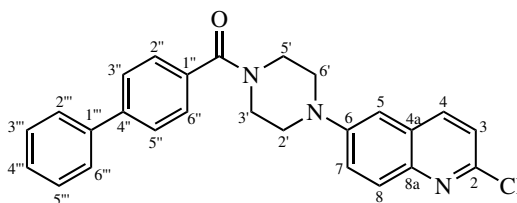
Triethylamine (0.07 mL, 0.502 mmol), **75b** (28.7 mg, 0.203 mmol) and **62** (52.1 mg, 0.210 mmol) in anhydrous DCM (3 mL) were reacted via General Method 7 for 1.5 hr. The product was purified by flash column chromatography on silica gel, eluting with 2% MeOH in DCM to afford the title compound as a yellow oil (45.8 mg, 64% over two steps). HRMS: C<sub>19</sub>H<sub>17</sub>ClN<sub>4</sub>O [M+H]<sup>+</sup> requires 353.1164 [<sup>35</sup>Cl] / 355.1134 [<sup>37</sup>Cl]; found 353.1164 / 355.1137. IR (neat); ν/cm<sup>-1</sup>: 1629, 1618, 1579, 1501, 1232, 1100, 728. <sup>1</sup>H NMR (CDCl<sub>3</sub>, 500 MHz); δ<sub>H</sub>: 3.14-3.54 [4H, m<sup>†</sup>, C(2')/6')H<sub>ax/eq</sub>], 3.52-4.22 [4H, m<sup>†</sup>, C(3')/5')H<sub>ax/eq</sub>], 7.04 [1H, d,  $J_{5,7} = 2.7$  Hz, C(5)H], 7.31 [1H, d,  $J_{3,4} = 8.6$  Hz, C(3)H], 7.41 [1H, dd,  $J_{5'',6''} = 7.8$  Hz;  $J_{5'',4''} = 4.9$  Hz, C(5'')H], 7.48 [1H, dd,  $J_{7,8} = 9.3$  Hz;  $J_{7,5} = 2.7$  Hz, C(7)H], 7.82 [1H, br dt,  $J_{6'',5''} = 7.8$  Hz;  $J_{6'',4''} = J_{6'',2''} = 1.5$  Hz, C(6'')H], 7.91 [1H, d,  $J_{8,7} = 9.3$  Hz, C(8)H], 7.94 [1H, d,  $J_{4,3} = 8.6$  Hz, C(4)H], 8.71 [1H, dd,  $J_{4'',5''} = 4.9$  Hz;  $J_{4'',6''} = 1.5$  Hz, C(4'')H], 8.73 [1H, d,  $J_{2'',6''} = 1.5$  Hz, C(2'')H]. <sup>13</sup>C NMR (CDCl<sub>3</sub>, 125 MHz); δ<sub>C</sub>: 41.7-42.9 [br s, C(3')\*/C(5')\*], 47.1-48.1 [br s, C(3')\*/C(5')\*], 49.0-50.4 [br d, C(2')/6')], 110.0 [C(5)], 122.8 [C(3)], 123.6 [C(7)], 123.7 [C(5'')], 128.0 [C(4a)], 129.6 [C(8)], 131.4 [C(1'')], 135.3 [C(6'')], 137.7 [C(4)], 143.6 [C(8a)], 148.1 [C(2'')], 148.3 [C(2)], 149.2 [C(6)], 151.2 [C(4'')], 167.9 [C=O].

\* denotes signals which could not be unambiguously assigned due to dynamics-induced signal broadening on the NMR-timescale.

**(4-(2-Chloroquinolin-6-yl)piperazin-1-yl)(pyridin-4-yl)methanone (64c)**

Triethylamine (0.07 mL, 0.502 mmol), **75c** (29.2 mg, 0.206 mmol) and **62** (49.0 mg, 0.198 mmol) in DCM (3 mL) were reacted via General Method 7 for 2.5 hr. The product was purified by flash column chromatography on silica gel, eluting with 2% MeOH in DCM to afford the title compound as a yellow oil (32.1 mg, 46% over two steps). HRMS: C<sub>19</sub>H<sub>17</sub>ClN<sub>4</sub>O [M+H]<sup>+</sup> requires 353.1164 [<sup>35</sup>Cl] / 355.1134 [<sup>37</sup>Cl]; found 353.1168 / 355.1146. IR (neat);  $\nu/\text{cm}^{-1}$ : 1635, 1619, 1579, 1499, 1232, 1100, 728. <sup>1</sup>H NMR (CDCl<sub>3</sub>, 500 MHz);  $\delta_{\text{H}}$ : 3.19-3.33 [2H, br s<sup>†</sup>, C(2'')H<sub>ax/eq</sub>\*/C(6'')H<sub>ax/eq</sub>\*], 3.33-3.48 [2H, br s<sup>†</sup>, C(2')H<sub>ax/eq</sub>\*/C(6')H<sub>ax/eq</sub>\*], 3.53-3.64 [2H, br s<sup>†</sup>, C(3'')H<sub>ax/eq</sub>\*/C(5'')H<sub>ax/eq</sub>\*], 3.92-4.15 [2H, m<sup>†</sup>, C(3')H<sub>ax/eq</sub>\*/C(5')H<sub>ax/eq</sub>\*], 7.03 [1H, d,  $J_{5,7} = 2.2$  Hz, C(5)H], 7.31 [1H, d,  $J_{3,4} = 8.6$  Hz, C(3)H], 7.34 [2H, m, C(2''/6'')H], 7.47 [1H, dd,  $J_{7,8} = 9.3$  Hz;  $J_{7,5} = 2.2$  Hz, C(7)H], 7.91 [1H, d,  $J_{8,7} = 9.3$  Hz, C(8)H], 7.94 [1H, d,  $J_{4,3} = 8.6$  Hz, C(4)H], 8.74 [2H, m, C(3''/5'')H]. <sup>13</sup>C NMR (CDCl<sub>3</sub>, 125 MHz);  $\delta_{\text{C}}$ : 41.7-42.2 [br s, C(3'')\*/C(5'')\*], 47.0-47.5 [br s, C(3')\*/C(5')\*], 49.0-49.5 [br s, C(2'')\*/C(6'')\*], 49.7-50.1 [br s, C(2')\*/C(6')\*], 110.1 [C(5)], 121.3 [C(2''/6'')], 122.8 [C(3)], 123.6 [C(7)], 128.0 [C(4a)], 129.6 [C(8)], 137.7 [C(4)], 143.1 [C(1'')], 143.7 [C(1'')], 148.3 [C(2)], 149.1 [C(6)], 150.6 [C(3''/5'')], 167.9 [C=O].

\* denotes signals which could not be unambiguously assigned due to dynamics-induced signal broadening on the NMR-timescale.

**[1,1'-Biphenyl]-4-yl(4-(2-chloroquinolin-6-yl)piperazin-1-yl)methanone (73)**

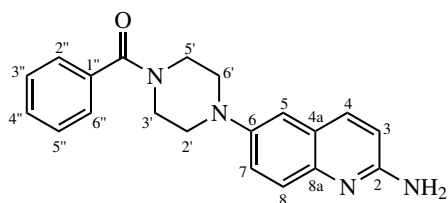
Triethylamine (0.05 mL, 0.359 mmol), biphenyl-4-carbonyl chloride (72.3 mg, 0.334 mmol) and **62** (69.7 mg, 0.281 mmol) in anhydrous DCM (3 mL) were reacted via General Method 7 for 2 hrs. The crude product was purified by flash column chromatography on silica gel, eluting with 2.5%

#### 6.4. SYNTHESIS OF SIMPLE 6-POSITION SUBSTITUTED 2-AMINOQUINOLINE LIGANDS

MeOH in DCM to afford the title compound as a yellow oil (14.1 mg, 11%). HRMS:  $C_{26}H_{22}ClN_3O$   $[M+H]^+$  requires 428.1524 [ $^{35}Cl$ ] / 430.1495 [ $^{37}Cl$ ]; found 428.1526 / 430.1497. IR (neat);  $\nu/cm^{-1}$ : 1627, 1616, 1578, 1505, 1434, 1235, 1099, 748.  $^1H$  NMR ( $CDCl_3$ , 500 MHz);  $\delta_H$ : 3.22-3.49 [4H, br s $^\dagger$ , C(2'/6)H $_{ax/eq}$ ], 3.65-4.14 [4H, m $^\dagger$ , C(3'/5') $_{ax/eq}$ ], 7.05 [1H, d,  $J_{5,7} = 2.6$  Hz, C(5)H], 7.32 [1H, d,  $J_{3,4} = 8.6$  Hz, C(3)H], 7.39 [1H, t $^\dagger$ ,  $J_{4''',5'''} = J_{4''',3'''} = 7.3$  Hz, C(4''')H], 7.45-7.54 [3H, m $^\wedge$ , C(7)H; C(3'''/5''')H], 7.53-7.56 [2H, m, C(2''/6'')H], 7.59-7.64 [2H, m, C(2'''/6''')H], 7.64-7.68 [2H, m, C(3''/5'')H], 7.92 [1H, d,  $J_{8,7} = 9.3$  Hz, C(8)H], 7.95 [1H, d,  $J_{4,3} = 8.6$  Hz, C(4)H].  $^{13}C$  NMR ( $CDCl_3$ , 125 MHz);  $\delta_C$ : 39.7-41.3 [br s, C(3')\*/C(5')\*] 45.4-46.7 [br s, C(3')\*/C(5')\*], 48.7-50.9 [br s, C(2'/6')], 109.8 [C(5)], 122.7 [C(3)], 123.5 [C(7)], 127.2 [C(2''/6'')], 127.3 [C(3''/5'')], 127.8 [C(2''/6'')], 127.91 [C(4''')], 127.93 [C(4a)], 128.9 [C(3'''/5''')], 129.5 [C(8)], 134.1 [C(1'')], 137 [C(4)], 140.2 [C(1''')], 143.0 [C(6'')], 143.5 [C(8a)], 148.1 [C(2)], 149.3 [C(6)], 170.3 [C=O].

\* denotes signals which could not be unambiguously assigned due to dynamics-induced signal broadening on the NMR-timescale.

#### (4-(2-Aminoquinolin-6-yl)piperazin-1-yl)(phenyl)methanone (60a)



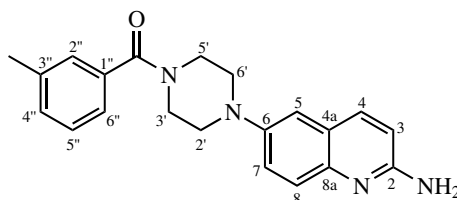
DavePhos (0.9 mg, 2.29  $\mu$ mol),  $Pd(dba)_2$  (0.8 mg, 1.39  $\mu$ mol), **63a** (33.3 mg, 94.6  $\mu$ mol) and LiH-MDS solution (1.0 M in THF, 0.25 mL, 0.25 mmol) in 1,4-dioxane (2 mL) were reacted via General Method 6 for 16 hrs. The crude product was purified by flash column chromatography on silica gel conditioned with TEA, eluting with 7.5% MeOH in DCM to afford the title compound as a yellow oil (5.6 mg, 18%). HRMS:  $C_{20}H_{20}N_4O$   $[M+H]^+$  requires 333.1710; found 333.1712. IR (neat);  $\nu/cm^{-1}$ : 3389, 3166, 1626, 1602, 1576, 1493, 1229, 1142, 1016.  $^1H$  NMR ( $CDCl_3$ , 500 MHz);  $\delta_H$ : 3.04-3.41 [4H, m $^\dagger$ , C(2'/6')H $_{ax/eq}$ ], 3.54-4.12 [4H, m $^\dagger$ , C(3'/5')H $_{ax/eq}$ ], 4.70 [2H, br s,  $NH_2$ ], 6.70 [1H, d,  $J_{3,4} = 8.8$  Hz, C(3)H], 6.98 [1H, d,  $J_{5,7} = 2.6$  Hz, C(5)H], 7.34 [1H, dd,  $J_{7,8} = 9.1$  Hz;  $J_{7,5} = 2.6$  Hz, C(7)H], 7.40-7.49 [5H, m, 5 x Ph H's], 7.60 [1H, d,  $J_{8,7} = 9.1$  Hz, C(8)H], 7.78 [1H, d,  $J_{4,3} = 8.8$  Hz, C(4)H].  $^{13}C$  NMR ( $CDCl_3$ , 125 MHz);  $\delta_C$ : 41.8-42.5 [br s, C(3')\*/C(5')\*], 47.2-48.2 [br s, C(3')\*/C(5')\*], 49.9-51.5 [br s, C(2'/6')], 111.9 [C(5)], 112.0 [C(3)], 123.3 [C(7)], 124.1 [C(4a)],

126.9 [C(8)], 127.1 [C(2'')/6'')\*/C(4'')\*/C(3'')/5'')\*], 128.6 [C(2'')/6'')\*/C(4'')\*/C(3'')/5'')\*], 129.9 [C(2'')/6'')\*/C(4'')\*/C(3'')/5'')\*], 135.6 [C(1'')], 137.3 [C(4)], 143.1 [C(8a)], 146.6 [C(6)], 155.7 [C(2)], 170.4 [C=O].

\* denotes signals which could not be unambiguously assigned due to dynamics-induced signal broadening on the NMR-timescale.

\*\* denotes overlapping signals in <sup>1</sup>H NMR spectra precluded unambiguous signal assignment in 2D NMR spectra.

**(4-(2-Aminoquinolin-6-yl)piperazin-1-yl)(3-tolyl)methanone (60b)**



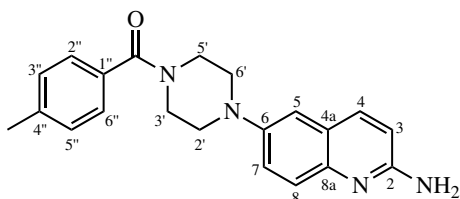
DavePhos (0.9 mg, 2.29  $\mu$ mol), Pd(dba)<sub>2</sub> (0.7 mg, 1.22  $\mu$ mol), **63b** (21.8 mg, 59.6  $\mu$ mol) and LiHMDS solution (1.0 M in THF, 0.14 mL, 0.14 mmol) in 1,4-dioxane (2 mL) were reacted via General Method 6 for 16 hrs. The crude product was purified by flash column chromatography on silica gel, eluting with 5% MeOH in DCM to afford the title compound as a yellow powder (7.8 mg, 38%). HRMS: C<sub>21</sub>H<sub>22</sub>N<sub>4</sub>O [M+H]<sup>+</sup> requires 347.1866; found 347.1867. IR (neat);  $\nu$ /cm<sup>-1</sup>: 3401, 3163, 1623, 1598, 1582, 1493, 1399, 1143, 1027. <sup>1</sup>H NMR (CDCl<sub>3</sub>, 600 MHz);  $\delta$ <sub>H</sub>: 2.39 [3H, s, CH<sub>3</sub>], 3.07-3.35 [4H, m<sup>†</sup>, C(2'')/6'')H<sub>ax/eq</sub>], 3.53-3.78 [2H, m<sup>†</sup>, C(3'')/5'')H<sub>ax/eq</sub>], 3.84-4.09 [2H, m<sup>†</sup>, C(3'')/5'')H<sub>ax/eq</sub>], 4.77 [2H, br s, NH<sub>2</sub>], 6.70 [1H, d,  $J_{3,4}$  = 8.8 Hz, C(3)H], 6.99 [1H, d,  $J_{5,7}$  = 2.7 Hz, C(5)H], 7.22-7.23 [1H, br d<sup>†</sup>,  $J_{6'',5''}$  = 7.5 Hz, C(6'')H], 7.23-7.27 [2H, m<sup>^</sup>, C(2'')H; C(4'')H], 7.31 [1H, t,  $J_{5'',6''}$  =  $J_{5'',4''}$  = 7.5 Hz, C(5'')H], 7.35 [1H, dd,  $J_{7,8}$  = 9.1 Hz;  $J_{7,5}$  = 2.7 Hz, C(7)H], 7.61 [1H, d,  $J_{8,7}$  = 9.1 Hz, C(8)H], 7.79 [1H, d,  $J_{4,3}$  = 8.8 Hz, C(4)H]. <sup>13</sup>C NMR (CDCl<sub>3</sub>, 150 MHz);  $\delta$ <sub>C</sub>: 21.4 [CH<sub>3</sub>], 41.6-42.6 [br s, C(3'')\*/C(5'')\*], 47.1-48.5 [br s, C(3'')\*/C(5'')\*], 49.7-51.3 [br s, C(2'')/6'')], 111.9 [C(5)], 112.0 [C(3)], 123.3 [C(7)], 124.0 [C(6'')], 124.0 [C(4a)], 126.7 [C(8)], 127.7 [C(2'')], 128.4 [C(5'')], 130.6 [C(4'')], 135.6 [C(1'')], 137.5 [C(4)], 138.5 [C(3'')], 142.9 [C(8a)], 146.6 [C(6)], 155.7 [C(2)], 170.6 [C=O].

\* denotes signals which could not be unambiguously assigned due to dynamics-induced signal broadening on the NMR-timescale.

#### 6.4. SYNTHESIS OF SIMPLE 6-POSITION SUBSTITUTED 2-AMINOQUINOLINE LIGANDS

---

##### (4-(2-Aminoquinolin-6-yl)piperazin-1-yl)(4-tolyl)methanone (**60c**)

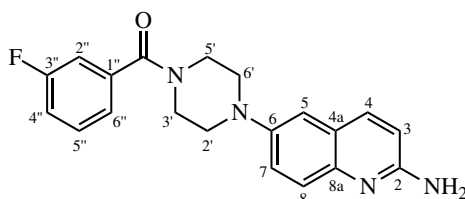


DavePhos (0.9 mg, 1.57  $\mu\text{mol}$ ), Pd(dba)<sub>2</sub> (0.9 mg, 2.29  $\mu\text{mol}$ ), **63c** (14.9 mg, 40.8  $\mu\text{mol}$ ) and LiH-MDS solution (1.0 M in THF, 0.1 mL, 0.10 mmol) in 1,4-dioxane (2 mL) were reacted via General Method 6 for 16 hrs. The crude product was purified by flash column chromatography on silica gel conditioned with TEA, eluting with 10% MeOH in DCM to afford the title compound as a yellow oil (8.9 mg, 63%\*). HRMS: C<sub>21</sub>H<sub>22</sub>N<sub>4</sub>O [M+H]<sup>+</sup> requires 347.1866; found 347.1868. IR (neat);  $\nu/\text{cm}^{-1}$ : 3393, 3145, 1623, 1603, 1569, 1506, 1401, 1229, 1150, 1015. <sup>1</sup>H NMR (CDCl<sub>3</sub>, 600 MHz);  $\delta_{\text{H}}$ : 2.39 [3H, s, CH<sub>3</sub>], 3.06-3.38 [4H, m<sup>†</sup>, C(2'/6')H<sub>ax/eq</sub>], 3.55-4.07 [4H, m<sup>†</sup>, C(3'/5')H<sub>ax/eq</sub>], 4.97 [2H, br s, NH<sub>2</sub>], 6.72 [1H, d, J<sub>3,4</sub> = 8.8 Hz, C(3)H], 6.98 [1H, d, J<sub>5,7</sub> = 2.5 Hz, C(5)H], 7.21-7.26 [2H, m, C(3''/5'')H], 7.32-7.38 [3H, m<sup>^</sup>, C(7); C(2''/6'')H], 7.61 [1H, d, J<sub>8,7</sub> = 9.1 Hz, C(8)H], 7.79 [1H, d, J<sub>4,3</sub> = 8.8 Hz, C(4)H]. <sup>13</sup>C NMR (CDCl<sub>3</sub>, 150 MHz);  $\delta_{\text{C}}$ : 21.4 [CH<sub>3</sub>], 41.7-42.8 [br s, C(3')\*/C(5')\*\*], 47.3-48.3 [br s, C(3'')\*/C(5'')\*\*], 49.9-51.3 [br s, C(2'/6')], 111.9 [C(5)], 112.1 [C(3)], 123.3 [C(7)], 123.9 [C(4a)], 126.3 [C(8)], 127.3 [C(2'')/C(6'')], 129.2 [C(3'')/C(5'')], 132.6 [C(1'')], 137.7 [C(4)], 140.1 [C(4'')], 142.1 [C(8a)], 146.7 [C(6)], 155.6 [C(2)], 170.6 [C=O].

\*Contained  $\leq$  10% TEA by NMR analysis, which was removed by micropipette column chromatography prior to SPR binding assays.

\*\* denotes signals which could not be unambiguously assigned due to dynamics-induced signal broadening on the NMR-timescale.

##### (4-(2-Aminoquinolin-6-yl)piperazin-1-yl)(3-fluorophenyl)methanone (**60d**)



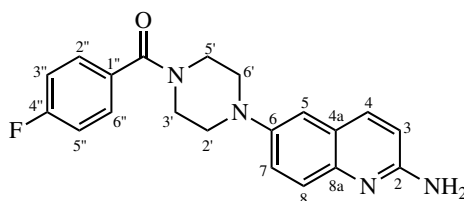
DavePhos (0.8 mg, 2.03  $\mu\text{mol}$ ), Pd(dba)<sub>2</sub> (1.1 mg, 1.91  $\mu\text{mol}$ ), **63d** (38.1 mg, 103  $\mu\text{mol}$ ) and LiH-MDS solution (1.0 M in THF, 0.24 mL, 0.24 mmol) in 1,4-dioxane (2 mL) were reacted via General

Method 6 for 16 hrs. The crude product was purified by flash column chromatography on silica gel, eluting with 5% MeOH in DCM to afford the title compound as a yellow powder (5.2 mg, 14%). HRMS:  $C_{20}H_{19}FN_4O$   $[M+H]^+$  requires 351.1616; found 351.1621. IR (neat);  $\nu/cm^{-1}$ : 3397, 3178, 1627, 1605, 1584, 1492, 1217, 1126, 1026.  $^1H$  NMR ( $CDCl_3$ , 500 MHz);  $\delta_H$ : 3.06-3.40 [4H, m $^\dagger$ , C(2'/6')H<sub>ax/eq</sub>], 3.52-4.14 [4H, m $^\dagger$ , C(3'/5')H<sub>eq/ax</sub>], 4.79 [2H, br s, NH<sub>2</sub>], 6.71 [1H, d,  $J_{3,4} = 8.8$  Hz, C(3)H], 6.99 [1H, d,  $J_{5,7} = 2.7$  Hz, C(5)H], 7.12-7.20 [2H, m $^\wedge$ , C(2''); C(4'')H], 7.21-7.25 [1H, m $^\dagger$ , C(6'')H], 7.34 [1H, dd,  $J_{7,8} = 9.1$  Hz;  $J_{7,5} = 2.7$  Hz, C(7)H], 7.42 [1H, td,  $J_{5'',4''} = J_{5'',6''} = 9.1$  Hz;  $J_{5'',F} = 2.7$  Hz, C(5'')H], 7.61 [1H, d,  $J_{8,7} = 9.1$  Hz, C(8)], 7.79 [1H, d,  $J_{4,3} = 8.8$  Hz, C(4)H].  $^{13}C$  NMR ( $CDCl_3$ , 125 MHz);  $\delta_C$ : 40.9-43.5 [br s, C(3')\*/C(5')\*], 46.8-49.0 [br s, C(3')\*/C(5')\*], 49.5-52.2 [br s, C(2'/6')], 112.1 [C(5)], 112.2 [C(3)], 114.6 [d,  $J_{2''/4'',F} = 22.8$  Hz, C(2'')\*\*/C(4'')\*\*], 117.1 [d,  $J_{2''/4'',F} = 21.1$  Hz, C(2'')\*\*/C(4'')\*\*], 122.9 [d,  $J_{6'',F} = 3.1$  Hz, C(6'')], 123.5 [C(7)], 124.2 [C(4a)], 126.9 [C(8)], 130.6,  $J_{5'',F} = 8.0$  Hz, C(5'')], 137.6 [C(4)], 137.8 [d,  $J_{1'',F} = 6.6$  Hz, C(1'')], 143.0 [C(8a)], 146.6 [C(6)], 155.9 [C(2)], 162.7 [d,  $J_{3'',F} = 248.4$  Hz, C(3'')], 169.1 [d,  $J_{C,F} = 2.3$  Hz, C=O].

\* denotes signals which could not be unambiguously assigned due to dynamics-induced signal broadening on the NMR-timescale.

\*\* denotes overlapping signals in  $^1H$  NMR precluded unambiguous signal assignment in 2D NMR spectra.

**(4-(2-Aminoquinolin-6-yl)piperazin-1-yl)(4-fluorophenyl)methanone (60e)**



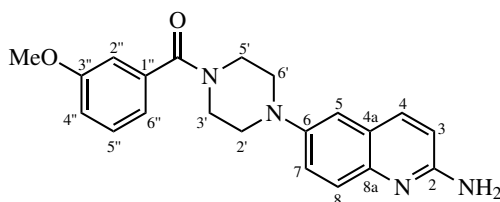
DavePhos (0.3 mg, 0.76  $\mu$ mol), Pd(dba)<sub>2</sub> (0.4 mg, 0.70  $\mu$ mol), **63e** (9.8 mg, 26.5  $\mu$ mol) and LiH-MDS solution (1.0 M in THF, 0.07 mL, 0.07 mmol) in 1,4-dioxane (2 mL) were reacted via General Method 6 for 16 hrs. The crude product was purified by flash column chromatography on silica gel, eluting with 5% MeOH in DCM to afford the title compound as a yellow powder (1.3 mg, 14%). HRMS:  $C_{20}H_{19}FN_4O$   $[M+H]^+$  requires 351.1616; found 351.1621. IR (neat);  $\nu/cm^{-1}$ : 3392, 3152, 1629, 1603, 1574, 1508, 1227, 1152, 1013.  $^1H$  NMR ( $CDCl_3$ , 500 MHz);  $\delta_H$ : 3.05-3.36 [4H, br s $^\dagger$ ,

#### 6.4. SYNTHESIS OF SIMPLE 6-POSITION SUBSTITUTED 2-AMINOQUINOLINE LIGANDS

C(2'/6')H<sub>ax/eq</sub>], 3.52-4.09 [4H, m<sup>†</sup>, C(3'/5')H<sub>ax/eq</sub>], 4.82 [2H, br s, NH<sub>2</sub>], 6.70 [1H, d,  $J_{3,4} = 8.8$  Hz, C(3)H], 6.99 [1H, d,  $J_{5,7} = 2.7$  Hz, C(5)H], 7.10-7.16 [2H, m, C(3''/5'')H], 7.35 [1H, dd,  $J_{7,8} = 9.1$  Hz;  $J_{7,5} = 2.7$  Hz, C(7)H], 7.44-7.51 [2H, m, C(2''/6'')H], 7.62 [1H, d,  $J_{8,7} = 9.1$  Hz, C(8)H], 7.79 [1H, d,  $J_{4,3} = 8.8$  Hz, C(4)H]. <sup>13</sup>C NMR (CDCl<sub>3</sub>, 125 MHz); δ<sub>C</sub>: 41.4-42.8 [br s, C(3')\*/C(5')\*], 46.5-47.6 [br s, C(3')\*/C(5')\*], 50.2-51.4 [br s, C(2'/6')], 112.1 [C(5)], 112.2 [C(3)], 115.8 [d,  $J_{3'/5'',F} = 21.8$  Hz, C(3'/5'')], 123.4 [C(7)], 124.2 [C(4a)], 126.9 [C(8)], 129.6 [d,  $J_{2''/6'',F} = 8.4$  Hz, C(2''/6'')], 131.8 [d,  $J_{1'',F} = 3.4$  Hz, C(1'')], 143.0 [C(8a)], 146.7 [C(6)], 155.9 [C(2)], 163.7 [d,  $J_{4'',F} = 250.1$  Hz, C(4'')], 169.7 [C=O].

\* denotes signals which could not be unambiguously assigned due to dynamics-induced signal broadening on the NMR-timescale.

#### (4-(2-Aminoquinolin-6-yl)piperazin-1-yl)(3-methoxyphenyl)methanone (60f)

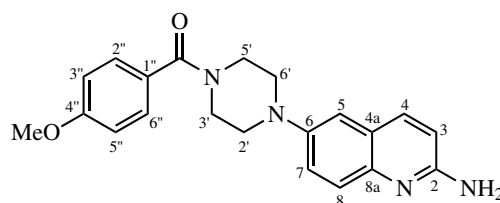


DavePhos (1.8 mg, 4.57 μmol), Pd(dba)<sub>2</sub> (2.4 mg, 4.17 μmol), **63f** (47.3 mg, 124 μmol) and LiHMDS solution (1.0 M in THF, 0.40 mL, 0.40 mmol) in 1,4-dioxane (2 mL) were reacted via General Method 6 for 16.5 hrs. The crude product was purified by flash column chromatography on silica gel, eluting with 6% MeOH in DCM to afford the title compound as a light orange powder (27.6 mg, 61%). IR (neat); ν/cm<sup>-1</sup>: 3329, 3198, 1621, 1604, 1580, 1490, 1464, 1230, 1132, 1018. HRMS: C<sub>21</sub>H<sub>22</sub>N<sub>4</sub>O<sub>2</sub> [M+H]<sup>+</sup> requires 363.1816; found 363.1818. <sup>1</sup>H NMR (CDCl<sub>3</sub>, 500 MHz); δ<sub>H</sub>: 3.08-3.37 [4H, br s<sup>†</sup>, C(2'/6')H<sub>ax/eq</sub>], 3.80-3.88 [4H, m<sup>†</sup>, C(3'/5')H<sub>ax/eq</sub>], 3.84 [3H, s, CH<sub>3</sub>], 5.42 [2H, br s, NH<sub>2</sub>], 6.69 [1H, d,  $J_{3,4} = 8.8$  Hz, C(3)H], 6.95-7.02 [4H, m<sup>^</sup>, C(5)H; C(2'')H\*/C(4'')H\*/C(6'')H\*], 7.31-7.37 [2H, m<sup>^</sup>, C(7)H; C(5'')H], 7.63 [1H, d,  $J_{8,7} = 9.4$  Hz, C(8)H], 7.79 [1H, d,  $J_{4,3} = 8.8$  Hz, C(4)H]. <sup>13</sup>C NMR (CDCl<sub>3</sub>, 125 MHz); δ<sub>C</sub>: 42.1-43.0 [br s, C(3')\*\*/C(5')\*\*], 46.6-48.7 [br s, C(3')\*\*/C(5')\*\*], 49.8-51.4 [br s, C(2'/6')], 55.6 [CH<sub>3</sub>], 112.1 [C(2'')\*/C(4'')\*/C(6'')\*/C(5)\*], 112.5 [C(3)], 112.7 [C(2'')\*/C(4'')\*/C(6'')\*/C(5)\*], 115.8 [C(2'')\*/C(4'')\*/C(6'')\*/C(5)\*], 119.3 [C(2'')\*/C(4'')\*/C(6'')\*/C(5)\*], 123.7 [C(4a)], 125.7 [C(8)], 129.8 [C(5'')], 137.0 [C(1'')], 138.1 [C(4)], 141.5 [C(8a)], 146.8 [C(6)], 155.8 [C(2)], 159.9 [C(3'')], 170.3 [C=O].

\* denotes overlapping signals in  $^1\text{H}$  NMR precluded unambiguous signal assignment in 2D NMR spectra.

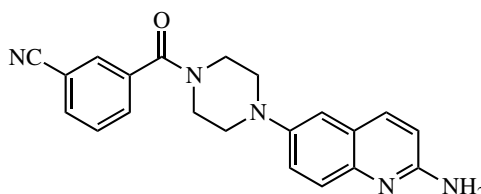
\*\* denotes signals which could not be unambiguously assigned due to dynamics-induced signal broadening on the NMR-timescale.

**(4-(2-Aminoquinolin-6-yl)piperazin-1-yl)(4-methoxyphenyl)methanone (60g)**



DavePhos (1.0 mg, 2.54  $\mu\text{mol}$ ),  $\text{Pd}(\text{dba})_2$  (1.4 mg, 2.43  $\mu\text{mol}$ ), **63g** (27.5 mg, 72.0  $\mu\text{mol}$ ) and LiHMDS solution (1.0 M in THF, 0.22 mL, 0.22 mmol) in 1,4-dioxane (2 mL) were reacted via General Method 6 for 16 hrs. The crude product was purified by flash column chromatography on silica gel, eluting with 4% MeOH in DCM to afford the title compound as a pale yellow powder (1.7 mg, 7%). HRMS:  $\text{C}_{21}\text{H}_{22}\text{N}_4\text{O}_2$   $[\text{M}+\text{H}]^+$  requires 363.1816; found 363.1817.  $^1\text{H}$  NMR ( $\text{CDCl}_3$ , 500 MHz);  $\delta_{\text{H}}$ : 3.11-3.42 [4H, br s $^\dagger$ , C(2'/6') $\text{H}_{\text{ax/eq}}$ ], 3.69-3.98 [4H, m $^\dagger$ , C(3'/5') $\text{H}_{\text{ax/eq}}$ ], 3.85 [3H, s,  $\text{CH}_3$ ], 4.83 [2H, br s,  $\text{NH}_2$ ], 6.70 [1H, d,  $J_{3,4} = 8.8$  Hz, C(3)H], 6.91-6.67 [2H, m, C(3''/5'')H], 6.99 [1H, d,  $J_{5,7} = 2.8$  Hz, C(5)H], 7.35 [1H, dd,  $J_{7,8} = 9.1$  Hz;  $J_{7,5} = 2.8$  Hz, C(7)H], 7.40-7.47 [2H, m, C(2''/6'')H], 7.61 [1H, d,  $J_{8,7} = 9.1$  Hz, C(8)H], 7.79 [1H, d,  $J_{4,3} = 8.8$  Hz, C(4)H].

**Attempted synthesis of 3-(4-(2-Aminoquinolin-6-yl)piperazine-1-carbonyl)benzonitrile (60h)**



*Synthetic pathway A:* DavePhos (0.3 mg, 0.76  $\mu\text{mol}$ ),  $\text{Pd}(\text{dba})_2$  (0.5 mg, 0.87  $\mu\text{mol}$ ), **63h** (20.8 mg, 55.2  $\mu\text{mol}$ ) and LiHMDS solution (1.0 M in THF, 0.13 mL, 0.13 mmol) in 1,4-dioxane (2 mL) were reacted via General Method 6 for 16 hrs. Workup as specified indicated only starting material was recovered.

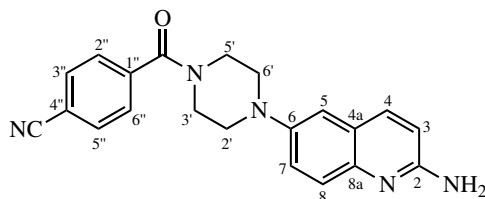


#### 6.4. SYNTHESIS OF SIMPLE 6-POSITION SUBSTITUTED 2-AMINOQUINOLINE LIGANDS

---

*Synthetic pathway B:* DavePhos (2.5 mg, 6.35  $\mu\text{mol}$ ), Pd(dba)<sub>2</sub> (3.7 mg, 6.43  $\mu\text{mol}$ ), **63h** (79.5 mg, 211  $\mu\text{mol}$ ) and LiHMDS solution (1.0 M in THF, 0.6 mL, 0.60 mmol) in 1,4-dioxane (2 mL) were reacted via General Method 6 for 16 hrs. Workup as specified indicated only starting material was recovered.

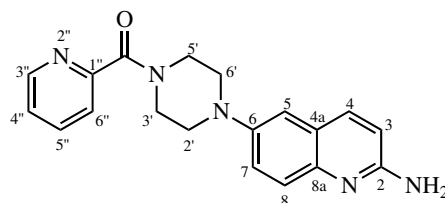
#### 4-(4-(2-Aminoquinolin-6-yl)piperazine-1-carbonyl)benzonitrile (**60i**)



DavePhos (2.3 mg, 5.84  $\mu\text{mol}$ ), Pd(dba)<sub>2</sub> (3.7 mg, 6.43  $\mu\text{mol}$ ), **63i** (74.2 mg, 197  $\mu\text{mol}$ ) and LiHMDS solution (1.0 M in THF, 0.6 mL, 0.6 mmol) in 1,4-dioxane (2 mL) were reacted via General Method 6 for 16 hrs. The crude product was purified by flash column chromatography on silica gel, eluting with 7.5% MeOH in DCM to afford the title compound as an orange powder (7.6 mg, 11%\*). HRMS: C<sub>21</sub>H<sub>19</sub>N<sub>5</sub>O [M+H]<sup>+</sup> requires 358.1662; found 358.1663. <sup>1</sup>H NMR (CDCl<sub>3</sub>, 500 MHz);  $\delta_{\text{H}}$ : 3.08-3.35 [4H, br s<sup>†</sup>, C(2'/6')H<sub>ax/eq</sub>], 3.49-3.63 [4H, m<sup>†</sup>, C(3'/5')H<sub>ax/eq</sub>\*\*], 3.90-4.08 [4H, m<sup>†</sup>, C(3'/5')H<sub>ax/eq</sub>\*\*], 5.30 [2H, br s, NH<sub>2</sub>], 6.73 [1H, d, J<sub>3,4</sub> = 8.8 Hz, C(3)H], 6.99 [1H, d, J<sub>5,7</sub> = 2.8 Hz, C(5)H], 7.34 [1H, dd, J<sub>7,8</sub> = 9.1 Hz; J<sub>7,5</sub> = 2.8 Hz, C(7)H], 7.54-7.59 [2H, m, C(2''/6'')H], 7.64 [1H, d, J<sub>8,7</sub> = 9.1 Hz, C(8)H], 7.73-7.77 [2H, m, C(3''/5'')H], 7.81 [1H, d, J<sub>4,3</sub> = 8.8 Hz, C(4)H]. <sup>13</sup>C NMR (CDCl<sub>3</sub>, 125 MHz);  $\delta_{\text{C}}$ : 41.9-42.9 [br s, C(3')\*\*/C(5')\*\*], 47.5-48.0 [br s, C(3'')\*\*/C(5'')\*\*], 50.1-51.2 [br s, C(2'/6')], 112.3 [C(5)], 112.5 [C(3)], 113.9 [C(4'')], 118.2 [C $\equiv$ N], 123.6 [C(7)], 123.8 [C(4a)], 125.9 [C(8)], 128.0 [C(2''/6'')], 132.7 [C(3''/5'')], 138.2 [C(4)], 140.0 [C(1'')], 141.6 [C(8a)], 146.7 [C(6)], 155.7 [C(2)], 168.6 [C=O].

\*<8% impurities present by <sup>1</sup>H NMR.

\*\* denotes signals which could not be unambiguously assigned due to dynamics-induced signal broadening on the NMR-timescale.

**(4-(2-Aminoquinolin-6-yl)piperazin-1-yl)(pyridin-2-yl)methanone (61a)**

DavePhos (1.7 mg, 4.32  $\mu\text{mol}$ ), Pd(dba)<sub>2</sub> (2.5 mg, 4.35  $\mu\text{mol}$ ), **61a** (50.0 mg, 142  $\mu\text{mol}$ ) and LiH-MDS solution (1.0 M in THF, 0.4 mL, 0.4 mmol) in 1,4-dioxane (2 mL) were reacted via General Method 6 for 16 hrs. The crude product was purified by flash column chromatography on silica gel, eluting with 6% MeOH in DCM to afford a 4:1 mixture of the title compound and **77** as a pale orange-brown powder (12.2 mg, <40%\*)

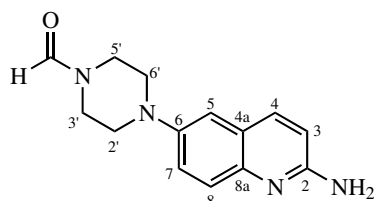
**61a**: HRMS: C<sub>19</sub>H<sub>19</sub>N<sub>5</sub>O [M+H]<sup>+</sup> requires 334.1662; found 334.1665. <sup>1</sup>H NMR (CDCl<sub>3</sub>, 500 MHz);  $\delta_{\text{H}}$ : 3.17-3.28 [2H, m<sup>†</sup>, C(2')H<sub>ax/eq</sub>\*\*/C(6')H<sub>ax/eq</sub>\*\*], 3.32 [2H, m<sup>†</sup>, C(2')H<sub>ax/eq</sub>\*\*/C(6')H<sub>ax/eq</sub>\*\*], 3.83 [2H, m<sup>†</sup>, C(3')H<sub>ax/eq</sub>\*\*/C(5')H<sub>ax/eq</sub>\*\*], 4.02 [2H, m<sup>†</sup>, C(3')H<sub>ax/eq</sub>\*\*/C(5')H<sub>ax/eq</sub>\*\*], 4.94 [2H, br s, NH<sub>2</sub>], 6.71 [1H, d, J<sub>3,4</sub> = 8.8 Hz, C(3)H], 6.99 [1H, d, J<sub>5,7</sub> = 2.8 Hz, C(5)H], 7.31-7.40 [2H, m<sup>^</sup>, C(7)H; C(4'')H], 7.61 [1H, d, J<sub>8,7</sub> = 9.1 Hz, C(8)H], 7.70 [1H, br d<sup>†</sup>, J<sub>6',5''</sub> = 7.7 Hz, C(6'')H], 7.78 [1H, d, J<sub>4,3</sub> = 8.8 Hz, C(4)H], 7.83 [1H, dt, J<sub>5'',4''</sub> = J<sub>5'',6''</sub> = 7.7 Hz; J<sub>5'',3''</sub> = 1.8 Hz, C(5'')H], 8.62 [1H, m<sup>†</sup>, C(3'')H]. <sup>13</sup>C NMR (CDCl<sub>3</sub>, 125 MHz);  $\delta_{\text{C}}$ : 42.6 [C(3'')\*\*/C(5'')\*\*], 47.3 [C(3'')\*\*/C(5'')\*\*], 50.3 [C(2'')\*\*/C(6'')\*\*], 50.9 [C(2'')\*\*/C(6'')\*\*], 112.0 [C(5)], 112.2 [C(3)], 123.5 [C(7)], 124.0 [C(4a)], 124.2 [C(6'')], 126.5 [C(8)], 137.3 [C(5'')], 137.8 [C(4)], 142.4 [C(8a)], 146.9 [C(6)], 148.5 [C(3'')], 154.0 [C(1'')], 155.8 [C(2)], 167.6 [C=O].

\* indicates maximum theoretical yield was calculated assuming pure **61a** had been isolated.

\*\* denotes signals which could not be unambiguously assigned due to dynamics-induced signal broadening on the NMR-timescale.

#### 6.4. SYNTHESIS OF SIMPLE 6-POSITION SUBSTITUTED 2-AMINOQUINOLINE LIGANDS

##### 4-(2-Aminoquinolin-6-yl)piperazine-1-carbaldehyde (**77**)

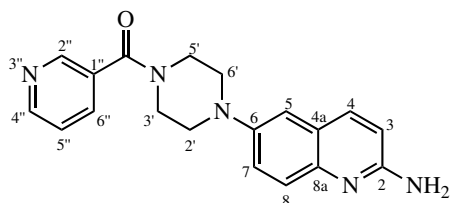


HRMS:  $C_{14}H_{16}N_4O$   $[M+H]^+$  requires 256.1319; found 256.1327.  $^1H$  NMR ( $CDCl_3$ , 500 MHz);  $\delta_H$ : 3.12-3.19 [2H, m, C(2'/6') $H_{ax/eq}$ ], 3.19-3.26 [2H, m, C(2'/6') $H_{ax/eq}$ ], 3.57 [2H, m, C(3'/5') $H_{ax/eq}$ ], 3.75 [2H, m, C(3'/5') $H_{ax/eq}$ ], 4.94 [2H, br s,  $NH_2$ ], 6.71 [1H, d,  $J_{3,4} = 8.8$  Hz, C(3)H], 6.98 [1H, d,  $J_{5,7} = 3.0$  Hz, C(5)H], 7.32-7.40 [1H, m $^\wedge$ , C(7)H], 7.61 [1H, d,  $J_{8,7} = 9.1$  Hz, C(8)H], 7.79 [1H, d,  $J_{4,3} = 8.8$  Hz, C(4)H], 8.12 [1H, s, CHO].  $^{13}C$  NMR ( $CDCl_3$ , 125 MHz);  $\delta_C$ : 40.2 [C(3')\*/C(5')\*], 45.8 [C(3')\*/C(5')\*], 50.2 [C(2')\*/C(6')\*], 51.4 [C(2')\*/C(6')\*], 112.3 [C(5); C(3)\*\*], 112.4 [C(5); C(3)\*\*], 123.7 [C(7)], 124.0 [C(4a)], 126.7 [C(8)], 137.7 [C(4)], 142.4 [C(8a)], 146.7 [C(6)], 155.9 [C(2)], 160.9 [C=O].

\* denotes signals which could not be unambiguously assigned due to dynamics-induced signal broadening on the NMR-timescale.

\*\* denotes signals in close proximity in  $^{13}C$  NMR spectra precluded unambiguous signal assignment in 2D NMR spectra.

##### (4-(2-Aminoquinolin-6-yl)piperazin-1-yl)(pyridin-3-yl)methanone (**61b**)



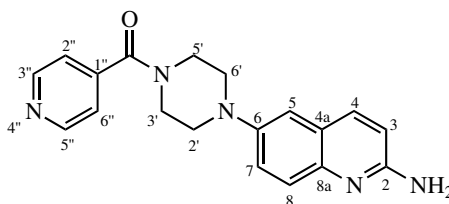
DavePhos (1.5 mg, 3.81  $\mu$ mol),  $Pd(dba)_2$  (2.3 mg, 4.00  $\mu$ mol), **64b** (45.8 mg, 130  $\mu$ mol) and LiH-MDS solution (1.0 M in THF, 0.4 mL, 0.4 mmol) in 1,4-dioxane (2 mL) were reacted via General Method 6 for 16 hrs. The crude product was purified by flash column chromatography on silica gel, eluting with 6% MeOH in DCM to afford the title compound as a pale yellow powder (6.0 mg, 14%) HRMS:  $C_{19}H_{19}N_5O$   $[M+H]^+$  requires 334.1662; found 334.1664.  $^1H$  NMR ( $CDCl_3$ , 500 MHz);  $\delta_H$ : 3.07-3.38 [4H, m $^\dagger$ , C(2'/6') $H_{ax/eq}$ ], 3.50-4.11 [4H, m $^\dagger$ , C(3'/5') $H_{ax/eq}$ ], 4.74 [2H, br s,  $NH_2$ ], 6.70 [1H, d,  $J_{3,4} = 8.7$  Hz, C(3)H], 6.99 [1H, d,  $J_{5,7} = 2.7$  Hz, C(5)H], 7.34 [1H, dd,  $J_{7,8} = 9.1$

Hz;  $J_{7,5} = 2.7$  Hz, C(7)H], 7.40 [1H, ddd,  $J_{5'',6''} = 7.9$  Hz;  $J_{5'',4''} = 4.9$  Hz;  $J_{5'',2''} = 0.9$  Hz, C(5'')H], 7.61 [1H, d,  $J_{8,7} = 9.1$  Hz, C(8)H], 7.79 [1H, d,  $J_{4,3} = 8.7$  Hz, C(4)H], 7.81 [1H, dt,  $J_{6'',5''} = 7.9$  Hz;  $J_{6'',4''} = J_{6'',2''} = 2.0$  Hz, C(6'')H], 8.70 [1H, dd,  $J_{4'',5''} = 4.9$  Hz;  $J_{4'',6''} = 2.0$  Hz, C(4'')H], 8.72 [1H, dd,  $J_{2'',6''} = -2.0$  Hz;  $J_{2'',5''} = 0.9$  Hz, C(2'')H].  $^{13}\text{C}$  NMR ( $\text{CDCl}_3$ , 125 MHz);  $\delta_{\text{C}}$ : 41.9-43.0 [br s, C(3')\*/C(5')\*], 47.4-48.8 [br s, C(3'')\*/C(5'')\*], 49.8-51.8 [br s, C(2'/6')], 112.2 [C(3); C(5)\*\*] 112.2 [C(3); C(5)\*\*], 123.4 [C(7)], 123.7 [C(5'')], 124.2 [C(4a)], 127.1 [C(8)], 131.6 [C(1'')], 135.3 [C(6'')], 137.5 [C(4)], 143.4 [C(8a)], 146.5 [C(6)], 148.2 [C(2'')], 151.1 [C(4'')], 156.0 [C(2)], 168.0 [C=O].

\* denotes signals which could not be unambiguously assigned due to dynamics-induced signal broadening on the NMR-timescale.

\*\* denotes signals in close proximity in  $^{13}\text{C}$  NMR spectra precluded unambiguous signal assignment in 2D NMR spectra.

**(4-(2-Aminoquinolin-6-yl)piperazin-1-yl)(pyridin-4-yl)methanone (61c)**



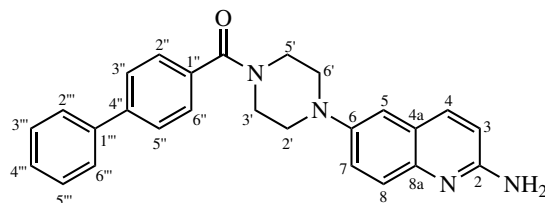
DavePhos (1.1 mg, 2.80  $\mu\text{mol}$ ),  $\text{Pd}(\text{dba})_2$  (1.6 mg, 2.78  $\mu\text{mol}$ ), **64c** (32.1 mg, 91.0  $\mu\text{mol}$ ) and LiH-MDS solution (1.0 M in THF, 0.28 mL, 0.28 mmol) in 1,4-dioxane (2 mL) were reacted via General Method 6 for 16 hrs. The crude product was purified by flash column chromatography on silica gel, eluting with 6% MeOH in DCM to afford the title compound as an orange crystalline solid (13.9 mg, 46%) HRMS:  $\text{C}_{19}\text{H}_{19}\text{N}_5\text{O}$   $[\text{M}+\text{H}]^+$  requires 334.1662; found 334.1663.  $^1\text{H}$  NMR ( $\text{CDCl}_3$ , 500 MHz);  $\delta_{\text{H}}$ : 3.17 [2H, br s $^\dagger$ , C(2') $\text{H}_{\text{ax/eq}}$ \*/C(6') $\text{H}_{\text{ax/eq}}$ \*], 3.31 [2H, br s $^\dagger$ , C(2'') $\text{H}_{\text{ax/eq}}$ \*/C(6'') $\text{H}_{\text{ax/eq}}$ \*], 3.58 [2H, br s $^\dagger$ , C(3') $\text{H}_{\text{ax/eq}}$ \*/C(5') $\text{H}_{\text{ax/eq}}$ \*], 3.99 [2H, br s $^\dagger$ , C(3'') $\text{H}_{\text{ax/eq}}$ \*/C(5'') $\text{H}_{\text{ax/eq}}$ \*], 5.60 [2H, br s,  $\text{NH}_2$ ], 6.74 [1H, d,  $J_{3,4} = 8.9$  Hz, C(3)H], 7.00 [1H, d,  $J_{5,7} = 2.7$  Hz, C(5)H], 7.31-7.36 [2H, m, C(2''/6'')H], 7.36 [1H, dd,  $J_{7,8} = 9.1$  Hz;  $J_{7,5} = 2.7$  Hz, C(7)H], 7.68 [1H, d,  $J_{8,7} = 9.1$  Hz, C(8)H], 7.84 [1H, d,  $J_{4,3} = 8.9$  Hz, C(4)H], 8.71-8.76 [2H, m, C(3''/5'')H].

\* denotes signals which could not be unambiguously assigned due to dynamics-induced signal broadening on the NMR-timescale.

#### 6.4. SYNTHESIS OF SIMPLE 6-POSITION SUBSTITUTED 2-AMINOQUINOLINE LIGANDS

---

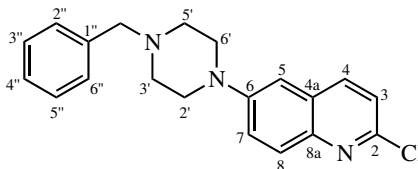
##### [1,1'-Biphenyl]-4-yl(4-(2-aminoquinolin-6-yl)piperazin-1-yl)methanone (76d)



DavePhos (0.3 mg, 0.762  $\mu\text{mol}$ ), Pd(dba)<sub>2</sub> (0.6 mg, 1.04  $\mu\text{mol}$ ), **73d** (14.1 mg, 32.9  $\mu\text{mol}$ ) and LiHMDS solution (1.0 M in THF, 0.08 mL, 0.08 mmol) in 1,4-dioxane (2 mL) were reacted via General Method 6 for 16 hrs. The crude product was purified by flash column chromatography on silica gel, eluting with 5% MeOH in DCM to afford the title compound as a yellow powder (8.4 mg, 66%). HRMS: C<sub>26</sub>H<sub>24</sub>N<sub>4</sub>O [M+H]<sup>+</sup> requires 409.2023; found 409.2023. IR (neat);  $\nu/\text{cm}^{-1}$ : 3409, 3127, 1617, 1602, 1572, 1492, 1433, 1230, 1155, 1008. <sup>1</sup>H NMR (CDCl<sub>3</sub>, 500 MHz);  $\delta_{\text{H}}$ : 3.09-3.41 [4H, br s<sup>†</sup>, C(2'/6')H<sub>ax/eq</sub>], 3.55-4.18 [4H, m<sup>†</sup>, C(3'/5')H<sub>ax/eq</sub>], 4.72 [2H, br s, NH<sub>2</sub>], 6.70 [1H, d,  $J_{3,4}$  = 8.8 Hz, C(3)H], 7.00 [1H, d,  $J_{5,7}$  = 2.7 Hz, C(5)H], 7.36 [1H, dd,  $J_{7,8}$  = 9.1 Hz;  $J_{7,5}$  = 2.7 Hz, C(7)H], 7.37-7.42 [1H, m<sup>†</sup>, C(4'')H], 7.44-7.50 [2H, m, C(3''/5'')H], 7.52-7.56 [2H, m, C(2''/6'')H], 7.59-7.64 [3H, m<sup>^</sup>, C(2'''/6''')H; C(8)H], 7.64-7.68 [2H, m, C(3'''/5''')H], 7.79 [1H, d,  $J_{4,3}$  = 8.8 Hz, C(4)H]. <sup>13</sup>C NMR (CDCl<sub>3</sub>, 125 MHz);  $\delta_{\text{C}}$ : 41.4-42.9 [br m, C(3')\*/C(5')\*], 47.1-48.6 [br m, C(3'')\*/C(5'')\*], 50.2-51.2 [br s, C(2'/6')], 111.9 [C(3)\*\*/C(5)\*\*], 112.0 [C(3)\*\*/C(5)\*\*], 123.3 [C(7)], 124.0 [C(4a)], 126.8 [C(8)], 127.2 [C(2''/6'')], 127.3 [C(3''/5'')], 127.8 [C(2''/6'')], 127.9 [C(4'')], 128.9 [C(3'''/5''')], 134.3 [C(1'')], 137.4 [C(4)], 140.2 [C(8a)], 142.85 [C(4')], 142.89 [C(8a)], 146.6 [C(6)], 155.7 [C(2)], 170.3 [C=O].

\* denotes signals which could not be unambiguously assigned due to dynamics-induced signal broadening on the NMR-timescale.

\*\* denotes signals could not be unambiguously assigned due to overlapping signals in 2D NMR spectra.

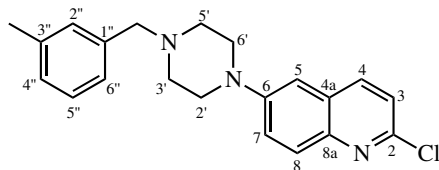
**6.4.2 Synthesis of simple 6-arylmethylpiperazinyl-2-aminoquinoline derivatives****6-(4-Benzylpiperazin-1-yl)-2-chloroquinoline (65a)<sup>47</sup>**

*Synthetic pathway A:* Benzaldehyde (30  $\mu$ L, 0.294 mM), **62** (59.5 mg, 0.240 mM), glacial acetic acid (40  $\mu$ mL, 0.699 mM) and NaBH(OAc)<sub>3</sub> (100 mg, 0.472 mmol) in anhydrous DCM (4 mL) were reacted via General Method 13 for 22 hrs. The product was purified by flash column chromatography on silica gel, eluting with 5% MeOH in DCM to afford the title compound as a yellow oil (13.7 mg, 17%). HRMS: C<sub>20</sub>H<sub>20</sub>ClN<sub>3</sub> [M+H]<sup>+</sup> requires 338.1419 [<sup>35</sup>Cl] / 340.1390 [<sup>37</sup>Cl], found 338.1418 / 340.1395. <sup>1</sup>H NMR (CDCl<sub>3</sub>, 500 MHz);  $\delta_{\text{H}}$ : 2.62-2.70 [4H, m, C(3'/5')H<sub>ax/eq</sub>], 3.27-3.37 [4H, m, C(2'/6')H<sub>ax/eq</sub>], 3.59 [2H, s, CH<sub>2</sub>], 6.99 [1H, d,  $J_{5,7} = 2.7$  Hz, C(5)H], 7.25-7.30 [2H, m<sup>^</sup>, C(3)H; C(4'')H], 7.32-7.40 [4H, m<sup>^</sup>, C(2''/6'')H; C(3''/5'')H], 7.48 [1H, dd,  $J_{7,8} = 9.3$  Hz;  $J_{7,5} = 2.7$  Hz, C(7)H], 7.87 [1H, d,  $J_{8,7} = 9.3$  Hz, C(8)H], 9.31 [1H, d,  $J_{4,3} = 8.6$  Hz, C(4)H]. <sup>13</sup>C NMR (CDCl<sub>3</sub>, 125 MHz);  $\delta_{\text{C}}$ : 49.1 [C(2'/6')], 53.0 [C(3'/5')], 63.2 [CH<sub>2</sub>], 108.9 [C(5)], 122.5 [C(3)], 123.2 [C(7)], 127.4 [C(4'')], 128.2 [C(4a)], 128.5 [C(3''/5'')], 129.3 [C(8)], 129.3 [C(2''/6'')], 137.6 [C(4)], 138.0 [C(1'')], 143.2 [C(8a)], 147.6 [C(2)], 149.8 [C(6)].

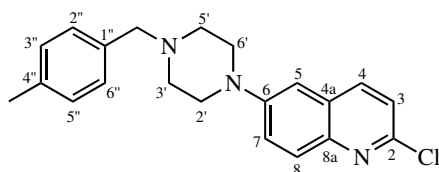
*Synthetic pathway B:* Benzaldehyde (21  $\mu$ L, 0.206 mM), **62** (46.0 mg, 0.186 mM), glacial acetic acid (20  $\mu$ L, 0.233 mM) and NaBH(OAc)<sub>3</sub> (100 mg, 0.472 mmol) in anhydrous DCM (4 mL) were reacted via General Method 13 for 20 hrs. The product was purified by flash column chromatography on silica gel, eluting with 5% MeOH in DCM to afford a 5:6 mixture containing the title compound and benzyl alcohol as a yellow oil (54.9 mg, <87%\*). Data for **65a** as above.

*Synthetic pathway C:* Benzyl bromide (0.3 mL, 0.25 mmol), **62** (51.3 mg, 0.21 mmol) and potassium carbonate (42.7 mg, 0.31 mmol) in anhydrous DCM (5 mL) were reacted via General Method 14 for 22 hr, The product was purified by flash column chromatography on silica gel, eluting with 10% EtOAc in DCM to afford the title compound as an off-white powder (12.6 mg, 18%). Data as above.

\* indicates maximum theoretical yield was calculated assuming pure **65a** was isolated.

**2-Chloro-6-(4-(3-methylbenzyl)piperazin-1-yl)quinoline (65b)**

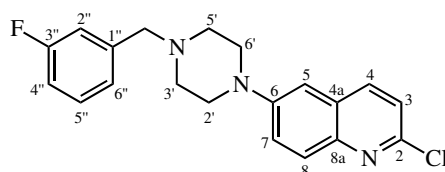
*m*-Tolualdehyde (27  $\mu$ L, 0.260 mM), **62** (49.6 mg, 0.200 mM), glacial acetic acid (22  $\mu$ L, 0.385 mM) and NaBH(OAc)<sub>3</sub> (92.6 mg, 0.437 mmol) in anhydrous DCM (6 mL) were reacted via General Method 13 for 19 hrs. The product was purified by flash column chromatography on silica gel, eluting with 10% EtOAc in DCM to afford the title compound as a pale yellow oil (34.7 mg, 49%). HRMS: C<sub>21</sub>H<sub>22</sub>ClN<sub>3</sub> [M+H]<sup>+</sup> requires 352.1575 [<sup>35</sup>Cl] / 354.1546 [<sup>37</sup>Cl], found 352.1564 / 354.1539. <sup>1</sup>H NMR (CDCl<sub>3</sub>, 500 MHz);  $\delta_{\text{H}}$ : 2.37 [3H, s, CH<sub>3</sub>], 2.62-2.68 [4H, m, C(3'/5')H<sub>ax/eq</sub>], 3.30-3.35 [4H, m, C(2'/6')H<sub>ax/eq</sub>], 3.56 [2H, s, CH<sub>2</sub>], 6.99 [1H, d,  $J_{5,7} = 2.7$  Hz, C(5)H], 7.10 [1H, br d<sup>†</sup>,  $J_{4'',5''} = 7.5$  Hz, C(4'')H], 7.16 [1H, br d<sup>†</sup>,  $J_{6'',5''} = 7.5$  Hz, C(6'')H], 7.18 [1H, br s<sup>†</sup>, C(2'')H], 7.23 [1H, t,  $J_{5'',4'} = J_{5'',6''} = 7.5$  Hz, C(5'')H], 7.27 [1H, d,  $J_{3,4} = 8.6$  Hz, C(3)H], 7.48 [1H, dd,  $J_{7,8} = 9.3$  Hz;  $J_{7,5} = 2.7$  Hz, C(7)H], 7.87 [1H, d,  $J_{8,7} = 9.3$  Hz, C(8)H], 7.91 [1H, d,  $J_{4,3} = 8.6$  Hz, C(4)H]. <sup>13</sup>C NMR (CDCl<sub>3</sub>, 125 MHz);  $\delta_{\text{C}}$ : 21.6 [CH<sub>3</sub>], 49.1 [C(2'/6')], 53.1 [C(3'/5')], 63.2 [CH<sub>2</sub>], 108.8 [C(5)], 122.5 [C(3)], 123.2 [C(7)], 126.4 [C(6'')], 128.1 [C(4'')], 128.2 [C(4a)], 128.3 [C(5'')], 129.3 [C(8)], 130.1 [C(2'')], 137.6 [C(4)], 137.9 [C(1'')], 138.1 [C(3'')], 143.2 [C(8a)], 147.6 [C(2)], 149.9 [C(6)].

**2-Chloro-6-(4-(4-methylbenzyl)piperazin-1-yl)quinoline (65c)**

*p*-Tolualdehyde (27  $\mu$ L, 0.229 mM), **62** (50.1 mg, 0.202 mM), glacial acetic acid (22  $\mu$ L, 0.385 mM) and NaBH(OAc)<sub>3</sub> (81.0 mg, 0.382 mmol) in anhydrous DCM (6 mL) were reacted via General Method 13 for 19 hrs. The product was purified by flash column chromatography on silica gel, eluting with 10% EtOAc in DCM to afford the title compound as a pale yellow oil (30.5 mg, 43%). HRMS: C<sub>21</sub>H<sub>22</sub>ClN<sub>3</sub> [M+H]<sup>+</sup> requires 352.1575 [<sup>35</sup>Cl] / 354.1546 [<sup>37</sup>Cl], found 352.1574 / 354.1549. <sup>1</sup>H NMR (CDCl<sub>3</sub>, 500 MHz);  $\delta_{\text{H}}$ : 2.35 [3H, s, CH<sub>3</sub>], 2.61-2.64 [4H, m, C(3'/5')H<sub>ax/eq</sub>], 3.27-3.34 [4H, m, C(2'/6')H<sub>ax/eq</sub>], 3.55 [2H, s, CH<sub>2</sub>], 6.98 [1H, d,  $J_{5,7} = 2.7$  Hz, C(5)H], 7.13-7.18

[2H, m, C(3''/5'')]H], 7.22-7.26 [2H, m, C(2''/6'')]H], 7.27 [1H, d,  $J_{3,4} = 8.6$  Hz, C(3)H], 7.48 [1H, dd,  $J_{7,8} = 9.3$  Hz;  $J_{7,5} = 2.7$  Hz, C(7)H], 7.87 [1H, d,  $J_{8,7} = 9.3$  Hz, C(8)H], 7.91 [1H, d,  $J_{4,3} = 8.6$  Hz, C(4)H].  $^{13}\text{C}$  NMR ( $\text{CDCl}_3$ , 125 MHz);  $\delta_{\text{C}}$ : 21.3 [CH<sub>3</sub>], 49.1 [C(2'/6')], 53.0 [C(3'/5')], 62.9 [CH<sub>2</sub>], 108.8 [C(5)], 122.5 [C(3)], 123.2 [C(7)], 128.2 [C(4a)], 129.15 [C(3''/5'')], 129.24 [C(8)], 129.3 [C(2''/6'')], 134.9 [C(1'')], 137.0 [C(4'')], 137.6 [C(4)], 143.2 [C(8a)], 147.6 [C(2)], 149.9 [C(6)].

### 2-Chloro-6-(4-(3-fluorolbenzyl)piperazin-1-yl)quinoline (65d)



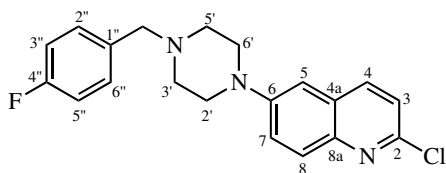
3-Fluorobenzaldehyde (30  $\mu\text{L}$ , 0.282 mM), **62** (61.3 mg, 0.247 mM), glacial acetic acid (26  $\mu\text{L}$ , 0.455 mM) and  $\text{NaBH}(\text{OAc})_3$  (114 mg, 0.539 mmol) in anhydrous DCM (6 mL) were reacted via General Method 13 for 22 hrs. The product was purified by flash column chromatography on silica gel, eluting with 10% EtOAc in DCM to afford the title compound as a pale yellow powder (43.6 mg, 50%). HRMS:  $\text{C}_{20}\text{H}_{19}\text{ClFN}_3$  [M+H]<sup>+</sup> requires 356.1324 [ $^{35}\text{Cl}$ ] / 358.1295 [ $^{37}\text{Cl}$ ], found 356.1327 / 358.1302.  $^1\text{H}$  NMR ( $\text{CDCl}_3$ , 500 MHz);  $\delta_{\text{H}}$ : 2.61-2.67 [4H, m, C(3'/5')H<sub>ax/eq</sub>], 3.29-3.34 [4H, m, C(2'/6')H<sub>ax/eq</sub>], 3.57 [2H, s, CH<sub>2</sub>], 6.94-7.00 [1H, m, C(4'')H], 6.98 [1H, d,  $J_{5,7} = 2.7$  Hz, C(5)H], 7.09-7.15 [2H, m, C(2'')H; C(6'')H], 7.26 [1H, d,  $J_{3,4} = 8.6$  Hz, C(3)H], 7.26-7.32 [1H, m, C(5'')H], 7.47 [1H, dd,  $J_{7,8} = 9.3$  Hz;  $J_{7,5} = 2.7$  Hz, C(7)H], 7.87 [1H, d,  $J_{8,7} = 9.3$  Hz, C(8)H], 7.90 [1H, d,  $J_{4,3} = 8.6$  Hz, C(4)H].  $^{13}\text{C}$  NMR ( $\text{CDCl}_3$ , 125 MHz);  $\delta_{\text{C}}$ : 49.0 [C(2'/6')], 53.0 [C(3'/5')], 62.5 [d,  $J_{\text{C,F}} = 1.8$  Hz, CH<sub>2</sub>], 108.9 [C(5)], 114.2 [d,  $J_{4'',\text{F}} = 21.2$  Hz, C(4'')], 115.8 [d,  $J_{2'',\text{F}} = 21.5$  Hz, C(2'')], 122.5 [C(3)], 123.2 [C(7)], 124.6 [d,  $J_{6'',\text{F}} = 2.8$  Hz, C(6'')], 128.2 [C(4a)], 129.2 [C(8)], 129.9 [d,  $J_{5'',\text{F}} = 8.2$  Hz, C(5'')], 137.6 [C(4)], 140.9 [d,  $J_{1'',\text{F}} = 7.0$  Hz, C(1'')], 143.2 [C(8a)], 147.6 [C(2)], 149.7 [C(6)], 163.1 [d,  $J_{3'',\text{F}} = 245.5$  Hz, C(3'')].



#### 6.4. SYNTHESIS OF SIMPLE 6-POSITION SUBSTITUTED 2-AMINOQUINOLINE LIGANDS

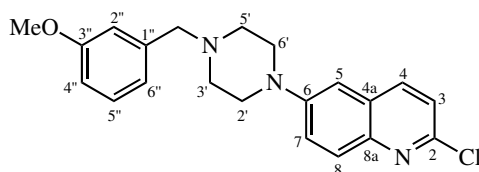
---

##### 2-Chloro-6-(4-(4-fluorobenzyl)piperazin-1-yl)quinoline (65e)



4-Fluorobenzaldehyde (25  $\mu$ L, 0.233 mM), **62** (50.2 mg, 0.203 mM), glacial acetic acid (22  $\mu$ L, 0.385 mM) and NaBH(OAc)<sub>3</sub> (105 mg, 0.496 mmol) in anhydrous DCM (6 mL) were reacted via General Method 13 for 18 hrs. The product was purified by flash column chromatography on silica gel, eluting with 10% EtOAc in DCM to afford the title compound as a pale yellow oil (27.9 mg, 39%). HRMS: C<sub>20</sub>H<sub>19</sub>ClFN<sub>3</sub> [M+H]<sup>+</sup> requires 356.1324 [<sup>35</sup>Cl] / 358.1295 [<sup>37</sup>Cl], found 356.1328 / 358.1292. <sup>1</sup>H NMR (CDCl<sub>3</sub>, 500 MHz);  $\delta_{\text{H}}$ : 2.60-2.66 [4H, m, C(3'/5')]H<sub>ax/eq</sub>], 3.29-3.34 [4H, m, C(2'/6')]H<sub>ax/eq</sub>], 3.55 [CH<sub>2</sub>], 6.99 [1H, d,  $J_{5,7} = 2.7$  Hz, C(5)H], 7.00-7.08 [2H, m, C(3''/5'')H], 7.27 [1H, d,  $J_{3,4} = 8.6$  Hz, C(3)H], 7.30-7.37 [2H, m, C(2''/6'')H], 7.48 [1H, dd,  $J_{7,8} = 9.3$  Hz;  $J_{7,5} = 2.7$  Hz, C(7)H], 7.87 [1H, d,  $J_{8,7} = 9.3$  Hz, C(8)H], 7.91 [1H, d,  $J_{4,3} = 8.6$  Hz, C(4)H]. <sup>13</sup>C NMR (CDCl<sub>3</sub>, 125 MHz);  $\delta_{\text{C}}$ : 49.1 [C(2'/6')], 53.0 [C(3'/5')], 62.3 [CH<sub>2</sub>], 108.9 [C(5)], 115.3 [d,  $J_{3''/5'',\text{F}} = 21.0$  Hz, C(3''/5'')], 122.5 [C(3)], 123.2 [C(7)], 128.2 [C(4a)], 129.3 [C(8)], 130.7 [d,  $J_{2''/6'',\text{F}} = 8.0$  Hz, C(2''/6'')], 133.7 [d,  $J_{1'',\text{F}} = 1.9$  Hz, C(1'')], 137.6 [C(4)], 143.2 [C(8a)], 147.6 [C(2)], 149.8 [C(6)], 162.2 [d,  $J_{4'',\text{F}} = 245.1$  Hz, C(4'')].

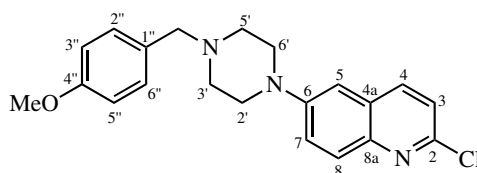
##### 2-Chloro-6-(4-(3-methoxybenzyl)piperazin-1-yl)quinoline (65f)



*m*-Anisaldehyde (32  $\mu$ L, 0.266 mM), **62** (56.1 mg, 0.226 mM), glacial acetic acid (25  $\mu$ L, 0.437 mM) and NaBH(OAc)<sub>3</sub> (99.4 mg, 0.469 mmol) in anhydrous DCM (6 mL) were reacted via General Method 13 for 19 hrs. The product was purified by flash column chromatography on silica gel, eluting with 10% EtOAc in DCM to afford the title compound as a pale yellow powder (42.3 mg, 51%). HRMS: C<sub>21</sub>H<sub>22</sub>ClN<sub>3</sub>O [M+H]<sup>+</sup> requires 368.1525 [<sup>35</sup>Cl] / 370.1595 [<sup>37</sup>Cl], found 368.1524 / 370.1491. <sup>1</sup>H NMR (CDCl<sub>3</sub>, 500 MHz);  $\delta_{\text{H}}$ : 2.62-2.68 [4H, m, C(3'/5')]H<sub>ax/eq</sub>], 3.29-3.34 [4H, m, C(2'/6')]H<sub>ax/eq</sub>], 3.56 [2H, s, CH<sub>2</sub>], 3.82 [3H, s, CH<sub>3</sub>], 6.82 [1H, dd,  $J_{4'',5''} = 8.2$  Hz;  $J_{4'',6''} = 2.5$  Hz, C(4'')H], 6.90-6.97 [2H, m, C(2'')H; C(6'')H], 6.98 [1H, d,  $J_{5,7} = 2.7$  Hz, C(5)H], 7.22-7.29

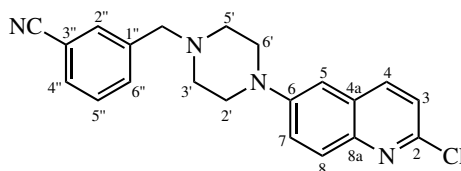
[2H, m<sup>^</sup>, C(3)H; C(5'')H], 7.47 [1H, dd,  $J_{7,8} = 9.3$  Hz;  $J_{7,5} = 2.7$  Hz, C(7)H], 7.86 [1H, d,  $J_{8,7} = 9.3$  Hz, C(8)H], 7.90 [1H, d,  $J_{4,3} = 8.6$  Hz, C(4)H]. <sup>13</sup>C NMR (CDCl<sub>3</sub>, 125 MHz); δ<sub>C</sub>: 49.0 [C(2'/6')], 53.0 [C(3'/5')], 55.3 [CH<sub>3</sub>], 63.0 [CH<sub>2</sub>], 108.8 [C(5)], 112.7 [C(4'')], 114.8 [C(2'')], 121.6 [C(6'')], 122.5 [C(3)], 123.1 [C(7)], 128.2 [C(4a)], 129.2 [C(8)], 129.4 [C(5'')], 137.6 [C(4)], 139.7 [C(1'')], 143.2 [C(8a)], 147.5 [C(2)], 149.8 [C(6)], 159.8 [C(3'')].

### 2-Chloro-6-(4-(4-methoxybenzyl)piperazin-1-yl)quinoline (65g)



*p*-Anisaldehyde (34 μL, 0.279 mM), **62** (61.3 mg, 0.247 mM), glacial acetic acid (26 μL, 0.455 mM) and NaBH(OAc)<sub>3</sub> (87.5 mg, 0.413 mmol) in anhydrous DCM (6 mL) were reacted via General Method 13 for 23 hrs. The product was purified by flash column chromatography on silica gel, eluting with 20% EtOAc in DCM to afford the title compound as a beige powder (25.3 mg, 28%). HRMS: C<sub>21</sub>H<sub>22</sub>ClN<sub>3</sub>O [M+H]<sup>+</sup> requires 368.1525 [<sup>35</sup>Cl] / 370.1595 [<sup>37</sup>Cl], found 368.1527 / 370.1505. <sup>1</sup>H NMR (CDCl<sub>3</sub>, 500 MHz); δ<sub>H</sub>: 2.61-2.66 [4H, m, C(3'/5')H<sub>ax/eq</sub>], 3.28-3.34 [4H, m, C(2'/6')H<sub>ax/eq</sub>], 3.53 [2H, s, CH<sub>2</sub>], 3.81 [3H, s, CH<sub>3</sub>], 6.85-6.91 [2H, m, C(3'')/5'')H], 6.98 [1H, d,  $J_{5,7} = 2.7$  Hz, C(5)H], 7.25-7.30 [3H, m<sup>^</sup>, C(3)H; C(2'')/6'')H], 7.48 [1H, dd,  $J_{7,8} = 9.3$  Hz;  $J_{7,5} = 2.7$  Hz, C(7)H], 7.86 [1H, d,  $J_{8,7} = 9.3$  Hz, C(8)H], 7.91 [1H, d,  $J_{4,3} = 8.7$  Hz, C(4)H]. <sup>13</sup>C NMR (CDCl<sub>3</sub>, 125 MHz); δ<sub>C</sub>: 49.1 [C(2'/6')], 52.9 [C(3'/5')], 55.4 [CH<sub>3</sub>], 62.5 [CH<sub>2</sub>], 108.8 [C(5)], 113.8 [C(3'')/5'')], 122.5 [C(3)], 123.2 [C(7)], 128.2 [C(4a)], 129.2 [C(8)], 130.0 [C(1'')], 130.5 [C(2'')/6'')], 137.6 [C(4)], 143.2 [C(8a)], 147.5 [C(2)], 149.8 [C(6)], 159.0 [C(4'')].

### 3-((4-(2-Chloroquinolin-6-yl)piperazin-1-yl)methyl)benzonitrile (65h)



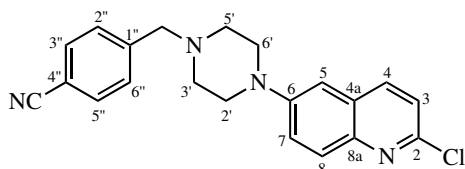
3-Formylbenzonitrile (58.0 mg, 0.442 mM), **62** (89.4 mg, 0.361 mM), glacial acetic acid (39 μL, 0.682 mM) and NaBH(OAc)<sub>3</sub> (121 mg, 0.569 mmol) in anhydrous DCM (8 mL) were reacted via General Method 13 for 25 hrs. The product was purified by flash column chromatography on sil-

#### 6.4. SYNTHESIS OF SIMPLE 6-POSITION SUBSTITUTED 2-AMINOQUINOLINE LIGANDS

ica gel, eluting with 10% EtOAc in DCM to afford the title compound as a pale yellow powder (73.6 mg, 56%). HRMS:  $C_{21}H_{19}ClN_4$   $[M+H]^+$  requires 363.1371 [ $^{35}Cl$ ] / 365.1342 [ $^{37}Cl$ ], found 363.1366 / 135.1345. IR (neat);  $\nu/cm^{-1}$ : 2226, 1619, 1574, 1506, 1235, 1097, 819.  $^1H$  NMR ( $CDCl_3$ , 500 MHz);  $\delta_H$ : 2.62-2.68 [4H, m, C(3'/5') $H_{ax/eq}$ ], 3.30-3.36 [4H, m, C(2'/6') $H_{ax/eq}$ ], 3.61 [2H, s,  $CH_2$ ], 7.00 [1H, d,  $J_{5,7} = 2.7$  Hz, C(5)H], 7.28 [1H, d,  $J_{3,4} = 8.6$  Hz, C(3)H], 7.45 [1H, t,  $J_{5'',6''} = J_{5'',4''} = 7.9$  Hz, C(5'')H], 7.48 [1H, dd,  $J_{7,8} = 9.3$  Hz;  $J_{7,5} = 2.7$  Hz, C(7)H], 7.57 [1H, d $^\dagger$ ,  $J_{4'',5''} = 7.9$  Hz, C(4'')H], 7.61 [1H, d $^\dagger$ ,  $J_{6'',5''} = 7.9$  Hz, C(6'')H], 7.71 [1H, s $^\dagger$ , C(2'')H], 7.88 [1H, d,  $J_{8,7} = 9.3$  Hz, C(8)H], 7.92 [1H, d,  $J_{4,3} = 8.6$  Hz, C(4)H].  $^{13}C$  NMR ( $CDCl_3$ , 125 MHz);  $\delta_C$ : 49.1 [C(2'/6')], 53.0 [C(3'/5')], 62.1 [ $CH_2$ ], 109.0 [C(5)], 112.3 [C(3'')], 119.0 [C $\equiv$ N], 122.5 [C(3)], 123.2 [C(7)], 128.1 [C(4a)], 129.3 [C(5'')\*]/C(8)\*], 129.3 [C(5'')\*]/C(8)\*], 131.1 [C(4'')], 132.5 [C(2'')], 133.5 [C(6'')], 137.6 [C(4)], 139.9 [C(1'')], 143.3 [C(8a)], 147.7 [C(2)], 149.7 [C(6)].

\* denotes signals could not be unambiguously assigned due to overlapping signals in 2D NMR spectra.

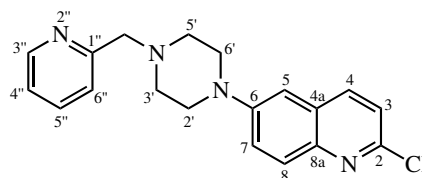
#### 4-((4-(2-Chloroquinolin-6-yl)piperazin-1-yl)methyl)benzonitrile (65i)



4-Formylbenzonitrile (61.2 mg, 0.467 mM), **62** (96.3 mg, 0.361 mM), glacial acetic acid (42  $\mu$ L, 0.682 mM) and  $NaBH(OAc)_3$  (146 mg, 0.569 mmol) in anhydrous DCM (8 mL) were reacted via General Method 13 for 25 hrs. The product was purified by flash column chromatography on silica gel, eluting with 10% EtOAc in DCM to afford the title compound as a pale yellow powder (94.7 mg, 67%). HRMS:  $C_{21}H_{19}ClN_4$   $[M+H]^+$  requires 363.1371 [ $^{35}Cl$ ] / 365.1342 [ $^{37}Cl$ ], found 363.1367 / 165.1347. IR (neat);  $\nu/cm^{-1}$ : 2226, 1619, 1574, 1506, 1235, 1098, 810.  $^1H$  NMR ( $CDCl_3$ , 500 MHz);  $\delta_H$ : 2.62-2.68 [4H, m, C(3'/5') $H_{ax/eq}$ ], 3.30-3.36 [4H, m, C(2'/6') $H_{ax/eq}$ ], 3.64 [2H, s,  $CH_2$ ], 7.00 [1H, d,  $J_{5,7} = 2.7$  Hz, C(5)H], 7.27 [1H, d,  $J_{3,4} = 8.6$  Hz, C(3)H], 7.45-7.53 [3H, m $^\wedge$ , C(7)H; C(2''/6'')H], 7.61-7.66 [2H, m, C(3''/5'')H], 7.87 [1H, d,  $J_{8,7} = 9.3$  Hz, C(8)H], 7.92 [1H, d,  $J_{4,3} = 8.6$  Hz, C(4)H].  $^{13}C$  NMR ( $CDCl_3$ , 125 MHz);  $\delta_C$ : 49.1 [C(2'/6')], 53.1 [C(3'/5')], 62.5 [ $CH_2$ ], 109.0 [C(5)], 111.2 [C(4'')], 119.0 [C $\equiv$ N], 122.6 [C(3)], 123.2 [C(7)], 128.2 [C(4a)],

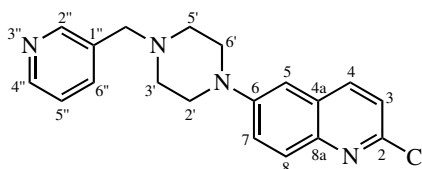
129.3 [C(8)], 129.6 [C(2''/6'')], 123.3 [C(3''/5'')], 137.6 [C(4)], 143.3 [C(8a)], 144.0 [C(1'')], 147.7 [C(2)], 149.6 [C(6)].

### 2-Chloro-6-(4-(pyridin-2-ylmethyl)piperazin-1-yl)quinoline (66a)



Picolinaldehyde (24  $\mu$ L, 0.252 mM), **62** (56.1 mg, 0.23 mM), glacial acetic acid (25  $\mu$ L, 0.437 mM) and NaBH(OAc)<sub>3</sub> (98 mg, 0.462 mmol) in anhydrous DCM (6 mL) were reacted via General Method 13 for 18 hrs. The product was purified by flash column chromatography on silica gel, eluting with 2% MeOH in DCM to afford the title compound as a pale yellow powder (39.5 mg, 51%). HRMS: C<sub>19</sub>H<sub>19</sub>ClN<sub>4</sub> [M+H]<sup>+</sup> requires 339.1371 [<sup>35</sup>Cl] / 341.1342 [<sup>37</sup>Cl], found 339.1370 / 341.1349. <sup>1</sup>H NMR (CDCl<sub>3</sub>, 500 MHz);  $\delta$ <sub>H</sub>: 2.70-2.76 [4H, m, C(3'/5')]H<sub>ax/eq</sub>], 3.33-3.38 [4H, m, C(2'/6')]H<sub>ax/eq</sub>], 3.75 [2H, s, CH<sub>2</sub>], 6.99 [1H, d,  $J_{5,7} = 2.7$  Hz, C(5)H], 7.20 [1H, ddd,  $J_{4'',5''} = 7.7$  Hz;  $J_{4'',3''} = 4.9$  Hz;  $J_{4'',6''} = 1.2$  Hz, C(4'')H], 7.27 [1H, d,  $J_{3,4} = 8.6$  Hz, C(3)H], 7.45 [1H, d<sup>†</sup>,  $J_{6'',5''} = 7.7$  Hz, C(6'')H], 7.48 [1H, dd,  $J_{7,8} = 9.3$  Hz;  $J_{7,5} = 2.7$  Hz, C(7)H], 7.68 [1H, dt,  $J_{5'',6''} = J_{5'',4''} = 7.7$  Hz;  $J_{5'',3''} = 1.8$  Hz, C(5'')H], 7.87 [1H, d,  $J_{8,7} = 9.3$  Hz, C(8)H], 7.91 [1H, d,  $J_{4,3} = 8.6$  Hz, C(4)H], 8.58-8.63 [1H, m, C(3'')H]. <sup>13</sup>C NMR (CDCl<sub>3</sub>, 125 MHz);  $\delta$ <sub>C</sub>: 49.0 [C(2'/6')], 53.2 [C(3'/5')], 64.7 [CH<sub>2</sub>], 108.8 [C(5)], 122.3 [C(4'')], 122.5 [C(3)], 123.1 [C(7)], 123.4 [C(6'')], 128.2 [C(4a)], 129.2 [C(8)], 136.6 [C(5'')], 137.6 [C(4)], 143.2 [C(8a)], 147.5 [C(2)], 149.5 [C(3'')], 149.8 [C(6)], 158.3 [C(1'')].

### 2-Chloro-6-(4-(pyridin-3-ylmethyl)piperazin-1-yl)quinoline (66b)

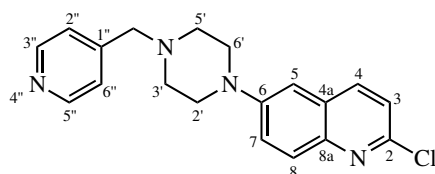


Nicotinaldehyde (21  $\mu$ L, 0.224 mM), **62** (48.7 mg, 0.383 mM), glacial acetic acid (22  $\mu$ L, 0.385 mM) and NaBH(OAc)<sub>3</sub> (81.2 mg, 0.383 mmol) in anhydrous DCM (6 mL) were reacted via General Method 13 for 22 hrs. The product was purified by flash column chromatography on silica gel, eluting with 2% MeOH in DCM to afford the title compound as a pale yellow powder (47.7 mg,

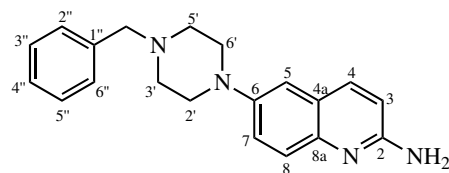
#### 6.4. SYNTHESIS OF SIMPLE 6-POSITION SUBSTITUTED 2-AMINOQUINOLINE LIGANDS

72%). HRMS:  $C_{19}H_{19}ClN_4$   $[M+H]^+$  requires 339.1371 [ $^{35}Cl$ ] / 341.1342 [ $^{37}Cl$ ], found 339.1367 / 341.1344. IR (neat);  $\nu/cm^{-1}$ : 1617, 1574, 1506, 1097, 816.  $^1H$  NMR ( $CDCl_3$ , 500 MHz);  $\delta_H$ : 2.63-2.69 [4H, m, C(3'/5') $H_{ax/eq}$ ], 3.29-3.35 [4H, m, C(2'/6') $H_{ax/eq}$ ], 3.60 [2H, s,  $CH_2$ ], 6.99 [1H, d,  $J_{5,7} = 2.7$  Hz, C(5)H], 7.25-7.32 [2H, m, C(3)H; C(5'')H], 7.48 [1H, dd,  $J_{7,8} = 9.3$  Hz;  $J_{7,5} = 2.7$  Hz, C(7)H], 7.72 [1H, br dt,  $J_{6'',5''} = 7.8$  Hz;  $J_{6'',4''} = J_{6'',2''} = 1.9$  Hz, C(6'')H], 7.87 [1H, d,  $J_{8,7} = 9.3$  Hz, C(8)H], 7.91 [1H, d,  $J_{4,3} = 8.6$  Hz, C(4)H], 8.54 [1H, dd,  $J_{4'',5''} = 4.8$  Hz;  $J_{4'',6''} = 1.9$  Hz, C(4'')H], 8.60 [1H, d,  $J_{2'',6''} = 1.9$  Hz, C(2'')H].  $^{13}C$  NMR ( $CDCl_3$ , 125 MHz);  $\delta_C$ : 49.0 [C(2'/6')], 53.0 [C(3'/5')], 62.3 [ $CH_2$ ], 109.0 [C(5)], 122.5 [C(3)], 123.2 [C(7)], 123.5 [C(5'')], 128.2 [C(4a)], 129.3 [C(8)], 133.5 [C(1'')], 136.8 [C(6'')], 137.6 [C(4)], 143.2 [C(8a)], 147.6 [C(2)], 148.9 [C(4'')], 149.7 [C(6)], 150.6 [C(2'')].

#### 2-Chloro-6-(4-(pyridin-4-ylmethyl)piperazin-1-yl)quinoline (66c)



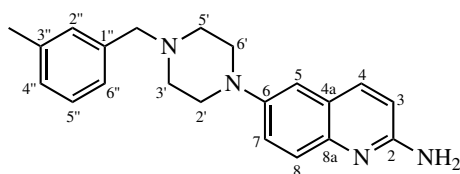
Isonicotinaldehyde (21  $\mu$ L, 0.234 mM), **62** (50.4 mg, 0.203 mM), glacial acetic acid (22  $\mu$ L, 0.385 mM) and  $NaBH(OAc)_3$  (85.2 mg, 0.402 mmol) in anhydrous DCM (6 mL) were reacted via General Method 13 for 22 hrs. The product was purified by flash column chromatography on silica gel, eluting with 2% MeOH in DCM to afford the title compound as a pale orange powder (50.2 mg, 73%). HRMS:  $C_{19}H_{19}ClN_4$   $[M+H]^+$  requires 339.1371 [ $^{35}Cl$ ] / 341.1342 [ $^{37}Cl$ ], found 339.1382 / 341.1358. IR (neat);  $\nu/cm^{-1}$ : 1620, 1576, 1497, 1097, 831.  $^1H$  NMR ( $CDCl_3$ , 500 MHz);  $\delta_H$ : 2.64-2.70 [4H, m, C(3'/5') $H_{ax/eq}$ ], 3.32-3.37 [4H, m, C(2'/6') $H_{ax/eq}$ ], 3.60 [2H, s,  $CH_2$ ], 7.01 [1H, d,  $J_{5,7} = 2.7$  Hz, C(5)H], 7.29 [1H, d,  $J_{3,4} = 8.6$  Hz, C(3)H], 7.31-7.35 [2H, m, C(2''/6'')H], 7.49 [1H, dd,  $J_{7,8} = 9.3$  Hz;  $J_{7,5} = 2.7$  Hz, C(7)H], 7.88 [1H, d,  $J_{8,7} = 9.3$  Hz, C(8)H], 7.93 [1H, d,  $J_{4,3} = 8.6$  Hz, C(4)H], 8.55-8.60 [2H, m, C(3''/5'')H].  $^{13}C$  NMR ( $CDCl_3$ , 125 MHz);  $\delta_C$ : 49.1 [C(2'/6')], 53.2 [C(3'/5')], 61.8 [ $CH_2$ ], 109.0 [C(5)], 122.6 [C(3)], 123.2 [C(7)], 124.0 [C(2''/6'')], 128.2 [C(4a)], 129.3 [C(8)], 137.6 [C(4)], 143.3 [C(8a)], 147.4 [C(1'')], 147.7 [C(2)], 149.7 [C(6)], 150.1 [C(3''/5'')].

**6-(4-Benzylpiperazin-1-yl)quinolin-2-amine (17a)**

DavePhos (1.4 mg, 3.56  $\mu\text{mol}$ ), Pd(dba)<sub>2</sub> (2.2 mg, 3.83  $\mu\text{mol}$ ), **65a** (<54.9 mg, <163\*  $\mu\text{mol}$ ) and LiHMDS solution (1.0 M in THF, 0.40 mL, 0.40 mmol) in 1,4-dioxane (2 mL) were reacted via General Method 6 for 16 hrs. The crude product was purified by flash column chromatography on silica gel, eluting with 7% MeOH in DCM to afford the title compound as a beige powder (25.6 mg, >51%\*). HRMS: C<sub>20</sub>H<sub>22</sub>N<sub>4</sub> [M+H]<sup>+</sup> requires 319.1917; found 319.1921. <sup>1</sup>H NMR (CDCl<sub>3</sub>, 500 MHz);  $\delta_{\text{H}}$ : 2.62-2.68 [4H, m, C(3'/5')H<sub>ax/eq</sub>], 3.20-3.25 [4H, m, C(2'/6')H<sub>ax/eq</sub>], 3.59 [2H, s, CH<sub>2</sub>], 5.90 [2H, br s, NH<sub>2</sub>], 6.69 [1H, d,  $J_{3,4} = 8.9$  Hz, C(3)H], 6.94 [1H, d,  $J_{5,7} = 2.7$  Hz, C(5)H], 7.26-7.39 [6H, m<sup>^</sup>, C(7)H; 5x Ph H's], 7.65 [1H, d,  $J_{8,7} = 9.1$  Hz, C(8)H], 7.77 [1H, d,  $J_{4,3} = 8.9$  Hz, C(4)H]. <sup>13</sup>C NMR (CDCl<sub>3</sub>, 125 MHz);  $\delta_{\text{C}}$ : 49.9 [C(2'/6')], 53.2 [C(3'/5')], 63.2 [CH<sub>2</sub>], 111.1 [C(5)], 112.5 [C(3)], 123.2 [C(7)], 123.7 [C(4a)], 124.6 [C(8)], 127.3 [C(3''/5'')\*\*/C(4'')\*\*], 128.4 [C(3''/5'')\*\*/C(4'')\*\*], 129.4 [C(2''/6'')], 138.0 [C(1'')], 138.7 [C(4)], 139.6 [C(8a)], 147.6 [C(6)], 155.2 [C(2)].

\* denotes the reagent contained residual benzyl alcohol, which could not be completely removed from the final product; theoretical minimum yield calculated assuming pure **65a** was used.

\*\* denotes signals could not be unambiguously assigned due to overlapping signals in 2D NMR spectra.

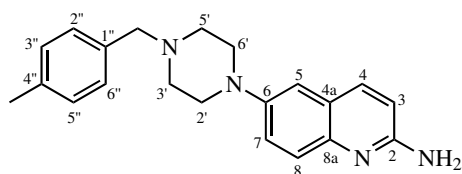
**6-(4-(3-Methylbenzyl)piperazin-1-yl)quinolin-2-amine (17b)**

DavePhos (2.1 mg, 5.33  $\mu\text{mol}$ ), Pd(dba)<sub>2</sub> (1.4 mg, 2.43  $\mu\text{mol}$ ), **65b** (34.7 mg, 98.6  $\mu\text{mol}$ ) and LiHMDS solution (1.0 M in THF, 0.24 mL, 0.24 mmol) in 1,4-dioxane (2 mL) were reacted via General Method 6 for 16 hrs. The crude product was purified by flash column chromatography on silica gel, eluting with 6% MeOH in DCM to afford the title compound as a beige powder (18.2

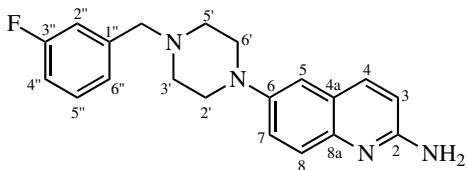
#### 6.4. SYNTHESIS OF SIMPLE 6-POSITION SUBSTITUTED 2-AMINOQUINOLINE LIGANDS

mg, 56%). HRMS:  $C_{21}H_{24}N_4$   $[M+H]^+$  requires 333.2074; found 333.2073.  $^1H$  NMR ( $CDCl_3$ , 500 MHz);  $\delta_H$ : 2.36 [3H, s,  $CH_3$ ], 2.62-2.68 [4H, m,  $C(3'/5')$  $H_{ax/eq}$ ], 3.21-3.36 [4H, m,  $C(2'/6')$  $H_{ax/eq}$ ], 3.55 [2H, s,  $CH_2$ ], 4.85 [2H, br s,  $NH_2$ ], 6.68 [1H, d,  $J_{3,4} = 8.8$  Hz,  $C(3)H$ ], 6.95 [H, d,  $J_{5,7} = 2.7$  Hz,  $C(5)H$ ], 7.09 [1H, br  $d^\dagger$ ,  $J_{4'',5''} = 7.5$  Hz,  $C(4'')H$ ], 7.16 [1H, br  $d^\dagger$ ,  $J_{6'',5''} = 7.5$  Hz,  $C(6'')H$ ], 7.18 [1H, br  $s^\dagger$ ,  $C(2'')H$ ], 7.23 [1H, t,  $J_{5'',4''} = J_{5'',6''} = 7.5$  Hz,  $C(5'')H$ ], 7.35 [1H, dd,  $J_{7,8} = 9.2$  Hz;  $J_{7,5} = 2.7$  Hz,  $C(7)H$ ], 7.58 [1H, d,  $J_{8,7} = 9.2$  Hz,  $C(8)H$ ], 7.77 [1H, d,  $J_{4,3} = 8.8$  Hz,  $C(4)H$ ].  $^{13}C$  NMR ( $CDCl_3$ , 125 MHz);  $\delta_C$ : 21.5 [ $CH_3$ ], 50.0 [ $C(2'/6')$ ], 53.3 [ $C(3'/5')$ ], 63.2 [ $CH_2$ ], 111.1 [ $C(5)$ ], 112.0 [ $C(3)$ ], 123.0 [ $C(7)$ ], 124.2 [ $C(4a)$ ], 1263 [ $C(8)$ ], 126.5 [ $C(6'')$ ], 128.0 [ $C(4'')$ ], 128.3 [ $C(5'')$ ], 130.1 [ $C(2'')$ ], 137.7 [ $C(4)$ ], 137.95 [ $C(1'')$ ], 138.0 [ $C(3'')$ ], 142.1 [ $C(8a)$ ], 147.3 [ $C(6)$ ], 155.5 [ $C(2)$ ].

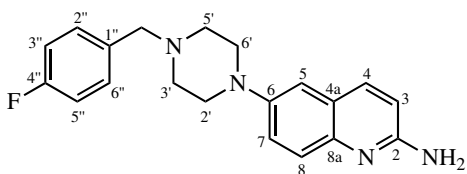
#### 6-(4-(4-Methylbenzyl)piperazin-1-yl)quinolin-2-amine (17c)



DavePhos (0.7 mg, 1.78  $\mu$ mol),  $Pd(dba)_2$  (1.3 mg, 2.26  $\mu$ mol), **65c** (30.5 mg, 86.7  $\mu$ mol) and LiH-MDS solution (1.0 M in THF, 0.21 mL, 0.21 mmol) in 1,4-dioxane (2 mL) were reacted via General Method 6 for 16 hrs. The crude product was purified by flash column chromatography on silica gel, eluting with 6% MeOH in DCM to afford the title compound as a beige-yellow powder (11.7 mg, 41%). HRMS:  $C_{21}H_{24}N_4$   $[M+H]^+$  requires 333.2074; found 333.2071.  $^1H$  NMR ( $CDCl_3$ , 500 MHz);  $\delta_H$ : 2.35 [3H, s,  $CH_3$ ], 2.62-2.67 [4H, m,  $C(3'/5')$  $H_{ax/eq}$ ], 3.20-3.25 [4H, m,  $C(2'/6')$  $H_{ax/eq}$ ], 3.55 [2H, s,  $CH_2$ ], 4.97 [2H, br s,  $NH_2$ ], 6.69 [1H, d,  $J_{3,4} = 8.8$  Hz,  $C(3)H$ ], 6.95 [H, d,  $J_{5,7} = 2.7$  Hz,  $C(5)H$ ], 7.13-7.18 [2H, m,  $C(3''/5'')$  $H$ ], 7.21-7.28 [2H, m,  $C(2''/6'')$  $H$ ], 7.35 [1H, dd,  $J_{7,8} = 9.2$  Hz;  $J_{7,5} = 2.7$  Hz,  $C(7)H$ ], 7.58 [1H, d,  $J_{8,7} = 9.2$  Hz,  $C(8)H$ ], 7.78 [1H, d,  $J_{4,3} = 8.8$  Hz,  $C(4)H$ ].  $^{13}C$  NMR ( $CDCl_3$ , 125 MHz);  $\delta_C$ : 21.3 [ $CH_3$ ], 50.0 [ $C(2'/6')$ ], 53.2 [ $C(3'/5')$ ], 62.9 [ $CH_2$ ], 111.1 [ $C(5)$ ], 112.1 [ $C(3)$ ], 123.1 [ $C(7)$ ], 124.2 [ $C(4a)$ ], 126.1 [ $C(8)$ ], 129.1 [ $C(3''/5'')$ ], 129.4 [ $C(2''/6'')$ ], 134.9 [ $C(1'')$ ], 136.9 [ $C(4'')$ ], 137.9 [ $C(4)$ ], 141.7 [ $C(8a)$ ], 147.4 [ $C(6)$ ], 155.4 [ $C(2)$ ].

**6-(4-(3-Fluorobenzyl)piperazin-1-yl)quinolin-2-amine (17d)**

DavePhos (1.2 mg, 3.05  $\mu\text{mol}$ ), Pd(dba)<sub>2</sub> (1.4 mg, 2.43  $\mu\text{mol}$ ), **65d** (43.6 mg, 123  $\mu\text{mol}$ ) and LiH-MDS solution (1.0 M in THF, 0.30 mL, 0.30 mmol) in 1,4-dioxane (2 mL) were reacted via General Method 6 for 16 hrs. The crude product was purified by flash column chromatography on silica gel, eluting with 6% MeOH in DCM to afford the title compound as a beige powder (26.5 mg, 64%). HRMS: C<sub>20</sub>H<sub>21</sub>FN<sub>4</sub> [M+H]<sup>+</sup> requires 337.1823; found 337.1826. <sup>1</sup>H NMR (CDCl<sub>3</sub>, 500 MHz);  $\delta_{\text{H}}$ : 2.62-2.67 [4H, m, C(3'/5')H<sub>ax/eq</sub>], 3.20-3.26 [4H, m, C(2'/6')H<sub>ax/eq</sub>], 3.57 [2H, s, CH<sub>2</sub>], 4.81 [2H, br s, NH<sub>2</sub>], 6.67 [1H, d,  $J_{3,4} = 8.8$  Hz, C(3)H], 6.90-7.03 [2H, m<sup>^</sup>, C(5)H; C(4'')H], 7.07-7.18 [2H, m<sup>^</sup>, C(2'')H; C(6'')H], 7.25-7.28 [1H, m<sup>^</sup>, C(5'')H], 7.34 [1H, dd,  $J_{7,8} = 9.2$  Hz;  $J_{7,5} = 2.8$  Hz, C(7)H], 7.58 [1H, d,  $J_{8,7} = 9.2$  Hz, C(8)H], 7.76 [1H, d,  $J_{4,3} = 8.8$  Hz, C(4)H]. <sup>13</sup>C NMR (CDCl<sub>3</sub>, 125 MHz);  $\delta_{\text{C}}$ : 50.1 [C(2'/6')], 53.2 [C(3'/5')], 62.5 [d,  $J_{\text{C,F}} = 1.9$  Hz, CH<sub>2</sub>], 111.1 [C(5)], 112.0 [C(3)], 114.1 [d,  $J_{4'',\text{F}} = 21.4$  Hz, C(4'')], 115.9 [d,  $J_{2'',\text{F}} = 21.3$  Hz, C(2'')], 123.0 [C(7)], 124.2 [C(4a)], 124.7 [d,  $J_{6'',\text{F}} = 2.8$  Hz, C(6'')], 126.5 [C(8)], 129.8 [d,  $J_{5'',\text{F}} = 8.2$  Hz, C(5'')], 137.6 [C(4)], 141.0 [d,  $J_{1'',\text{F}} = 7.2$  Hz, C(1'')], 142.4 [C(8a)], 147.2 [C(6)], 155.6 [C(2)], 163.1 [d,  $J_{3'',\text{F}} = 245.5$  Hz, C(3'')].

**6-(4-(4-Fluorobenzyl)piperazin-1-yl)quinolin-2-amine (17e)**

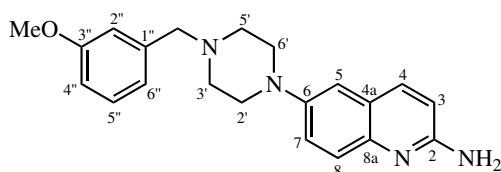
DavePhos (0.7 mg, 0.178  $\mu\text{mol}$ ), Pd(dba)<sub>2</sub> (0.9 mg, 1.57  $\mu\text{mol}$ ), **65e** (27.9 mg, 78.4  $\mu\text{mol}$ ) and LiHMDS solution (1.0 M in THF, 0.19 mL, 0.19 mmol) in 1,4-dioxane (2 mL) were reacted via General Method 6 for 16 hrs. The crude product was purified by flash column chromatography on silica gel, eluting with 6% MeOH in DCM to afford the title compound as a beige powder (14.4 mg, 55%). HRMS: C<sub>20</sub>H<sub>21</sub>FN<sub>4</sub> [M+H]<sup>+</sup> requires 337.1823; found 337.1818. <sup>1</sup>H NMR (CDCl<sub>3</sub>, 500 MHz);  $\delta_{\text{H}}$ : 2.60-2.66 [4H, m, C(3'/5')H<sub>ax/eq</sub>], 3.20-3.25 [4H, m, C(2'/6')H<sub>ax/eq</sub>], 3.55 [2H, s, CH<sub>2</sub>], 5.14 [2H, br s, NH<sub>2</sub>], 6.70 [1H, d,  $J_{3,4} = 8.8$  Hz, C(3)H], 6.95 [H, d,  $J_{5,7} = 2.8$  Hz, C(5)H],



#### 6.4. SYNTHESIS OF SIMPLE 6-POSITION SUBSTITUTED 2-AMINOQUINOLINE LIGANDS

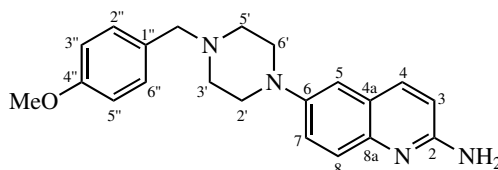
6.99-7.06 [2H, m, C(3''/5'')H], 7.29-7.38 [3H, m<sup>^</sup>, C(7)H; C(2''/6'')H], 7.59 [1H, d,  $J_{8,7} = 9.1$  Hz, C(8)H], 7.78 [1H, d,  $J_{4,3} = 8.8$  Hz, C(4)H]. <sup>13</sup>C NMR (CDCl<sub>3</sub>, 125 MHz);  $\delta_C$ : 50.0 [C(2''/6'')], 53.2 [C(3''/5'')], 62.3 [CH<sub>2</sub>], 111.1 [C(5)], 112.2 [C(3)], 115.2 [d,  $J_{3''/5'',F} = 21.0$  Hz, C(3''/5'')], 123.1 [C(7)], 124.1 [C(4a)], 125.8 [C(8)], 130.8 [d,  $J_{2''/6'',F} = 8.0$  Hz, C(2''/6'')], 133.8 [d,  $J_{1'',F} = 3.0$  Hz, C(1'')], 138.1 [C(4)], 141.2 [C(8a)], 147.4 [C(6)], 155.4 [C(2)], 132.2 [d,  $J_{4'',F} = 244.7$  Hz, C(4'')].

#### 6-(4-(3-Methoxybenzyl)piperazin-1-yl)quinolin-2-amine (17f)

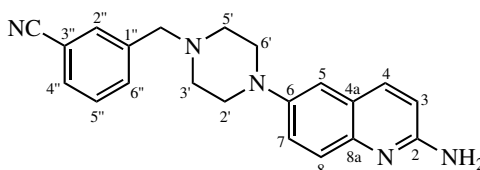


DavePhos (1.1 mg, 2.80  $\mu$ mol), Pd(dba)<sub>2</sub> (1.4 mg, 2.43  $\mu$ mol), **65f** (34.5 mg, 93.8  $\mu$ mol) and LiH-MDS solution (1.0 M in THF, 0.21 mL, 0.21 mmol) in 1,4-dioxane (2 mL) were reacted via General Method 6 for 16 hrs. The crude product was purified by flash column chromatography on silica gel, eluting with 6% MeOH in DCM to afford the title compound as a pale yellow powder (15.4 mg, 47%). HRMS: C<sub>21</sub>H<sub>24</sub>N<sub>4</sub>O [M+H]<sup>+</sup> requires 349.2023; found 349.2021. <sup>1</sup>H NMR (CDCl<sub>3</sub>, 600 MHz);  $\delta_H$ : 2.63-2.68 [4H, m, C(3''/5'')H<sub>ax/eq</sub>], 3.21-3.26 [4H, m, C(2''/6'')H<sub>ax/eq</sub>], 3.57 [2H, s, CH<sub>2</sub>], 3.82 [3H, s, CH<sub>3</sub>], 4.84 [2H, br s, NH<sub>2</sub>], 6.68 [1H, d,  $J_{3,4} = 8.8$  Hz, C(3)H], 6.82 [1H, ddd,  $J_{4'',5''} = 8.0$  Hz;  $J_{4'',6''} = 2.6$  Hz;  $J_{4'',2''} = 1.1$  Hz, C(4'')H], 6.94-6.97 [3H, m<sup>^</sup>, C(5)H; C(2'')H; C(6'')H\*], 7.25 [1H, t,  $J_{5'',4''} = J_{5'',6''} = 8.0$  Hz, C(5'')H], 7.35 [1H, dd,  $J_{7,8} = 9.2$  Hz;  $J_{7,5} = 2.8$  Hz, C(7)H], 7.58 [1H, d,  $J_{8,7} = 9.2$  Hz, C(8)H], 7.77 [1H, d,  $J_{4,3} = 8.8$  Hz, C(4)H]. <sup>13</sup>C NMR (CDCl<sub>3</sub>, 150 MHz);  $\delta_C$ : 50.1 [C(2''/6'')], 53.3 [C(3''/5'')], 55.4 [CH<sub>3</sub>], 63.1 [CH<sub>2</sub>], 111.1 [C(5)], 112.0 [C(3)], 112.7 [C(4'')], 114.8 [C(2'')], 121.6 [C(6'')], 123.0 [C(7)], 124.2 [C(4a)], 126.3 [C(8)], 129.4 [C(5'')], 137.7 [C(4)], 139.8 [C(1'')], 142.1 [C(8a)], 147.3 [C(6)], 155.5 [C(2)], 159.8 [C(3'')].

\* denotes signals could not be unambiguously assigned due to overlapping signals in 2D NMR spectra.

**6-(4-(4-Methoxybenzyl)piperazin-1-yl)quinolin-2-amine (17g)**

DavePhos (1.0 mg, 0.254  $\mu\text{mol}$ ), Pd(dba)<sub>2</sub> (1.3 mg, 2.26  $\mu\text{mol}$ ), **65g** (25.3 mg, 68.8  $\mu\text{mol}$ ) and LiHMDS solution (1.0 M in THF, 0.18 mL, 0.18 mmol) in 1,4-dioxane (2 mL) were reacted via General Method 6 for 16 hrs. The crude product was purified by flash column chromatography on silica gel, eluting with 7.5% MeOH in DCM to afford the title compound as a pale yellow powder (16 mg, 67%). HRMS: C<sub>21</sub>H<sub>24</sub>N<sub>4</sub>O [M+H]<sup>+</sup> requires 349.2023; found 349.2014. <sup>1</sup>H NMR (CDCl<sub>3</sub>, 600 MHz);  $\delta_{\text{H}}$ : 2.61-2.66 [4H, m, C(3'/5')H<sub>ax/eq</sub>], 3.20-3.25 [4H, m, C(2'/6')H<sub>ax/eq</sub>], 3.53 [2H, s, CH<sub>2</sub>], 4.93 [2H, br s, NH<sub>2</sub>], 6.68 [1H, d,  $J_{3,4} = 8.8$  Hz, C(3)H], 6.85-6.91 [2H, m, C(3''/5'')H], 6.95 [1H, d,  $J_{5,7} = 2.7$  Hz, C(5)H], 7.24-7.30 [2H, m, C(2''/6'')H], 7.34 [1H, dd,  $J_{7,8} = 9.2$  Hz;  $J_{7,5} = 2.7$  Hz, C(7)H], 7.58 [1H, d,  $J_{8,7} = 9.2$  Hz, C(8)H], 7.77 [1H, d,  $J_{4,3} = 8.8$  Hz, C(4)H]. <sup>13</sup>C NMR (CDCl<sub>3</sub>, 150 MHz);  $\delta_{\text{C}}$ : 50.0 [C(2'/6')], 53.1 [C(3'/5')], 55.4 [CH<sub>3</sub>], 62.7 [CH<sub>2</sub>], 111.1 [C(5)], 112.1 [C(3)], 113.8 [C(3''/5'')], 123.1 [C(7)], 124.2 [C(4a)], 126.1 [C(8)], 130.0 [C(1'')], 130.6 [C(2''/6'')], 137.8 [C(4)], 141.8 [C(8a)], 147.4 [C(6)], 155.4 [C(2)], 158.9 [C(4'')].

**3-((4-(2-Aminoquinolin-6-yl)piperazin-1-yl)methyl)benzonitrile (17h)**

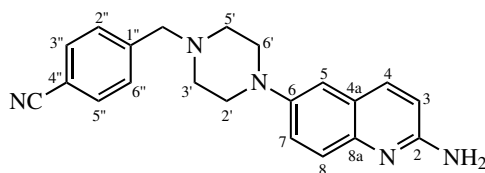
DavePhos (2.3 mg, 5.84  $\mu\text{mol}$ ), Pd(dba)<sub>2</sub> (3.5 mg, 6.09  $\mu\text{mol}$ ), **65h** (69.7 mg, 192  $\mu\text{mol}$ ) and LiHMDS solution (1.0 M in THF, 0.58 mL, 0.58 mmol) in 1,4-dioxane (2 mL) were reacted via General Method 6 for 16 hrs. The crude product was purified by flash column chromatography on silica gel, eluting with 6% MeOH in DCM to afford the title compound as a yellow powder (22.8 mg, 35%). HRMS: C<sub>21</sub>H<sub>21</sub>N<sub>5</sub> [M+H]<sup>+</sup> requires 344.1870; found 344.1861. IR (neat);  $\nu/\text{cm}^{-1}$ : 3441, 3122, 2226. <sup>1</sup>H NMR (CDCl<sub>3</sub>, 500 MHz);  $\delta_{\text{H}}$ : 2.62-2.67 [4H, m, C(3'/5')H<sub>ax/eq</sub>], 3.21-3.27 [4H, m, C(2'/6')H<sub>ax/eq</sub>], 3.61 [2H, s, CH<sub>2</sub>], 4.86 [2H, br s, NH<sub>2</sub>], 6.70 [1H, d,  $J_{3,4} = 8.8$  Hz, C(3)H], 6.97 [1H, d,  $J_{5,7} = 2.7$  Hz, C(5)H], 7.35 [1H, dd,  $J_{7,8} = 9.2$  Hz;  $J_{7,5} = 2.7$  Hz, C(7)H], 7.44 [1H, t,  $J_{5'',4''} = J_{5'',6''} = 7.7$  Hz, C(5'')H], 7.57 [1H, d<sup>†</sup>,  $J_{4'',5''} = 7.7$  Hz, C(4'')H], 7.59 [1H, d,  $J_{8,7} = 9.2$

#### 6.4. SYNTHESIS OF SIMPLE 6-POSITION SUBSTITUTED 2-AMINOQUINOLINE LIGANDS

---

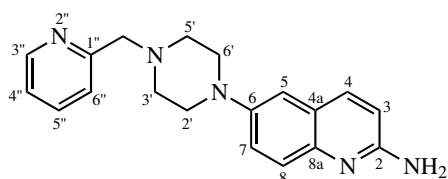
Hz, C(8)H], 7.61 [1H, d<sup>†</sup>,  $J_{6'',5''} = 7.7$  Hz, C(6'')H], 7.70 [1H, s<sup>†</sup>, C(2'')H], 7.78 [1H, d,  $J_{4,3} = 8.8$  Hz, C(4)H]. <sup>13</sup>C NMR (CDCl<sub>3</sub>, 125 MHz); δ<sub>C</sub>: 50.1 [C(2'/6')], 53.3 [C(3'/5')], 62.2 [CH<sub>2</sub>], 111.2 [C(5)], 112.1 [C(3)], 112.6 [C(3'')], 119.1 [C≡N], 123.1 [C(7)], 124.2 [C(4a)], 126.4 [C(8)], 129.3 [C(5'')], 131.1 [C(4'')], 132.6 [C(2'')], 133.5 [C(6'')], 137.8 [C(4)], 140.0 [C(1'')], 142.1 [C(8a)], 147.2 [C(6)], 155.5 [C(2)].

#### 4-((4-(2-Aminoquinolin-6-yl)piperazin-1-yl)methyl)benzonitrile (17i)



DavePhos (3.1 mg, 7.88 μmol), Pd(dba)<sub>2</sub> (4.4 mg, 7.65 μmol), **65i** (91.1 mg, 251 μmol) and LiH-MDS solution (1.0 M in THF, 0.75 mL, 0.75 mmol) in 1,4-dioxane (2 mL) were reacted via General Method 6 for 16 hrs. The crude product was purified by flash column chromatography on silica gel, eluting with 6% MeOH in DCM to afford the title compound as a beige powder (24.2 mg, 28%). HRMS: C<sub>21</sub>H<sub>21</sub>N<sub>5</sub> [M+H]<sup>+</sup> requires 344.1870; found 344.1869. IR (neat); ν/cm<sup>-1</sup>: 3294, 3177, 2226. <sup>1</sup>H NMR (CDCl<sub>3</sub>, 500 MHz); δ<sub>H</sub>: 2.62-2.68 [4H, m, C(3'/5')H<sub>ax/eq</sub>], 3.21-3.27 [4H, m, C(2'/6')H<sub>ax/eq</sub>], 3.63 [2H, s, CH<sub>2</sub>], 4.78 [2H, br s, NH<sub>2</sub>], 6.69 [1H, d,  $J_{3,4} = 8.8$  Hz, C(3)H], 6.96 [1H, d,  $J_{5,7} = 2.7$  Hz, C(5)H], 7.35 [1H, dd,  $J_{7,8} = 9.2$  Hz;  $J_{7,5} = 2.7$  Hz, C(7)H], 7.48-7.53 [2H, m, C(2''/6'')H], 7.59 [1H, d,  $J_{8,7} = 9.2$  Hz, C(8)H], 7.61-7.68 [2H, m, C(3''/5'')H], 7.78 [1H, d,  $J_{4,3} = 8.8$  Hz, C(4)H]. <sup>13</sup>C NMR (CDCl<sub>3</sub>, 125 MHz); δ<sub>C</sub>: 50.1 [C(2'/6')], 53.4 [C(3'/5')], 62.6 [CH<sub>2</sub>], 111.1 [C(4'')], 111.2 [C(5)], 112.1 [C(3)], 119.1 [C≡N], 123.1 [C(7)], 124.3 [C(4a)], 126.5 [C(8)], 129.7 [C(2''/6'')], 132.3 [C(3''/5'')], 137.7 [C(4)], 142.4 [C(8a)], 144.2 [C(1'')], 147.1 [C(6)], 155.5 [C(2)].

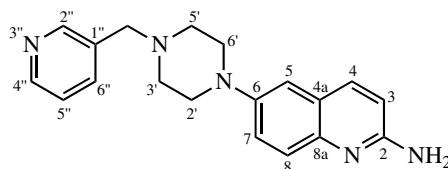
#### 6-(4-(Pyridin-2-ylmethyl)piperazin-1-yl)quinolin-2-amine (59a)



DavePhos (0.8 mg, 2.03 μmol), Pd(dba)<sub>2</sub> (1.2 mg, 2.09 μmol), **66a** (30.3 mg, 89.4 μmol) and LiHMDS solution (1.0 M in THF, 0.22 mL, 0.22 mmol) in 1,4-dioxane (2 mL) were reacted via

General Method 6 for 16 hrs. The crude product was purified by flash column chromatography on silica gel, eluting with 8% MeOH in DCM to afford the title compound as a yellow-orange powder (3.1 mg, 11%). HRMS: C<sub>19</sub>H<sub>21</sub>N<sub>5</sub> [M+H]<sup>+</sup> requires 320.1870; found 320.1866. <sup>1</sup>H NMR (CDCl<sub>3</sub>, 500 MHz); δ<sub>H</sub>: 2.60-2.81 [4H, m, C(3'/5')H<sub>ax/eq</sub>], 3.20-3.31 [4H, m, C(2'/6')H<sub>ax/eq</sub>], 3.76 [2H, s, CH<sub>2</sub>], 5.57 [2H, br s, NH<sub>2</sub>], 6.71 [1H, d, J<sub>3,4</sub> = 8.9 Hz, C(3)H], 6.96 [1H, d, J<sub>5,7</sub> = 2.7 Hz, C(5)H], 7.20 [1H, dd, J<sub>4'',5''</sub> = 7.6 Hz; J<sub>4'',3''</sub> = 4.9 Hz, C(4'')H], 7.37 [1H, dd, J<sub>7,8</sub> = 9.1 Hz; J<sub>7,5</sub> = 2.7 Hz, C(7)H], 7.45 [1H, d, J<sub>6'',5''</sub> = 7.6 Hz, C(6'')], 7.62 [1H, d, J<sub>8,7</sub> = 9.1 Hz, C(8)H], 7.68 [1H, dt, J<sub>5'',6''</sub> = J<sub>5'',4''</sub> = 7.6 Hz; J<sub>5'',3''</sub> = 1.8 Hz, C(5'')H], 7.82 [1H, d, J<sub>4,3</sub> = 8.9 Hz, C(4)H], 8.60 [1H, d<sup>†</sup>, J<sub>3'',4''</sub> = 4.9 Hz, C(3'')H].

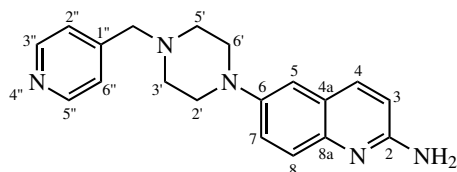
#### 6-(4-(Pyridin-3-ylmethyl)piperazin-1-yl)quinolin-2-amine (59b)



DavePhos (1.1 mg, 2.80 μmol), Pd(dba)<sub>2</sub> (1.5 mg, 2.61 μmol), **66b** (47.7 mg, 0.141 mmol) and LiHMDS solution (1.0 M in THF, 0.34 mL, 0.34 mmol) in 1,4-dioxane (2 mL) were reacted via General Method 6 for 16 hrs. The crude product was purified by flash column chromatography on silica gel, eluting with 10% MeOH in DCM to afford the title compound as a beige powder (6.6 mg, 15%). HRMS: C<sub>19</sub>H<sub>21</sub>N<sub>5</sub> [M+H]<sup>+</sup> requires 320.1870; found 320.1873. <sup>1</sup>H NMR (CDCl<sub>3</sub>, 500 MHz); δ<sub>H</sub>: 2.63-2.69 [4H, m, C(3'/5')H<sub>ax/eq</sub>], 3.21-3.26 [4H, m, C(2'/6')H<sub>ax/eq</sub>], 3.60 [2H, s, CH<sub>2</sub>], 4.73 [2H, br s, NH<sub>2</sub>], 6.68 [1H, J<sub>3,4</sub> = 8.8 Hz, C(3)H], 6.96 [1H, d, J<sub>5,7</sub> = 2.7 Hz, C(5)H], 7.28 [1H, dd, J<sub>5'',6''</sub> = 7.8 Hz; J<sub>5'',4''</sub> = 4.8 Hz, C(5'')H], 7.35 [1H, dd, J<sub>7,8</sub> = 9.2 Hz; J<sub>7,5</sub> = 2.7 Hz, C(7)H], 7.58 [1H, d, J<sub>8,7</sub> = 9.2 Hz, C(8)H], 7.71 [1H, br d<sup>†</sup>, J<sub>6'',5''</sub> = 7.8 Hz, C(6'')H], 7.77 [1H, d, J<sub>4,3</sub> = 8.8 Hz, C(4)H], 8.53 [1H, d<sup>†</sup>, J<sub>4'',5''</sub> = 4.8 Hz, C(4'')H], 8.60 [1H, s<sup>†</sup>, C(2'')H]. <sup>13</sup>C NMR (CDCl<sub>3</sub>, 150 MHz); δ<sub>C</sub>: 49.8 [C(2'/6')], 53.1 [C(3'/5')], 60.3 [CH<sub>2</sub>], 111.2 [C(5)], 112.5 [C(3)], 123.4 [C(7)], 123.5 [C(5'')], 123.7 [C(4a)], 124.3 [C(8)], 133.6 [C(1'')], 136.9 [C(6'')], 139.2 [C(4)], 147.8 [C(6)], 148.9 [C(4'')], 150.6 [C(2'')], 154.8 [C(2)].

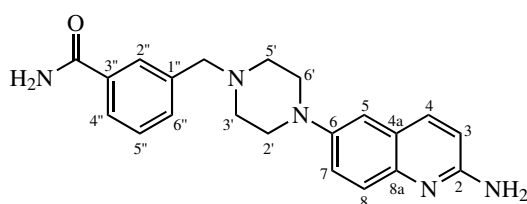
#### 6.4. SYNTHESIS OF SIMPLE 6-POSITION SUBSTITUTED 2-AMINOQUINOLINE LIGANDS

##### 6-(4-(Pyridin-4-ylmethyl)piperazin-1-yl)quinolin-2-amine (59c)



DavePhos (1.2 mg, 3.05  $\mu\text{mol}$ ), Pd(dba)<sub>2</sub> (1.7 mg, 2.96  $\mu\text{mol}$ ), **66c** (50.2 mg, 0.148 mmol) and LiHMDS solution (1.0 M in THF, 0.36 mL, 0.36 mmol) in 1,4-dioxane (2 mL) were reacted via General Method 6 for 16 hrs. The crude product was purified by flash column chromatography on silica gel, eluting with 10% MeOH in DCM to afford the title compound as a beige powder (15.9 mg, 34%). HRMS: C<sub>19</sub>H<sub>21</sub>N<sub>5</sub> [M+H]<sup>+</sup> requires 320.1870; found 320.1872. <sup>1</sup>H NMR (CDCl<sub>3</sub>, 500 MHz);  $\delta_{\text{H}}$ : 2.63-2.68 [4H, m, C(3'/5')H<sub>ax/eq</sub>], 3.21-3.27 [4H, m, C(2'/6')H<sub>ax/eq</sub>], 3.59 [2H, s, CH<sub>2</sub>], 5.56 [2H, br s, NH<sub>2</sub>], 6.72 [1H, d,  $J_{3,4} = 8.8$  Hz, C(3)H], 6.96 [1H, d,  $J_{5,7} = 2.8$  Hz, C(5)H], 7.28-7.38 [2H, m, C(2''/6'')H], 7.34 [1H, dd,  $J_{7,8} = 9.1$  Hz;  $J_{7,5} = 2.8$  Hz, C(7)H], 7.60 [1H, d,  $J_{8,7} = 9.1$  Hz, C(8)H], 7.78 [1H, d,  $J_{4,3} = 8.8$  Hz, C(4)H], 8.54-8.59 [2H, m, C(3''/5'')H]. <sup>13</sup>C NMR (CDCl<sub>3</sub>, 150 MHz);  $\delta_{\text{C}}$ : 49.9 [C(2'/6')], 53.3 [C(3'/5')], 61.8 [CH<sub>2</sub>], 111.2 [C(5)], 112.5 [C(3)], 123.2 [C(7)], 123.8 [C(4a)], 124.0 [C(2''/6'')], 124.9 [C(8)], 138.5 [C(4)], 140.0 [C(8a)], 147.4 [C(6)], 147.6 [C(1'')], 150.0 [C(3''/5'')], 155.3 [C(2)].

##### 3-((4-(2-Aminoquinolin-6-yl)piperazin-1-yl)methyl)benzamide (17j)

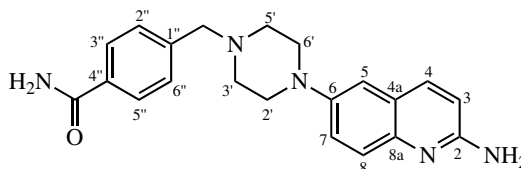


Potassium hydroxide (16.8 mg, 0.299 mmol), **17h** (10.3 mg, 30.0  $\mu\text{mol}$ ) in *t*-butanol (0.8 mL) were reacted via General Method 15 for 2 hrs. The crude product was purified by micropipette column chromatography on silica gel, eluting with 12% MeOH in DCM to afford the title compound as a yellow powder (5.7 mg, 53%). HRMS: C<sub>21</sub>H<sub>23</sub>N<sub>5</sub>O [M+H]<sup>+</sup> requires 362.1975; found 362.1973. IR (neat);  $\nu/\text{cm}^{-1}$ : 3333, 3189, 2924, 2819, 1603. <sup>1</sup>H NMR (CDCl<sub>3</sub>, 500 MHz);  $\delta_{\text{H}}$ : 2.64-2.68 [4H, m, C(3'/5')H<sub>ax/eq</sub>], 3.19-3.27 [4H, m, C(2'/6')H<sub>ax/eq</sub>], 3.64 [2H, s, CH<sub>2</sub>], 4.83 [2H, br s, NH<sub>2</sub>], 5.59 [1H, br s, amide NH], 6.11 [1H, br s, amide NH], 6.68 [1H, d,  $J_{3,4} = 8.8$  Hz, C(3)H], 6.96 [1H, d,  $J_{5,7} = 2.7$  Hz, C(5)H], 7.35 [1H, d<sup>†</sup>,  $J_{7,8} = 9.3$  Hz, C(7)H], 7.43 [1H, t,  $J_{5'',4''} = J_{5'',6''} = 7.7$  Hz, C(5'')H],

7.55 [1H, d<sup>†</sup>,  $J_{6'',5'} = 7.7$  Hz, C(6'')H], 7.59 [1H, d,  $J_{8,7} = 9.3$  Hz, C(8)H], 7.72 [1H, d<sup>†</sup>,  $J_{4'',5''} = 7.7$  Hz, C(4'')H], 7.78 [1H, d,  $J_{4,3} = 8.8$  Hz, C(4)H], 7.84 [1H, s<sup>†</sup>, C(2'')H]. <sup>13</sup>C NMR (CDCl<sub>3</sub>, 150 MHz); δ<sub>C</sub>: 50.1 [C(2'/6')], 53.3 [C(3'/5')], 62.8 [CH<sub>2</sub>], 111.2 [C(5)], 112.1 [C(3)], 123.1 [C(7)], 124.2 [C(4a)], 126.4 [C(8); C(4'')\*], 126.4 [C(8); C(4'')\*], 128.2 [C(2'')], 128.8 [C(5'')], 132.9 [C(6'')], 133.4 [C(3'')], 137.8 [C(4)], 139.0 [C(1'')], 142.0 [C(8a)], 147.2 [C(6)], 155.4 [C(2)], 169.2 [C=O].

\* denotes signals could not be unambiguously assigned due to overlapping signals in the <sup>13</sup>C NMR spectrum.

#### 4-((4-(2-Aminoquinolin-6-yl)piperazin-1-yl)methyl)benzamide (17k)

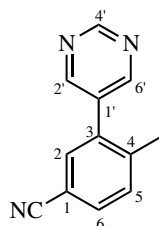


Potassium hydroxide (8.0 mg, 0.143 mmol), **17i** (9.5 mg, 27.7 μmol) in *t*-butanol (1 mL) were reacted via General Method 15 for 3 hrs. The crude product was purified by micropipette column chromatography on silica gel, eluting with 12% MeOH in DCM to afford the title compound as a beige powder (4.3 mg, 43%). HRMS: C<sub>21</sub>H<sub>23</sub>N<sub>5</sub>O [M+H]<sup>+</sup> requires 362.1975; found 362.1976. IR (neat); ν/cm<sup>-1</sup>: 3347, 3204, 2925, 2821, 2604. <sup>1</sup>H NMR (CDCl<sub>3</sub>, 500 MHz); δ<sub>H</sub>: 2.63-2.68 [4H, m, C(3'/5')H<sub>ax/eq</sub>], 3.20-3.28 [4H, m, C(2'/6')H<sub>ax/eq</sub>], 3.64 [2H, s, CH<sub>2</sub>], 5.17 [2H, br s, NH<sub>2</sub>], 5.55 [1H, br s, amide NH], 5.94 [1H, br s, amide NH], 6.68 [1H, d,  $J_{3,4} = 8.8$  Hz, C(3)H], 6.96 [1H, d,  $J_{5,7} = 2.7$  Hz, C(5)H], 7.35 [1H, dd,  $J_{7,8} = 9.2$  Hz;  $J_{7,5} = 2.7$  Hz, C(7)H], 7.44-7.49 [2H, m, C(2''/6'')H], 7.61 [1H, d,  $J_{8,7} = 9.2$  Hz, C(8)H], 7.77-7.82 [3H, m<sup>^</sup>, C(4)H; C(3''/5'')H].

## 6.5 Synthesis of complex 6-substituted-2-aminoquinoline ligands

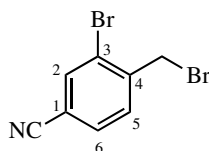
### 6.5.1 Synthesis of a complex 6-benzylpiperidinyl 2-aminoquinoline ligand containing biaryl and nitrile components

#### 4-Methyl-3-(pyrimidin-5-yl)benzonitrile (98)



3-Bromo-4-methylbenzonitrile (1.00 g, 5.15 mmol), pyrimidin-5-ylboronic acid (0.800 g, 6.45 mmol), Pd(OAc)<sub>2</sub> (71.2 mg, 0.32 mmol), triphenylphosphine (85.8 mg, 0.33 mmol) and potassium carbonate (0.925 g, 6.69 mmol) 1:1 toluene/ethanol (2.5 mL) were reacted via General Method 17 for 13 hrs. The crude product was recrystallised from ethanol to afford the title compound as a fluffy, off-white powder, m.p. 149-151 °C (0.484 g, 48%). HRMS: C<sub>12</sub>H<sub>9</sub>N<sub>3</sub> [M+H]<sup>+</sup> requires 196.0869; found 196.0871. <sup>1</sup>H NMR (CDCl<sub>3</sub>, 500 MHz); δ<sub>H</sub>: 2.36 [3H, s, CH<sub>3</sub>], 7.46 [1H, d, J<sub>5,6</sub> = 7.9 Hz, C(5)H], 7.52 [1H, d, J<sub>2,6</sub> = 1.8 Hz, C(2)H], 7.65 [1H, dd, J<sub>6,5</sub> = 7.9 Hz; J<sub>6,2</sub> = 1.8 Hz, C(6)H], 8.73 [2H, s, C(2'/6')H], 9.28 [1H, s, C(4')H]. <sup>13</sup>C NMR (CDCl<sub>3</sub>, 125 MHz); δ<sub>C</sub>: 20.9 [CH<sub>3</sub>], 111.0 [C(1)], 118.3 [C≡N], 131.9 [C(5)], 132.5 [C(6)], 133.3 [C(2)], 133.5 [C(1')], 135.8 [C(3)], 141.8 [C(4)], 156.6 [C(2'/6')], 158.3 [C(4')].

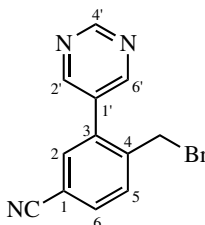
#### 3-Bromo-4-(bromomethyl)benzonitrile (104)



*N*-Bromosuccinimide (1.02 g, 5.72 mmol), 3-bromo-4-methylbenzonitrile (1.01 g, 5.17 mmol), benzoyl peroxide (41.7 mg, 0.172 mmol) in BTF (10 mL) were reacted via General Method 18 for 19 hr at 80°C. The crude product was purified by flash column chromatography on silica gel, eluting with 30% DCM in hexane to afford the title compound as a white powder (0.752 g, 53%). <sup>1</sup>H NMR (CDCl<sub>3</sub>, 500 MHz); δ<sub>H</sub>: 4.58 [2H, s, CH<sub>2</sub>], 7.57 [1H, d, J<sub>5,6</sub> = 8.0 Hz, C(5)H], 7.60 [1H, dd, J<sub>6,5</sub> = 8.0 Hz; J<sub>6,2</sub> = 1.5 Hz, C(6)H], 7.88 [1H, d, J<sub>2,6</sub> = 1.5 Hz, C(2)H]. <sup>13</sup>C NMR (CDCl<sub>3</sub>, 125

MHz);  $\delta_{\text{C}}$ : 31.7 [CH<sub>2</sub>], 114.0 [C(1)], 117.0 [C≡N], 124.9 [C(3)], 131.6 [C(6)], 131.8 [C(5)], 136.7 [C(2)], 142.5 [C(4)].

#### 4-(Bromomethyl)-3-(pyrimidin-5-yl)benzonitrile (**92**)

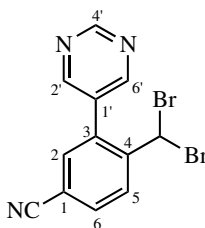


*N*-Bromosuccinimide (0.554 g, 3.11 mmol), **98** (0.498 g, 0.767 mmol), benzoyl peroxide (13.5 mg, 55.7  $\mu\text{mol}$ ) in BTF (9 mL) were reacted via General Method 18 for 20 hr at 60°C. The crude product was purified by flash column chromatography on silica gel, eluting with 2.5% EtOAc in DCM to afford a 5:6 mixture of the title compound and **98** as a white powder (108 mg, <15%\*) and **106** as a colourless, transparent oil (6.8 mg, <1%).

\* maximum theoretical yield calculated assuming pure **92** was isolated.

**92**: HRMS: C<sub>12</sub>H<sub>8</sub>BrN<sub>3</sub> [M+H]<sup>+</sup> requires 273.9975 [<sup>79</sup>Br] / 275.9954 [<sup>81</sup>Br]; found 273.9975 / 275.9955. <sup>1</sup>H NMR (CDCl<sub>3</sub>, 500 MHz);  $\delta_{\text{H}}$ : 4.34 [2H, s, CH<sub>2</sub>], 7.56 [1H, d,  $J_{2,6} = 1.7$  Hz, C(2)H], 7.69 [1H, d,  $J_{5,6} = 8.0$  Hz, C(5)H], 7.76 [1H, dd,  $J_{6,5} = 8.0$  Hz;  $J_{6,2} = 1.7$  Hz, C(6)H], 8.86 [2H, s, C(2'/6')H], 9.34 [1H, s, C(4')H]. <sup>13</sup>C NMR (CDCl<sub>3</sub>, 125 MHz);  $\delta_{\text{C}}$ : 29.0 [CH<sub>2</sub>] 113.4 [C(1)]. 117.6 [C≡N], 132.2 [C(1')], 132.2 [C(5)], 133.1 [C(6)], 134.2 [C(2)], 136.1 [C(3)], 141.3 [C(4)], 156.3 [C(2'/6')], 158.9 [C(4')].

#### 4-(Dibromomethyl)-3-(pyrimidin-5-yl)benzonitrile (**106**)



HRMS: C<sub>12</sub>H<sub>7</sub>Br<sub>2</sub>N<sub>3</sub> [M+H]<sup>+</sup> requires 351.9079 [<sup>79</sup>Br,<sup>79</sup>Br] / 353.9060 [<sup>79</sup>Br,<sup>81</sup>Br] / 355.9039 [<sup>81</sup>Br, <sup>81</sup>Br] found 351.9080 / 353.9058 / 355.9039. <sup>1</sup>H NMR (CDCl<sub>3</sub>, 500 MHz);  $\delta_{\text{H}}$ : 6.42 [1H, s, CH], 7.49 [1H, d,  $J_{2,6} = 1.7$  Hz, C(2)H], 7.87 [1H, dd,  $J_{6,5} = 8.3$  Hz;  $J_{6,2} = 1.7$  Hz, C(6)H], 8.27



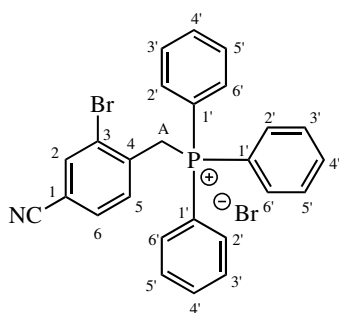
## 6.5. SYNTHESIS OF COMPLEX 6-SUBSTITUTED-2-AMINOQUINOLINE LIGANDS

[1H, d,  $J_{5,6} = 8.3$  Hz, C(5)H], 8.83 [2H, s, C(2'/6')H], 9.38 [1H, s, C(4')H].  $^{13}\text{C}$  NMR ( $\text{CDCl}_3$ , 125 MHz);  $\delta_{\text{C}}$ : 35.4 [CH], 114.3 [C(1)], 117.2 [C $\equiv$ N], 131.3 [C(3)\*/C(1')\*], 131.5 [C(3)\*/C(1')\*], 131.9 [C(5)], 133.6 [C(2)\*\*; C(6)\*\*], 144.6 [C(4)], 156.2 [C(2'/6')], 159.3 [C(4')].

\* denotes signals could not be unambiguously assigned due to overlapping signals in 2D NMR spectra.

\*\* denotes overlapping signals in  $^{13}\text{C}$  NMR spectra.

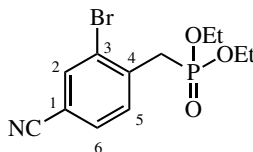
### (2-Bromo-4-cyanobenzyl)triphenylphosphonium bromide (107)



A mixture of **104** and 3-bromo-4-methylbenzonitrile (1.55 g, <5.65 mmol\*) and triphenylphosphine (1.79 g, 6.83 mmol) in toluene (25 mL) were reacted via General Method 16 for 17 hr to afford the title compound as an off-white solid (1.72 g, >57%\*\*).  $^1\text{H}$  NMR ( $\text{CDCl}_3$ , 600 MHz);  $\delta_{\text{H}}$ : 5.95 [2H, d,  $J_{\text{H,P}} = 15.1$  Hz,  $\text{CH}_2$ ], 7.50 [1H, dt,  $J_{6,5} = 8.0$  Hz;  $J_{6,2} = J_{6,\text{P}} = 1.3$  Hz, C(6)H], 7.63-7.72 [7H, m $^\wedge$ , C(2)H; C(3'/5')H], 7.72-7.80 [6H, m, C(2'/6')H], 7.80-7.87 [3H, m, C(4')H], 7.91 [1H, dd,  $J_{5,6} = 8.0$  Hz;  $J_{5,\text{P}} = 2.7$  Hz, C(5)H].  $^{13}\text{C}$  NMR ( $\text{CDCl}_3$ , 150 MHz);  $\delta_{\text{C}}$ : 31.2 [d,  $J_{\text{C,P}} = 48.5$  Hz,  $\text{CH}_2$ ], 114.1 [d,  $J_{1,\text{P}} = 4.1$  Hz, C(1)], 116.7 [d,  $J_{\text{C,P}} = 2.5$  Hz, C $\equiv$ N], 117.1 [d,  $J_{1',\text{P}} = 86.1$  Hz, C(1')], 127.6 [d,  $J_{3,\text{P}} = 6.6$  Hz, C(3)], 130.6 [d,  $J_{3'/5',\text{P}} = 12.7$  Hz, C(3'/5')], 131.8 [d,  $J_{4,\text{P}} = 3.6$  Hz, C(6)], 134.1 [d,  $J_{4,\text{P}} = 8.8$  Hz, C(4)], 134.5 [d,  $J_{2'/6',\text{P}} = 10.1$  Hz, C(2'/6')], 134.5 [d,  $J_{5,\text{P}} = 4.9$  Hz, C(5)], 135.6 [d,  $J_{4',\text{P}} = 3.1$  Hz, C(4')], 135.9 [d,  $J_{2,\text{P}} = 3.3$  Hz, C(2)].

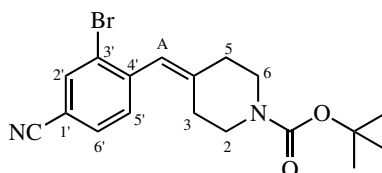
\* indicates maximum theoretical number of moles, assuming pure **104** was used.

\*\* indicates minimum theoretical yield was calculated assuming pure **104** was used as the limiting reagent in the reaction.

**Diethyl 2-bromo-4-cyanobenzylphosphonate (111)**

A solution of **104** (0.813 g, 2.96 mmol) in triethylphosphite (3.5 mL, 20.4 mmol) was heated at reflux for 16 hrs. The reaction mixture was cooled to room temperature, and excess triethylphosphite was removed via short-path distillation under reduced pressure to afford a mixture of the title compound and triethylphosphite as a yellow oil, which used without further purification (0.660 g, <67%\*).  $^1\text{H}$  NMR ( $\text{CDCl}_3$ , 500 MHz);  $\delta_{\text{H}}$ : 1.28 [6H, t,  $J_{\text{H,H}} = J_{\text{H,P}} = 7.1$  Hz, 2 x  $\text{CH}_3$ ], 3.46 [2H, d,  $J_{\text{H,P}} = 22.7$  Hz,  $\text{CH}_2$ ], 4.07-4.35 [4H, m $^\dagger$ , 2 x  $\text{OCH}_2$ ], 7.58 [2H, br s $^{*\dagger}$ , C(5)H; C(6)H], 7.87 [1H, br s $^\dagger$ , C(2)H].  $^{13}\text{C}$  NMR ( $\text{CDCl}_3$ , 125 MHz);  $\delta_{\text{C}}$ : 16.4 [d,  $J_{\text{C,P}} = 6.1$  Hz,  $\text{CH}_3$ ], 34.0 [d,  $J_{\text{C,P}} = 138.1$  Hz,  $\text{CH}_2$ ], 62.8 [d,  $J_{\text{C,P}} = 6.7$  Hz,  $\text{OCH}_2$ ], 117.2 [d,  $J_{\text{C,P}} = 2.3$  Hz,  $\text{C}\equiv\text{N}$ ], 125.3 [d,  $J_{3,\text{P}} = 8.7$  Hz, C(3)], 130.7 [d,  $J_{6,\text{P}} = 6.7$  Hz, C(6)], 130.9 [d,  $J_{1,\text{P}} = 3.6$  Hz, C(1)], 132.3 [d,  $J_{5,\text{P}} = 5.2$  Hz, C(5)], 136.2 [d,  $J_{2,\text{P}} = 3.3$  Hz, C(2)], 138.0 [d,  $J_{4,\text{P}} = 9.4$  Hz, C(4)].

\* indicates theoretical maximum yield was calculated assuming pure **111** had been isolated.

***tert*-Butyl 4-(2-bromo-4-cyanobenzylidene)piperidine-1-carboxylate (108)**

*Synthetic method A:* Under an atmosphere of nitrogen, LiHMDS (1.0 M in THF, 6.4 mL, 6.4 mmol) was added to **107** (1.70 g, 3.12 mmol) in anhydrous THF (5 mL), and stirred at room temperature for 15 minutes. A solution of *N*-Boc-4-piperidone (791 mg, 3.97 mmol) in anhydrous THF (2 mL) was added dropwise, and the reaction stirred at room temperature for 19 hrs. Work-up as specified afforded the crude product as a red-orange oil. Analysis of the crude product  $^1\text{H}$  NMR spectrum indicated the main product present was the reduced product 3-bromo-4-methylbenzonitrile, with only trace amounts of the desired title compound. Product was not purified.

*Synthetic method B:* Under an atmosphere of nitrogen, LiHMDS (1.0 M in THF, 4.0 mL, 4.0 mmol) was added to **111** (0.660 g, <1.99 mmol\*) in anhydrous THF (5 mL), and stirred at room tem-

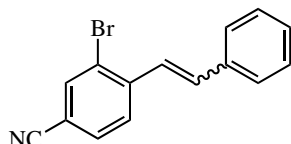
## 6.5. SYNTHESIS OF COMPLEX 6-SUBSTITUTED-2-AMINOQUINOLINE LIGANDS

perature for 15 minutes. A solution of *N*-Boc-4-piperidone (503 mg, 2.52 mmol) in anhydrous THF (2 mL) was added dropwise, and the reaction stirred at room temperature for 24 hrs. The reaction mixture was quenched with water (10 mL) and extracted with ethyl acetate (3 x 40 mL). The organic extracts were combined, dried over MgSO<sub>4</sub>, filtered and concentrated under reduced pressure. The crude product was purified by flash column chromatography on silica gel, eluting with 10% EtOAc/hexanes to afford the title compound as a white solid, m.p. 133-135 °C (294 mg, >39%\*). HRMS: C<sub>18</sub>H<sub>21</sub>BrN<sub>2</sub>O<sub>2</sub> [(M-C(CH<sub>3</sub>)<sub>3</sub>)+H]<sup>+</sup> requires 321.0233 [<sup>79</sup>Br] / 323.0213 [<sup>81</sup>Br], found 321.0232 / 323.0213. IR (neat); ν/cm<sup>-1</sup>: 2229, 1695, 1696, 1231, 590. <sup>1</sup>H NMR (CDCl<sub>3</sub>, 600 MHz); δ<sub>H</sub>: 1.48 [9H, s, C(CH<sub>3</sub>)<sub>3</sub>], 2.28 [2H, t,  $J_{3ax,3eq} = J_{3ax/3eq,2ax,2eq} = 5.8$  Hz, C(3)H<sub>ax/eq</sub>], 2.39 [2H, t,  $J_{5ax,5eq} = J_{5ax/5eq,6ax/6eq} = 5.8$  Hz, C(5)H<sub>ax/eq</sub>], 3.42 [2H, t,  $J_{2ax,2eq} = J_{2ax/2eq,3ax/3eq} = 5.8$  Hz, C(2)H<sub>ax/eq</sub>], 3.55 [2H, t,  $J_{6ax,6eq} = J_{6ax/6eq,5ax/5eq} = 5.8$  Hz, C(6)H<sub>ax/eq</sub>], 6.31 [1H, s, C(A)H], 7.28 [1H, d,  $J_{5',6'} = 7.8$  Hz, C(5')H], 7.55 [1H, dd,  $J_{6',5'} = 7.8$  Hz;  $J_{6',2'} = 1.7$  Hz, C(6')H], 7.87 [1H, d,  $J_{2',6'} = 1.7$  Hz, C(2')H]. <sup>13</sup>C NMR (CDCl<sub>3</sub>, 150 MHz); δ<sub>C</sub>: 28.6 [CH<sub>3</sub>], 29.7 [C(5)], 36.2 [C(3)], 43.8-46.4 [br m<sup>^</sup>, C(2'); C(6')], 80.0 [C(CH<sub>3</sub>)<sub>3</sub>], 111.9 [C(1')], 117.5 [C≡N], 123.1 [C(A)], 124.7 [C(3')], 130.6 [C(6')], 131.4 [C(5')], 136.0 [C(2')], 142.8 [C(4)\*\*; C(4')\*\*], 142.8 [C(4)\*\*; C(4')\*\*], 154.8 [C=O].

\* indicates residual triethylphosphite was present in the reagent; theoretical minimum yield was calculated assuming pure **111** was used.

\*\* denotes that overlapping signals in <sup>13</sup>C NMR spectra precluded unambiguous signal assignment in 2D NMR spectra.

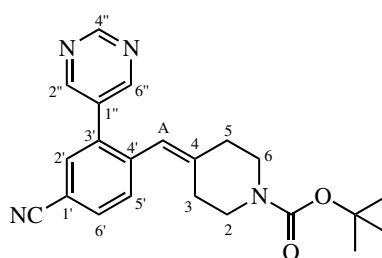
### (*E*)-3-Bromo-4-styrylbenzonitrile (**110**)



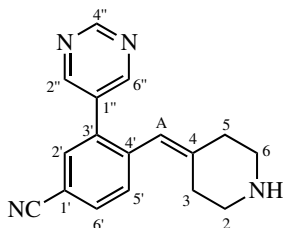
**107** (0.256 g, 0.477 mmol) was suspended in anhydrous THF (5 mL) and stirred under an atmosphere of nitrogen. The suspension was cooled to 0°C, and LiHMDS (1.0 M in THF, 0.95 mL, 0.95 mmol) was added dropwise. The reaction mixture was warmed to room temperature, and stirred for 15 mins. Benzaldehyde (0.06 mL, 0.588 mmol) was added dropwise, and the reaction mixture was then stirred for 18 hrs. The reaction mixture was quenched with MeOH (30 mL), then concentrated

under reduced pressure. The resulting residue was suspended in a 2:3 mixture of EtOAc/hexanes (40 mL) and filtered, then the filtrate was concentrated under reduced pressure to afford the crude product as an orange oily solid. Analysis of the crude product  $^1\text{H}$  NMR spectrum indicated that the title compound had formed, through identification of two distinctive doublets integrating to 1H displaying characteristic di-substituted alkene coupling constant values ( $J = 12.1$  Hz). Product was not purified.

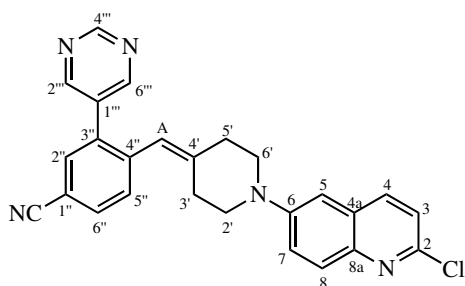
***tert*-Butyl 4-(4-cyano-2-(pyrimidin-5-yl)benzylidene)piperidine-1-carboxylate (94)**



Pyrimidin-5-ylboronic acid (115 mg, 0.930 mmol), **108** (292 mg, 0.775 mmol), Pd(OAc)<sub>2</sub> (6.5 mg, 29.0  $\mu\text{mol}$ ), triphenylphosphine (21.9 mg, 83.5  $\mu\text{mol}$ ) and potassium carbonate (193 mg, 1.39 mmol) 1:1 toluene/ethanol (2 mL) were reacted via General Method 17 for 13 hrs. The crude product was purified by flash column chromatography on silica gel, eluting with 20% EtOAc in hexanes to afford the title compound as a pale yellow oil (146 mg, 50%). HRMS: C<sub>24</sub>H<sub>26</sub>N<sub>2</sub>O<sub>2</sub> [M+H]<sup>+</sup> requires 377.1972; found 377.1981.  $^1\text{H}$  NMR (CDCl<sub>3</sub>, 600 MHz);  $\delta_{\text{H}}$ : 1.46 [9H, s, C(CH<sub>3</sub>)<sub>3</sub>], 2.17-2.31 [4H, m<sup>^</sup>, C(3)H<sub>ax/eq</sub>; C(5)H<sub>ax/eq</sub>], 3.32 [2H, br s<sup>†</sup>, C(2)H<sub>ax/eq</sub>], 3.45 [2H, t,  $J_{6\text{ax},6\text{eq}} = J_{6\text{ax}/6\text{eq},5\text{ax}/5\text{eq}} = 5.8$  Hz, C(6)H<sub>ax/eq</sub>], 6.13 [1H, s, C(A)H], 7.42 [1H, d,  $J_{5',6'} = 8.0$  Hz, C(5')H], 7.63 [1H, d,  $J_{2',6'} = 1.7$  Hz, C(2')H], 7.70 [1H, dd,  $J_{6',5'} = 8.0$  Hz;  $J_{6',2'} = 1.7$  Hz, C(6')H], 8.75 [2H, s, C(2''/6'')H], 9.24 [1H, s, C(4'')H].  $^{13}\text{C}$  NMR (CDCl<sub>3</sub>, 150 MHz);  $\delta_{\text{C}}$ : 28.5 [CH<sub>3</sub>], 29.7 [C(3)], 36.1 [C(5)], 43.3-46.7 [br m<sup>^</sup>, C(2); C(6)], 80.1 [C(CH<sub>3</sub>)<sub>3</sub>], 111.7 [C(1')], 118.2 [C $\equiv$ N], 121.7 [C(A)], 131.7 [C(5')], 132.2 [C(2')], 135.2 [C(3')], 141.0 [C(1')], 143.3 [C(4)], 154.6 [C=O], 156.8 [C(2''/6'')], 158.1 [C(4'')].

**4-(Piperidin-4-ylidenemethyl)-3-(pyrimidin-5-yl)benzotrile (95)**

Trifluoroacetic acid (1 mL, 13.1 mmol), **94** (125 mg, 0.331 mmol) in DCM (6 mL) were reacted essentially via General Method 4 for 2 hr, except the reaction mixture was extracted with 3:1 chloroform/isopropanol (3 x 20 mL), to afford the title compound as a yellow-orange oil (93.9 mg, 100%). HRMS:  $C_{17}H_{16}N_4$   $[M+H]^+$  requires 277.1448; found 277.1442.  $^1H$  NMR ( $CDCl_3$ , 600 MHz);  $\delta_H$ : 2.37 [2H, t,  $J_{3ax,3eq} = J_{3ax/3eq,2ax,2eq} = 5.8$  Hz, C(3) $H_{ax/eq}$ ], 2.39-2.48 [2H, m $^\dagger$ , C(5) $H_{ax/eq}$ ], 2.88 [2H, t,  $J_{2ax,2eq} = J_{2ax/2eq,3ax/3eq} = 5.8$  Hz, C(2) $H_{ax/eq}$ ], 3.08 [2H, t,  $J_{6ax,6eq} = J_{6ax/6eq,5ax/5eq} = 5.8$  Hz, C(6) $H_{ax/eq}$ ], 5.40 [1H, br s, NH], 6.16 [1H, s, C(A)H], 7.42 [1H, d,  $J_{5',6'} = 8.0$  Hz, C(5')H], 7.64 [1H, d,  $J_{2',6'} = 1.7$  Hz, C(2')H], 7.72 [1H, dd,  $J_{6',5'} = 8.0$  Hz;  $J_{6',2'} = 1.7$  Hz, C(6')H], 8.75 [2H, s, C(2''/6'')H], 9.25 [1H, s, C(4'')H].  $^{13}C$  NMR ( $CDCl_3$ , 150 MHz);  $\delta_C$ : 28.9 [C(3)], 35.3 [C(5)], 45.9 [C(2)], 46.7 [C(6)], 112.0 [C(1')], 118.1 [C $\equiv$ N], 122.2 [C(A)], 131.6 [C(5')], 132.3 [C(6')], 133.0 [C(1'')], 133.3 [C(2')], 135.3 [C(3')], 140.5 [C(4')], 141.2 [C(4)], 156.8 [C(2''/6'')], 158.2 [C(4'')].

**4-((1-(2-Chloroquinolin-6-yl)piperidin-4-ylidene)methyl)-3-(pyrimidin-5-yl)benzotrile (96)**

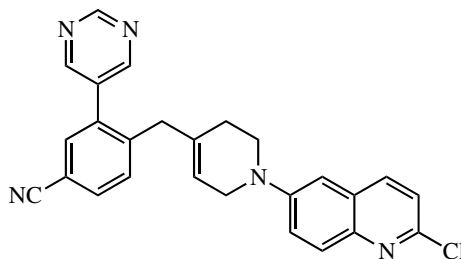
Sodium *tert*-butoxide (56.7 mg, 437  $\mu$ mol), **95** (93.9 mg, 340  $\mu$ mol), **26** (106 mg, 437  $\mu$ mol), cataCXium<sup>®</sup> A (4.0 mg, 11.2  $\mu$ mol), Pd(OAc)<sub>2</sub> (4.0 mg, 17.8  $\mu$ mol) in anhydrous BTF (2 mL) were reacted via General Method 5 for 16 hr. The crude product was purified by flash column chromatography on silica gel, eluting with 0.5 % MeOH in DCM to afford a mixture of the title compound with trace amounts of its tetrahydropyridine isomer **113**<sup>\*</sup> as an orange oil (47.3 mg, 32%), and **112** as an orange oil (4.6 mg, 3%).

## 6.5. SYNTHESIS OF COMPLEX 6-SUBSTITUTED-2-AMINOQUINOLINE LIGANDS

**96:** HRMS:  $C_{26}H_{20}ClN_5$   $[M+H]^+$  requires 438.1480 [ $^{35}Cl$ ] / 440.1451 [ $^{37}Cl$ ]; found 438.1485 / 440.1475.  $^1H$  NMR ( $CDCl_3$ , 600 MHz);  $\delta_H$ : 2.45 [2H, t,  $J_{3'ax,3'eq} = J_{3'ax/3'eq,2'ax,2'eq} = 5.8$  Hz,  $C(3')H_{ax/eq}$ ], 2.49 [2H, t,  $J_{5'ax,5'eq} = J_{5'ax/5'eq,6'ax/6'eq} = 5.7$  Hz,  $C(5')H_{ax/eq}$ ], 3.27 [2H, t,  $J_{2'ax,2'eq} = J_{2'ax/2'eq,3'ax/3'eq} = 5.8$  Hz,  $C(2')H_{ax/eq}$ ], 3.40-3.43 [2H, m $^\dagger$ ,  $C(6')H_{ax/eq}$ ], 6.18 [1H, s, C(A)H], 6.99 [1H, d,  $J_{5,7} = 2.7$  Hz, C(5)H], 7.29 [1H, d,  $J_{3,4} = 8.6$  Hz, C(3)H], 7.46-7.49 [2H, m $^\wedge$ , C(7)H; C(5'')H], 7.65 [1H, d,  $J_{2'',6''} = 1.7$  Hz, C(2'')H], 7.72 [1H, dd,  $J_{6'',5''} = 8.0$  Hz;  $J_{6'',2''} = 1.7$  Hz, C(6'')H], 7.87 [1H, d,  $J_{8,7} = 9.3$  Hz, C(8)H], 7.91 [1H, d,  $J_{4,3} = 8.6$  Hz, C(4)H], 8.78 [2H, s, C(2''')/6''')H], 9.24 [1H, s, C(4''')H].  $^{13}C$  NMR ( $CDCl_3$ , 150 MHz);  $\delta_C$ : 29.4 [C(3')], 35.7 [C(5')], 50.1 [C(2')], 50.9 [C(6')], 109.4 [C(5)], 111.7 [C(1'')], 118.2 [C $\equiv$ N], 121.4 [C(A)], 122.6 [C(3)], 123.6 [C(7)], 128.2 [C(4a)], 129.5 [C(8)], 131.7 [C(5'')], 132.2 [C(6'')], 133.1 [C(1''')], 133.3 [C(2'')], 135.2 [C(3'')], 137.5 [C(4)], 141.0 [C(4'')], 143.1 [C(4')], 143.2 [C(8a)], 147.8 [C(2)], 149.0 [C(6)], 156.9 [C(2''')/6''')], 158.1 [C(4''')].

\* Presence of the tetrahydropyridine isomer **113** was supported by identification of distinctive tetrahydropyridine ring signals in  $^1H$  NMR spectra, and comparison to data reported previously.<sup>56</sup>

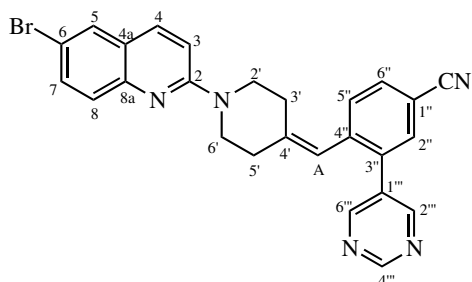
*4-((1-(2-Chloroquinolin-6-yl)-1,2,3,6-tetrahydropyridin-4-yl)methyl)-3-(pyrimidin-5-yl)benzonitrile (113)*



The tetrahydropyridine isomer **113** was not isolated for full characterisation by spectroscopic methods (see above).

## 6.5. SYNTHESIS OF COMPLEX 6-SUBSTITUTED-2-AMINOQUINOLINE LIGANDS

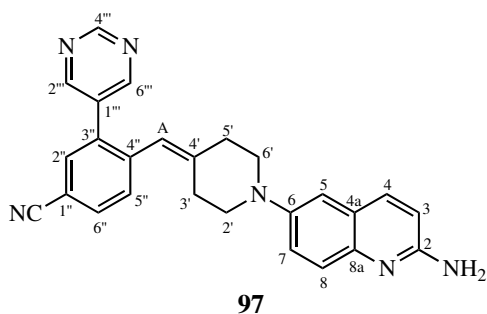
### 4-((1-(6-Bromoquinolin-2-yl)piperidin-4-ylidene)methyl)-3-(pyrimidin-5-yl)benzotrile (**112**)



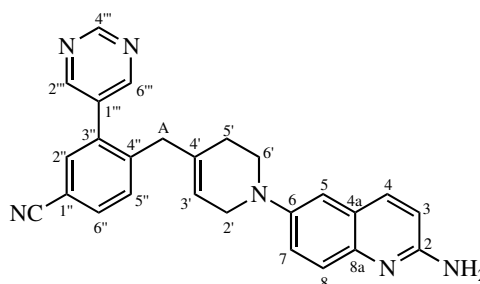
HRMS:  $C_{26}H_{20}BrN_5$   $[M+H]^+$  requires 482.0975 [ $^{79}Br$ ] / 484.0955 [ $^{81}Br$ ], found 482.0968 / 484.0958.

$^1H$  NMR ( $CDCl_3$ , 500 MHz);  $\delta_H$ : 2.35-2.44 [2H, m $\wedge$ , C(3') $H_{ax/eq}$ ; C(5') $H_{ax/eq}$ ], 3.71 [2H, t,  $J_{2'ax,2'eq} = J_{2'ax/2'eq,3'ax/3'eq} = 5.9$  Hz, C(2') $H_{ax/eq}$ ], 3.81 [2H, t,  $J_{6'ax,6'eq} = J_{6'ax/6'eq,5'ax/5'eq} = 5.9$  Hz, C(5') $H_{ax/eq}$ ], 6.18 [1H, s, C(A)H], 7.00 [1H, d,  $J_{3,4} = 9.2$  Hz, C(3)H], 7.46 [1H, d,  $J_{5'',6''} = 7.9$  Hz, C(5'')H], 7.54 [1H, d,  $J_{8,7} = 9.0$  Hz, C(8)H], 7.59 [1H, dd,  $J_{7,8} = 9.0$  Hz;  $J_{7,5} = 2.1$  Hz, C(7)H], 7.65 [1H, br s $^\dagger$ , C(2'')H], 7.72 [1H, d $^\dagger$ ,  $J_{6'',5''} = 7.9$  Hz, C(6'')H], 7.73 [1H, d,  $J_{5',7} = 2.1$  Hz, C(5)H], 7.80 [1H, d,  $J_{4,3} = 9.2$  Hz, C(4)H], 8.78 [2H, s, C(2''')/6''')H], 9.23 [1H, s, C(4''')H].

### 4-((1-(2-Aminoquinolin-6-yl)piperidin-4-ylidene)methyl)-3-(pyrimidin-5-yl)benzotrile (**97**) and 4-((1-(2-Aminoquinolin-6-yl)-1,2,3,6-tetrahydropyridin-4-yl)methyl)-3-(pyrimidin-5-yl)benzotrile (**157**)



**97**



**114**

DavePhos (1.9 mg, 4.23  $\mu$ mol),  $Pd(dba)_2$  (2.3 mg, 4.00  $\mu$ mol), **96** (47.3 mg, 108  $\mu$ mol) and LiHMDS solution (1.0 M in THF, 0.33 mL, 0.33 mmol) in 1,4-dioxane (2 mL) were reacted via General Method 6 for 16 hrs. The crude product was purified by flash column chromatography on silica gel, eluting with 5% MeOH in DCM to afford an inseparable 6:1 mixture of the title compound and **114**\* as an orange powder (3.7 mg, 8% $^{\$}$ ).

**97**: HRMS:  $C_{26}H_{22}N_6$   $[M+H]^+$  requires 419.1979; found 419.1981.  $^1H$  NMR ( $CDCl_3$ , 600 MHz);  $\delta_H$ : 2.45 [2H, t,  $J_{3'ax,3'eq} = J_{3'ax/3'eq,2'ax,2'eq} = 5.7$  Hz, C(3') $H_{ax/eq}$ ], 2.48 [2H, t,  $J_{5'ax,5'eq} = J_{5'ax/5'eq}$ ,

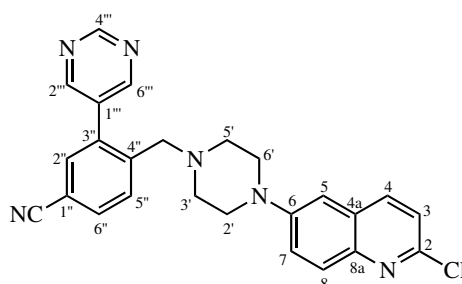
$\delta_{\text{ax/6'eq}} = 5.7$  Hz, C(5')H<sub>ax/eq</sub>], 3.12-3.21 [2H, m<sup>†</sup>, C(2')H<sub>ax/eq</sub>], 3.26-3.36 [2H, m<sup>†</sup>, C(6')H<sub>ax/eq</sub>], 5.43 [2H, br s, NH<sub>2</sub>], 6.15 [1H, s, C(A)H], 6.68 [1H, d,  $J_{3,4} = 8.8$  Hz, C(3)H], 6.95 [1H, d,  $J_{5,7} = 2.7$  Hz, C(5)H], 7.34 [1H, dd,  $J_{7,8} = 9.1$  Hz;  $J_{7,5} = 2.7$  Hz, C(7)H], 7.47 [1H, d,  $J_{5'',6''} = 8.0$  Hz, C(5'')H], 7.61 [1H, d,  $J_{8,7} = 9.1$  Hz, C(8)H], 7.65 [1H, d,  $J_{2'',6''} = 1.7$  Hz, C(2'')H], 7.72 [1H, dd,  $J_{6'',5''} = 8.0$  Hz;  $J_{6'',2''} = 1.7$  Hz, C(6'')H], 7.79 [1H, d,  $J_{4,3} = 8.8$  Hz, C(4)H], 8.78 [2H, s, C(2''')/6''')H], 9.24 [1H, s, C(4''')H]. <sup>13</sup>C NMR (CDCl<sub>3</sub>, 150 MHz);  $\delta_{\text{C}}$ : 29.6 [C(3')], 36.1 [C(5')], 51.3 [C(2')], 52.0 [C(6')], 111.7 [C(1'')], 112.0 [C(5)], 112.4 [C(3)], 118.3 [C $\equiv$ N], 121.1 [C(A)], 123.9 [C(7)], 123.9 [C(4a)], 125.5 [C(8)], 131.8 [C(5'')], 132.3 [C(6'')], 133.2 [C(1'')], 133.3 [C(2'')], 135.2 [C(3'')], 138.3 [C(4)], 140.9 [C(8a)], 141.2 [C(4'')], 143.6 [C(4')], 146.9 [C(6)], 155.6 [C(2)], 156.9 [C(2''')/6''')], 158.1 [C(4''')].

§ indicates combined yield of **97** and **114**.

\* Full spectroscopic characterisation of **114** by analysis of NMR spectra was not possible due to overlapping signals with **97** and a poor signal-to-noise ratio caused by low abundance, however distinctive tetrahydropyridine ring H signals were observed and consistent with those reported previously.<sup>56</sup>

### 6.5.2 Synthesis of a complex 6-benzylpiperazinyl 2-aminoquinoline ligand containing biaryl and nitrile components

#### 4-((4-(2-Chloroquinolin-6-yl)piperazin-1-yl)methyl)-3-(pyrimidin-5-yl)benzonitrile (**99**)



Potassium carbonate (33.0 mg, 0.239 mmol), **62** (43.2 mg, 0.174 mmol) and a 5:6 mixture of **92** and **98** (0.107 g) in DCM (5 mL) were reacted via General Method 14 for 21 hrs. The crude product was purified by flash column chromatography on silica gel, eluting with 1% MeOH in DCM to afford the title compound as a yellow oil (38 mg, 49%\*). HRMS: C<sub>25</sub>H<sub>21</sub>ClN<sub>6</sub> [M+H]<sup>+</sup> requires 441.1589 [<sup>35</sup>Cl] / 443.1560 [<sup>37</sup>Cl]; found 441.1591 / 443.1574. <sup>1</sup>H NMR (CDCl<sub>3</sub>, 600 MHz);  $\delta_{\text{H}}$ : 2.49-2.54

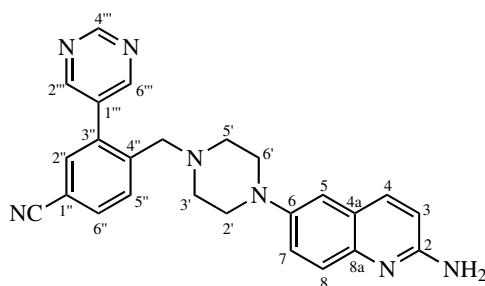


## 6.5. SYNTHESIS OF COMPLEX 6-SUBSTITUTED-2-AMINOQUINOLINE LIGANDS

[4H, m, C(3'/5')H<sub>ax/eq</sub>], 3.17-3.21 [4H, m, C(2'/6')H<sub>ax/eq</sub>], 3.45 [2H, s, CH<sub>2</sub>], 6.94 [1H, d,  $J_{5,7} = 2.7$  Hz, C(5)H], 7.26 [1H, d,  $J_{3,4} = 8.6$  Hz, C(3)H], 7.41 [1H, dd,  $J_{7,8} = 9.3$  Hz;  $J_{7,5} = 2.7$  Hz, C(7)H], 7.57 [1H, d,  $J_{2'',6''} = 1.7$  Hz, C(2'')H], 7.64 [1H, d,  $J_{5'',6''} = 8.0$  Hz, C(5'')H], 7.73 [1H, dd,  $J_{6'',5''} = 8.0$  Hz;  $J_{6'',2''} = 1.7$  Hz, C(6'')H], 7.83 [1H, d,  $J_{8,7} = 9.3$  Hz, C(8)H], 7.89 [1H, d,  $J_{4,3} = 8.6$  Hz, C(4)H], 8.82 [2H, s, C(2'''/6''')H], 9.25 [1H, s, C(4''')H]. <sup>13</sup>C NMR (CDCl<sub>3</sub>, 150 MHz); δ<sub>C</sub>: 49.1 [C(2'/6')], 52.6 [C(3'/5')], 60.3 [CH<sub>2</sub>], 109.2 [C(5)], 112.3 [C(1'')], 118.1 [C≡N], 122.6 [C(3)], 123.2 [C(7)], 128.1 [C(4a)], 129.3 [C(8)], 131.7 [C(5'')], 132.4 [C(6'')], 133.1 [C(1''')], 133.9 [C(2'')], 137.1 [C(3'')], 137.6 [C(4)], 141.8 [C(4'')], 143.3 [C(8a)], 147.8 [C(6)], 149.5 [C(2)], 156.5 [C(2'''/6''')], 158.2 [C(4''')].

\* Yield calculated based upon consumption of the limiting reagent **62**.

### 4-((4-(2-Aminoquinolin-6-yl)piperazin-1-yl)methyl)-3-(pyrimidin-5-yl)benzonitrile (**100**)



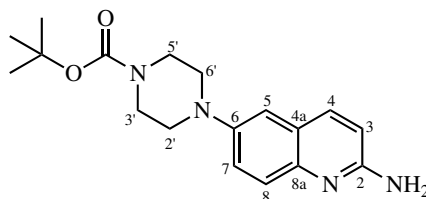
DavePhos (1.0 mg, 2.54 μmol), Pd(dba)<sub>2</sub> (1.5 mg, 2.61 μmol), **99** (38.0 mg, 86.2 μmol) and LiH-MDS solution (1.0 M in THF, 0.28 mL, 0.28 mmol) in 1,4-dioxane (2 mL) were reacted via General Method 6 for 16 hrs. The crude product was purified by flash column chromatography on silica gel, eluting with 8% MeOH in DCM to afford the title compound as a brown powder (6 mg, 17%). HRMS: C<sub>25</sub>H<sub>23</sub>N<sub>7</sub> [M+H]<sup>+</sup> requires 422.2088; found 422.2090. <sup>1</sup>H NMR (CDCl<sub>3</sub>, 600 MHz); δ<sub>H</sub>: 2.49-2.55 [4H, m, C(3'/5')H<sub>ax/eq</sub>], 3.09-3.14 [4H, m, C(2'/6')H<sub>ax/eq</sub>], 3.46 [2H, s, CH<sub>2</sub>], 4.99 [2H, br s, NH<sub>2</sub>], 6.69 [1H, d,  $J_{3,4} = 8.8$  Hz, C(3)H], 6.92 [1H, d,  $J_{5,7} = 2.7$  Hz, C(5)H], 7.30 [1H, dd,  $J_{7,8} = 9.1$  Hz;  $J_{7,5} = 2.7$  Hz, C(7)H], 7.58 [1H, d,  $J_{2'',6''} = 1.8$  Hz, C(2'')H], 7.58 [1H, d,  $J_{8,7} = 9.1$  Hz, C(8)H], 7.65 [1H, d,  $J_{5'',6''} = 7.9$  Hz, C(5'')H], 7.74 [1H, dd,  $J_{6'',5''} = 7.9$  Hz;  $J_{6'',2''} = 1.8$  Hz, C(6'')H], 7.77 [1H, d,  $J_{4,3} = 8.8$  Hz, C(4)H], 8.84 [2H, s, C(2'''/6''')H], 9.26 [1H, s, C(4''')H]. <sup>13</sup>C NMR (CDCl<sub>3</sub>, 150 MHz); δ<sub>C</sub>: 50.1 [C(2'/6')], 52.9 [C(3'/5')], 60.4 [CH<sub>2</sub>], 111.4 [C(5)], 112.2 [C(3); C(1'')\*], 112.3 [C(3); C(1'')\*], 118.2 [C≡N], 123.2 [C(7)], 124.1 [C(4a)], 126.1 [C(8)], 131.8

## 6.5. SYNTHESIS OF COMPLEX 6-SUBSTITUTED-2-AMINOQUINOLINE LIGANDS

[C(5'')], 132.4 [C(6'')], 133.2 [C(1''')], 133.9 [C(2'')], 137.1 [C(3'')], 137.9 [C(4)], 141.8 [C(8a)], 142.0 [C(4'')], 147.1 [C(6)], 155.5 [C(2)], 156.6 [C(2'''/6''')], 158.2 [C(4''')].

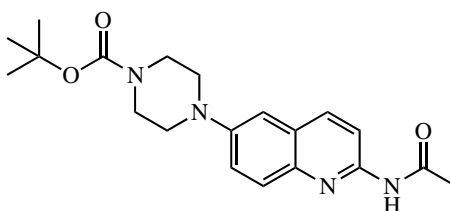
\* denotes signals could not be unambiguously assigned due to overlapping signals in 2D NMR spectra.

### *tert*-Butyl 4-(2-aminoquinolin-6-yl)piperazine-1-carboxylate (**117**)<sup>47</sup>



DavePhos (1.1 mg, 2.80  $\mu$ mol), Pd(dba)<sub>2</sub> (1.4 mg, 2.43  $\mu$ mol), **67** (72.0 mg, 0.207 mmol) and LiHMDS solution (1.0 M in THF, 0.52 mL, 0.52 mmol) in 1,4-dioxane (2 mL) were reacted via General Method 6 for 16 hrs. The crude product was purified by flash column chromatography on silica gel, eluting with 10% MeOH in DCM to afford the title compound as a yellow-brown powder (68.4 mg, 100%). HRMS: C<sub>18</sub>H<sub>24</sub>N<sub>4</sub>O<sub>2</sub> [M+H]<sup>+</sup> requires 329.1972; found 329.1974. <sup>1</sup>H NMR (CDCl<sub>3</sub>, 500 MHz);  $\delta_{\text{H}}$ : 1.49 [9H, s, C(CH<sub>3</sub>)<sub>3</sub>], 3.15 [4H, t,  $J_{2'\text{ax}/6'\text{ax}, 2'\text{eq}/6'\text{eq}} = J_{2'\text{ax}/6'\text{ax}, 3'\text{ax}/5'\text{ax}} = 5.1$  Hz, C(2'/6')H<sub>ax/eq</sub>], 3.62 [4H, t,  $J_{3'\text{ax}/5'\text{ax}, 3'\text{eq}/5'\text{eq}} = J_{3'\text{ax}/5'\text{ax}, 2'\text{ax}/6'\text{ax}} = 5.1$  Hz, C(3'/5')H<sub>ax/eq</sub>], 4.69 [2H, br s, NH<sub>2</sub>], 6.69 [1H, d,  $J_{3,4} = 8.8$  Hz, C(3)H], 6.97 [1H, d,  $J_{5,7} = 2.7$  Hz, C(5)H], 7.34 [1H, dd,  $J_{7,8} = 9.1$  Hz;  $J_{7,5} = 2.7$  Hz, C(7)H], 7.59 [1H, d,  $J_{8,7} = 9.1$  Hz, C(8)H], 7.77 [1H, d,  $J_{4,3} = 8.8$  Hz, C(4)H].

### Attempted synthesis of *tert*-butyl 4-(2-acetamidoquinolin-6-yl)piperazine-1-carboxylate (**119**)

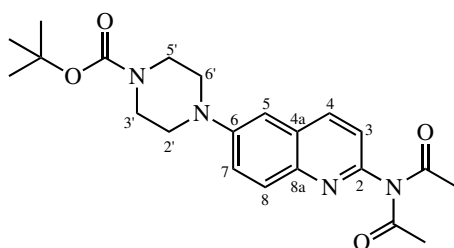


Under an atmosphere of N<sub>2</sub>, dry triethylamine (45  $\mu$ L, 0.323 mmol) was added to **117** (68.4 mg, 0.208 mmol) in DCM (6 mL). The reaction mixture was cooled to 0 °C, and acetyl chloride (20.0  $\mu$ L, 0.280 mmol) was added dropwise. The reaction mixture was warmed to room temperature, and stirred at room temperature for 10 mins, monitoring by TLC (10% MeOH in DCM). The reaction mixture was washed with sat. NaHCO<sub>3(aq)</sub> (10 mL), then the organic products were extracted

## 6.5. SYNTHESIS OF COMPLEX 6-SUBSTITUTED-2-AMINOQUINOLINE LIGANDS

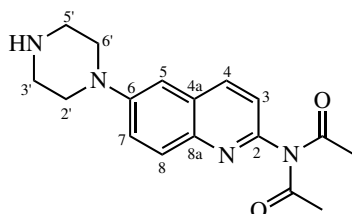
with 3:1 chloroform/isopropanol (2 x 20 mL), washed with 1N HCl (10 mL), and extracted with 3:1 chloroform/isopropanol (2 x 20 mL). The organic phases were combined, dried over MgSO<sub>4</sub>, filtered and concentrated under reduced pressure. The crude product was purified by flash column chromatography on silica gel, eluting with 1% MeOH in DCM, to afford **120** as an orange solid (67.6 mg, 88%).

*tert*-Butyl 4-(2-(*N*-acetylacetamido)quinolin-6-yl)piperazine-1-carboxylate (**120**)



HRMS: C<sub>22</sub>H<sub>28</sub>N<sub>4</sub>O<sub>4</sub> [M+H]<sup>+</sup> requires 413.2183; found 413.2184. <sup>1</sup>H NMR (CDCl<sub>3</sub>, 600 MHz); δ<sub>H</sub>: 1.50 [9H, s, C(CH<sub>3</sub>)<sub>3</sub>], 2.32 [6H, s, CH<sub>3</sub>], 3.30 [4H, t,  $J_{2'ax/6'ax,2'eq/6'eq} = J_{2'ax/6'ax,3'ax/5'ax} = 5.2$  Hz, C(2'/6')H<sub>ax/eq</sub>], 3.65 [4H, t,  $J_{3'ax/5'ax,3'eq/5'eq} = J_{3'ax/5'ax,2'ax/6'ax} = 5.2$  Hz, C(3'/5')H<sub>ax/eq</sub>], 7.08 [1H, d,  $J_{5,7} = 2.7$  Hz, C(5)H], 7.22 [1H, d,  $J_{3,4} = 8.6$  Hz, C(3)H], 7.53 [1H, dd,  $J_{7,8} = 9.3$  Hz;  $J_{7,5} = 2.7$  Hz, C(7)H], 7.94 [1H, d,  $J_{8,7} = 9.3$  Hz, C(8)H], 8.12 [1H, d,  $J_{4,3} = 8.6$  Hz, C(4)H]. <sup>13</sup>C NMR (CDCl<sub>3</sub>, 150 MHz); δ<sub>C</sub>: 26.9 [CH<sub>3</sub>], 28.6 [C(CH<sub>3</sub>)<sub>3</sub>], 42.2-44.6 [br m, C(3'/5')], 49.2 [C(2'/6')], 80.3 [C(CH<sub>3</sub>)<sub>3</sub>], 109.3 [C(5)], 121.7 [C(3)], 123.5 [C(7)], 129.0 [C(4a)], 130.1 [C(8)], 137.7 [C(4)], 143.0 [C(8a)], 149.6 [C(2)], 150.3 [C(6)], 154.8 [C=O (Boc)], 173.0 [C=O (amide)].

*N*-(6-(Piperazin-1-yl)quinolin-2-yl)acetamide (**121**)

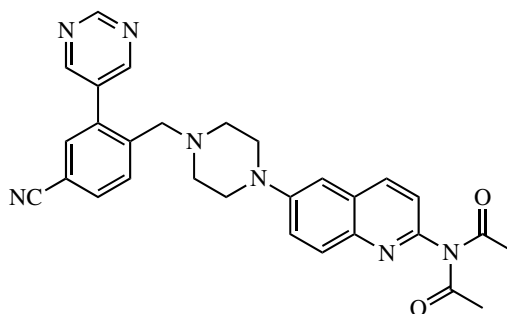


Trifluoroacetic acid (1 mL, 13.1 mmol), **120** (67.6 mg, 0.164 mmol) in DCM (6 mL) were essentially reacted via General Method 4 for 1 hr, except the reaction mixture was extracted with 3:1 chloroform/isopropanol (3 x 20 mL), to afford the title compound as a yellow-orange oily solid (39.9 mg, 90%). HRMS: C<sub>17</sub>H<sub>20</sub>N<sub>4</sub>O<sub>2</sub> [M+H]<sup>+</sup> requires 313.1659; found 313.1660. <sup>1</sup>H NMR (CDCl<sub>3</sub>, 600 MHz); δ<sub>H</sub>: 2.17 [3H, s, CH<sub>3</sub>], 2.24 [3H, br s, CH<sub>3</sub>], 3.22-3.27 [2H, m, C(2')H<sub>ax/eq</sub>\*/C(6')H<sub>ax/eq</sub>\*],

3.26-3.31 [2H, m, C(2')H<sub>ax/eq</sub>\*/C(6')H<sub>ax/eq</sub>\*], 3.65-3.75 [2H, m, C(3')H<sub>ax/eq</sub>\*/C(5')H<sub>ax/eq</sub>\*], 3.80-3.88 [2H, m, C(3')H<sub>ax/eq</sub>\*/C(5')H<sub>ax/eq</sub>\*], 7.05 [1H, d,  $J_{5,7} = 2.7$  Hz, C(5)H], 7.45 [1H, dd,  $J_{7,8} = 9.2$  Hz;  $J_{7,5} = 2.7$  Hz, C(7)H], 7.74 [1H, d,  $J_{8,7} = 9.2$  Hz, C(8)H], 8.04 [1H, d,  $J_{4,3} = 9.1$  Hz, C(4)H], 8.35 [1H, br d,  $J_{3,4} = 9.1$  Hz, C(3)H], 8.47 [1H, br s, NH]. <sup>13</sup>C NMR (CDCl<sub>3</sub>, 150 MHz);  $\delta_C$ : 21.5 [CH<sub>3</sub>], 25.0 [CH<sub>3</sub>], 41.4 [C(3')\*/C(5')\*], 46.3 [C(3')\*/C(5')\*], 49.7 [C(2')\*/C(6')\*], 50.0 [C(2')\*/C(6')\*], 110.6 [C(5)], 114.8 [C(3)], 123.7 [C(7)], 127.2 [C(4a)], 128.1 [C(8)], 137.7 [C(4)], 141.9 [C(8a)], 148.2 [C(6)], 149.4 [C(2)], 169.1 [C=O], 169.2 [C=O].

\* denotes signals which could not be unambiguously assigned due to dynamics-induced signal broadening on the NMR-timescale.

**Attempted synthesis of *N*-(6-(4-(4-Cyano-2-(pyrimidin-5-yl)benzyl)piperazin-1-yl)quinolin-2-yl) acetamide (123)**

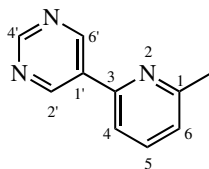


*Synthetic method A*: Potassium carbonate (11.8 mg, 85.4  $\mu$ mol), **121** (19.6 mg, 62.7  $\mu$ mol) and **92** (18.4 mg, 67.1  $\mu$ mol) in DCM (6 mL) were reacted via General Method 14 for 23 hrs. Workup as specified afforded a yellow-brown oily solid. <sup>1</sup>H NMR analysis of the crude reaction mixture revealed minimal conversion of reactants, with only trace amounts of the desired product present. Product was not purified.

*Synthetic method B*: Triethylamine (15  $\mu$ L, 0.108 mmol), **121** (19.6 mg, 62.7  $\mu$ mol) and **92** (18.4 mg, 67.1  $\mu$ mol) in DCM (5 mL) were reacted via General Method 14 for 23 hrs. Workup as specified to afford a brown-orange oil. <sup>1</sup>H NMR analysis of the crude reaction mixture revealed consumption of **92**, and no product formation.

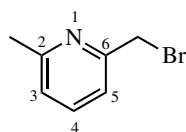
### 6.5.3 Synthesis of a complex 6-arylmethylpiperidine ligand containing biaryl and 2-pyridyl components

#### 5-(6-Methylpyridin-2-yl)pyrimidine (133)



3-Bromo-6-methylpyridine (0.66 mL, 5.81 mmol), pyrimidin-5-ylboronic acid (0.881 g, 7.11 mmol), Pd(OAc)<sub>2</sub> (65.0 mg, 0.29 mmol), triphenylphosphine (97.4 mg, 0.371 mmol) and potassium carbonate (1.24 g, 8.95 mmol) 1:1 toluene/ethanol (2.5 mL) were reacted via General Method 17 for 13 hrs. The crude product was purified by flash column chromatography on silica gel, eluting with 2.5% MeOH in DCM to afford the title compound as an off-white powder, m.p. 91-93 °C (lit.,<sup>139</sup> 100-102 °C), (0.490 g, 49%). HRMS: C<sub>10</sub>H<sub>9</sub>N<sub>3</sub> [M+NH<sub>4</sub>]<sup>+</sup> requires 189.1135; found 189.1128. <sup>1</sup>H NMR (CDCl<sub>3</sub>, 600 MHz); δ<sub>H</sub>: 2.63 [3H, s, CH<sub>3</sub>], 7.20 [1H, d, J<sub>6,5</sub> = 7.7 Hz, C(6)H], 7.55 [1H, d, J<sub>4,5</sub> = 7.7 Hz, C(4)H], 7.70 [1H, t, J<sub>5,4</sub> = J<sub>5,6</sub> = 7.7 Hz, C(5)H], 9.24 [1H, s, C(4')H], 9.32 [2H, s, C(2'/6')H]. <sup>13</sup>C NMR (CDCl<sub>3</sub>, 150 MHz); δ<sub>C</sub>: 24.5 [CH<sub>3</sub>], 117.4 [C(4)], 123.1 [C(6)], 132.5 [C(1')], 137.2 [C(5)], 151.2 [C(3)], 155.0 [C(2'/6')], 158.3 [C(4')], 159.3 [C(1)].

#### 2-(Bromomethyl)-6-methylpyridine (136)

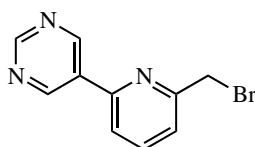


*N*-Bromosuccinimide (919 mg, 5.16 mmol), 2,6-lutidine **135** (0.53 mL, 4.61 mmol) and benzoyl peroxide (16.3 mg, 67.3 μmol) in BTF (8 mL) were reacted via General Method 18 for 23 hr at 60°C. Work-up as specified afforded a yellow-orange, oily solid. The crude product was purified by flash column chromatography on silica gel, eluting with 40% EtOAc in hexanes to afford the title compound as a yellow powder (14.4 mg, 2%<sup>S</sup>). HRMS: C<sub>7</sub>H<sub>8</sub>BrN [M+H]<sup>+</sup> requires 185.9913 [<sup>79</sup>Br] / 187.9892 [<sup>81</sup>Br]; found 185.9914 / 187.9896. <sup>1</sup>H NMR (CDCl<sub>3</sub>, 500 MHz); δ<sub>H</sub>: 2.60 [3H, s, CH<sub>3</sub>], 4.57 [2H, s, CH<sub>2</sub>], 7.11 [1H, d, J<sub>3/5,4</sub> = 7.7 Hz, C(3)H\*/C(5)H\*], 7.29 [1H, d, J<sub>3/5,4</sub> = 7.7 Hz, C(3)H\*/C(5)H\*], 7.63 [1H, t, J<sub>4,5</sub> = J<sub>4,3</sub> = 7.7 Hz, C(4)H].

§ indicates isolated yield only; only a portion of the crude product was successfully purified by flash column chromatography due to limited solubility in the mobile phase during column loading.

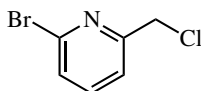
\*\* indicates that signals could not be unambiguously assigned in the absence of 2D NMR spectra.

#### Attempted synthesis of 5-(6-(Bromomethyl)pyridin-2-yl)pyrimidine (**126**)



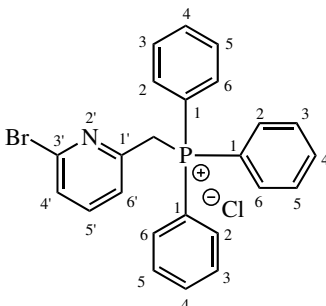
*N*-Bromosuccinimide (0.576 g, 3.24 mmol), **133** (0.467 g, 2.74 mmol) and benzoyl peroxide (44.7 mg, 0.185 mmol) in BTF (5 mL) were reacted via General Method 18 for 17 hr at 80°C. Work-up as specified afforded a brown, oily solid. <sup>1</sup>H NMR analysis of the crude product mixture revealed starting material **133** was present, with only trace amounts of the title compound.

#### 2-Bromo-6-(chloromethyl)pyridine (**137**)



*N*-Chlorosuccinimide (0.430 g, 3.22 mmol), 3-bromo-6-methylpyridine (0.33 mL, 2.90 mmol) and benzoyl peroxide (39.2 mg, 0.162 mmol) in BTF (10 mL) were reacted via General Method 19 for 23 hr at 80 °C. After work-up as specified, the product was immediately used without further purification.

#### ((6-Bromopyridin-2-yl)methyl)triphenylphosphonium chloride (**127**)

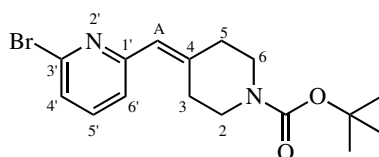


Crude **137** (0.599 g, 2.90 mmol) suspended in toluene (20 mL), and triphenylphosphine (0.957 g, 3.65 mmol) were reacted via General Method 16 for 20 hr to afford the title compound as a brown

## 6.5. SYNTHESIS OF COMPLEX 6-SUBSTITUTED-2-AMINOQUINOLINE LIGANDS

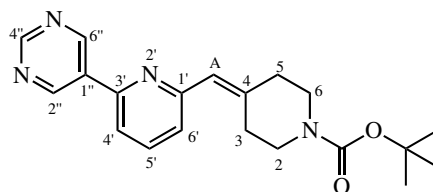
solid, used without further purification (0.524 g, 39% over 2 steps).  $^1\text{H}$  NMR ( $\text{CDCl}_3$ , 600 MHz);  $\delta_{\text{H}}$ : 5.78 [2H, d,  $J_{\text{H,P}} = 14.4$  Hz,  $\text{CH}_2$ ], 7.26 [1H, d,  $J_{4',5'} = 7.8$  Hz, C(4')H], 7.46 [1H, t,  $J_{5',4'} = J_{5',6'} = 7.8$  Hz, C(5')H], 7.60-7.68 [6H, m, C(3/5)H], 7.75 [3H, t,  $J_{4,5} = J_{4,3} = 7.5$  Hz, C(4)H], 7.81-7.94 [6H, m, C(2/6)H], 8.15 [1H, d,  $J_{6',5'} = 7.8$  Hz, C(6')H].  $^{13}\text{C}$  NMR ( $\text{CDCl}_3$ , 150 MHz);  $\delta_{\text{C}}$ : 32.3 [d,  $J_{\text{C,P}} = 52.4$  Hz,  $\text{CH}_2$ ], 118.8 [d,  $J_{1,\text{P}} = 87.6$  Hz, C(1)], 126.4 [d,  $J_{6',\text{P}} = 7.9$  Hz, C(6')], 127.3 [d,  $J_{4',\text{P}} = 2.2$  Hz, C(4')], 130.1 [d,  $J_{3/5,\text{P}} = 12.9$  Hz, C(3/5)], 134.4 [d,  $J_{2/6,\text{P}} = 10.3$  Hz, C(2/6)], 134.8 [d,  $J_{4,\text{P}} = 3.0$  Hz, C(4)], 139.9 [C(5')], 140.4 [d,  $J_{3',\text{P}} = 2.1$  Hz, C(3')], 151.3 [d,  $J_{1',\text{P}} = 8.6$  Hz, C(1')].

### *tert*-Butyl 4-((6-bromopyridin-2-yl)methylene)piperidine-1-carboxylate (**129**)

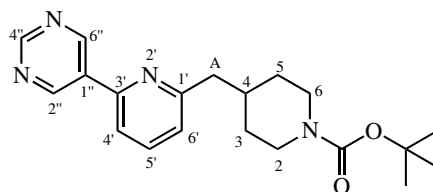


**127** (0.524 g, 1.12 mmol), LiHMDS (1.0 M in THF, 2.3 mL, 2.3 mmol) and *N*-Boc-4-piperidone (0.278 g, 1.40 mmol) were reacted via General Method 2 for 22 hr at room temperature. The crude product was purified by flash column chromatography on silica gel, eluting with 10% EtOAc in hexanes to afford the title compound as a yellow oil (0.146 g, 37%). HRMS:  $\text{C}_{16}\text{H}_{21}\text{BrN}_2\text{O}_2$  [ $\text{M}+\text{H}$ ] $^+$  requires 353.0859 [ $^{79}\text{Br}$ ] / 355.0839 [ $^{81}\text{Br}$ ]; found 353.0856 / 355.0839.  $^1\text{H}$  NMR ( $\text{CDCl}_3$ , 600 MHz);  $\delta_{\text{H}}$ : 1.48 [9H, s,  $(\text{CH}_3)_3$ ], 2.36 [2H, br  $\text{t}^\dagger$ ,  $J_{5_{\text{ax}},5_{\text{eq}}} = J_{5_{\text{ax}},5_{\text{eq}},6_{\text{ax}},6_{\text{eq}}} = 5.8$  Hz, C(5) $\text{H}_{\text{ax/eq}}$ ], 2.80-2.94 [2H, br  $\text{s}^\dagger$ , C(3) $\text{H}_{\text{ax/eq}}$ ], 3.47 [2H, t,  $J_{2_{\text{ax}},2_{\text{eq}}} = J_{2_{\text{ax}},2_{\text{eq}},3_{\text{ax}},3_{\text{eq}}} = 5.9$  Hz, C(2) $\text{H}_{\text{ax/eq}}$ ], 3.53 [2H, br  $\text{t}^\dagger$ ,  $J_{6_{\text{ax}},6_{\text{eq}}} = J_{6_{\text{ax}},6_{\text{eq}},5_{\text{ax}},5_{\text{eq}}} = 5.8$  Hz, C(6) $\text{H}_{\text{ax/eq}}$ ], 6.29 [1H, s, C(A)H], 7.08 [1H, d,  $J_{6',5'} = 7.7$  Hz, C(6')H], 7.27 [1H, d,  $J_{4',5'} = 7.7$  Hz, C(4')H], 7.47 [1H, t,  $J_{5',4'} = J_{5',6'} = 7.7$  Hz, C(5')H].  $^{13}\text{C}$  NMR ( $\text{CDCl}_3$ , 150 MHz);  $\delta_{\text{C}}$ : 28.6 [ $\text{CH}_3$ ], 29.4 [C(3)], 36.8 [C(5)], 42.5-46.5 [br  $\text{m}^\wedge$ , C(6); C(2)], 79.8 [ $\text{C}(\text{CH}_3)_3$ ], 122.8 [C(A);\* C(6')\*], 125.3 [C(4')], 138.5 [C(5')], 141.4 [C(3')], 144.7-146.0 [br m, C(4)], 154.9 [C=O], 157.6 [C(1')].

\* denotes overlapping signals in  $^{13}\text{C}$  NMR spectra.

***tert*-Butyl 4-((6-(pyrimidin-5-yl)pyridin-2-yl)methylene)piperidine-1-carboxylate (**130**)**

Pyrimidin-5-ylboronic acid (80.1 mg, 0.646 mmol), **129** (0.187 g, 0.646 mmol), Pd(OAc)<sub>2</sub> (4.4 mg, 19.6 μmol), triphenylphosphine (22.4 mg, 85.4 μmol) and potassium carbonate (118 mg, 0.852 mmol) 1:1 toluene/ethanol (2 mL) were reacted via General Method 17 for 13 hrs. The crude product was purified by flash column chromatography on silica gel, eluting with 50% EtOAc in hexanes to afford the title compound as an off-white powder (0.148 g, 80%). HRMS: C<sub>20</sub>H<sub>24</sub>N<sub>4</sub>O<sub>2</sub> [M+H]<sup>+</sup> requires 353.1972; found 353.1974. <sup>1</sup>H NMR (CDCl<sub>3</sub>, 600 MHz); δ<sub>H</sub>: 1.50 [9H, s, (CH<sub>3</sub>)<sub>3</sub>], 2.40-2.45 [2H, m, C(5)H<sub>ax/eq</sub>], 3.00-3.14 [2H, br s<sup>†</sup>, C(3)H<sub>ax/eq</sub>], 3.50-3.55 [2H, m, C(2)H<sub>ax/eq</sub>], 3.55-3.60 [2H, m, C(6)H<sub>ax/eq</sub>], 6.41 [1H, s, C(A)H], 7.20 [1H, d<sup>†</sup>, J<sub>6',5'</sub> = 7.8 Hz, C(6')H], 7.59 [1H, dd, J<sub>4',5'</sub> = 7.8 Hz; J<sub>4',6'</sub> = 0.9 Hz, C(4')H], 7.78 [1H, t, J<sub>5',6'</sub> = J<sub>5',4'</sub> = 7.8 Hz, C(5')H], 9.26 [1H, s, C(4'')H], 9.34 [2H, s, C(2''/6'')]. <sup>13</sup>C NMR (CDCl<sub>3</sub>, 150 MHz); δ<sub>C</sub>: 28.5 [CH<sub>3</sub>], 29.8 [C(3)], 36.9 [C(5)], 43.1-46.4 [br m<sup>^</sup>, C(2); C(6)], 79.7 [C(CH<sub>3</sub>)<sub>3</sub>], 117.6 [C(4')], 123.3 [br s, C(A)], 124.2 [C(6')], 132.6 [C(1'')], 137.5 [C(5')], 144.5-145.7 [br m, C(4)], 151.3 [C(3')], 154.8 [C=O], 155.1 [C(2''/6'')], 157.3 [C(1')], 158.6 [C(4'')].

***tert*-Butyl 4-((6-(pyrimidin-5-yl)pyridin-2-yl)methyl)piperidine-1-carboxylate (**138**)**

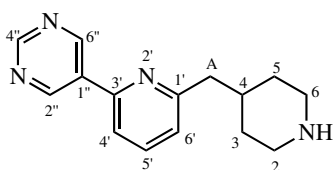
A catalytic amount of 10% Pd on carbon was added to **130** (0.118 g, 0.335 mmol) in MeOH (10 mL), and reacted via General Method 3 for 20 hrs. After workup as specified, the crude product was purified by flash column chromatography on silica gel, eluting with EtOAc to afford the title compound as a colourless, transparent oil (90.9 mg, 77%). HRMS: C<sub>20</sub>H<sub>26</sub>N<sub>4</sub>O<sub>2</sub> [M+H]<sup>+</sup> requires 355.2129; found 355.2127. <sup>1</sup>H NMR (CDCl<sub>3</sub>, 600 MHz); δ<sub>H</sub>: 1.25 [2H, dq, J<sub>3ax/5ax,3eq/5eq</sub> = J<sub>3ax/5ax,4ax</sub> = J<sub>3ax/5ax,2ax/6ax</sub> = 12.5 Hz; J<sub>3ax/5ax,2eq/6eq</sub> = 4.3 Hz, C(3/5)H<sub>ax</sub>], 1.46 [9H, s, (CH<sub>3</sub>)<sub>3</sub>], 1.64-1.71 [2H, m<sup>†</sup>, C(3/5)H<sub>eq</sub>], 1.99-2.10 [1H, m<sup>†</sup>, C(4)H<sub>ax</sub>], 2.63-2.76 [2H, br s<sup>†</sup>, C(2/6)H<sub>ax</sub>],



## 6.5. SYNTHESIS OF COMPLEX 6-SUBSTITUTED-2-AMINOQUINOLINE LIGANDS

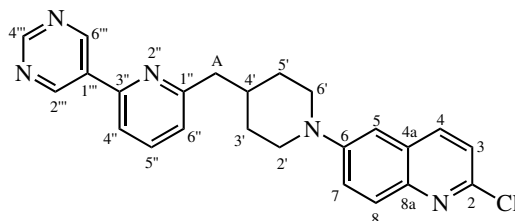
3.95-4.22 [2H, br s<sup>†</sup>, C(2/6)H<sub>eq</sub>], 7.16 [1H, dd,  $J_{6',5'} = 7.7$  Hz;  $J_{6',4'} = 0.9$  Hz, C(6')H], 7.60 [1H, dd,  $J_{4',5'} = 7.7$  Hz;  $J_{4',6'} = 0.9$  Hz, C(4')H], 7.74 [1H, t,  $J_{5',4'} = J_{5',6'} = 7.7$  Hz, C(5')H], 9.26 [1H, s, C(4'')H], 9.34 [2H, s, C(2''/6'')H]. <sup>13</sup>C NMR (CDCl<sub>3</sub>, 150 MHz); δ<sub>C</sub>: 28.6 [CH<sub>3</sub>], 31.9-32.4 [br s<sup>^</sup>, C(3); C(5)], 36.7 [C(4)], 43.2-45.0 [br m<sup>^</sup>, C(2); C(6)], 45.3 [C(A)], 79.4 [C(CH<sub>3</sub>)<sub>3</sub>], 1180 [C(4')], 123.7 [C(6')], 132.7 [C(1'')], 137.4 [C(5')], 151.6 [C(3')], 155.0 [C=O], 155.3 [C(2''/6'')], 158.6 [C(4'')], 161.4 [C(1')].

### 5-(6-(Piperidin-4-ylmethyl)pyridin-2-yl)pyrimidine (131)



Trifluoroacetic acid (1 mL, 13.1 mmol), **138** (90.9 mg, 256 μmol) in DCM (6 mL) were reacted essentially via General Method 4 for 2 hr, except the reaction mixture was extracted with 3:1 chloroform/isopropanol (3 x 20 mL), to afford the title compound as a colourless, transparent oil (51.2 mg, 79%). HRMS: C<sub>15</sub>H<sub>18</sub>N<sub>4</sub> [M+H]<sup>+</sup> requires 255.1604; found 255.1606. <sup>1</sup>H NMR (CDCl<sub>3</sub>, 600 MHz); δ<sub>H</sub>: 1.50-1.64 [2H, m<sup>†</sup>, C(3/5)H<sub>ax</sub>], 1.81-1.87 [2H, m, C(3/5)H<sub>eq</sub>], 2.12-2.22 [1H, m, C(4)H<sub>ax</sub>], 2.80 [2H, td,  $J_{2ax/6ax,2eq/6eq} = J_{2ax/6ax,3ax/5ax} = 12.8$  Hz;  $J_{2ax/6ax,3eq/5eq} = 3.2$  Hz, C(2/6)H<sub>ax</sub>], 2.84 [2H, d,  $J_{A,4ax} = 7.1$  Hz, C(A)H], 3.31 [2H, td,  $J_{2eq/6eq,2ax/6ax} = J_{2eq/6eq,3eq/5eq} = 12.8$  Hz;  $J_{2eq/6eq,3ax/5ax} = 3.2$  Hz, C(2/6)H<sub>eq</sub>], 6.79 [1H, br s, NH], 7.17 [1H, dd,  $J_{6',5'} = 7.7$  Hz;  $J_{6',4'} = 0.9$  Hz, C(6')H], 7.61 [1H, dd,  $J_{4',5'} = 7.7$  Hz;  $J_{4',6'} = 0.9$  Hz, C(4')H], 7.75 [1H, t,  $J_{5',4'} = J_{5',6'} = 7.7$  Hz, C(5')H], 9.25 [1H, s, C(4'')H], 9.33 [2H, s, C(2''/6'')H]. <sup>13</sup>C NMR (CDCl<sub>3</sub>, 150 MHz); δ<sub>C</sub>: 30.0 [C(3/5)], 35.1 [C(4)], 44.8 [C(A)\*C(2/6)\*], 44.8 [C(A)\*C(2/6)\*], 118.2 [C(4')], 123.8 [C(6')], 132.6 [C(1'')], 137.6 [C(5')], 151.7 [C(3')], 155.2 [C(2''/6'')], 158.7 [C(4'')], 160.5 [C(1')].

\* denotes overlapping signals in <sup>13</sup>C NMR spectra precluded unambiguous signal assignment in 2D NMR spectra.

**2-Chloro-6-(4-((6-(pyrimidin-5-yl)pyridin-2-yl)methyl)piperidin-1-yl)quinoline (132)**

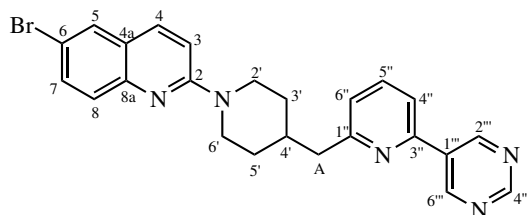
Sodium *tert*-butoxide (28.1 mg, 0.292 mmol), **131** (48.6 mg, 0.191 mmol), **26** (56.6 mg, 0.233 mmol), cataCXium® A (7.7 mg, 21.5  $\mu$ mol), Pd(OAc)<sub>2</sub> (4.9 mg, 21.8  $\mu$ mol) in anhydrous BTF (2 mL) were reacted via General Method 5 for 16 hr. The crude product was purified by flash column chromatography on silica gel, eluting with 2% MeOH in DCM to afford the title compound as a yellow powder (30.3 mg, 55%) and **139** as a yellow oil (6.3 mg, 7%).

**132**: HRMS: C<sub>24</sub>H<sub>22</sub>ClN<sub>5</sub> [M+H]<sup>+</sup> requires 416.1636 [<sup>35</sup>Cl] / 418.1607 [<sup>37</sup>Cl]; found 416.1630 / 418.1617. <sup>1</sup>H NMR (CDCl<sub>3</sub>, 600 MHz);  $\delta$ <sub>H</sub>: 1.55 [2H, dq,  $J_{3'ax/5'ax,3'eq/5'eq} = J_{3'ax/5'ax,2'ax/6'ax} = J_{3'ax/5'ax,4'ax} = 12.3$  Hz;  $J_{3'ax/5'ax,2'eq/6'eq} = 4.1$  Hz, C(3'/5')H<sub>ax</sub>], 1.87 [2H, br d<sup>†</sup>,  $J_{3'eq/5'eq,3'ax/5'ax} = 12.3$  Hz, C(3'/5')H<sub>eq</sub>], 2.08-2.19 [1H, m, C(4')H<sub>ax</sub>], 2.83 [2H, td,  $J_{2'ax/6'ax,2'eq/6'eq} = J_{2'ax/6'ax,3'ax/5'ax} = 12.3$  Hz;  $J_{2'ax/6'ax,3'eq/5'eq} = 2.6$  Hz, C(2'/6')H<sub>ax</sub>], 2.87 [2H, d,  $J_{A,4'ax} = 7.6$  Hz, C(A)H], 3.83 [2H, br d<sup>†</sup>,  $J_{2eq/6eq,2ax/6ax} = 12.3$  Hz, C(2'/6')H<sub>eq</sub>], 7.00 [1H, d,  $J_{5,7} = 2.7$  Hz, C(5)H], 7.20 [1H, dd,  $J_{6'',5''} = 7.7$  Hz;  $J_{6'',4''} = 0.9$  Hz, C(6'')H], 7.27 [1H, d,  $J_{3,4} = 8.6$  Hz, C(3)H], 7.50 [1H, dd,  $J_{7,8} = 9.3$  Hz;  $J_{7,5} = 2.7$  Hz, C(7)], 7.62 [1H, dd,  $J_{4'',5''} = 7.7$  Hz;  $J_{4'',6''} = 0.9$  Hz, C(4'')H], 7.76 [1H, t,  $J_{5'',6''} = J_{5'',4''} = 7.7$  Hz, C(5'')H], 7.86 [1H, d,  $J_{8,7} = 9.3$  Hz, C(8)H], 7.91 [1H, d,  $J_{4,3} = 8.6$  Hz, C(4)H], 9.26 [1H, s, C(4''')H], 9.36 [2H, s, C(2'''/6''')H]. <sup>13</sup>C NMR (CDCl<sub>3</sub>, 150 MHz);  $\delta$ <sub>C</sub>: 32.0 [C(3'/5')], 36.4 [C(4')], 45.2 [C(A)], 49.8 [C(2'/6')], 109.0 [C(5)], 118.0 [C(4'')], 122.5 [C(3)], 123.7 [C(7)\*C(6'')\*], 123.8 [C(7)\*C(6'')\*], 128.3 [C(4a)], 129.2 [C(8)], 132.7 [C(1'')], 134.5 [C(5'')\*C(4)\*], 134.5 [C(5'')\*C(4)\*], 143.1 [C(8a)], 147.4 [C(2)], 150.1 [C(6)], 151.6 [C(3'')], 155.3 [C(2'''/6''')], 158.7 [C(4''')], 161.4 [C(1'')].

\* denotes signals could not be unambiguously assigned due to overlapping signals in 2D NMR spectra.

## 6.5. SYNTHESIS OF COMPLEX 6-SUBSTITUTED-2-AMINOQUINOLINE LIGANDS

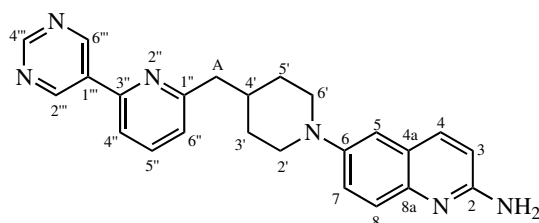
### 6-Bromo-2-(4-((6-(pyrimidin-5-yl)pyridin-2-yl)methyl)piperidin-1-yl)quinoline (139)



HRMS:  $C_{24}H_{22}BrN_5$   $[M+H]^+$  requires 460.1131 [ $^{79}Br$ ]/462.1111 [ $^{81}Br$ ]; found 460.1126/462.1113.

$^1H$  NMR ( $CDCl_3$ , 600 MHz);  $\delta_H$ : 1.34-1.48 [2H,  $m^\dagger$ ,  $C(3'/5')$  $H_{ax}$ ], 1.83 [2H,  $br\ d^\dagger$ ,  $J_{3'eq/5'eq,3'ax/5'ax} = 12.8$  Hz,  $C(3'/5')$  $H_{eq}$ ], 2.17-2.28 [1H,  $m$ ,  $C(4')$  $H_{ax}$ ], 2.84 [2H,  $d$ ,  $J_{A,4'ax} = 7.1$  Hz,  $C(A)H$ ], 2.96 [2H,  $td$ ,  $J_{2'ax/6'ax,2'eq/6'eq} = J_{2'ax/6'ax,3'ax/5'ax} = 12.8$  Hz;  $J_{2'ax/6'ax,3'eq/5'eq} = 2.7$  Hz,  $C(2'/6')$  $H_{ax}$ ], 4.55 [2H,  $br\ d^\dagger$ ,  $J_{2eq/6eq,2ax/6ax} = 12.8$  Hz,  $C(2'/6')$  $H_{eq}$ ], 6.99 [1H,  $d$ ,  $J_{3,4} = 9.3$  Hz,  $C(3)H$ ], 7.18 [1H,  $dd$ ,  $J_{6'',5''} = 7.7$  Hz;  $J_{6'',4''} = 0.9$  Hz,  $C(6'')H$ ], 7.53 [1H,  $d$ ,  $J_{8,7} = 8.9$  Hz,  $C(8)H$ ], 7.56 [1H,  $dd$ ,  $J_{7,8} = 8.9$  Hz;  $J_{7,5} = 2.2$  Hz,  $C(7)H$ ], 7.61 [1H,  $d^\dagger$ ,  $J_{4'',5''} = 7.7$  Hz,  $C(4'')H$ ], 7.70 [1H,  $d$ ,  $J_{5,7} = 2.2$  Hz,  $C(5)H$ ], 7.72-7.78 [2H,  $m^\wedge$ ,  $C(5'')H$ ;  $C(4)H$ ], 9.26 [1H,  $s$ ,  $C(4''')H$ ], 9.36 [2H,  $s$ ,  $C(2'''/6''')H$ ].  $^{13}C$  NMR ( $CDCl_3$ , 150 MHz);  $\delta_C$ : 32.1 [ $C(3'/5')$ ], 37.0 [ $C(4')$ ], 45.3 [ $C(A)$ ], 45.6 [ $C(2'/6')$ ], 110.7 [ $C(3)$ ], 114.9 [ $C(6)$ ], 118.0 [ $C(4'')$ ], 123.7 [ $C(5'')$ ], 124.1 [ $C(4a)$ ], 128.4 [ $C(8)$ ], 129.3 [ $C(5)$ ], 132.7 [ $C(7)$ ], 132.7 [ $C(1''')$ ], 136.4 [ $C(4)$ ], 137.4 [ $C(5'')$ ], 147.0 [ $C(8a)$ ], 151.6 [ $C(3'')$ ], 155.3 [ $C(2'''/6''')$ ], 157.5 [ $C(2)$ ], 158.7 [ $C(4''')$ ], 161.4 [ $C(1'')$ ].

### 6-(4-((6-(Pyrimidin-5-yl)pyridin-2-yl)methyl)piperidin-1-yl)quinolin-2-amine (88)



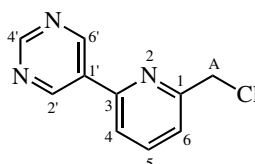
DavePhos (0.4 mg, 1.02  $\mu$ mol),  $Pd(dba)_2$  (0.3 mg, 0.521  $\mu$ mol), **132** (12.3 mg, 29.6  $\mu$ mol) and LiHMDS solution (1.0 M in THF, 0.07 mL, 70.0  $\mu$ mol) in 1,4-dioxane (2 mL) were reacted via General Method 6 for 16 hrs. The crude product was purified by flash column chromatography on silica gel, eluting with 8% MeOH in DCM to afford the title compound as a dark yellow powder (2.7 mg, 23%). HRMS:  $C_{24}H_{24}N_6$   $[M+H]^+$  requires 397.2135; found 397.2142.  $^1H$  NMR ( $CDCl_3$ , 600 MHz);  $\delta_H$ : 1.57 [2H,  $dq$ ,  $J_{3'ax/5'ax,3'eq/5'eq} = J_{3'ax/5'ax,2'ax/6'ax} = J_{3'ax/5'ax,4'ax} = 12.0$  Hz;  $J_{3'ax/5'ax,2'eq/6'eq} = 3.9$  Hz,  $C(3'/5')$  $H_{ax}$ ], 1.74-1.89 [2H,  $m^\dagger$ ,  $C(3'/5')$  $H_{eq}$ ], 2.02-2.13 [1H,  $m$ ,

$C(4')H_{ax}$ ], 2.75 [2H, td,  $J_{2'ax/6'ax,2'eq/6'eq} = J_{2'ax/6'ax,3'ax/5'ax} = 12.0$  Hz;  $J_{2'ax/6'ax,3'eq/5'eq} = 2.6$  Hz,  $C(2'/6')H_{ax}$ ], 2.87 [2H, d,  $J_{A,4ax} = 7.1$  Hz, C(A)H], 3.66-3.76 [2H, m<sup>†</sup>,  $C(2'/6')H_{eq}$ ], 4.92 [2H, br s, NH<sub>2</sub>], 6.68 [1H, d,  $J_{3,4} = 8.8$  Hz, C(3)H], 6.98 [1H, d,  $J_{5,7} = 2.7$  Hz, C(5)H], 7.20 [1H, dd,  $J_{6'',5''} = 7.8$  Hz;  $J_{6'',4''} = 0.9$  Hz, C(6'')H], 7.37 [1H, dd,  $J_{7,8} = 9.2$  Hz;  $J_{7,5} = 2.7$  Hz, C(7)H], 7.58 [1H, d,  $J_{8,7} = 9.2$  Hz, C(8)H], 7.61 [1H, dd,  $J_{4'',5''} = 7.8$  Hz;  $J_{4'',6''} = 0.9$  Hz, C(4'')H], 7.75 [1H, t,  $J_{5'',4''} = J_{5'',6''} = 7.8$  Hz, C(5'')H], 7.78 [1H, d,  $J_{4,3} = 8.8$  Hz, C(4)H], 9.26 [1H, s, C(4''')H], 9.35 [2H, s, C(2'''/6''')H]. <sup>13</sup>C NMR (CDCl<sub>3</sub>, 150 MHz); δ<sub>C</sub>: 32.3 [C(3'/5')], 36.4 [C(4')], 45.3 [C(A)], 50.9 [C(2'/6')], 111.5 [C(5)], 112.0 [C(3)], 118.0 [C(4'')], 123.8 [C(6'')], 123.9 [C(7)], 124.2 [C(4a)], 126.0 [C(8)], 132.8 [C(1''')], 137.4 [C(5'')], 137.9 [C(4)], 141.6 [C(8a)], 147.9 [C(6)], 151.6 [C(3'')], 155.3 [C(2'''/6''')\*]/C(2)\*], 155.3 [C(2'''/6''')\*]/C(2)\*], 158.6 [C(4''')], 161.6 [C(1'')].

\* denotes overlapping signals in <sup>13</sup>C NMR spectra precluded unambiguous assignment in 2D NMR spectra.

#### 6.5.4 Synthesis of a complex 6-arylmethylpiperazinyl ligand containing biaryl and 2-pyridyl components

##### 5-(6-(Chloromethyl)pyridin-2-yl)pyrimidine (140)



*Synthetic pathway A:* *N*-Chlorosuccinimide (0.204 g, 1.53 mmol), **133** (0.231 g, 1.35 mmol) and benzoyl peroxide (40.7 mg, 0.168 mmol) in BTF (6 mL) were reacted via General Method 19 for 25 hr at 75 °C. After work-up as specified, the crude product was used without further purification.

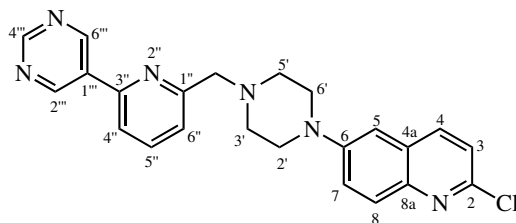
*Synthetic pathway B:* *N*-Chlorosuccinimide (0.325 g, 2.43 mmol), **133** (0.354 g, 2.07 mmol) and benzoyl peroxide (28.3 mg, 0.117 mmol) in BTF (6 mL) were reacted via General Method 19 for 23 hr at 75 °C. Work-up as specified, and the filtrate was concentrated under reduced pressure. The crude product was purified by flash column chromatography on silica gel, eluting with 1% MeOH in DCM to afford the title compound as a white powder (7.9 mg, 2%)<sup>\*</sup>. HRMS: C<sub>10</sub>H<sub>8</sub>ClN<sub>3</sub> [M+H]<sup>+</sup>

## 6.5. SYNTHESIS OF COMPLEX 6-SUBSTITUTED-2-AMINOQUINOLINE LIGANDS

requires 206.0480 [ $^{35}\text{Cl}$ ] / 208.0450 [ $^{37}\text{Cl}$ ]; found 206.0482 / 208.0453.  $^1\text{H}$  NMR ( $\text{CDCl}_3$ , 600 MHz);  $\delta_{\text{H}}$ : 4.76 [2H, s,  $\text{CH}_2$ ], 7.57 [1H, dd,  $J_{6,5} = 7.8$  Hz;  $J_{6,4} = 0.9$  Hz, C(6)H], 7.72 [1H, dd,  $J_{4,5} = 7.8$  Hz;  $J_{4,6} = 0.9$  Hz, C(4)H], 7.89 [1H, t,  $J_{5,6} = J_{5,4} = 7.8$  Hz, C(5)H], 9.28 [1H, s, C(4')H], 9.36 [2H, s, C(2'/6')H].  $^{13}\text{C}$  NMR ( $\text{CDCl}_3$ , 150 MHz);  $\delta_{\text{C}}$ : 46.7 [ $\text{CH}_2$ ], 119.8 [C(4)], 122.8 [C(6)], 132.1 [C(1')], 138.5 [C(5)], 151.7 [C(3)], 155.4 [C(2'/6')], 157.7 [C(1)], 158.9 [C(4')].

\* indicates the purified product was contaminated with residual succinimide (i.e., pyrrolidine-2,5-dione).

### 2-Chloro-6-(4-((6-(pyrimidin-5-yl)pyridin-2-yl)methyl)piperazin-1-yl)quinoline (134)

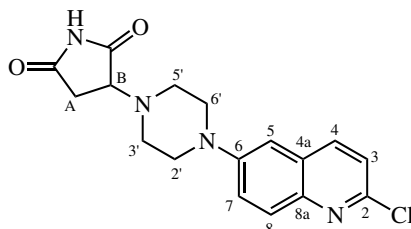


*Synthetic method A:* Potassium carbonate (57.2 mg, 0.414 mmol), **62** (81.4 mg, 0.329 mmol) and **140** (76.4 mg, 0.372 mmol) in DCM (6 mL) were reacted via General Method 14 for 19 hrs. The crude product was purified by flash column chromatography on silica gel, eluting with 2% MeOH in DCM to afford the title compound as an off-white powder (83.0 mg, 61%). HRMS:  $\text{C}_{23}\text{H}_{21}\text{ClN}_6$  [ $\text{M}+\text{H}$ ] $^+$  requires 417.1589 [ $^{35}\text{Cl}$ ] / 419.1560 [ $^{37}\text{Cl}$ ], found 417.1589 / 419.1569.  $^1\text{H}$  NMR ( $\text{CDCl}_3$ , 600 MHz);  $\delta_{\text{H}}$ : 2.77-2.87 [4H, m, C(3'/5') $\text{H}_{\text{ax/eq}}$ ], 3.35-3.42 [4H, m, C(2'/6') $\text{H}_{\text{ax/eq}}$ ], 3.85 [2H, s,  $\text{CH}_2$ ], 7.02 [1H, d,  $J_{5,7} = 2.7$  Hz, C(5)H], 7.28 [1H, d,  $J_{3,4} = 8.6$  Hz, C(3)H], 7.50 [1H, dd,  $J_{7,8} = 9.3$  Hz;  $J_{7,5} = 2.7$  Hz, C(7)H], 7.57 [1H, dd,  $J_{4'',5''} = 7.8$  Hz;  $J_{4'',6''} = 1.0$  Hz, C(4'')H], 7.67 [1H, dd,  $J_{6'',5''} = 7.8$  Hz;  $J_{6'',4''} = 1.0$  Hz, C(6'')H], 7.84 [1H, t,  $J_{5'',4''} = J_{5'',6''} = 7.8$  Hz, C(5'')H], 7.88 [1H, d $^\dagger$ ,  $J_{8,7} = 9.3$  Hz, C(8)H], 7.93 [1H, dd,  $J_{4,3} = 8.6$  Hz;  $J_{4,8} = 0.7$  Hz, C(4)H], 9.26 [1H, s, C(4''')H], 9.35 [2H, s, C(2'''/6''')H].  $^{13}\text{C}$  NMR ( $\text{CDCl}_3$ , 150 MHz);  $\delta_{\text{C}}$ : 49.1 [C(2'/6')], 53.2 [C(3'/5')], 64.4 [ $\text{CH}_2$ ], 109.0 [C(5)], 119.1 [C(4'')], 122.6 [C(3)], 123.1 [C(6'')], 123.2 [C(7)], 128.2 [C(4a)], 129.3 [C(8)], 132.6 [C(1''')], 137.6 [C(4)], 137.8 [C(5'')], 143.3 [C(8a)], 147.6 [C(6)], 149.7 [C(2)], 151.5 [C(3'')], 155.3 [C(2'''/6''')], 158.7 [C(4''')], 159.6 [C(1'')].

*Synthetic method B:* Potassium carbonate (56.3 mg, 0.407 mmol), **62** (58.6 mg, 0.237 mmol) and crude **140** (0.684 mg, 0.274 mmol) in DCM (5 mL) were reacted via General Method 14 for 22 hrs. The crude product was purified by flash column chromatography on silica gel, eluting with 2%

MeOH in DCM to afford a 3:2 mixture of the title compound and **141** as an off-white powder (12.3 mg). Data for **134** as above.

*3-(4-(2-Chloroquinolin-6-yl)piperazin-1-yl)pyrrolidine-2,5-dione (141)*

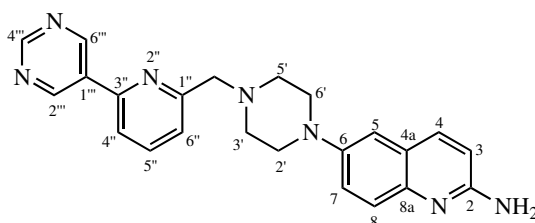


HRMS:  $C_{17}H_{17}ClN_4O_2$   $[M+H]^+$  requires 345.1113 [ $^{35}Cl$ ] / 347.1084 [ $^{37}Cl$ ], found 345.1114 / 347.1095.  $^1H$  NMR ( $CDCl_3$ , 600 MHz);  $\delta_H$ : 2.75-2.84 [3H, m $^\wedge$ , C(3')H $_{ax/eq}$ \*/C(5')H $_{ax/eq}$ \*; C(A)H], 2.94 [1H, dd,  $J_{A,A} = 18.6$  Hz;  $J_{A,B} = 9.1$  Hz, C(A)H], 3.05 [2H, dt,  $J_{3'ax/5'ax,3'eq/5'eq} = 10.5$  Hz;  $J_{3'ax/eq/5'ax/eq,2'ax/eq/6'ax'eq} = 5.0$  Hz, C(3')H $_{ax/eq}$ \*/C(5')H $_{ax/eq}$ \*], 3.35 [4H, t,  $J_{2'ax/eq/6'ax'eq,3'ax/eq/5'ax/eq} = 5.0$  Hz, C(2'/6')H $_{ax/eq}$ ], 3.94 [1H, dd,  $J_{B,A} = 9.1$  Hz;  $J_{B,A} = 5.2$  Hz, C(B)H], 7.01 [1H d,  $J_{5,7} = 2.8$  Hz, C(5)H], 7.30 [1H, d,  $J_{3,4} = 8.6$  Hz, C(3)H], 7.47 [1H, dd,  $J_{7,8} = 9.3$  Hz;  $J_{7,5} = 2.8$  Hz, C(7)H], 7.89 [1H, d,  $J_{8,7} = 9.3$  Hz, C(8)H], 7.93 [1H, d,  $J_{4,3} = 8.6$  Hz, C(4)H], 8.23 [1H, br s, NH].  $^{13}C$  NMR ( $CDCl_3$ , 150 MHz);  $\delta_C$ : 32.7 [C(A)], 49.2 [C(2'/6')\*\*; C(3'/5')\*\*], 63.7 [C(B)], 109.4 [C(5)], 122.7 [C(3)], 123.4 [C(7)], 128.1 [C(4a)], 129.4 [C(8)], 137.7 [C(4)], 143.4 [C(8a)], 147.9 [C(6)], 149.5 [C(2)], 174.4 [C=O], 175.8 [C=O].

\* denotes the signals could not be unambiguously assigned due to overlapping signals in 2D NMR spectra.

\*\* denotes overlapping signals in  $^{13}C$  NMR spectra.

**6-(4-((6-(Pyrimidin-5-yl)pyridin-2-yl)methyl)piperazin-1-yl)quinolin-2-amine (89)**



DavePhos (1.6 mg, 4.07  $\mu$ mol), Pd(dba) $_2$  (1.7 mg, 2.96  $\mu$ mol), **134** (38.9 mg, 93.3  $\mu$ mol) and LiHMDS solution (1.0 M in THF, 0.30 mL, 0.30 mmol) in 1,4-dioxane (2 mL) were reacted via

## 6.5. SYNTHESIS OF COMPLEX 6-SUBSTITUTED-2-AMINOQUINOLINE LIGANDS

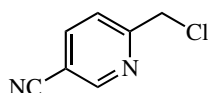
---

General Method 6 for 16 hrs. The crude product was purified by flash column chromatography on silica gel, eluting with 10% MeOH in DCM to afford the title compound as a yellow-orange solid (13.3 mg, 36%). HRMS:  $C_{23}H_{23}N_7$   $[M+H]^+$  requires 398.2088; found 398.2085.  $^1H$  NMR ( $CDCl_3$ , 600 MHz);  $\delta_H$ : 2.72-2.87 [4H, m, C(3'/5') $H_{ax/eq}$ ], 3.25-3.43 [4H, m, C(2'/6') $H_{ax/eq}$ ], 3.87 [2H, s,  $CH_2$ ], 4.77 [2H, br s,  $NH_2$ ], 6.69 [1H, d,  $J_{3,4} = 8.8$  Hz, C(3)H], 6.98 [1H, d,  $J_{5,7} = 2.7$  Hz, C(5)H], 7.37 [1H, dd,  $J_{7,8} = 9.1$  Hz;  $J_{7,5} = 2.7$  Hz, C(7)H], 7.57 [1H, dd,  $J_{4'',5''} = 7.8$  Hz;  $J_{4'',6''} = 0.9$  Hz, C(4'')H], 7.60 [1H, d,  $J_{8,7} = 9.1$  Hz, C(8)H], 7.66 [1H, dd,  $J_{6'',5''} = 7.8$  Hz;  $J_{6'',4''} = 0.9$  Hz, C(6'')H], 7.79 [1H, d,  $J_{4,3} = 8.8$  Hz, C(4)H], 7.84 [1H, t,  $J_{5'',4''} = J_{5'',6''} = 7.8$  Hz, C(5'')H], 9.26 [1H, s, C(4''')H], 9.35 [2H, s, C(2'''/6''')H].  $^{13}C$  NMR ( $CDCl_3$ , 150 MHz);  $\delta_C$ : 50.2 [C(2'/6')], 53.5 [C(3'/5')], 64.5 [ $CH_2$ ], 111.2 [C(5)], 112.0 [C(3)], 119.0 [C(6'')], 123.1 [C(4'')\*]; C(7)\*], 124.3 [C(4a)], 126.5 [C(8)], 132.6 [C(1''')], 137.7 [C(4)], 137.8 [C(5'')], 142.3 [C(8a)], 147.2 [C(6)], 151.5 [C(3'')], 155.3 [C(2'''/6''')], 155.5 [C(2)], 158.7 [C(4'')], 159.8 [C(1'')].

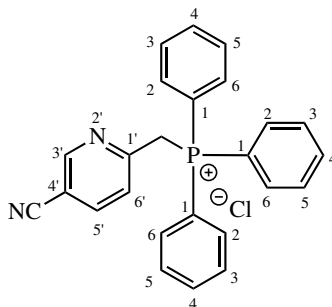
\* denotes overlapping signals in  $^{13}C$  NMR spectra.

### 6.5.5 Towards the synthesis of a 6-arylmethylpiperidinyl 2-aminoquinoline ligand containing 4-amido and 2-pyridyl components

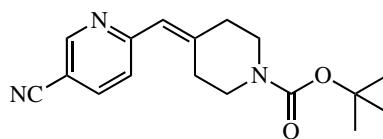
#### 6-(Chloromethyl)nicotinonitrile (142)



*N*-Chlorosuccinimide (0.821 g, 6.15 mmol), 6-methylnicotinonitrile (0.637 g, 5.39 mmol) and benzoyl peroxide (7.07 mg, 0.292 mmol) in BTF (10 mL) were reacted via General Method 19 for 23 hr at 75 °C. After work-up as specified, the product was immediately used without further purification.

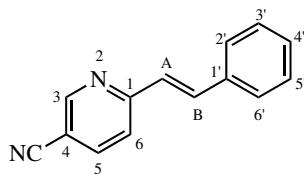
**((5-Cyanopyridin-2-yl)methyl)triphenylphosphonium chloride (143)**

Crude **142** (0.823 g, 5.39 mmol) suspended in toluene (10 mL), and triphenylphosphine (2.23 g, 8.51 mmol) were reacted via General Method 16 for 19 hr to afford the title compound as a brown solid, which was used without further purification (1.36 g, 61% over 2 steps).  $^1\text{H}$  NMR ( $\text{CDCl}_3$ , 600 MHz);  $\delta_{\text{H}}$ : 6.02 [2H,  $J_{\text{H,P}} = 15.0$  Hz, C(A)H], 7.64 [6H, td,  $J_{3/5,2/6} = J_{3/5,4} = 7.8$  Hz;  $J_{3/5,\text{P}} = 3.6$  Hz, C(3/5)H], 7.72-7.79 [3H, m, C(4)H], 7.83 [1H, ddd,  $J_{5',6'} = 8.2$  Hz;  $J_{5',3'} = 2.2$  Hz;  $J_{5',\text{P}} = 0.9$  Hz, C(5')H], 7.84-7.90 [6H, m, C(2/6)H], 8.40 [1H, dd,  $J_{6',5'} = 8.2$  Hz;  $J_{6',\text{P}} = 1.3$  Hz, C(6')H], 8.50 [1H, d,  $J_{3',5'} = 2.2$  Hz, C(3')H].  $^{13}\text{C}$  NMR ( $\text{CDCl}_3$ , 150 MHz);  $\delta_{\text{C}}$ : 32.7 [d,  $J_{\text{C,P}} = 51.7$  Hz, C(A)], 109.1 [d,  $J_{4',\text{P}} = 2.5$  Hz, C(4')], 116.4 [d,  $J_{\text{C,P}} = 1.5$  Hz,  $\text{C}\equiv\text{N}$ ], 118.6 [d,  $J_{1,\text{P}} = 87.6$  Hz, C(1)], 127.9 [d,  $J_{6',\text{P}} = 7.6$  Hz, C(6')], 130.2 [d,  $J_{3/5,\text{P}} = 12.9$  Hz, C(3/5)], 134.3 [d,  $J_{2/6,\text{P}} = 10.4$  Hz, C(2/6)], 135.0 [d,  $J_{4,\text{P}} = 3.0$  Hz, C(4)], 140.4 [C(5')], 151.4 [d,  $J_{3',\text{P}} = 2.1$  Hz, C(3')], 155.3 [d,  $J_{1',\text{P}} = 8.6$  Hz, C(1')].

**Attempted synthesis of *tert*-Butyl 4-((5-cyanopyridin-2-yl)methylene)piperidine-1-carboxylate (144)**

**143** (1.36 g, 3.28 mmol), LiHMDS (1.0 M in THF, 6.6 mL, 6.6 mmol) and *N*-Boc-4-piperidone (0.853 g, 4.28 mmol) in THF (6 mL) were reacted via General Method 2 for 23 hr. Work-up as specified afforded the crude product as an orange oil. Analysis of the crude product  $^1\text{H}$  NMR spectrum indicated the main product present was the reduced product 6-methylnicotinonitrile, with only trace amounts of the desired title compound. Product was not purified.

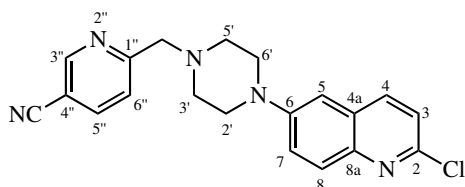


**(E)-6-Styrylnicotinonitrile (150)**

**143** (0.298 g, 0.718 mmol) was suspended in anhydrous THF (5 mL) and stirred under an atmosphere of nitrogen. The suspension was cooled to 0°C, and LiHMDS (1.0 M in THF, 1.0 mL, 1.0 mmol) was added dropwise. The reaction mixture was warmed to room temperature, and stirred for 15 mins. Benzaldehyde (0.06 mL, 0.588 mmol) was added dropwise, and the reaction mixture was then stirred for 20 hrs. The reaction mixture was quenched with MeOH (30 mL), then concentrated under reduced pressure. The resulting residue was suspended in a 2:3 mixture of EtOAc/hexanes (40 mL) and filtered, then the filtrate was concentrated under reduced pressure. The crude product was purified by flash column chromatography on silica gel, eluting with 10% EtOAc in hexanes to afford the title compound as a white crystalline solid (69.7 mg, 57%). <sup>1</sup>H NMR (CDCl<sub>3</sub>, 600 MHz); δ<sub>H</sub>: 7.16 [1H, d, *J*<sub>A,B</sub> = 16.0 Hz, C(A)H], 7.33-7.38 [1H, m, C(4')H], 7.41-7.45 [2H, m, C(3'/5')H], 7.43 [1H, dd, *J*<sub>6,5</sub> = 8.2 Hz; *J*<sub>6,3</sub> = 0.9 Hz, C(6)H], 7.57-7.62 [2H, m, C(2'/6')H], 7.80 [1H, d, *J*<sub>B,A</sub> = 16.0 Hz, C(B)H], 7.89 [1H, dd, *J*<sub>5,6</sub> = 8.2 Hz; *J*<sub>5,3</sub> = 2.2 Hz, C(5)H], 8.83 [1H, dd, *J*<sub>3,5</sub> = 2.2 Hz; *J*<sub>3,6</sub> = 0.9 Hz, C(3)H]. <sup>13</sup>C NMR (CDCl<sub>3</sub>, 150 MHz); δ<sub>C</sub>: 107.3 [C(4)], 117.3 [C≡N], 121.8 [C(6)], 126.2 [C(A)], 127.7 [C(2'/6')], 129.0 [C(3'/5')], 129.5 [C(4')], 135.8 [C(1')], 137.2 [C(B)], 139.7 [C(5)], 152.5 [C(3)], 159.0 [C(1)].

### 6.5.6 Towards the synthesis of a 6-arylmethylpiperazinyl 2-aminoquinoline ligand containing 4-amido and 2-pyridyl components

#### 6-((4-(2-Chloroquinolin-6-yl)piperazin-1-yl)methyl)nicotinonitrile (148)

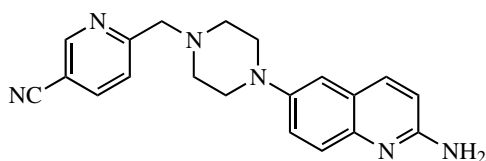


Potassium carbonate (51.3 mg, 0.407 mmol), **62** (71.8 mg, 0.237 mmol) and crude **142** (51.0 mg, 0.334 mmol) in DCM (6 mL) were reacted via General Method 14 for 22 hrs. The crude product was purified by flash column chromatography on silica gel, eluting with 1% MeOH in DCM to

afford the title compound as a yellow-brown oil (25.3 mg, 50% over 2 steps). HRMS:  $C_{20}H_{18}ClN_5$  requires 364.1323 [ $^{35}Cl$ ] / 366.1294 [ $^{37}Cl$ ]; found 364.1325 / 366.1303.  $^1H$  NMR ( $CDCl_3$ , 600 MHz);  $\delta_H$ : 2.72-2.77 [4H, m, C(3'/5') $H_{ax/eq}$ ], 3.30-3.47 [4H, m, C(2'/6') $H_{ax/eq}$ ], 3.83 [2H, s,  $CH_2$ ], 7.01 [1H, d,  $J_{5,7} = 2.7$  Hz, C(5)H], 7.29 [1H, d,  $J_{3,4} = 8.6$  Hz, C(3)H], 7.49 [1H, dd,  $J_{7,8} = 9.3$  Hz;  $J_{7,5} = 2.7$  Hz, C(7)H], 7.67 [1H, br  $d^\dagger$ ,  $J_{6'',5''} = 8.1$  Hz, C(6'')H], 7.88 [1H,  $d^\dagger$ ,  $J_{8,7} = 9.3$  Hz, C(8)H], 7.93 [1H, dd,  $J_{4,3} = 8.6$  Hz;  $J_{8,4} = 0.7$  Hz, C(4)H], 7.97 [1H, dd,  $J_{5'',6''} = 8.1$  Hz;  $J_{5'',3''} = 2.2$  Hz, C(5'')H], 8.87 [1H, dd,  $J_{3'',5''} = 2.2$  Hz;  $J_{3'',6''} = 0.9$  Hz, C(3'')H].  $^{13}C$  NMR ( $CDCl_3$ , 150 MHz);  $\delta_C$ : 49.0 [C(2'/6')], 53.2 [C(3'/5')], 64.1 [ $CH_2$ ], 108.5 [C(4'')], 109.1 [C(5)], 116.8 [ $C\equiv N$ ], 122.6 [C(3)], 123.1 [C(6''); C(7)\*], 123.2 [C(6''), C(7)\*], 128.1 [C(4a)], 129.2 [C(8)], 137.6 [C(4)], 139.8 [C(5'')], 143.3 [C(8a)], 147.7 [C(2)], 149.6 [C(6)], 152.2 [C(3'')], 163.2 [C(1'')].

\* denotes signals could not be unambiguously assigned due to overlapping signals in 2D NMR spectra.

#### Attempted synthesis of 6-((4-(2-Aminoquinolin-6-yl)piperazin-1-yl)methyl)nicotinonitrile (**149**)



DavePhos (1.0 mg, 2.54  $\mu$ mol),  $Pd(dba)_2$  (1.9 mg, 3.30  $\mu$ mol), **148** (24.7 mg, 67.9  $\mu$ mol) and LiHMDS solution (1.0 M in THF, 0.22 mL, 0.22 mmol) in 1,4-dioxane (2 mL) were reacted via General Method 6 for 16 hrs. Work-up as specified afforded the crude product as a brown oily solid.  $^1H$  NMR analysis of the crude product mixture revealed starting material with only trace amounts of the title compound were present, which could not be separated by chromatographic methods.

## 6.6 Protein Methods: Expression and purification

### 6.6.1 Comment on general protein methods

Reagents and technical details of methods are provided in advance of the general procedure for protein preparation (Section 6.6.2). They are included here as a detailed reference and for completeness.

### 6.6.1.1 Common buffers and solutions

Milli-Q water at 18.2 m $\Omega$  was used for the preparation of all buffers and procedures requiring aqueous conditions. Hereafter, water refers to Milli-Q water at 18.2 m $\Omega$ .

TBS (Tris-buffered saline): tris(hydroxymethyl)aminomethane (Tris) (25 mM), sodium chloride (150 mM), dissolved in water, adjusted to pH  $\sim$ 8.0, filtered through 0.2  $\mu$ m polyethersulfone (PES) membrane.

TTBS: 0.1% v/v Triton-X dissolved in TBS, adjusted to pH  $\sim$ 8.0, filtered through 0.2  $\mu$ m polyethersulfone (PES) membrane.

TGS (Tris glycine SDS): tris(hydroxymethyl)aminomethane (Tris) (25 mM), glycine (190 mM) and SDS (3 mM), dissolved in water.

PBS (Phosphate Buffered saline): disodium hydrogen phosphate (12 mM), sodium chloride (150 mM) dissolved in water, filtered through 0.2  $\mu$ m nylon membrane filter.

Rapid Coomassie stain: Coomassie (Brilliant) Blue (2 g), methanol (400 mL), acetic acid (glacial, 100 mL) and water (500 mL).

Rapid de-stain: Methanol (400 mL), acetic acid (glacial, 100 mL) and water (500 mL).

### 6.6.1.2 Purification of GST-SH3 fusion proteins by agarose/glutathione column chromatography

GST-SH3 Fusion proteins were purified from bacterial lysate using a Pharmacia XK26/20 (i.d. 26 mm) column loaded with glutathione sepharose 4B (GE Healthcare), attached to either a GE Healthcare ÄKTA Pure<sup>®</sup> Fast Protein Liquid Chromatography system fitted with a GE Healthcare F9-R Fraction collector at room temperature, or a Bio-Rad NGC Quest 10 chromatography system fitted with a Bio-Rad BioFrac fraction collector, at 4°C. In either case, the column was equilibrated with at least two column volumes of TBS, followed by at least two column volumes of TTBS. The column was then loaded with no more than 4 mL of bacterial lysate if using the ÄKTA Pure<sup>®</sup> Fast Protein Liquid Chromatography system, or 10 mL if using the Bio-Rad NGC Quest 10 chromatography system. The buffer was pumped at a flow rate of 4 ml/min, collecting fractions with volumes

of 10 mL. The column was washed with TTBS, until all lysate had eluted (two column volumes), then washed extensively with TBS (four column volumes). Bound GST-SH3 fusion protein was eluted by washing with 10 mM reduced glutathione in TBS (pH ~8), and the fraction volume was reduced to 5 mL. An example chromatographic trace is provided in Chapter 2, Figure 2.10A. Progress of the column was monitored by SDS-PAGE (see Chapter 2, Figure 2.10B), and the appropriate fractions combined. Protein samples were stored at 4 °C.

Upon completion of the chromatographic procedure, the column was washed with several column volumes of water, followed by 0.5 M NaOH solution, then 20% ethanol. The column was stored in 20% ethanol.

### **6.6.1.3 Determination of protein concentration using Bradford dye binding assay**

10 Microlitres of standard solutions of bovine serum albumin (BSA; cat. no. 10735086001 Roche Diagnostics) with concentrations of 0-2 mg/mL in either TBS or PBS, and appropriately diluted protein samples in either TBS or PBS were pipetted into 96 well flat-bottomed clear plates, before the addition of a 4:1 dilution of protein assay concentrate (BIORAD cat. no. #5000006, diluted with either TBS or PBS) to each standard or sample, to a total volume of 210  $\mu$ L. The solutions were homogenised by gently swirling the plate, followed by sealing the plate and allowing it to equilibrate at room temperature for 5-10 mins. Absorbances at 600 nm were then recorded with a Multiskan Ascent 354 plate reader (Thermo Fisher), using Ascent Software Version 2.4. Readings for samples and standards were obtained in duplicate, and the averages for the standards were used to derive a standard curve. The standard curve was then used to calculate the concentrations of the protein samples.

### **6.6.1.4 PD10 buffer exchange chromatography**

PD10 Columns (GE Healthcare) were equilibrated with ~25 mL of the appropriate buffer prior to loading the protein sample (up to 2.5 mL) as per the manufacturer's instructions. The column was washed with 3.5 mL of the appropriate buffer, and the protein-containing elute was collected. Complete elution of the protein was determined by analysing additional column washings via Bradford dye binding assay.

### 6.6.1.5 Thrombin digestion

Purified GST-SH3 fusion protein in TBS was diluted to  $\sim 2$  mg/mL. Thrombin (Sigma T7009, 3 units/mg GST-SH3),  $\text{CaCl}_2$  (to resultant concentration of 2.5 mM) and  $\text{NaN}_3$  (to resultant concentration of 0.01% w/v) were added to the diluted protein, and the resultant mixture incubated at room temperature, inverting occasionally. After at least 18 hours, the progress of the digestion was confirmed by SDS-PAGE (Figure 6.1).

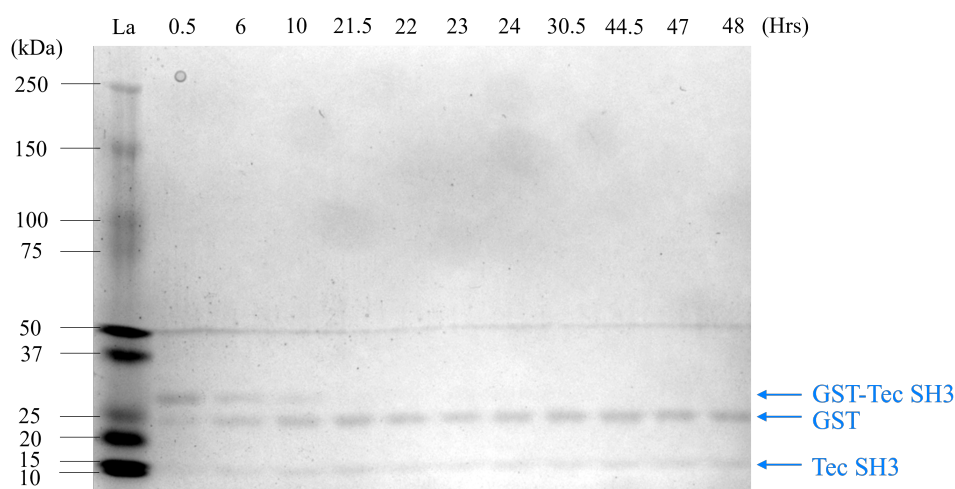


Figure 6.1: SDS-PAGE analysis of protein samples at different timepoints during thrombin digest. Reference ladder indicated by 'La', with size of reference proteins labelled (in kDa). Column labels refer to the time (hrs) since beginning the digest. Suggested protein identities indicated by blue arrows, labelled in blue.

### 6.6.1.6 Size exclusion chromatography

The crude protein was concentrated to  $\sim 3$  mL using either a 10 kDa or 3 kDa MWCO filter (as appropriate), and purified using either a GE Healthcare HiLoad™ 16/600 Superdex™ 75 pg column, attached to a GE Healthcare ÄKTA Pure® Fast Protein Liquid Chromatography system fitted with a GE Healthcare F9-R Fraction collector, or a GE Healthcare HiPrep™ 26/60 Sephacryl S-200 HR column attached to a Bio-Rad NGC Quest 10 chromatography system fitted with a Bio-Rad BioFrac fraction collector, at 4°C. The column was equilibrated with at least two column volumes of TBS, before loading no more than 2 mL of the crude protein if using the ÄKTA Pure® Fast Protein Liquid Chromatography system, or 10 mL if using the Bio-Rad NGC Quest 10 chromatography system. The buffer was pumped at a flow rate of  $\sim 1$  mL/min, and fractions with volumes of 8 mL were collected. An example chromatographic trace is provided in Chapter 2, Figure 2.11A. The progress

of the column was monitored by SDS-PAGE (see Chapter 2, Figure 2.11B), and the appropriate fractions combined. Protein samples were stored at 4°C.

Upon completion of the chromatographic procedure, the column was washed with several column volumes of water, followed by 0.5 M NaOH solution, then 20% ethanol. The column was stored in 20% ethanol.

### 6.6.1.7 SDS-PAGE: sodium dodecyl sulfate-polyacrylamide gel electrophoresis

#### Gel buffers

Running buffer: 1 x TGS

Loading buffer stock (makes 46 mL): 0.5 M Tris-HCl (pH 6.8) (14 mL), Bromophenyl blue (0.02 g), glycerol (16 mL) and 10% SDS (16 mL).

Reducing loading buffer (makes 1 mL): Loading buffer stock (800 µL) and DTT (1M, 200 µL).

#### Composition of SDS-PAGE gels

Gels were either poured using a BIO-RAD Mini-PROTEAN® Tetra Cell casting stand, or purchased as pre-cast gels (BIO-RAD 4-20% Mini-PROTEAN® TGX™ Precast Protein Gels, 10-well, 50 µL, cat. no. 4561094). For gels which were poured in-house, their composition was as follows:

Resolving gel (12%): acrylamide (40%, 3.0 mL), tris-HCl pH 8.8 (3.75 mL), SDS (10%, 100 µL), water (3.1 mL), ammonium persulfate (10%, 20 µL), TEMED (20 µL).

Stacking gel (4%): acrylamide (40%, 340 µL), tris-HCl pH 6.8 (1.25 mL), SDS (10%, 38 µL), water (2.1 mL), ammonium persulfate (10%, 8 µL), TEMED (8 µL).

#### Electrophoresis protocol

Protein samples were diluted 1:1 with reducing loading buffer to a final volume of 30 µL, and heated at 100°C for 5 mins, and given a “flick” spin prior to loading the gel. BIO-RAD Precision Plus Protein™ Standards (#161-0374) were used as a reference. Gels were run at 140 V, 400 mA using a discontinuous buffer system, where the discontinuous buffer system involves loading of the sample into a non-restrictive large pore gel (i.e., stacking gel), before moving into a gel containing

smaller pores (i.e., resolving gel) for improved resolution.<sup>140</sup> Gels were run until the dye front reached the bottom of the gel.

Completed gels were stained using Rapid Coomassie stain with gentle agitation for at least 60 mins at room temperature. Gels were then de-stained with gentle agitation using Rapid de-stain over at least 12 hours, then imaged using a BIO-RAD Chemidoc™ XRS+ system.

### 6.6.2 Protein preparation methods

#### 6.6.2.1 Bacterial growth media

Luria broth (LB), per 1 L: Sodium chloride (5 g/L), Bacto yeast extract (5 g/L) and Bacto tryptone (10 g/L) in water, adjusted to pH ~7 prior to autoclaving.

#### 6.6.2.2 Procedure for preparation of GST-Tec SH3 fusion proteins for SPR experiments and x-ray crystallography

All GST-SH3 fusion proteins were prepared based closely upon previously reported methods.<sup>3,46</sup> *Escherichia coli* (*E. coli*) strain BL-21-DE3 transformed with a pGEX-4T-2 expression vector encoding GST, connected by a thrombin cleavage site to amino acids of either 181-245 of the murine Tec IV SH3 domain, or 181-245 of the murine Tec IV domain domain containing a single amino acid variation at position 196, had been previously prepared.<sup>3,46,54</sup>

An agar plate (LB Lennox 1.5% agar + ampicillin, 0.1 mg/mL) was inoculated with the a glycerol stock of *E. coli* BL21-DE3 p-GEX 4T-2, and incubated overnight at 37° C. Two colonies were sub-cultured into LB (+ ampicillin, 0.1 mg/mL), and incubated overnight at 37° C on an orbital shaker. The overnight culture was then diluted 1:10 into pre-warmed LB (+ ampicillin, 0.1 mg/mL), and incubated at 37° C on an orbital shaker until the culture reached an optical density (at 600 nm) of 0.6-0.8. Protein expression was induced by the addition of isopropyl- $\beta$ -D-thiogalactoside (IPTG) solution (0.5 M, to resultant concentration of 0.2 mM). The cultures were incubated for a further 4 hours at 37° C on an orbital shaker, before transferring into 500 mL centrifuge pots, and spinning at 5000 xg at 4° C for 15 mins. The supernatants were discarded, and the pellets were stored at -20° C for at least 18 hours. The pellets were resuspended in TTBS, and subjected to at least two freeze-thaw cycles before warming to room temperature and cell lysis via sonication with addition of

PMSF in ethanol (100 mM, to resultant concentration of 1 mM). The lysate was then spun at 11200 xg at 4° C for 20 mins, and the resulting supernatant was filtered through a 0.45 µm cellulose-acetate membrane. The filtered lysate was purified on an agarose/glutathione affinity column, as described in Section 6.6.1.2 (Chapter 2, Figure 2.10). After affinity chromatography, appropriate fractions were combined and concentrated using a 10 kDa MWCO filter. The concentrated sample was purified further using a size-exclusion column, as described in Section 6.6.1.6 (Chapter 2, Figure 2.11). Following purification, the concentration of the GST-SH3 fusion protein was determined via Bradford dye binding assay (Section 6.6.1.3). From a 2 L culture, typically a 3-6 mL fraction was obtained containing ~20 mg/mL purified GST-SH3 fusion protein. If not used immediately, aliquots of the concentrated fusion protein were snap-frozen and stored at -80°C.

For GST-SH3 fusion protein to be used in SPR experiments, the concentrated fusion protein was exchanged into PBS using a PD10 desalting column, and stored at either -20°C or -80°C.

### **6.6.3 Procedure for preparation of Tec SH3 protein for x-ray crystallography experiments**

Purified GST-SH3 protein in TBS was treated with thrombin as described in Section 6.6.1.5 (Figure 6.1). The crude digested protein was concentrated to ~2 mL using a 3 kDa MWCO filter, then filtered through a 0.22 µm cellulose acetate-membrane prior to purification by size-exclusion chromatography as described in Section 6.6.1.6, eluting with TBS (see Chapter 2, Figure 2.14). Fractions containing SH3 protein were analysed by SDS-PAGE. The appropriate fractions were combined then concentrated to ~6 mL using a 3 kDa MWCO filter, to a concentration of ~6 mg/mL in TBS.

A portion of the concentrated SH3 protein was then exchanged into PBS using a PD10 desalting column, and stored at either -20°C or -80°C.

## **6.7 Protein Methods: SPR ligand binding assays**

### **6.7.1 Preparation of GST protein**

Lypophilised GST from equine liver (Sigma G6511) (4 mg) was reconstituted with MQ water (1 mL). The resulting suspension was centrifuged at 2000 xg for 10 mins. The supernatant was removed



from the resulting pellet, then buffer exchanged into PBS using PD-10 desalting columns as per the manufacturer's instructions. Protein concentrations of the collected fractions were determined via Bradford assay, and appropriate fractions combined before determining the final protein concentration via Bradford assay. The protein solution was supplemented with  $\text{Na}_3\text{N}$  to a final concentration of 0.02% v/v, and aliquots snap-frozen in preparation for SPR assays.

### 6.7.2 Ligand-binding assays with GST-SH3 fusion proteins and Tec SH3 domain using SPR experiments

SPR assays were conducted using a Biacore S200 system (GE Healthcare), using Biacore S200 Evaluation Software to display and analyse assay results.

All buffers were prepared in-house, unless otherwise stated. N-Hydroxysuccinimide (NHS), 1-ethyl-3-(3-dimethylaminopropyl) carbodiimide hydrochloride (EDC) and ethanolamine (1.0 M, pH 8.5) were purchased from GE Healthcare and prepared as aqueous stock solutions as per the manufacturer's instructions. TWEEN<sup>®</sup>20 was purchased from Sigma Aldrich. Dimethyl sulfoxide was purchased from Chem-Supply. Serial dilutions were completed manually as 1/2 dilutions. All data processing was completed using Biacore S200 Evaluation Software, Version 1.0 (Build: 20) (GE Healthcare).

Series S CM5 Sensor chips (GE Healthcare/Cytiva) were pre-conditioned with two sequential injections (50 sec) of NaOH (50 mM), HCl (10mM), SDS (0.1 % v/v),  $\text{H}_3\text{PO}_4$  (0.85 % w/v) and glycine (50 mM, pH 9.5) at a flow rate of 10  $\mu\text{L}/\text{min}$  with a short interval (30 sec) between each injection. Proteins were immobilised to the pre-conditioned chip using amine coupling chemistry, to a target concentration of  $\sim 0.75$  mg/mL in the surface matrix. The immobilisation running buffer consisted of PBS (pH 7.4) with TWEEN<sup>®</sup>20 (0.05 % v/v). The appropriate flow channel surfaces were activated with a 1:1 mixture of NHS (100 mM) and EDC (390 mM), injected over 15 minutes at a flow rate of 10  $\mu\text{L}/\text{min}$ . For GST, GST-Tec SH3 or GST-Tec SH3 D196A, protein stock solutions in PBS were each diluted in sodium acetate solution (10 mM, pH 4.96) to  $\sim 1$   $\mu\text{M}$  immediately prior to injection over activated sensor chip surface. The protein was injected at a flow rate of 2  $\mu\text{L}/\text{min}$ . Once a suitable amount of protein had bound (typically 6000-9000 RU), the flow rate was increased to 10  $\mu\text{L}/\text{min}$ , and the sensor chip surface was then blocked with two consecutive injections of ethanolamine (1.0 M, pH 8.5), lasting 3.5 mins each. Similarly, following flow channel surface

activation with NHS and EDC as described above, Tec SH3 protein stock solutions in PBS were diluted in sodium acetate solution (10 mM, pH 3.98) to  $\sim 2 \mu\text{M}$  immediately prior to injection over the sensor chip surface. The protein was injected at a flow rate of  $2 \mu\text{L}/\text{min}$ . Once a suitable amount of protein had bound (aiming for  $\sim 2500$  RU, but typically achieving  $\sim 500$  RU), the sensor chip surface was blocked with two consecutive injections of ethanolamine (1.0 M, pH 8.5) as described above.

For each ligand binding assay, the running buffer was replaced with fresh running buffer containing PBS (pH 7.4), DMSO (5 % v/v) and TWEEN<sup>®</sup>20 (0.05 % v/v) immediately prior to starting the assay. Ligand stocks prepared in DMSO (typically 100 mM) were diluted to 500  $\mu\text{M}$  stocks in running buffer, prior to serial dilution to the desired assay concentrations, with running buffer.

Assays were completed at 25 °C with a buffer flow rate of  $30 \mu\text{L}/\text{min}$ . Ligand association and dissociation times for each assay run were typically 45 seconds each, unless otherwise stated. The sensor chip surface was briefly washed with 50% DMSO in water after each injection to remove any non-specifically bound ligands from the sensor chip surface. To ensure the protein binding capacity and sensor chip surface architecture was not impacted by each 50% DMSO wash, baseline RU values were monitored for consistency throughout all assay runs, and inter-assay variability in  $\text{RU}_{\text{max}}$  values for each ligand was monitored.

Following sample injection, the response recorded for the reference flow channel was subtracted from the response for the target flow channel, to correct for non-specific binding interactions and baseline drift. The data was solvent corrected for bulk response (refractive index) differences, and blank injections were utilised as a double reference. The data was molecular weight normalised for each ligand, and  $K_{\text{d}}$  values were determined by steady-state analysis for those ligands which had achieved saturation binding. Screening assays were completed with ligand concentrations of 0, 6.25, 12.5, 25, 50 and 100  $\mu\text{M}$ . Ligands that recorded saturation binding with the target protein, as well as moderate binding affinity ( $K_{\text{d}} \leq 20 \mu\text{M}$ ), were selected for further investigation in optimised binding assays. Optimisation of binding assays was achieved by altering the range of ligand concentrations assayed, as per equation 6.1, where  $[L]_{\text{max}}$  refers to maximum ligand concentration for optimised SPR binding assays, and  $K_{\text{d}(\text{screen})}$  refers to the dissociation constant determined from the screening assays.

$$[L]_{\max} \leq 10K_d(\text{screen}) \quad (6.1)$$

Optimised SPR binding assays for ligands that reached saturation binding were completed in triplicate, and an average  $K_d$  value calculated. This method was used for  $K_d$  calculation by SPR methods in this thesis, and describes the derivation of those values discussed in the main text.

### 6.7.3 Optimisation of protein pre-concentration conditions by pH scouting

The flow channels of a Series S CM5 sensor chip were pre-conditioned as described previously (see Section 6.7.2). The protein of interest (i.e., to be immobilised) was diluted to the desired concentration (typically starting at  $\sim 1 \mu\text{M}$ ) in the specified buffer, and injected over a single flow channel at a flow rate of  $10 \mu\text{L}$  for a period of 60 sec. Following this,  $50 \text{ mM NaOH}$  was then injected over the flow channel surface at a flow rate of  $10 \mu\text{L}$  for a period of 60 sec, to remove residual protein from the flow channel surface. The process was repeated until protein concentration and buffer conditions were identified which yielded strong attraction to the sensor chip surface, represented as a substantial increase in RU upon protein injection. Upon identification of favourable protein pre-concentration conditions, protein immobilisation was conducted as described in Section 6.7.2.

## 6.8 Protein Methods: X-ray crystallography

### 6.8.1 Automated preparation of screening trays

Using a Crystal Phoenix dispensing instrument (Art Robbins Instruments),  $80 \mu\text{L}$  of screening buffers from a 96-well deep block was dispensed into the reservoirs of an Intelli-Plate (Art Robbins Instruments, catalog number 102-0011-11). Screening experiments were conducted via vapour diffusion sitting drop method, where  $1 \mu\text{L}$  of protein solution and  $1 \mu\text{L}$  screening buffer were dispensed and mixed in the appropriate screening well. As a control for salt crystals,  $1 \mu\text{L}$  of screening buffer was also dispensed into the appropriate adjacent screening well. The plate was immediately sealed with Crystal Clear sealing tape (Hampton Research, HR4-506), then incubated at  $16^\circ\text{C}$  to encourage crystal growth.

### **6.8.2 Manual preparation of screening trays**

Volumes and consumables as per Section 6.8.1, but solutions were dispensed using a multichannel pipette (8 channels). To minimise evaporation of protein-buffer solutions, the buffer reservoir was used as the negative control solution for salt crystals.

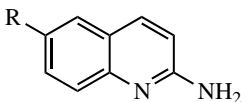
### **6.8.3 Preparation of optimisation trays**

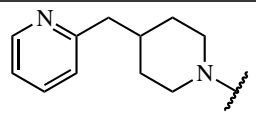
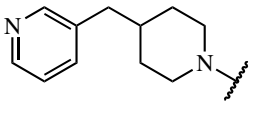
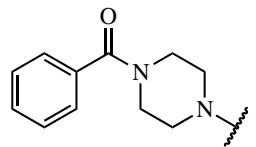
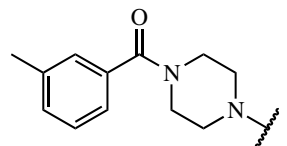
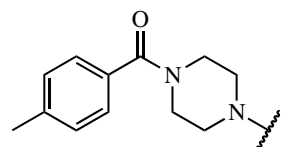
All optimisation trays were completed using clear 24-well flat bottom plates. All buffers were filtered through 0.45  $\mu\text{m}$  syringe filters prior to use. The rims of the wells were coated in vacuum grease (Hampton Research, HR3-510) and the appropriate buffers, precipitants and MQ water were combined to a total reservoir volume of 500  $\mu\text{L}$  in each well, and mixed via pipetting to ensure homogeneity. Crystallisation experiments were conducted through vapour diffusion via hanging drop, with varying drop ratios. The trays were incubated at 16°C to encourage crystal growth.

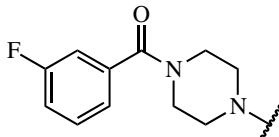
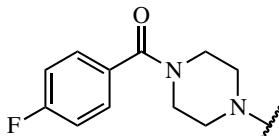
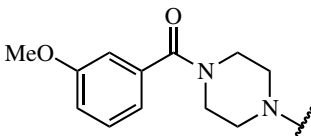
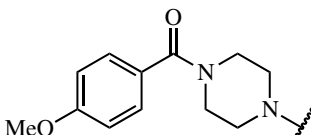
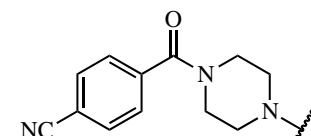
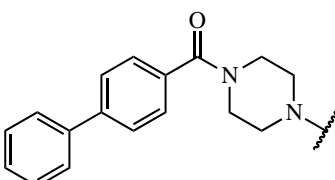
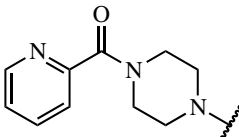
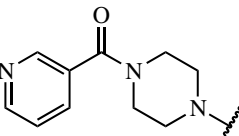
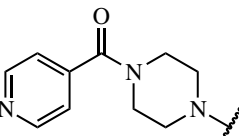
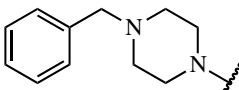
# Appendix A: Summary of SPR-derived ligand binding affinities

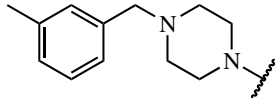
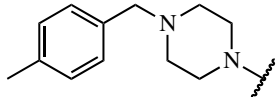
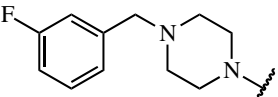
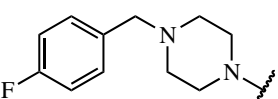
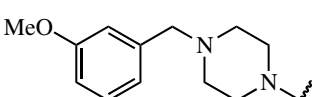
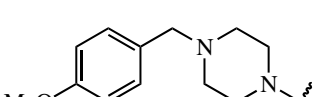
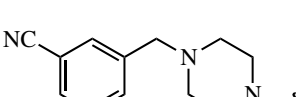
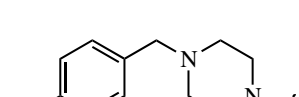
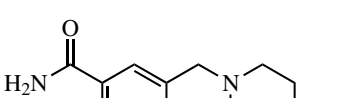
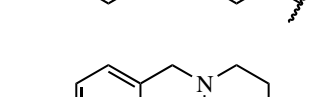
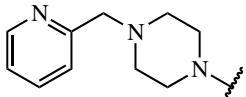
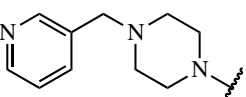
## Ligand binding affinities for GST-Tec SH3

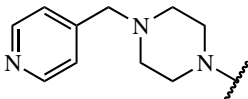
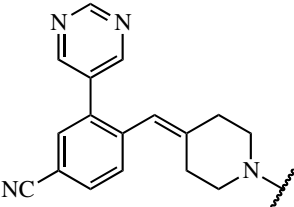
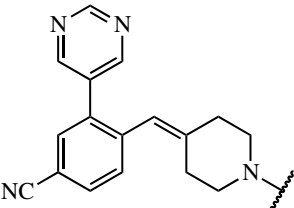
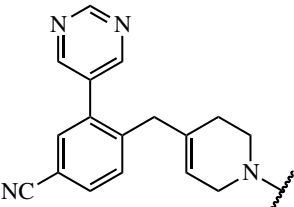
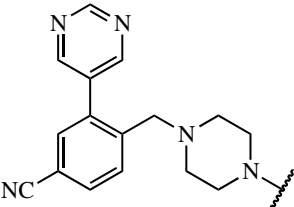
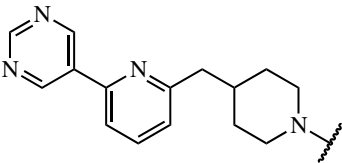
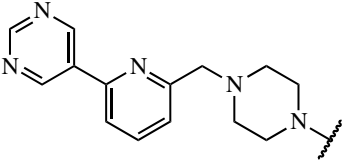
Table A.1: Binding affinities of ligands synthesised in this work, as determined by SPR for binding to GST-Tec SH3. <sup>a</sup> indicates assays (in triplicate) were completed within a single run. <sup>b</sup> indicates previous  $K_d$  values were determined by NMR binding assays. <sup>c</sup> indicates only a screening  $K_d$  value was obtained. <sup>d</sup> indicates binding isotherms had not reached plateau, as the ligand showed precipitation at high concentrations, therefore the highest data point was removed. <sup>e</sup> indicates ligand exhibited some off-site binding to reference channel protein. N/A denotes not applicable, as the ligand has not previously been reported in the literature. N.D. denotes not determined as the ligand was not soluble under the assay conditions.



Compound	R =	$K_d \pm SD$ ( $\mu\text{M}$ )	$K_d \pm SD$ ( $\mu\text{M}$ )
		(this work)	(previous work)
18a		$5.5 \pm 0.9$	$5 \pm 1^{56}$
18b		$3.0 \pm 0.7$	$2.8 \pm 1^{66}$
60a		$8.2 \pm 0.5$	N/A
60b		N.D.	N/A
60c		$5.3 \pm 0.6$	N/A

60d		$6.6 \pm 0.7$	N/A
60e		$7.2 \pm 0.5$	N/A
60f		$7.8 \pm 0.2$	N/A
60g		$5.4 \pm 0.2$	N/A
60i		$10.3 \pm 0.8$	N/A
76		N.D.	N/A
61a		$7.8 \pm 0.2^a$	N/A
61b		$8.6 \pm 0.4$	N/A
61c		$8.6 \pm 0.6$	N/A
17a		$9.2 \pm 0.6$	$28 \pm 8^b$

17b		27.4 <sup>c</sup>	N/A
17c		4.1 ± 0.6 <sup>d,e</sup>	N/A
17d		18.9 ± 2.5	N/A
17e		10.6 ± 1.9	N/A
17f		11.1 ± 3.6 <sup>d</sup>	N/A
17g		6.7 ± 0.5	N/A
17h		13.0 ± 1.4	N/A
17i		29.9 <sup>c</sup>	N/A
17j		9.2 ± 0.4	N/A
17k		6.8 ± 0.1	N/A
59a		5.2 ± 0.9 <sup>a</sup>	N/A
59b		10.6 ± 0.7	N/A

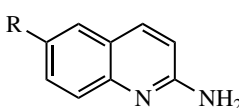
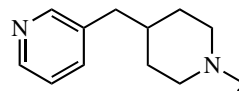
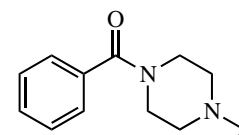
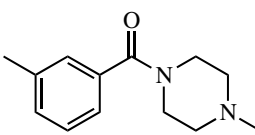
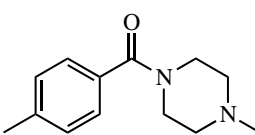
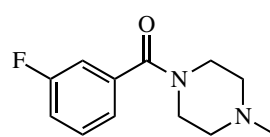
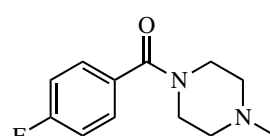
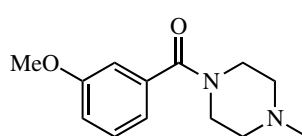
<b>59c</b>		$11.6 \pm 1.3$	N/A
<b>97</b>		$8.4 \pm 1.2$	N/A
<b>97 &amp; 114 (3:1)</b>		$8.3 \pm 1.5$	N/A
			
<b>100</b>		$20.6 \pm 3.4$	N/A
<b>88</b>		$7.3 \pm 1.0$	N/A
<b>89</b>		$18.1 \pm 1.3$	N/A

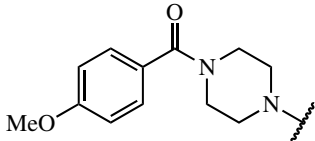
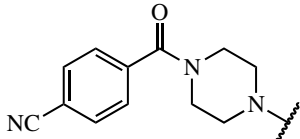
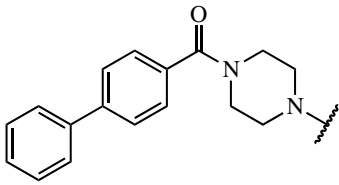
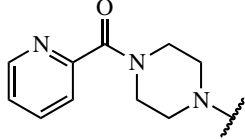
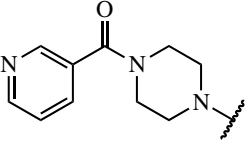
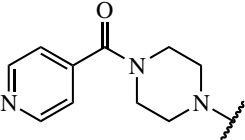
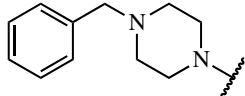
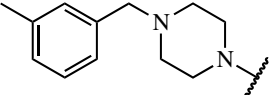
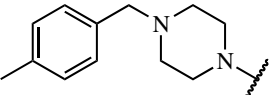
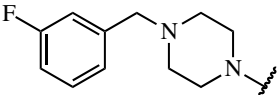
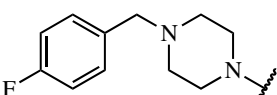
---

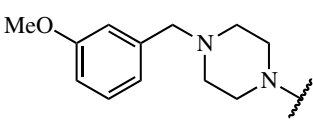
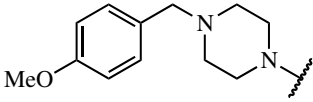
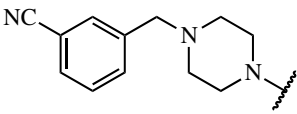
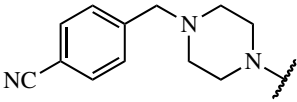
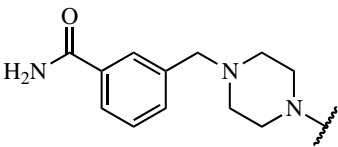
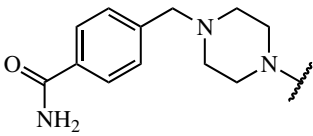
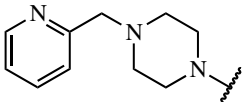
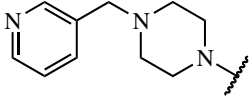
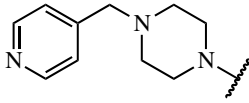


## Ligand binding affinities for GST-Tec SH3 D196A

Table A.2: Binding affinities of ligands synthesised in this work, as determined by SPR for binding to GST-Tec SH3 D196A. N.D. denotes not determined as the ligand was not soluble under the assay conditions.

Compound	R =	$K_d \pm SD$ ( $\mu\text{M}$ )
18a		no binding
18b		no binding
60a		no binding
60b		N.D.
60c		no binding
60d		no binding
60e		no binding
60f		no binding

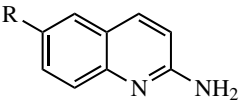
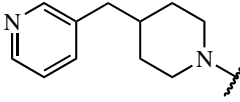
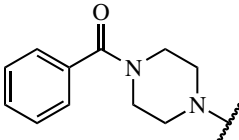
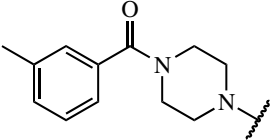
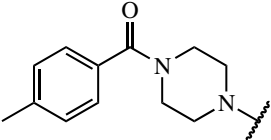
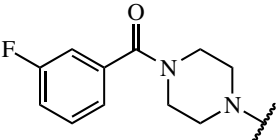
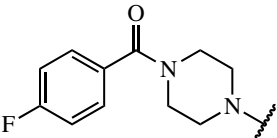
<b>60g</b>		no binding
<b>60i</b>		no binding
<b>76</b>		N.D.
<b>61a</b>		no binding
<b>61b</b>		no binding
<b>61c</b>		no binding
<b>17a</b>		no binding
<b>17b</b>		no binding
<b>17c</b>		no binding
<b>17d</b>		no binding
<b>17e</b>		no binding

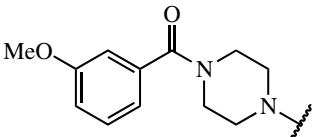
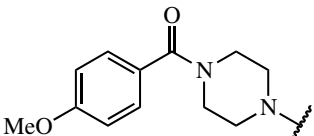
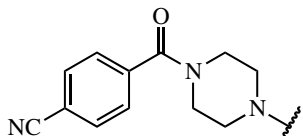
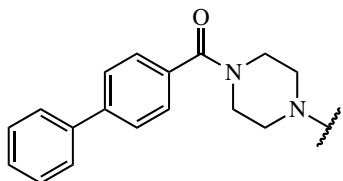
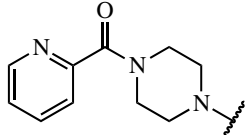
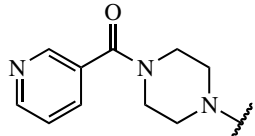
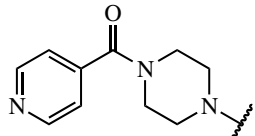
<b>17f</b>		no binding
<b>17g</b>		no binding
<b>17h</b>		no binding
<b>17i</b>		no binding
<b>17j</b>		no binding
<b>17k</b>		no binding
<b>59a</b>		no binding
<b>59b</b>		no binding
<b>59c</b>		no binding

---

## Comparison of ligand binding affinities for GST-Tec SH3 and Tec SH3

Table A.3: Comparison of binding affinities of compounds synthesised in this work, as determined by SPR for binding to either GST-Tec SH3 or Tec SH3. N.D. denotes not determined as the ligand was not soluble under the assay conditions. <sup>a</sup> indicates assays (in triplicate) were completed within a single run.

Compound	R =	GST-Tec SH3	Tec SH3
		$K_d \pm SD$ ( $\mu\text{M}$ )	$K_d \pm SD$ ( $\mu\text{M}$ )
18a		$5.5 \pm 0.9$	$6.6 \pm 0.6$
18b		$3.0 \pm 0.7$	$4.3 \pm 0.4$
60a		$8.2 \pm 0.5$	$10.1 \pm 0.3$
60b		N.D.	N.D.
60c		$5.3 \pm 0.6$	$8.2 \pm 0.4$
60d		$6.6 \pm 0.7$	$8.3 \pm 0.3$
60e		$7.2 \pm 0.5$	$9.0 \pm 0.5$

<b>60f</b>		$7.8 \pm 0.2$	$11.8 \pm 0.8$
<b>60g</b>		$5.4 \pm 0.2$	$8.7 \pm 0.3$
<b>60i</b>		$10.3 \pm 0.8$	$11.6 \pm 1.0$
<b>76</b>		N.D.	N.D.
<b>61a</b>		$7.8 \pm 0.2^a$	$11.5 \pm 1.7^a$
<b>61b</b>		$8.6 \pm 0.4$	$7.4 \pm 0.3$
<b>61c</b>		$8.6 \pm 0.6$	$9.5 \pm 0.8$

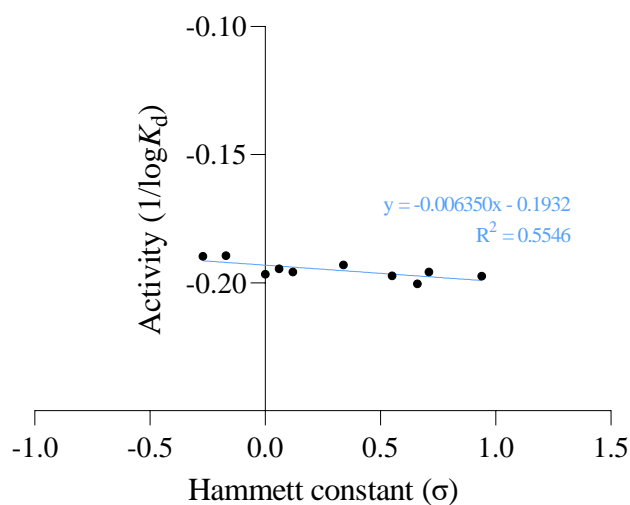
---

## Appendix B: Hansch plot analysis of trends in SPR binding assay data with GST-Tec SH3

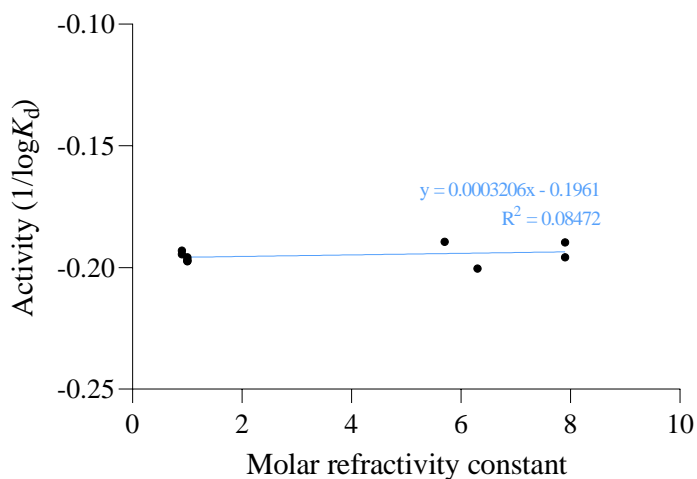
### Binding studies with 6-arylamidopiperazinyl-2-aminoquinoline derivatives

The following graphs in Figure B.1 represent Hansch plots between **60** and **61** ligand binding activity, and either electronic character (as Hammett constants,  $\sigma$ ),<sup>108–110</sup> volume (as molar refractivity constants)<sup>111</sup> and overall ligand hydrophobicity (as *clogP* values).<sup>61,112</sup> Therefore, using the available Hammett & molar refractivity constant tables in the literature,<sup>108–111</sup> and *clogP* values<sup>61</sup> the binding affinities (where available) were plotted, a simple linear regression fitted using GraphPad Prism v 9.0.0(121).<sup>51</sup>

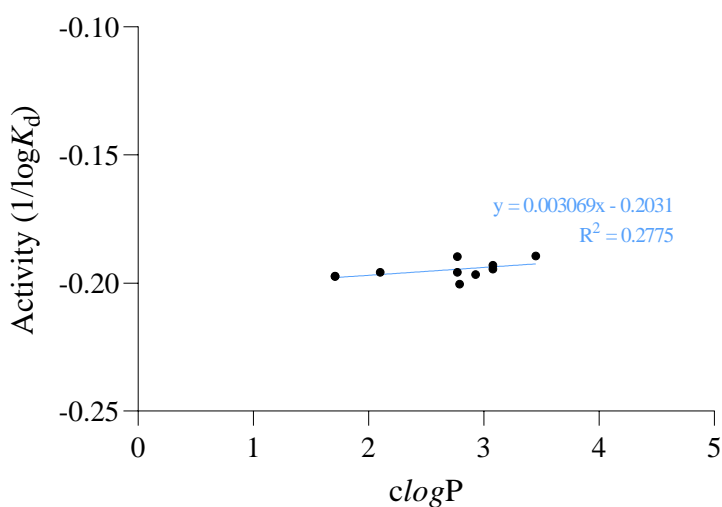
Similarly to above, the graphs in Figure B.2 represent Hansch plots between **17** and **59** ligand binding activity, and either electronic character (as Hammett constants,  $\sigma$ ),<sup>108–110</sup> volume (as molar refractivity constants)<sup>111</sup> and overall ligand hydrophobicity (as *clogP* values).<sup>61,112</sup> Again, using the available Hammett & molar refractivity constant tables in the literature,<sup>108–111</sup> and *clogP* values<sup>61</sup> the binding affinities (where available) were plotted, a simple linear regression fitted using GraphPad Prism v 9.0.0(121).<sup>51</sup>



**A**



**B**



**C**

Figure B.1: Hansch plots displaying relationship between binding activity of **60** and **61** ligands and the: (A) electronic nature of substituent (as Hammett constant,  $\sigma$ );<sup>108-110</sup> (B) volume of substituent (as molar refractivity constant);<sup>111</sup> or (C) overall ligand hydrophobicity (as  $clogP$  value).<sup>61,112</sup> Fitted linear equations and corresponding function over relevant datapoint range shown in blue, goodness of fit indicated by  $R^2$  value.

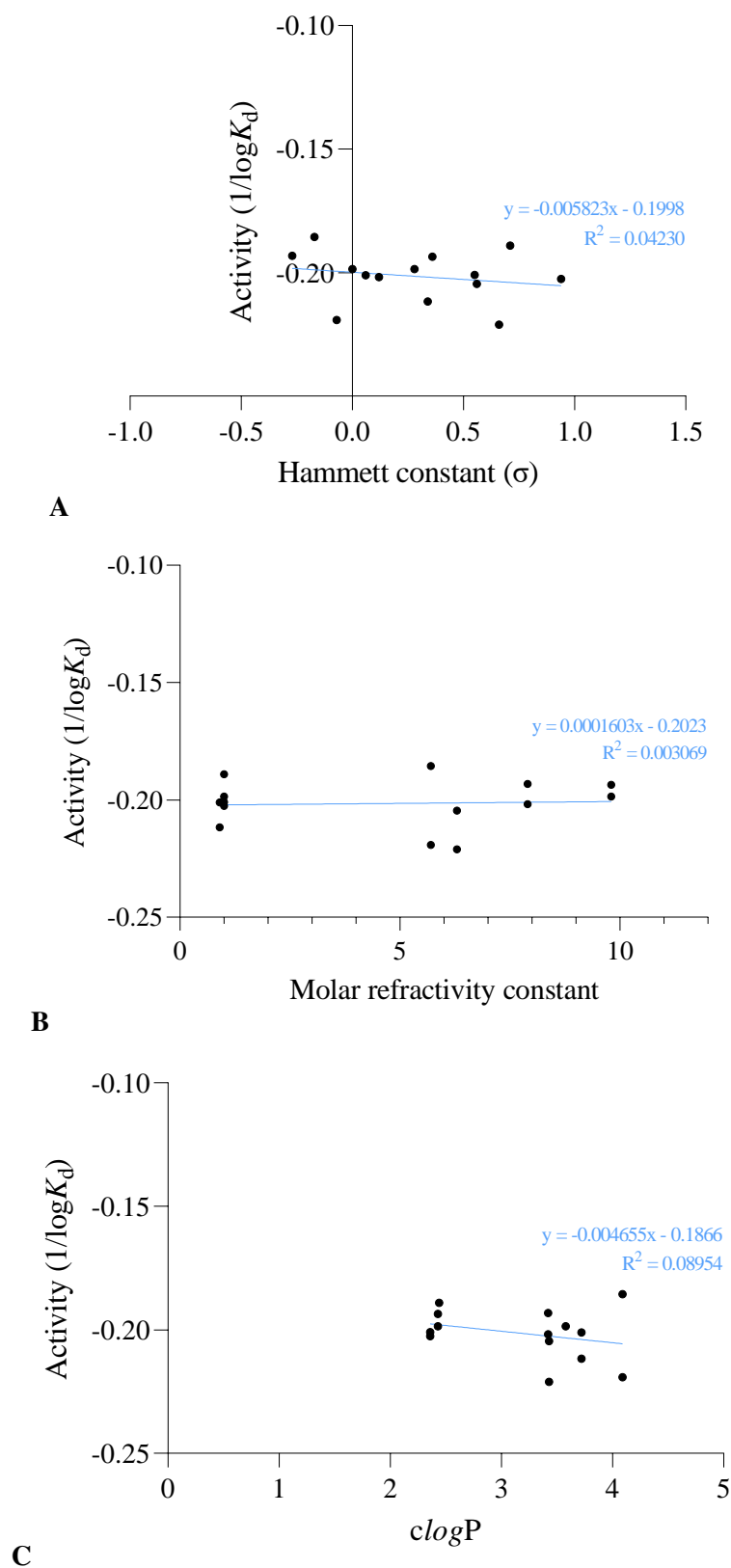


Figure B.2: Hansch plots displaying relationship between binding activity of **17** and **59** ligands and the: (A) electronic nature of substituent (as Hammett constant,  $\sigma$ );<sup>108–110</sup> (B) volume of substituent (as molar refractivity constant);<sup>111</sup> or (C) overall ligand hydrophobicity (as  $clogP$  value).<sup>61,112</sup> Fitted linear equations and corresponding function over relevant datapoint range shown in blue, goodness of fit indicated by  $R^2$  value.





# Bibliography

- (1) Berg, L. J.; Finkelstein, L. D.; Lucas, J. A.; Schwartzberg, P. L. *Annu. Rev. Immunol.* **2005**, *23*, 549–600.
- (2) Vihinen, M.; Nilsson, L.; Smith, C. *FEBS Lett.* **1994**, *350*, 263–265.
- (3) Pursglove, S. E.; Mulhern, T. D.; Mackay, J. P.; Hinds, M. G.; Booker, G. W. *J. Biol. Chem.* **2002**, *277*, 755–762.
- (4) Lu, X.-L.; Cao, X.; Liu, X.-Y.; Jiao, B.-H. *Curr. Med. Chem.* **2010**, *17*, 1117–1124.
- (5) Mano, H. *Cytokine Growth Factor Rev.* **1999**, *10*, 267–280.
- (6) Sato, K.; Mano, H.; Ariyama, T.; Inazawa, J.; Yazaki, Y.; Hirai, H. *Leukemia* **1994**, *8*, 1663–1672.
- (7) Byrd, J. C.; Furman, R. R.; Coutre, S. E.; Flinn, I. W.; Burger, J. A.; Blum, K. A.; Grant, B.; Sharman, J. P.; Coleman, M.; Wierda, W. G.; Jones, J. A.; Zhao, W.; Heerema, N. A.; Johnson, A. J.; Sukbuntherng, J.; Chang, B. Y.; Clow, F.; Hedrick, E.; Buggy, J. J.; James, D. F.; O'Brien, S. *N. Engl. J. Med.* **2013**, *369*, 32–42.
- (8) Schaeffer, E. M.; Schwartzberg, P. L. *Curr. Opin. Immunol.* **2000**, *12*, 282–288.
- (9) Ellmeier, W.; Jung, S.; Sunshine, M. J.; Hatam, F.; Xu, Y.; Baltimore, D.; Mano, H.; Littman, D. R. *J. Exp. Med.* **2000**, *192*, 1611–1624.
- (10) De Bruijn, M. J. W.; Rip, J.; van der Ploeg, E. K.; van Greuningen, L. W.; Ta, V. T. B.; Kil, L. P.; Langerak, A. W.; Rimmelzwaan, G. F.; Ellmeier, W.; Hendriks, R. W.; Corneth, O. B. *J. Immunol.* **2017**, *198*, 3058–3068.
- (11) Zwolanek, F.; Riedelberger, M.; Stolz, V.; Jenull, S.; Istel, F.; Köprülü, A. D.; Ellmeier, W.; Kuchler, K. *PLoS Pathog.* **2014**, *10*, 1–17.
- (12) Nguyen, J. T.; Porter, M.; Amoui, M.; Miller, W. T.; Zuckermann, R. N.; Lim, W. A. *Chem. Biol.* **2000**, *7*, 463–473.
- (13) Dalgarno, D. C.; Botfield, M. C.; Rickles, R. J. *Pept. Sci.* **1997**, *43*, 383–400.
- (14) Kay, B. K.; Williamson, M. P.; Sudol, M. *FASEB J.* **2000**, *14*, 231–241.
- (15) Smith, C. I. E.; Islam, T. C.; Mattsson, P. T.; Mohamed, A. J.; Nore, B. F.; Vihinen, M. *BioEssays* **2001**, *23*, 436–446.
- (16) Berg, T. *Angew. Chem. Int. Ed.* **2017**, *56*, 12048–12050.

- (17) Jenkins, M. K.; Taylor, P. S.; Norton, S. D.; Urdahl, K. B. *J. Immunol.* **1991**, *147*, 2461–2466.
- (18) Yang, W.-C.; Ghiotto, M.; Barbarat, B.; Olive, D. *J. Biol. Chem.* **1999**, *274*, 607–617.
- (19) Andreotti, A.; Bunnell, S.; Feng, S.; Berg, L.; Schreiber, S. *Nature* **1997**, *385*, 93–97.
- (20) Hansson, H.; Smith, C.; Härd, T. *FEBS Lett.* **2001**, *508*, 11–15.
- (21) Erlanson, D. A.; Davis, B. J.; Jahnke, W. *Cell Chem. Bio.* **2019**, *26*, 9–15.
- (22) Murakami, Y.; Tripathi, L. P.; Prathipati, P.; Mizuguchi, K. *Curr. Opin. Struct. Biol.* **2017**, *44*, 134–142.
- (23) Gao, Q.; Yang, L.; Zhu, Y. *Curr. Comput.-Aided Drug Des.* **2010**, *6*, 37–49.
- (24) Magee, T. V. *Bioorg. Med. Chem. Lett.* **2015**, *25*, 2461–2468.
- (25) Fuller, J. C.; Burgoyne, N. J.; Jackson, R. M. *Drug Discov. Today* **2009**, *14*, 155–161.
- (26) Mayer, J. P.; DiMarchi, R. D. *Cell Chem. Biol.* **2005**, *12*, 860–861.
- (27) Wells, J. A.; McClendon, C. L. *Nature* **2007**, *430*, 1001–1009.
- (28) Wu, B.; Barile, E.; De, S. K.; Wei, J.; Purves, A.; Pellicchia, M. *Curr. Top. Med. Chem.* **2015**, *15*, 2032–2042.
- (29) Choi, S.; Choi, K.-Y. *Expert Opin. Drug Discov.* **2017**, *12*, 293–303.
- (30) Scott, D. E.; Bayly, A. R.; Abell, C.; Skidmore, J. *Nat. Rev. Drug Discov.* **2016**, *15*, 533–550.
- (31) Lu, H.; Zhou, Q.; He, J.; Jiang, Z.; Peng, C.; Tong, R.; Shi, J. *Signal Transduct. Target. Ther.* **2020**, *5*, 1–23.
- (32) Lipinski, C. A. *J. Pharmacol. Toxicol. Methods* **2000**, *44*, 235–249.
- (33) Lipinski, C. A. *Adv. Drug Deliv. Rev.* **2016**, *101*, 34–41.
- (34) Congreve, M.; Carr, R.; Murray, C.; Jhoti, H. *Drug Discov. Today* **2003**, *8*, 876–877.
- (35) Veber, D. F.; Johnson, S. R.; Cheng, H.-Y.; Smith, B. R.; Ward, K. W.; Kopple, K. D. *J. Med. Chem.* **2002**, *45*, 2615–2623.
- (36) Bickerton, G. R.; Paolini, G. V.; Besnard, J.; Muresan, S.; Hopkins, A. L. *Nat. Chem.* **2012**, *4*, 90–98.
- (37) Baell, J.; Walters, M. A. *Nature* **2014**, *513*, 481–483.
- (38) Hopkins, A. L.; Groom, C. R.; Alex, A. *Drug Discov. Today* **2004**, *9*, 430–431.
- (39) Hopkins, A. L.; Keserü, G. M.; Leeson, P. D.; Rees, D. C.; Reynolds, C. H. *Nat. Rev. Drug Discov.* **2014**, *13*, 105–121.

- (40) Kenny, P. W.; Leitão, A.; Montanari, C. A. *J. Comput.-Aided Mol. Des.* **2014**, *28*, 699–710.
- (41) Murray, C. W.; Erlanson, D. A.; Hopkins, A. L.; Keserü, G. M.; Leeson, P. D.; Rees, D. C.; Reynolds, C. H.; Richmond, N. J. *ACS Med. Chem. Lett.* **2014**, *5*, 616–618.
- (42) Shultz, M. D. *ACS Med. Chem. Lett.* **2014**, *5*, 2–5.
- (43) Berman, H. M.; Westbrook, J.; Feng, Z.; Gilliland, G.; Bhat, T. N.; Weissig, H.; Shindyalov, I. N.; Bourne, P. E. *Nucleic Acids Res.* **2000**, *28*, 235–242.
- (44) Pursglove, S. E.; Mulhern, T. D.; Hinds, M. G.; Norton, R. S.; Booker, G. W. *J. Biomol. NMR* **1998**, *12*, 461–462.
- (45) Böhm, H.-J. *J. Comput.-Aided Mol. Des.* **1992**, *6*, 61–78.
- (46) Inglis, S. R.; Stojkoski, C.; Branson, K. M.; Cawthray, J. F.; Fritz, D.; Wiadrowski, E.; Pyke, S. M.; Booker, G. W. *J. Med. Chem.* **2004**, *47*, 5405–5417.
- (47) Smith, J. A.; Jones, R. K.; Booker, G. W.; Pyke, S. M. *J. Org. Chem.* **2008**, *72*, 8880–8892.
- (48) Jones, R. PhD Thesis, The University of Adelaide, 2007.
- (49) Ziarek, J. J.; Peterson, F. C.; Lytle, B. L.; Volkman, B. F. In *Methods in Enzymology*; Elsevier: 2011, pp 241–275.
- (50) Inglis, S. PhD Thesis, The University of Adelaide, 2004.
- (51) GraphPad Prism for Windows, 9.0.0, GraphPad Software, 2020.
- (52) Pettersen, E. F.; Goddard, T. D.; Huang, C. C.; Couch, G. S.; Greenblatt, D. M.; Meng, E. C.; Ferrin, T. E. *J. Comput. Chem.* **2004**, *25*, 1605–1612.
- (53) Inglis, S. R.; Jones, R. K.; Booker, G. W.; Pyke, S. M. *Bioorg. Med. Chem. Lett.* **2006**, *16*, 387–390.
- (54) Stojkoski, C. Honours Thesis, The University of Adelaide, 2001.
- (55) Martin, S. C.; Ball, Z. T. *ACS Med. Chem. Lett.* **2019**, *10*, 1380–1385.
- (56) Jayne, S. PhD Thesis, The University of Adelaide, 2019.
- (57) Foo, T. Honours Thesis, The University of Adelaide, 2005.
- (58) Inglis, S. R.; Jones, R.; Fritz, D.; Stojkoski, C.; Booker, G.; Pyke, S. *Org. Biomol. Chem.* **2005**, *3*, 2543–2557.
- (59) Altschul, S. F.; Gish, W.; Miller, W.; Myers, E. W.; Lipman, D. J. *J. Mol. Biol.* **1990**, *215*, 403–410.
- (60) Smith, J. A. PhD Thesis, The University of Adelaide, 2009.
- (61) ChemAxon, Marvin, 19.8.0, 2019.

- (62) Sezonov, G.; Joseleau-Petit, D.; D'Ari, R. *J. Bacteriol.* **2007**, *189*, 8746–8749.
- (63) Azatian, S. B.; Kaur, N.; Latham, M. P. *J. Biomol. NMR* **2019**, *73*, 11–17.
- (64) Cytiva, *Biacore™ Sensor Surface Handbook*; Cytiva: Marlborough, Massachusetts, USA, 2022.
- (65) Cytiva, *Biacore S200: Software Handbook*; Cytiva: Marlborough, Massachusetts, USA, 2021.
- (66) Limongelli, J. Honours Thesis, The University of Adelaide, 2020.
- (67) GE Healthcare Life Sciences, *Biacore™ Assay Handbook*; General Electric Company: Uppsala, Sweden, 2012.
- (68) Harper, S.; Speicher, D. W. In *Methods in Molecular Biology*; Humana Press: 2010, pp 259–280.
- (69) Wang, K.; Zhang, L.; Sheng, X.; Qin, Y.; Li, S.; Shen, Q. DNA Construct Design System, WO2019201276A1, 2019.
- (70) Marty, M. T.; Baldwin, A. J.; Marklund, E. G.; Hochberg, G. K. A.; Benesch, J. L. P.; Robinson, C. V. *Anal. Chem.* **2015**, *87*, 4370–4376.
- (71) Schasfoort, R. B. M. In *Handbook of Surface Plasmon Resonance (2)*; The Royal Society of Chemistry: London, United Kingdom: 2017, pp 1–26.
- (72) Watts, B. *Guide to Running an SPR Experiment*; Duke Human Vaccine Institute: Durham, North Carolina, USA, 2019.
- (73) GE Healthcare Life Sciences, *Biacore Training Courses: Biacore Training*; General Electric Company: Uppsala, Sweden, 2015.
- (74) Anjaneyulu, P.; Staros, J. V. *Int. J. Pept. Protein Res.* **1987**, *30*, 117–124.
- (75) Johnsson, B.; Löfås, S.; Lindquist, G. *Anal. Biochem.* **1991**, *198*, 268–277.
- (76) Gasteiger, E.; Hoogland, C.; Gattiker, A.; Duvaud, S.; Wilkins, M. R.; Appel, R. D.; Bairoch, A. In *Protein Identification and Analysis Tools on the ExPASy Server*; Walker, J. M., Ed.; Humana Totowa, New Jersey: 2005; Chapter 52, pp 571–607.
- (77) Drescher, D. G.; Drescher, M. J.; Ramakrishnan, N. A. In *Methods in Molecular Biology*; Humana Press: 2009, pp 323–343.
- (78) GE Healthcare Life Sciences, *Biacore™: Sensor Surface Handbook*; General Electric Company: Buckinghamshire, United Kingdom, 2017.
- (79) Kyte, J.; Doolittle, R. F. *J. Mol. Biol.* **1982**, *157*, 105–132.

- (80) Ye, Q.; Singh, V. K.; Blonde, J. D.; Jia, Z. *Acta Crystallogr. Sect. F: Struct. Biol. Cryst. Commun.* **2004**, *61*, 62–64.
- (81) Bucher, M. H.; Evdokimov, A. G.; Waugh, D. S. *Acta Crystallogr. Sect. D: Biol. Crystallogr.* **2002**, *58*, 392–397.
- (82) Kuge, M.; Fujii, Y.; Shimizu, T.; Hakoshima, T.; Hirose, F.; Matsukage, A. *Protein Sci.* **1997**, *6*, 1783–1786.
- (83) Prade, L.; Huber, R.; Manoharan, T. H.; Fahl, W. E.; Reuter, W. *Structure* **1997**, *5*, 1287–1295.
- (84) Manoharan, T.; Gulick, A.; Puchalski, R.; Servais, A.; Fahl, W. *J. Biol. Chem.* **1992**, *267*, 18940–18945.
- (85) Cardoso, R. M.; Daniels, D. S.; Bruns, C. M.; Tainer, J. A. *Proteins: Struct. Funct. Bioinf.* **2003**, *51*, 137–146.
- (86) McTigue, M. A.; Bernstein, S. L.; Williams, D. R.; Tainer, J. A. *Proteins: Struct. Funct. Bioinf.* **1995**, *22*, 55–57.
- (87) Reinemer, P.; Prade, L.; Hof, P.; Neufeind, T.; Huber, R.; Zettl, R.; Palme, K.; Schell, J.; Koelln, I.; Bartunik, H. D.; Bieseler, B. *J. Mol. Biol.* **1996**, *255*, 289–309.
- (88) Grahn, E.; Novotny, M.; Grehn, L.; Olin, B.; Madsen, D.; Wahlberg, M.; Jakobsson, E.; Gustafsson, A.; Mannervik, B.; Kleywegt, G. *Acta Crystallogr. Sect. D: Biol. Crystallogr.* **2006**, *62*, 197–207.
- (89) Gustafsson, A.; Mannervik, B. *J. Mol. Biol.* **1999**, *288*, 787–800.
- (90) Berndt, S.; Gurevich, V. V.; Iverson, T. M. *PLoS ONE* **2019**, *14*, 1–10.
- (91) Merő, B.; Radnai, L.; Gógl, G.; Tőke, O.; Leveles, I.; Koprivanacz, K.; Szeder, B.; Dülk, M.; Kudlik, G.; Vas, V.; Cserkaszkzy, A.; Sipeki, S.; Nyitray, L.; Vértessy, B. G.; Buday, L. *J. Biol. Chem.* **2019**, *294*, 4608–4620.
- (92) Aldehaiman, A.; Momin, A. A.; Restouin, A.; Wang, L.; Shi, X.; Aljedani, S.; Opi, S.; Lugari, A.; Shahul Hameed, U. F.; Ponchon, L.; Morelli, X.; Huang, M.; Dumas, C.; Collette, Y.; Arold, S. T. *Biochem. J.* **2021**, *478*, 1525–1545.
- (93) Bolgov, A.; Korban, S.; Luzik, D.; Zhemkov, V.; Kim, M.; Rogacheva, O.; Bezprozvanny, I. *Acta Crystallogr. Sect. F: Struct. Biol. Cryst. Commun.* **2020**, *76*, 263–270.
- (94) Johnston, K. M.; Luker, R. M.; Williams, G. H. *J. Chem. Soc., Perkin Trans. 1* **1972**, 1648–1652.

- (95) Alabaster, C. T.; Bell, A. S.; Campbell, S. F.; Ellis, P.; Henderson, C. G.; Roberts, D. A.; Ruddock, K. S.; Samuels, G. M. R.; Stefaniak, M. H. *J. Med. Chem.* **1988**, *31*, 2048–2056.
- (96) Schlummer, B.; Scholz, U. *Adv. Synth. Catal.* **2004**, *346*, 1599–1626.
- (97) Loones, K. T. J.; Maes, B. U. W.; Rombouts, G.; Hostyn, S.; Diels, G. S. M. *Tetrahedron* **2005**, *61*, 10338–10348.
- (98) Kóródi, F. *Synth. Commun.* **1991**, *21*, 1841–1846.
- (99) Dorel, R.; Grugel, C. P.; Haydl, A. M. *Angew. Chem.* **2019**, *131*, 17276–17287.
- (100) Fitzner, M.; Wuitschik, G.; Koller, R. J.; Adam, J.-M.; Schindler, T.; Reymond, J.-L. *Chem. Sci.* **2020**, *11*, 13085–13093.
- (101) Leggio, A.; Belsito, E. L.; De Luca, G.; Di Gioia, M. L.; Leotta, V.; Romio, E.; Siciliano, C.; Liguori, A. *RSC Adv.* **2016**, *6*, 34468–34475.
- (102) Mai, S.; Rao, C.; Chen, M.; Su, J.; Du, J.; Song, Q. *Chem. Commun.* **2017**, *53*, 10366–10369.
- (103) Kudelko, A.; Wróblowska, M. *Tetrahedron Lett.* **2014**, *55*, 3252–3254.
- (104) Schwab, J. M.; Ray, T.; Ho, C. K. *J. Am. Chem. Soc.* **1989**, *111*, 1057–1063.
- (105) Gazvoda, M.; Kočevár, M.; Polanc, S. *Eur. J. Org. Chem.* **2013**, *2013*, 5381–5386.
- (106) Rauk, A.; Allen, L. C.; Mislow, K. *Angew. Chem. Int. Ed. Engl.* **1970**, *9*, 400–414.
- (107) Wodtke, R.; Steinberg, J.; Köckerling, M.; Löser, R.; Mamat, C. *RSC Adv.* **2018**, *8*, 40921–40933.
- (108) Hammett, L. P. *J. Am. Chem. Soc.* **1937**, *59*, 96–103.
- (109) Bowden, K. In *Comprehensive Medicinal Chemistry: The Rational Design, Mechanistic Study & Therapeutic Applications of Chemical Compounds*; Pergamon Press: 1990; Vol. 4, pp 205–240.
- (110) Blanch, J. H. *J. Chem. Soc. B* **1966**, 937–939.
- (111) Taylor, P. J. In *Comprehensive Medicinal Chemistry: The Rational Design, Mechanistic Study & Therapeutic Applications of Chemical Compounds*; Pergamon Press: 1990; Vol. 4, pp 295–320.
- (112) Sarkar, A.; Kellogg, G. *Curr. Top. Med. Chem.* **2010**, *10*, 67–83.
- (113) Swan, E. Honours Thesis, The University of Adelaide, 2018.
- (114) Ozawa, M.; Shiro, T.; Takaaki, S.; Mari, I. Cyclic Aminoalkylcarboxamide Derivative pat., WO2008029924A1, 2008.

- (115) Hall, J. H.; Gisler, M. *J. Org. Chem.* **1976**, *41*, 3769–3770.
- (116) Wiberg, K. B. *J. Am. Chem. Soc.* **1953**, *75*, 3961–3964.
- (117) *SPR-Pages*, <https://www.sprpages.nl/> (accessed 5 Aug 2022).
- (118) Reichardt, C., *Solvents and Solvent Effects in Organic Chemistry*, Third; Reichardt, C., Ed.; Wiley-VCH Verlag GmbH & Co.: 2003.
- (119) Selig, W. *Microchem. J.* **1978**, *23*, 466–468.
- (120) Podgoršek, A.; Stavber, S.; Zupan, M.; Iskra, J. *Tetrahedron Lett.* **2006**, *47*, 7245–7247.
- (121) Robiette, R.; Richardson, J.; Aggarwal, V. K.; Harvey, J. N. *J. Am. Chem. Soc.* **2006**, *128*, 2394–2409.
- (122) Byrne, P. A.; Gilheany, D. G. *Chem. Eur. J.* **2016**, *22*, 9140–9154.
- (123) Qiuyun, D.; Mingxin, D.; Shibo, J.; Lu, H. 1-(3-Aminopropyl) piperazine-4-aminoamide compound as well as preparation method and application thereof Patent Application, CN101921224A, 2010.
- (124) Greene, T. W.; Wuts, P. G. M. In *Protective Groups in Organic Synthesis*; John Wiley & Sons, Ltd: 1999; Chapter 7, pp 494–653.
- (125) Abraham, M. H.; Grellier, P. L. *J. Chem. Soc., Perkin Trans. 2* **1976**, 1735–1741.
- (126) Bremner, D. H.; Dunn, A. D.; Wilson, K. A. *Synthesis* **1992**, *1992*, 528–530.
- (127) Newkome, G. R.; Kiefer, G. E.; Xia, Y.-J.; Gupta, V. K. *Synthesis* **1984**, *1984*, 676–679.
- (128) Rajalingam, D.; Kathir, K. M.; Ananthamurthy, K.; Adams, P. D.; Kumar, T. K. S. *Anal. Biochem.* **2008**, *375*, 361–363.
- (129) Pursglove, S. E. PhD Thesis, The University of Adelaide, 2001.
- (130) Waugh, D. S. *Protein Expr. Purif.* **2011**, *80*, 283–293.
- (131) Smyth, D. R.; Mrozkiewicz, M. K.; McGrath, W. J.; Listwan, P.; Kobe, B. *Protein Sci.* **2003**, *12*, 1313–1322.
- (132) Bruzzoni-Giovanelli, H.; Alezra, V.; Wolff, N.; Dong, C.-Z.; Tuffery, P.; Rebollo, A. *Drug Discov. Today* **2018**, *23*, 272–285.
- (133) Truong, J.; George, A.; Holien, J. K. *RSC Med. Chem.* **2021**, *12*, 1731–1749.
- (134) Chalmers, B. A.; Xing, H.; Houston, S.; Clark, C.; Ghassabian, S.; Kuo, A.; Cao, B.; Reitsma, A.; Murray, C.-E. P.; Stok, J. E.; Boyle, G. M.; Pierce, C. J.; Littler, S. W.; Winkler, D. A.; Bernhardt, P. V.; Pasay, C.; De Voss, J. J.; McCarthy, J.; Parsons, P. G.; Walter, G. H.;



Smith, M. T.; Cooper, H. M.; Nilsson, S. K.; Tsanaktsidis, J.; Savage, G. P.; Williams, C. M. *Angew. Chem. Int. Ed.* **2016**, *55*, 3580–3585.

- (135) Eaton, P. E. *Angew. Chem. Int. Ed. Engl.* **1992**, *31*, 1421–1436.
- (136) Falkiner, M. J.; Littler, S. W.; McRae, K. J.; Savage, G. P.; Tsanaktsidis, J. *Org. Process Res. Dev.* **2013**, *17*, 1503–1509.
- (137) Dauben, H. J.; McCoy, L. L. *J. Am. Chem. Soc.* **1959**, *81*, 4863–4873.
- (138) Virgil, S. C.; Hughes, T. V. In *Encyclopedia of Reagents for Organic Synthesis*; John Wiley & Sons, Ltd: 2006.
- (139) Cook, X. A. F.; Pantaine, L. R. E.; Blakemore, D. C.; Moses, I. B.; Sach, N. W.; Shavnya, A.; Willis, M. C. *Angew. Chem. Int. Ed.* **2021**, *60*, 22461–22468.
- (140) Ornstein, L. *Ann. N.Y. Acad. Sci.* **1964**, *121*, 321–349.